Intergovernmental Oceanographic Commission
Workshop report no. 17 - supplement

Papers submitted to the Joint IOC/WMO Seminar on Oceanographic Products and the IGOSS Data Processing and Services System

Moscow, 2-6 April 1979

Intergovernmental Oceanographic Commission

Workshop report No. 17
Supplement

Papers submitted to the Joint IOC/WMO Seminar on Oceanographic Products and the IGOSS Data Processing and Services System

Moscow, 2-6 April 1979

UNESCO 1979

Workshop report No. 17
Supplement

The Scientific Workshops of the Intergovernmental Oceanographic Commission are usually jointly sponsored with other intergovernmental or non-governmental bodies. In each case, by mutual agreement, one of the sponsoring bodies assumes responsibility for publication of the final report. Copies may be requested from the publishing bodies as listed below or from the Secretary IOC, Unesco, Place de Fontenoy, 75700 Paris, France.

No.	Title	Publishing Body	Languages
1	CCOP-IOC, 1974, Metallogenesis, Hydrocarbons and Tectonic Patterns in Eastern Asis /Report of the IDOE Workshop on/; Bangkok, Thailand, 24-29 September 1973 UNDP (CCOP), 138 p.	Office of the Project Manager UNDP/CCOP c/o ESCAP Sala Santitham Bangkok 2, Thailand	English
2	CICAR Ichthyplankton Workshop, Mexico City, 16-27 July 1974. (Unesco Technical Paper in Marine Science, No. 20)	Division of Marine Sciences, Unesco Place de Fontenoy, 75700 Paris, France	English Spanish
3	Report of the IOC/GFCM/ICSEM International Workshop on Marine Pollution in the Mediterranean, Monte Carlo, 9-14 September 1974.	IOC, Unesco Place de Fontenoy 75700 Paris, France	English French Spanish
4	Report of the Workshop on the Phenomenon known as "El Nino", Guyaquil, Ecuador 4-12 December 1974	FAO Via delle Terme di Caracalla, 00100 Rome, Italy	English Spanish
5	IDOE International Workshop on Marine Geology and Geophysics of the Caribbean Region and its Resources, Kingston, Jamaica, 17-22 February 1975	IOC, Unesco Place de Fontenoy 75700 Paris, France	English Spanish
6	Report of the CCOP/SOPAC-IOC IDOE International Workshop on Geology, Mineral Resources and Geophysics of the South Pacific, Suva, Fiji, 1-6 September 1975	IOC, Unesco Place de Fontenoy 75700 Paris, France	English
7	Report of the Scientific Workshop to initiate planning for a co-operative investigation in the North and Central Western Indian Ocean, organized within the IDOE under the sponsorship of IOC/FAO (IOFC)/UNESCO/EAC, Nairobi, Kenya, 25 March - 2 April 1976.	IOC, Unesco Place de Fontenoy 75700 Paris, France	Full text (English only) Extract and Recommendations: French Spanish Russian

No.	Title	Publishing body	Languages
8	Joint IOC/FAO (IPFC)/UNEP International Workshop on Marine Pollution in East Asian Waters, Penang, 7-13 April 1976	IOC, Unesco Place de Fontenoy 75700 Paris, France	English
9	IOC/CMG/SCOR Second International Workshop on Marine Geoscience, Mauritius, 9-13 August 1976	IOC, Unesco Place de Fontenoy 75700 Paris, France	English French Spanish Russian
10	IOC/WMO Second Workshop on Marine Pollution (Petroleum) Monitoring, Monaco, 14-18 June 1976	IOC, Unesco Place de Fontenoy 75700 Paris, France	English French Spanish Russian
11	Report of the IOC/FAO/UNEP International Workshop on Marine Pollution in the Caribbean and Adjacent Regions, Port of Spain, Trinidad, 13-17 December 1976	IOC, Unesco Place de Fontenoy 75700 Paris, France	English Spanish
11 Suppl.	Collected contributions of invited lecturers and authors to the IOC/FAO/UNEP International Workshop on Marine Pollution in the Caribbean and Adjacent Regions, Port of Spain, Trinidad, 13-17 December 1976	IOC, Unesco Place de Fontenoy 75700 Paris, France	English Spanish
12	Report of the IOCARIBE Interdisciplinary Workshop on scientific programmes in support of fisheries projects, Fort-de-France, Martinique, 28 November - 2 December 1977	IOC, Unesco Place de Fontenoy 75700 Paris, France	English Spanish
13	Report of the IOCARIBE Workshop on Environmental Geology of the Caribbean Coastal Area, 16-18 January 1978	IOC, Unesco Place de Fontenoy 75700 Paris, France	English Spanish
14	IOC/FAO/WHO/UNEP International Workshop on Marine Pollution in the Gulf of Guinea and adjacent areas, Abidjan, Ivory Coast, 2-9 May 1978	UNEP Palais des Nations 1211 Geneva 20 Switzerland	English French
15	CPPS/FAO/IOC/UNEP International Workshop on Marine Pollution in the Southeast Pacific Santiago de Chile 6-10 November 1978	IOC, Unesco Place de Fontenoy 75700 Paris, France CPPS Dir. de Soberania Maritima Ministerio de Relaciones Exteriores Lima Peru	English Spanish

Workshop report No. 17
Supplement

No.	Title	Publishing Body	Languages
16	Workshop on the Western Pacific	IOC, Unesco Place de Fontenoy 75700 Paris, France	English French Russian
17	Report of the Joint IOC/WMO Workshop on Oceanographic Products and the IGOSS Data Processing and Services System (IDPSS), Moscow, 9-11 April 1979	IOC, Unesco Place de Fontenoy 75700 Paris, France	English
17 Suppl.	Papers presented at the Joint IOC/WMO Seminar on Oceanographic Products and the IGOSS Data Processing and Services System (IDPSS), Moscow, 2-6 April 1979	IOC, Unesco Place de Fontenoy 75700 Paris, France	English

CONTENTS

* Presentation was based on slide projections, hence only a summary of the paper is reproduced herewith.

FOREWORD

The Joint IOC/WMO Seminar/Workshop on Oceanographic Products and the IGOSS Data Processing and Services System (IDPSS) was held in Moscow from 2 to 11 April 1979 within the framework of the Integrated Global Ocean Station System (IGOSS), in co-operation with the U.S.S.R. State Committee for Hydrometeorology and the Control of the Environment.

The Integrated Global Ocean Station System (IGOSS) is a joint IOC/WMO operational service programme for the supply of timely information on the state of the oceans to various marine activities and to support the scientific study of the oceans and the atmosphere. The IGOSS Data Processing and Services System (IDPSS) constitutes, together with the IGOSS observing system and data exchange system, a basic element of IGOSS the purpose of which is to make available to users the basic processed observational data and analyses needed for real-time and near-real-time application.

The need for a Seminar/Workshop was first identified by the Joint IOC/WMO Planning Group for IGOSS in 1976 and subsequently endorsed by the IOC Executive Council (Res. EC-X.12) and the WMO Executive Committee (Res. 4 (EC-XXVIII)) with the objective of considering the requirements of marine user groups for oceanographic services and for exchange of knowledge and experience among the specialists on oceanographic product formulation and methods used for their preparation.

The Seminar/Workshop was intended to provide a sound scientific and practical basis for the development of the IGOSS Data Processing and Services System and to encourage the participation of Member States in the IGOSS programme.

The Seminar, held from 2 to 6 April 1979, included presentations of papers on the following subjects:

- Identification of applications and benefits of existing and possible future products by various marine user groups;

- Review and evaluation of existing oceanographic products;

- Review of methods and techniques being used for the preparation of oceanographic products;

- Data processing, including quality control and standardization of methods and techniques of processing;

- Identification of data base required for the preparation of oceanographic products as well as means to ensure that data base.

Thirty-three papers were presented at the Seminar in which 55 participants from 14 countries and international organizations took part.

The Seminar was followed by a Workshop (9-11 April 1979) which identified types of guides and supporting documentation needed for the development of IDPSS and prepared guidelines for manuals and guides on IDPSS. Specific recommendations were formulated with regard to the content of the Guide on IDPSS, the Glossary of terms related to IGOSS, as well as further development of IDPSS in certain oceanic areas (see Workshop Report No. 17).

Preparations for the Seminar/Workshop were undertaken with the help of the Organizing Committee consisting of Dr. K.P. Vasiliev (U.S.S.R.) (Conference Co-ordinator), Mr. C. Fons (France), Dr. J. Masuzawa (Japan), Captain R.E. Nawratil (Argentina), Mr. B. Thompson (U.S.A.), Prof. Dr. H. Walden (Federal Republic of Germany). These members also served as discussion leaders for certain topics.

It was the general feeling of the participants at the Workshop that such types of Seminars were of great value in order to ensure that IGOSS is developed in an efficient and rational manner and that similar Seminars should be organized in future on other specific subjects related to IGOSS.

The participants at the Workshop expressed their appreciation to the U.S.S.R. State Committee for Hydrometeorology and the Control of the Environment, Hydrometeorological Centre of the U.S.S.R., and particularly to Dr. K.P. Vasiliev (Conference Co-ordinator) and his colleagues, for the excellent arrangements made for the meetings.

We wish to address the sincere thanks of IOC and WMO to all the individual experts who contributed papers, to the members of the Organizing Committee for the Seminar/Workshop, and to the U.S.S.R. State Committee for Hydrometeorology and the Control of the Environment for hosting the Seminar/ Workshop and for their great efforts to ensure the success of the meetings.

Desmond P.D. Scott
Secretary IOC

for (G.K. Weiss)
Secretary-General of WMO

INTRODUCTORY SPEECH BY MR. Y. TREGLOS, CHAIRMAN OF THE JOINT IOC/WMO WORKING COMMITTEE FOR THE INTEGRATED GLOBAL OCEAN STATION SYSTEM (JWC-IGOSS)

The Integrated Global Ocean Station System (IGOSS) is the joint responsibility of the Intergovernmental Oceanographic Commission (IOC) of Unesco and the World Meteorological Organization (WMO). It is designed as a global system whose purpose is to collect, analyse and disseminate oceanographic data and products in a timely manner.

Why has such a system been set up? A large number of human activities are centred on the ocean. Without listing them all,mention may be made first of all of fishing which, in order for it to be profitable and effective, calls for sound knowledge of surface and sub-surface conditions at those levels at which the desired species are most likely to be found.

The ocean also plays a leading role in the transport of goods and persons, and has done so for a very long time. But it cannot always be counted on to afford a safe passage and it is necessary to know in advance how it is going to behave and hence to build up knowledge about it. To achieve this, a considerable number of scientific studies have to be carried out. A signal example of such studies is the World Climate Programme.

Human activities in their turn affect the state of the ocean: marine pollution is not a myth and constant attention has to be given to it. Here again an untiring effort has to be made to monitor, measure, analyse, predict and make known the situation, past, present or future.

In order for an attempt to be made to solve this vast set of problems - and those mentioned so far do not purport to give a full picture - a system must be devised which is commensurate with the task. The necessary information will have to be able to be collected by means of a complex array of resources and then will have to be adequately transmitted within time-limits adapted to the specific phenomenon observed to a centre that is capable of using it; there it will be processed, analysed, "digested" and set out in proper form; it then becomes a "product" that has to be disseminated in turn through suitable channels and within appropriate time-limits.

The first stage therefore consists in the collection of relevant data. The meteorologist and the oceanographer have at their disposal for this purpose an entire arsenal of conventional and well-known tools, involving ships and coastal stations. These are now supplemented by a number of buoys, of every shape, size and destination. Some carry sub-surface equipment, like currentmeters for instance. Others, moored in carefully chosen places, record all kinds of meteorological and oceanic parameters. Others, smaller in size and more limited in range, but considerably cheaper and less cumbersome, drift across the surface of the oceans. They perhaps represent one of the great hopes of synoptic oceanography in the years to come. It will one day be as natural for an oceanographer to use them as it is today for a

meteorologist to send out a sounding balloon.

Other methods of data collection may appear less sophisticated, but nothing that works should be neglected. What is more effective, for instance, than a neuston net for extracting tar particles from the sea's surface?

We would perhaps be by-passing the essential if we were to forget about satellites and their possible uses for observation. At present, infra-red images are the ones that are most commonly used. But soon perhaps microwaves will enable us to "see" the surface of the ocean even through clouds.

Once these data have been collected, they have to be transmitted. For this purpose, WMO places its services at the disposal of IGOSS, and in particular the Global Telecommunications System (GTS). Messages concerning IGOSS are conveyed through the same well-tried channels as traditional meteorological messages. This is true in particular of observations of temperature, salinity or currents according to depth under the BATHY/TESAC programme. The volume of such messages increased fourfold between 1972 and 1978. Such a development requires no commentary.

These messages originate from a great variety of sources. They are received from traditional shipping lanes, that is to say from those stretches of the ocean where there is dense traffic. They are also sent out, as a matter of course, by stationary weather ships. Others originate from oceanographic research vessels effecting campaigns away from the normal routes. All are useful, but the latter, whose rarity is matched by their excellent quality, are the only ones (before buoys made their appearance) that provide information concerning zones where there is not much traffic. They are invaluable and should be warmly encouraged.

Lastly, there are the products themselves, which provide the reason for our meeting here today. A number of them relate to the surface temperature of the sea, a parameter that has long been included in surface observation messages sent out by ships and one that is easy to observe, even if not always perfectly. The processing of such data is now a routine matter for countries possessing sufficiently powerful computers.

These products often deal with a particular sector of the oceans to which the "manufacturer" gives special attention or that corresponds to a stated need. Others are geared to a less well-defined sector but concern all the oceans in the world. They are usually intended to serve for weather forecasting models and prove to be of use to fishermen.

Some products, even more finely attuned to the requirements of fishermen, relate to sub-surface sea temperatures. They may take the form of maps showing temperature distribution along a particular isobath. Another form they may assume, and one that is more adapted to scientific research in general, is so designed as to show the depth of an interesting isotherm.

It should not be thought that IGOSS is interested only in the sea's temperature. This is an important parameter, but others, more difficult to determine, are proving to be just as essential where knowledge of the ocean is concerned. A highly topical example may be found within the framework of the FGGE. Among other special observation systems, use is made in this experiment of drifting buoys distributed at mean and high latitudes of the Southern Hemisphere. They transmit data relating to sea surface temperature, as might be expected, but also to atmospheric pressure. In addition, it is possible, by keeping track of the routes they follow, to obtain interesting information concerning mean winds and surface circulation in that part of the world.

In order for this vast series of programmes to be carried out, the collaboration of the largest possible number of countries is necessary. They should collaborate in the programme, but also among themselves, so that they can, more specially, assist those who have not had the good fortune to attain the same degree of development. Training, education and mutual assistance (TEMA) are, and will remain, an essential aspect of IGOSS: the Vice-Chairman of the Joint IOC/WMO Working Committee for IGOSS, Dr. K.P. Vasiliev, has personal responsibility here.

It remains for me to express the wish that everyone will set their hearts on making a contribution that is commensurate with the project and that perhaps, one day, the great map of the world that shows all of the individual nations that are participating in our work will show no more than the oceans and the continents.

DETERMINATION OF SURFACE DRIFT PATTERNS AFFECTING FISH STOCKS IN THE CALIFORNIA CURRENT UPWELLING REGION

by

Andrew Bakun, Craig S. Nelson,* Richard H. Parrish

Pacific Environmental Group, Southwest Fisheries Center,
National Marine Fisheries Service, NOAA, Monterey, California 93940

Abstract

Surface marine observations are used to infer the large-scale seasonal patterns of ocean surface drift near the coast in the California Current. Striking conformities are noted between these patterns and regional faunal groupings. In the Pacific Northwest coastal fish species having pelagic larvae tend to spawn during the winter season when surface wind drift is generally directed toward the coast, rather than during the more productive upwelling season. In the region of vigorous upwelling off Northern California, which is characterized by strong offshore surface transport through most of the year, there is a paucity of locally spawning species. Rather, the fish stocks which harvest the massive productivity of that region are mainly migrating species which spawn under the more favorable drift conditions of the Southern California Bight. Closed gyral circulations in the Southern California Bight and off southern Baja California appear to foster favorable spawning conditions, leading to distinct faunal assemblages.

The apparent dependence of spawning strategies upon surface drift conditions suggests the hypothesis that anomalies in surface drift patterns could be a cause of the observed wide variations in spawning success of the major fishery species of the California Current region. Geostrophic currents tend to parallel coastal boundaries; thus a reasonable assumption is that major anomalies in the onshore-offshore component of surface transport are related to fluctuations in the surface wind drift. Indices of surface Ekman flux are derived from wind reports from ships at sea.

Other biologically important index series can be derived from related information. Offshore-directed surface Ekman flux can be linked to locally wind-induced coastal upwelling. Ekman flux divergence offshore of the coastal boundary zone may control concentration or dispersion of fish larvae, food organisms, and predator organisms. Wind mixing energy added to the water column can destroy vertical stratification of food particles, thought to be important to survival of first feeding fish larvae. Such index series have been applied to studies of the variations of such stocks as Pacific mackerel, Dungeness crab, English and Dover soles, northern anchovy, rockfish and Atlantic menhaden.

* Present address: NOAA Ship Townsend Cromwell, National Ocean Survey, NOAA, 1125-B Ala Moana Blvd., Honolulu, Hawaii 96814

Introduction

The California Current is a highly productive upwelling system, containing important fishery resources. The coastal fisheries have historically been subject to extreme fluctuations which have resulted in economic hardships. The Pacific sardine fishery expanded rapidly in the early 1930's to become the region's most important fishery, with 774,000 MT landed in the 1936-37 season. Thereafter the stocks declined to the point that the fishery had virtually disappeared by the late 1960's. Similarly, Pacific mackerel landings reached a peak of 66,500 MT in 1935-36, only to decline to a level near 1,100 MT by 1969. Estimates of northern anchovy spawning biomass off Southern California indicate an explosive increase from 267,000 MT in 1951 to 5,635,000 MT in 1965 and a recent decline to 1,180,000 MT in 1978. The lack of obvious relationships between stock size and recruitment in these and other pelagic species indicates an important effect of environmental conditions on the viability of the stocks. Truly effective management of the fishery resources of the region will require a capability to predict and allow for the effects of environmental variability. Recently, some promising hypotheses have been formulated, and environmental index time series suitable for testing the hypotheses are being developed.

Surface Ekman transport

Winter and summer distributions of surface Ekman transport, computed from the wind stress summaries of Nelson (1977), are presented in Figures 1 and 2. In these presentations summaries of stress computations from each available surface wind observation in the surface marine observation file (TDF-11) were made for each one-degree areal quadrangle. Each vector symbol represents a discrete sample which is completely independent of every other sample. No spatial smoothing has been applied.

During the winter (Figure 1) Cape Mendocino marks a division between generally onshore-directed Ekman transport to the north and offshore-directed transport to the south. Strongest offshore transport occurs off central Baja California. During the summer (Figure 2) Ekman transport tends to be directed offshore throughout the region, most strongly from Cape Blanco to Point Conception. The Southern California Bight, south of Point Conception appears as a local minimum in offshore transport.

Since offshore Ekman flux is the primary driving force for locally wind induced coastal upwelling (Figure 3), the area south of Cape Mendocino is characterized by coastal upwelling throughout the year. To the north, there is a seasonal alternation, with coastal upwelling predominating in summer and downwelling predominating during winter.

In these presentations (Figures 1 and 2) spatial detail has been achieved by compositing all available data in a given season from a large number of years, basically on the grounds that seasonal variability in temperate latitudes is generally large compared to interyear variability. Such spatial

resolution is never available in a synoptic sampling (Figure 4). For most practical applications a time series of variations in transport is required. However in forming time series from sparse observations which are sporadically distributed in time and space, the variability introduced by random errors in measurement or by changes in spatial distribution of reports may be as large as the variability in the processes themselves. Some method of objective analysis which filters out the small scale variability is required to produce homogeneous time series. Well developed objective analysis techniques are routinely employed by meteorological agencies.

One approach to producing time series indicators of Ekman transport is Bakun's (1975) upwelling indices. These are computed from synoptic surface atmospheric pressure analyses generated at the U.S. Navy's Fleet Numerical Weather Central. Wind reports are included in these analyses as equivalent pressure gradients according to the "Fields by information blending" methodology (Holl and Mendenhall, 1972). A geostrophic approximation and a simplified treatment of the planetary boundary layer are used to estimate the sea surface stress and resulting Ekman transport (Bakun, 1973). The component of Ekman transport perpendicular to the coast is resolved, positive values indicating offshore transport and negative values indicating onshore transport. A one-year sample of daily means of the 6-hourly synoptic computations (Figure 5) illustrates the characteristic seasonal and shorter scale variability.

Off the coasts of the states of Washington and Oregon (48N and 45N latitudes) the seasonal pattern is dominated by short intense bursts of onshore Ekman flux caused by winter storms. The summer season exhibits much lower energy pulsations, chiefly in the offshore direction. Off the state of California (39N, 36N) the summer is characterized by intense bursts of upwelling-producing offshore transport; the winter season is a more equal mix of onshore and offshore transport events. Off the state of Baja California in Mexico (30N, 27N) a lower level but steadier succession of offshore transport pulses continues throughout the year; the maximum intensity of upwelling producing offshore Ekman flux tends to occur in the early spring rather than in the late spring and early summer as is the case further north. At all the locations a large amount of the variance occurs in the "atmospheric event" frequency range, encompassing periods from greater than a day to several weeks.

Reproductive Strategies of Fishes

On the large time and space scales involved in the larval drift of a fish stock, the surface flow field can be adequately viewed as being a linear combination of the geostrophic flow field and the surface drift caused by the stress of the wind on the sea surface. A satisfactory approximation to the surface wind drift is provided by the Ekman transport. The conceptual picture, then, is of a thin surface layer of Ekman drift which varies in phase with atmospheric weather patterns, superimposed on a deeper, more slowly varying geostrophic flow field (Parrish, Nelson and Bakun, manuscript). Geostrophic flow in the California Current tends to parallel the coast; in the Southern California Bight south of Pt. Conception a cyclonic gyral circulation exists most of the year (Reid, Roden and Wyllie, 1958). A similar cyclonic circulation

tends to occur off southern Baja California, south of Punta Eugenia (Bakun and Nelson, in press).

The flow patterns that can be inferred from the combined Ekman and geostrophic fields suggest that, for purposes of larval transport, the California Current system can be divided into four regions:

(1) The Pacific Northwest region (north of Cape Blanco),
(2) The region of maximum upwelling (Cape Blanco to Pt. Conception),
(3) The Southern California Gyre (Pt. Conception to central Baja California),
(4) The southern Baja California region.

The correspondence of the reproductive strategies of California Current fishes to this regional subdivision is striking.

(1) In the Pacific Northwest region, the surface Ekman drift is predominently offshore during the summer upwelling season, and strongly onshore during the winter. Nearly all the dominant commercial Pacific Northwest fishes have a late winter spawning period. This is not the expected spawning period for a temperate fish fauna as it comes well before the maximum plankton blooms. In contrast most of the north Atlantic cold temperate fish fauna has short spawning periods coincident with the spring plankton blooms (Cushing, 1975). Evidently, in the Pacific Northwest the necessity for avoidance of loss of epipelagic eggs and larvae from the favorable near-coastal zone outweighs the necessity for high food availability. Another common adaptation for reducing larval loss in Pacific Northwest fishes is the avoidance of epipelagic eggs. A common example is the spawning of demersal eggs in protected inshore waters (e.g. herring, lingcod, cottids, and most of the other intertidal and littoral fishes of this region). Other strategies include livebearing (rockfishes and embiotocids), anadromous spawning (salmonids and osmerids), deep water spawning (pleuronectids and sablefish), and extensive migrations to areas of more favorable larval transport (hake, sardine, albacore).

(2) In the region of maximum upwelling, between Cape Blanco and Point Conception, Ekman transport is generally offshore, intensely so during the spring and summer. The adaptations to avoid larval loss found in the temperate component of the fauna are similar to those described for the Pacific Northwest. There is probably a continuous colonization of the upwelling region by larvae which are advected into the region from the Pacific northwest region. The subtropical component of the fish fauna in this region is principally composed of adults which use this region as a feeding ground, but do not spawn there (i.e. hake, sardine, bonito, white seabass, Pacific mackerel, and albacore). Very few coastal fishes have their center of abundance in the upwelling maxima region; bocaccio, Sebastes paucispinis, and chilepepper, Sebastes goodei, (both live bearers) appear to be the best examples. Apparently, coastal species with pelagic eggs and larvae have great difficulty in maintaining large resident populations in this region of strongest offshore transport and upwelling. Rather, the commercially important harvesters of the massive

organic production of this area are migrating species which spawn under the more favorable transport conditions of the Southern California Gyre.

(3) In the Southern California Gyre, south of Point Conception there is a local minimum of offshore Ekman transport near the coast at all seasons of the year. The geostrophic component of flow forms a closed gyre. The dominant pelagic fishes of the California Current System (i.e. those which have supported large fisheries) all spawn in this region. The adult sardine, hake, jack mackerel and Pacific mackerel migrate to the northward areas for feeding. The central stock of the northern anchovy, probably because of limited swimming ability due to their small size, remains principally within the Southern California Gyre.

(4) In the southern Baja California region a number of pelagic fishes have subpopulations which are distinct from those in the Southern California Bight. These include sardine (Clark 1947), Pacific mackerel (Roedel 1952) and northern anchovy (Vrooman and Smith 1971). In addition, a large tropical component appears in the fauna of this region due to northward warm water advection along the coast and proximity to the warm Gulf of California.

This general pattern of correspondence between reproduction strategies and ocean flow characteristic suggests that the necessity for minimization of offshore loss of reproductive products by seaward transport processes must have exerted a particularly strong control on the development of spawning characteristics. This in turn implies an important effect of transport conditions upon reproductive success, leading directly to the hypothesis that deviations from "normal" transport conditions, to which reproductive strategies are adapted, may be a cause of the very large recruitment variations observed in the coastal fisheries of the California Current.

A major problem in defining the environmental-biological relationships which are required to construct useful predictive models for fishery management is that there are generally available only very small time series samples with which to work. Fishery data characteristically yield one data point per year and the period over which the time series can be considered homogeneous does not normally exceed ten to twenty years. To sort out a multitude of possible environmental effects from a series with ten to twenty data points is a statistically impossible task. It is necessary therefore to either find the means to reduce the multitude of environmental factors to one, or at most several, indices of integrated environmental state, or to hope that one or perhaps two environmental factors will have such a dominant effect as to be discernible through the "noise level" generated by the other environmental effects not accounted for. The considerations presented above suggest that surface drift during the early egg and larval period may be such a dominant environmental factor for some of the major coastal fishery species of the California Current.

Wind stress curl

At a coastal boundary, the divergence in the surface Ekman transport is controlled by the offshore component, as indicated in Figure 3. In the open ocean, away from the vicinity of the boundary, Ekman divergence is controlled by the wind stress curl (Fofonoff, 1963). Positive wind stress curl induces Ekman divergence; negative curl induces convergence. Thus there are four possible combinations of convergence or divergence within a narrow coastal boundary zone and offshore of that zone (Figure 6). Certainly there could be a significant biological difference between the two coastal upwelling situations (types C and D in Figure 6). In the former (type C) there would be continued divergence and lower intensity upwelling offshore of the coastal upwelling zone. In the latter (type D), convergence and downwelling prevail offshore; formation of convergent surface fronts where organisms would tend to be concentrated would be favored. These could be areas either of good feeding success or of high vulnerability to predation.

There are no routine measurements of wind stress curl. However, since forming the curl of a vector field is a linear operation, the curl of a mean field should resemble the mean of the corresponding curl field. The curl fields (Figures 7 and 8) corresponding to the winter and summer stress fields (Figures 1 and 2) were computed by forming finite difference derivatives among neighboring one-degree squares (Nelson, 1977). Much of the smaller scale detail, particularly in the northern portion of the winter distribution (Figure 7) can be attributed to sampling errors which are amplified when derivatives are taken. However the coherent larger scale features are certainly significant, appearing consistently in Nelson's (1977) long term monthly fields.

Negative wind stress curl, or surface convergence, predominates in the offshore region throughout the year. From this offshore region, a lobe of negative wind stress curl extends shoreward to the central Baja California Coast between Punta Baja and Punta Eugenia. This feature appears consistently during all seasons of the year. In this same area of coast there is a consistent local maximum in the offshore Ekman Transport (Bakun and Nelson, in press). Thus the area from Punta Baja to Punta Eugenia represents a type "D" situation (Figure 6) with vigorous coastal upwelling coupled with convergence and downwelling offshore of the coastal upwelling zone.

To the north and south of this lobe of negative curl are regions of positive wind stress curl, or surface divergence, which extend from 100 to 300 km offshore. Particularly strong positive curl characterizes the Southern California Bight. This strong positive curl area expands northward, following the northward seasonal progression of coastal upwelling, to occupy virtually the entire coast during summer (type C, Figure 6).

During the spring upwelling maximum off Baja California, sea surface flow is parallel to the coast and strongly equatorward in response to the pressure gradients established by the upwelling of denser waters near shore. When the upwelling relaxes in the fall, the surface circulation tends to separate into semi-independent cyclonic gyres (Figure 9) in the regions of positive

wind stress curl. From Punta Baja to Punta Eugenia, where the curl is negative, flow remains equatorward along the coast (Bakun and Nelson, in press). Possible explanations for this correspondence of flow and wind curl patterns include (a) the existence of some approximate "Sverdrup balance" near the coast (Nelson, 1977), and (b) the effect of surface Ekman pumping whereby the pressure gradients set up between areas of surface convergence and divergence would induce geostrophic currents parallel to stress curl contours. This is a matter of ongoing research at out laboratory. In either case fluctuations in wind stress curl pattern would be related to variations in current pattern.

The lobe of negative curl which appears to separate the gyres of Figure 9, is located also at the separation between the Southern California Gyre and Southern Baja California faunal regions, discussed in the previous section. An example of the faunal separation is the existence of separate subpopulations of northern anchovy (Figure 10). It is possible that fluctuations in the strength of the negative curl lobe could influence exchanges between the central and southern anchovy populations.

There is a lack of sufficient data density (Figure 3) to resolve features of the size of the negative curl lobe in any synoptic sampling in order to form time series to test and utilize this possibility. Presently we are forced to rely on an untested assumption that the small scale features would fluctuate in the same general sense as the much larger scale which can be resolved by the available data (Bakun and Nelson, in press). Satellite systems, with wind stress sensors yielding the 50-km resolution designed for SEASAT-A would seem to allow us, for the first time, to view wind stress patterns on the same scale that they may actually affect fishery stocks.

Applications

Computed upwelling indices (Bakun 1973) which estimate the fluctuations in offshore Ekman transport, and offshore divergence indices (Bakun and Nelson, in press) which reflect variations in the large scale wind stress curl pattern, are beginning to be utilized in studies of California Current fishery stocks. A statistical model which explained less than twenty percent of the variance in Pacific mackerel recruitment was improved to explain seventy-eight percent of the variance (Figure 11) by the addition of two environmental variables, the upwelling index and offshore divergence index series in the vicinity of the negative curl lobe off Baja California (Parrish and MacCall, in press). Apparent relationships with upwelling index series have also been demonstrated for anchovy (Anon., 1978), Dungeness Crab (Peterson, 1973, Botsford and Wickham, 1975), Coho salmon (Gonsolus, 1978), English and Dover sole (Hayman, 1978), and rockfish (Parrish, et al., manuscript). A similar computation of the onshore Ekman transport near Cape Hatteras, accounted for nearly sixty percent of the variance from a fitted stock-recruitment curve for the Atlantic menhaden fishery (Nelson, Ingham and Schaaf, 1977).

Concluding remarks

In defining the effect of the environment on fishery stocks we must deal with a space-time continuum of processes; the necessary coverage is generally not available from research vessel operations. Recently, progress has been made using routinely-collected maritime data. Composite long term seasonal summaries of surface wind and ship drift observations have revealed features not resolvable in available synoptic samplings. Comparisons of these features to known biological features have motivated testable hypotheses. Consistent time series on the lower resolution scale that is available synoptically have been generated from analyzed meteorological fields. These have been used to test hypotheses and establish fishery-environmental relationships suitable for management purposes.

Important new findings on the sensitivity of pelagic fish stocks to the breaking up of fine-scale food strata by wind mixing during early larval feeding (Lasker, 1978) have not been discussed here. However, their application in fishery management will similarly require consistent time series indicators of the effect of wind acting on the sea surface.

References

Anonymous, 1978 - Northern anchovy fishery management plan. Pacific Fishery Council, Portland, Oregon, 103 p. + 8 appendices.

Bakun, A., 1973 - Coastal upwelling indices, west coast of North America, 1946-71. U.S. Dep. Commer., NOAA Tech. Rep. NMFS SSRF-671, 103 p.

Bakun, A., 1975 - Daily and weekly upwelling indices, west coast of North America, 1967-73. U.S. Dep. Commer., NOAA Tech. Rep. NMFS SSRF-693, 114 p.

Bakun, A., and Nelson, C.S., in press - Climatology of upwelling related processes off Baja California. Calif. Coop. Oceanic Fish. Invest., Prog. Rep.

Botsford, L.W., and Wickham, D.E., 1975 - Correlation of upwelling index and Dungeness crab catch. Fish. Bull. U.S., 73(4), 901-907.

Clark, F.N., 1947 - Analysis of the populations of the Pacific sardine on the basis of vertebral counts. Calif. Dept. Fish and Game, Fish. Bull. 65, 26 p.

Cushing, D.H., 1975 - Marine Ecology and Fisheries. Cambridge University Press, Cambridge--New York, 124 p.

Fofonoff, N.P., 1963 - Dynamics of ocean currents. In, The Sea. M.N. Hill, ed., Interscience Pub., New York, 1, 323-395.

Gonsolus, R.T., 1978 - The status of Oregon coho and recommendations for managing the production, harvest, and escapement of wild and hatchery-reared stocks. Oregon Dept. of Fish and Wildlife, Columbia Region, 59 p.

Hayman, R.A., 1978 - Environmental fluctuation and cohort strength of Dover sole (Microstomus pacificus) and English sole (Parophrys Vetulus). Ph. D. Thesis. Oregon State Univ.

Holl, M.M., and Mendenhall, B.R., 1972 - Fields by information blending, sea level pressure version. Fleet Numerical Weather Central Tech. Note 72-2, Monterey, California, 66 p.

Lasker, R., 1978 - The relation between oceanographic conditions and larval anchovy food in the California Current: identification of factors leading to recruitment failure. Rapp. P.-v. Reun. Cons. Int. Explor. Mer., 173, 212-230.

Nelson, C.S., 1977 - Wind stress and wind stress curl over the California Current. U.S. Dep. Commer., NOAA Tech. Rep. NMFS SSRF-714, 87 p.

Nelson, W.H., Ingham, M.C., and Schaff, W.E., 1977 - Larval transport and year class strength of Atlantic menhaden, Brevoortia tyrannus. Fish. Bull. U.S., 75(1), 23-42.

Parrish, R.H. and MacCall, A.D., in press - Climatic variation and exploitation in the Pacific mackerel fishery. Calif. Dept. Fish and Game, Fish. Bull., 167 p.

Parrish, R.H., Nelson, C.S., and Bakun, A., manuscript - Larval transport mechanisms and reproductive success of fishes in the California Current. Submitted to Fish. Bull. U.S.

Peterson, W.T., 1973 - Upwelling indices and annual catches of Dungeness crab, Cancer magister, along the west coast of the United States. Fish. Bull. U.S., 71(3), 902-910.

Reid, J. L. Jr., Roden, G.I., and Wyllie, J.G., 1958 - Studies of the California Current system. Calif. Coop. Oceanic Fish. Invest., Prog. Rep., 1 July 1956 to 1 January 1958, 27-57.

Roedel, P.M., 1952 - A raciel study of the Pacific mackerel. Calif. Dept. Fish and Game, Fish. Bull., 84, 53 p.

Vrooman, A.M., and Smith, P.E., 1971 - Biomass of the subpopulations of northern anchovy Engraulis mordax Girard. Calif. Coop. Oceanic Fish. Invest., Prog. Rep. 15, 49-51.

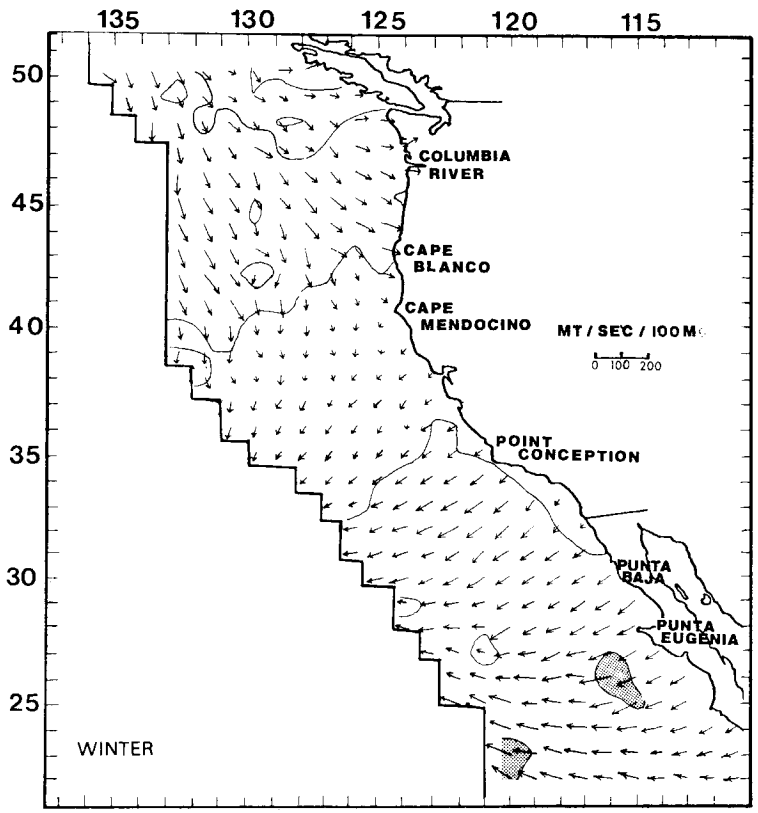

FIGURE 1. SURFACE EKMAN TRANSPORT DURING WINTER (DECEMBER THROUGH FEBRUARY LONG TERM 1° MEANS). CONTOUR INTERVAL IS 50 METRIC TONS PER SECOND ACROSS EACH 100 M WIDTH. AREAS OF TRANSPORT GREATER THAN 100 MT/SEC/100 M ARE SHADED. STRESS ESTIMATES WERE COMPUTED FROM EACH AVAILABLE SURFACE WIND OBSERVATION AS THE PRODUCT OF THE SQUARE OF THE WIND SPEED, THE DENSITY OF AIR (CONSIDERED A CONSTAND EQUAL TO 0.00122 GM/CM^3), AND A CONSTAND DRAG COEFFICIENT (0.0013) AND VECTORIALLY AVERAGED BY ONE-DEGREE "SQUARE" AREA. THE EKMAN TRANSPORT, DIRECTED NINETY DEGREES TO THE RIGHT OF THE MEAN STRESS, WAS CALCULATED BY DIVIDING BY THE LOCAL CORIOLIS PARAMETER.

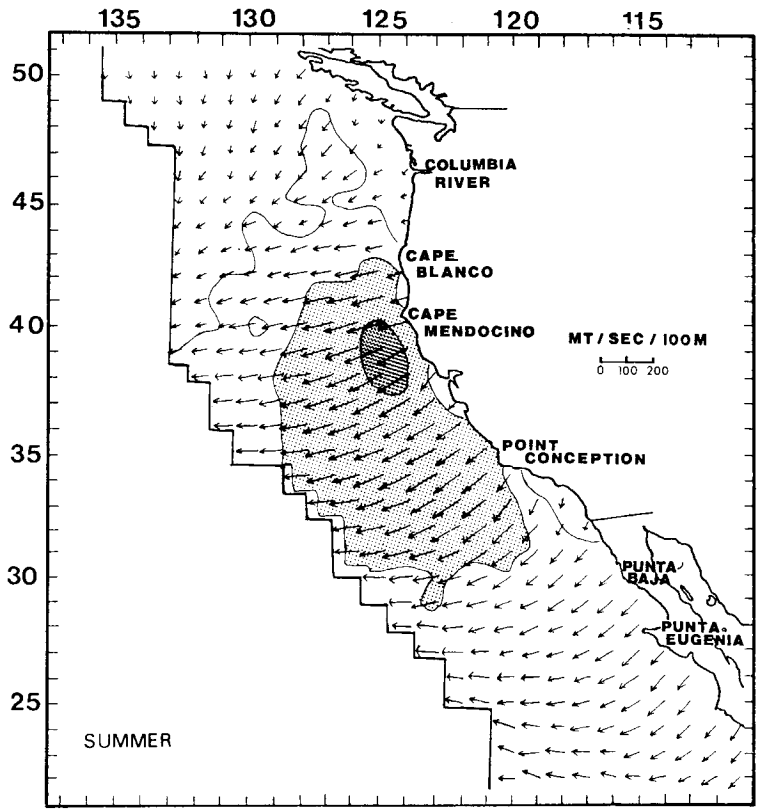

FIGURE 2. SURFACE EKMAN TRANSPORT DURING SUMMER (JUNE THROUGH AUGUST LONG TERM 1° MEANS).

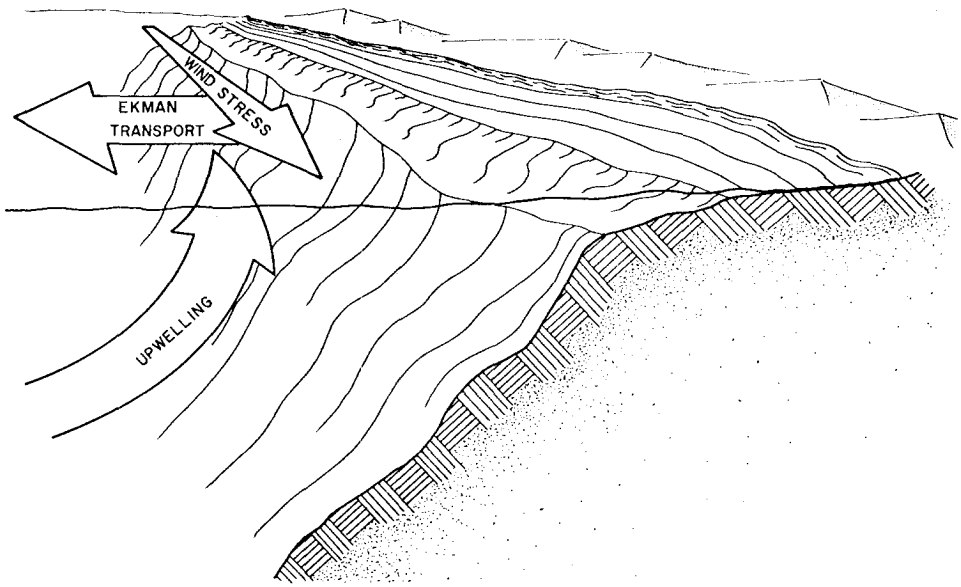

FIGURE 3. A CONCEPTUAL DIAGRAM FOR LOCALLY WIND INDUCED COASTAL UPWELLING. A COMPONENT OF WIND STRESS PARALLEL TO THE COAST AND DIRECTED EQUATORWARD INDUCES OFFSHORE TRANSPORT IN THE SURFACE EKMAN LAYER OF THE OCEAN. TO THE EXTENT THAT THIS OFFSHORE FLUX IS NOT BALANCED BY INFLUX OF HORIZONTAL SURFACE FLOW, THE BALANCE IS MAINTAINED BY UPWELLING OF DEEPER WATERS.

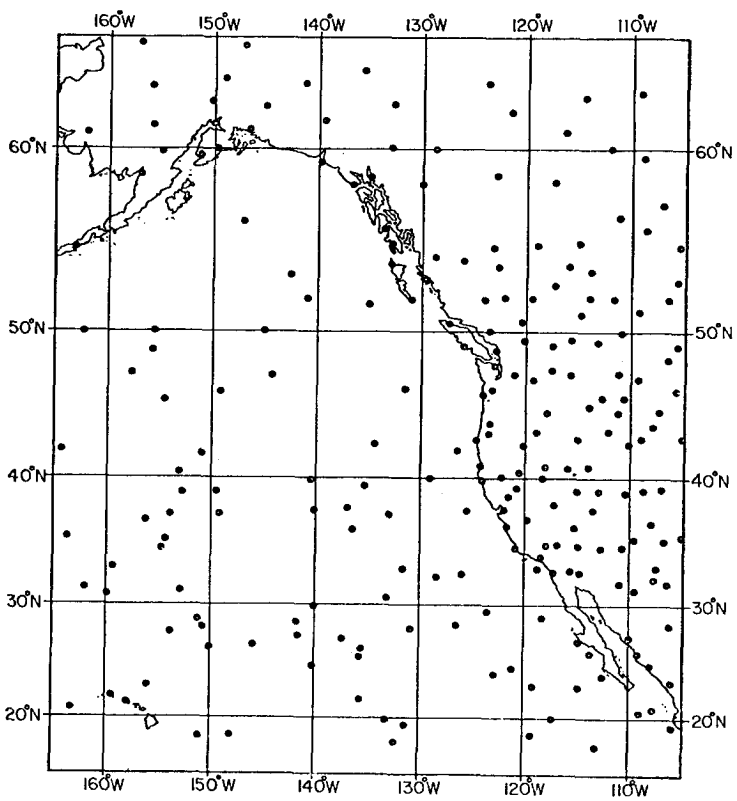

FIGURE 4. A TYPICAL DISTRIBUTION OF REPORTS AVAILABLE FOR A SYNOPTIC SURFACE ATMOSPHERIC WIND-PRESSURE ANALYSIS. THIS PARTICULAR DISTRIBUTION IS FOR 1800 GMT ON 5 JANUARY 1974.

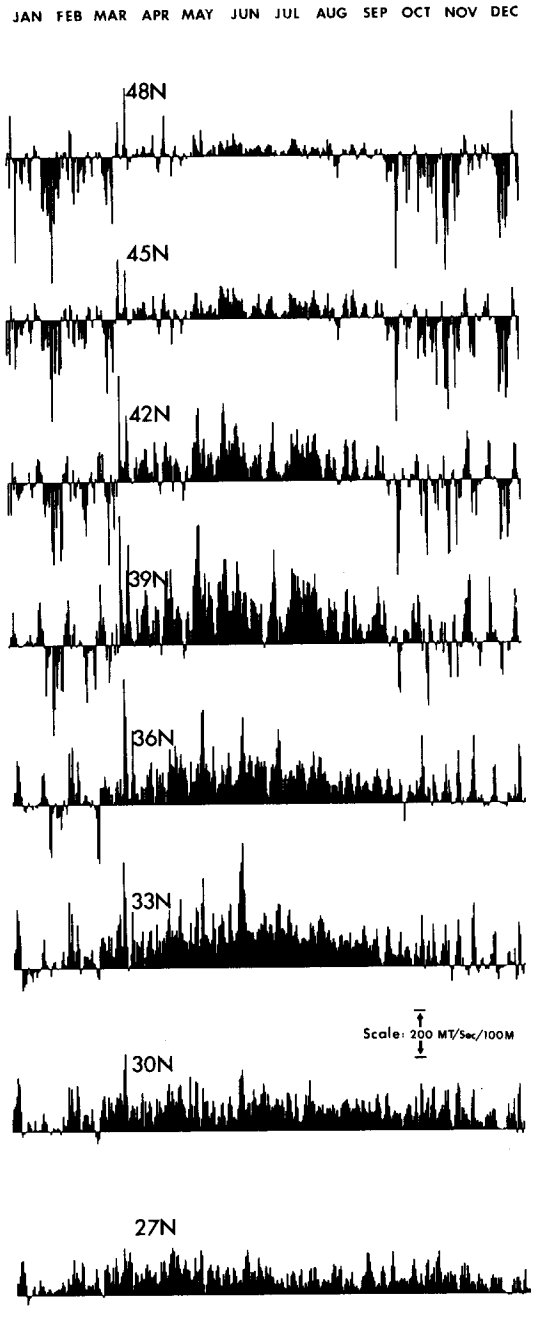

FIGURE 5. DAILY UPWELLING INDICES FOR 1975 AT 3-DEGREE INTERVALS FROM THE WASHINGTON COAST TO CENTRAL BAJA CALIFORNIA. THE MAGNITUDE OF THE ALONGSHORE WIND STRESS IS INDICATED BY THE LENGTH OF THE BARS; THE SCALE IS SHOWN ON THE FIGURE. UNITS ARE METRIC TONS PER SECOND PER 100 M LENGTH OF COAST. BARS EXTENDING UPWARD INDICATE SOUTHWARD STRESS EVENTS, WHICH CAUSE OFFSHORE EKMAN FLUX AND PRODUCE UPWELLING; THOSE EXTENDING DOWNWARD INDICATE SOUTHWARD STRESS EVENTS, WHICH PRODUCE ONSHORE EKMAN TRANSPORT AND RESULTANT COASTAL DOWNWELLING.

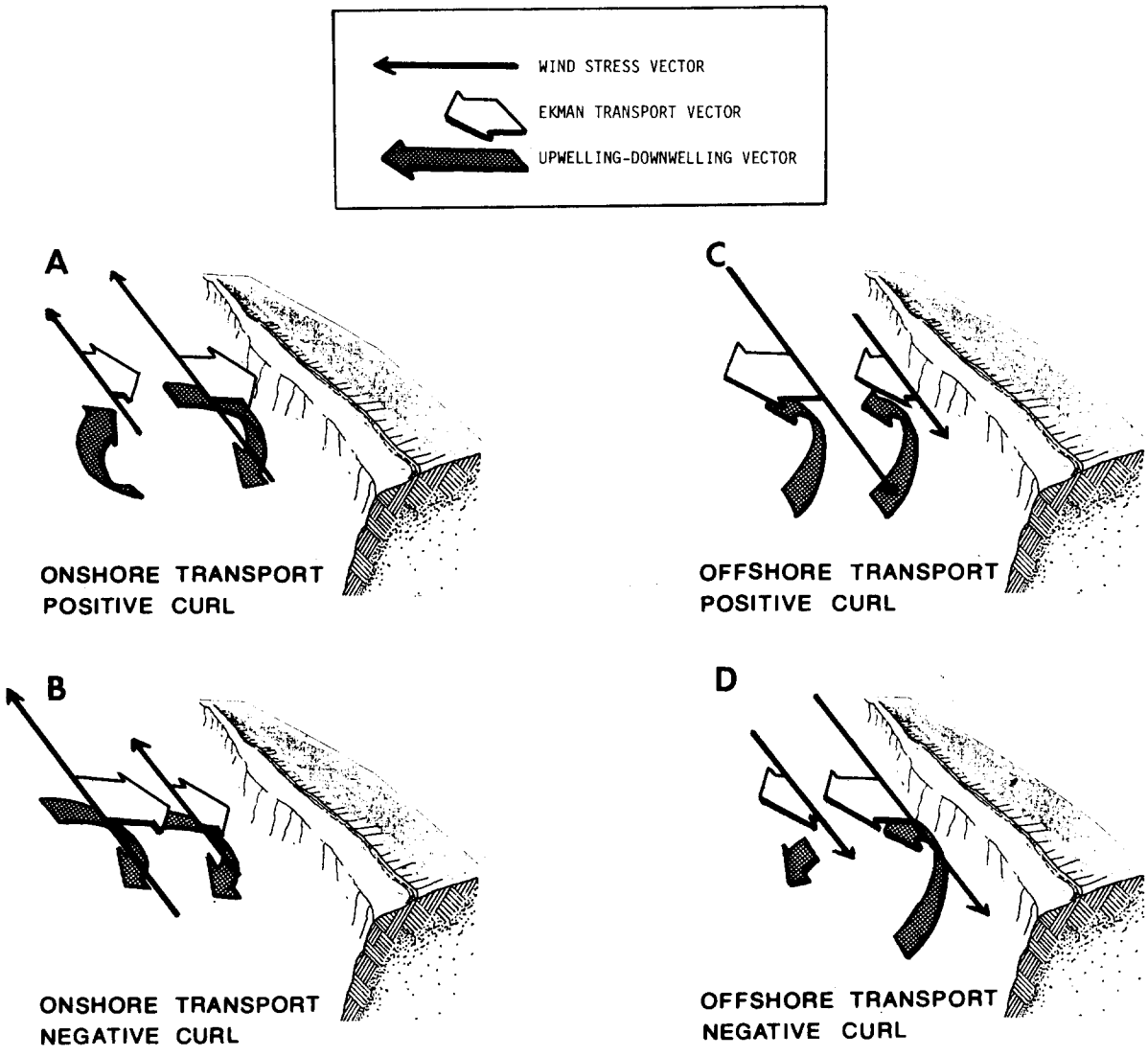

FIGURE 6. CLASSIFICATION OF WIND STRESS EVENTS ACCORDING TO COMBINATION OF COASTAL AND OFFSHORE CONVERGENCE OR DIVERGENCE. A. ONSHORE EKMAN TRANSPORT AND POSITIVE WIND STRESS CURL; CONVERGENCE AND DOWNWELLING AT THE COAST, DIVERGENCE AND UPWELLING OFFSHORE. B. ONSHORE EKMAN TRANSPORT AND NEGATIVE WIND STRESS CURL; CONVERGENCE AND DOWNWELLING AT THE COAST, CONTINUED CONVERGENCE OFFSHORE. C. OFFSHORE EKMAN TRANSPORT AND POSITIVE WIND STRESS CURL; DIVERGENCE AND UPWELLING AT THE COAST, CONTINUED DIVERGENCE OFFSHORE. D. OFFSHORE EKMAN TRANSPORT AND NEGATIVE WIND STRESS CURL; DIVERGENCE AND UPWELLING AT THE COAST, CONVERGENCE OFFSHORE.

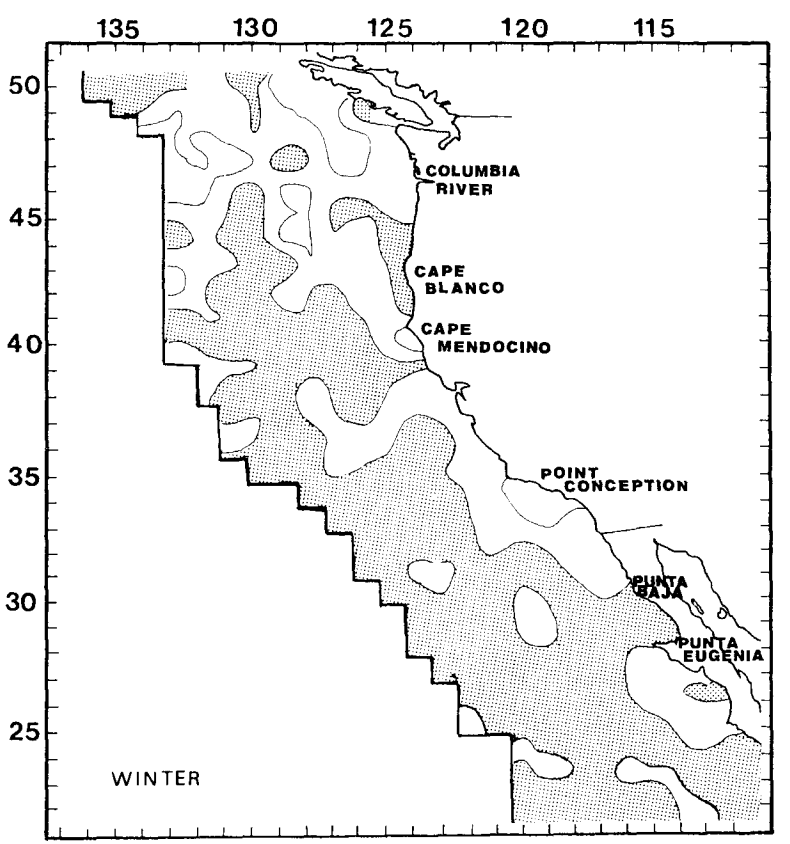

FIGURE 7. WIND STRESS CURL DISTRIBUTION DURING WINTER (DECEMBER THROUGH FEBRUARY LONG TERM MEANS). CONTOUR INTERVAL IS 0.25 DYNES CM^{-2} PER 100 KM. NEGATIVE CURL VALUES ARE SHADED; I.E. SHADED AREAS INDICATE SURFACE EKMAN CONVERGENCE, UNSHADED AREAS INDICATE EKMAN DIVERGENCE.

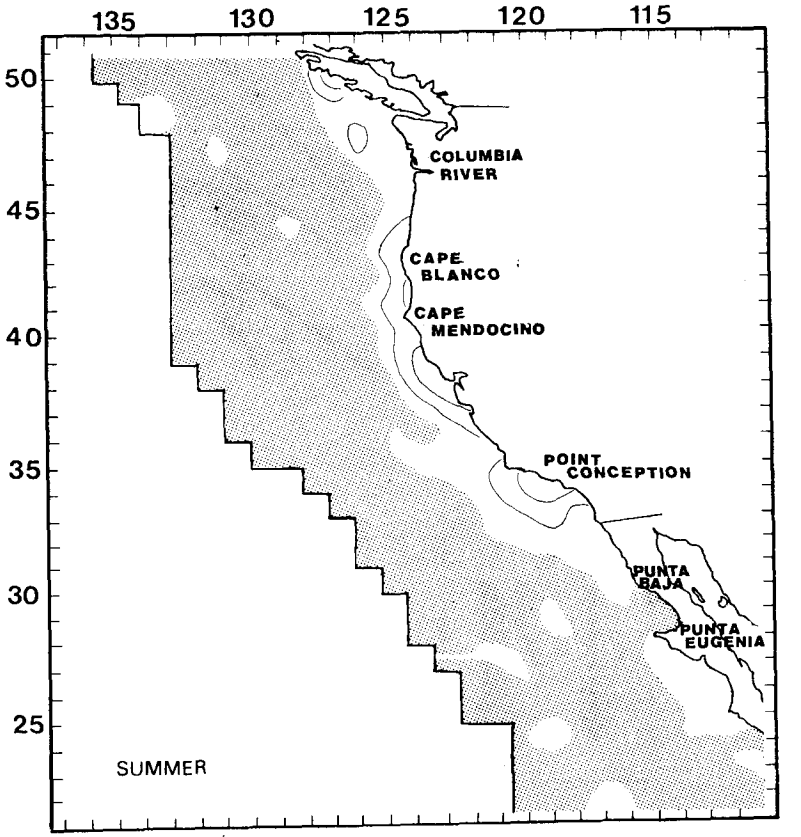

FIGURE 8. WIND STRESS DISTRIBUTION DURING SUMMER (JUNE THROUGH AUGUST LONG TERM MEANS). CONVERGENT AREAS ARE SHADED; DIVERGENT AREAS ARE UNSHADED.

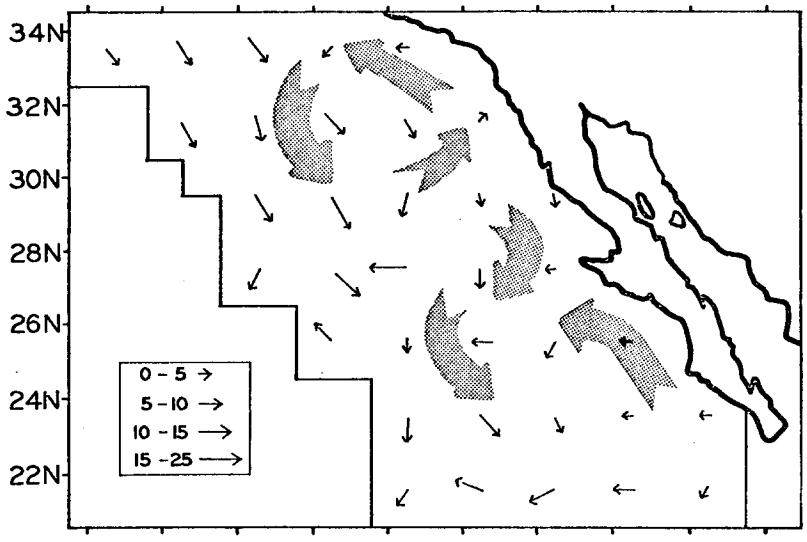

FIGURE 9. SHIP DRIFT DURING OCTOBER, NOVEMBER, AND DECEMBER. OBSERVATIONS WERE SUMMARIZED BY 2° "SQUARE" AREAS FROM THE NAVOCEANO SHIP DRIFT FILE. THE SMALL ARROWS, INDICATING MEAN DRIFT, ARE SCALED ACCORDING TO THE KEY AT THE LOWER LEFT. LARGE ARROWS SUGGEST THE INFERRED CIRCULATION PATTERN. SHIP DRIFT OBSERVATIONS ARE DERIVED FROM DIFFERENCES IN DEAD-RECKONING AND VERIFIED POSITIONS ASSEMBLED FROM SHIP'S LOGBOOKS.

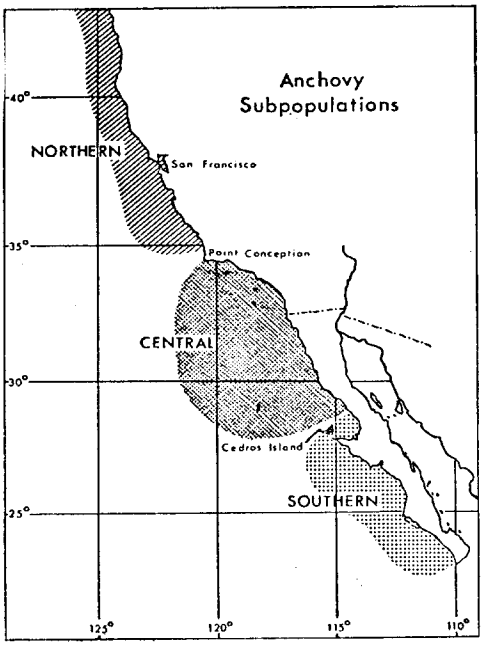

FIGURE 10. THE WINTER DISTRIBUTIONS OF ANCHOVIE SUBPOPULATIONS IN THE CALIFORNIA CURRENT (AFTER VROOMAN AND SMITH, 1971).

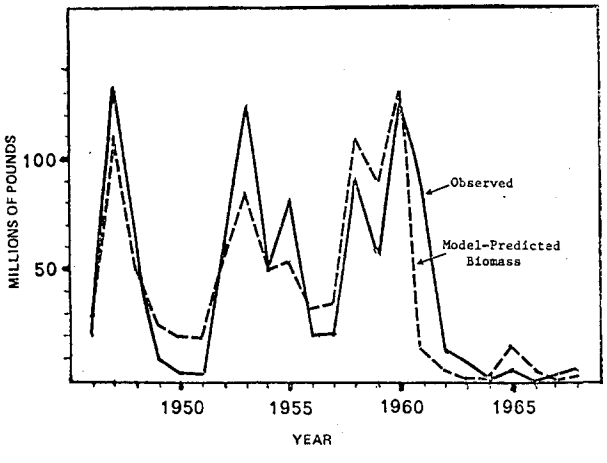

FIGURE 11. YEAR-CLASS SIZE IN THE CALIFORNIA STOCK OF PACIFIC MACKEREL.

DRIFTING BUOY PRODUCTS FROM THE FIRST GARP GLOBAL EXPERIMENT (FGGE): A PROGRESS REPORT

N.E.J. Boston and J.A. Helbig

Beak Consultants Limited
Suite 602, 1550 Alberni St.
Vancouver, Canada
V6G 1A5

R. Keely, J. Thomas and J.R. Wilson

Marine Environmental Data Service
Fisheries and Environment Canada
240 Sparks Street
Ottawa, Canada
K1A 0E6

TABLE OF CONTENTS

FORWARD

This discussion paper is a joint effort between Beak Consultants Limited and the Marine Environmental Data Service. This work is not funded but some portions fall within contract K4297, the FGGE Drifting Buoy System.

The results are necessarily of a preliminary nature. The first special observing period, from 5 January to 5 March 1979, has only recently concluded. The second observing period (1 May to 30 June) has not yet begun. As a result, the data have not been digested and manipulated. They are presented in basically a raw form. However, due to the magnitude of the Global Experiment and the timing of the IGOSS Seminar/Workshop, even the preliminary results were considered of sufficient interest and importance for presentation. We have in fact a discussion of a program presently underway. Comments and suggestions made here could influence the handling of the data though not the operation of the program which has been in planning for several years.

We review the drifting buoy system and discuss four IGOSS products produced by the Marine Environmental Data Service, Ottawa. Examples are presented and possible conclusions to be obtained from them discussed. Two derived products are suggested and possible application of drifting buoy products discussed. Recommendations are made of drifting buoy studies which could be fruitfully carried out at the conclusion of the Global Experiment.

ACKNOWLEDGEMENTS

Dr. J.F. Garrett
MEDS
G.L. Holland, Marine Sciences information Directorate

THE DRIFTING BUOY SYSTEM

Background

The objectives of the First GARP Global Experiment require a reasonably uniform global coverage of meteorological data. This is particularly difficult to obtain in the Southern Hemisphere with its vast array of ocean largely untravelled by ships. The most practical method for obtaining data from these ocean areas is by a combination of satellite methods for obtaining vertical profiles and a network of buoy stations providing observations of atmospheric pressure and sea surface temperature. These meteorological buoys, some of which are and will be drouged, transmit their data by means of a satellite link so that they are available in time for operational use as well as for storage for future research needs. By keeping the buoys small and simple their deployment has been done so far by the few ships that operate in the oceans of the Southern Hemisphere. If the locations and times of deployment have been suitably chosen, some buoys will eventually drift into most regions of the ocean.

The buoy system now in place was developed by Canada for operation in the belt 20S - 65S during the Global Experiment. A total of about 300 drifting buoys of several different types have been supplied by participating countries. Ships of these and other countries have been assisting in the deployment of buoy array; the plan for making optimum use of such assistance was the responsibility of N.E.J. Boston. A special location and data collection system has been developed to assimilate, process and distribute these data. The development was and operation of the system is undertaken by France and is called System Argos. System Argos is a cooperative project between the Centre National d'Etudes Spatiales (CNES), France, the National Aeronautics and Space Administration (NASA), USA, and the National Oceanic and Atmospheric Administration (NOAA, USA). System Argos consists of a central control centre at Toulouse, France, equipment packages on satellites and ground based systems which transmit to the Toulouse centre.

The management and planning for this system has been carried out by a Committee of Participants for the Southern Hemisphere Drifting Buoy System. This committee reports to the WMO through the GARP Activities Office in Geneva. The Committee of Participants was responsible for ensuring that the proposed buoys met the necessary requirements of accuracy and reliability and for overseeing the planning and logistics of the deployment together with the planning and monitoring of the data handling system. The actual planning and coordination of the deployment is carried out by the Logistics and Deployment Centre (Vancouver) while the Data Processing and monitoring is carred out by the Data Processing and Control Centre (Toulouse).

To aid in the design of an optimal buoy deployment plan, Bjorheim and Guddal (1978) of Det Norske Meteorologiske Institutt developed a model to simulate buoy trajectories. These were computed by integration in time over the buoy velocity, $\underline{V}_{sur} + k\underline{v}_{wind}$ $\underline{v} = \underline{v}_{sur} + k\underline{v}_{wind}$, where $\underline{v}_{sur}$ represents the sea surface

current field, $\underline{v}_{wind}$ is the surface wind field, and k is a drift factor. The surface currents were read from charts and were set equal to zero away from coastal boundaries. Surface winds were obtained by clockwise rotation at the geostrophic wind as computed from the surface atmosphere pressure field. The rotation angle was an increasing function of wind speed and was fixed to lie between 10^{0} and 25^{0}. The surface pressure field was obtained from monthly mean maps in climatological atlases. In order to minimize manual effort, only the mean pressure fields for January, April, July, and October were determined. At each horizontal grid point a Fourier series in time was fit to these four values, thus enabling the "instantaneous" geostrophic wind to be calculated at each step of the trajectory analysis.

The drift factor k was chosen as .03 for undrouged buoys and was reduced to .01 or .02 for drouged buoys depending on the depth of the drouge. As a test, the model was run with these values to simulate tracks observed by Garrett (1978) and qualitative agreement was obtained (figure available). The model was then run using various deployment arrays and the results were used to design a deployment plan.

Present Status

During SOP-I the FGGE buoy array performed more or less as planned, keeping in mind that only one satellite equipped with the Argos Data Collection and Platform Location System (TIROS-N) is operating. Deployments were slightly behind schedule resulting in reduced coverage at the beginning of the SOP. Several failures in the same region produced a significant gap in one area. Difficulties were experienced in meeting the schedule for Level II-a data production for one of the four synoptic times. However, the deployments were on schedule by the start of the Intensive Observation Period; most of the ocean area from 20^{o}S to 65^{o}S was always within 500 km of a buoy sending good pressure data; level II-a data was generally available in meteorological centres in time for use in regional analyses and level II-b data production, including quality control procedures, was on schedule.

The evolution of the drifting buoy system south of 20^{o}S is summarized in Table 1. At the beginning of the SOP-I a significant number of buoys still had not yet been deployed. Later the effects of buoy drift and failure can be seen. Nevertheless, at least 65% of the ocean area from 20^{o}S to 65^{o}S was within 500 km of a buoy reporting good pressure data during the Intensive Observing Period (15 January to 15 February) and at least 50% of the area was covered by buoy data for the entire SOP-I. The coverage of data in the southern hemisphere is reflected best in the actual spatial distribution of buoys as shown in Figure 1. A number of platforms were also launched in the tropics and the Arctic. By the end of the SOP-I there were 18 buoys sending good data from the Arctic Ocean and 6 sending good data from equatorial regions (Figures 2a, b and c).

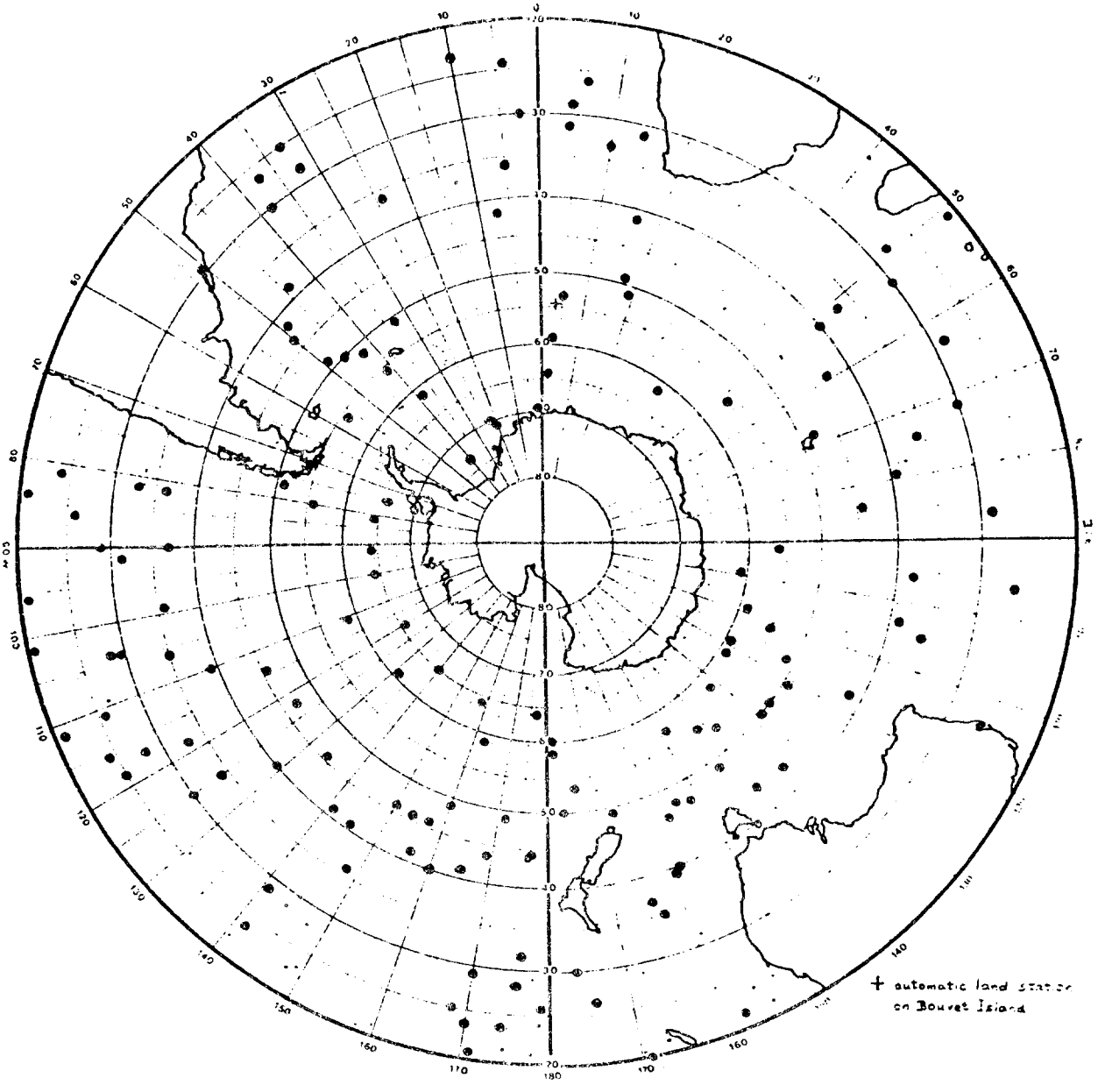

Figure 1. Distribution of operational Southern Hemisphere Drifting Buoys as of 19 February in the area south of 20°S latitude.

In this distribution approximately 60 percent of area is within 500 km. of a good data producing buoy. (See Table 1.)

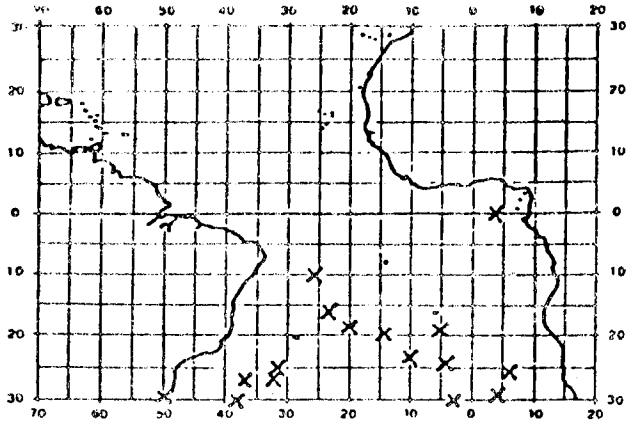

(a)

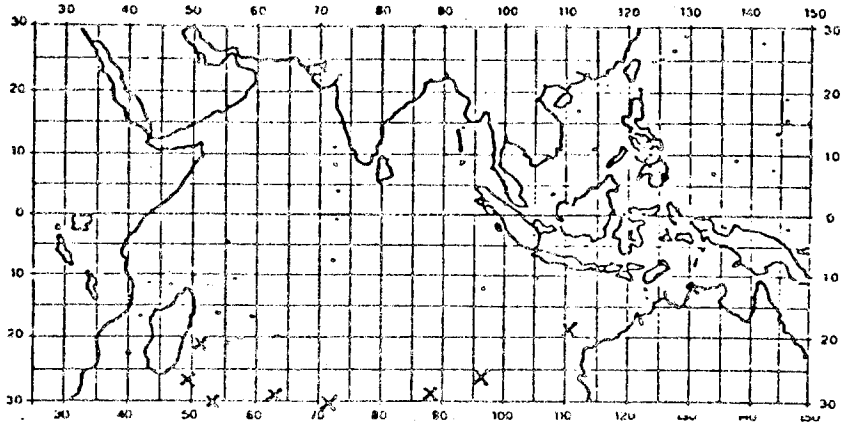

(b)

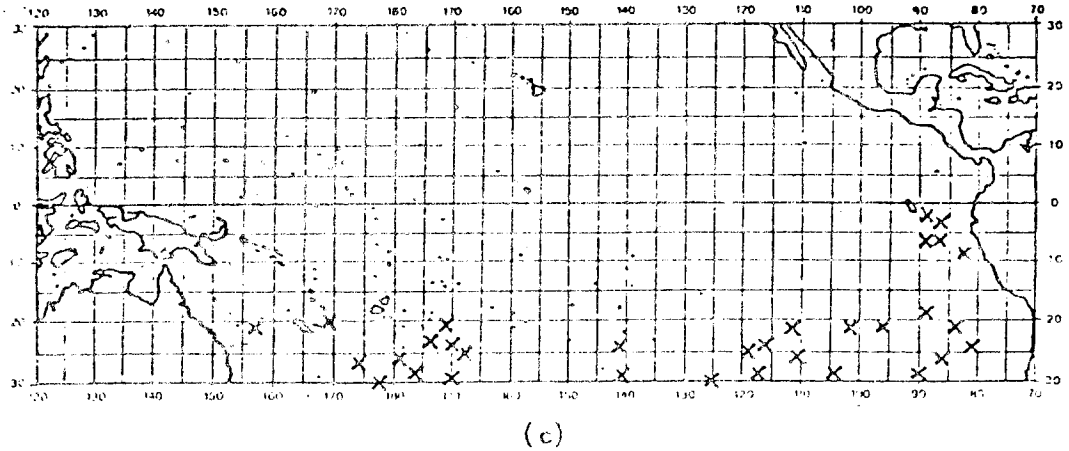

(c)

Figure 2. Distribution of the drifting buoys in the tropical region transmitting good data on 19 February 1979.

(a) Tropical Atlantic Ocean
(b) Tropical Indian Ocean
(c) Tropical Pacific Ocean

Table 1: FGGE Buoys South of 20^{o} During SOP-I

Date (1979)	Number Launched	Number with Good Pressures	Number on GTS	% of area within 500 km. of good buoy
5 January	125	106	100	52%
15 January	147	126	108	64%
29 January	174	143	144	70%
12 February	189	161	152	67%
28 February	198	156	162	59%
5 March	204	152	156	-

The failure rate for the buoys has been somewhat higher than expected. About 14% of the buoys experienced a failure of some sort (one or more sensors, or transmitter) during the first 10 days after launch. After the first few days in the water the failure rate is about one failure per 380 buoy days. These figures are for the array as a whole - some types of buoys are much better than average. For example the 23 French buoys launched for SOP-I have experienced only one failure, a temperature sensor, during a cumulative total of more than 1,900 days of operation.

Level II-a data has been routinely produced and distributed over the GTS four times per day as planned. Most of the time data for the synoptic periods around 00Z, 12Z and 18Z are distributed in the appropriate collection of GTS bulletins, sent from Toulouse about 3 hours 40 minutes after each synoptic hour. However communication problems leading to delays in the delivery in Toulouse of the raw satellite data have usually prevented the data from the 06Z synoptic period from being distributed in the bulletins sent out at 0940Z. Typically the GTS data arrives in Ottawa, Canada 20 minutes after it is sent from Toulouse and in Melbourne, Australia 2 hours 20 minutes after it is sent.

Level II-b data is being produced within the anticipated 2 month delay. A variety of quality control procedures are used to detect and flag or correct erroneous values. Four to five man days of effort were required at the FGGE Buoy Control Centre to prepare the Level II-b data for each week. Participation in the SOP-I End-to-End Systems Test included hand delivery of a provisional data tape to the Level II-b centre and participation in the evaluation sessions held at ECMWF.

During SOP-I data from the buoy array has been used in operational meteorological analyses in a number of centres, including Melbourne, Washington NMC and Bracknell. Experimental oceanographic products based on the buoy motion and sea surface temperature data are being prepared routinely in Washington and Ottawa (MEDS).

An average of about 180 observations is available every six hours from drifting buoys in the higher latitudes of the southern hemisphere. Fewer than 180 buoys were deployed in the 15-19 January time period, but some of them report twice or even three times in six hours. The pressure data are good, consistent with each other and with ship data in the few cases when comparisons were possible. In some areas with good coverage of drifting buoy sea surface temperatures and satellite sea-surface temperatures, intercomparisons between the two systems could be made. The agreement was within $\pm$ 1^{o}C.

FGGE DRIFTING BUOY PRODUCTS

Overview

The Marine Environmental Data Service (Canada) is preparing a set of three near-realtime products for IGOSS during the FGGE operational year. The products are buoy tracks, temperature anomaly maps, and sea surface temperature maps. These maps, on polar stereographic projection, are produced for 5-day periods and are distributed as soon as possible after the end of each 5-day period.

The technique used to generate the anomaly maps and the SST charts is "optimum interpolation", as described by Gandin (1965), Bretherton, et al. (1976), and Freeland, et al. (1975). This technique requires essentially a set of initial conditions, which can be chosen in various ways.

For the analyses of the drifting buoy data, the initial conditions have been chosen as the climatological mean. The dataset used was obtained from the U.S. National Climatic Center, Ashville, North Carolina, and included all available sea surface temperatures by 5^{o} square and by month.

There are about 3 million temperature readings for each of the 12 months. The information in each 5^{o} square consists of average temperature, sample size, the standard deviation in the mean of the temperature, and the average position. In generating the maps, these data are interpolated in space, as necessary, using the optimum interpolation technique, and in time using simple linear interpolation.

Generally, the climatic temperature grid was blanked in regions where the expected error was greater than $1C^{o}$. This mainly eliminated doubtful extrapolations southward from the southern most data in the Antarctic, and worked well for the months of November through March. However, from April onward, occasional "holes" in the data coverage began to appear, mainly south of latitude $55^{o}S$. In these holes, the interpolated values were allowed to remain, even though the expected error exceeded $1C^{o}$, provided the interpolation in a hole appeared to be essentially linear, and rough agreement with the 1978 U.S.S.R. Oceanographic Atlas was maintained.

The optimum interpolation technique also requires as input a spatial correlation function and an estimate of noise. The spatial correlation function and noise estimate used was derived by fitting a Gaussian curve to the first eight 5-day sets of data. The noise value is related to some combination of the accuracy or sensitivity of the instrument and to the fact that the field is not perfectly sampled and spatial aliasing exists. The noise value arrived at was $0.58C^{o}$. The correlation scales for the climatological and buoy data were 3,800 km and 900 km respectively.

The validity of the estimated correlation function and noise can be partially checked by comparing the RMS actual and expected residuals at the data points. For the eight 5-day periods between December 28, 1978, and February 5, 1979, an

average ratio of actual to expected residuals of 1.07 was obtained, with 95% confidence limits of .99 and 1.15. Ideally this ratio should be 1.0, so we have some confirmation of our estimates.

The purpose of producing the temperature anomaly map was to effect some quality control on the drifting buoy data: buoys which differed dramatically from climatology could be found with ease on these maps. However, it soon became obvious that the maps were rather more interesting than the SST maps themselves. It was therefore decided to include the anomaly map as a product. Comments have also been prepared on the features found in the anomaly maps and are sent out with the maps. When reading these comments, one must realize that the words "warmer" and "colder" are in reference to the climatological dataset described above, and the conclusions reached are only as good as that dataset.

Product 1 - Buoy Tracks

Buoy tracks, generally over a 5-day period, are shown with a large dot representing the last position. The annotations include (top and bottom) buoy number, average SST over the five days, and the difference between the average SST and the climatological average for the date and average position corresponding to the observation. A positive temperature indicates the temperature as reported by the buoy is warmer than the climatological value.

Because drift velocities are typically small (a few km per day), the 5-day buoy tracks transfer limited information. Mid-ocean temporal scales exceed 5 days and spatial scales exceed a few kilometres. Plots over longer periods (59 days, Fig. 3) are required to demonstrate the variety and scales of motion of the drifting buoys. In the two-month track chart shown, gaps in reliable positions are filled by a linear interpolation. Dates beneath buoy numbers display the start and end reporting times of the buoy. A record starting in January and ending in February has the two dates separated by an = sign, starting in January and ending in January by a - sign, and starting in February and ending in February by a + sign. Descretion must be used in visually inspecting these tracks since all are not over the same length of time.

The tracks illustrate an anticlockwise gyre in the South Atlantic. The long tracks along 20S indicate uniform buoy movement westward of 15 to 17 km per day (about 1/3 knot). Along the western side of the South Atlantic, the tracks indicate a rather confused motion - two tracks cross nearly at right angles and two others move more or less parallel but in opposite directions. The time history of the individual buoys would have to be examined in detail in order to resolve these problems.

Another conspicuous feature is the confirmation of the Antarctic Circumpular circulation. Although indicating the general eastward trend, the tracks are not without their individual wrinkles. Buoy 56639 had a particularly interesting start-up history (Fig. 4). There is a suggestion of a fort-nightly oscillation in the tracks directly south of Australia. This periodicity is hinted at in a number of other areas as well.

FIGURE 3

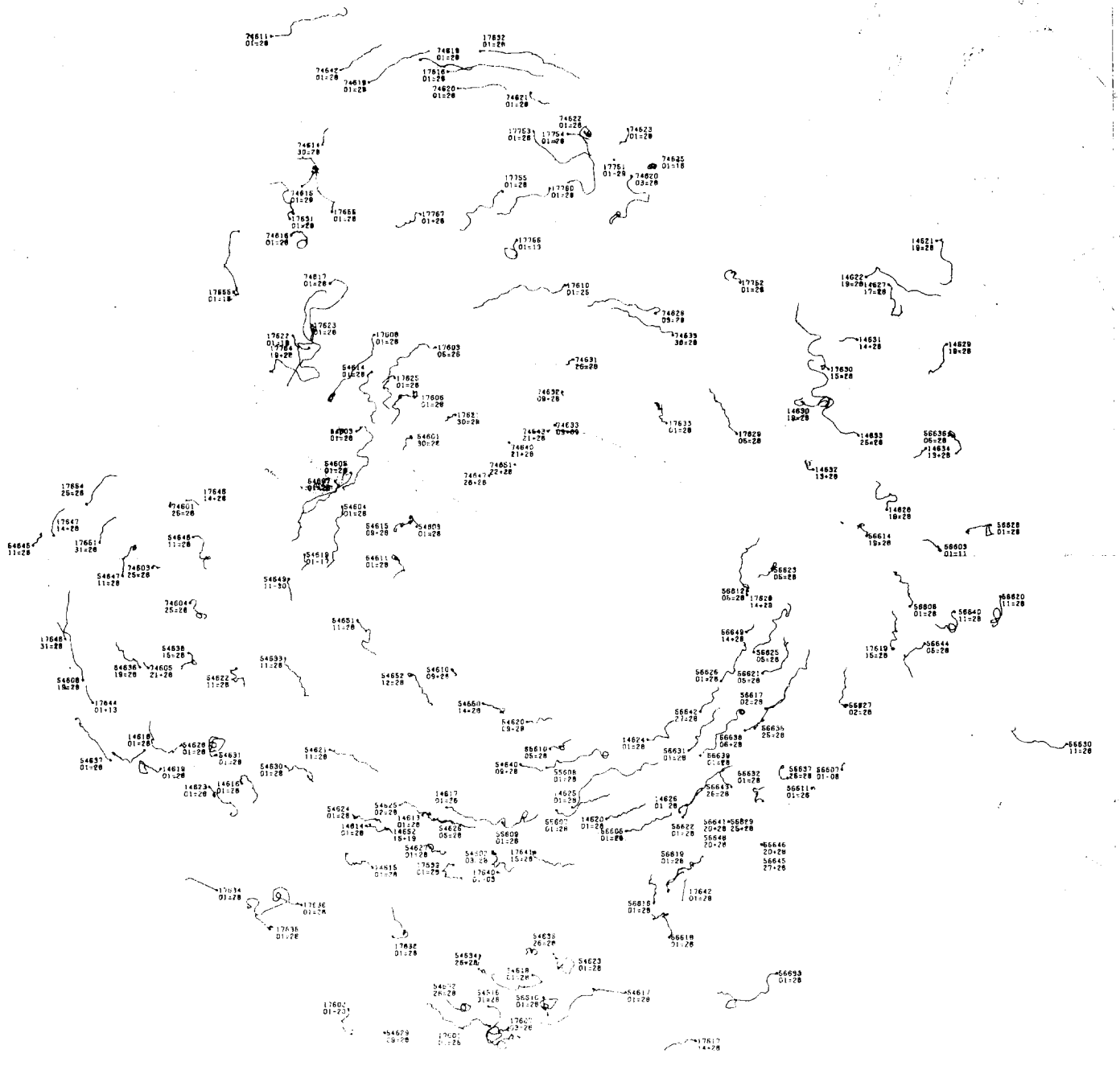

JAN 01 - FEB 28/79 BUOY TRACKS ... LABEL SHOWS BUOY NUMBER AND DAY OF FIRST/LAST POSITION (FIRST = LAST = BOTH MONTHS)

INTEGRATED GLOBAL OCEAN STATION SYSTEM (IGOSS) PRODUCT IN SUPPORT OF THE FIRST GARP GLOBAL EXPERIMENT (FGGE) BY THE MAP OF METEOROLOGICAL DATA SERVICE, CANADA

BUOY OF THE MONTH - JANUARY 1979

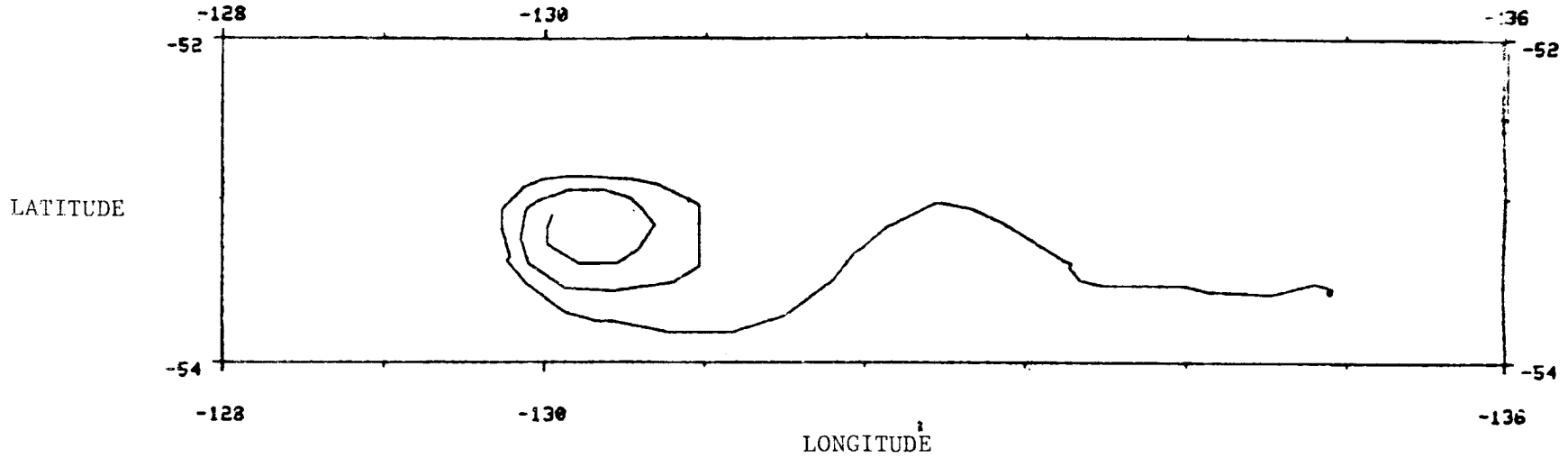

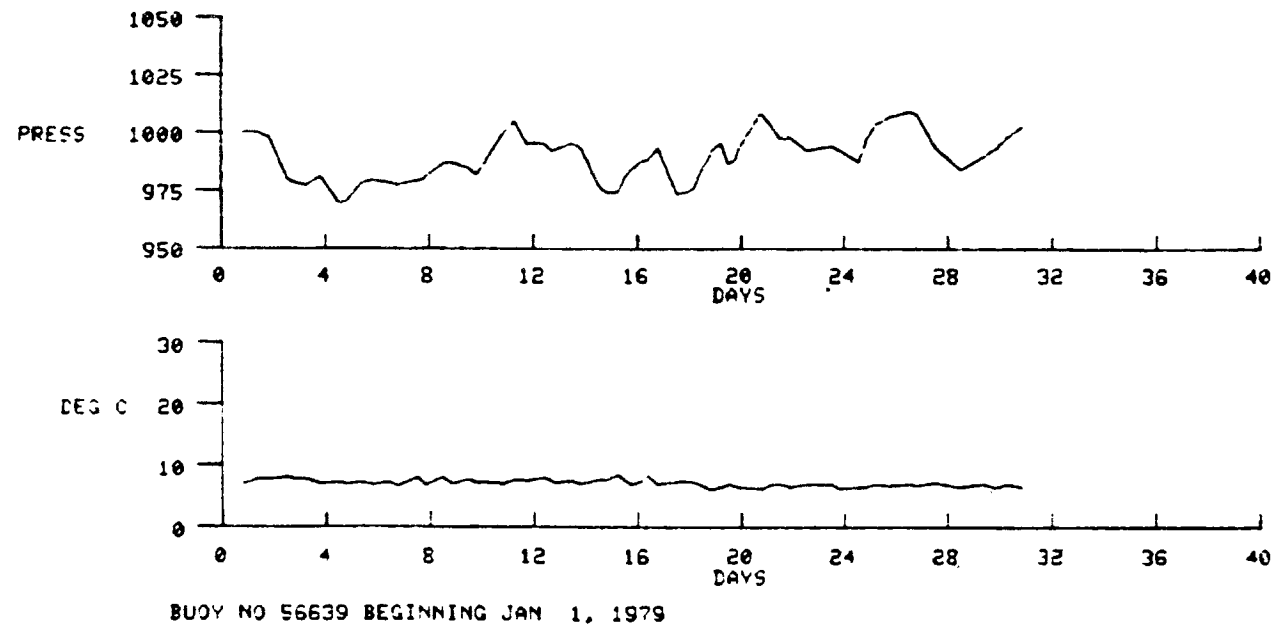

Figure 4

Some of the largest drift rates have been encountered in the Atlantic and Indian Oceans along latitude 50S. Buoy 74639 traversed approximately 700 km in 24 days for an average drift velocity of 0.5 kts.

The lowest drift velocities have occurred in the eastern portion of the South Pacific. Other than uncertain movement, the tracks in this region have no distinguishing characteristics.

There would appear to be considerable information on surface currents embedded in these motions but not extractable without some detailed studies. These would include comparison of motion of drouged and undrouged buoys, comparison of motions of different buoy types, examination of time histories of drift in which wind is included.

These tracks are for the first two months only. The additional information on drift motion accumulated by the end of the Global Experiment should provide sufficient information to fruitfully carry out such studies.

Product 2- Temperature Anomaly Contour Maps

The temperature anomaly of a buoy over a 5-day period is taken as the difference between the average temperature reported by the buoy in that period and the climatic temperature at the central time of the period and at the average buoy position. When the climatic temperature is not available, the anomaly is not calculated.

With the anomaly temperatures at the average buoy positions as control (or data) points, optimum interpolation is used to calculate the anomaly at positions defined in latitude and longitude by grid points in a 61 x 61 grid laid over a south polar stereographic map of the part of the world south of 15^{o}S.

On the anomaly map, the anomaly values are posted at average buoy positions, and the contour lines are drawn as solid lines for positive anomalies, dashed for negative, and heavy for zero. The faint dashed lines are contours of expected error in the anomaly. Note that, because of noise, the contoured surface does not exactly pass through the data values. However, if the correlation and noise have been well chosen, the surface should be close to the best estmate of the "true" anomaly surface, and the plot of expected error should be valid as well.

Three examples of this product are given in Figures 5-7; the accompanying descriptions for each map that are provided by MEDS follow. These examples illustrate some of the problems associated with either poor spatial coverage or possibly faulty sensors.

SST Anomaly Map: February 1-5, 1979

The number of reporting buoys is 133. The average sea surface temperature anomaly is 0.66^{o}C. A major change this time has been buoy 14633 (43^{o}S, 55^{o}E) reporting a negative anomaly in the Indian Ocean. This is now in the neighbourhood of buoy 14630 and apparently confirms the existence of this

feature. The warm anomaly east of Argentina (40°S, 50°W) has extended to the east, and in the east, both north and south as well. This is primarily because buoys 17755, 17610 and 17760 all report warmer anomalies. The cold anomaly in the Weddell Sea region (55°S, 50°W) has shifted westward to include all of Drake Passage. Negative anomalies reported by buoys 54607 and 54603 appear to be responsible. Finally, the cold anomaly of the western Pacific (25°S, 135° - 165°W) appears to be moving northward. Those buoys still reporting cold anomalies have warmed about 0.5°C. Buoy 54607 appears to have grounded on the islands of Cape Horn.

SST Anomaly Map: February 6-10, 1979

The number of reporting buoys is 139. The average sea surface temperature is 0.69°C. The most outstanding changes have occurred in the Indian Ocean. A very warm anomaly has appeared at 40°S, 45°E. Peak anomalies exceeding +4°C are reported by buoys 14633 and 17630. Previously, buoy 14633 reported a -2.4°C anomaly. This wide variation casts some doubt on the quality of the temperature sensor. Other features have also appeared in the Indian Ocean and the ocean just south of Australia. The warm anomaly near Argentina (40°S, 50°W) has warmed in its eastern regions, with buoy 17767 reporting an anomaly 0.6°C warmer. A consequent areal reduction in the cold Atlantic anomaly (20°S, 0° - 50°W) has occurred. Finally, the cold anomaly off Antarctica (55°S, 140°W) has all but vanished, with buoy 54652 reporting 0.7°C warmer than last time, and a new buoy (54610) close by reporting a slightly positive anomaly.

SST Anomaly Map - February 11-15, 1979

The number of reporting buoys is 144. The average sea surface temperature anomaly is 0.70°C. A noticeable change has been the western extension of the warm anomaly east of New Zealand (40°S, 145°W). This is due to increased anomalies, both north and west of New Zealand. The very warm anomaly in the Indian Ocean (40°S, 45°E) has cooled considerably. Buoy 14633 reports a 4.2°C cooler anomaly, and buoy 17630 a 2.3° cooler anomaly than last time. The whole tip of South Africa has water 1.5° warmer than the climatic mean. The cold anomaly of the Atlantic (20°S, 15°W) shows a greatly reduced area, primarily because buoy 17655 failed to report reliable temperatures. The westward extension of this anomaly was caused by the cold values reported by this buoy alone. The other features have remained fairly stable compared to last time.

Product 3 - SST Contour Maps

The SST contour map is obtained by adding the climatic temperature to the gridded anomaly values. The average buoy temperature readings are posted at the average buoy positions.

In regions where a reliable climatic temperature is unavailable, the SST contours are omitted. The average buoy temperature is still posted in this case, but is underlined with asterisks to indicate that it did not take part in the contour generations.

FIGURE 5

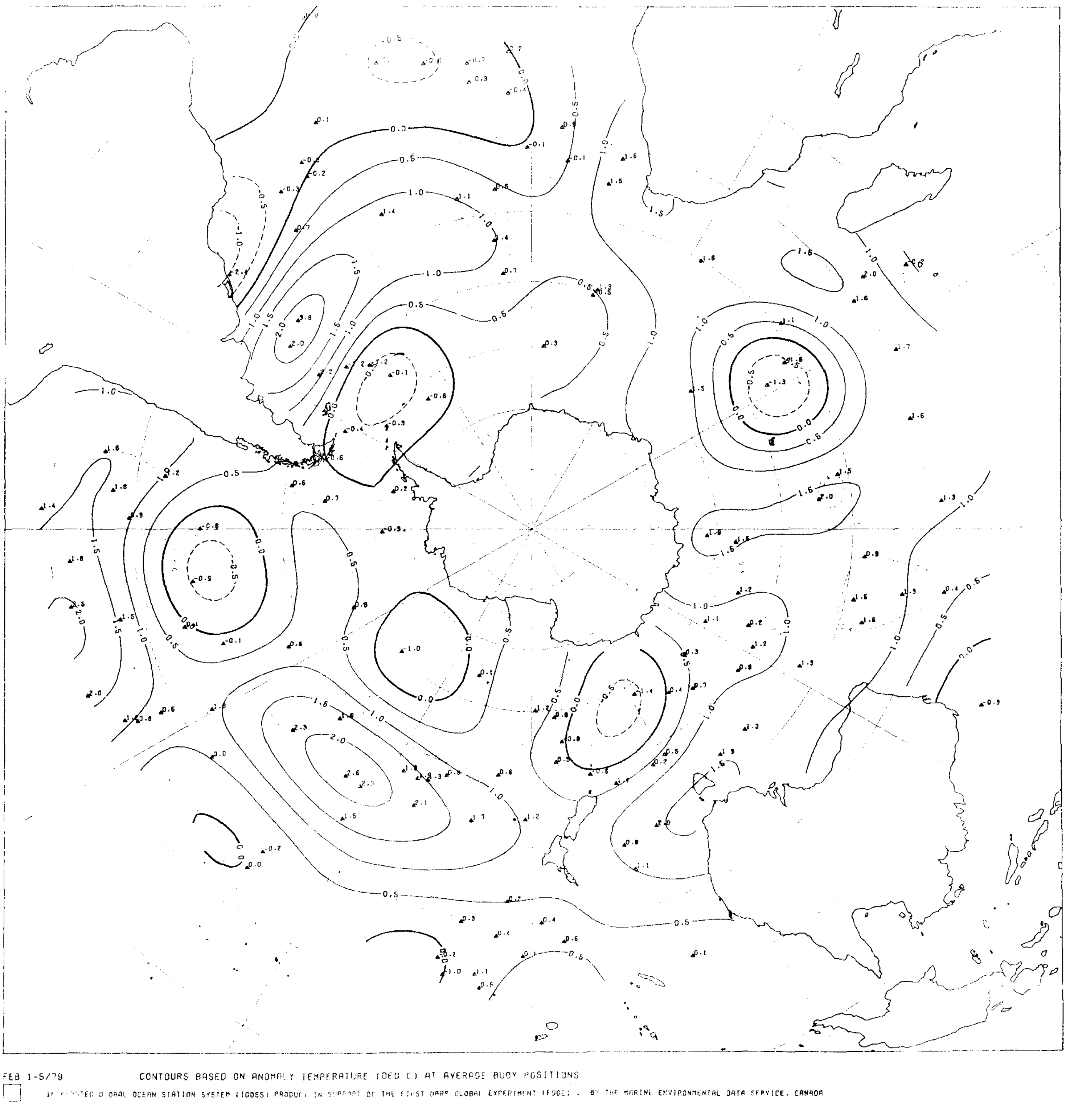

FEB 1-5/79 CONTOURS BASED ON ANOMALY TEMPERATURE (DEG C) AT AVERAGE BUOY POSITIONS

INTEGRATED GLOBAL OCEAN STATION SYSTEM (IGOSS) PRODUCT IN SUPPORT OF THE FIRST GARP GLOBAL EXPERIMENT (FGGE) . BY THE MARINE ENVIRONMENTAL DATA SERVICE, CANADA

FIGURE 6

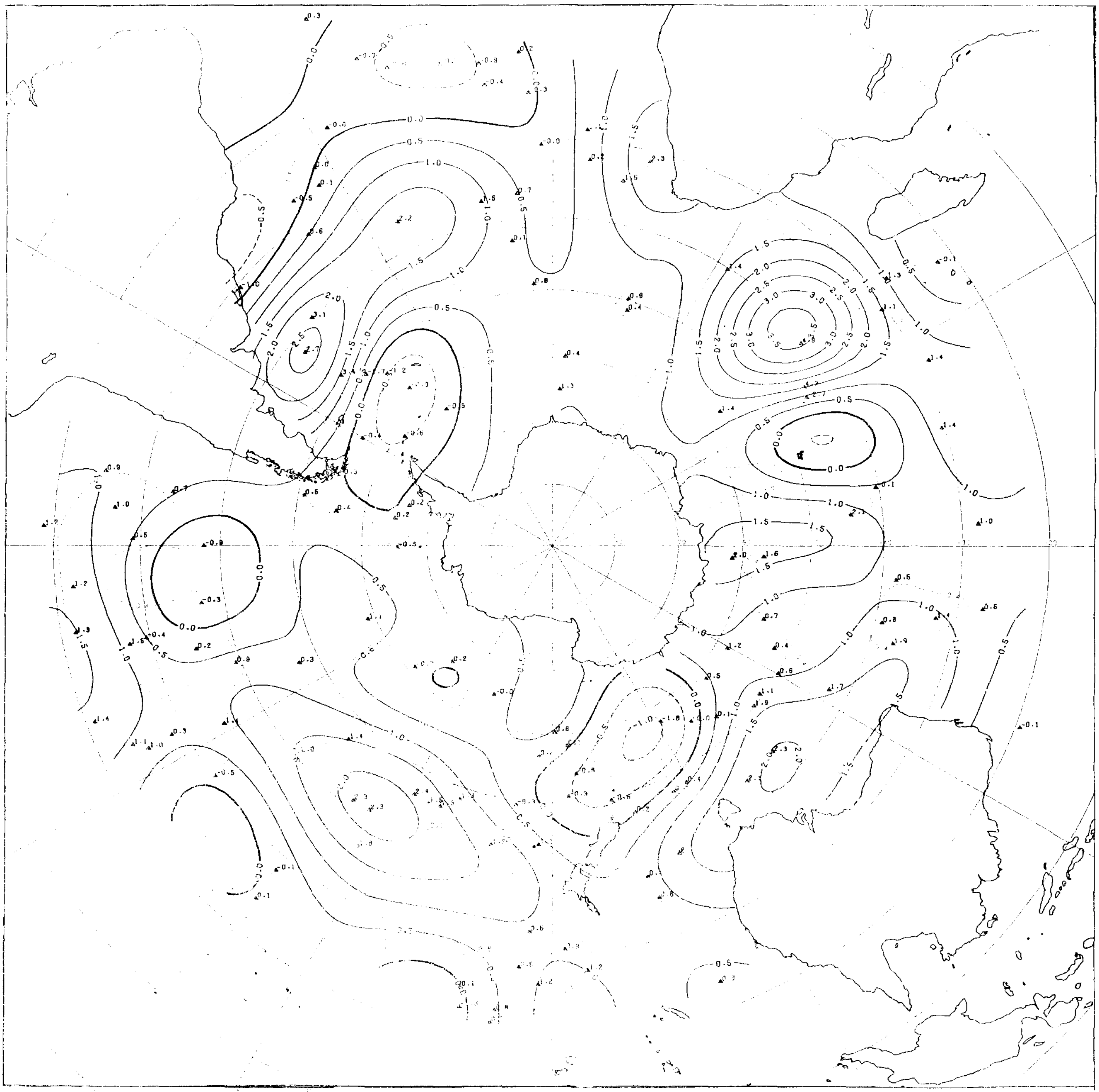

FEB 6-10/73 CONTOURS BASED ON ANOMALY TEMPERATURE ... AVERAGE BUOY POSITIONS

INTEGRATED GLOBAL OCEAN STATION SYSTEM (IGOSS) PRODUCT IN SUPPORT OF THE FIRST GARP GLOBAL EXPERIMENT (FGGE) , BY THE MARINE ENVIRONMENTAL DATA SERVICE, CANADA

FIGURE 7

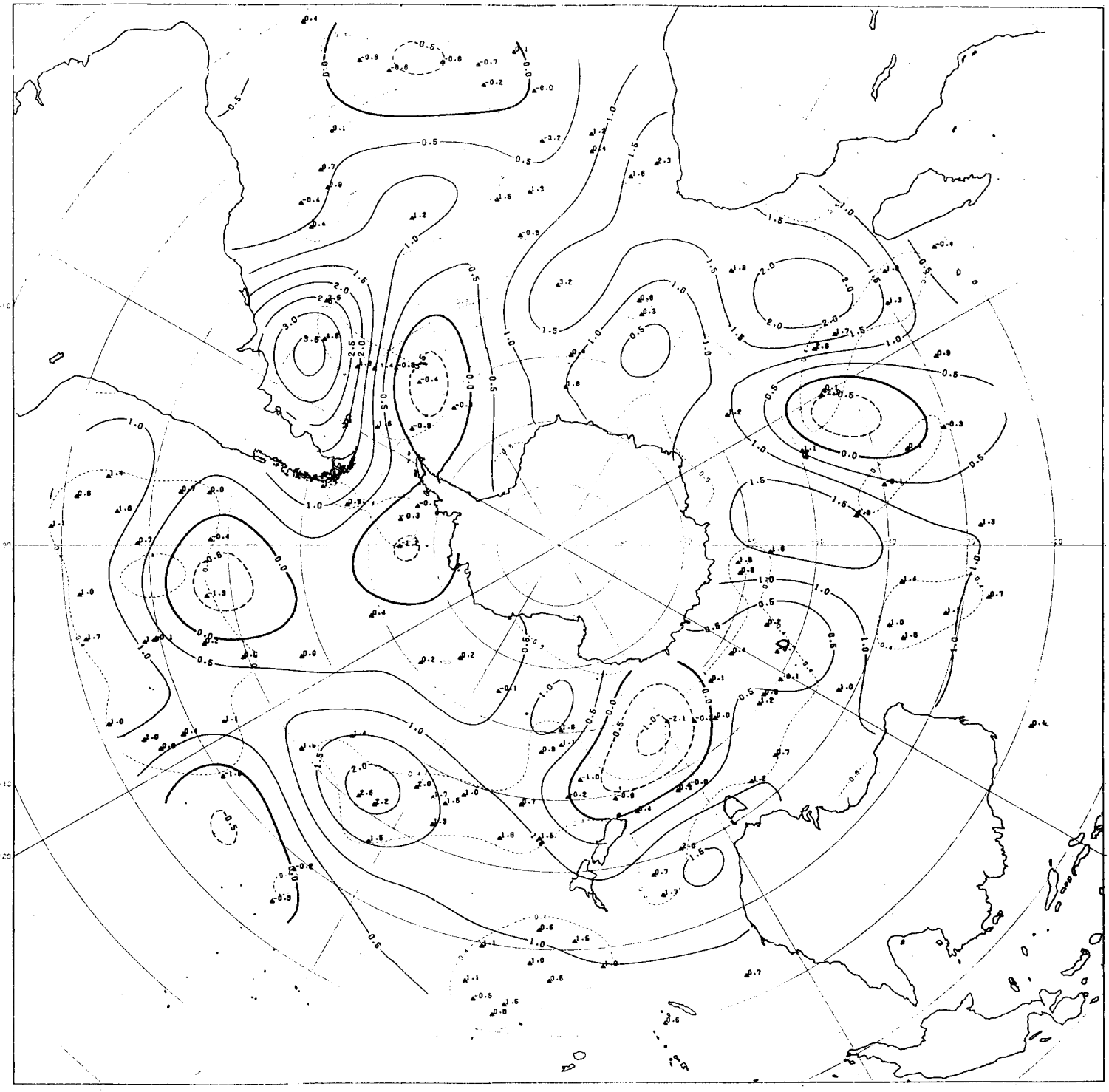

FEB 11-15/79 CONTOURS BASED ON HOURLY TEMPERATURE (DEG C) AT AVERAGE BUOY POSITIONS

INTEGRATED GLOBAL OCEAN/STATION SY... ...OF THE FIRST GARP GLOBAL EXPERIMENT (FGGE) ... ENVIRONMENTAL DATA SERVICE, CANADA

For the first few 5-day periods, the expected error contours of the anomaly were plotted on the SST map as faint dashed lines. These will give an underestimate of the expected error in SST, except in regions where the climatic temperatures are very accurate. This feature was discontinued after the first few periods.

The SST contour maps are perhaps the least interesting of the MEDS products. This is because the buoy separation is too large to allow the resolution of sharp or even moderate temperature gradients which form so much of the interest in the interleaving water of the antarctic region (fronts and convergences). Instead, the temperature data indicate basically that the water is warmer near the tropics than it is near the Antarctic. For such information we don't need buoys. However the SST anomaly charts, originally produced as a quality control on the SST charts, prove to be much more valuable.

SST Map February 6-11, 1979

This figure is typical of sea surface temperature maps in that it conveys very little immediately useful information. In particular, features such as the relatively warm pool of water off Argentina, are not discernible here.

Product 4 - Surface Pressure Contour Maps

In addition to the buoy tracks, temperature anomaly contour maps, and SST contour maps intended for relatively wide distribution, MEDS is also producing contour maps of 5-day averaged, surface atmospheric pressure. As before optimum interpolation technique is used. Presently land-based pressure observations are not utilized, but they could be readily incorporated into the scheme.

The 5-day averaging period was chosen for compatability with other products, but this choice may be inappropriate depending on the spectral characteristics of the pressure field. If the characteristic period of storms is less than 5 days, important features might be lost in the averaging and not appear in the charts. Clearly more work is necessary to produce a reliable and useful product.

Surface Pressure Maps February 1-5 and February 6-10, 1979

Figures 9 and 10 are included as examples of this product, and illustrate the variability from one 5-day period to the next. Some features, such as the high pressure system in the Atlantic are comparatively stable (as shown on these and other figures). However others, such as the low pressure system southeast of Australia in Figure 9 appear transitory. As mentioned, of course, a 5-day averaging period might be totally inappropriate. The interested reader might enjoy trying to correlate features in these plots with the corresponding SST-anomaly maps.

FIGURE 8

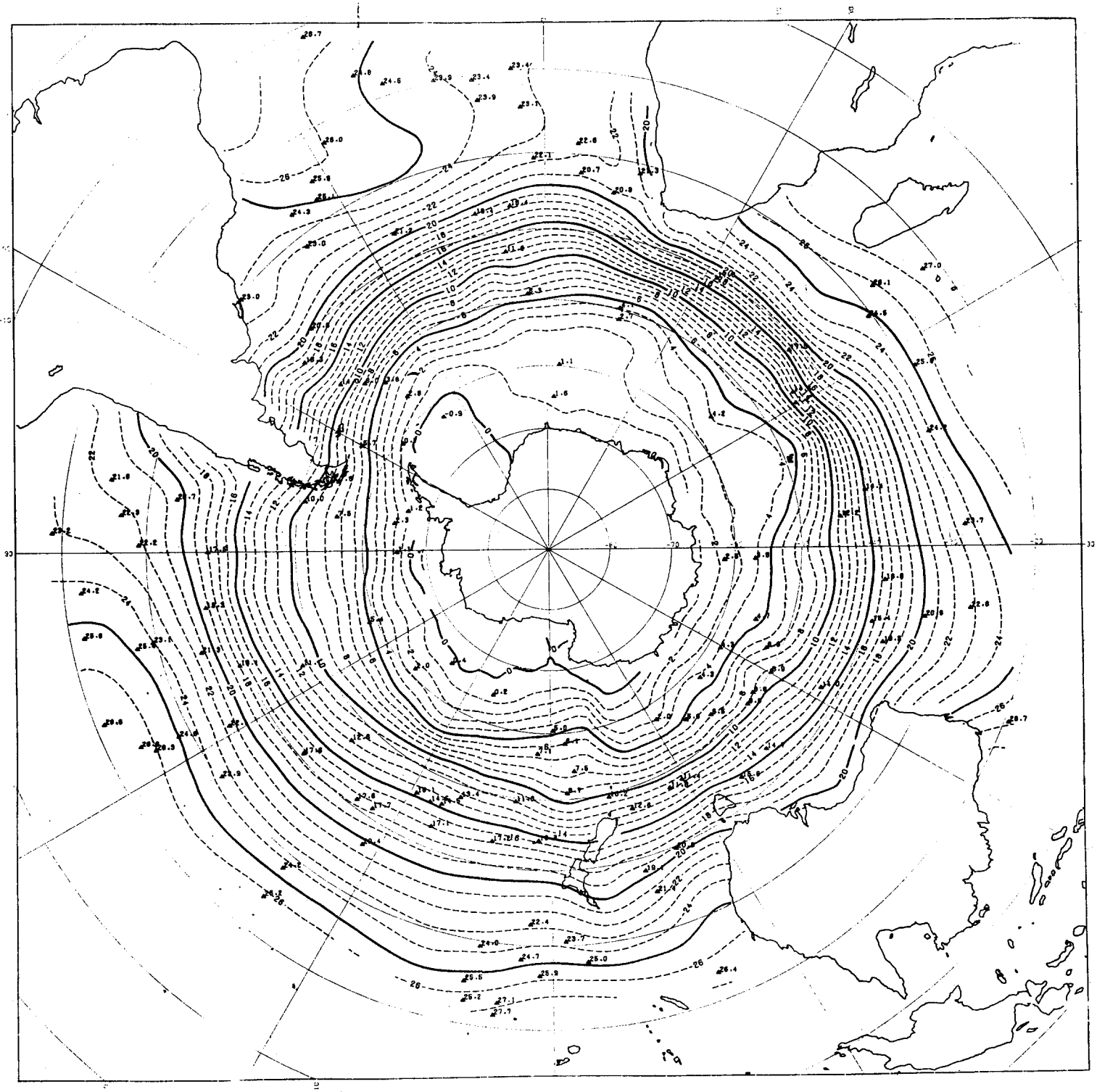

FEB 6-10/79 CONTOURS BASED ON AVERAGE TEMPERATURE (DEG C) AT AVERAGE BUOY POSITIONS

INTEGRATED GLOBAL OCEAN STATION SYSTEM (IGOSS) PRODUCT IN SUPPORT OF THE FIRST GARP GLOBAL EXPERIMENT (FGGE). BY THE MARINE ENVIRONMENTAL DATA SERVICE, CANADA

FIGURE 9

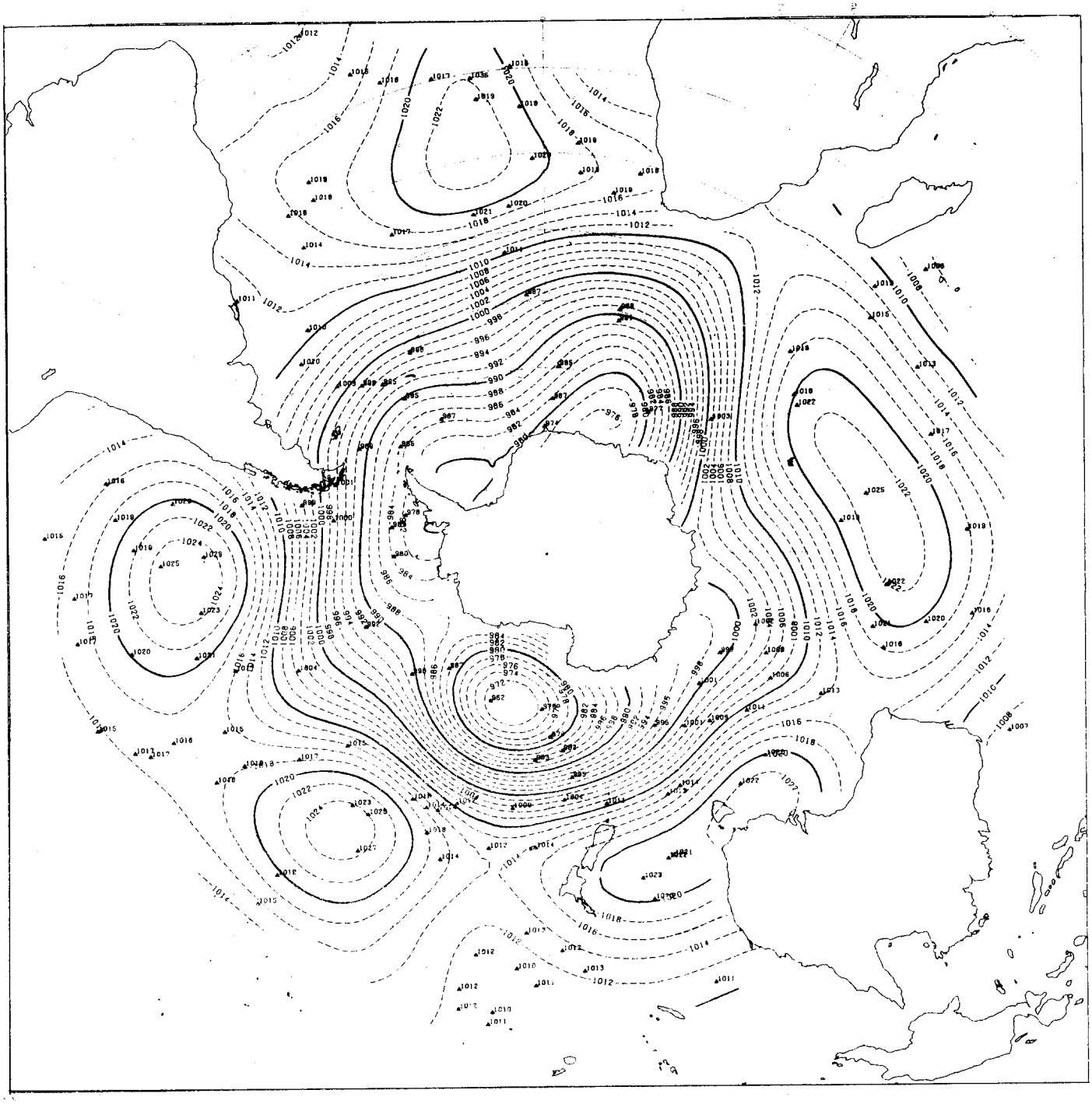

FEB 06 - FEB 10/79 CONTOURS BASED ON AVERAGE PRESSURE (MILLIBAR) AT AVERAGE BUOY POSITIONS

INTEGRATED GLOBAL OCEAN STATION SYSTEM (IGOSS) PRODUCT IN SUPPORT OF THE FIRST GARP GLOBAL EXPERIMENT (FGGE). BY THE MARINE ENVIRONMENTAL DATA SERVICE, CANADA

FIGURE 10

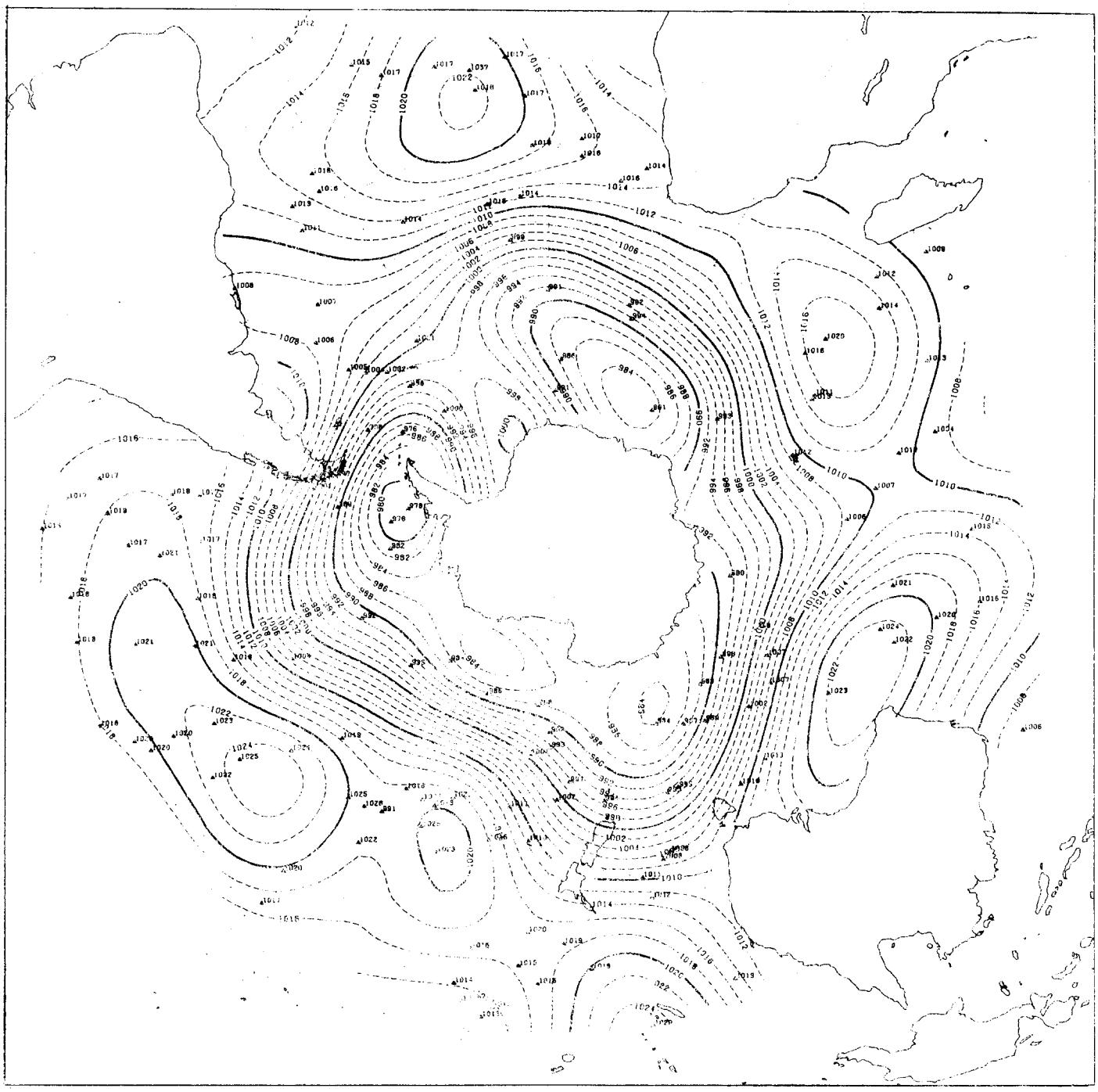

FEB 11 - FEB 15/79 CONTOURS BASED ON AVERAGE PRESSURE (MILLIBARS) AT AVERAGE BUOY POSITIONS

INTEGRATED GLOBAL OCEAN STATION SYSTEM (IGOSS) PRODUCT IN SUPPORT OF THE FIRST GARP GLOBAL EXPERIMENT (FGGE) BY THE MARINE ENVIRONMENTAL DATA SERVICE, CANADA

DERIVED PRODUCTS

Geostrophic Wind

Once the atmospheric pressure field has been successfully determined, it may be used in the derivation of other useful products. In particular, the geostrophic wind $\underline{v}_{geo}$ is given as the spatial derivative of the pressure field. As such, it is more sensitive to errors in measurement than is the pressure field. Although one also must measure buoy position and air density (and hence temperature) in addition to pressure, the latter is the limiting measurement. For FGGE buoys it is determined to an accuracy of at best 0.5 mb. Since $\underline{v}_{geo}$ is calculated from pressure differences between adjacent buoys which may only be a few mb, a sizeable error might be expected. The optimum interpolation should help minimize this problem however.

Surface winds are calculated by rotating the geostrophic wind clockwise (in the southern hemisphere) through an angle α and reducing it in magnitude to approximate frictional effects. Several methods are commonly used to determine α (which may be as large as 30^0) and to estimate the reduction in velocity. For example, in the calculation of Coastal Upwelling Indices, Bakun (1973) fixes α at 15^0 and reduces the wind speed by 30%. On the other hand, Roden and Paskausky (1978) and Bjørheim and Guddal (1978) use wind speed dependent formulations for α but do not reduce $|\underline{v}_{geo}|$. In general, α depends on the wind speed, the stability of the boundary layer above the ocean surface, and on the sea surface state (eg: Arya, 1975). In view of the problems associated with the accurate determination of $\underline{v}_{geo}$, the problem of specifying a rotation angle lessens in significance, and our initial intention is to simply use $\underline{v}_{geo}$ for the surface wind. (In the determination of surface currents, the factor expressing the reduced magnitude of $\underline{v}_{geo}$ may be incorporated into k; see below.)

A potential problem exists in the use of $\underline{v}_{geo}$ to determine the surface wind $\underline{v}_{wind}$. At times and in some regions, non-geostrophic effects (eg: local accelerations) may be important. That is the winds may not be in geostrophic balance; however, this requires further investigation.

Surface Currents

A valuable oceanographic product that may be extracted from the buoy tracks and geostrophic wind is the ocean surface current field. For undrouged buoys, Kirwan *et al.* (1975) has demonstrated that the buoy velocity $\underline{v}$ is closely approximated by $\underline{v} = \underline{v}_{sur} + k\underline{v}_{wind}$ where $\underline{v}_{sur}$ is the surface current, $\underline{v}_{wind}$ is the wind velocity, and k is a drift factor. Although $\underline{v}$ is readily obtained by differentiating the buoy trajectory, the determination of k and $\underline{v}_{wind}$ is not as straightforward. In principal, k is a function of $\underline{v}_{wind}$, but in practice it is usually fixed as a constant between .01 and .10. Its value depends on the buoy design and it should be determined experimentally for each buoy type. The above relation is often used operationally for drouged buoys, but with a reduced drift factor.

Of more fundamental significance is the relationship between currents deduced from measurements at or close to the air-sea interface and those at some depth isolated from direct wind forcing; that is the flow commonly referred to as the surface circulation by oceanographers. Near the surface the direct, wind induced drift might comprise a significant component of the total current. Of course, the problem to which the deduced currents are to be applied determine which flow is of interest. For example, if one were concerned with oil spill dynamics, the surface currents would be required. However, if one wished to estimate mass transports or to compare observed currents with computed geostrophic velocities, wind drift contamination might present a serious problem. In regions of large velocity shear, a moderate wind drift component could drive a buoy into a region of significantly different ambient current. This could pose a serious problem in a study of buoy dispersion (Kirwan, et al., 1975).

Having raised these potentially serious obstacles to the successful extraction of surface currents from observed buoy tracks and computed wind fields, we note that recent results indicate that these problems may not be overly significant. In the study of undrouged buoys deployed in the North Pacific in October, 1975, Kirwan, et al. (1978b) found that application of the wind corrections of Kirwan, et al. (1975) led to unrealistic results, especially at high wind speeds. Kirwan, et al. (1978c) concluded that this was also true for buoys drouged at 30 m and deployed in the North Pacific during June and September, 1976, and they therefore used uncorrected buoy tracks in their analysis. Kirwan, et al. (1978a) noted that there was no obvious change in the trajectories or velocities of these buoys when the drouges fell off. Clearly these results demonstrate the need for field studies to determine the relationship between surface winds and the motions of drouged and undrouged drifting buoys.

APPLICATIONS OF PRODUCTS

One of the most promising applications of drifting buoy systems is their potential use in conjunction with remote sensing systems. Presently, the most widely used oceanographic products routinely obtained from satellite systems are sea surface temperatures. Although the temperature resolution of infrared and buoy systems are comparable, the former is capable of resolving spatial features of the order of 1 km. This means that remotely sensed SST's are preferable for a variety of purposes, for example in the detection of oceanic fronts which have characteristic length scales of a few km (Legeckis, 1978). Unfortunately, infrared instruments are unable to sample cloud covered areas since their signals are effectively absorbed by atmospheric moisture. Furthermore, even in relatively cloud free areas, extensive processing is required to filter out the effects of limited absorbence.

Buoy based SST measurements could be used for two purposes. First they would extend observations to cloud covered areas, and second, they could be used to calibrate remote measurements. Indeed Brown has reported (in Gower, 1978) that the use of SST's measured from a research ship in conjunction with remote observations permits the generation of accurate SST maps.

The most popular oceanographic application of remotely sensed SST's has been the tracking of ocean currents or of eddies shed from these currents. These studies could be significantly enhanced if one or more drifting buoys were deployed in the area of interest. In addition to providing direct velocity information, they would provide SST measurements during cloudy periods.

In the future, microwave techniques may be regularly used to sense SST, surface salinity, and surface wind speed. The need for surface truth data to allow the development of more accurate microwave measurement has been expressed by the Inter Union Commission of Radio Meteorology (Gower, 1978). Drifting buoy systems may provide an ideal mechanism to do so.

A direct application of drifting buoy data is to ship routing. Clearly the movement of the upper layer is that which most influences deep ocean ships. Whereas gains would not be great, on a nominally 10-day run a gain (or loss) or half to one day could be realized by taking advantage of (or bucking) known drifts.

The buoy information could also be used to assist in the construction of a large scale baroclinic model aimed at describing the dynamics of the upper layer. Depending upon the degree of sophistication and the success of such a model, it could be used in a predictive scheme to predict the motion of oil spills and as an aid in search and rescue operations.*

*this could become tiresome

RECOMMENDATIONS AND CONCLUSIONS

In this study we have briefly examined and given examples of products that are being produced or may be produced in the future using data obtained from the FGGE Drifting Buoy System. To enhance these products we recommend that the following studies be undertaken:

(1) An intercomparison of the different types of pressure and temperature sensors employed on FGGE buoys.

(2) The determination of wind drift factors for each buoy type under a variety of wind conditions.

(3) A detailed intercomparison of the motions of drouged and undrouged buoys.

(4) The determination of the spectral characteristics of the surface pressure field.

(5) The extraction of sea surface currents using the method outlined previously.

REFERENCES CITED

Arya, S.P.S., 1975: Geostrophic Drag and Heat Transfer Relations for the Atmospheric Boundary Layer. Quart. J.R. Met. Soc., 101, 147-161.

Bakun, A., 1973: Coastal Upwelling Indices, West Coast of North America, 1946-71. U.S. Dep. Commer., NOAA Tech. Rep. NMFS SSRF-671, 103 pp.

Bjørheim, K. & J. Guddal, 1978: Simulation of Drifting Buoys Trajectories. Technical Report No. 34. Det Norske Meteorologiske Institutt.

Bretherton, F.P., R.E. Davis & C.B. Fandry, 1976: A Technique for Objective Analysis and Design of Oceanographic Experiments Applied to MODE-73. Deep-Sea Research, 23, 559-582.

Freeland, H.J., P.B. Rhines, & T. Rossby, 1975: Statistical Observations of the Trajectories of Neutrally Buoyant Floats in the North Atlantic. Journal of Marine Research, 33, 383-404.

Gandin, L.S., 1965: Objective Analysis of Meteorological Fields, Israel Program for Scientific Translations.

Garrett,J., 1978: Canadian FGGE Buoy Project. Annex 4, Appendix 3. Third Session of the Committee of Participants for the Drifting Buoy System for the FGGE. Melbourne.

Gower, J.F.R., 1978: Editor, Passive Radiometry of the Ocean, Working Group Reports. Pacific Marine Science Report 78-28. Institute of Ocean Sciences, Patricia Bay, Sidney, B.C. Canada, unpublished manuscript, 43 pp. (The full proceedings of this colloquium are to be published in Boundary Layer Meteorology.)

Kirwan, A.D., G.J. McNally, E. Renya, & W.J. Merrell, 1978a: The Near-Surface Circulation of the Eastern North Pacific. J. Phys. Oceanogr. 8, 937-945.

Kirwan, A.D., G. McNally, & S. Pazan, 1978b: Wind Drag and Relative Seperations of Undrouged Drifters. J. Phys. Oceanogr. 8, 1146-1150.

Kirwan, A.D., G. McNally, S. Pazan, & R. West, 1978c: Analysis of Surface Current Response to Wind. Submitted to J. Phys. Oceanogr.

Kirwan, A.D., G. McNally, M.S. Chang, & R. Molinari, 1975: The Effect of Wind and Surface Currents on Drifters. J. Phys. Oceanogr. 5, 361-368.

Legeckis, R., 1978: A Survey of Worldwide Sea Surface Temperature Fronts Detected by Environmental Satellites. J. Geophys. Res., 83, 4501-4522.

Roden, G.I. & D.F. Paskausky, 1978: Estimation of Rates of Frontogenesis and Frontolysis in the North Pacific Ocean Using Satellite and Surface Meteorological Data from January 1977. J. Geophys. Res., 83, 4545-4550.

RESULTS AND PROSPECTS PROVIDED BY THE CONTINUAL MONITORING OF THE OCEANS BY MERCHANT VESSELS

by J.R. Donguy, C. Henin *

Summary

ORSTOM has been concerned with the continual monitoring of the oceans through the voluntary aid of merchant ships since 1958: in the Atlantic (1958 and 1977-1978), in the Indian Ocean (1966-1967) and in the Pacific (1958-1964 and 1969-1978). Oceanographic, hydroclimatic and economic data have been gathered.

The principal surface water masses encountered have been defined and information about their formation has been collected. Frontal phenomena (convergences and divergences) have been recognized. A study of the thermocline depth will make it possible to monitor circulation at the surface and results may be checked by means of certain chemical parameters (silicates).

In the Pacific, the El Niño phenomenon may be monitored closely, along with the hydroclimatic disturbances related to it upstream and downstream. The thermal content of the Pacific Ocean, which is essential for weather forecasting, will be known by 1979 through the use of bathythermographs with expandable heads (XBT).

Chlorophyll measurements and zooplankton samplings made since 1977 give some indication of the productivity of the tropical Pacific Ocean. The localization of frontal areas constitutes an important element of information for tuna fishing. Determination of the environment in which fish and their larvae live is an important factor for their survival and growth. Lastly, considerations might be given to continual monitoring of pollution of the oceans.

Other applications might be proposed, such as the checking of satellite data and the determination of the oceanographic context of cruises.

---

* ORSTOM Centre, New Caledonia

Use of Historical Data to Compute Density and Dynamic Height from Temperature Profiles

by

W. J. Emery

INTRODUCTION

In 1918 Helland-Hansen made a fundamental discovery in observing that the relationship between temperature and salinity, the TS curve, was often constant in space and time. This constancy of TS curves is related to the quasi-stationary distribution of water masses and the mixing processes which operate at water mass boundaries. The conservative nature of the TS curves has been widely used as a quality control procedure for oceanographic data. The TS relationship, for an individual hydrographic station, can be compared with the accepted standard TS curve, for the region in question, and any marked deviations from the standard may be considered as erroneous data. Such standard TS curves have also been widely used to fill in missing salinity values when only temperatures were available.

With the development of temperature profiles, such as the bathythermograph (BT) and its modern counterpart, the expendable bathythermograph (XBT), the constancy of the TS relation has offered a mechanism to infer salinity from temperature measurements alone. These inferred salinities, combined with the temperature observations, can be used to compute density and dynamic height. The central problem in this procedure is to determine what the standard TS relation is, and if that relation is indeed constant.

The continued archival of hydrographic data has provided us with a fairly large number of hydrographic casts in many parts of the world's ocean. It may be reasoned that if the TS relation is in fact constant, a spatial average of some of these hydrographic data should yield a mean TS curve representative of the standard TS relation for the region selected. A test of this assumption is made by computing the standard deviation in salinity as a function of temperature. Where the standard deviation is small the mean curve is most likely constant, at least within the limits of the available data coverage. Mean TS curves with small salinity deviations can then be used to infer salinity from temperature.

It should be noted here that mean TS curves differ from the standard TS curves employed by earlier investigators. These mean curves combine many different hydrographic stations which may have had specific temperature-salinity pairs at different depth levels. Taken together as a mean TS curve this depth information no longer applies and thus the mean curves no longer provide any specific depth information. This is important since the theory of TS curves has been based on curves taken from individual hydrographic stations for which an explicit relationship between T, S and Z (depth) exists.

Mean TS curves have been computed for 10° squares in the North Pacific between 20°S and 40°N. In much of this zonal band these mean TS curves can be used to infer salinity from temperature observations for reliable dynamic height computations. North of this region the TS curves display large standard deviations in salinity and test calculations at ocean weather station Papa (50°N, 145°W) demonstrated that mean TS curves cannot be used for computations of reliable values of inferred dynamic height. At higher latitudes in the Pacific some conservative relation, other than the mean TS curve, must be employed for the inference of salinities from temperature profiles. The only possible alternative is a mean salinity profile (salinity versus depth or SZ profile) from which salinities could be taken to match the depths on an observed temperature profile. Test calculations, again at station Papa, revealed the conservative nature of the SZ profile and its usefulness in inferred dynamic height computations.

A combination of mean TS and SZ curves has been used to compute 0/500m inferred dynamic height in the central North Pacific from an XBT temperature structure climatology. Monthly maps of these dynamic height values reveal changes in the geostrophic circulation.

DATA

Historical hydrographic data have been used for the computation of both TS and SZ curves. An appreciation of the distribution of these data can best be gained by a map showing individual stations as dots (Fig. 1) for the North Pacific. One can readily identify the positions of the weather stations along with station locations of major data collection programs. The tendency for research programs to collect data along meridians is also readily apparent. Equally as striking are the regions of the south central Pacific which contain only a very limited number of stations. Realizing that only a small percentage of these stations are comprehensive stations that extend to the ocean bottom, the available data on temperature and salinity are definitely inadequate in many parts of the North Pacific.

TS DYNAMIC HEIGHT AT WEATHER STATIONS

To avoid such data limitations initial computations were performed at three Pacific Ocean weather stations: Papa, Victor and November (Fig. 2). Mean TS curves at November and Victor revealed that most of the salinity variance was limited to the upper 100m (Emery, 1975). Seasonal TS curves computed for station Victor (Fig. 3) all displayed the same general pattern seen in the annual average. These curves along with the annual mean at station November all showed a decrease in salinity variance at the deeper, low temperature range. The mean TS curve at Papa, however, exhibited a large salinity variance between 100 and 1000m. To test the effect of these differences true dynamic heights (d) and inferred dynamic heights (d') were computed. Histograms of the differences between these heights appear normally distributed with a small rms difference at both Victor and November. Papa, however, has a large rms difference and a histogram skewed to one side. This non-gaussian behaviour was later found to be due to the presence

of inversions in the temperature profile, and the local formation of the upper water mass.

TS DYNAMIC HEIGHT, 20 TO 40°N

Restricting the study area to the Pacific between 20°S and 40°N mean TS curves were computed (Emery and Wert, 1976) for each 10° square (Fig. 5). This combination of curves clearly depicts the distribution of the major Pacific water masses. Most obvious is the zone between 10 and 20°N where an increase in the mid-temperature range salinity variance indicates the juncture of Antarctic and Subarctic Intermediate Waters. A closer look at the 10° square around Hawaii (Kuksa and Emery, 1975) revealed the added presence of California Intermediate Water in this zone. The meeting of surface waters from the north and south is also clearly shown by the increased salinity variance at the higher temperatures for latitudes between 0 and 10°N.

Care must be exercised in the preparation of the mean TS curves as the inclusion of erroneous data will severely affect the shape of the curve and the magnitude of the salinity variance. As a method of quality control the individual TS pairs were plotted as a scatter plot along with the mean TS curves (Fig. 6). This procedure allowed the identification of stations that were incorrectly located and thus had strikingly different TS characteristics. This scatter plot also clearly demonstrates the termination of the Antarctic Intermediate Water in this square by the abrupt shift at about 12°C to lower salinity associated with water from the Subarctic.

As could be predicted from the magnitude of the salinity deviations for the individual TS curves the rms differences between 0/500m true and inferred dynamic heights (Fig. 7) were large along the central zone (010°N) and off the west coast of North America. In many regions, however, rms differences were between 1 and 4 dyn/cm which is within the accuracy of an individual calculation of true dynamic height. Therefore, in these regions mean TS curves could be used to infer salinity from observed temperature profiles for the computation of inferred dynamic height.

MEAN SALINITY PROFILES

Returning to latitudes north of 40°N an effort was made to investigate climatological relations, other than mean TS curves, for the inference of salinity. As before, initial computations were carried out at ocean station Papa where a program of oceanographic data collection has provided a substantial data base. Studies (Tabata, 1960, 1961) of these data indicated the consistency of salinity profiles; therefore, a mean SZ curve, down to 500m, was computed along with the standard deviation in salinity (Fig. 8). The important feature of this curve is that the majority of the salinity variance is restricted to the region in and above the halocline. Below this the salinity deviation decreases rapidly. A computation of seasonal SZ profiles also demonstrated that the shape of the mean annual SZ curve remains constant below the halocline.

To evaluate the application of the mean SZ profile to inferred dynamic height computation, salinities were inferred from the SZ curve and combined with the temperature profiles to give values of 0/500m SZ inferred dynamic height. The differences between these values and true dynamic height, plotted as a histogram (Fig. 10), demonstrate an apparent normal behaviour and a relatively small rms difference of 3 dyn/cm. Compared to the analogous rms difference of 10 dyn/cm computed at Papa using the mean TS curve, this is a substantial improvement.

TS AND SZ CURVES NORTH OF 30°N

A comprehensive comparison of inferred dynamic heights, computed from mean TS and SZ curves, required the preparation of these curves from all available data (Emery and O'Brien, 1978). As shown here in Figure 9 there are a fairly large number of archived hydrographic stations available. Therefore, it was decided that the mean curves should be computed for 5° squares rather than 10° squares as were used previously. To properly examine the changes which occur at 40°N, due to the presence of the Subarctic Front, the analysis was extended south to 30°N.

Mean TS curves in the 0 to 500m layer, computed for all 5° squares north of 30°N, clearly demonstrated the role of the Subarctic Front. Looking at the curves in the eastern half of the ocean (Fig. 10) a dramatic shift in the salinity variance can be seen to occur at 40°N. South of this latitude the TS curves in the central ocean are almost linear with a fairly small salinity variance. To the north of 40°N the mean TS curves show a shift to lower salinities at midrange temperatures. This shift is accompanied by a rapid increase in the salinity variance. Farther north this shift leads to a strong inflection in the TS curves with a continued large standard deviation in salinity.

These features in the mean TS curves result in predictably large values of the rms differences between TS inferred and true dynamic heights as shown in Fig. 11. These values given for all 5° squares, along with the number of hydrographic stations used in the computation, identify the central North Pacific, primarily south of 40°N as the region where TS inferred dynamic height might be used with some confidence.

A similar treatment of the mean salinity profiles (Fig. 12) revealed, as hoped, the conservative nature of many of the SZ curves north of 40°N. Unfortunately, however, most of the SZ curves near the coast did not exhibit a reduction in salinity variance in the deeper layers. Surprisingly, even the curve just south of the location of station Papa (50°N, 145°W) had a salinity variance which remained large below the halocline. These features must reflect the increased vertical convection that occurs at these squares. In other squares the salinity variance is limited to the upper 200m indicating the restriction of salinity changes to the upper ocean. This is the case both in the high salinity surface waters south of 40°N and the sharply lower salinity waters north of this latitude.

Dynamic heights computed using salinities inferred from these mean SZ curves were again differenced with true dynamic heights and the rms differences define the regions where SZ inferred dynamic heights might be considered reliable (Fig. 13). Here the white squares are those with an rms difference less than 4 dyn/cm. Their relative abundance in the eastern and central regions identify these as the areas where the SZ curve might be used to compute inferred dynamic height In the western North Pacific the dominance of temperature in establishing the stratification results in large rms differences since the SZ method will not reflect the compensation between temperature and salinity.

Histograms of the inferred minus true dynamic height values for both SZ and TS methods reveal the different processes at different latitudes. In most squares north of 40°N the SZ method results in quasi-normal populations while the TS histograms are bi-modal. The reverse is true of most of the squares south of this latitude.

COMPUTATION OF INFERRED DYNAMIC HEIGHT MAPS

For temperature profiles in the region spanning 40°N a combination of methods should be used for the computation of inferred dynamic height. A thermal climatology was prepared from all available XBT data by White and Bernstein (1978) for the North Pacific in the area from 20 to 50°N, 130°W to 150°E. These XBT data were objectively mapped on a grid of 2 by 10° squares over depths from the surface to 500m. Using mean TS and SZ curves where most appropriate, inferred 0/500m dynamic heights were computed for each month of this temperature climatology. The first six months (Fig. 14) of these maps reveal a lot of detail in the geostrophic flow of the North Pacific Current. Most interesting is the easternmost part between 30 and 40°N where the current separates, some going south to join the California Current, and the remainder flowing north to become part of the Alaskan Gyre. Significant changes occur at this point especially in the amount of flow which does or does not turn south. It must be realized that even a minor change in the spacing of these isolines is associated with an increase of several centimetres per second in the geostrophic flow. The appearance of small cyclonic and anti-cyclonic eddies at this separation indicates the changes in vorticity associated with the flow turning.

A second six months (Fig. 15) also demonstrates some important changes especially in the northwest corner. Here the pattern appears to have shifted north and perhaps a little west. There is some concern for the small wiggles near 40°N as in general the method of salinity inference changes here. It is interesting, however, that no sharp discontinuity in dynamic height is apparent to belie the boundary between methods. The smooth transition between procedures is additional evidence to the reliability of applying these methods to such computations.

Another more rigid evaluation is a comparison between these maps and similar maps of true dynamic height. In 1975 Wyrtki published a report which contained bi-monthly maps of 0/500m dynamic height for the Pacific,

computed from all available hydrographic data. The combination of data into bi-monthly periods was due to the paucity of data in individual months. We thus averaged individual months together of the inferred dynamic height maps and compared them with Wyrtki's maps (Fig. 16). The inferred maps appear very smooth in contrast to Wyrtki's but have the same general range and trend. Even the subtle northward and southward shifts of the patterns are well represented by the inferred maps. In the latter part of the year the inferred dynamic heights tend to turn south a little less sharply than Wyrtki's true topographies.

It must be remembered here that the true dynamic topographies contoured by Wyrtki stem from hydrographic data collected mainly before 1970. The XBT climatology, on the other hand, are based on data whose collection only began in 1966 and are concentrated in the time after 1970. Also, the hydrographic data may be relatively few compared to the many XBT profiles now available. The favorable comparison between such different climatologies emphasizes both the reliability of the TS and SZ inferred dynamic height methods, and the stationary nature of the climatological mean geostrophic flow.

REFERENCES

Emery, W.J., 1975: Dynamic height from temperature profiles. J. Phys. Oceanogr., 5, 369-375.

Emery, W.J., and R.T. Wert, 1976: Temperature-salinity curves in the Pacific and their application to dynamic height computation. J. Phys. Oceanogr., 6, 613-617.

Emery, W.J. and A. O'Brien, 1978: Inferring salinity from temperature or depth for dynamic height computations in the North Pacific. Atmosphere-Oceans, 16, 4.

Kuksa, V.I. and W.J. Emery, 1976: A short study of the transition zone between Pacific Intermediate Water masses. Oceanology, 4, 594-597.

Tabata, S., 1960: Characteristics of water and variations of salinity, temperature and dissolved oxygen content of the water at ocean weather station "P" in the Northeast Pacific Ocean. J. Fish. Res. Board Can., 17, 353-370.

Tabata, S., 1961: Temporal changes of salinity, temperature and dissolved oxygen content of the water at station "P" in the Northeast Pacific Ocean and some of their determining factors. J. Fish. Res. Board Can., 18, 1073-1124.

White, W.B. and R.L. Bernstein, 1978: Design of an oceanographic network in the mid-latitude North Pacific. J. Phys. Oceanogr. (in press).

Wyrtki, K., 1974: The dynamic topography of the Pacific Ocean and its fluctuations. Hawaii Institute of Geophys., Rept. H16-74-5.

LIST OF FIGURES

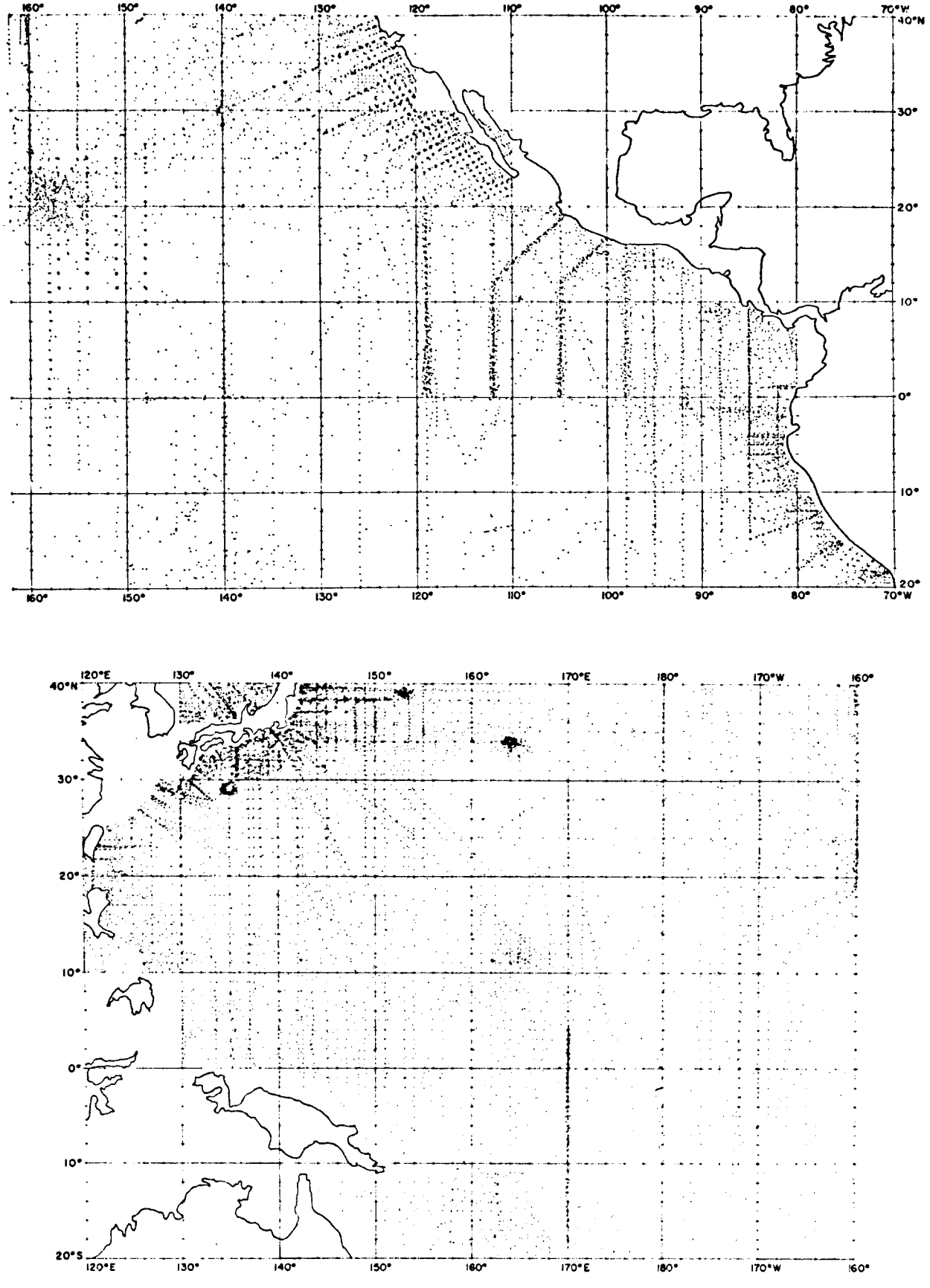

Fig. 1 - Available hydrographic stations in the Pacific from 20°S to 40°N.

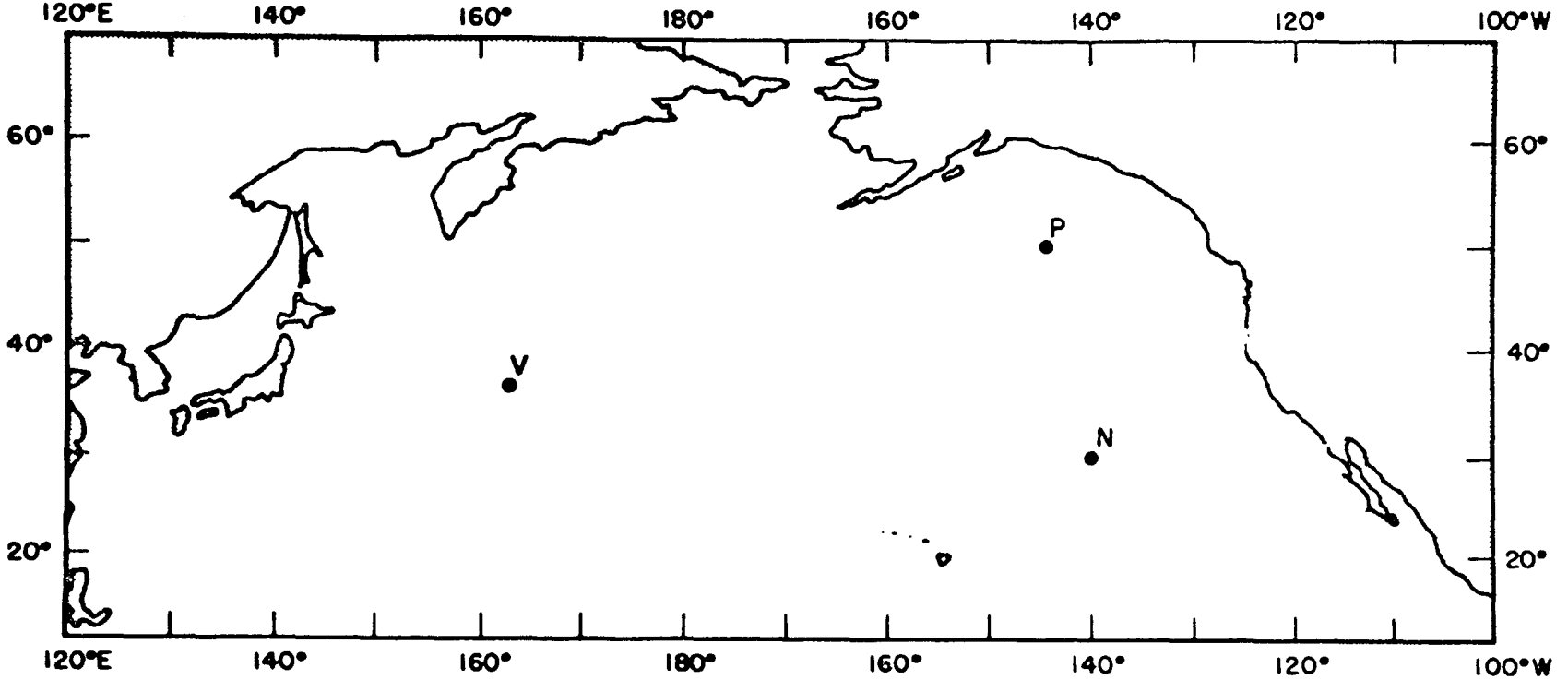

Fig. 2 - Positions of Pacific Ocean weather stations Papa (P), November (N), and Victor (V).

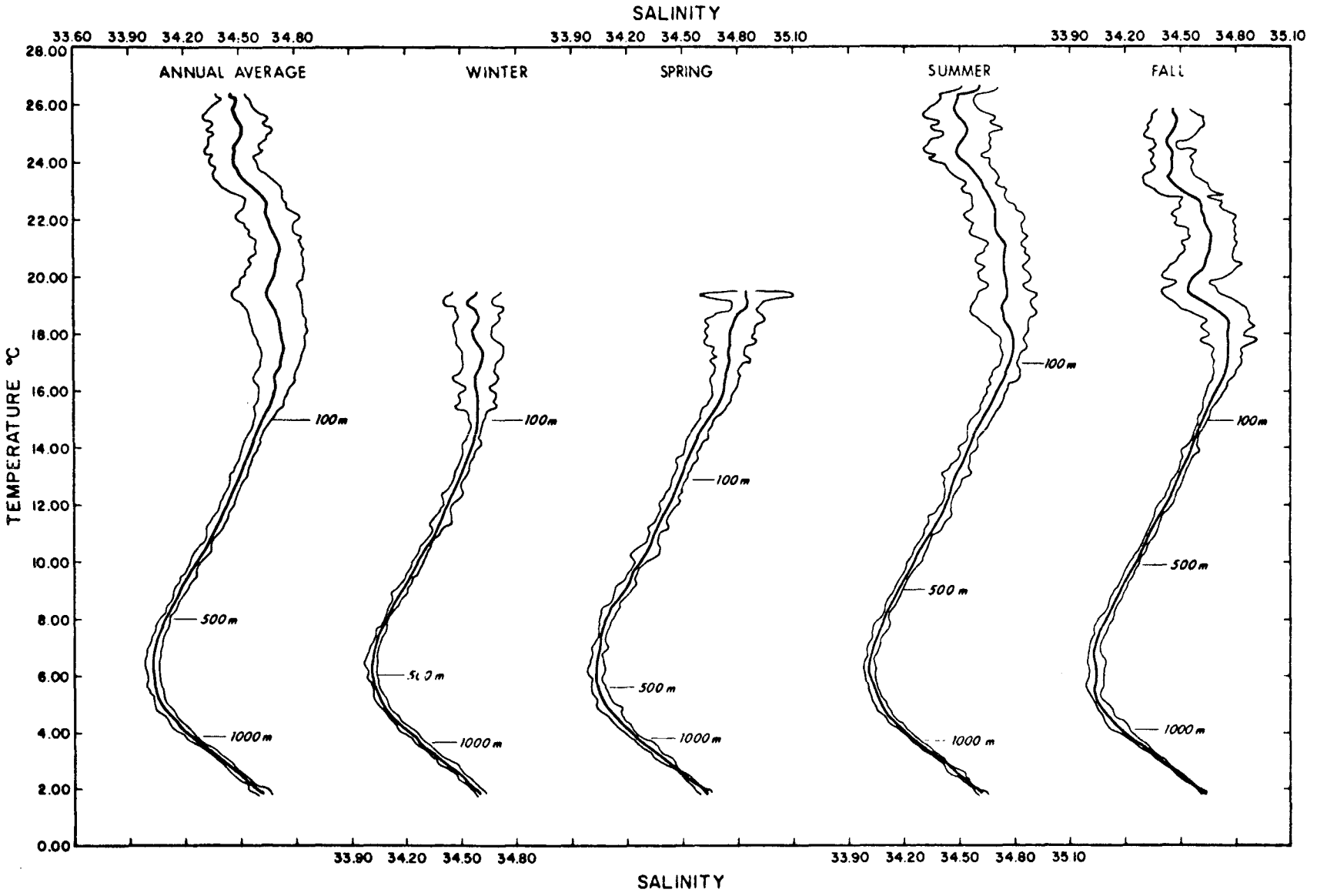

Fig. 3 - Seasonal and annual mean TS curves at station Victor.

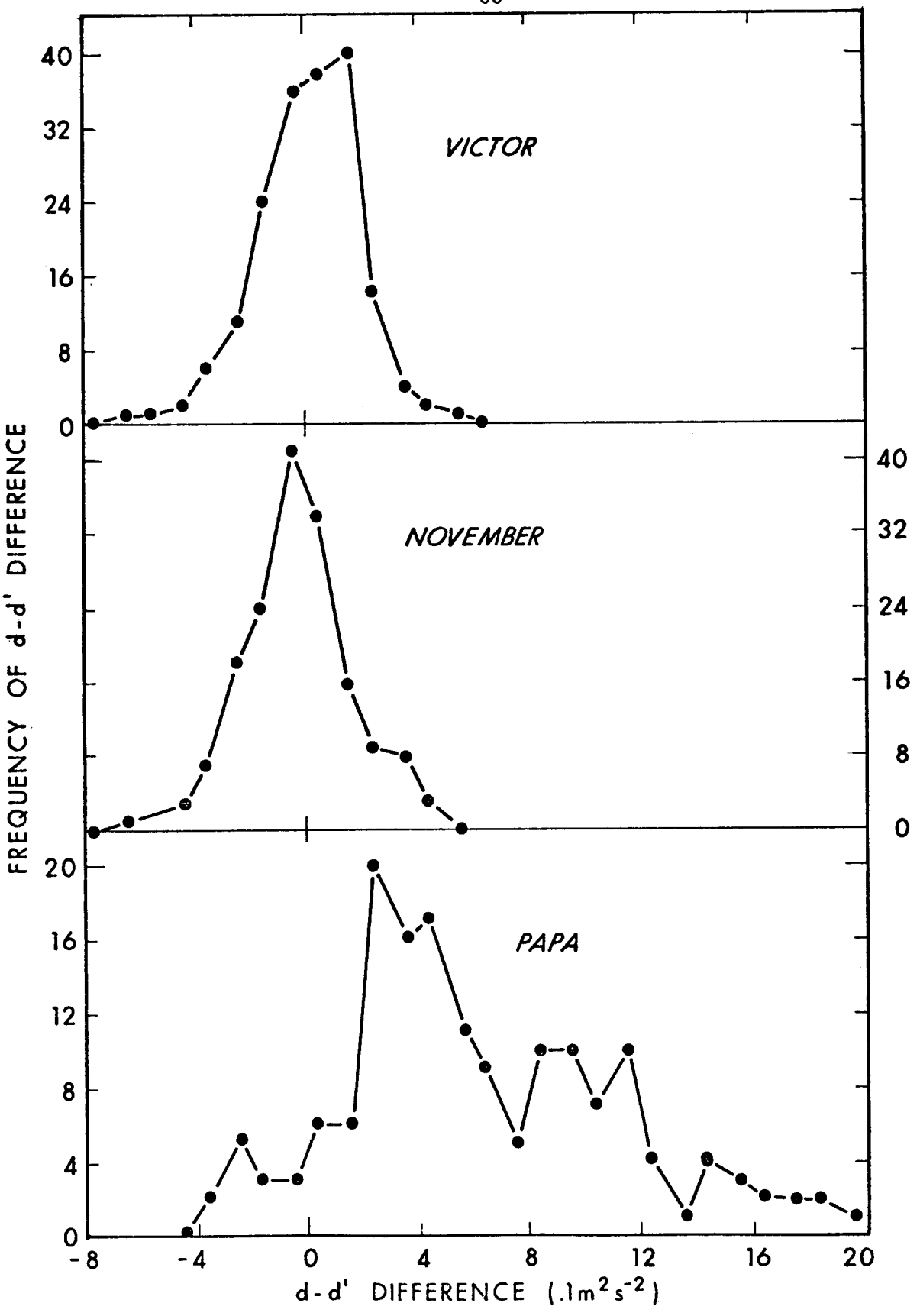

Fig. 4 - Histograms of the differences (dyn/cm) betwee true (d) and TS inferred (d') dynamic heights at the three weather stations.

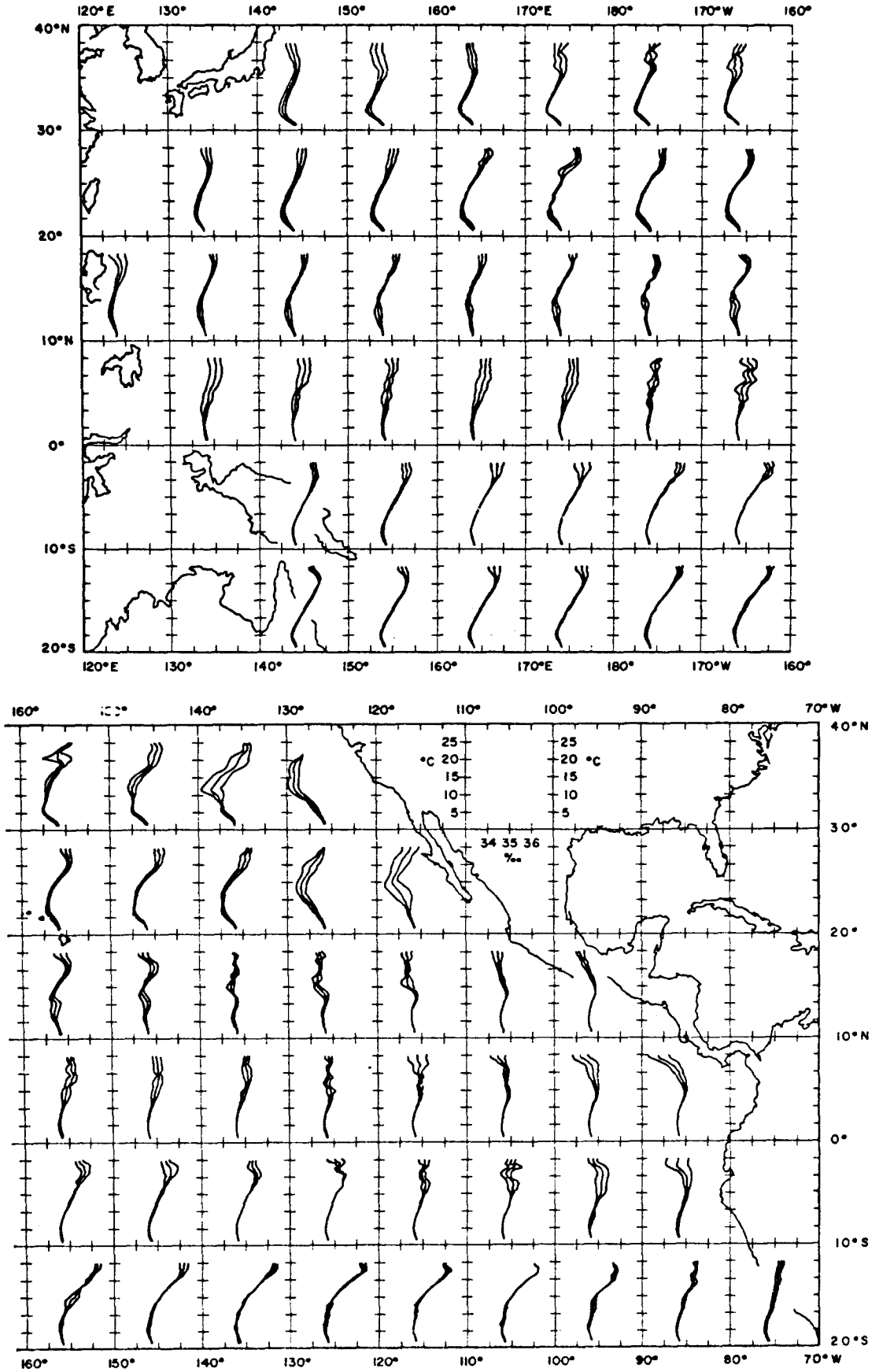

Fig. 5 - Mean TS curve by 10° squares bracketed by the standard deviation in salinity.

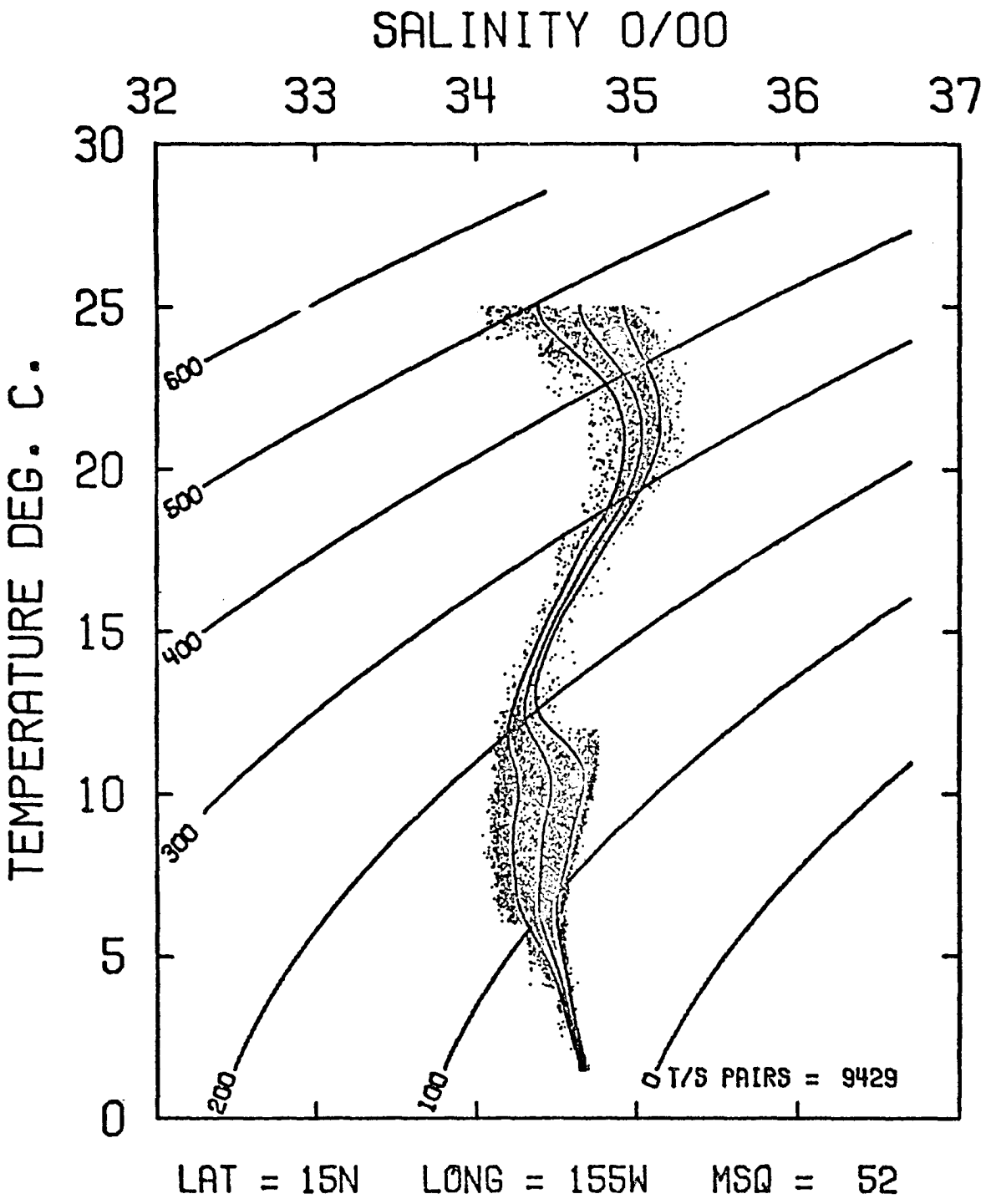

Fig. 6 - Mean TS curve, salinity deviation and individual TS pairs (dots) in the 10° square near Hawaii.

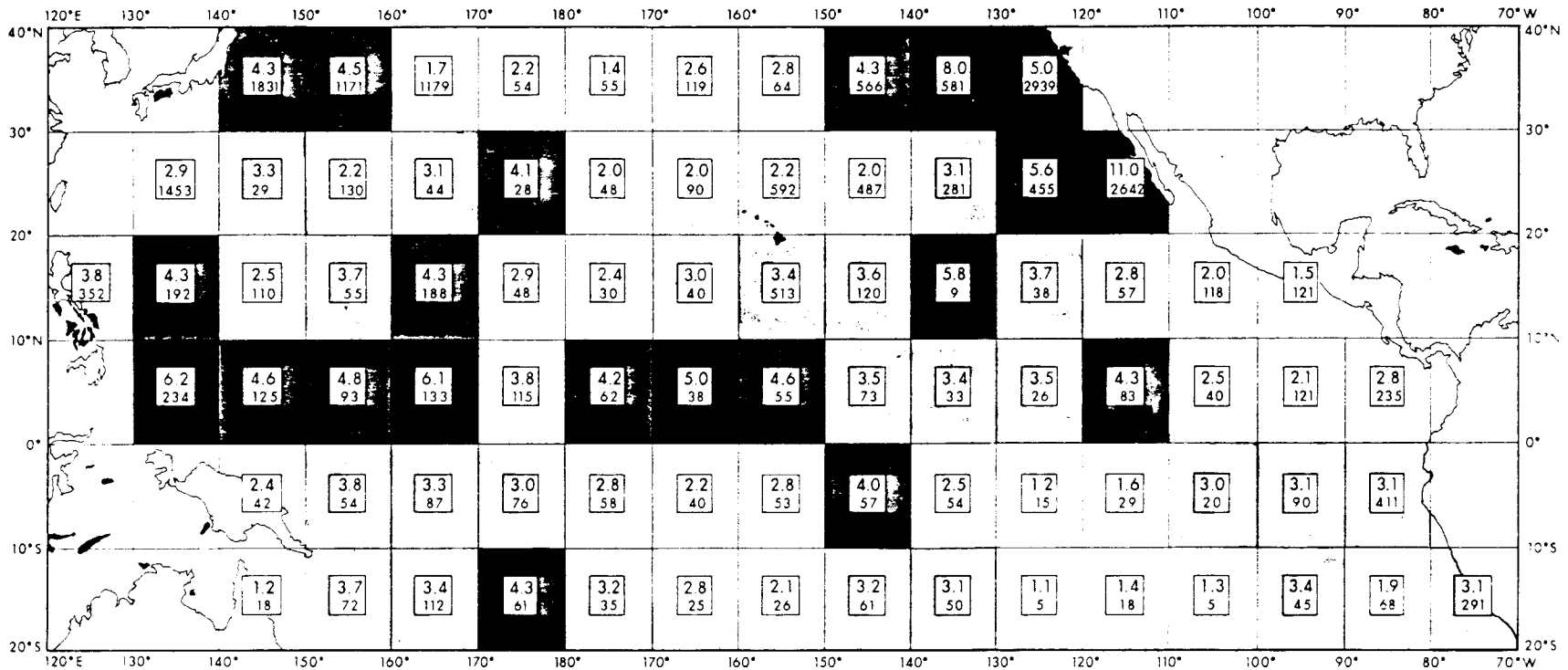

Fig. 7 - RMS differences (dyn/cm) between 0/500m true and TS inferred dynamic heights by 10° squares. Differences greater than 4 dyn/cm are darkly shaded. The lower value in each square is the number of the hydrographic station used to calculate differences.

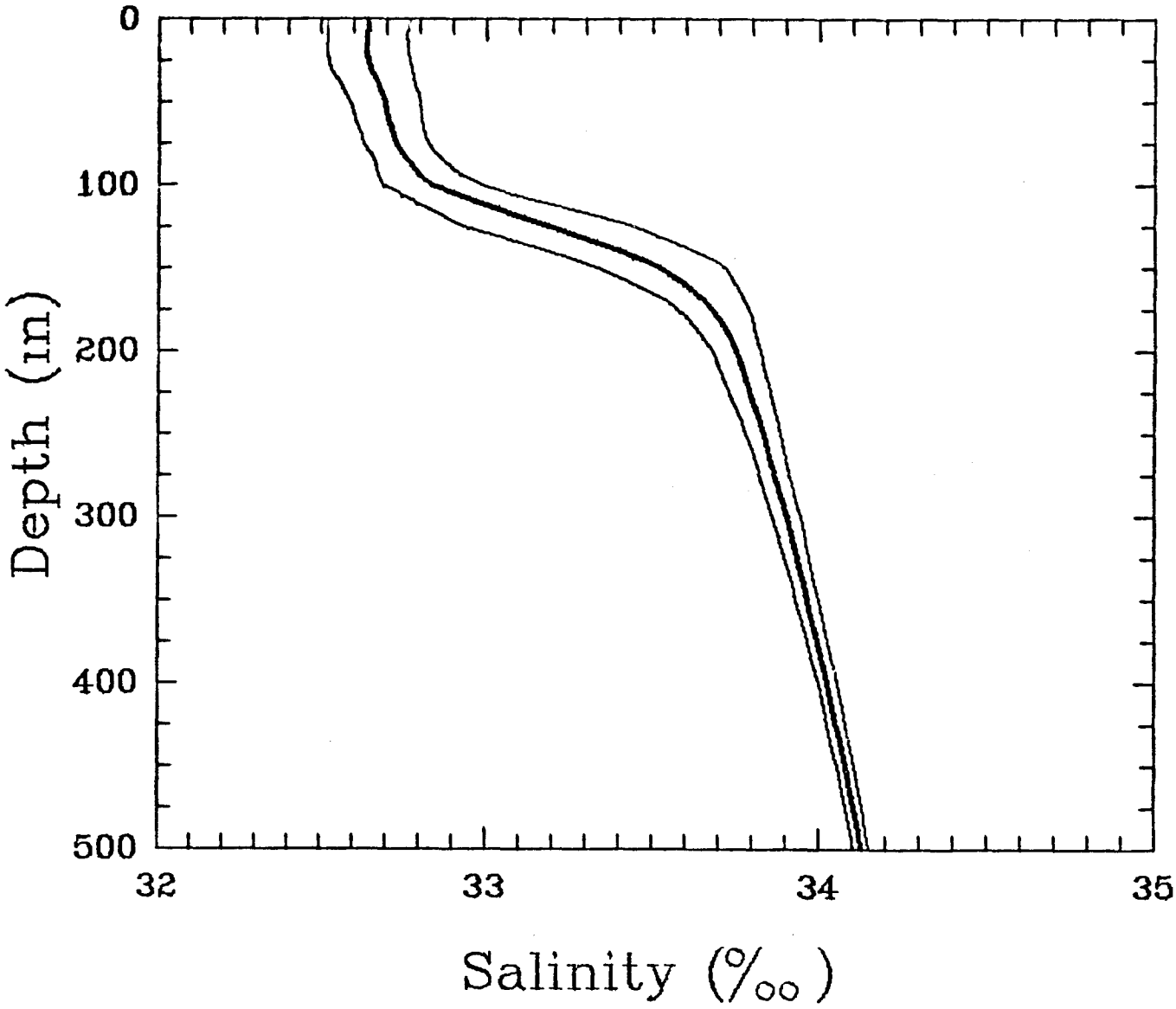

Fig. 8 - Mean salinity profile to 500m (SZ curve) at weather station Papa. Mean curve is bracketed by the standard deviation in salinity.

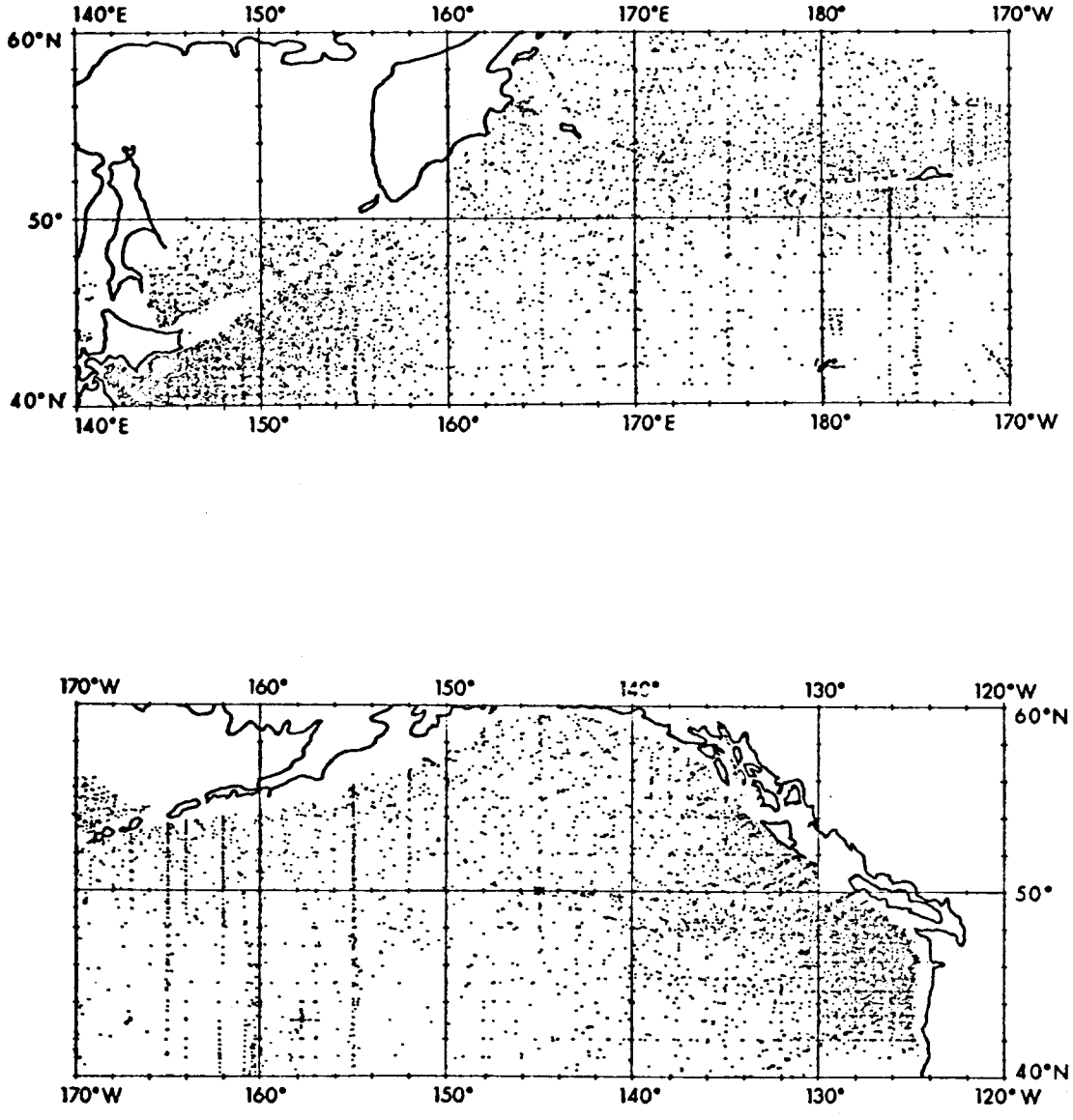

Fig. 9 - Available hydrographic stations in the Pacific north of 40°N.

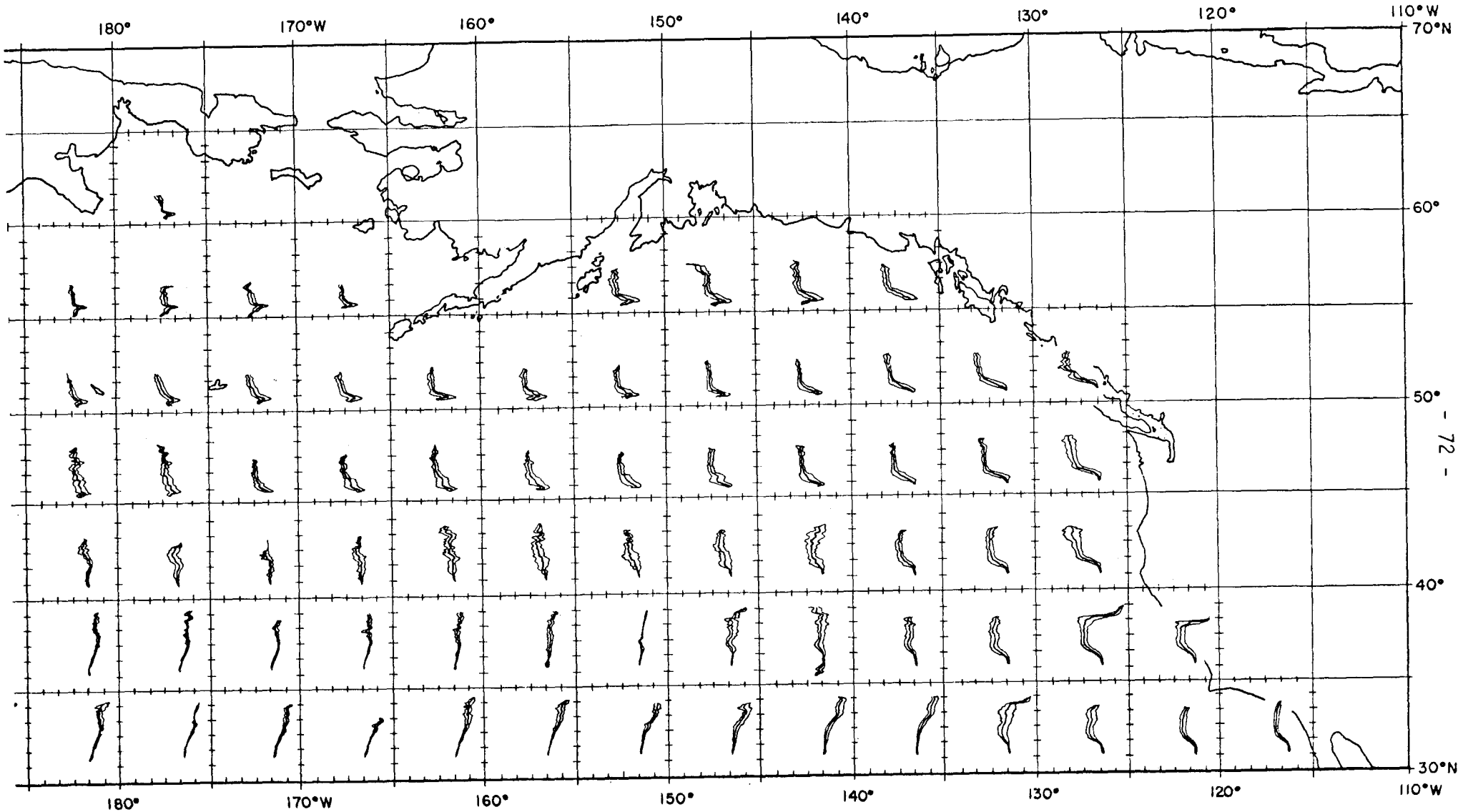

Fig. 10 - Mean TS curves by 5° square in the Northeast Pacific north of 30°N. Mean curves are bracketed by the standard deviations in salinity.

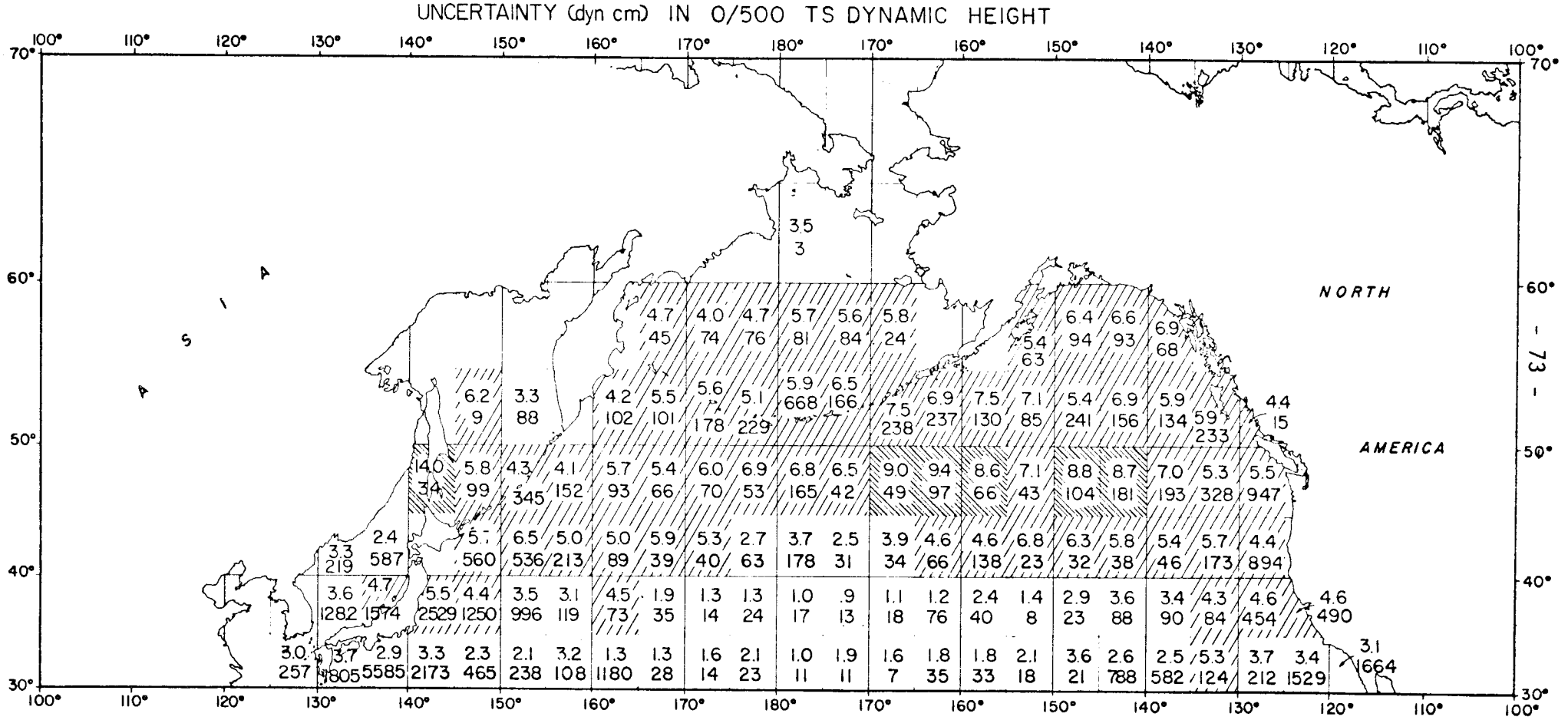

Fig. 11 - RMS differences (dyn/cm) between 0/500m true and TS inferred dynamic heights. The number of hydrographic lasts is also given as the lower value in each square.

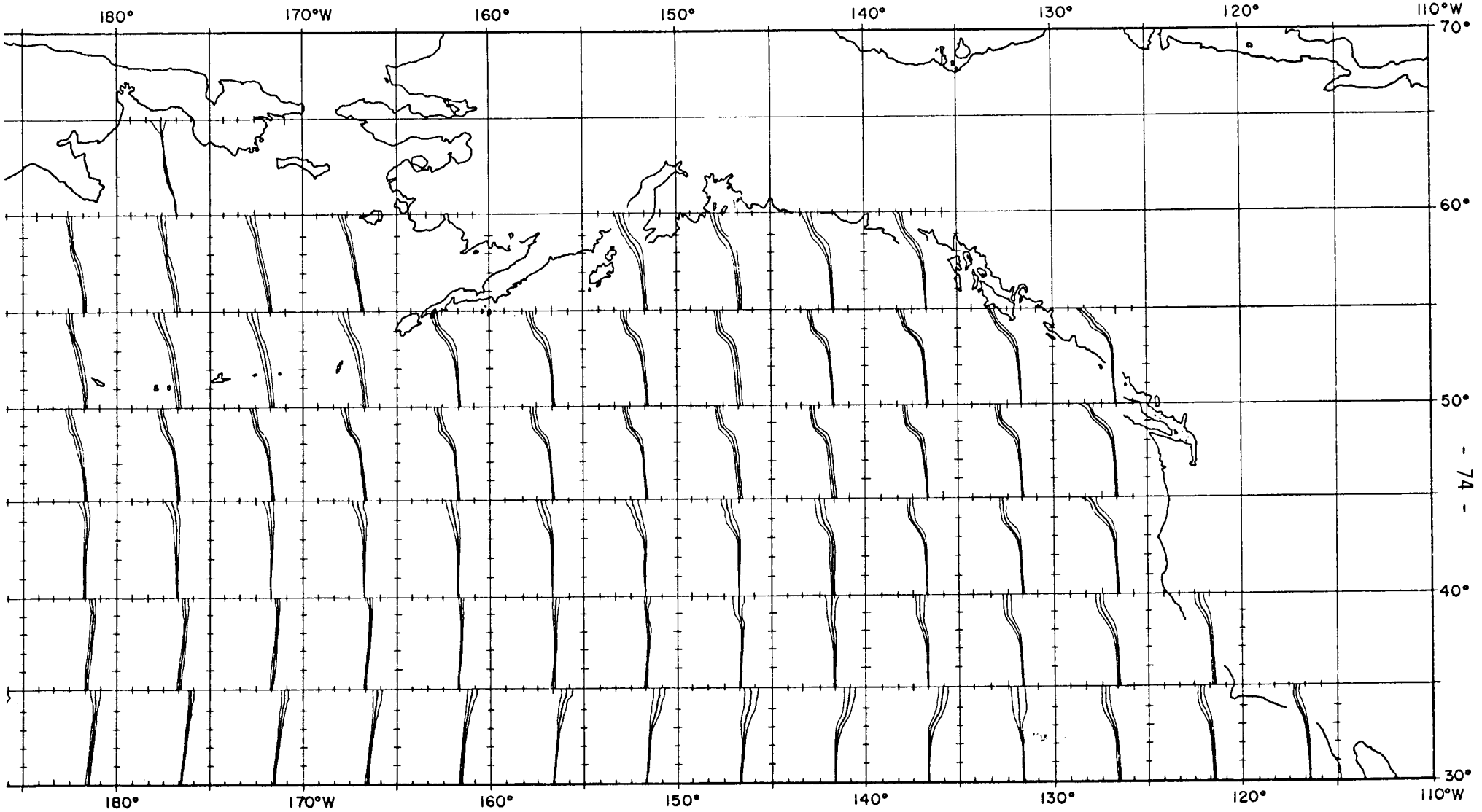

Fig. 12 - Mean SZ curves by 5° square in the Northeast Pacific north of 30°N. Mean curves are bracketed by the standard deviations in salinity.

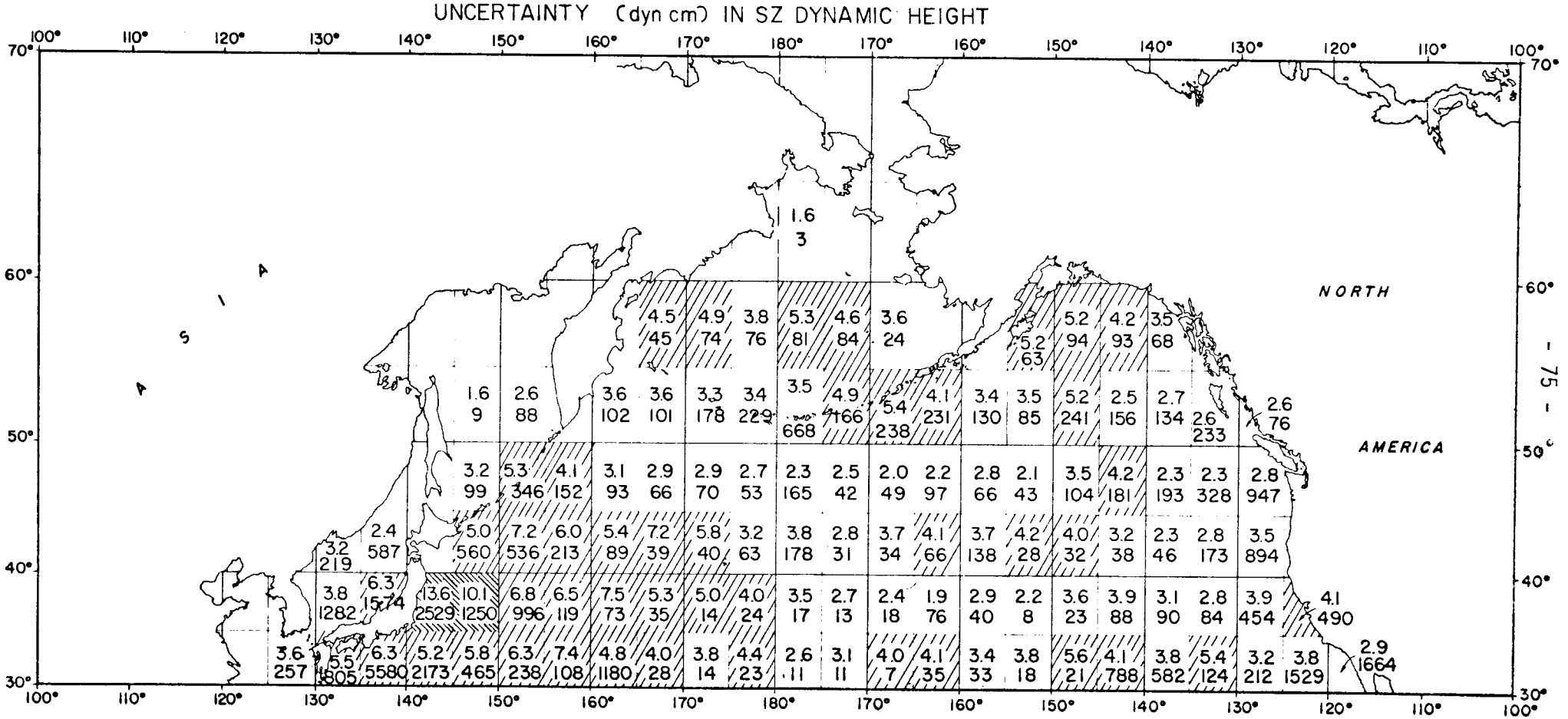

Fig. 13 - RMS differences (dyn/cm) between 0/500m true and SZ inferred dynamic heights. Values are as in Fig. 11.

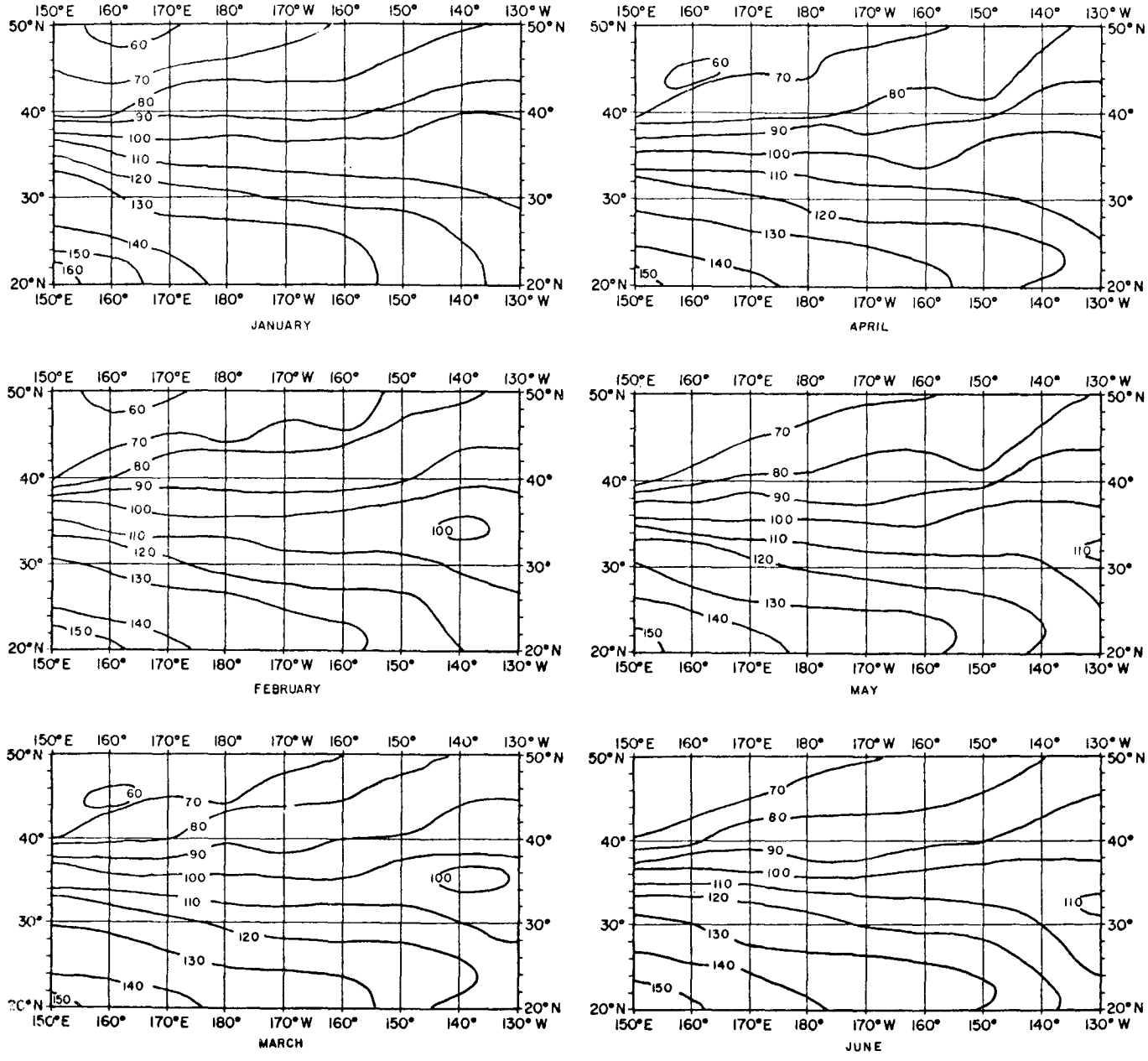

- Maps of 0/500m inferred dynamic height (dyn/cm) between 30 and 50°N, 130°W and 150°E, for climatological January through June.

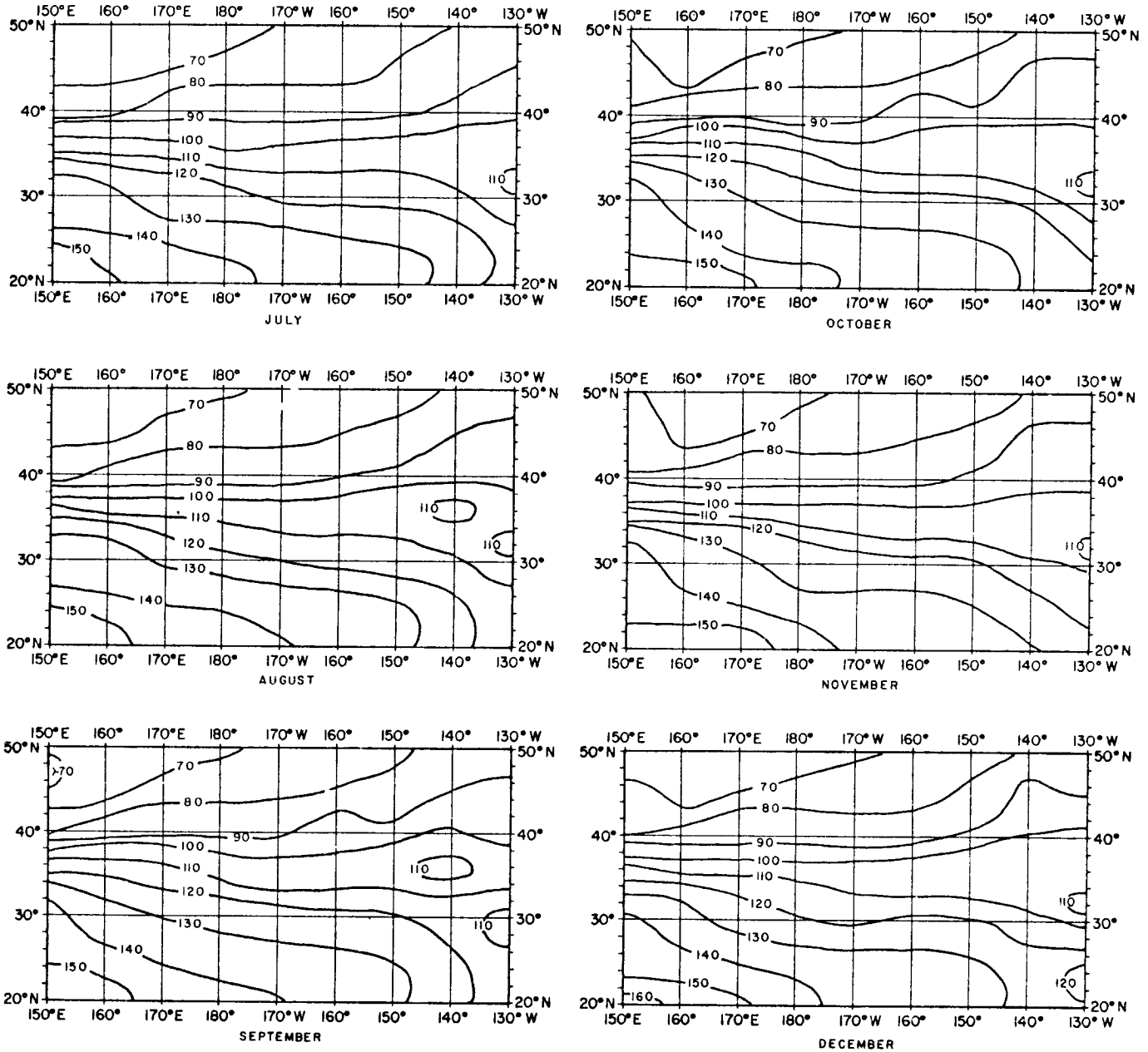

Fig. 15 - As in Fig. 14 for July through December.

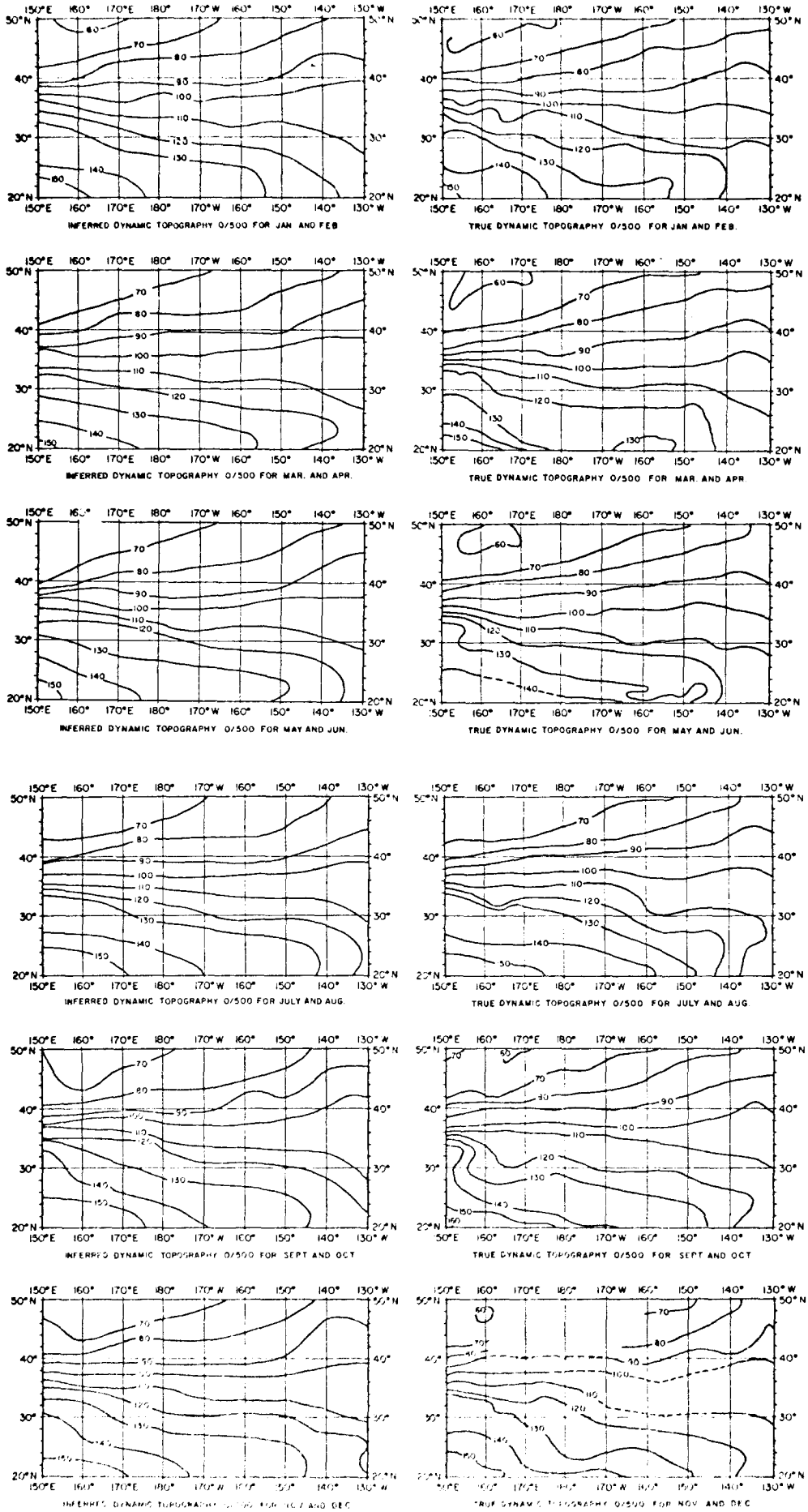

Fig. 16 - Comparison between true and inferred 0/500m dynamic height maps from 30 to 50°N, 130°W to 150°E for bi-monthly climatological periods.

CONTRIBUTION TO THE STUDY OF THE INTERACTIONS BETWEEN THE OCEAN AND THE ATMOSPHERE

C. FONS

"The ocean is as fuel to the atmosphere"
J. Malkus

In the last decade research workers have shown an increasing interest in the problems of ocean-atmosphere interaction. This has now become an established area of research, even though the results so far seem rather disappointing.

I intend here to tackle this study by considering a period extending from 25 November to 10 December 1976, during which a large number of important cyclogeneses occurred. Sea surface heat variations during that period will also be examined in an attempt to gain an understanding of heat exchanges through the study of radiosonde patterns relating to lower atmosphere layers.

It should be recalled that the best criterion for identifying an air mass is its wet-bulb (pseudo-adiabatic) potential temperature, designated by $\theta'w$. This temperature varies only when there is an exchange of heat between an air particle for which $\theta'w$ has been computed and the environment.

$\theta'w$ increases when there is an input of heat, either in the form of real heat or in the form of latent heat of vaporization.

$\theta'w$ decreases when the air particle considered yields heat to the environment.

Two cases are then to be considered:

1) Evolution of an air mass through heating at the base

Let us assume that a cold air mass moves across a warm ocean, reflected in the air temperatures of the lower atmosphere layers being lower than those of the surface layers of the ocean.

A heat flow is established from the ocean towards the atmosphere. The surface temperature of the sea decreases. Convection rapidly occurs within the ocean and the heat lost to the atmosphere is soon replaced by heat from the deeper layers.

In the atmosphere water vapour plays an important role as it affects heat exchanges in the form of latent heat of vaporization. The air particles in the vicinity of the sea's surface tend to take on the same temperature as the water and then to become saturated through evaporation

of the seawater. This process necessitates a certain quantity of heat which, pumped into the ocean, is then carried by the air particles in the form of latent heat of vaporization. The quantity of heat involved is enormous and constitutes the major part of the heat abosrbed by the atmosphere from the oceans. Convection currents carry this water vapour towards the upper air where, upon condensation, the latent heat of vaporization is released at a level far higher than that at which it was absorbed by the atmopshere. The heat thus released generally helps to produce convection.

In this case, a rise is noted in the $\theta'w$ of the lower layers. This is reflected in the radiosonde patterns by a curve showing rapid growth. This rapidly fades out with altitude. When heat convection occurs, the thickness of the heated layer increases and consequently the input also increases.

2) Evolution of an air mass through cooling at the base

Let us assume that a relatively warm air mass is situated over an ocean whose surface temperatures are lower than those of the air. Heat immediately starts to flow from the lower atmosphere layers, the temperatures of which decrease, towards the surface layers of the ocean, the temperatures of which increase. As in the former case, the quantity of heat lost tends to be replaced by a heat flow from the upper air. Such a flow can be generated only by conduction and radiation and by turbulence if there is a wind. The temperatures of the lower layers of the atmosphere decrease and tend to become the same as those of the surface layers of the sea. In the water the heat given up by the atmosphere creates a flow of heat towards the deeper layers of the ocean. The temperature of the sea surface layers consequently increases rapidly until it is the same as that of the air. The heat flow very quickly decreases.

At the level of the lower atmosphere layers, the $\theta'w$ decreases. This entire process is summarized in Figure 1 which shows the two foregoing cases in their final phase of transformation.

Ia shows radiosonde patterns (curve $\theta'w$) resulting from heating at the base. The initial sounding ends at the temperature point T_1, while the originating bathythermograph ends, above the thermocline, at the point of Sea Surface Temperature 1 (SST_1). During the exchange that takes place from the ocean towards the atmosphere, the SST decreases to point SST_2. The triangle drawn with dotted lines shows a "cooling" of the surface water mass. The quantity of heat thus exchanged with the atmosphere has the effect of heating the air mass and the base temperature rises to T_2. The hatched area represents the "heating". Point M represents the furthermost point of the heat transfer which, in fact, shows the difference between the initial temperatures of the sea and of the atmosphere.

Ib shows radiosonde patterns (curve $\theta'w$) resulting from cooling at the base. The initial sounding ends at the temperature point T_1, while the originating bathythermograph ends, above the thermocline, at the surface temperature point SST_1. During the exchange that takes place from the atmosphere towards the ocean, the air temperature drops to temperature T_2, resulting in a triangle representing the "cooling" of the air mass. The quantity of heat absorbed by the water causes the surface temperature to rise to SST_2, which helps to bring about the temporary formation of a secondary thermocline. The hatched area represents the "heating" of the water. The furthermost point of the heat transfer can

can also be revealed by showing the difference between the initial temperatures of the air and of the seawater.

Study of the meteorological and oceanographic situation during the period from 25 November to 10 December

During this period four large-scale cyclogeneses were observed. We shall first consider, on a comparative basis, the isobaric topography and ocean surface temperature variations over 24 hours.

The depression D_1, which was the first to be produced from an undulation in a cold front moved towards an area off the east shore of Ireland and became deeper (charts of 25 and 26 November). During these two days D_1 moved over a zone of negative sea surface temperature variation, i.e. between two charts separated by 24 hours, the surface temperature dropped and consequently there was an exchange from the ocean to the atmosphere. This variation in surface temperature may be marked by a time lag. When a certain quantity of heat is thus abosrbed by the atmosphere, the phenomenon of cyclogenesis may continue through the action of other factors, and in particular as a result of conflicting air masses of different origins and, consequently, with different characteristics. In this case, the initial exchange of heat acts so to speak like a catalyst.

On the 27th at 12 U.T., the depression D_1 was still proceeding over a zone of negative temperature variation. But as from the 28th at 12 U.T. D_1 started to move over stretches of water where the temperature variations were positive. From that time on, the cyclogenesis can be said to be practically over and that, barring any further input of energy, D_1 would begin to level out more or less rapidly.

Depression D_2 started on 30 November at 12 U.T. as a result of an undulation in a cold front shifting over a zone where, in 24 hours, pronounced variations in the surface temperature of the ocean were noted. The heat exchange, in this case as well, was in the direction ocean-atmosphere.

On 1 December at 12 U.T. the depression, fully formed, had become centred on the immediate vicinity of the west of Ireland. As it was a small-scale depression, it was bound to be very violent. Still at the same time, it was noted that D_2 had just emerged from the zone of ocean to atmosphere exchange since it was now over a zone of positive temperature variation. Still on 1 December at 12 U.T., it was noted that the anticyclone centred on the south-west region of Newfoundland was beginning to move over the ocean at the exact point where there was a zone of negative sea surface temperature variation. On 2 December at 12 U.T. the negative variation became more pronounced, and on 3 December at 12 U.T., D_3 came into being, once again over an area of negative variation. This depression continued to deepen on 4 December while moving towards the Davis Strait where it ran into a zone of positive variation (this case is to be compared with the first one referred to). Finally, on 7 December at 12 U.T., once again an anticyclone became centred on the southern region of Newfoundland where there exists a zone of highly negative 24-hour surface temperature variation. A violent exchange probably occurred at this stage and on 8 December at 12 U.T. depression D_4 came into being, but this depression was far more complex than those of the previous depression systems; in the first instance, it divided up into two parts which evolved independently (chart

of 9 December). But it was the southern part of D_4 that was to achieve maximum development by becoming centred on a zone of negative variation.

Let us now consider the same sequence of cyclogeneses but taking a look at, on the one hand, the variation of the mean $\theta'w$ for the stretch of the atmosphere between 1000 and 900 millibars (figures Nos. 2 and 2 bis) and, on the other, when they are known, temperature variations in the stretch between the ocean surface and 80 metres below.

The $\theta'w$ variations are studied for four fixed points of the ocean for which radiosoundings are regularly effected. The different curves show marked variations in this parameter which, it is to be recalled, is responsive to heat exchanges either in the form of real heat or in that of latent heat of vaporization.

Let us consider the curve of $\theta'w$ relating to the fixed point 38° N and 71°W. We have shown on this curve the characteristic irregularities in the $\theta'w$ pattern by means of letters. Let us at the same time consider the ocean temperature pattern in the initial 80 metres.

Point A: On 28 November at 00 U.T. a peak is observed in the evolution of $\theta'w$ which increases from 14 degrees on the 27th at 12 U.T. to 18 degrees on the 28th at 00 U.T. This increase should, according to what was said earlier, correspond to a cooling of the water. Comparison of the bathythermographs of the 27th at 12 U.T. and the 28th at 00 U.T. shows a slight cooling which does not seem to be very significant but which nevertheless exists (Fig. 3 and 4).

Point B: Between the 28th at 00 U.T. and the 28th at 12 U.T. a drop in the $\theta'w$ is noted of approximately 4 degrees. There should be an exchange in the direction atmosphere-ocean and hence a heating of the water. Comparison of the bathythermographs between the 28th at 00 U.T. and at 12 U.T. reveals a heating of the water layer considered.

Point C: Further peak in the evolution of the $\theta'w$ on the 29th at 00 U.T. There is no trace of cooling of the ocean layer in the initial 80 metres.

Point D: Between 29 November at 12 U.T. and the 30th at 12 U.T. a dramatic drop in the $\theta'w$ of approximately 14 degrees is observed. This drop in the $\theta'w$ should have dramatic repercussions within the water layer. And this is what is seen to occur when one considers the bathythermographs of the 29th and the 30th at 12 U.T., which show considerable heating.

Point E: Between 30 November at 12 U.T. and 1 December at the same time, a further drop in the $\theta'w$ is observed. The bathythermographs of the 1st at 00 U.T. and of the 2nd at 00 U.T. again show a rise in the temperature of the water layer considered.

Point F: The evolution of the $\theta'w$ shows a further peak on 3 December at 00 U.T. This rise in temperature results in a lowering of the water temperature revealed by comparing the progression of the bathythermographs between the 2nd and the 3rd at 00 U.T.

Point G: A further considerable drop in the $\theta'w$ between the 3rd at 00 U.T. and 12 U.T. The atmosphere imparts heat to the water. This is what one observes when one considers the bathythermographs of the 3rd at 00 U.T. and at 12 U.T. A rise in the temperature of the water mass in the initial 80 metres is observed.

Point H: Further peak in the variation of the $\theta'w$ on 5 December at 00 U.T. There is therefore heat exchange in the direction ocean-atmosphere. The progression of the bathythermographs between 4 and 5 December at 00 U.T. reveals a marked drop in oceanic temperatures.

Point I: Further decrease in the $\theta'w$ but the phenomenon is in process. This perhaps explains why there is no rise in temperature in the initial 80 metres.

Let us now consider what occurs at the stationary point C (Figure 5).

Point a: From the 26th at 12 U.T. an increase in the $\theta'w$ is observed up to the 27th at 00 U.T. An exchange therefore occurs in the direction ocean-atmosphere. This exchange is reflected in a lowering of temperature in the initial 80 metres. This cooling is less marked than in the previous cases but the stationary point C is located geographically at higher latitudes than the previous fixed point and, in addition, the favoured area for Atlantic cyclogeneses tends, rather, to be around Newfoundland.

Point b: On the 27th at 00 U.T. the $\theta'w$ decreases rapidly until 12 U.T. then more slowly until the 28th at 00 U.T. This decrease is accompanied by an exchange in the direction atmosphere-ocean, reflected in a rise in the temperature of the water, particularly marked in the initial 50 metres.

Point c: On the 29th at 00 U.T., further "heating" reflected in a drop in temperature in the first 80 metres.

Point d: The previous increase in the $\theta'w$ is followed immediately by a decrease in this parameter as from the 29th at 12 U.T. This is reflected in a rise in temperature in the first 80 metres of the ocean.

Point e: On the 3rd at 12 U.T. the $\theta'w$ goes down to a very low level. This drop is reflected in a slight cooling in the first 80 metres.

Point f: The $\theta'w'$ rapidly goes up again, this being reflected in a fairly marked cooling of the oceanic surface layer.

Point g: The first decrease in the $\theta'w'$ between the 6th at 12 U.T. and the 7th at 00 U.T. results in a rise in temperature in the initial 80 metres.

Let us now consider developments at the stationary point L (Figure 6). For irregularities in the evolution of the $\theta'w'$, the same observations as before will be found to apply: a decrease in the $\theta'w'$ is reflected in a rise in temperature in the first 80 metres of the ocean and vice versa.

CONCLUSION

This short study serves to highlight a number of difficulties that may be smoothed out in the future, particularly through the adoption of a policy for the consistent and simultaneous measurement of certain oceanographic and meteorological parameters. The technique employed for the measurement of sea surface temperature via satellite provides a more accurate indication of the variations to which this parameter is subject in time, but this technique is not self-sufficient for, in the event of cloud cover, no further measurement is possible.

A great deal remains to be done to achieve complete understanding of the processes of exchange between the ocean and the atmosphere. A possible line of research may consist in examination of the progression of the $\theta'w'$ of the lower atmosphere layers and comparison with the evolution of bathythermographs relating to the oceanic surface layer.

SUMMARY

This contribution to the study of ocean-atmosphere exchanges covers the period extending from 25 November to 10 December 1976, during which a large number of cyclogeneses were formed. The problem is tackled in two ways:

- comparison of the topography of the isobaric field and variations in sea surface temperatures over 24 hours;

- comparison of the evolution of the $\theta'w$ of the atmosphere layer between 1000 and 900 millibars at different fixed points of the Atlantic with the progression of bathythermographs relating to the layer between the surface and a depth of 80 metres recorded at the same fixed points or at points close to the initial points.

ANNEX

Figures 7, 8 and 9:

Diagrams showing radiosonde patterns in the layer between 1000 and 700 millibars.

The curve marked with a continuous line shows the evolution of air temperature.

The curve marked with a broken line shows the progression of the $O'x$.

Figure 10:

Section of the Gulf Stream on 8 December 1976.

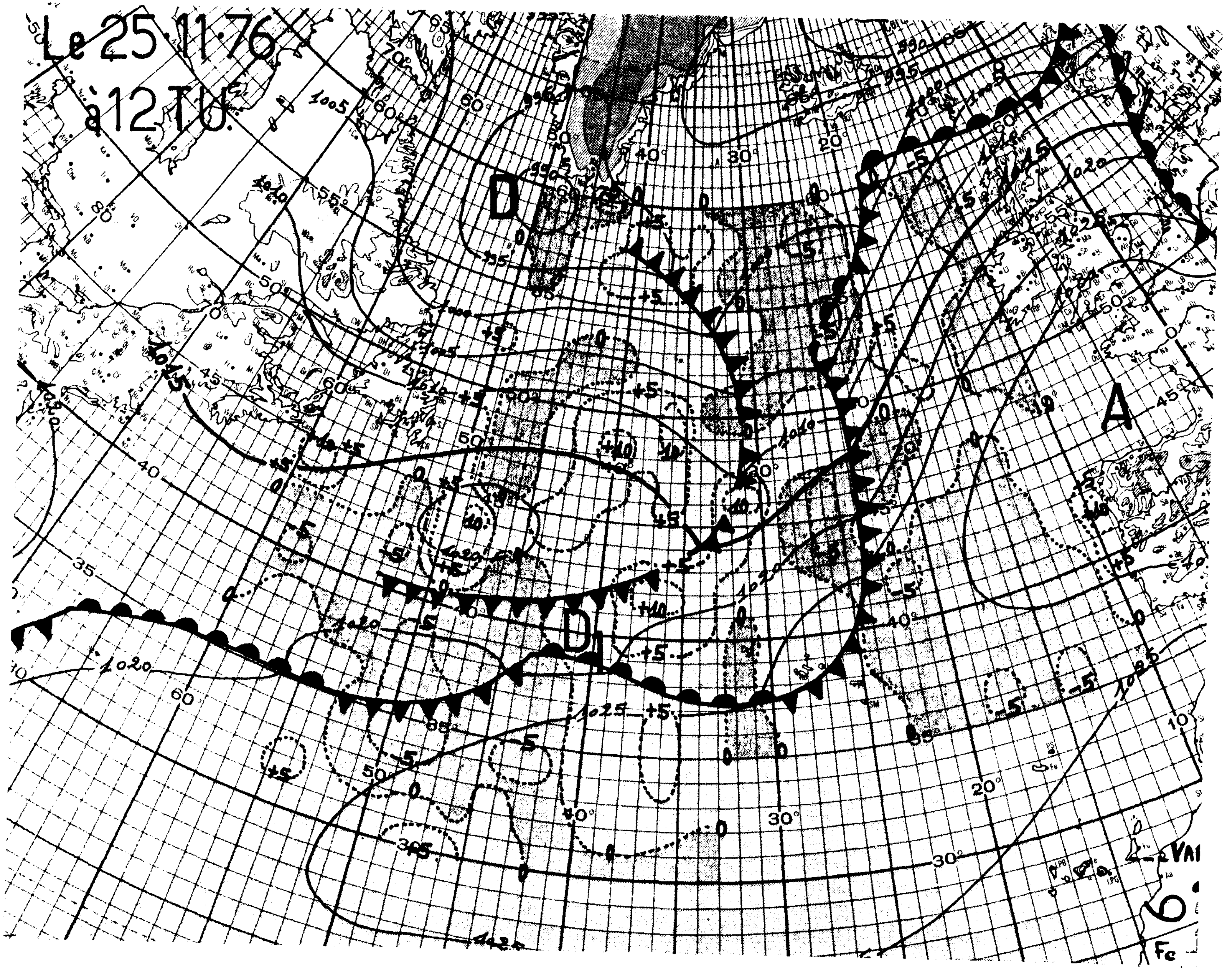
Le 25.11.76
à 12 TU.
D
D1
A

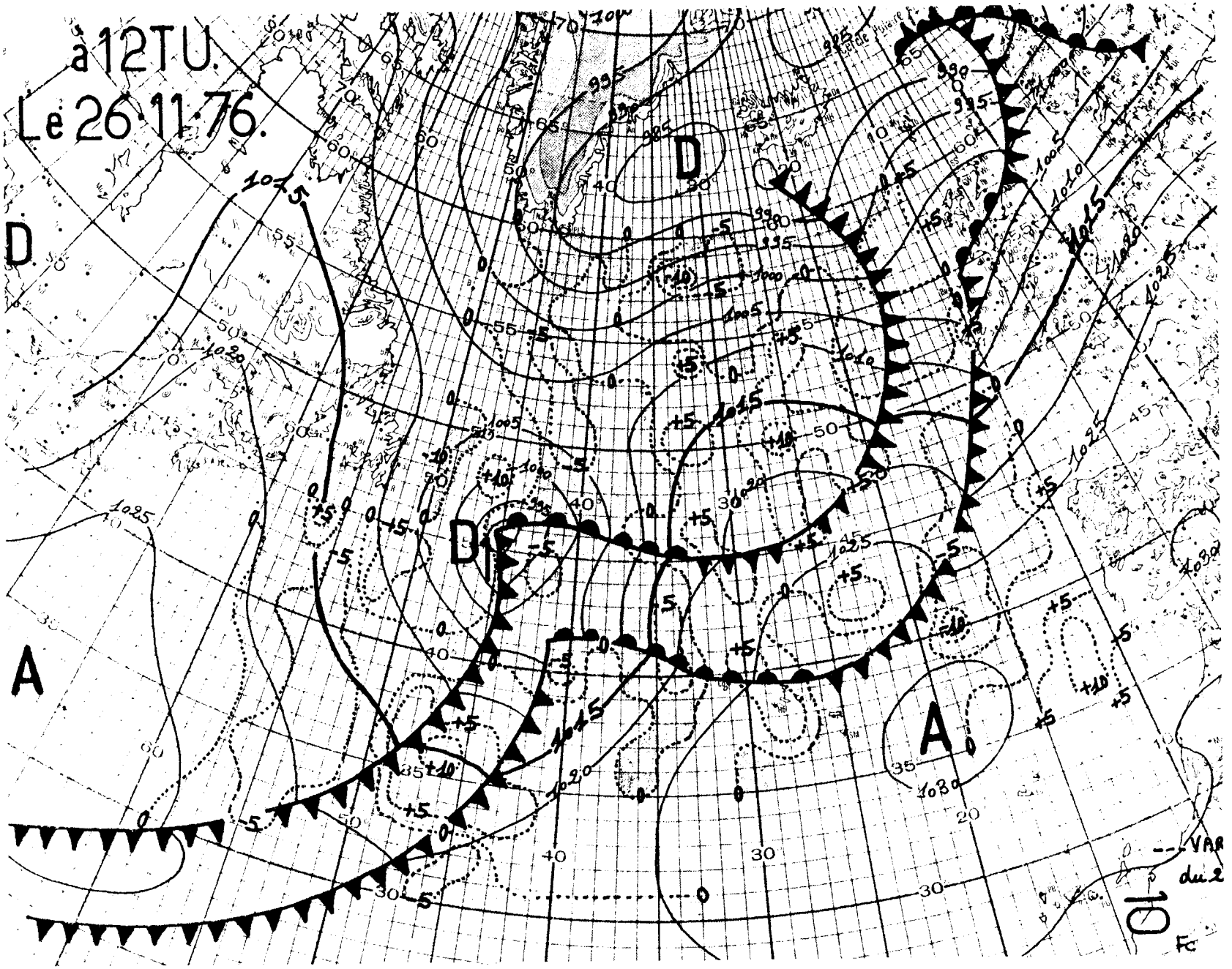
à 12 TU.
Le 26-11-76.
D
D
D
A
A

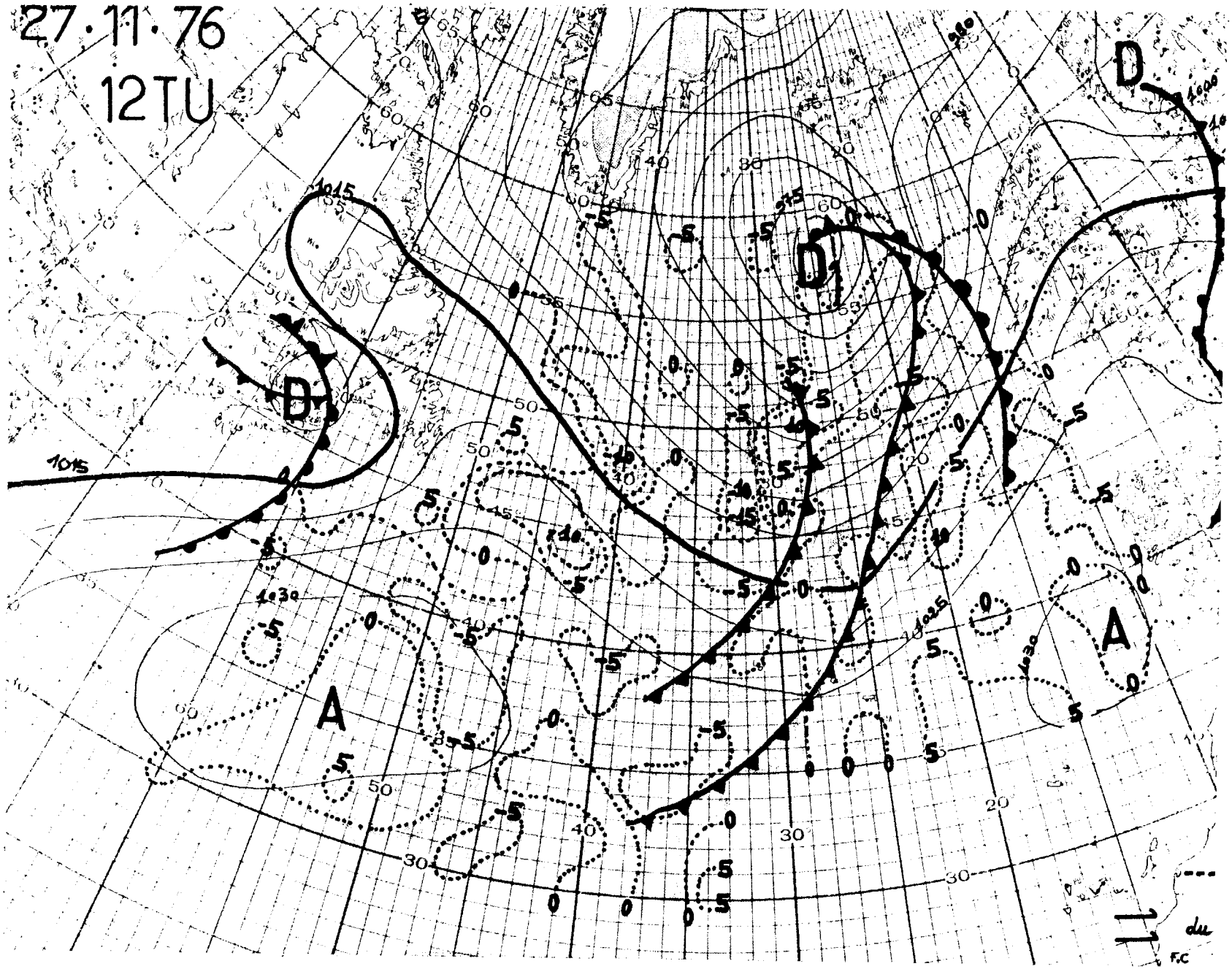
27·11·76
12TU
D
D
D
A
A
1015
1015
1030
1025
1030
F.C

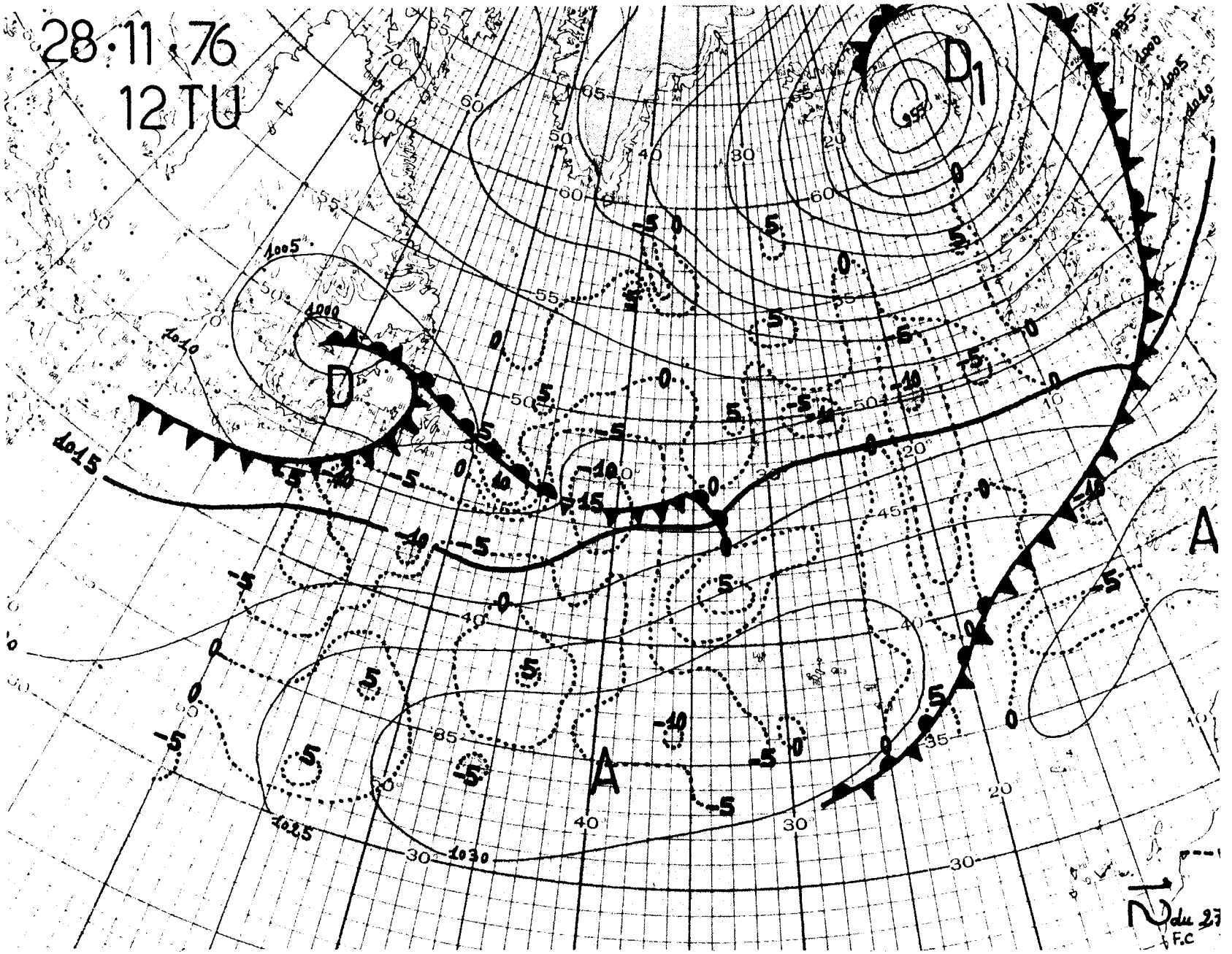
28·11·76
12 TU
P1
D
A
A
1005
1000
1010
1015
1025
1030
du 27
F.C

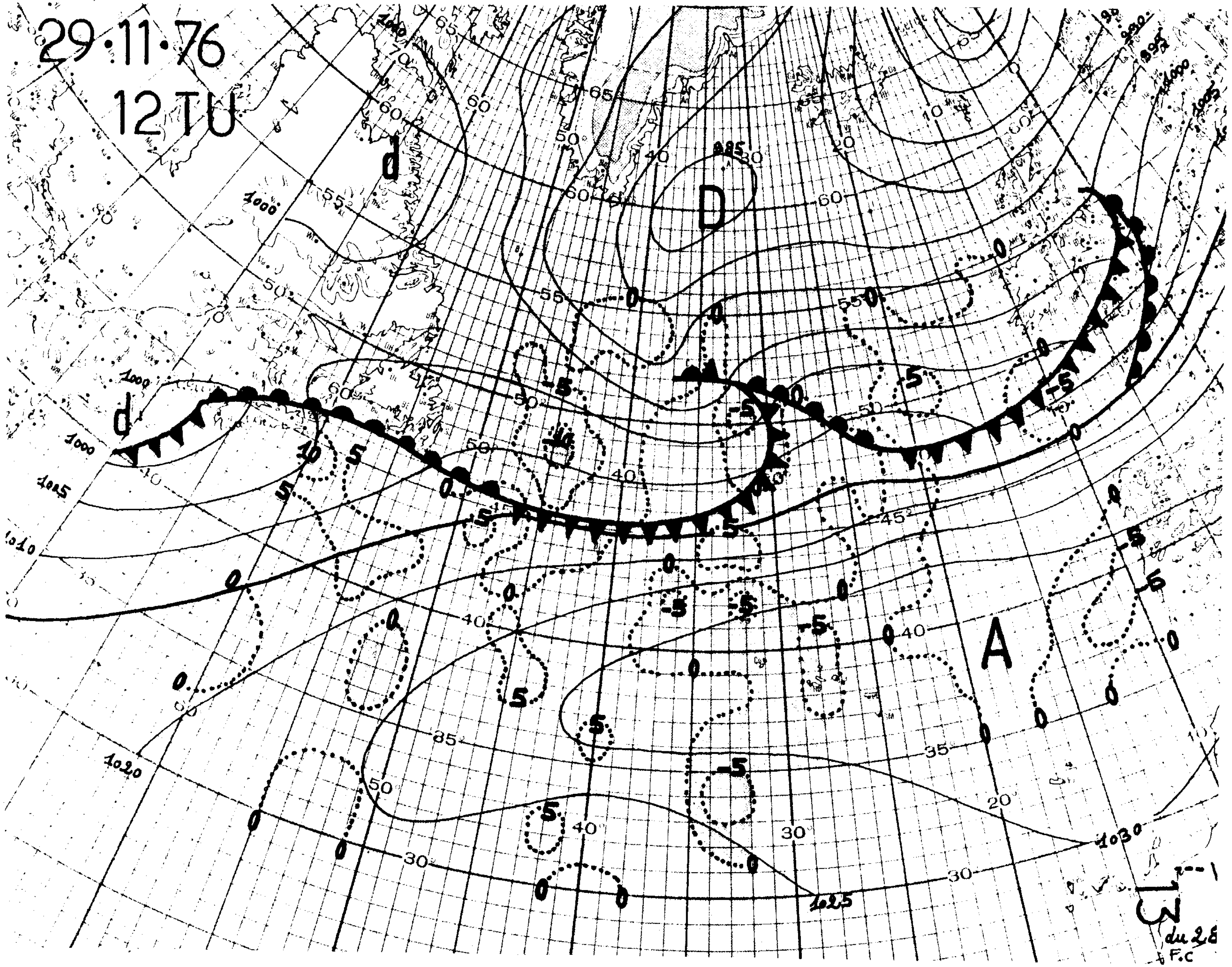
29·11·76
12 TU
D
A
d
d
1000
1005
1010
1020
1025
1030
du 28
F.c

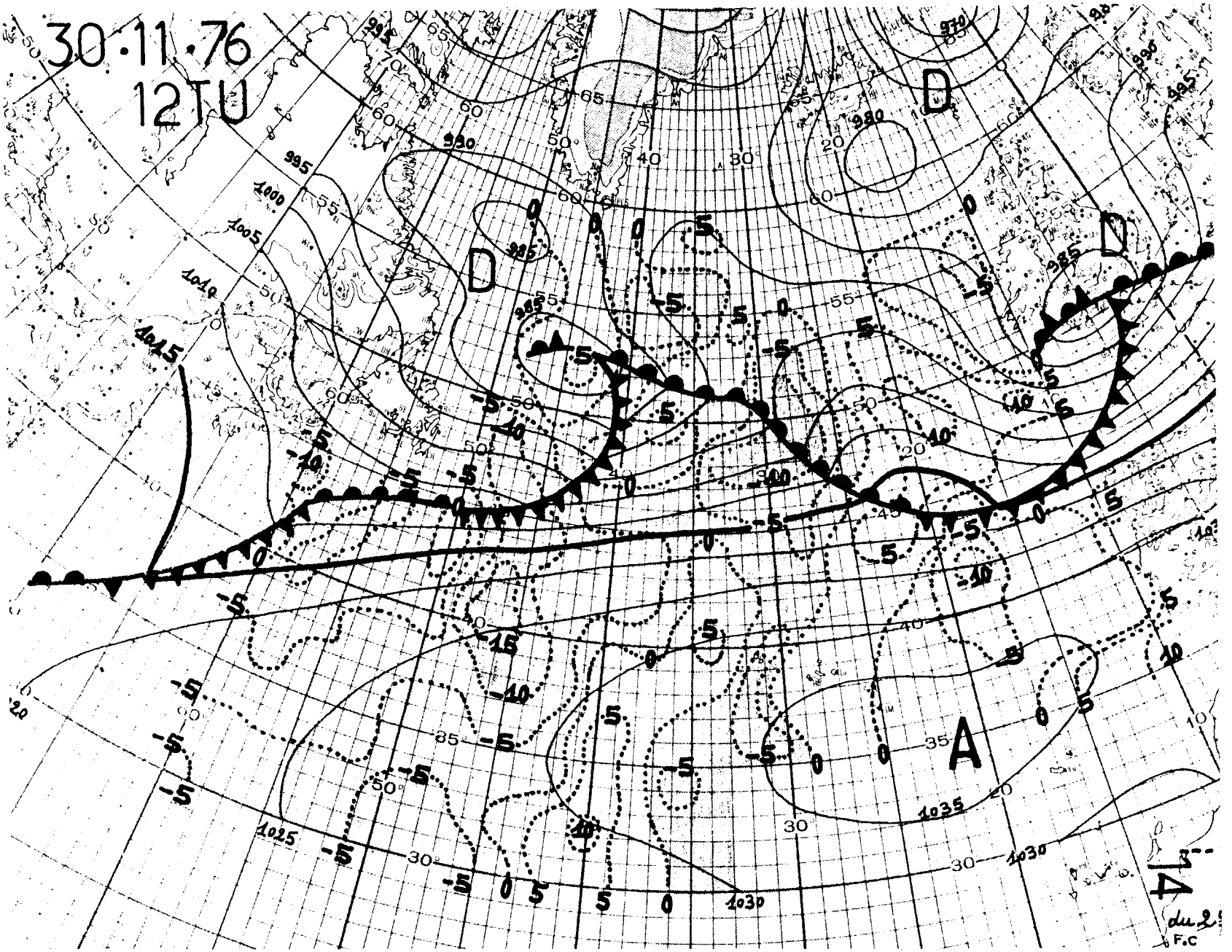
30·11·76
12TU
D
D
D
A
1035
1030
1025
1020
1015
1010
1005
1000
995
990
985
980
970
14
F.C

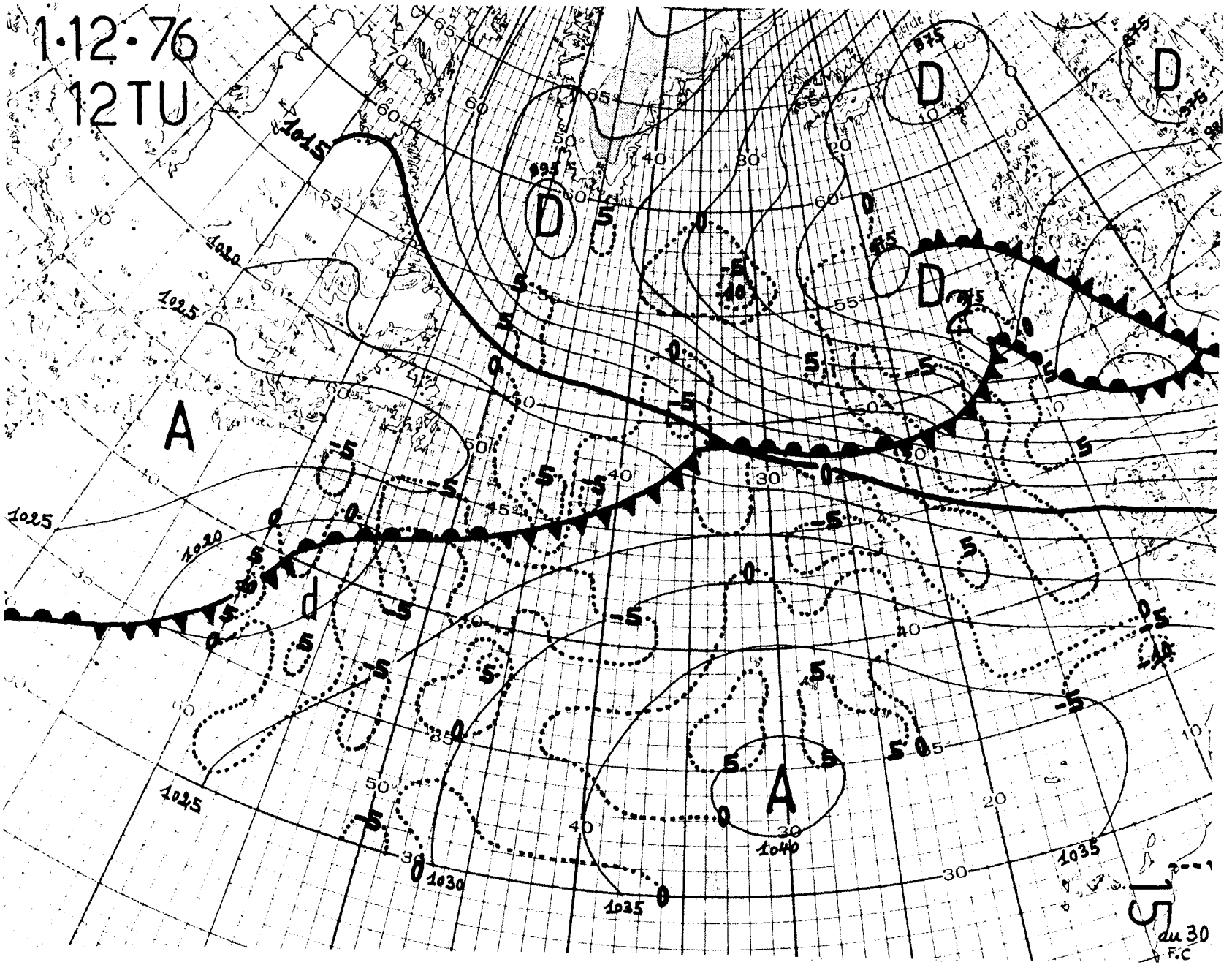
1·12·76
12 TU
D
D
D
A
d
A
1015
1020
1025
1030
1035
1040
15
du 30
F.C

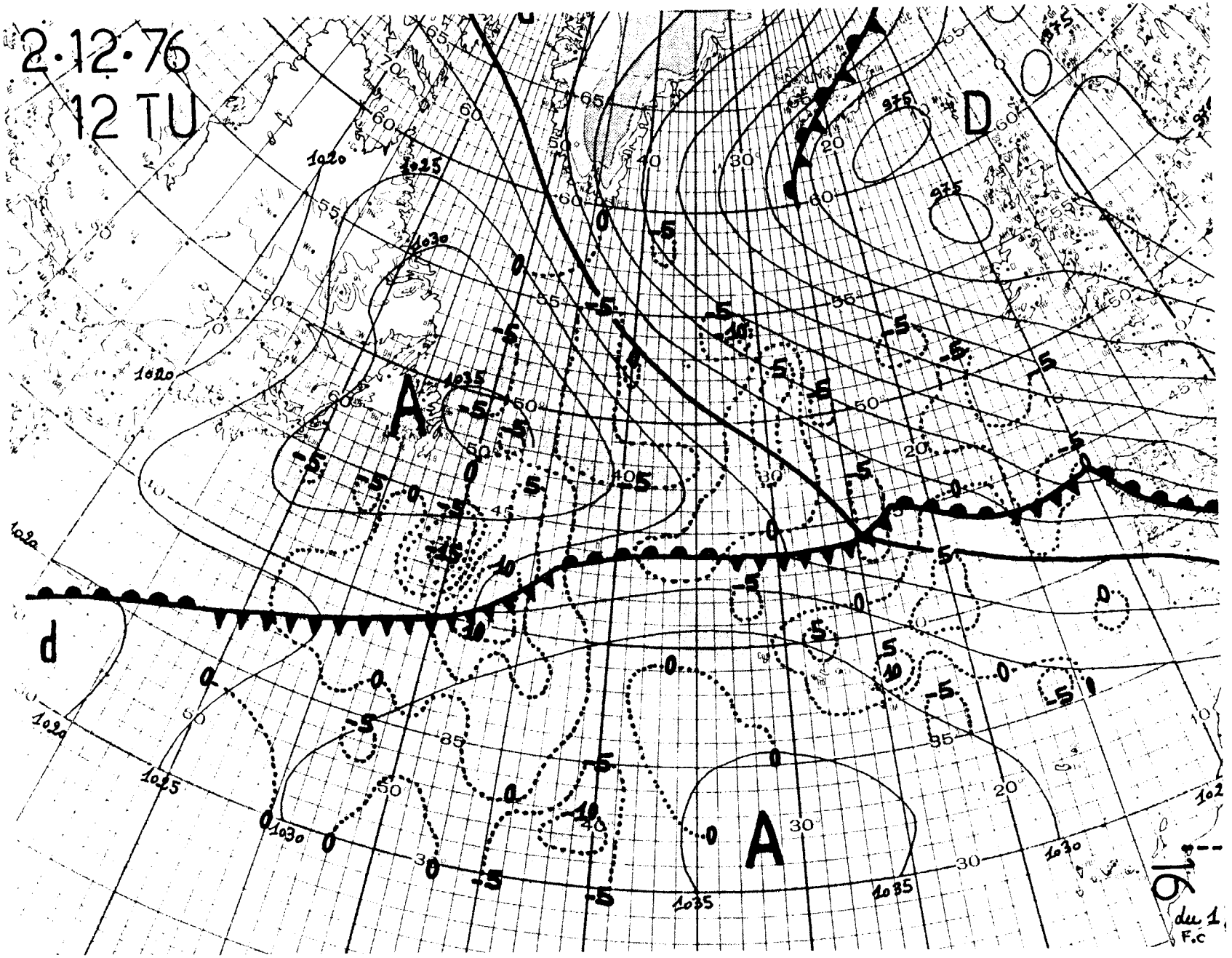
2·12·76
12 TU
D
A
d
A

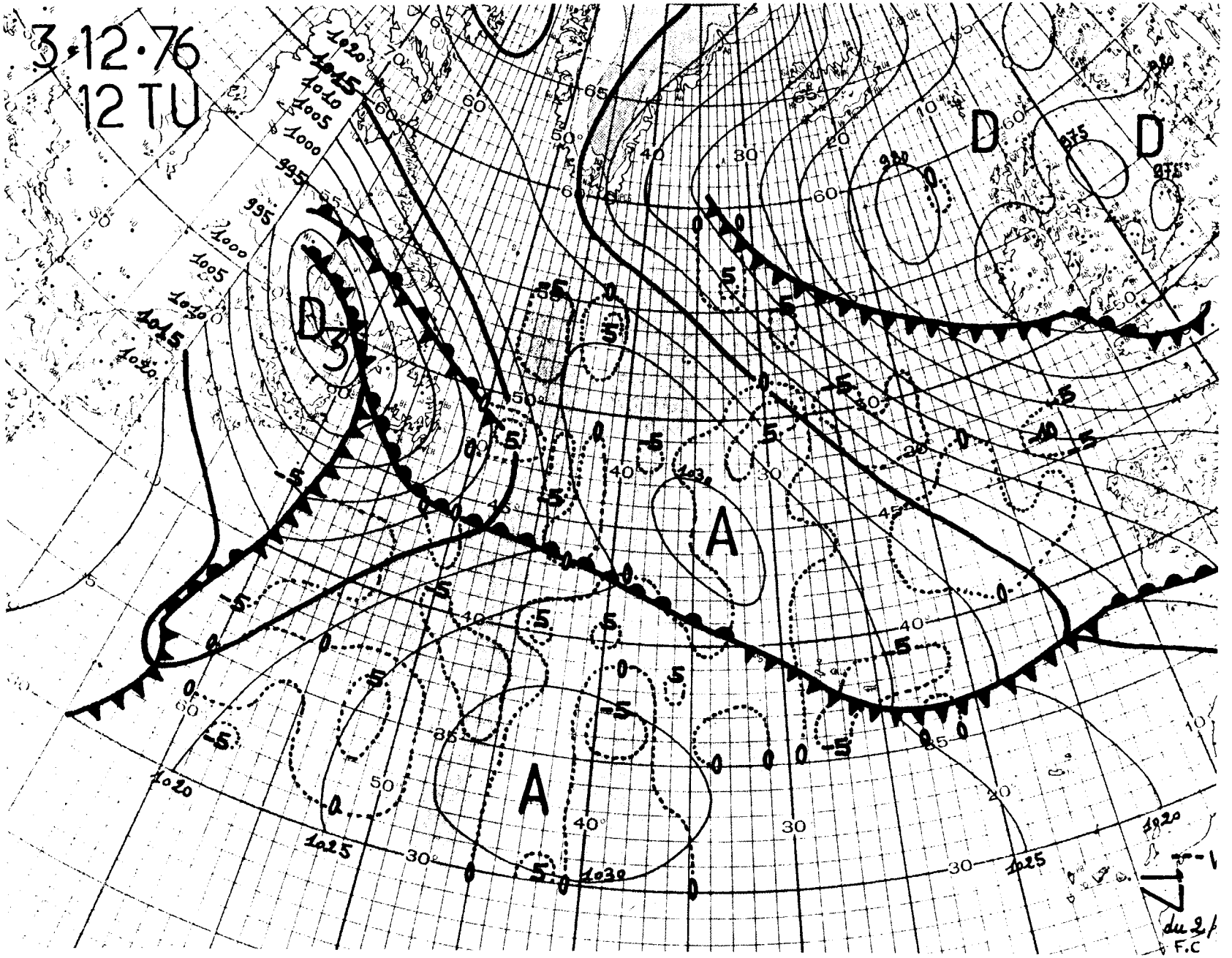
3·12·76
12 TU
D
D
D
A
A

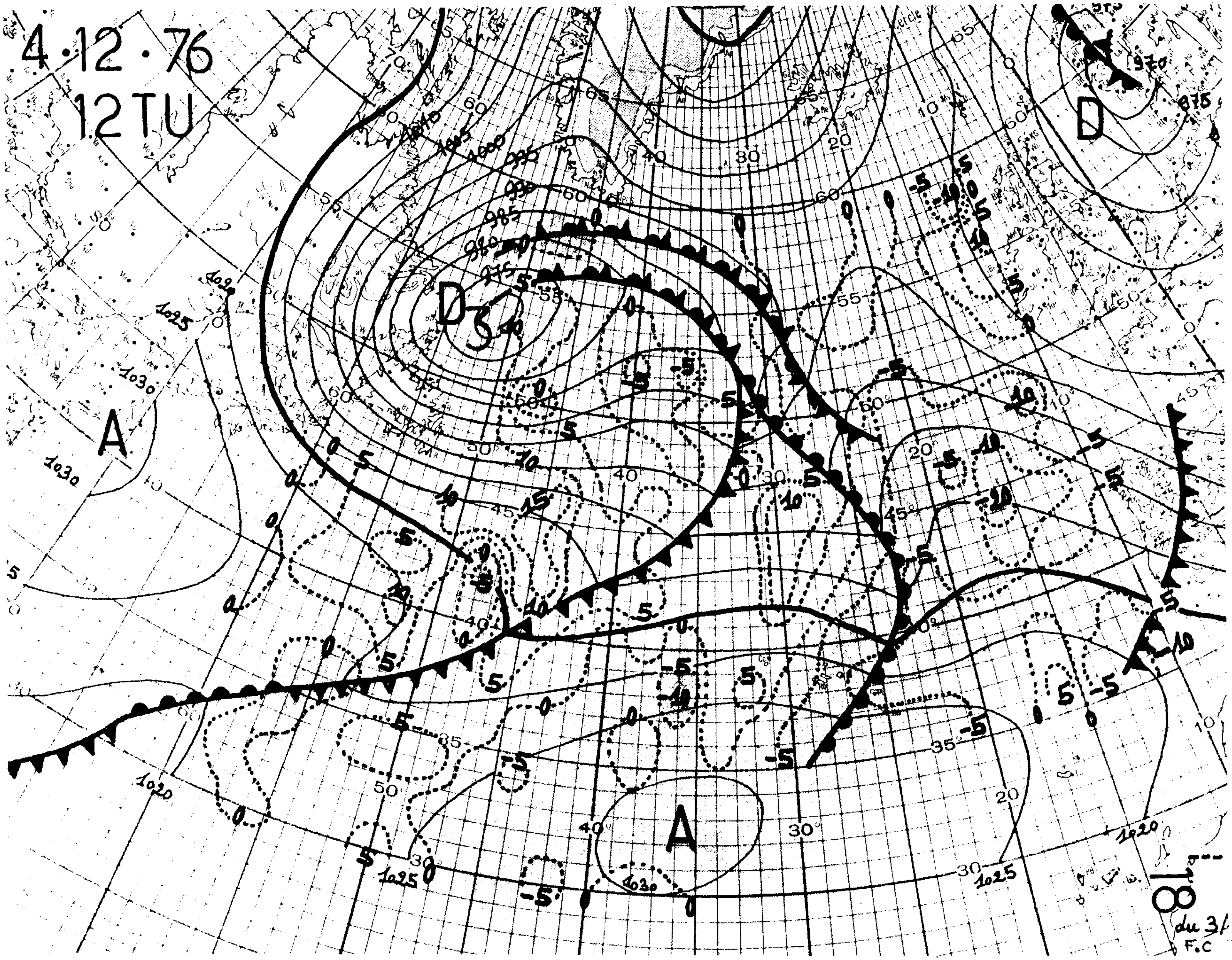
4.12.76
12TU
D
D
A
A
18
du 3/
F.C

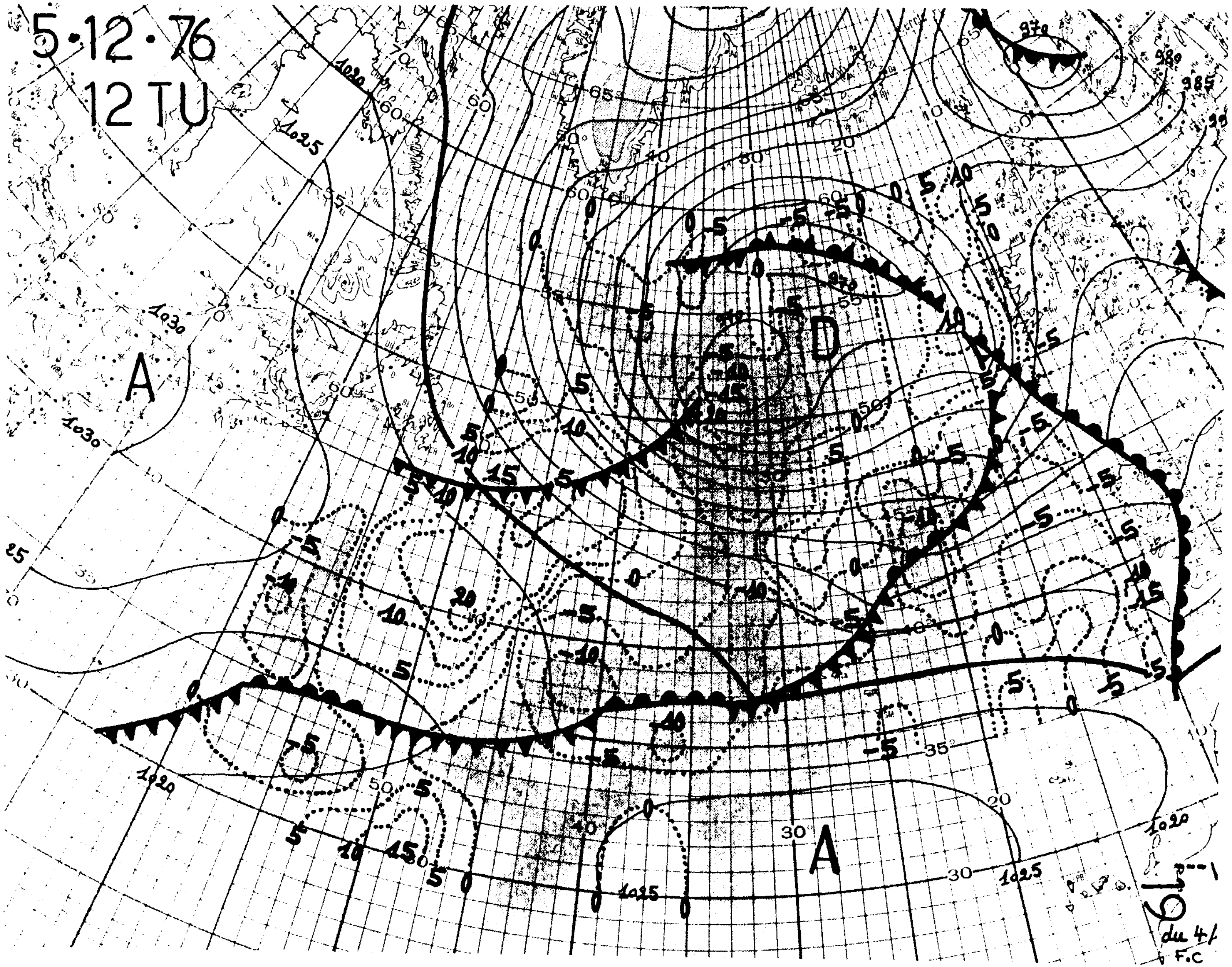
5·12·76
12 TU
A
D
A
1020
1025
1030
970
980
985
du 4/
F.C

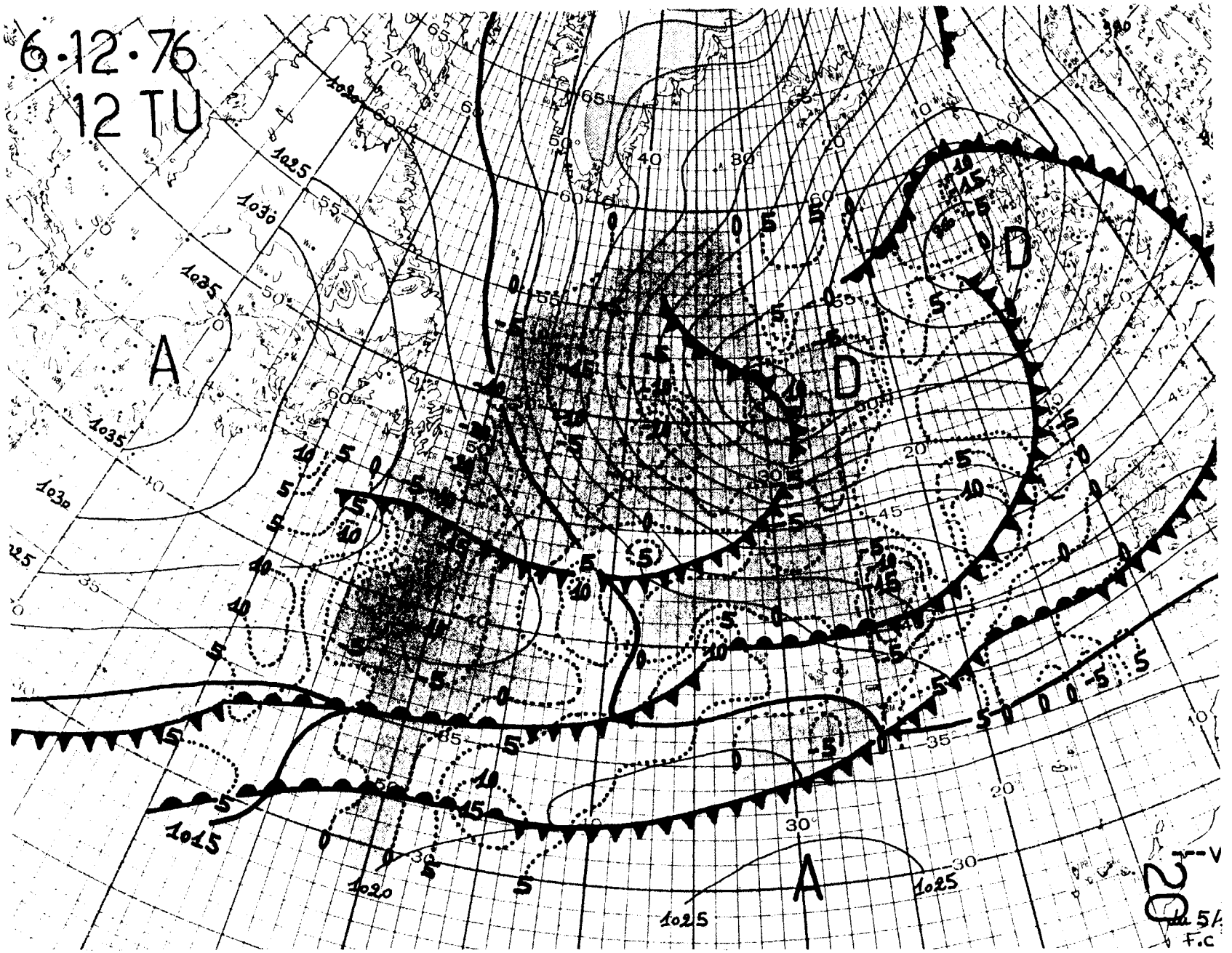
6·12·76
12 TU
A
D
D
A
1025
1030
1035
1020
1015
1025
1020
1025

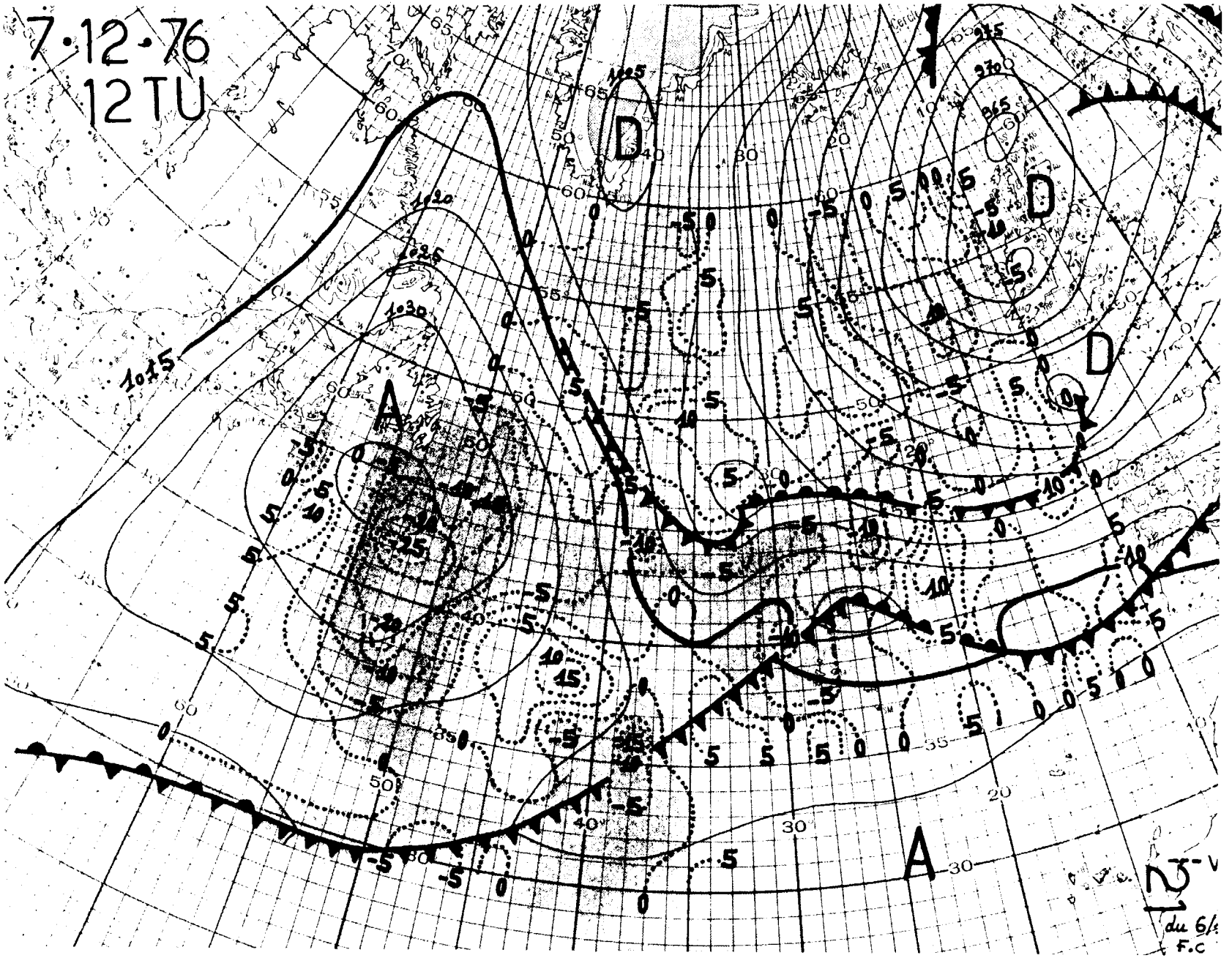
7·12·76
12 TU
D
D
D
A
A
1005
1020
1025
1030
1015
du 6/
F.C

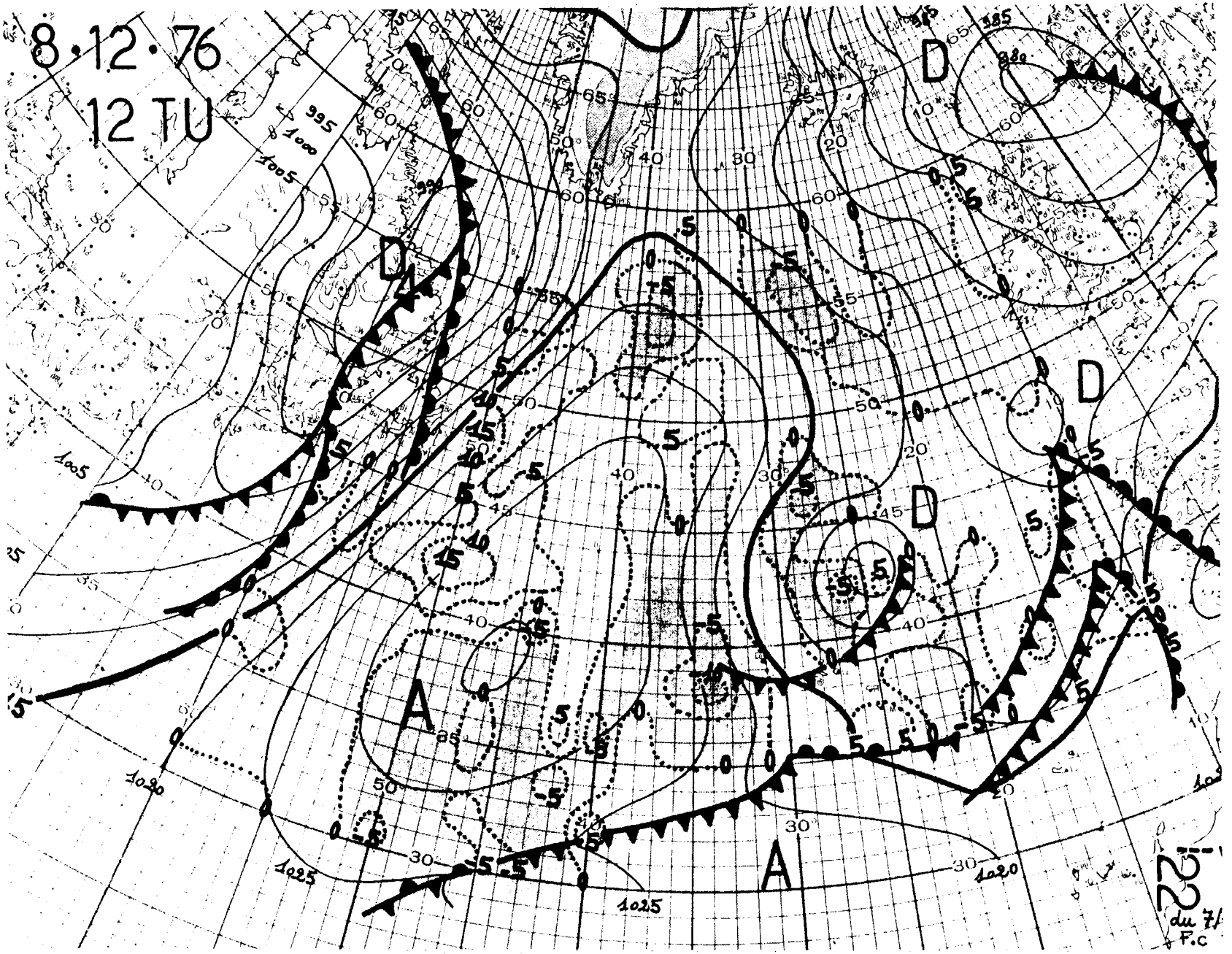
8.12.76
12 TU
995
1000
1005
1020
1025
1025
1020
D
D
D
D
A
A
du 7/
F.C

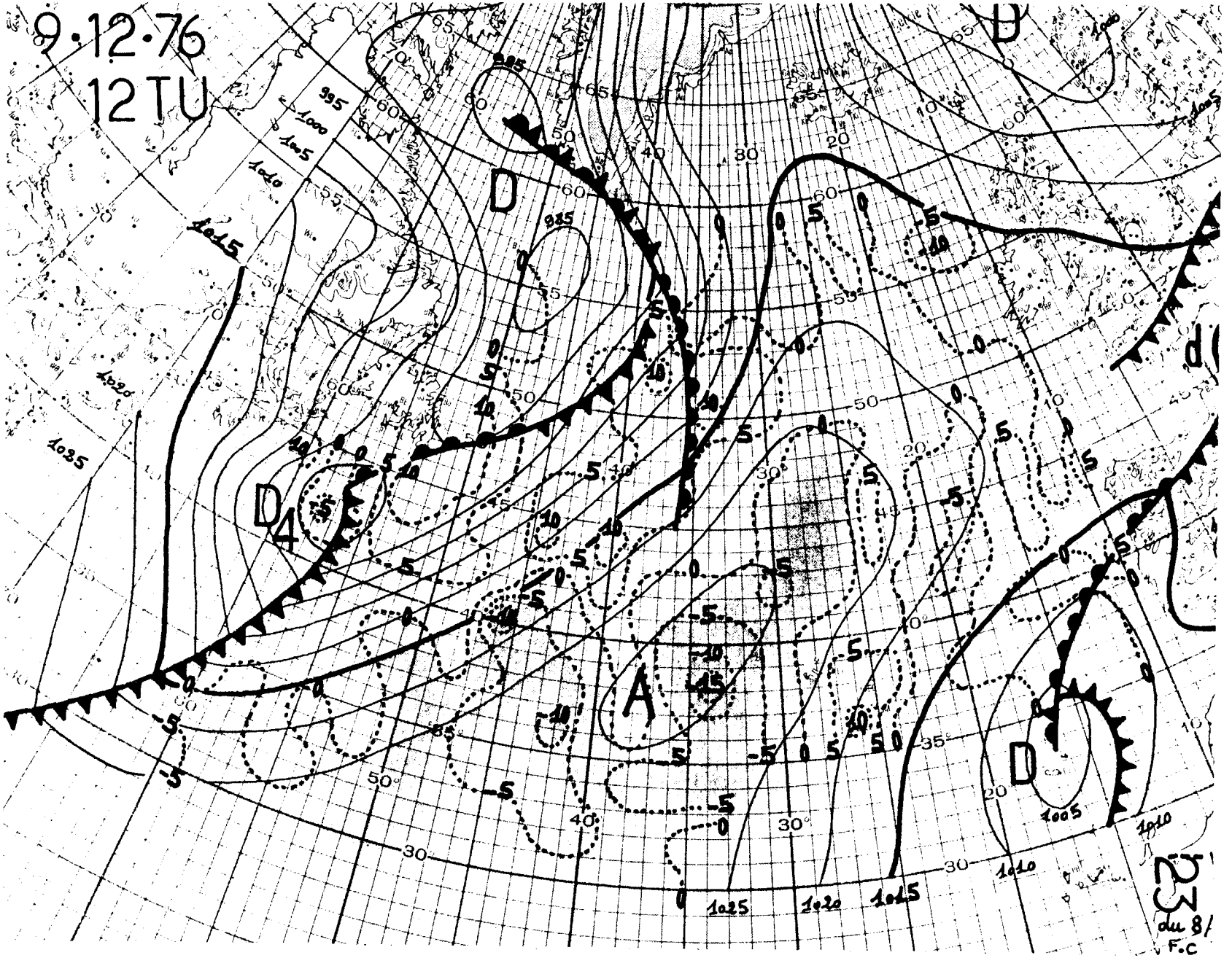
9·12·76
12 TU
D
D
D4
A
D
d
985
995
1000
1005
1010
1015
1020
1025
23
du 8/
F.C

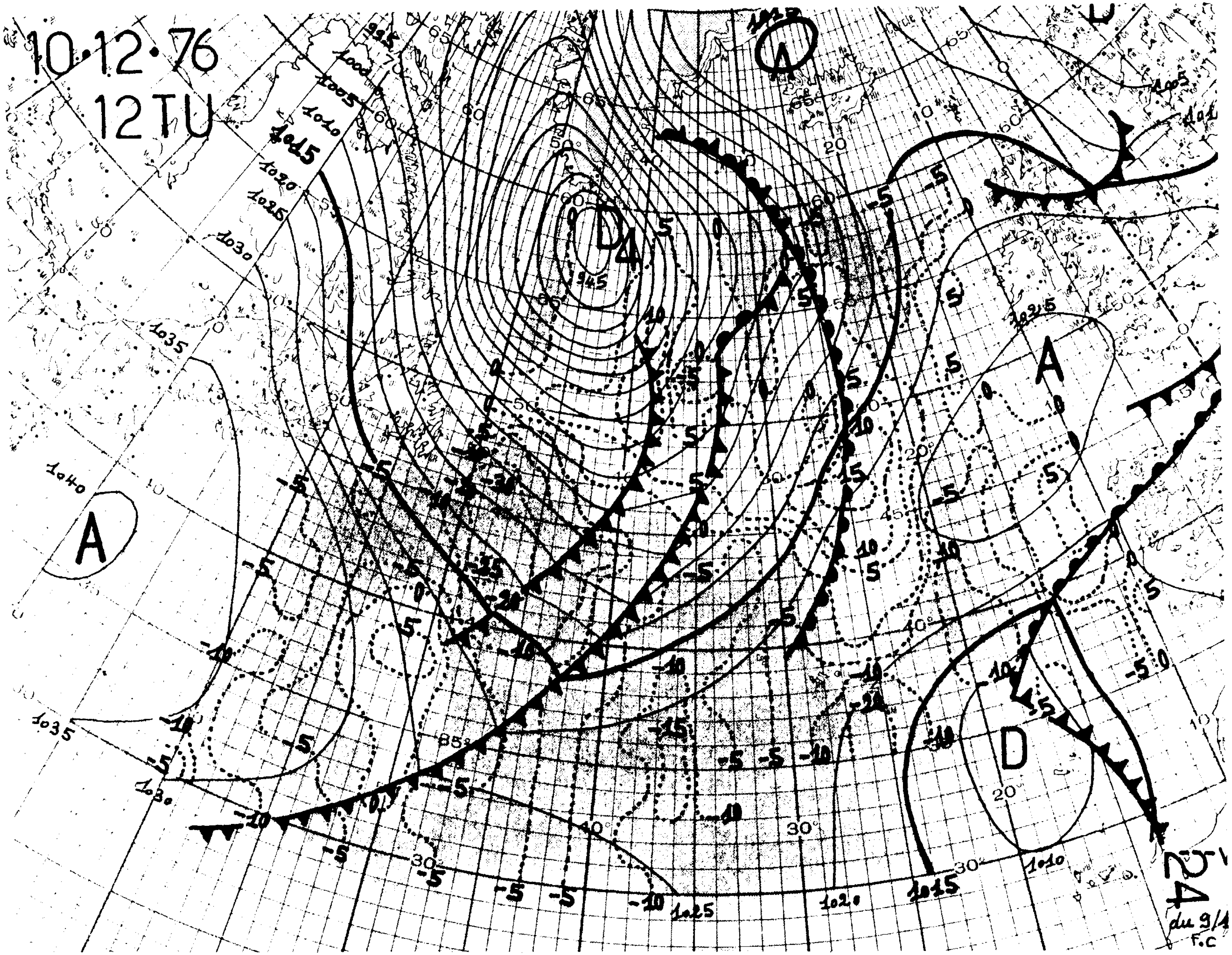
10.12.76
12TU
D
945
A
A
A
D
1005
1010
1015
1020
1025
1030
1035
1040
24
du 9/1
F.C

Fig 1

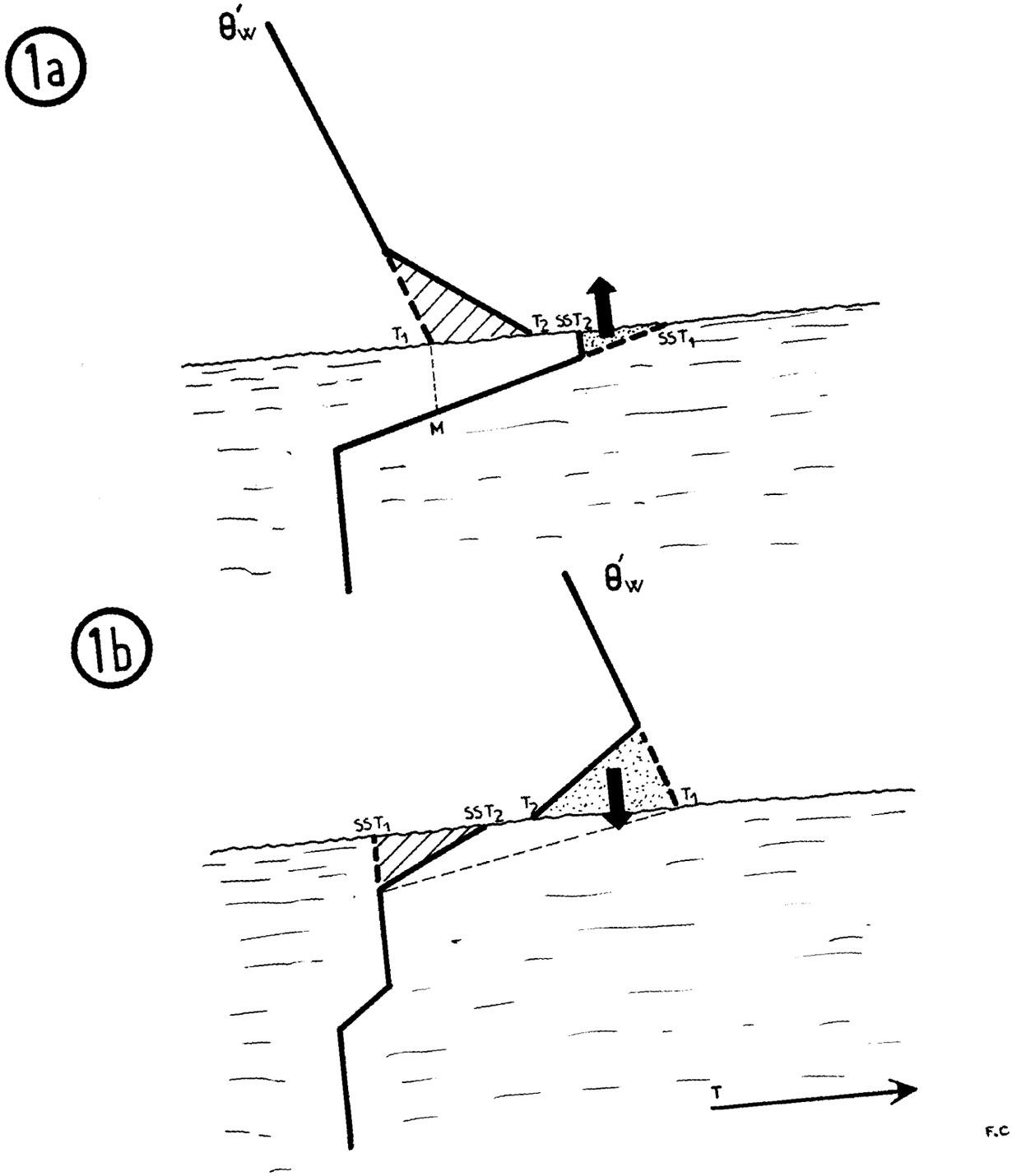

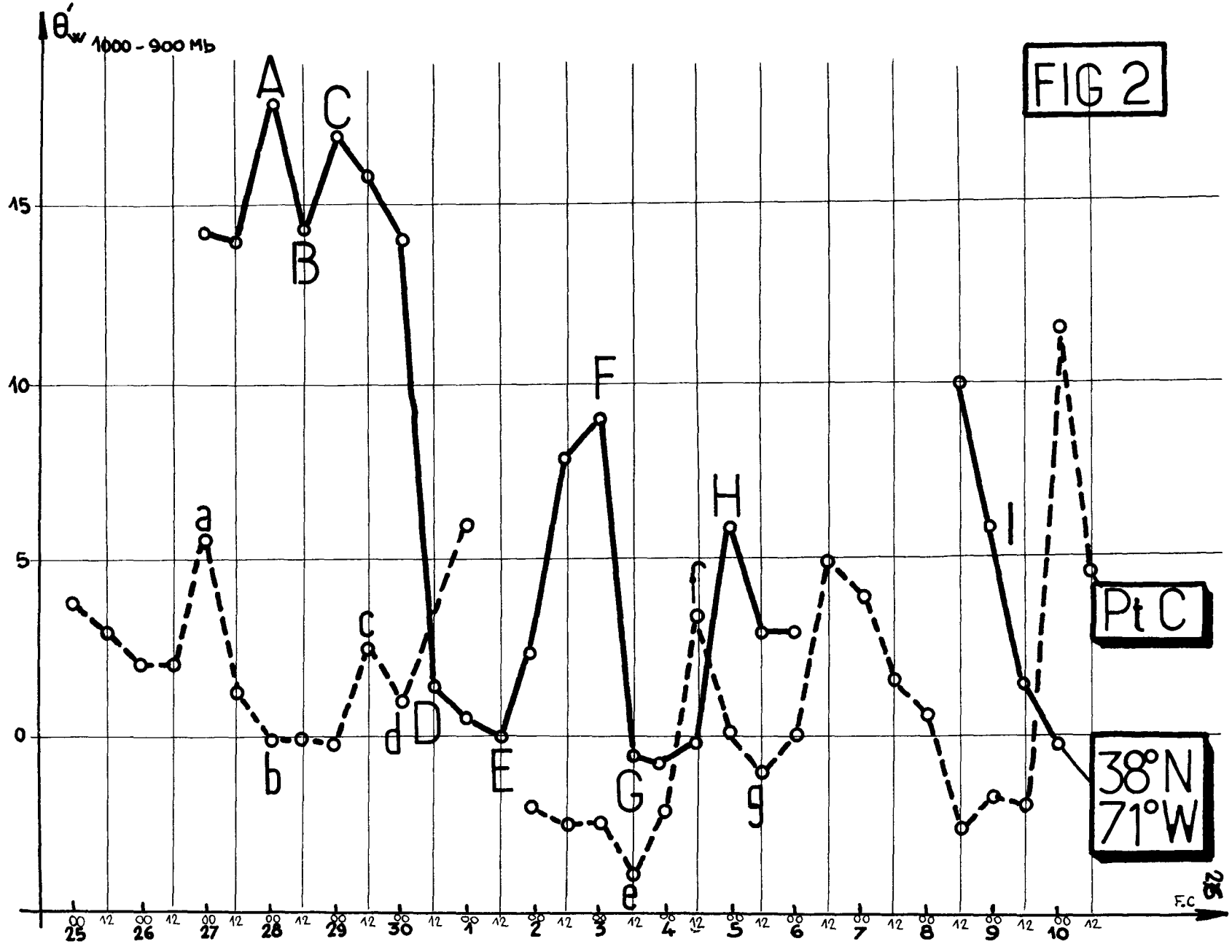
θ'w 1000 - 900 Mb
FIG 2
15
10
5
0
A
B
C
D
E
F
G
H
I
a
b
c
d
e
f
g
Pt C
38°N
71°W
F.C
25
26
27
28
29
30
1
2
3
4
5
6
7
8
9
10

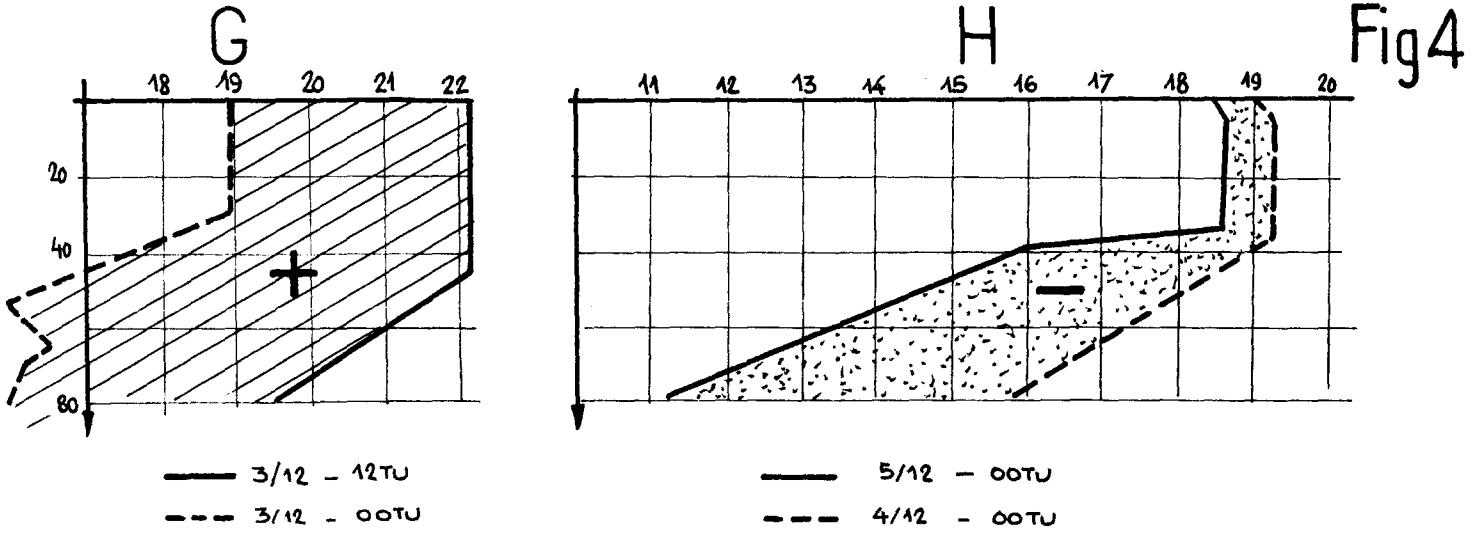
G
18
19
20
21
22
20
40
80
3/12 - 12TU
3/12 - 00TU
H
11
12
13
14
15
16
17
18
19
20
5/12 - 00TU
4/12 - 00TU
I
14
15
16
17
18
20
40
60
80
9/12 - 00TU
8/12 - 12TU
POINT 38N-70W
BATHY FINAL
BATHY INITIAL

Fig4

F.c

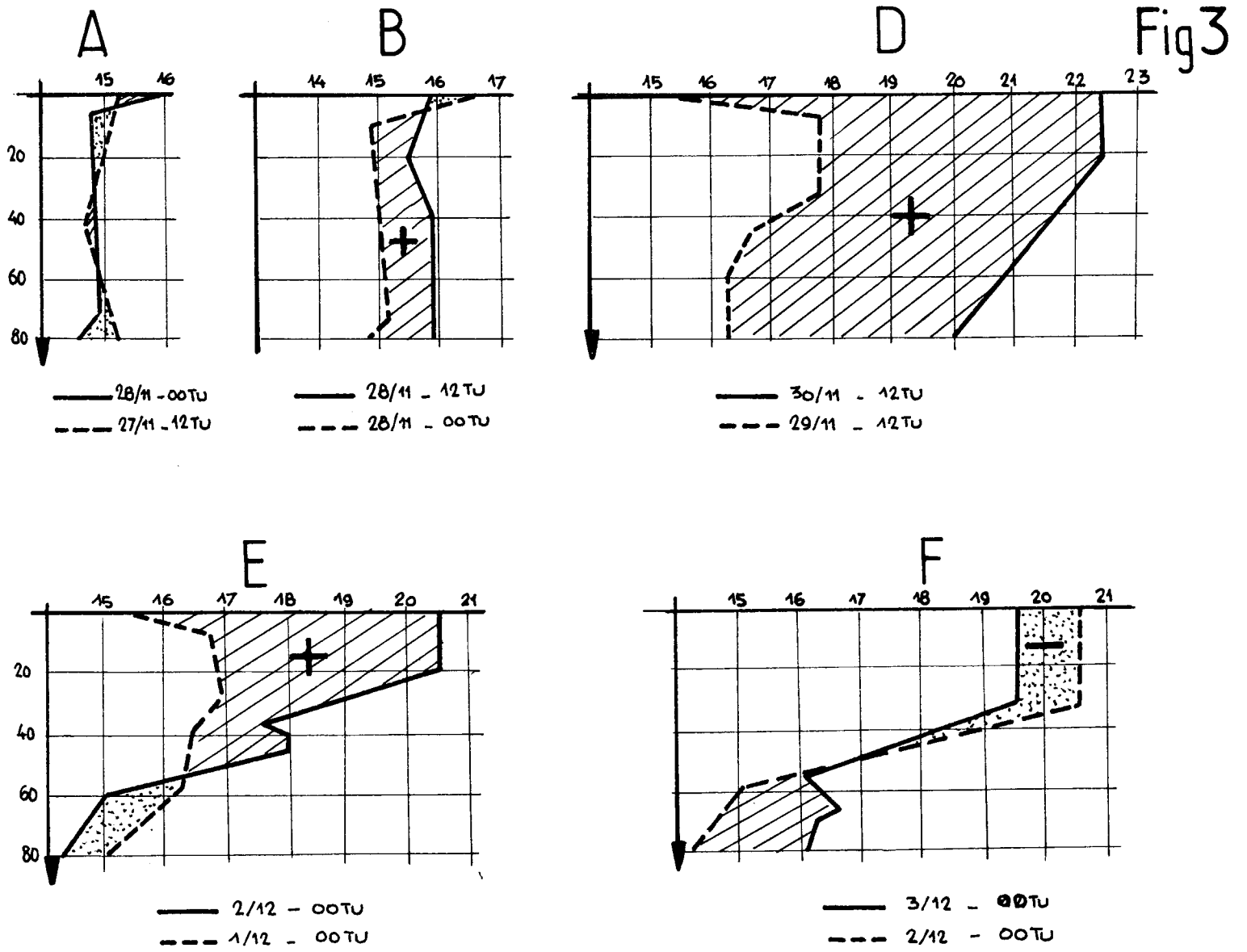
A
B
D
E
F
Fig3
15
16
17
18
19
20
21
22
23
14
20
40
60
80
28/11 - 00TU
27/11 - 12TU
28/11 - 12TU
28/11 - 00TU
30/11 - 12TU
29/11 - 12TU
2/12 - 00TU
1/12 - 00TU
3/12 - 00TU
2/12 - 00TU

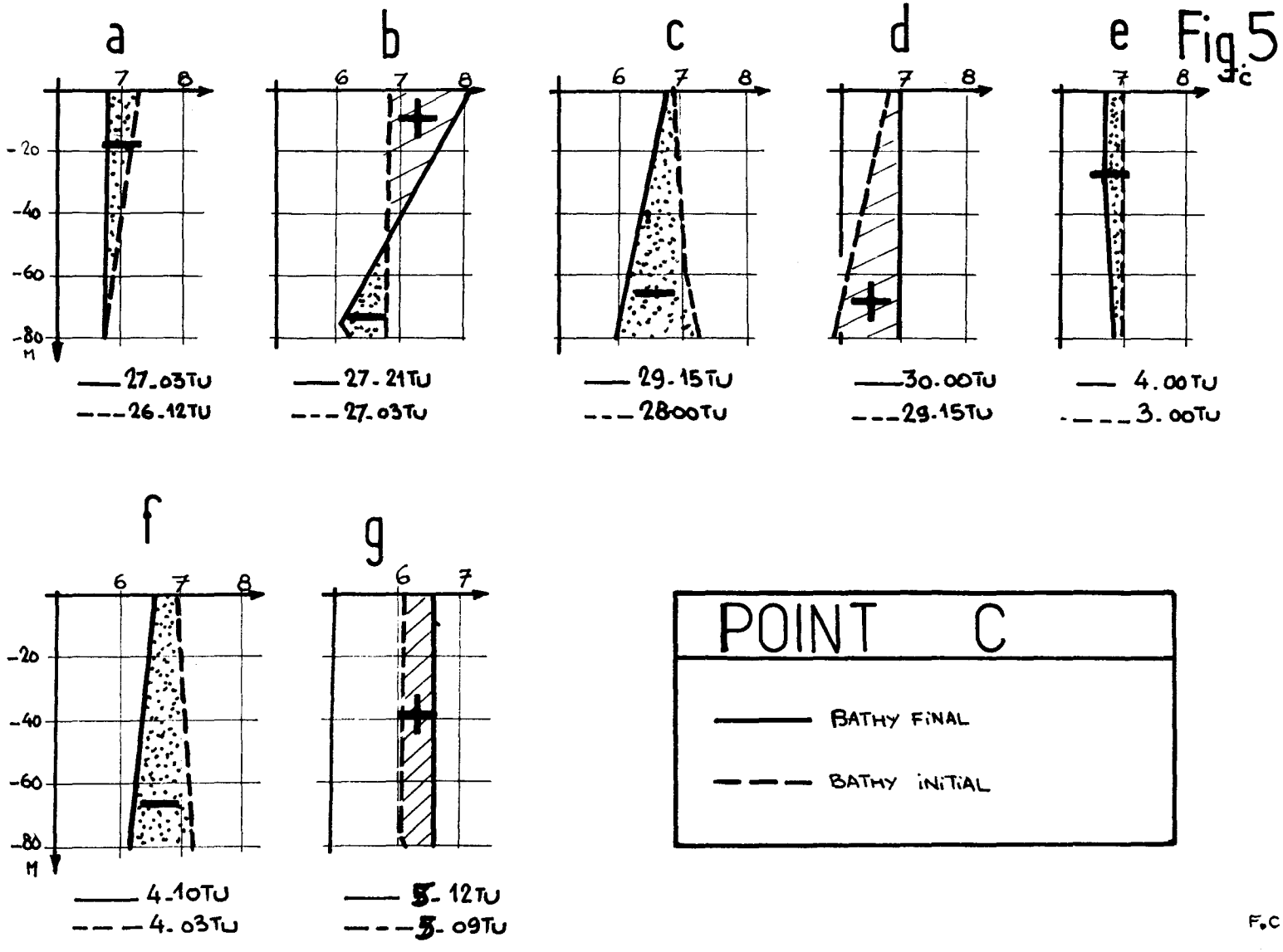
a
b
c
d
e
f
g
Fig 5c
7
8
6
-20
-40
-60
-80
M
27.03TU
26.12TU
27.21TU
27.03TU
29.15TU
28.00TU
30.00TU
29.15TU
4.00TU
3.00TU
4.10TU
4.03TU
5.12TU
5.09TU
POINT C
BATHY FINAL
BATHY INITIAL
F.C

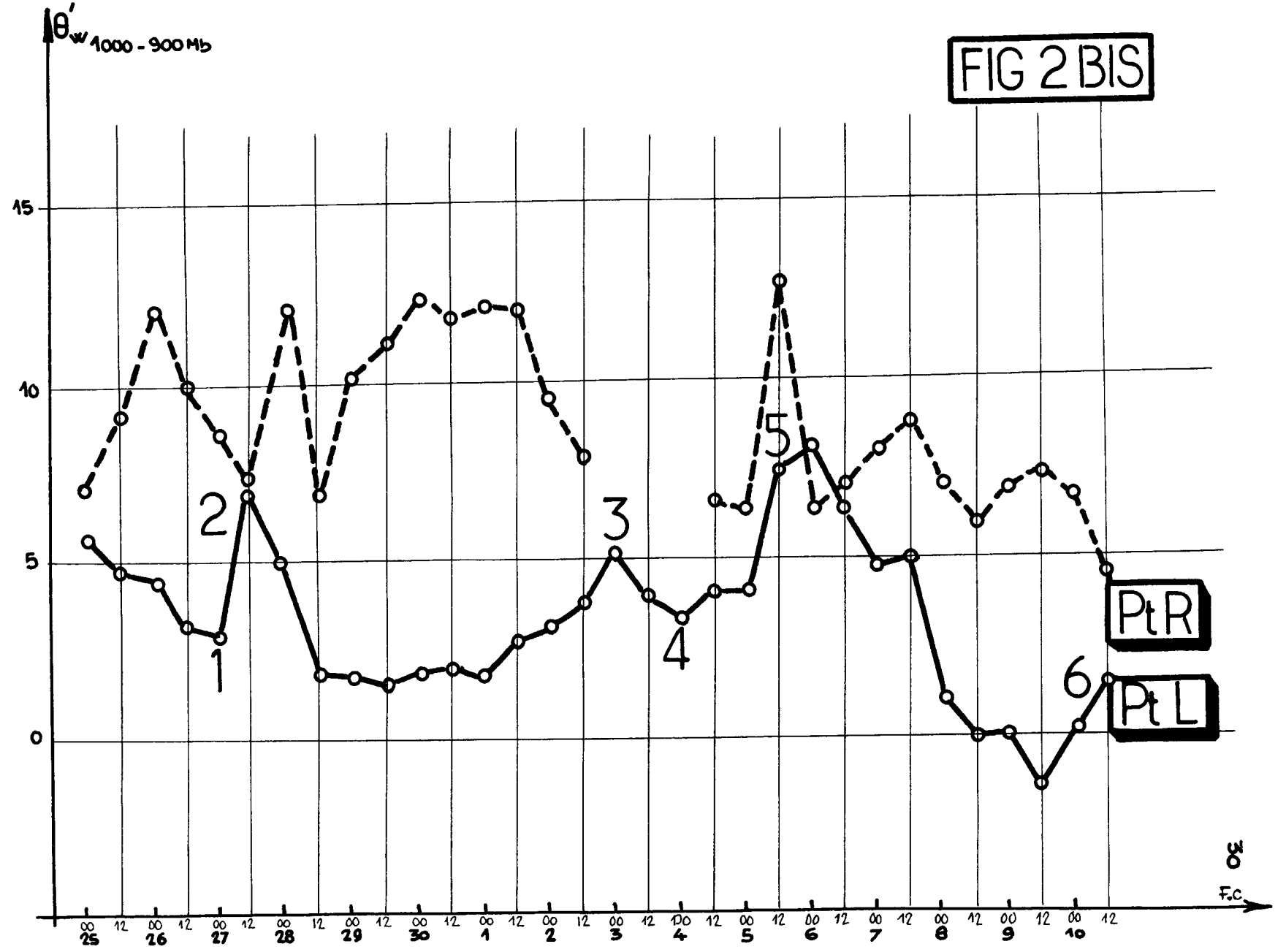
FIG 2 BIS
θ'w 1000 - 900 Mb
15
10
5
0
1
2
3
4
5
6
PtR
PtL
F.C.
00 12 00 12 00 12 00 12 00 12 00 12 00 12 00 12 00 12 00 12 00 12 00 12 00 12 00 12 00 12 00 12 00 12
25 26 27 28 29 30 1 2 3 4 5 6 7 8 9 10

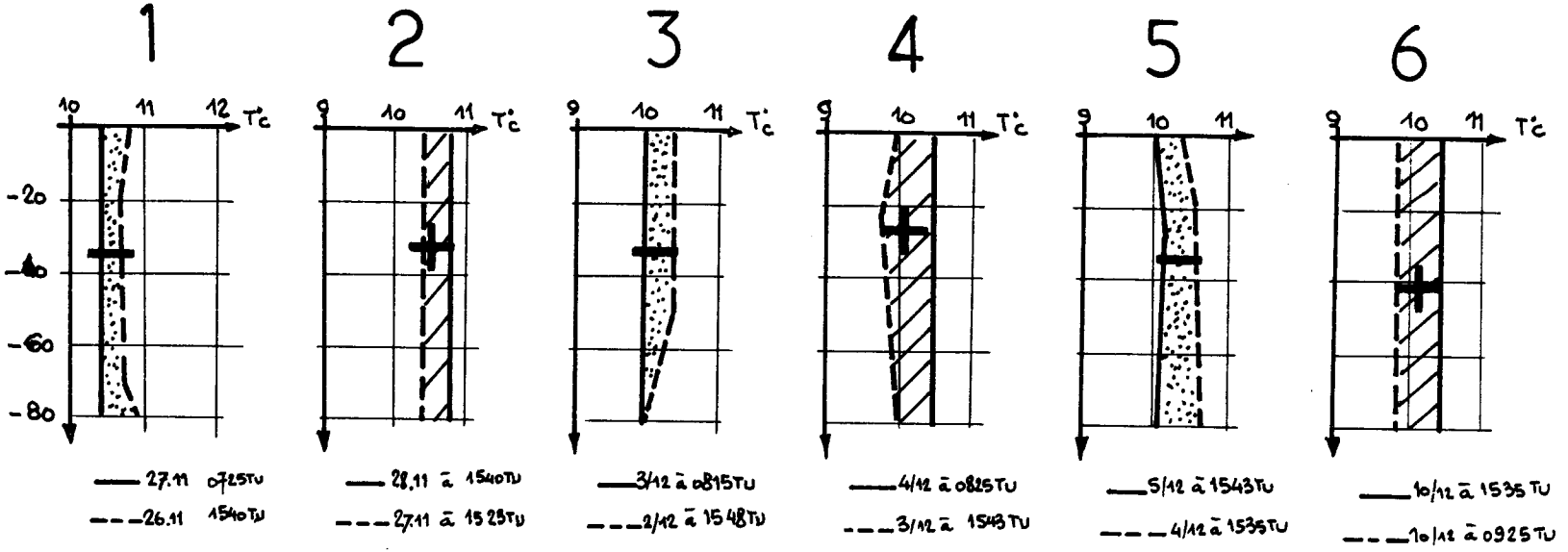
1
2
3
4
5
6
10
11
12
9
T°C
-20
-40
-60
-80
27.11 à 25TU
26.11 1540TU
28.11 à 1540TU
27.11 à 1525TU
3/12 à 0815TU
2/12 à 1548TU
4/12 à 0825TU
3/12 à 1548TU
5/12 à 1543TU
4/12 à 1535TU
10/12 à 1535 TU
10/12 à 0925 TU

Fig 6

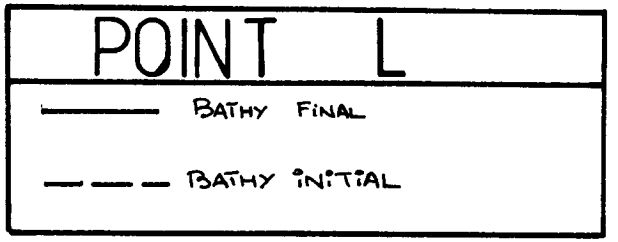
POINT L
BATHY FINAL
BATHY INITIAL

57°N
20°W

28·11
à 12 TU

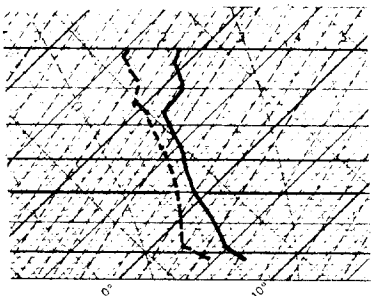

28·11
à 00 TU

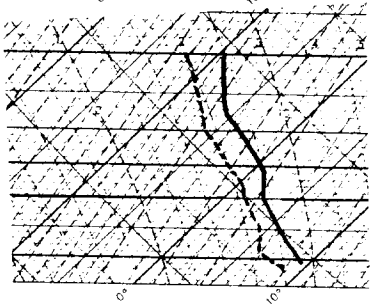

27·11
à 12 TU

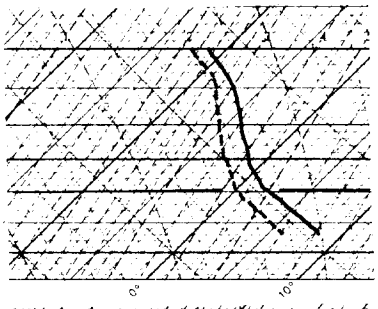

27·11
à 00 TU

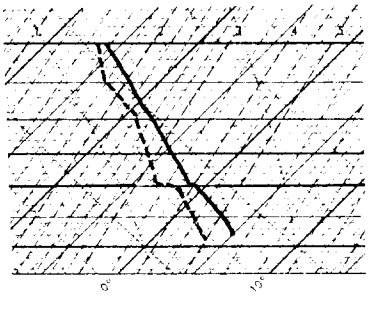

47°N
17°W

32

28·11
à 12 TU

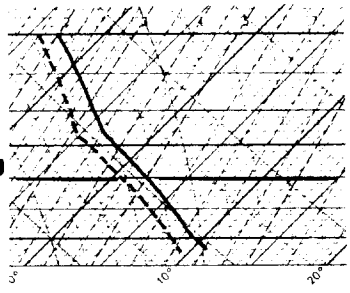

28·11
à 00 TU

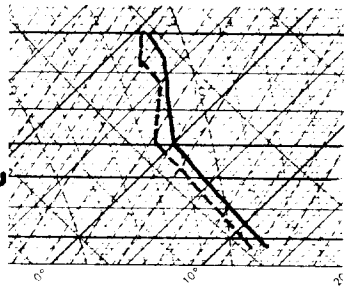

27·11
à 12 TU

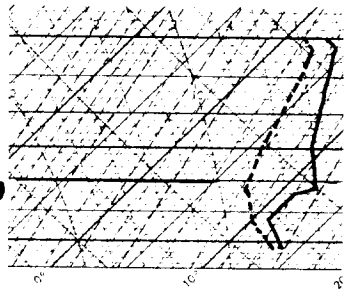

27·11
à 00 TU

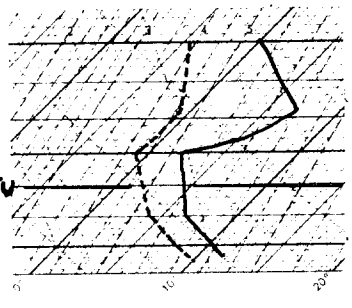

Fig 7

52°5 N
35°5 W

28·11
à 00 TU

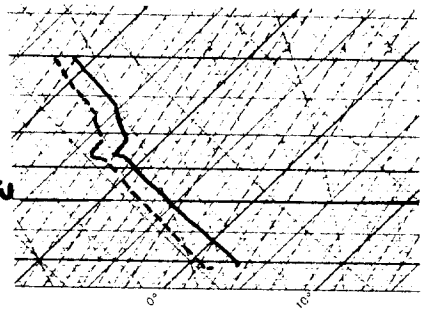

27·12
à 12 TU

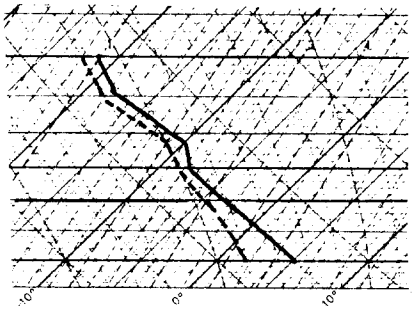

27·0(
à 00 TU

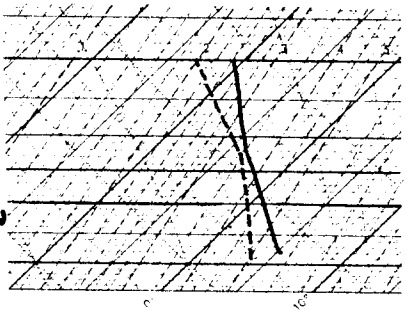

26·11
à 12 TU

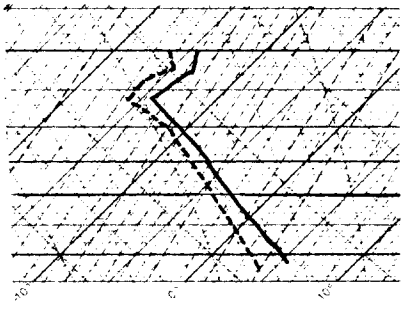

52°5 N
35°5 W

33

1·12
à 12 TU

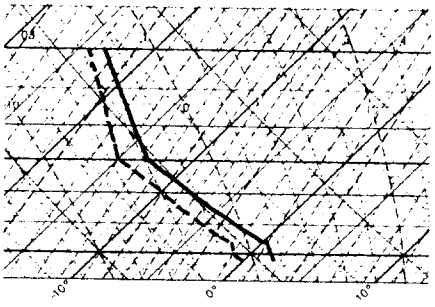

1·12
à 00 TU

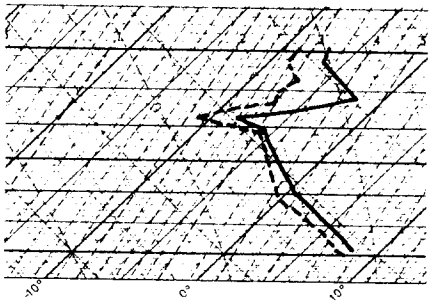

30·12
à 12 TU

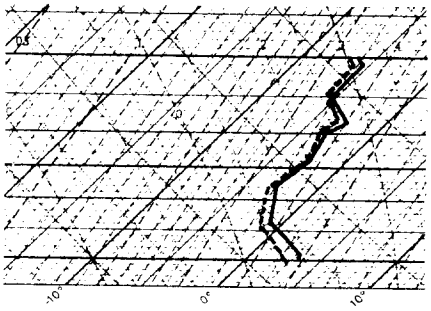

30·12
à 00 TU

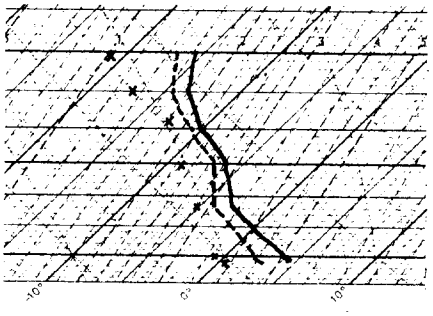

Fig 8

34

52°5 N
35°5 W

10.12 à 12 TU

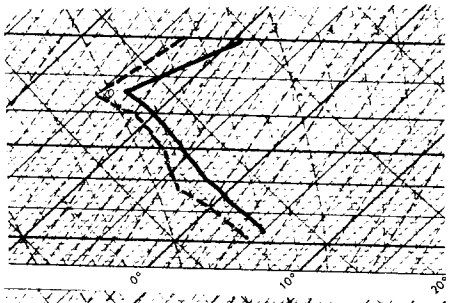

10.12 à 00 TU

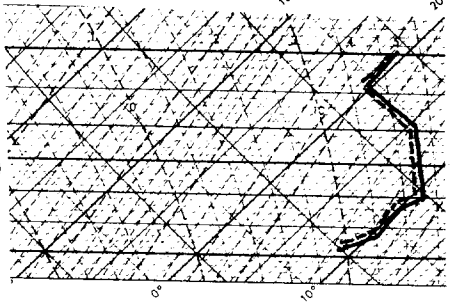

9.12 à 00 TU

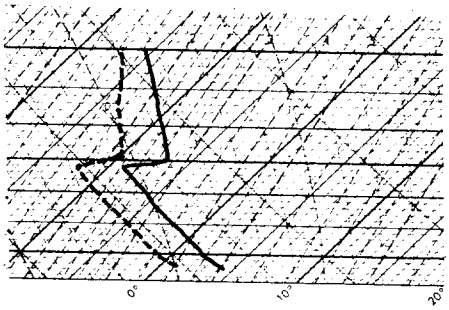

8.12 à 12 TU

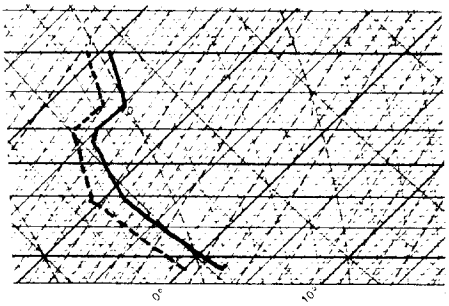

38°0 N
71°0 W

3.12 à 12 TU

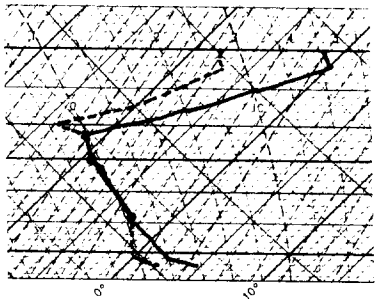

3.12 à 00 TU

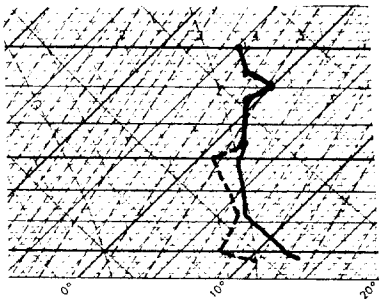

2.12 à 12 TU

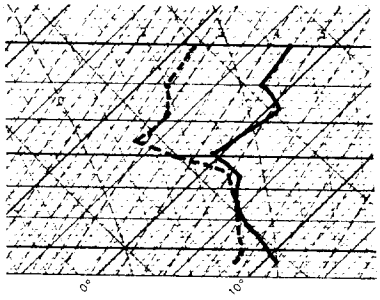

2.12 à 00 TU

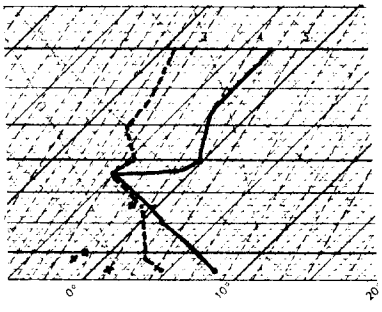

Fig 9

35

NRDT

Coupe du Gulf Stream

Fig 10

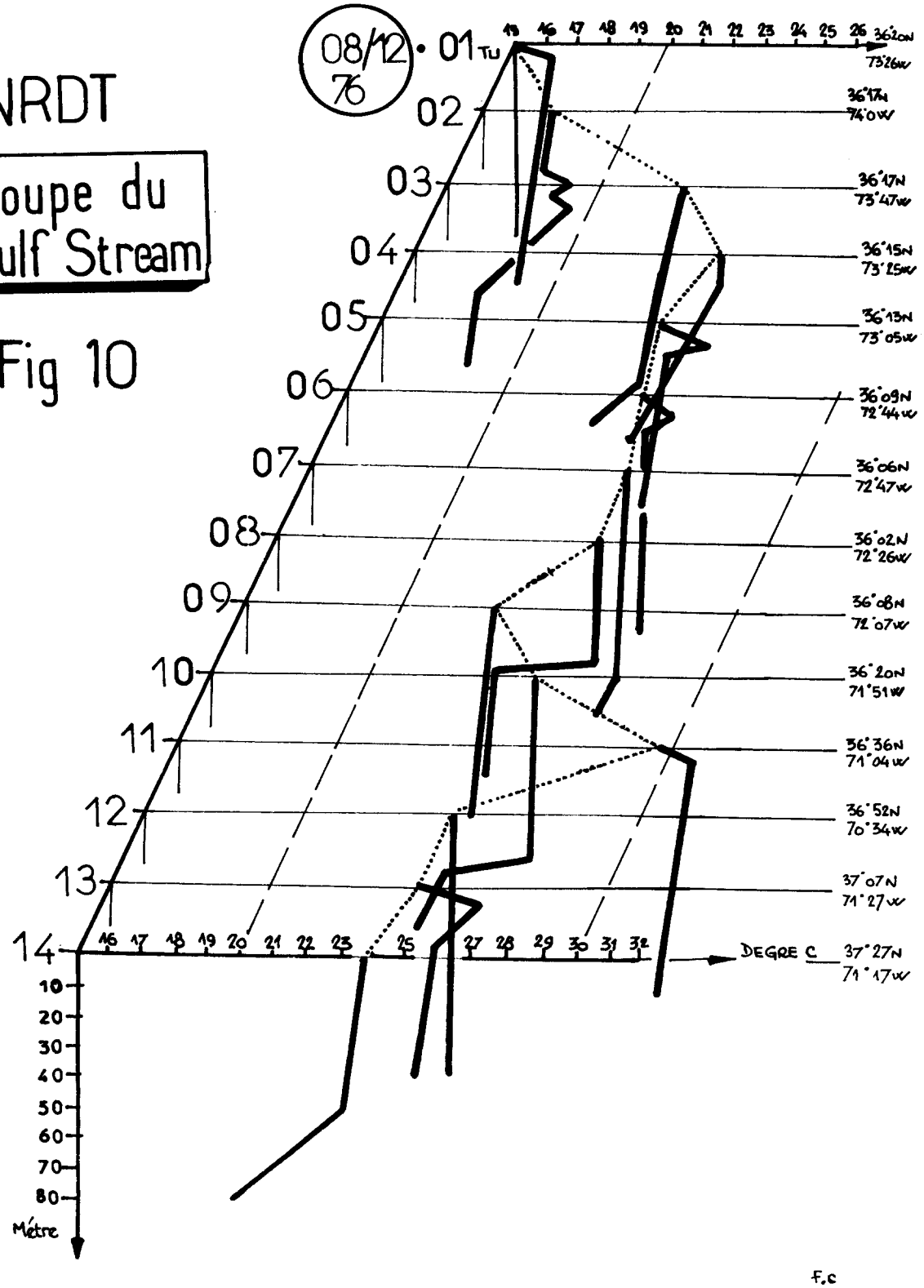

F.c

REAL TIME OCEAN THERMAL STRUCTURE ANALYSIS

by

William Gemmill and Sigurd Larson

National Meteorological Center
National Weather Service/NOAA
Washington, D. C. 20233

I. Introduction

In 1975, a small, ad hoc group was formed at the National Meteorological Center (NMC) near Washington, D. C., to provide improved oceanographic and marine products to the public. This group acts as a center for real-time data processing, analysis, and dissemination of ocean related products in much the same manner as NMC serves meteorological needs. Contoured maps, grid point values and data collectives are transmitted to the user by mail, radio facsimile, and the Global Telecommunication System (GTS). This material is also used as guidance by Weather Service Offices responsible for preparation of forecasts for the coastal, offshore and high seas areas. Functions of the NMC Oceanography group include the daily analysis of the global ocean surface temperature used in NMC numerical weather prediction and in long range monthly and seasonal weather forecasts, the development of an expanded oceanographic data base, objective analysis of ocean variables in addition to temperature, and adapting numerical and statistical ocean forecasting techniques to the real-time NMC operation.

The group to date has delt primarily with the thermal structure of the upper ocean. Both regional and global sea surface temperature analyses are being generated operationally, a regional subsurface subjective analysis is routinely produced and a new processing system for BATHY/TESAC data (temperature and depth data/temperature, salinity and depth data) is being implemented for data transmission and monitoring. Statistical summaries of IGOSS participation by GTS center and by ship are submitted to the WMO twice yearly. During the intensive expendable bathythermograph (XBT) program of POLYMODE, NMC acted as a "real-time" POLYMODE analysis center. Data were passed through NMC to POLYMODE headquarters, and were accessed at NMC where the data were plotted and analysed before being distributed to interested scientists.

II. Sea Surface Temperature Measurements

A variety of world-wide oceanographic data are transmitted to NMC in real-time. Direct sea surface temperatures are obtained from ship weather reports, fixed and drifting buoys, BATHY/TESAC reports, and remote measurements are obtained from satellites.

These data do not constitute a "homogeneous" set however; they differ in instrument accuracy, position accuracy, measurement depth and areal extent. SST data transmitted by ships in their routine weather reports are measured at sea water intakes located on the ship's hull, 4 to 8 meters below the water line. Fixed buoys provide reliable temperatures within one meter of the surface but are confined to coastal regions. Drifting buoys also measure temperatures less than a meter below the surface and are expected to provide valuable information in the data sparse Southern oceans. BATHY/TESAC reports provide the most accurate data available for ocean surface temperatures, but these measurements are concentrated in areas of special projects such as POLYMODE, NORPAX and along shipping lanes. Satellite measurements are the most satisfactory in terms of distribution and quantity. They exhibit less variability than ship "intake" temperatures over a region but at the same time they may reveal an areal bias. Further, there are many ocean areas around the world that are obscured by clouds for extended periods of time, severely limiting the number of satellite observations. The anticipated number of observations from each source during a 24 hour period during 1979 is given in Table 1.

Unfortunately, the two largest sets of data, ship reports and satellite derived reports, also exhibit the largest errors. The accuracies assigned to fixed buoys, drifting buoys and BATHY/TESAC reports are based on ideal laboratory calibration. It is anticipated that the accuracy of real-time data will deteriorate because of instrument errors, transmission errors, and position errors.

The quality of sea surface temperature reports from merchant ships were recently evaluated by Tabata (1978). Fixed buoy and ocean station P data, averaged over 3 1/2 day periods, were compared with ship data in their vicinity in the N. E. Pacific Ocean. Ship data were found to be $0.2° \pm 1.5°$ warmer than the buoy and station data (Tabata states that the buoys are comparable to ocean station P which was determined to have an accuracy of $\pm$ 0.2°C). These results agree closely with James and Fox (1972) who made a comparison of intake temperatures vs. bucket temperatures using data taken under the auspices of the WMO. They reported that for 13876 observations, ship intake temperatures were $+0.3° \pm 1.3°$C warmer than bucket temperatures. Tabata's study was based on data received on a teletype receiver at the local weather station, whereas James and Fox used data recorded on log forms.

The quality of the satellite retrievals is much more difficult to determine. The satellite estimates the average temperature over a 100 km square, whereas the other sensors measure temperature at a "spot." A set of edited ship reports when compared with satellite data within 100 km and a 24 hour period produced global daily mean differences during July, August and September 1978, which ranged between -0.2°to +0.8°C, with an RMS deviation near $\pm$ 2.5°C (Casely, 1978).

III. Regional Analysis

A). Sea Surface Temperature

1). Method of Analysis

Routine sea surface temperature analyses are being produced for three regions contiguous to the continental United States: the Western North Atlantic, the Gulf of Mexico and the Gulf of Alaska. These analyses are generated on a polar steorographic grid (1/16 of the standard NMC 381 km grid true at 60°N) from a composit of 5 days of ship, buoy, XBT and satellite data using an objective analysis procedure.

Objective analyses methods are used to quickly transform a large set of irregularly space data into a set of regularly spaced data points, through interpolation, removal of errors and smoothing. The objective analysis scheme for the regional analysis is a successive correction technique frequently used by meteorologists (Cressman, 1959). The analysis uses the observations to make successive corrections to an initial guess. Each correction pass using all the data is called a scan.

The analysis procedure starts with a gridded first guess (G°_{ij}) which is usually the previous analysis, but may be climatology. For each observation location, an interpolated first guess value is determined. The difference between the observation (O) and interpolated (I) value is called a correction (C), and is given by: $C(x,y) = O(x,y) - I(x,y)$, where (x,y) is the position of the observation. The correction (C) is compared to the correction tolerance set for the scan. If it exceeds the limit, the correction is rejected. A weight (W), $W = (R^2 - r^2)/(R^2 + r^2)$ is computed at all grid points within the radius of influence (R) of an acceptable observation. The radius of influence (R) is a constant for each scan. The distance between a grid point (i,j) and an observation location (x,y) within R is defined as $r^2 = (i-x)^2 + (j-y)^2$, the weighting function, however, is defined as zero for $r \geq R$. The corrections are weighted and accumulated at grid points. The mean weighted correction is determined at each grid point by: $\bar{C} = (\Sigma WC/\Sigma W)*Wmax$. Wmax is the maximum of all weights applied at a given point. This modification was necessary to reduce undue influence when only a few distant observations are available to correct a grid point. The new grid point value then becomes $G^{n}_{ij} = \bar{C}_{ij} + G^{\circ}_{ij}$. A flow diagram of the steps in the regional analysis is shown in Figure 1.

Initially, data are allowed to have a large influence radius and a large correction tolerance, but on successive scans the influence radius and correction tolerance is reduced. The initial radius is chosen to approximate the extent of data void areas. The final radius is set equal to 1 and the weight is equal to 1 everywhere within the influence radius. A modification has been made to compensate for rapid changes in strong gradients of the Gulf Stream, by increasing correction tolerances as a function of the strong gradients. The influence radius and correction tolerance are given in Table 2.

2). Discussion of Regional Analyses

The fishing industry, oil and gas activities and marine meteorology need detailed synoptic information concerning ocean water temperatures and its changes. Ocean regions adjacent to continents exhibit more complex structure and variability than do mid-ocean areas. And, it is in the continental shelf regions that human activity is increasing rapidly.

It is in these areas that air-sea interaction is the most intense and most variable. Ocean surface thermal gradients are largest during winter and become weak during summer. During the winter, cold continental air mass pass over adjacent waters extracting heat. These air masses modify rapidly as they move far offshore, thereby having a diminished effect on ocean temperatures. During summer, features are masked at the ocean surface by solar isolation and diminished air mass contrast.

i) The Western North Atlantic Ocean

The dramatic seasonal variability in this area is evident by comparing figures 2a and 2b. The Gulf Stream is identified as the warm edge of the strong temperature gradient zone. It follows the coast from Florida to Cape Hatteras and then meanders northeastward into the Atlantic. Satellite data is not used in this analysis because its 100 km resolution is too large for Gulf Stream depiction. These analyses utilized about 800 observations from ship and buoys over a five day period. Because of the composit period there is a smearing effect of Gulf Stream meandering. However, if a shorter period were used there would be less data and thereby a loss of accuracy in the analysis.

The high gradient zone along the western and northern edge of the Gulf Stream is much too broad. In this analysis the maximum gradient is 7°C/30km, where the true gradient is 10°C/20km. This is due not only to the composit data, but also to the distribution of the data on the fine grid. There is small scale detail to the south of the stream in the Sargasso Sea, but the data distribution is not adequate to depict it with any certainty. The summer map shows the influence of strong solar heating across most of the area and surface gradient of the Gulf Stream is evident only northeast of Cape Hatteras.

ii) Gulf of Mexico

In the winter, the major features of the Gulf of Mexico are identified in Figures 3a and 3b. The warm loop current flows north past Yukatan, loops toward the U. S. Gulf Coast and flows out through the Florida Straights to become the Gulf Stream. Waters adjacent to the U. S. Gulf Coast are cold due to river outflow and cooling by continental air masses. In contrast the summer analysis shows little structure in the sea surface temperature (Figure 36). The various types of data used in these analysis averages 250 observations.

iii) The Gulf of Alaska

The Northeast Pacific (Figures 4a and 4b) is less influenced by continential air masses than those areas previously decribed. For a typical 5 day period, 1000 observations are combined to form the analysis of the region. Most air masses in this area have been over water for some time, and are more or less in equilibrium with the sea. The main feature here is the west wind drift, which is near 48°N. There is a cyclonic gyre in the Gulf of Alaska, centered near 52°N,146°W. To the south along the coast of Washington, cold upwelling is present. The basic pattern in the Northeastern Pacific does not undergo the dramatic seasonal change as observed in the previously discussed regions, although its annual change is on the order of 8°C.

B). Depth of 17.5°C Isotherm Analysis

An experimental analyses is being produced for the depth of the 17.5°C isotherm in the Western North Atlantic. There are on the average of 180 ship reports per day in the analysis area (25°N to 45°N and 55°W to the U. S. Coast), but only 15 XBT reports in the same area (an exception was during POLYMODE when that many were reported with a 5° square). The region was chosen because of the active interest and studies of the Gulf Stream, numerous Coastal Guard and Fisheries surveys along the continental shelf and the extensive POLYMODE experiment in the Sargasso Sea. The depth of the 17.5°C isotherm was chosen because it is the top (500m) of the main thermocline in the Sargasso Sea. It rises rapidly across the Gulf Stream to a depth of 100m in slope water (summer) and outcrops along the Gulfstream during winter. The topography of this surface can also be used to identify warm and cold eddies.

The analysis consists of a composit of 2 weeks of subsurface reports. However, because these data are poorly distributed, the analysis is supplimented with the most current satellite imagery of the Western North Atlantic Ocean to locate the Gulf Stream and eddies (Kniskern and Thompson, 1975). The surface position of the 17.5°C isotherm is determined from the regional SST analysis. An example of the 17.5°C analysis produced during the POLYMODE experiment is shown in Figure 5.

IV. Global Sea Surface Temperature Analysis

A). Method of Analysis

The Global Sea Surface temperature analysis is generated using techniques developed for the U. S. Navy by Carstensen (1962) and used operationally by Wolff, et. al. (1965) and Perdue (1969). Analyses are performed on alternate days for the Northern and Southern Hemispheres on a 129x129 polar stereographic grid which has a mesh length of 202.6km at 80° (N/S) and 102.1 km at the equator.

Observations taken from surface platforms (ship reports, fixed and drifting buoy reports, BATHY and TESAC reports) are partitioned from satellite observations within the analysis. The final analysed field however reflects the mixture of both surface and satellite observations. This approach was

taken to allow monitoring of any systematic difference which may exist between the two types of data. This partitioning of the data was accomplished by executing the analysis scheme first for all surface data and then a second time for satellite observations.

The initial step of the analysis procedure, shown in Figure 6, is to form a first guess field by subtracting from the previous analysis, a long term average temperature (Alexander and Mobley, 1976) at each point on the grid. This first guess field serves the "standard" against which to compare the observations. To insure that the first guess field is reliable, large differences with climatology (anomalies) are reduced unless they are supported by observations during the past ten days. The observations are weighted relative to each other based on the type and age of the report. Table 3 shows the weights given to each type of report. These weights are then sumed at each grid point having more than one report over the past ten days and the total "coverage value" is used in limiting the first guess anomalies. The actual limits imposed on these anomalies and the "coverage" required to support them are given in Table 4.

The anomaly field is then smoothed to remove any abrupt spatial changes and added to the climatology field to form the first guess. The data is then analyzed in a series of five passes through the procedure shown in Figure 7. In each pass, the first guess field is interpolated at the location of each report through a non-linear interpolation scheme. The analysed field resulting from each pass becomes the first guess for the next pass.

At the location of each observation, a difference is formed by subtracting the interpolated first guess value from the report. The difference is then compared to a tolerance which varies with each pass and for each type of report. These tolerances are given in Table 5. If the tolerance is exceeded, the report is rejected for the current pass. All reports are checked during each pass. Because the resulting analysed field is used as the first guess for the next pass, reports initially rejected may be accepted, if the previously accepted reports have modified the temperature field in such a way as to reduce the difference between it and the rejected report.

For each accepted observation, the difference is weighted relative to others on the basis of its age and type. A percentage of this weighted difference is used to correct the first guess at the four grid points surrounding the observation. The actual percentage of the difference is inversely proportional to the distance between the grid point and the observation. At each grid point, the weighted differences from each report lying within one mesh length are accumulated, averaged and added to the first guess to form the new value of the temperature field. The influence of the accepted reports is spread to grid points not corrected by data through the conditional relaxation method of Carstensen.

The mathematical formulation for the conditional relaxation procedure is given below:

$$T_n = T_{n-1} + \alpha (\nabla^2 T_{n-1} - \nabla^2 T_o)$$

where

T_n is the temperature for the Nth relaxtion interation at a non boundry, non corrected grid point

T_{n-1} is the temperature at the grid point for the previous (n-1) relaxation interation

∇^2 To is the Laplacian of the first guess field and is equal to:

$$T_o (i,j+1) + T_o (i,j-1) + T_o (i-1,j) + T_o (i+1,j) - 4\, T_o (i,j)$$

$\nabla^2 T_{n-1}$ is the Laplacian of the temperature at the grid point for the n-1 relaxation iteration

α is a relaxation coefficient equal to 0.32.

The relaxation technique is performed in a series of iterations (denoted by n) in which a residual equal to $(\nabla^2 T_{n-1} - \nabla^2 T_o)$ is calculated at each grid point non-corrected by observations. This residual is then added to the value at the non-corrected grid point and the procedure is repeated at each uncorrected grid point. If the residual at each grid point is less than a small, pre-determined number everywhere on the grid, the relaxation is considered to have "converged" to a correct solution. If this is not the case, additional iterations (denoted by n+1) are performed until the convergence criterion is met.

This procedure preserves the "shape" of the temperature field by imposing the condition that the change, over the time since the previous analysis, in the divergence of the temperature gradient is very small ie.

$$\partial/\partial t (\nabla \cdot \nabla T) = 0 \text{ for non-corrected grid points}$$

The number of reports which were accepted in the final pass at each grid point are stored as a coverage field to be used to constrain the first guess in latter analyse.

The entire analysis procedure is then executed again for satellite data and the difference between the surface data only analysis and combined surface and satellite analysis is stored as a satellite data impact field. An example of a Northern Hemisphere analysis is shown in Figure 8 and a Southern Hemisphere analysis in Figure 9.

B). Statistical Data Summaries

All the data processed in the hemispheric analysis is summarized statistically each time the analysis is run. An example of such a summary for ship reports and satellite data is shown in Figure 10 and 11. This summary will be used to "tune" the analysis through modification of the weighting and tolerance limits. It will also provide quantative information on possible systematic differences between surface and satellite data. Such a systematic difference is indicated by Figure 12. This is a plot of the frequency of occurence of the difference between the observation and first guess. The data are from the period between 7 to 17 November 1978 and suggest a systematic difference of ship data being about 0.5° to 1°C warmer than satellite data overall. The BATHY data which are considered to be the most accurate,show a symmetric peak between -0.5°and +0.5°C. It should be noted that 50% of this type of data lie between -0.5° and +0.5°C and that 75% lie between -1°C and +1°C of the first guess field during the period.

V. The POLYMODE Experiment

A). Purpose

POLYMODE was a joint US/USSR oceanographic experiment designed to study meso-scaled ocean eddies in the upper ocean. Part of the experiment emphasized intensive synoptic oceanic measurements to map the evolution and movement of mid ocean flow patterns. The area of study was 1000 km east of Florida within an 8-degree rectangle centered near 29°N and 70°W.

A pilot project was designed to evaluate the capability of NMC to act as a real-time national center during the POLYMODE experiment for the acquisition and transmission of XBT data and the analysis and dissemination of special ocean charts to the POLYMODE center near Boston. On the larger scale, the purpose of the IGOSS/POLYMODE project was to test the operational components of IGOSS (data collection, product formulation and dissemination) during a controlled experiment and provide POLYMODE participants with the capability to exchange data and receive oceanographic analysis.

B). The Role of NMC

In July of 1977, Soviet ships began taking temperatures and salinity observations in the POLYMODE region. These data were transmitted to U. S. Coast Guard receiving stations, and relayed directly to NMC via landline. Data were coded and handled using standard IGOSS procedures for collection of temperature (BATHY) and temperature/salinity (TESAC) data. A rudimentory check of the data was made at NMC to eliminate obvious error, before twice daily transmissions to Boston. A limited number of observations were received from non-POLYMODE ships transversing the experiment area. All data were transmitted by NMC worldwide via the Global Telecommunications System of the World Weather Watch. During the year ending in June 1978, NMC handled 3,063 BATHY messages for POLYMODE from U. S. and USSR ships. In general 5-20 reports were received on any particular day.

The depth of the 15°C isotherm was extracted from BATHY reports and was analysed subjectively. The latest 10-18 days (synoptic period) of data were plotted thrice weekly, contoured and the analysis transmitted to sea for facsimile reception aboard ship. A copy was also telecopied directly to the POLYMODE center, from which distribution was made.

The quantity and quality of BATHY data was sufficient to study the evolution of deep ocean meso-circulation features. In general, a trough-ridge-trough (or vice versa) pattern appeared to drift in a westerly direction in agreement with the upper thermocline circulation of the region (Figure 13) and major features were monitored as they moved through the region (Figure 14).

C). Conclusion of NMC's Participation

The emphasis by NMC was to provide these analyses in a timely manner so that participating scientists could have a quick, preliminary look at the thermal structure of the experiment area.

The following conclusions can be stated concerning the project:

1. the use of Specialized Oceanographic Centers (in this case NMC) is an effective way to provide regional IGOSS products.

2. the IGOSS System (Coastal Radio Stations, NMC, GTS) was capable of handling the increased data.

3. Oceanographic features, such as eddies, can be mapped in near-real time and disseminated to users, when data of sufficient quantity and quality are available.

4. IGOSS support for FGGE in data collection and product formulation should prove to be benefitial to service agencies and researchers alike.

The willingness of the POLYMODE participants to provide NMC with data in real-time was essential to the success of the IGOSS/POLYMODE project. An underlying reason for the project's success was that user (POLYMODE scientists) had a need, and a system (IGOSS) which could provide the needed services was already in place.

VI. Summary and Comments

The National Meteorological Center (USA) is now expanding its capabilities to provide real-time ocean services. The primary system of distribution is by mail, but the regional Atlantic and Pacific analyses are now being transmitted on a weekly basis on national facsimile. The Atlantic analysis is

transmitted to sea by radio facsimile twice a week. The global analysis are to be transmitted over the GTS on a daily basis. Our present temperature products are summarized in Table 6.

Future plans include regional and hemispheric automated subsurface analysis; a new program system for the transmission and monitoring of BATHY/TESAC data, subsurface climatological fields and diagnostic models of mixed layer depth or other parameters.

References

1) Alexander, R. C. and R. L. Mobley, 1976: Monthly Average Sea-Surface Temperatures and Ice-Pack Limits on a 1° Global Grid. Monthly Weather Review, 104 (2), 143-148.

2) Carstensen, L., 1962: Progress Report, Fleet Numerical Weather Facility; U. S. Naval Post-Graduate School, Monterey, Ca.

3) Casely, G., 1978: Satellite Derived SST Quarterly Report, July - September 1978. Unpubl. report, U. S. Department of Commerce, NOAA, NESS, Washington D. C., 3 pp.

4) Cressman, G. P., 1959: An Operational Objective Analysis System, Monthly Weather Review, 87 (10); 367-374.

5) James, R. W., and P. J. Fox, 1972: Comparative Sea Surface Temperature Measurements. Report No. 5, Reports on Marine Science Affairs, 27 pp.

6) Kalinowski, J. K., Signore, T. L., Pichel, W. G., Walton, C. C., Brower, R. L., Brown, S. R. and Bennenkamper, K. G., 1977: Present and Future Operational NOAA Satellite Oceanography Products: An Introduction. Proceedings 11th International Symposium Sensing of Environment, April 25-29, 1977, Ann Arbor, Mich., 625-633.

7) Kniskern, F. E. and Thompson, B. J., 1975: Some Oceanographic Service Products Derived from Satellite Data. Internation Council for the Exploration of the Sea. Reykjavik, Iceland, 27 pp.

8) National Oceanic and Atmospheric Administration, 1978: IGOSS/POLYMODE Experiment Final Report; Oceanographic Services Branch, NWS, Washington, D. C., 15 pp.

9) Perdue, James, N., 1970: Documentation of Subroutine Analysis; Contract Report No. N66314 - 70-C-0217, Fleet Numerical Weather Central, Monterey, Ca.

10) Tabata, S., 1978: Comparison of Observations of Sea Surface Temperature at Ocean Station P and NOAA Buoy Stations and Those Made by Merchant Ships Traveling in Their Vicinities, in the Northeast Pacific Ocean. Journal of Applied Meteorology, 17 (2): 374-385.

11) Wolff, P. M., Carstensen, L. P., and Laevastu, T., 1965: Analysis and Forecasting of Sea Surface Temperature (SST), Technical Note No. 8, Fleet Numerical Weather Facility, Monterey, Ca.

Table 1. Anticipated Number and Accuracy of Measurement of SST for Various Sources During a 24 Hour Period During 1979.

DATA SOURCE	QUANTITY	ACCURACY	REMARKS
1) Ship observations	2800	± 1.5°C	90% in Northern Hemisphere
2) Fixed buoy observations	80	± 0.2°C	Located in Coastal regions
3) Drifting buoy observations	200	± 0.2°C	Primarily in Southern Oceans
4) BATHY/TESAC observations	150	± 0.2°C	Limited to special regional projects, and shipping lanes.
5) Satellite observations	40,000*	± 1.5°C	Distributed between hemispheres, limited by clouds

*It is expected that by 1979 the temperature retrievals will have a 50 km resolution after TIROS-N Satellite becomes operational (Kalinowski, et al, 1977).

Table 2. Scan Radii and Correction Tolerance Limits for Regional Analyses

	Scan				
	1	2	3	4	5
Scan Radii (Grid intervals)	20	10	5	3	1
Correction Tolerance (°C)	5	4	4	3.5	2.5

Table 3. Coverage Weight Given to Each Type of Report Based on its Age

Report Type	Age of Report in Days				
	0-2	3-4	5-6	7-8	9-10
Northern Surface	10	8	7	6	5
Satellite	5	4	4	3	2
Southern Surface	15	12	10	9	7
Satellite	5	4	4	3	2

Table 4. Limits on First Guess Anomaly Based on Total Coverage Supporting That Anomaly

Total Coverage	Limit Imposed on First Guess Anomaly
< 2	$\pm$ 2.5°C
< 61	$\pm$ 2.5°C
< 121	$\pm$ 3.5°C
< 181	$\pm$ 4.5°C
≥ 181	$\pm$ 5.5°C

Table 5. Acceptable Difference (°C) Between Report and Interpolated First Guess for Each Pass

Record Type	PASS				
	1	2	3	4	5
Northern Surface	$\pm$2.75	$\pm$2.50	$\pm$2.40	$\pm$2.25	$\pm$2.00
Satellite	$\pm$1.55	$\pm$1.40	$\pm$1.35	$\pm$1.25	$\pm$1.15
Southern Surface	$\pm$2.85	$\pm$2.60	$\pm$2.50	$\pm$2.35	$\pm$2.10
Satellite	$\pm$1.35	$\pm$1.20	$\pm$1.15	$\pm$1.10	$\pm$0.95

Table 6. Real-Time Ocean Products at NMC

Region	Type	Grid* Interval (KM)	Number of Days of Data	Frequency Produced	Method	Method of Transmission
NW Atlantic	SST	23.8	5	Twice	SCT**	Fax/Mail
Gulf of Mexico	SST	23.8	5	Weekly	SCT	Mail
NE Pacific	SST	23.8	5		SCT	Fax/Mail
Northern Hemisphere	SST	190.5	2	Every Other Day	CRM***	GTS/Mail
Southern Hemisphere	SST	190.5	2		CRM	GTS/Mail
NW Atlantic	17.5°C		14	Weekly	Subjec-tive	Fax/Mail

*The grid is based on a polar stereographic projection which is true at 60°N.

**SCT - Successive correction technique

***CRM - Conditional relaxation method

ANALYSIS PROCEDURE

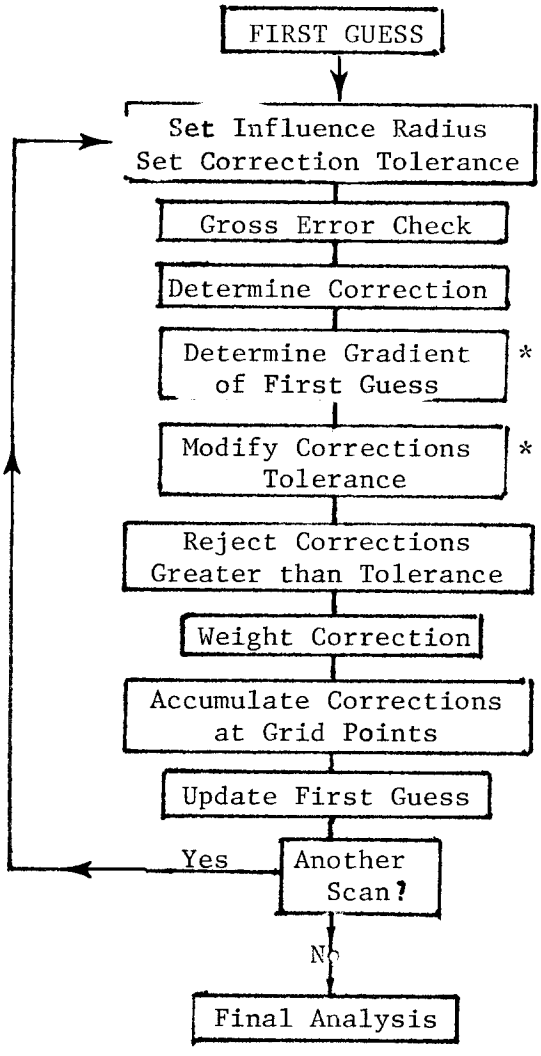

Figure 1. Flow Diagram of Regional Analyses

*Correction Tolerance modified only in high gradients region of the Gulf Stream.

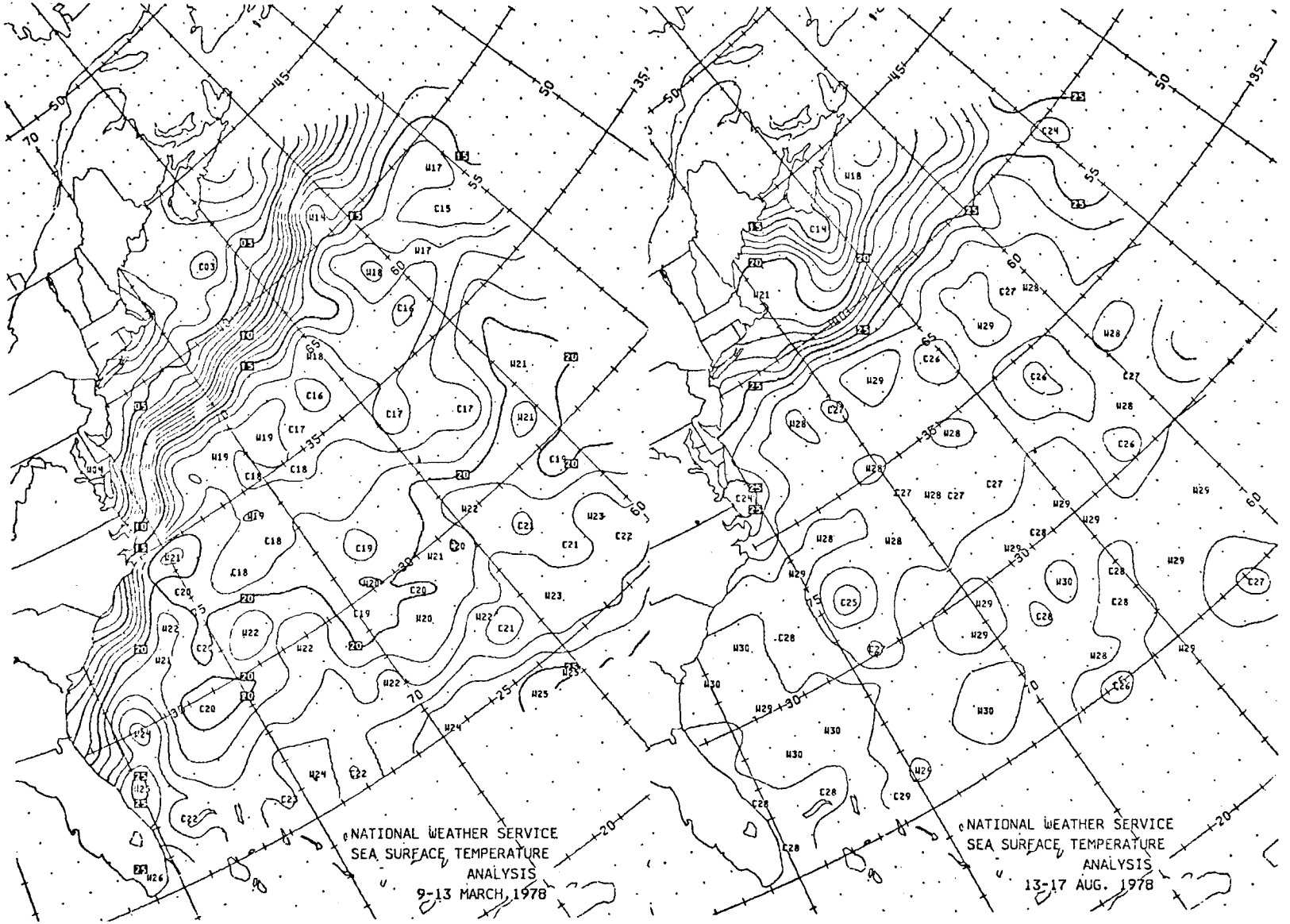

(a) (b)

Figure 2. Northwest Atlantic Analysis

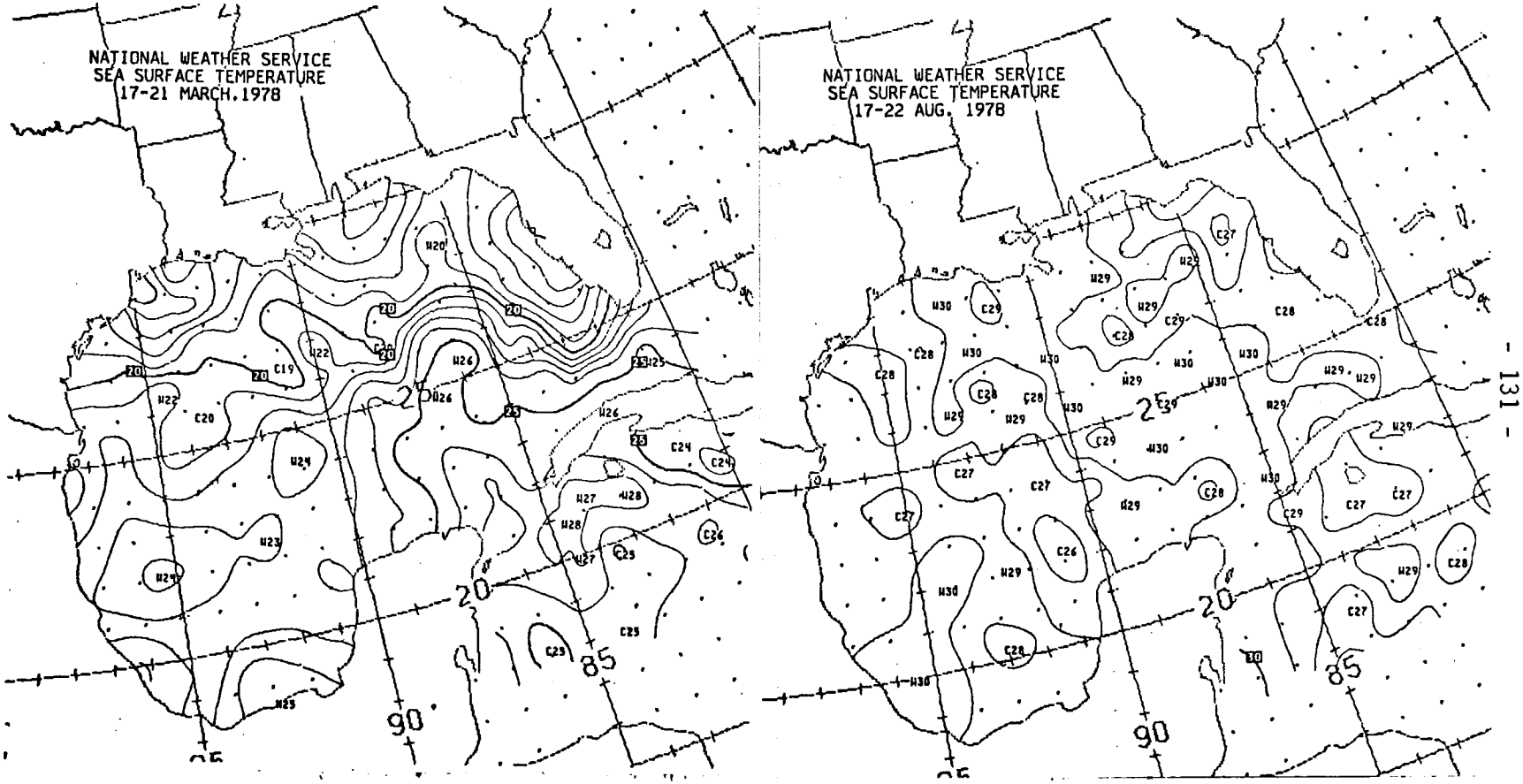

(a) (b)

Figure 3. Gulf of Mexico Analysis

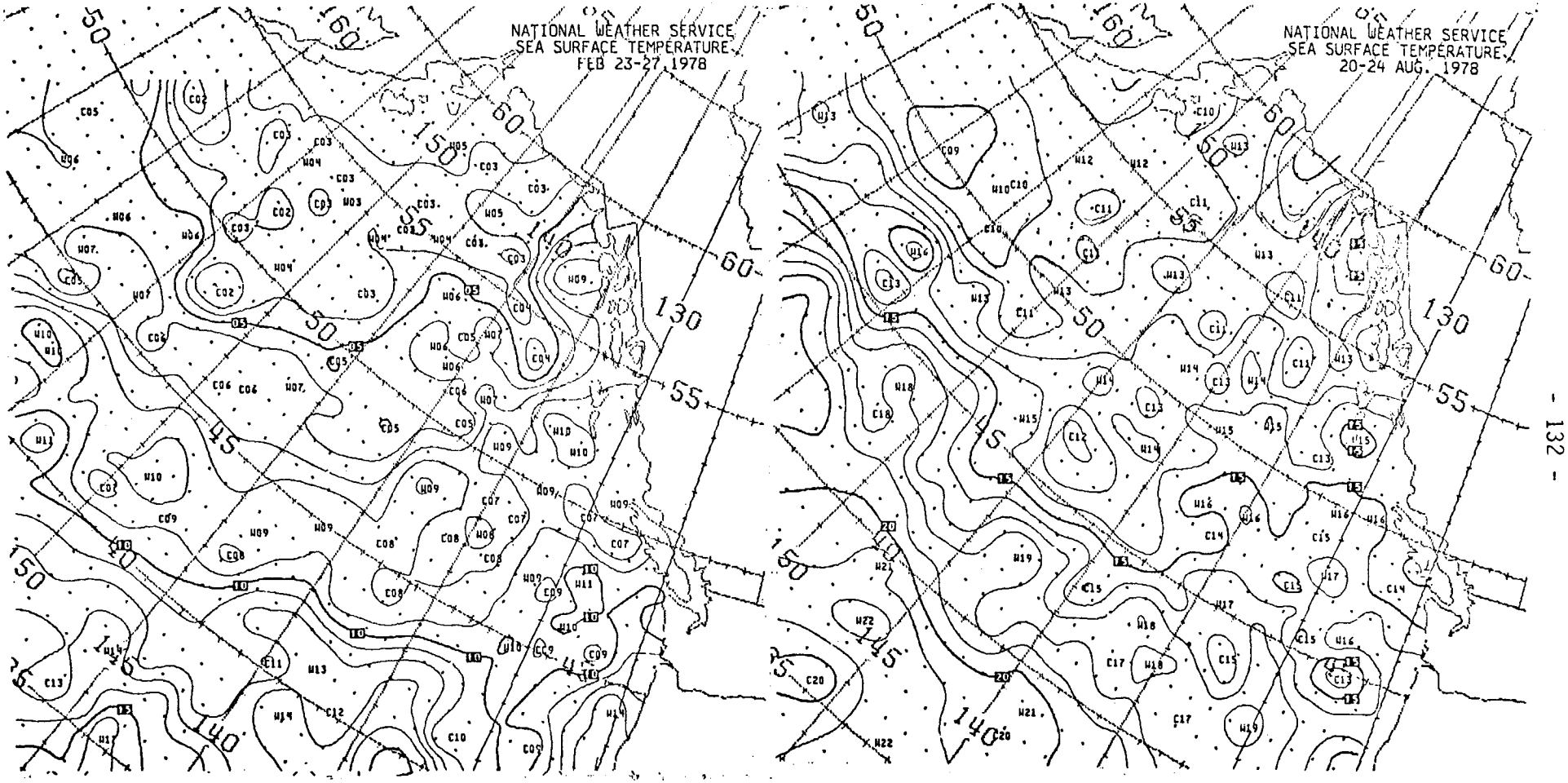

(a) (b)

Figure 4. Gulf of Alaska Analysis

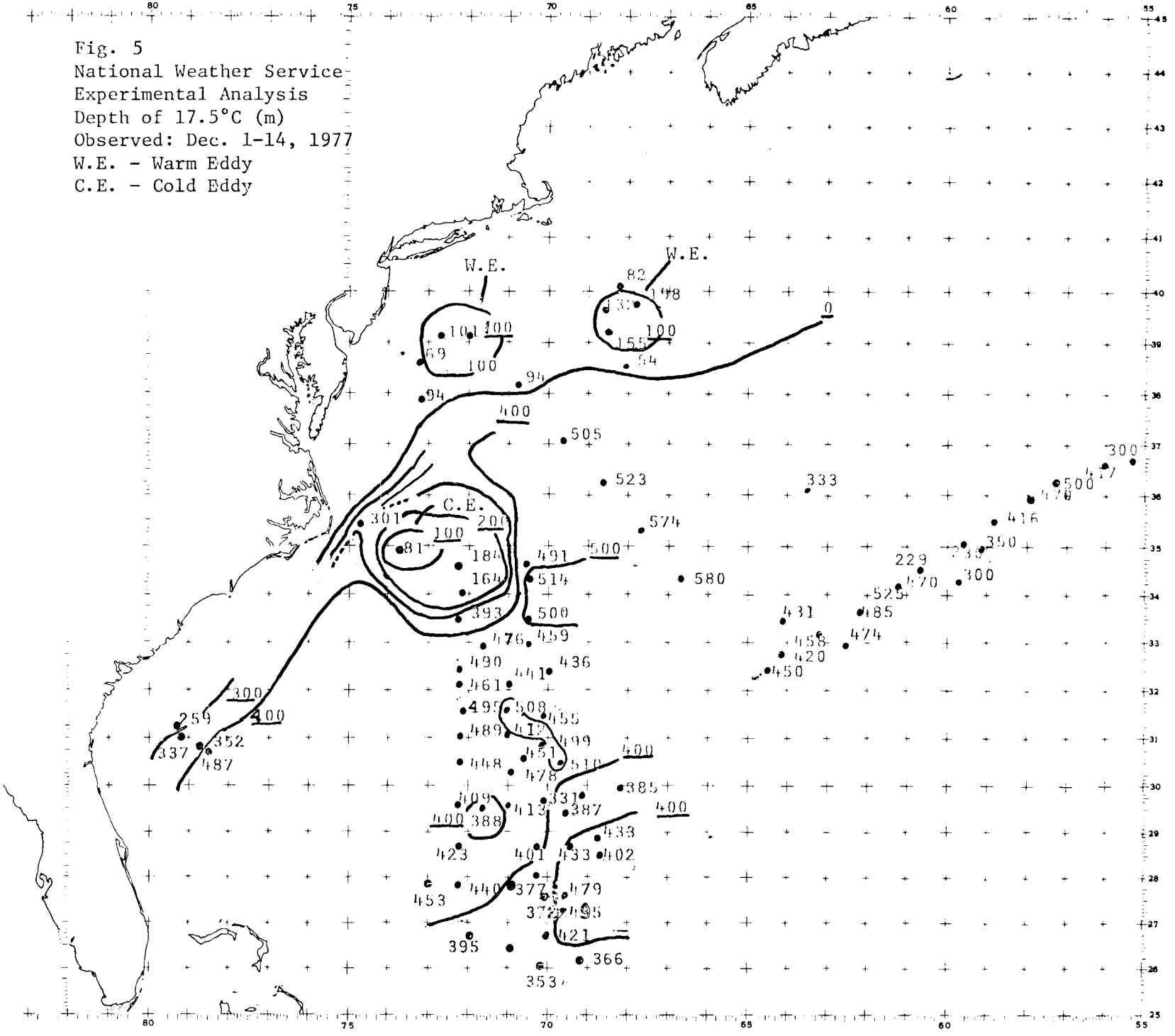

Fig. 5
National Weather Service
Experimental Analysis
Depth of 17.5°C (m)
Observed: Dec. 1-14, 1977
W.E. - Warm Eddy
C.E. - Cold Eddy

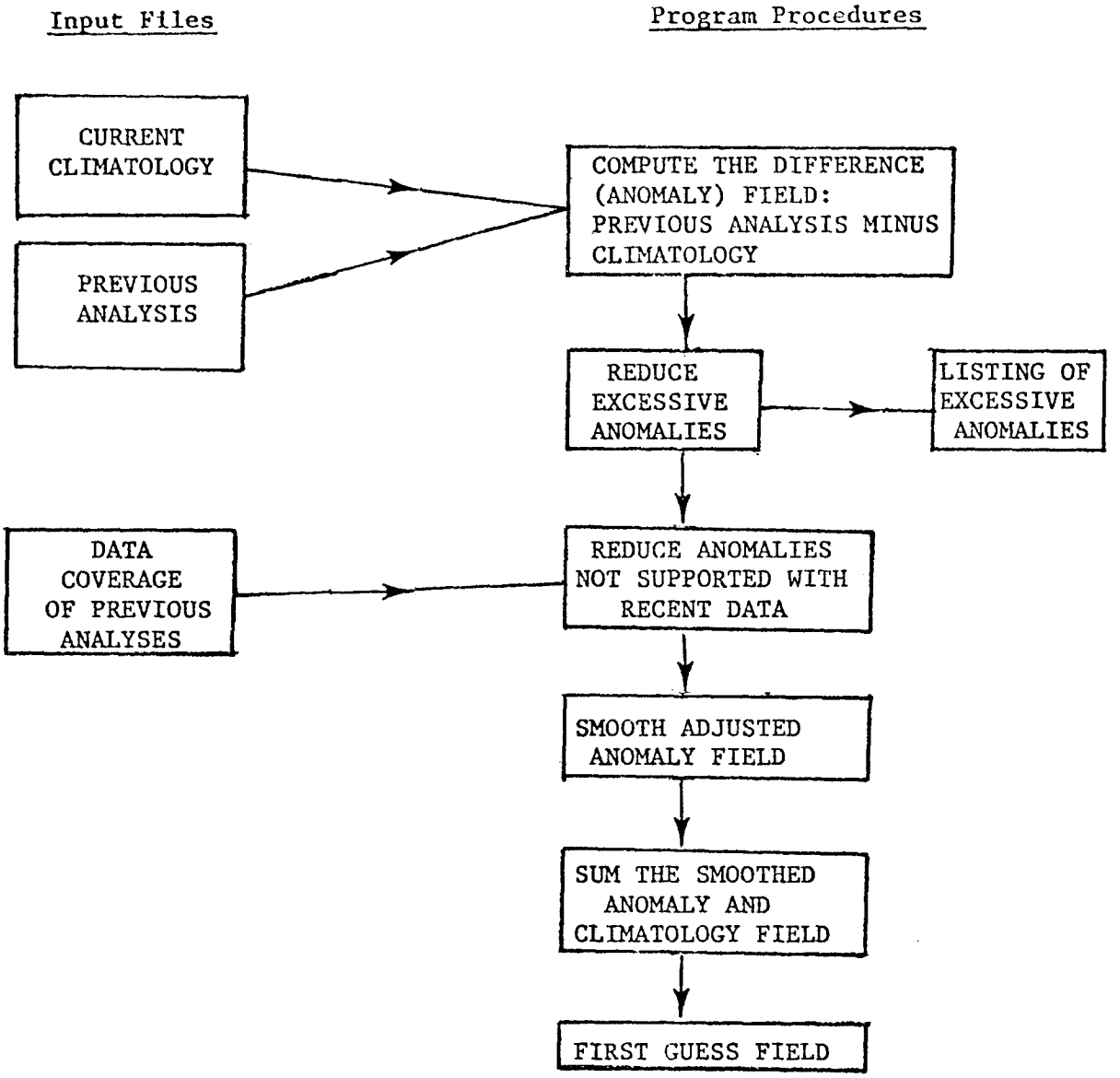

Figure 6. FLOW DIAGRAM OF THE FIRST GUESS STEP

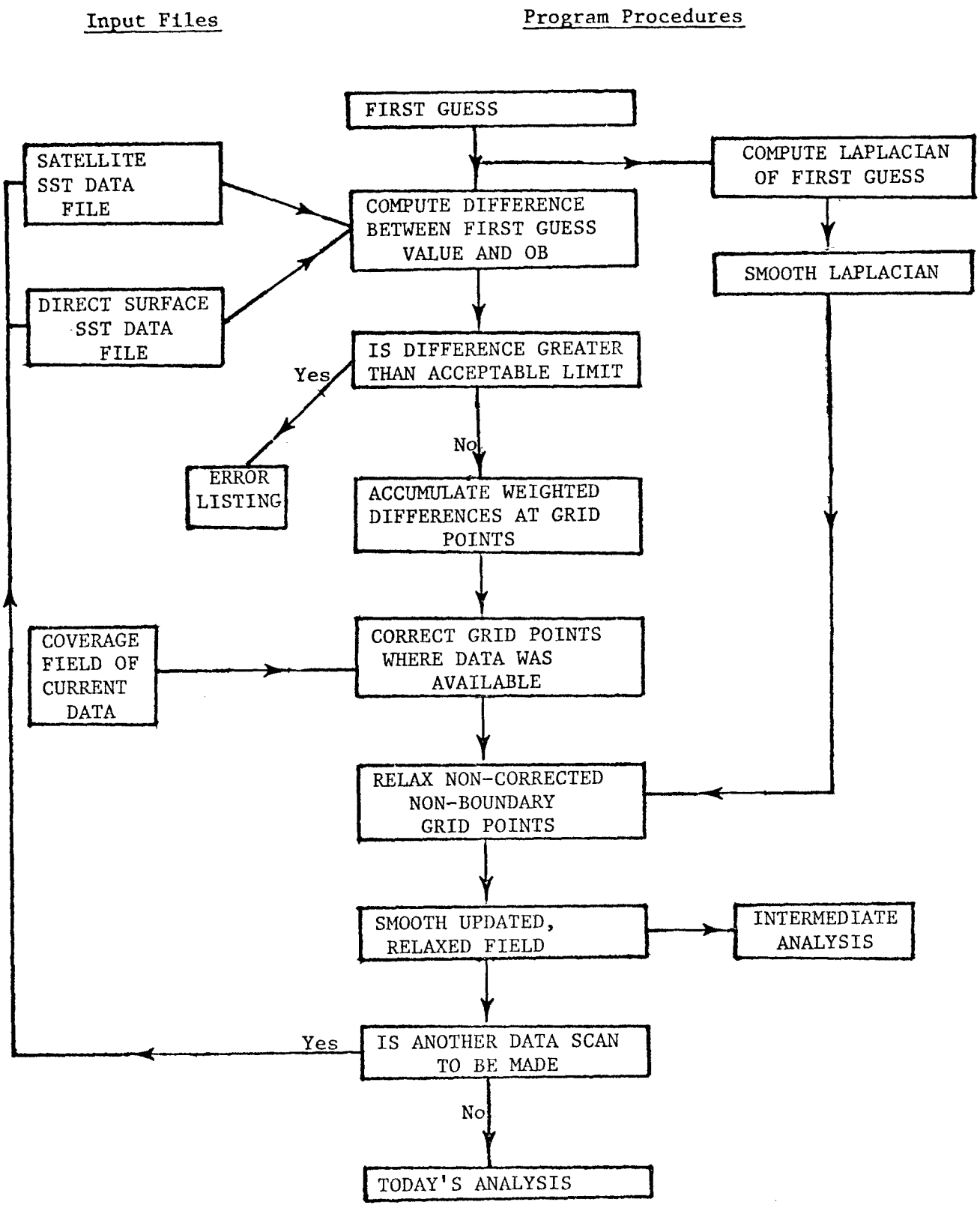

Figure 7.FLOW DIAGRAM OF ANALYSIS STEP

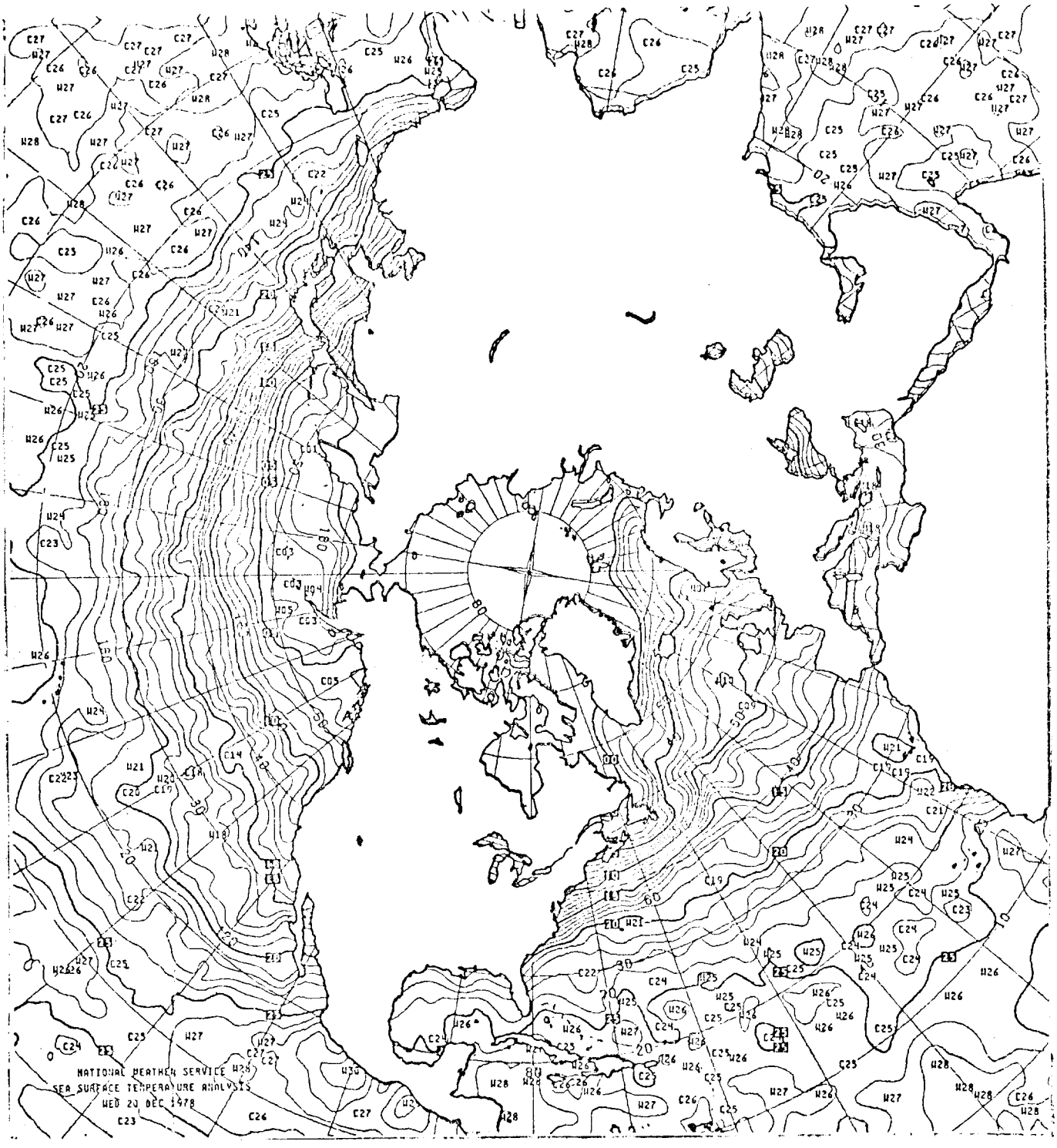

Figure 8. Northern Hemisphere Analysis

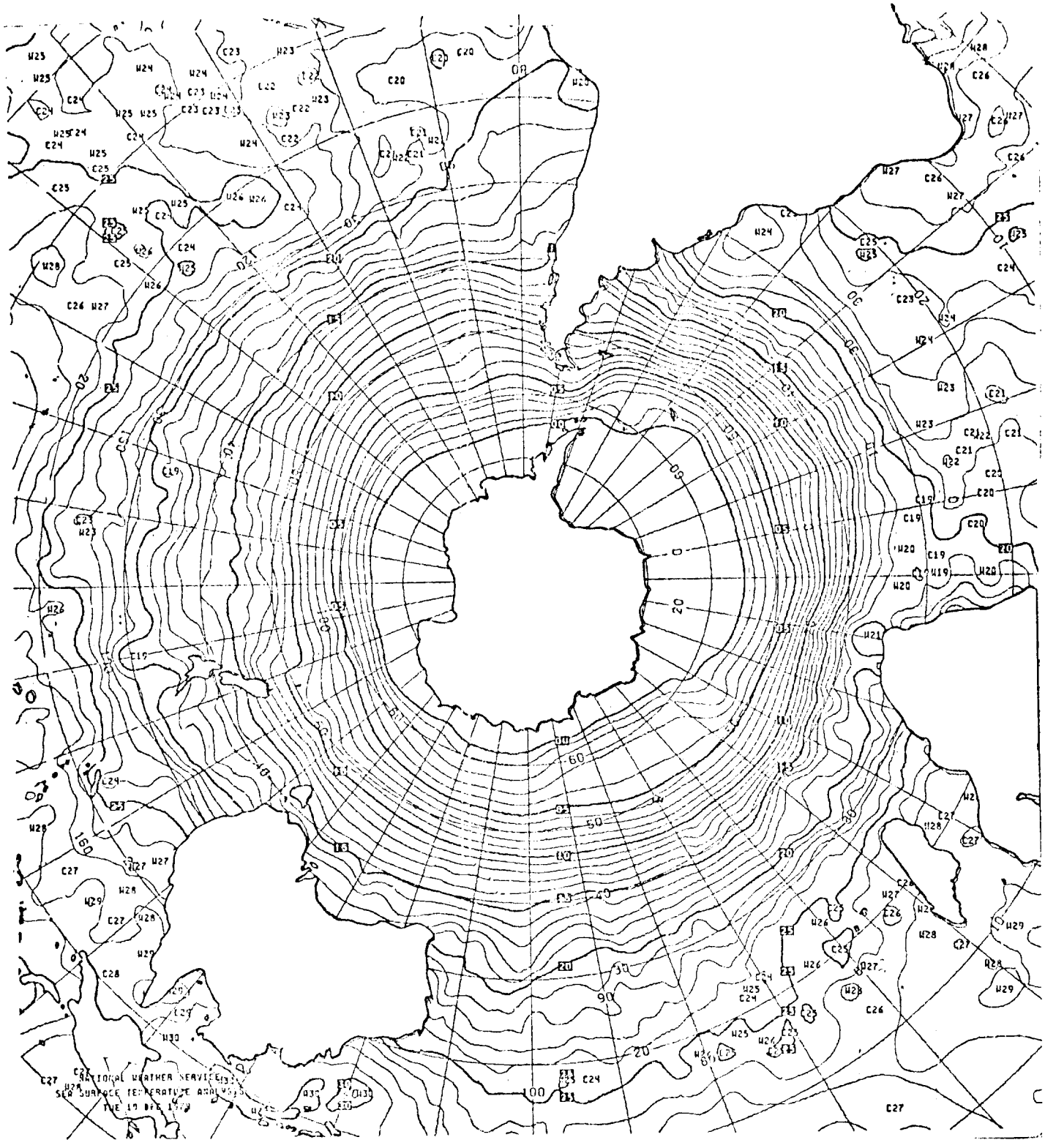

Figure 9. Southern Hemisphere Analysis

```
**** STATISTICS FOR NORTHERN HEMISPHERE   SURFACE    DATA FOR 20 DEC  1976 ****
     PASS NO.  1 WITH ACCEPTANCE WINDOW =   2.75 DEGREES

NO. OF   SURFACE SHIP REPORTS     3772 ...NO. ACCEPTED =  3263 .....% = 86.51
        ******** ANALYSIS OF DIFFERENCES (OBS - FIRST GUESS)  **********

        MEAN DIFFERENCE     =  0.13
        STANDARD DEVIATION  =  2.62
        SKEWNESS            = -1.39
        KURTOSIS            = 22.56

        ***** RANGE = 49.87 ..... MAX = 24.89 ..... MIN =-24.98
        % POSITIVE = 58.70 ..... % NEGITIVE = 41.30

        FREQUENCY DISTRIBUTION..... NO.  LESS THAN -10.00 =    28 .... % =  0.74
                                    NO. BETWEEN -10.00 AND  -8.00 =    17 .... % =  0.45
                                    NO. BETWEEN  -8.00 AND  -6.00 =    29 .... % =  0.77
                                    NO. BETWEEN  -6.00 AND  -5.00 =    21 .... % =  0.56
                                    NO. BETWEEN  -5.00 AND  -4.00 =    52 .... % =  1.38
                                    NO. BETWEEN  -4.00 AND  -3.00 =    74 .... % =  1.96
                                    NO. BETWEEN  -3.00 AND  -2.00 =   148 .... % =  3.92
                                    NO. BETWEEN  -2.00 AND  -1.50 =   141 .... % =  3.74
                                    NO. BETWEEN  -1.50 AND  -1.00 =   213 .... % =  5.65
                                    NO. BETWEEN  -1.00 AND  -0.75 =   154 .... % =  4.08
                                    NO. BETWEEN  -0.75 AND  -0.50 =   193 .... % =  5.12
                                    NO. BETWEEN  -0.50 AND  -0.25 =   229 .... % =  6.07
                                    NO. BETWEEN  -0.25 AND   0.0  =   259 .... % =  6.87
                                    NO. BETWEEN   0.0  AND   0.25 =   282 .... % =  7.48
                                    NO. BETWEEN   0.25 AND   0.50 =   255 .... % =  6.76
                                    NO. BETWEEN   0.50 AND   0.75 =   280 .... % =  7.42
                                    NO. BETWEEN   0.75 AND   1.00 =   240 .... % =  6.36
                                    NO. BETWEEN   1.00 AND   1.50 =   406 .... % = 10.76
                                    NO. BETWEEN   1.50 AND   2.00 =   275 .... % =  7.29
                                    NO. BETWEEN   2.00 AND   3.00 =   273 .... % =  7.24
                                    NO. BETWEEN   3.00 AND   4.00 =    96 .... % =  2.55
                                    NO. BETWEEN   4.00 AND   5.00 =    47 .... % =  1.25
                                    NO. BETWEEN   5.00 AND   6.00 =    20 .... % =  0.53
                                    NO. BETWEEN   6.00 AND   8.00 =    18 .... % =  0.48
                                    NO. BETWEEN   8.00 AND  10.00 =    11 .... % =  0.29
                                       NO. GREATER THAN    10.00 =    11 .... % =  0.29
```

Figure 10. Statistical Summary of Surface Ship Reports

**** STATISTICS FOR NORTHERN HEMISPHERE SATELLITE DATA FOR 29 DEC 1978 ****

PASS NO. 1 WITH ACCEPTANCE WINDOW = 1.55 DEGREES

NO. OF SATELLITE RETRIVALS 5334 ...NO. ACCEPTED = 3319 .....% = 62.22

******** ANALYSIS OF DIFFERENCES (OBS - FIRST GUESS) **********

MEAN DIFFERENCE = -1.06
STANDARD DEVIATION = 1.45
SKEWNESS = -0.10
KURTOSIS = 3.40

***** RANGE = 10.93 ..... MAX = 5.19 ..... MIN = -5.74
% POSITIVE = 22.55 ..... % NEGITIVE = 77.45

FREQUENCY DISTRIBUTION.....								
NO.	LESS THAN	-10.00	=	0	....	%	=	0.0
NO.	BETWEEN	-10.00 AND -8.00	=	0	....	%	=	0.0
NO.	BETWEEN	-8.00 AND -6.00	=	0	....	%	=	0.0
NO.	BETWEEN	-6.00 AND -5.00	=	29	....	%	=	0.54
NO.	BETWEEN	-5.00 AND -4.00	=	117	....	%	=	2.19
NO.	BETWEEN	-4.00 AND -3.00	=	377	....	%	=	7.07
NO.	BETWEEN	-3.00 AND -2.00	=	763	....	%	=	14.30
NO.	BETWEEN	-2.00 AND -1.50	=	619	....	%	=	11.60
NO.	BETWEEN	-1.50 AND -1.00	=	762	....	%	=	14.29
NO.	BETWEEN	-1.00 AND -0.75	=	385	....	%	=	7.22
NO.	BETWEEN	-0.75 AND -0.50	=	381	....	%	=	7.14
NO.	BETWEEN	-0.50 AND -0.25	=	349	....	%	=	6.54
NO.	BETWEEN	-0.25 AND 0.0	=	349	....	%	=	6.54
NO.	BETWEEN	0.0 AND 0.25	=	320	....	%	=	6.00
NO.	BETWEEN	0.25 AND 0.50	=	241	....	%	=	4.52
NO.	BETWEEN	0.50 AND 0.75	=	171	....	%	=	3.21
NO.	BETWEEN	0.75 AND 1.00	=	137	....	%	=	2.57
NO.	BETWEEN	1.00 AND 1.50	=	150	....	%	=	2.81
NO.	BETWEEN	1.50 AND 2.00	=	99	....	%	=	1.86
NO.	BETWEEN	2.00 AND 3.00	=	64	....	%	=	1.20
NO.	BETWEEN	3.00 AND 4.00	=	13	....	%	=	0.24
NO.	BETWEEN	4.00 AND 5.00	=	5	....	%	=	0.09
NO.	BETWEEN	5.00 AND 6.00	=	3	....	%	=	0.06
NO.	BETWEEN	6.00 AND 8.00	=	0	....	%	=	0.0
NO.	BETWEEN	8.00 AND 10.00	=	0	....	%	=	0.0
NO.	GREATER THAN	10.00	=	0	....	%	=	0.0

Figure 11. Statistical Summary of Satellite Data

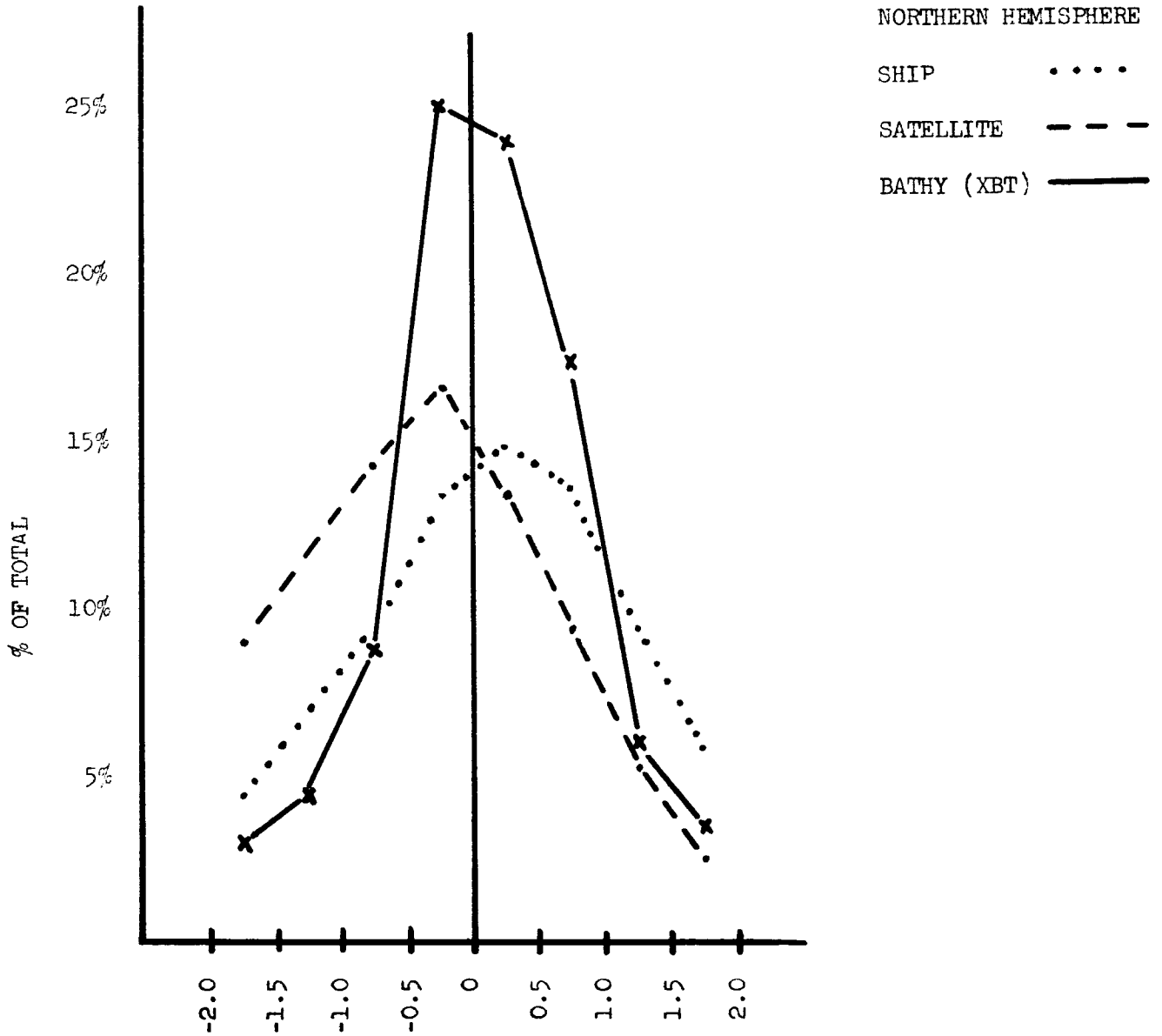

Figure 12. DIFFERENCE BETWEEN REPORT AND 1st GUESS

FREQUENCY DISTRIBUTION OF REPORTS BETWEEN 7NOV.-17NOV.

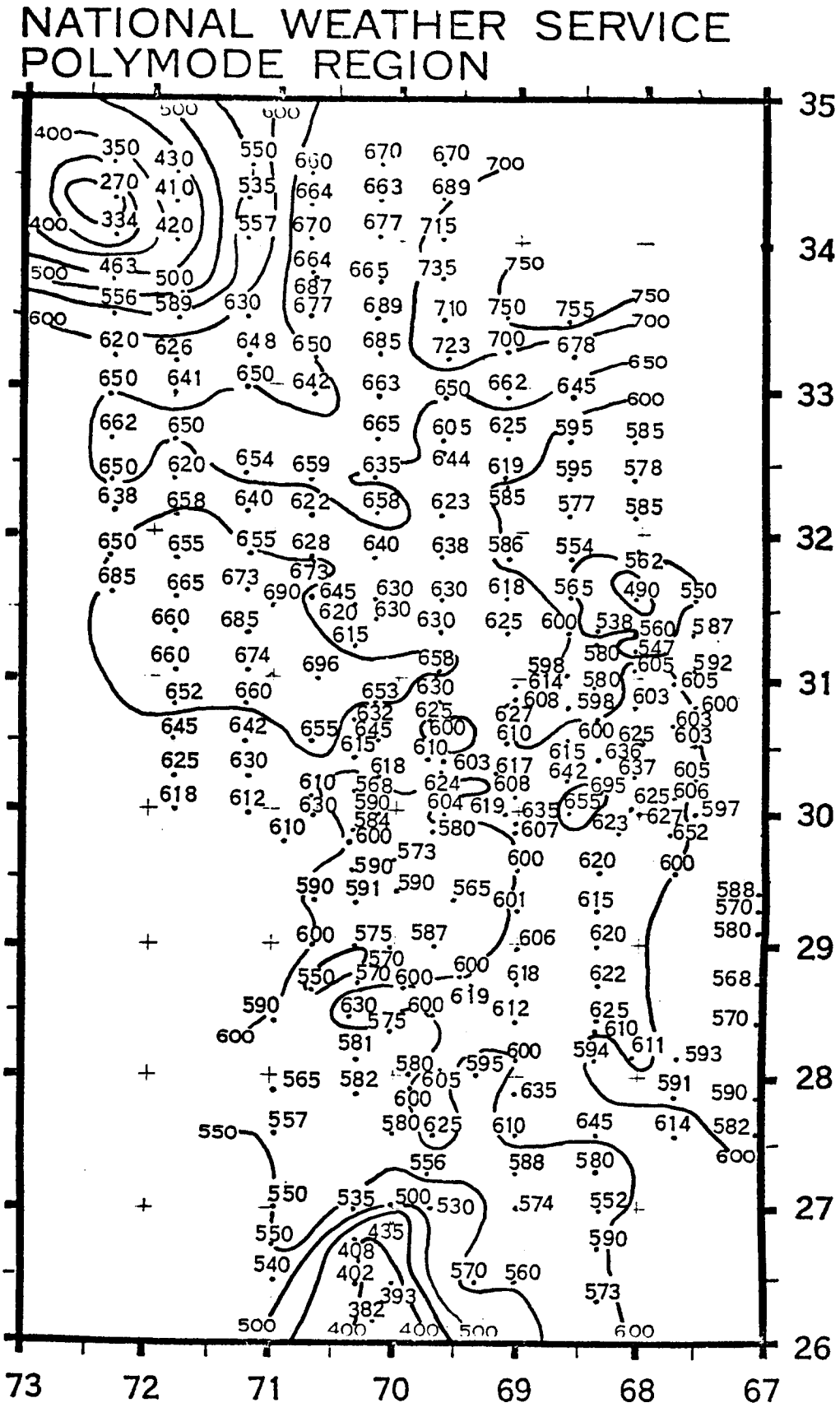

Figure 13. Depth of 15°C Isotherm Analysis
December 10-22,1977

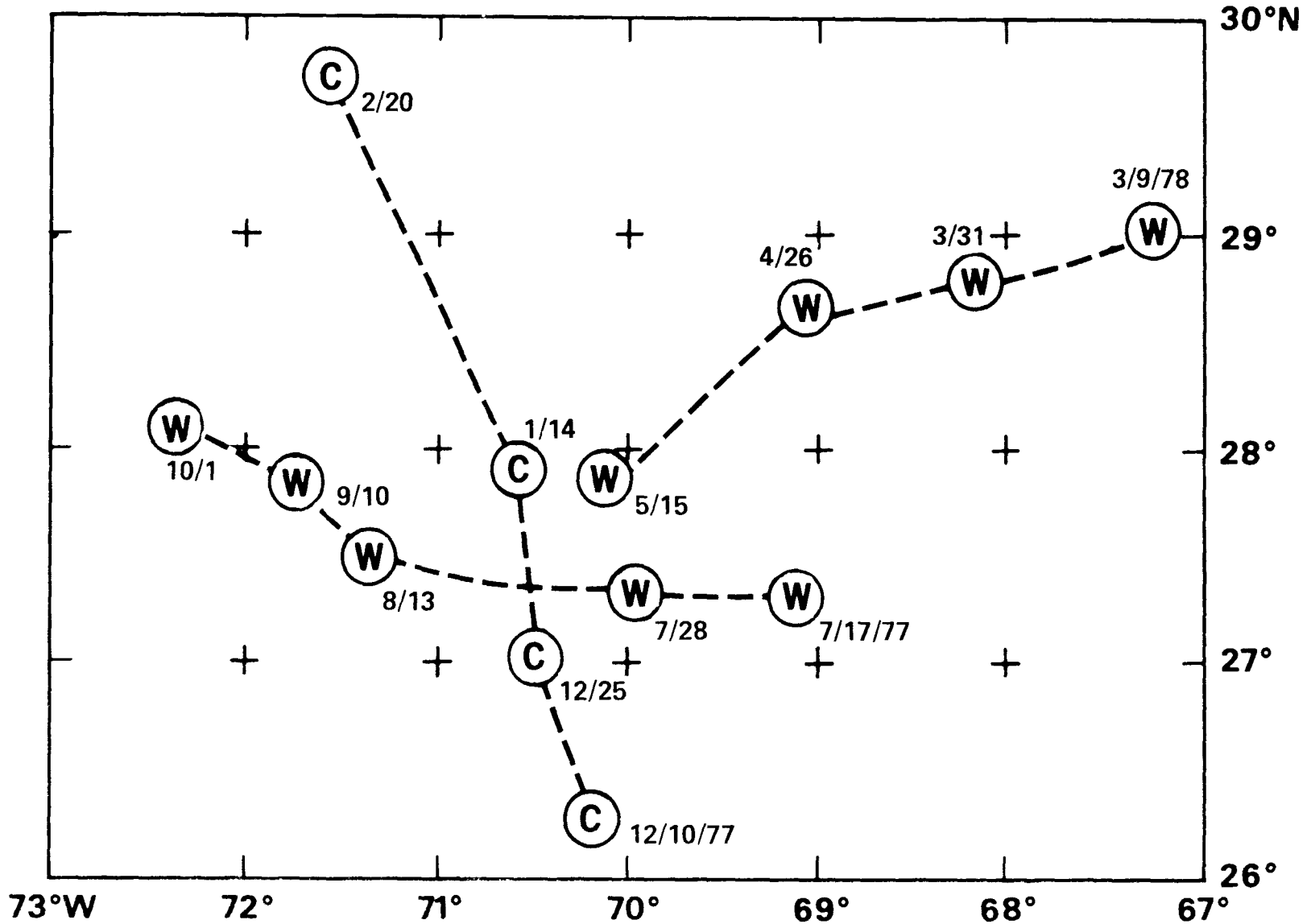

Figure 14. Tracks of major warm (W) and cold (C) eddies identified using BATHY data submitted via radio during POLYMODE to the National Weather Service. Eddy locations for each date were determined by depth of the 15°C isotherm.

LOCATION OF OCEANIC FRONTS FROM DIGITAL SATELLITE TEMPERATURE DATA BY AUTOMATED PATTERN ANALYSIS

BY

D. GERSON, E. KHEDOURI, AND P. GABORSKI

U. S. NAVAL OCEANOGRAPHIC OFFICE
NSTL STATION
BAY ST. LOUIS, MISSISSIPPI 39522

1. INTRODUCTION

Detailed charts of major oceanic fronts, such as the Gulf Stream, are presently prepared on a regular basis by professional oceanographers using satellite imagery as a prime source of data. Use of automation is primarily for enhancement of imagery to visually aid the analyst in his interpretation effort. Fully automated products have until now been oriented toward large area temperature analyses which tend to smooth out fronts rather than detect them.

The purpose of this paper is to describe an objective, fully automated procedure, for locating ocean fronts and other major ocean features from satellite imagery. The proposed procedure consists mainly of imagery pattern recognition methods such as those described by Haralick et al. (1973), Duda and Hart (1973), and Gerson (1975). The pattern recognition features used for frontal identification are automatically evaluated for their effectiveness, and the best feature set is then selected for a particular case. Because an infinite number of potential pattern recognition features exist, an exhaustive study is impossible. The features tested, however, are relatively complete and their evaluation clearly indicates the most useful ones.

2. DATA

Digital infra-red data from the GOES II (Geostationary Operational Environmental Satellite) were used for this study. A sample of the full disc image is shown in figure 1. Five such pictures are available daily in digital form on magnetic tape. The satellite is centered at the equator and 75°W and covers an area of approximately 89° of latitude and 99° of longitude. The spatial resolution is approximately 8 km; that is, each pixel (picture element) represents the average temperature over an 8 x 8 km square on earth surface. There are 256 gray scales for each pixel; when converted to temperatures, they cover a range from -110.2°C to +56.8°C. It is, therefore, possible to truncate both the high and low ends without affecting the temperature resolu-

tion and obtain a useful temperature range of approximately 32°C.

A package of computer programs known as XAP was used for manipulating the satellite pictures. Details are described in Hayes (1975). These programs facilitate operations such as: selecting an area of specified size from a picture, adding, subtracting or algebraically combining pictures, etc. These programs were very important in developing the techniques for this project.

3. CLOUD REDUCTION

Clouds present a problem in automated frontal detection as they do in the manual operation. A technique has been developed, however, to reduce their effect. In the Gulf Stream region, clouds are almost always colder than water. We can, therefore, select a temperature threshold and identify clouds; but this gives no information about the sea surface temperatures below. Fortunately clouds move much more rapidly than sea surface features. We can, therefore, reduce clouds by overlaying several daily pictures and compositing them by selecting the warmest temperature at each point. Using this method we have been able to remove the clouds entirely in many pictures or reduce them substantially. When the clouds are extremely persistent, we can extend the overlay process to several days. This latter process may degrade the results because corresponding points can represent temperatures from different days but it has produced useable images from very poor data. A similar technique has been successfully applied by Waters and Baig (1977).

A sample picture from February 26, 1977, is shown in figure 2 and a composite picture, produced from five images for that day, is shown in figure 3. It can be seen that a substantial amount of clouds were removed by this method. In this case, a sizable segment of the Gulf Stream seen on the composite picture, was not evident in any of the individual images. Note that these pictures are actually computer printouts, and the shading is produced by over-printing letters. The quality of the pictures is immaterial because the final results are not dependent on visual effects. These type pictures are only used to examine some interim results.

The disadvantage of the above method is that sometimes cold features embedded in warm water, such as cold eddies, become suppressed because compositing consists of selecting the warmest temperature from each picture and it is, therefore, possible for a cold eddy to be masked because of afternoon heating. To avoid this problem the above method can be supplemented in the following manner. Each point identified as a cloud, is set to maximum temperature in every picture. The pictures are then composited using minimum temperature at each point. In this method the cold features are accentuated rather than suppressed.

4. PATTERN RECOGNITION

Once a relatively cloud free picture is produced, it is subdivided into overlapping 16 x 16 pixel (approximately 128 x 128 km) frames and each frame is evaluated in sequences shown in the hierarchical decision tree depicted in figure 4. The first step is to decide whether a frame, because of its geographical position, could possibly contain the Gulf Stream; this is done by using a priori knowledge about Gulf Stream location and movement. The next step is to examine the promising frames and decide whether they do, in fact, contain the Stream; this is done by water mass classification. Development of a classification scheme for this step was the major experimental effort and involved the use of pattern recognition techniques including decision theory necessary to evaluate and implement the classification scheme. The third step in the decision tree is pixel evaluation. In this step, each pixel within the frames which are known to contain the Stream, is evaluated to pin-point the exact frontal location.

Step 1 - A Priori Frame Selection.

Because the historical geographical boundaries of the Gulf Stream are known, we can simply eliminate all the frames which are outside those boundaries. Similarly, by knowing the previous position of the front, and knowing the maximum possible fluctuation within the time period involved, we can further eliminate frames which could not possibly contain the Gulf Stream. Figure 5 shows the frames which are selected after eliminating all the frames which could not possibly contain the front.

Step 2 - Frame Evaluation.

Several statistical features were evaluated to decide which of the frames selected in step 1, do in fact, contain the Stream. The statistical features were evaluated for their ability to classify imagery into three classes: (1) Gulf Stream Water; (2) Slope Water (water north and west of the Gulf Stream); and (3) Sargasso Water (water south and east of the Stream). To evaluate the ability of a particular statistical feature to accomplish the above, Fisher's linear discriminant was used. The choice was based on its computational simplicity and availability of computer programs.

(a) Fisher's Linear Discriminant

A complete discussion of the discriminant is given in Duda and Hart (1973). The method can briefly be described as follows. Suppose we have two classes (crosses and circles) as shown in figure 6. If the samples are projected onto a correctly oriented line, there will be a good separation between the clusters, but if they are projected onto an arbitrary line, the separation will not be evident. To evaluate a pattern being tested, it is necessary to know how well

the clusters of data projected onto a correctly oriented line are separated. The best statistical features are those which result in greatest separation between classes and smallest dispersion within a class. A convenient measure for the above two criteria is the Fisher distance (FD) defined as follows:

$$FD_{1,2} = \frac{|M_1 - M_2|}{S_1 - S_2}$$

where M_1 and M_2 are the mean values of the projected points and S_1 and S_2 are the standard deviations. The statistical features giving the largest Fisher distance for two classes, will be taken to be the best statistics to discriminate between those two classes. The minimum error classification into two classes is obtained using the threshold value (T) defined as follows:

$$T_{1,2} = \frac{M_1 S_2 + M_2 S_1}{S_1 + S_2}$$

all points falling on one side of T are identified with one class, while those on the other side are identified with the second class.

(b) Statistical Features

Statistical features evaluated by Fisher's discriminant for this study are summarized in table 1. Complete description of each statistic is given in Gerson and Gaborski (1977), a brief description is as follows:

Mean and Standard Deviation - Two very simple, though sometimes very effective, statistics are mean and standard deviation of the temperature values. These statistics should give good results in separating Slope Water from Sargasso Water where there is a consistent difference in temperatures between the water masses and small variation in temperature within the water masses.

Histogram Analysis - Examination of histograms of frames containing the Gulf Stream, shows that skewness changes from positive to negative as the Gulf Stream is crossed from east to west. Skewness measures the asymmetrical distortion about the mean.

Power Spectrum - If a picture is considered to be a function of two variables, its Fourier transform can be obtained and thus its power spectrum. The power spectrum plot of a picture shows the low frequencies, such as flat unchanging areas, near the center of the plot. Any high frequencies such as sharp edges or rapidly changing temperatures would appear further from the center.

TABLE 1

STATISTICS USED FOR WATER MASS CLASSIFICATION

Mean

Standard Deviation

Histogram Analysis

Power Spectrum Analysis

Co-occurrence Matrix Analysis

(1) Angular Second Moment
(2) Contrast
(3) Correlation
(4) Entropy

Gradient Statistics
Mean and Standard Deviation of:

(1) Horizontal differences
(2) Vertical differences
(3) Maximum differences

Difference Histogram

(1) Mean
(2) Contrast
(3) Angular Second Moment
(4) Entropy
(5) Maximum
(6) Mode
(7) Inverse Difference Moment

Co-occurrence Matrix Analysis - A useful method for examining the texture of a picture is to study the co-occurrence of temperature values. A co-occurrence matrix is an ordered arrangement of the frequencies with which the various possible temperatures occur adjacent to, or at some fixed distance from one another. Four types of matrices are formed depending on the direction of the adjacency: horizontal, vertical, left diagonal, and right diagonal. These matrices can be analyzed using several statistics. Four features selected in this case were: angular second moment, contrast, correlation, and entropy. For a complete discussion see Haralich et al. (1973).

Gradient Analysis - An analysis of gradients in a picture can provide information which may be useful in classification. Gradient statistics computed were: mean and standard deviation of horizontal, vertical, and maximum differences.

Difference Histograms - Another set of features selected were difference histogram statistics. Difference histograms, similar to co-occurrence matrices, measure the frequency with which temperature differences occur adjacent to or at a fixed distance between pixels. These histograms can be computed over four directions: horizontal, vertical, right diagonal, and left diagonal. Seven statistics were generated from these difference histograms: mean, contrast, angular second moment, entropy, maximum, mode and inverse difference moment.

(c) Results

The above statistics were applied to experimental data consisting of 85 samples which were classified by an experienced analyst into three classes: Gulf Stream, Sargasso Water, and Slope Water. Fisher distances and classification error rates were calculated for all the statistical features and are given in Gerson and Gaborski (1977). Statistics giving the best results (greatest Fisher distances and smallest error rates) are summarized in Table 2. The statistic "mean" gave the best results with Fisher distance of 2.08 and an error rate of 2 percent for classifying Stream and Slope Water. The implication is that the two water masses have consistently different temperatures. Several statistics gave good results in separating Stream and Sargasso waters. The best was "difference histogram maximum entropy" which gave a Fisher distance of 1.78 and error rate of 2 percent. "Standard deviation" gave a Fisher distance of 1.76 and zero error rate. Finally for separation of Sargasso and Slope Waters, statistic "mean" gave a Fisher distance of 2.84 and zero error rate. This is obviously hard to surpass, but several of the difference histogram features also gave high Fisher distances and low error rates.

While it should be technically correct to test all possible pairs and

TABLE 2

SAMPLE OF BEST CLASSIFICATION STATISTICS

WATER MASSES	STATISTIC	FISHER DISTANCE	PERCENT ERROR
Gulf Stream vs. Slope	Mean	2.08	2
Gulf Stream vs. Sargasso	Difference Histogram Maximum Entropy	1.78	2
	Standard Deviation	1.76	0
Sargasso vs. Slope	Mean	2.84	0

triplets of features, computational limits preclude such extensive tests. Several of the most promising pairs and triplets were tested, however, and the best results were obtained with triplet "mean", "standard deviation" and "difference histogram maximum entropy". The results gave 100 percent correct classification for all three water masses.

Once the best feature set is determined, it is applied to each frame previously tagged as "possibly containing Gulf Stream". Fisher's discriminant is then used for classifications. Results are depicted in figure 7, where each frame shown is now known to contain the Stream. This constitutes the second step in the hierarchical decision approach. To accomplish the third step, it is now necessary to locate the Stream within each frame by evaluating each pixel.

Step 3 - Pixel Evaluation

(a) Procedure

This step was successfully accomplished by scanning each frame with a 5 x 5 pixel square and applying some of the statistical features discussed previously. The scanning process is illustrated in figure 8. Of the statistics tested, it was found that skewness of the histogram which changes from negative to positive as the Gulf Stream is crossed from west to east gave the best results. The procedure developed and illustrated in figures 8 and 9 is as follows:

First, scan each 16 x 16 pixel frame using a 5 x 5 pixel square and calculate the histogram and skewness of the 25 points.

Next, set all positive values of skewness to '1' and all negative values to '0'. The result is the binary picture 9b obtained from 9a.

Finally, apply an edge detector to the binary picture. The edge detector puts a frame of 1's around the binary picture and then tests all internal 1's; if the 1's are situated next to 0's, they are edge points. Isolated or pairs of 0's in the binary picture are ignored since they would be surrounded by an edge. This procedure produced the edges shown in figure 9c from 9b.

(b) Results

The edge picture in figure 9c shows the northern and southern edges of the Gulf Stream. This completes all the steps in the hierarchical decision approach. The only remaining step is to connect the points from all the frames for the desired front. For example, if the location of the Gulf Stream northern edge is desired, all the edge points from the left side of every frame are connected

producing the result shown in figure 10.

5. DISCUSSIONS AND CONCLUSIONS

The results based on 85 samples show that it is possible to use an automated system to obtain frontal locations identical to those depicted by a trained analyst. Comparison of results with ground-truth from other sources of data would not be a meaningful test of the automated method because any discrepancy will include other errors inherent in satellite imagery which may give wrong frontal locations. Whether it is possible to improve on the manual method is a subject for future investigation. It is entirely possible, for example, that some surface manifestation of a front may not be readily apparent to the eye, but may respond to some statistics such as co-occurrence matrix analysis, which detect fine variations in the texture.

Although the statistical features derived here are applicable only to the Gulf Stream region, the proposed method has the inherent flexibility to be applied to any major front. Also the method is applicable if different criteria are used to determine what constitutes a front. In the case of the Gulf Stream, for example, the deep front is better correlated to maximum surface temperature than it is to the surface gradient as described by Khedouri et al. (1976). This could be built into the system by determining which statistical features will give best results for finding the front based on these criteria and revising the required threshold values for Fisher's discriminant.

The entire procedure described here could be implemented on any large computer. It could also be hard-wired on a small specialized computer or on a satellite computer. This of course is the subject of future work.

The following conclusions can be reached from work completed up to this point:

1) In the Gulf Stream region, clouds can be reduced or removed entirely by compositing several satellite pictures.

2) Fisher's linear discriminant is a simple and effective way to evaluate the statistical features for their ability to classify water masses.

3) The triplet composed of "mean", "standard deviation" and "difference histogram maximum entropy" resulted in 100 percent correct classification on the 85 test samples.

4) Change in skewness of the temperature histogram, from positive to negative as the Gulf Stream is crossed from east to west, is an effective statistical feature for determining the exact frontal location.

ACKNOWLEDGEMENTS

The authors acknowledge the efforts of Mr. M.K. Shank, Jr. and Dr. R.W. James for their administrative support and technical guidance; Mr. W. George for his assistance in computer programming; Mr. G. Voorheis for the final illustrations; and Mrs. L. Allen for preparation of the manuscript.

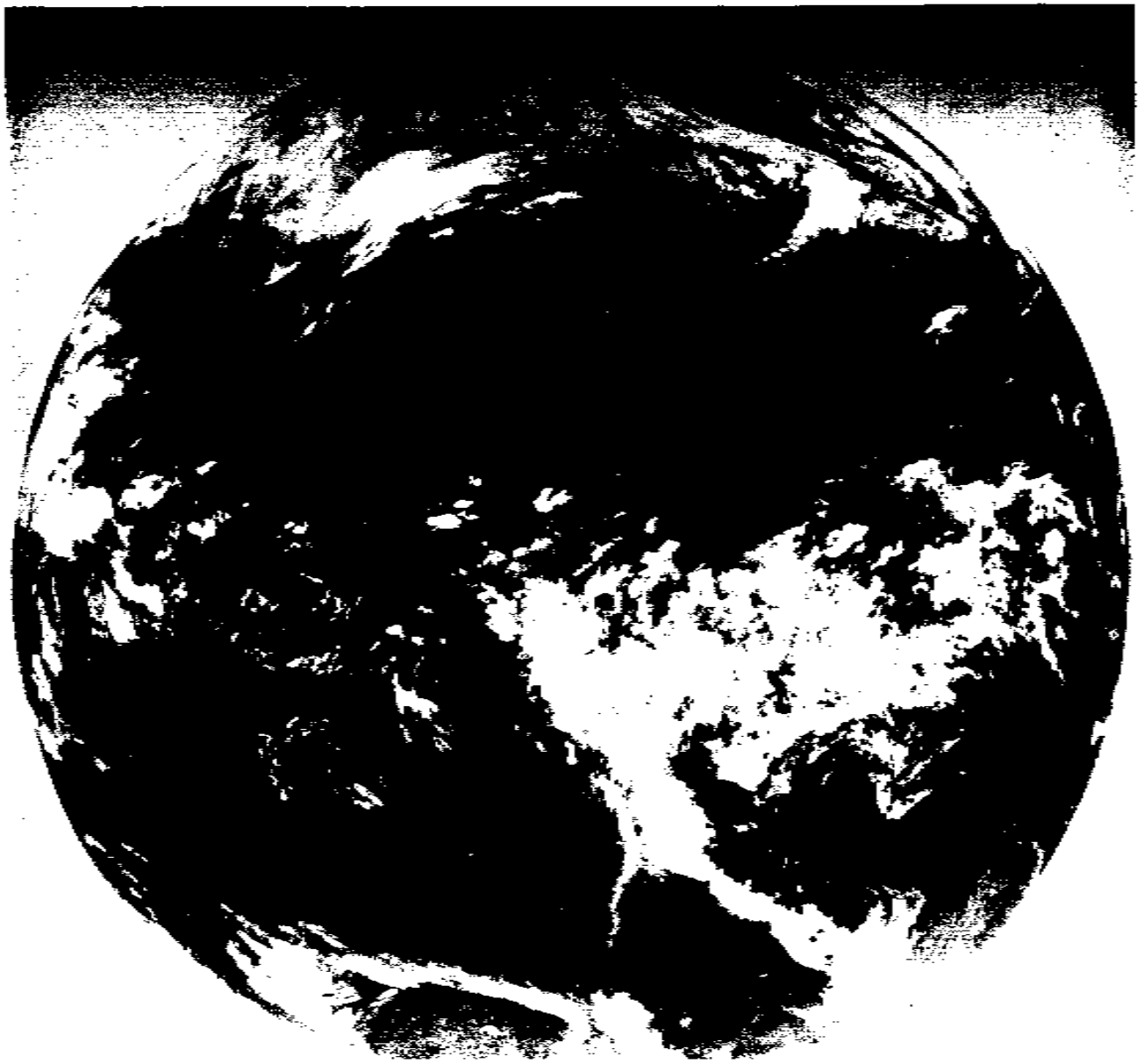

Figure 1. GOES SMS-2 infra-red image for 26 February 1977

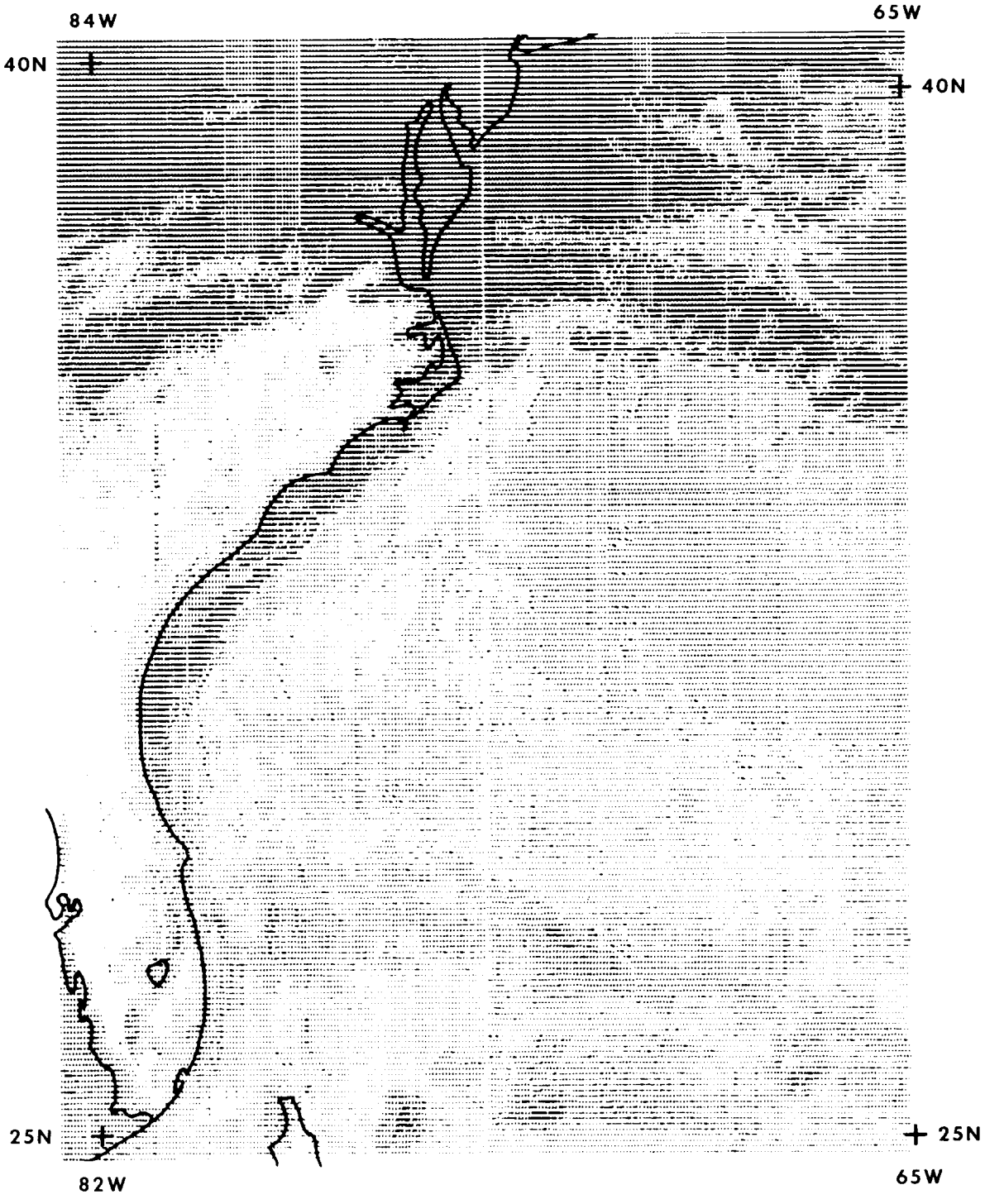

Figure 2. Sample picture produced from GOES digital data for 26 February 1977

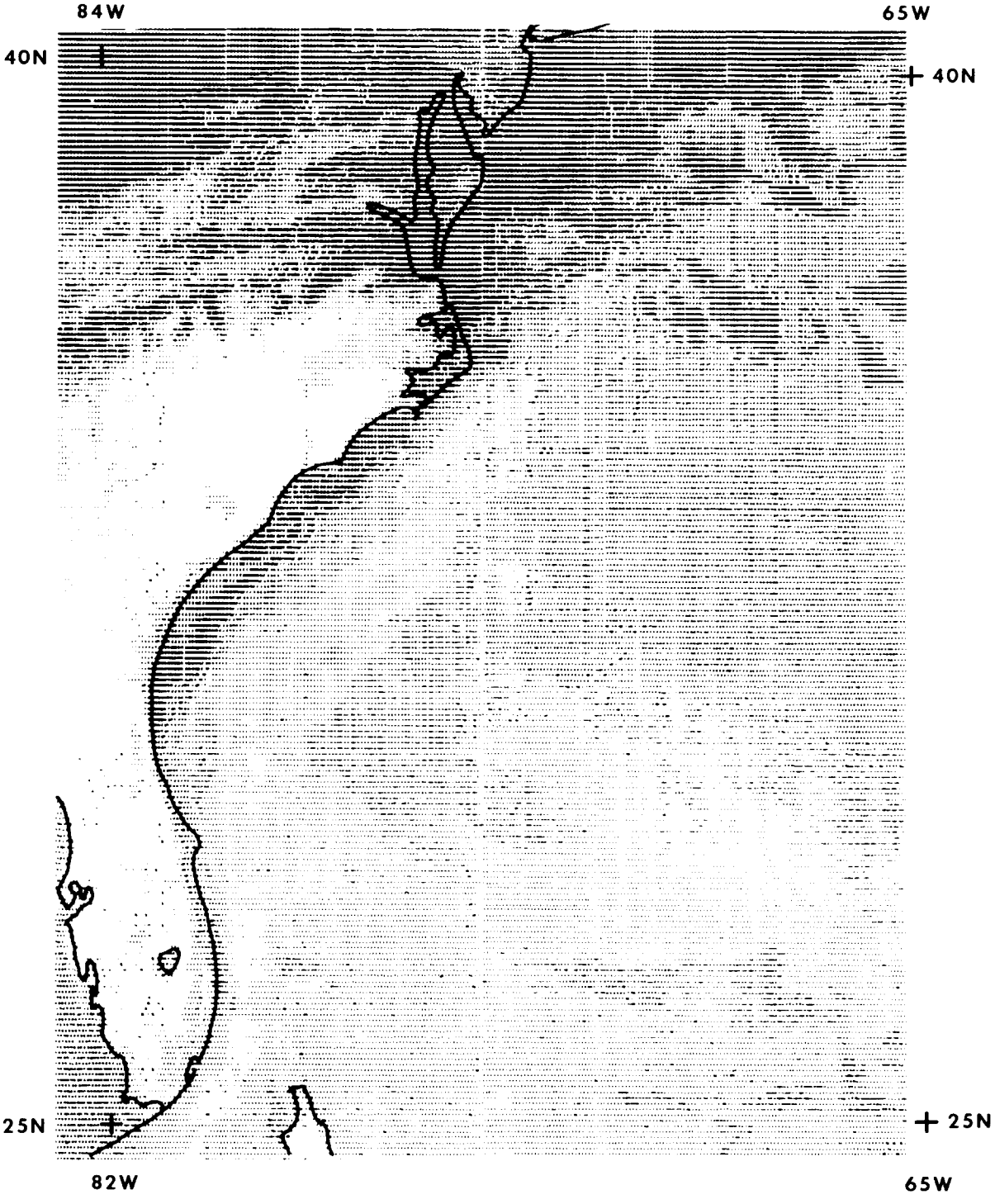

Figure 3. Sample of cloud reduced picture produced by compositing five pictures for 26 February 1977

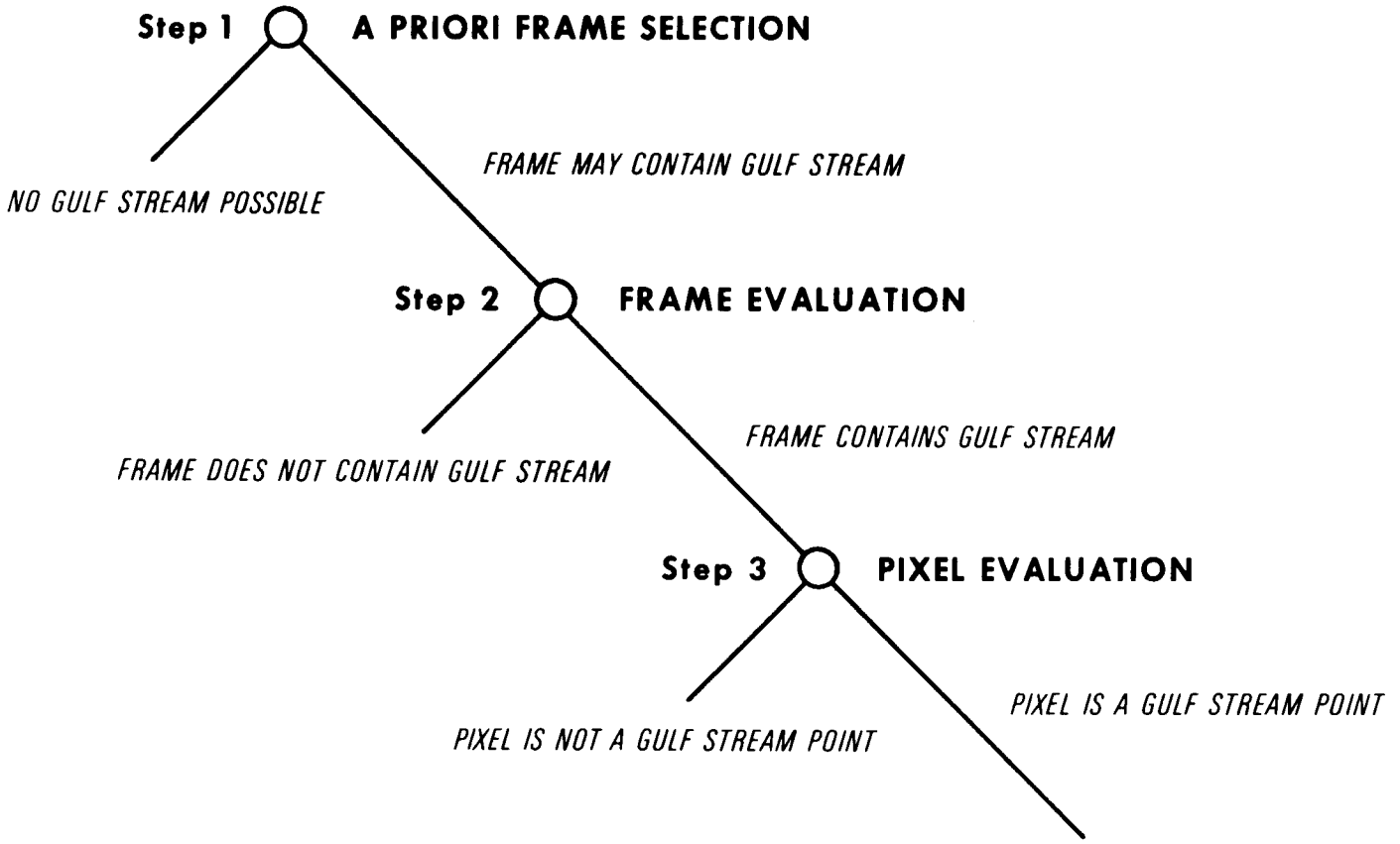

Figure 4. Hierarchical decision tree

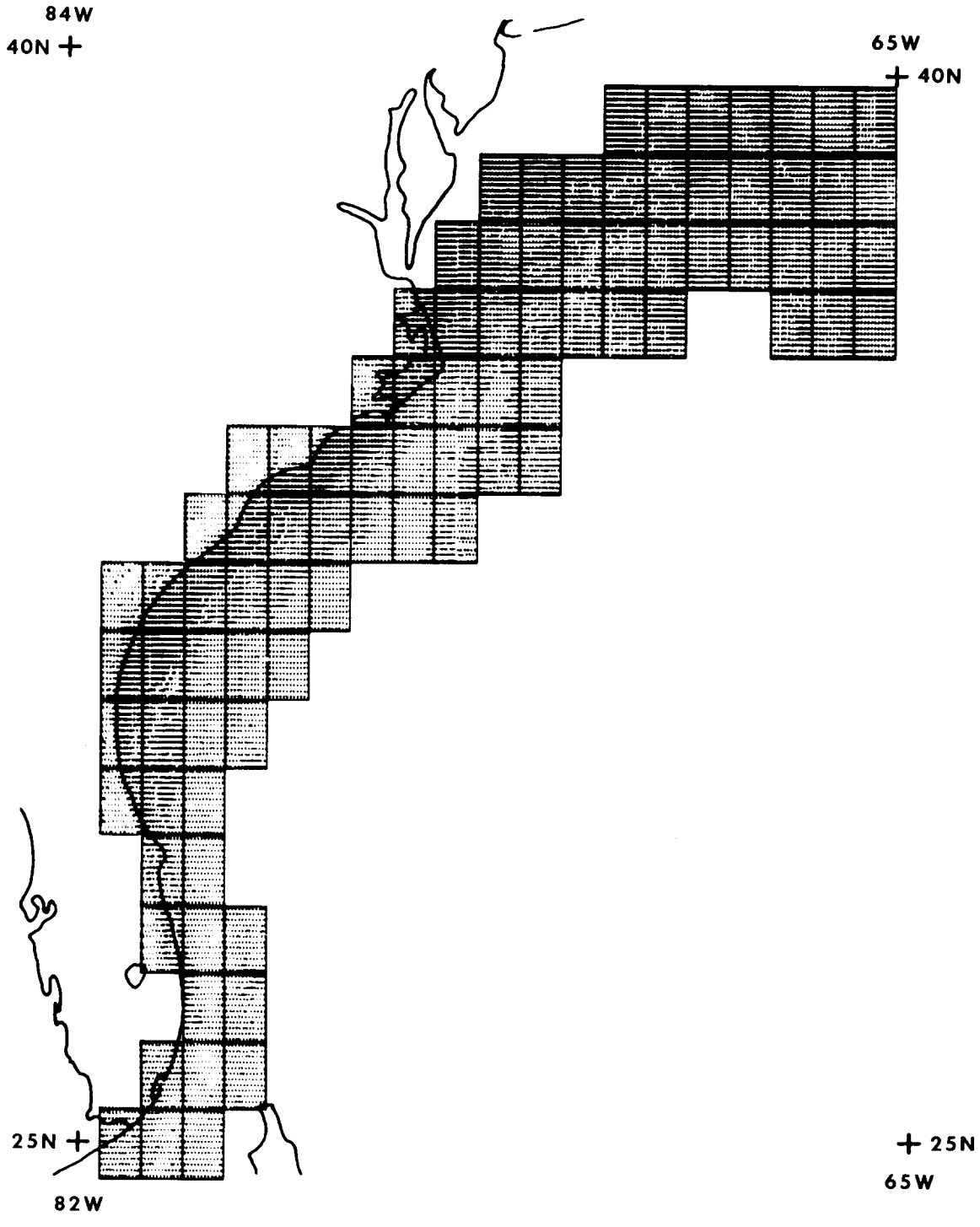

Figure 5. Frames which could possibly contain the Gulf Stream based on a priori information

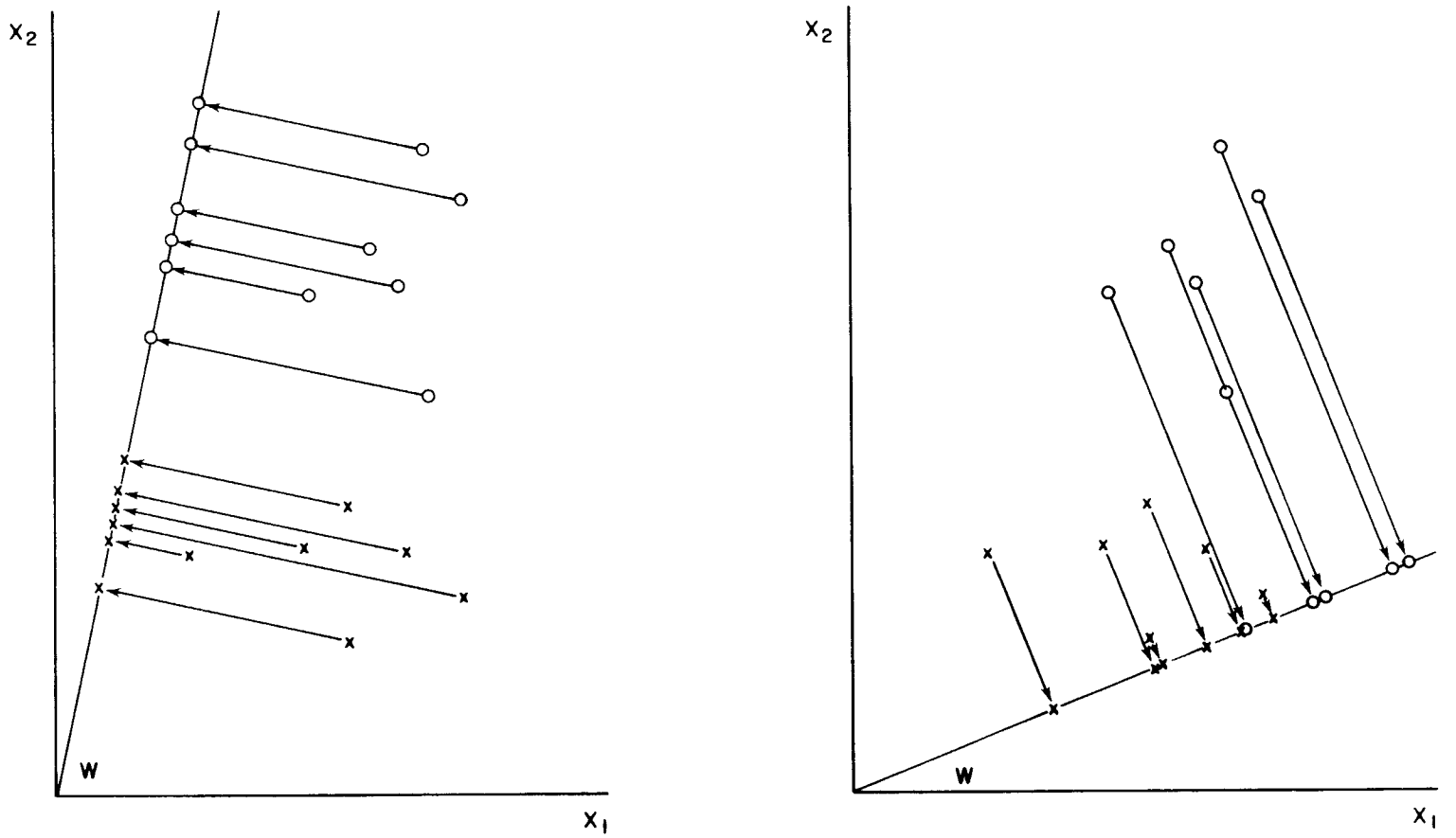

(from Duda and Hart)

Figure 6. Projection of sample onto a line

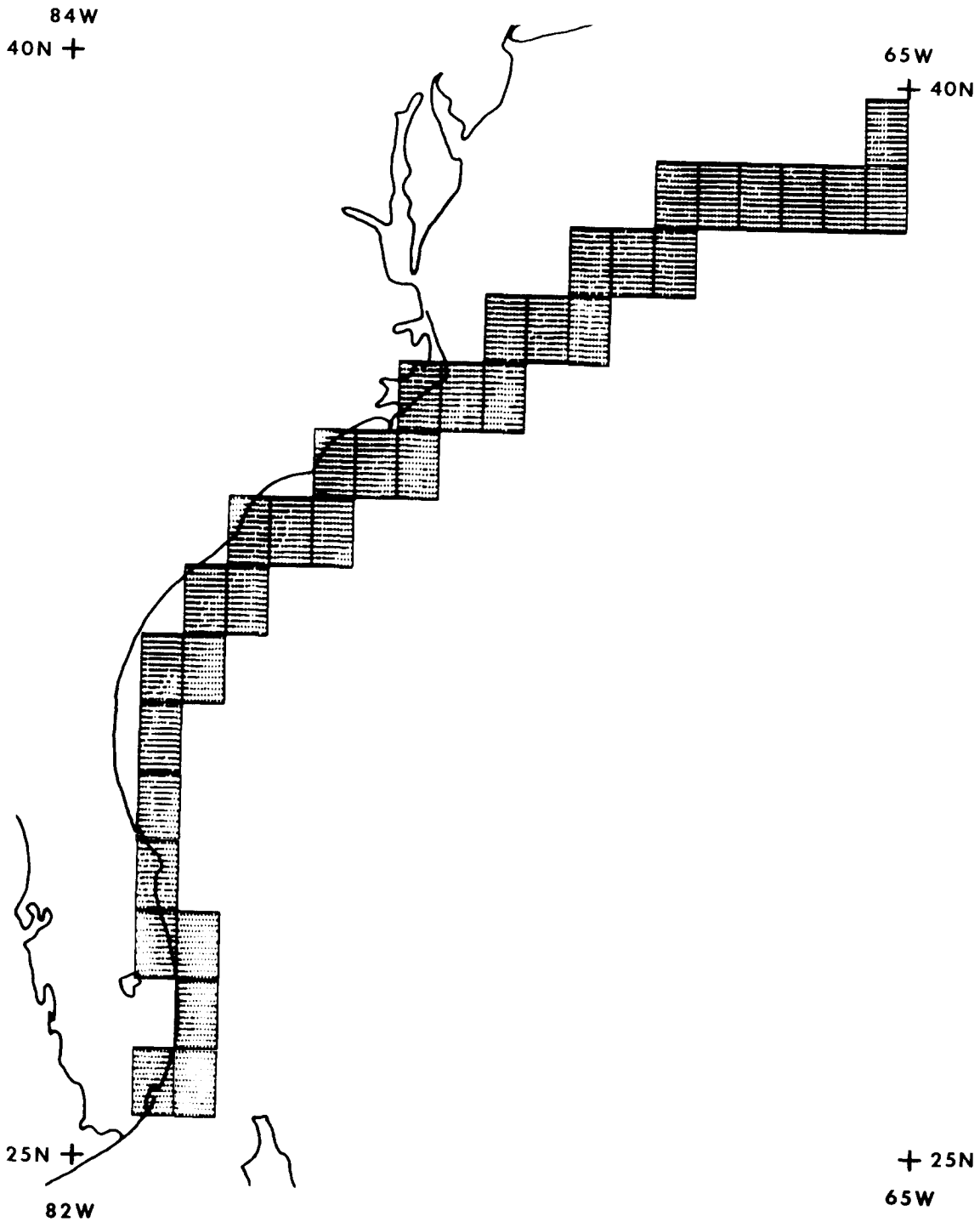

Figure 7. Frames determined by pattern analysis to contain the Gulf Stream

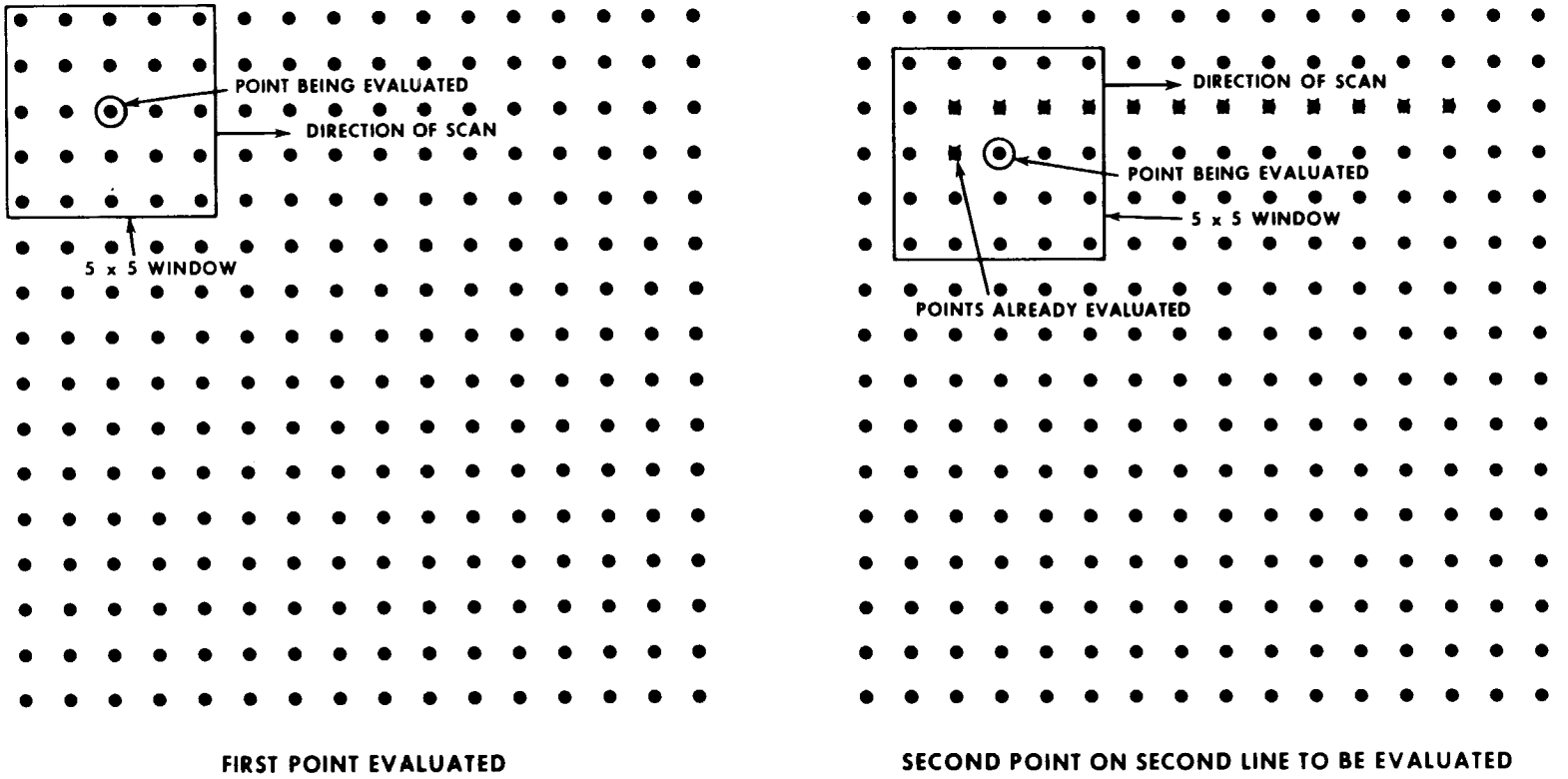

Figure 8. Scanning procedure for pixel evaluation

a. ORIGINAL FRAME

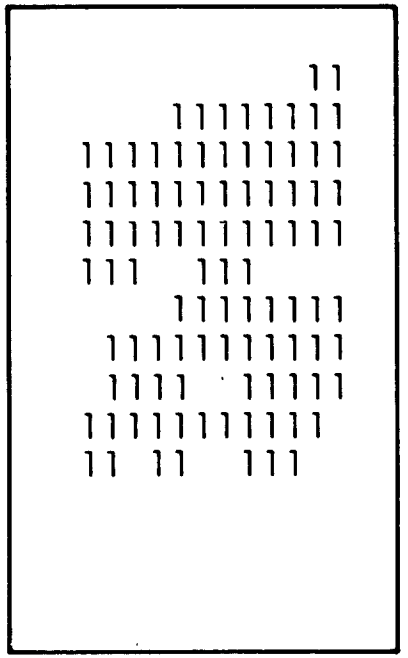

b. AFTER SCANNING AND THRESHOLDING AT ZERO SKEWNESS

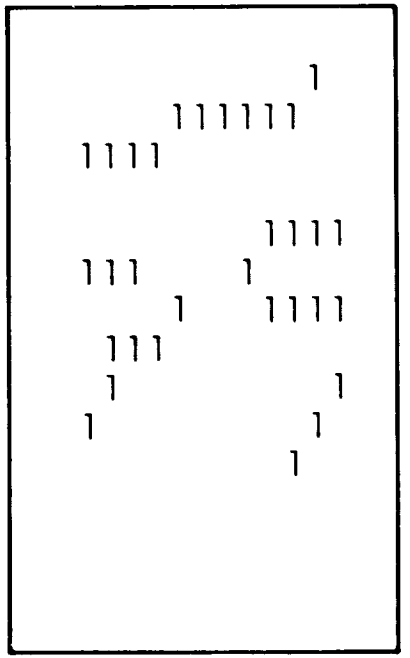

c. AFTER EDGE DETECTION

Figure 9. Pixel evaluation and edge detection

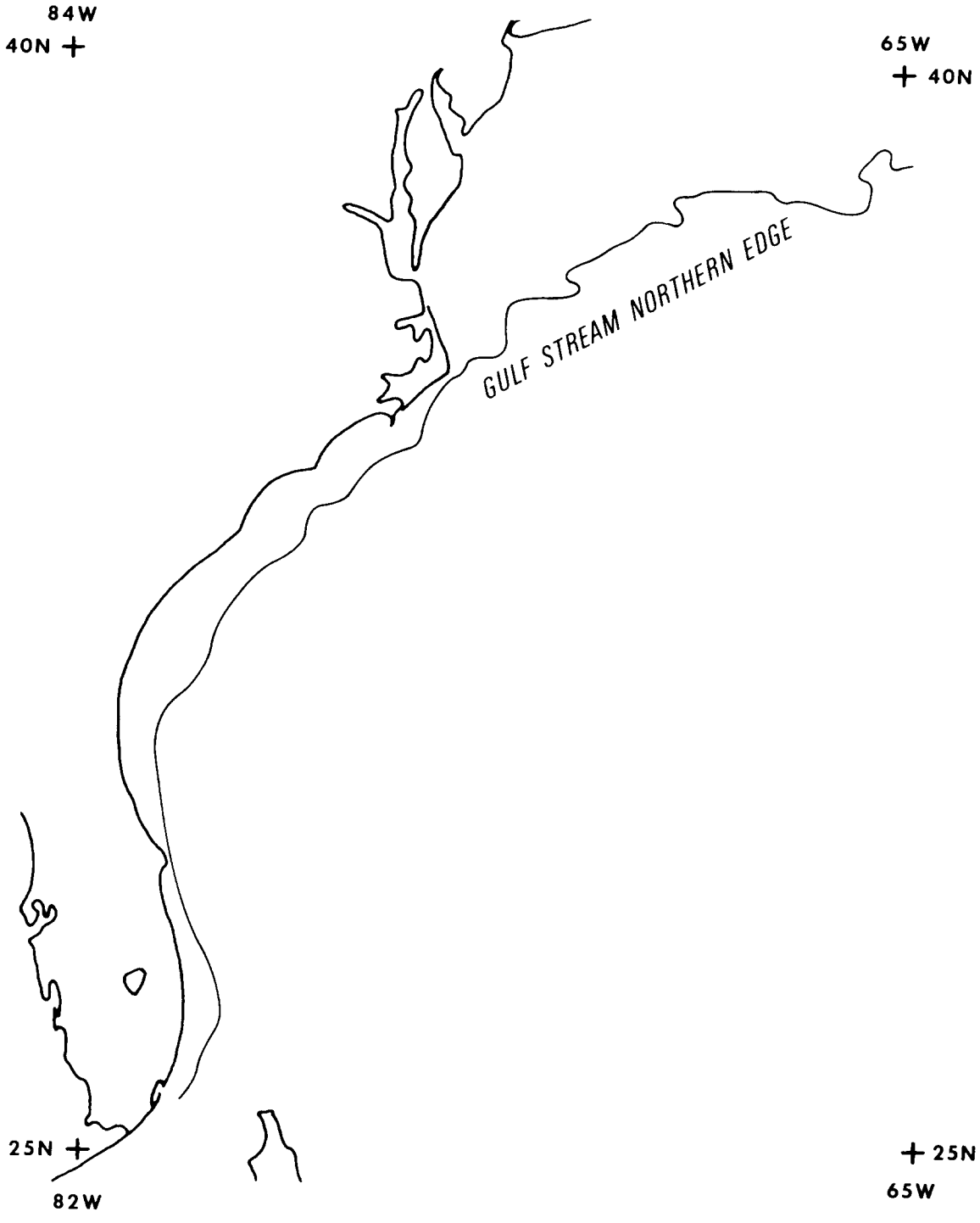

Figure 10. Gulf Stream location for 26 February 1977

REFERENCES

Duda, R.O., and P.E. Hart, Pattern Classification and Scene Analysis, J. Wiley & Sons, New York (1973).

Gerson, D.J., Computer Estimation of the Presence of Sea Ice in Satellite Pictures, University of Maryland Computer Science Center, Technical Report 366, College Park, Maryland (1975).

Gerson, D.J., and P. Gaborski, Pattern Analysis for Automatic Location of Ocean Fronts in Digital Satellite Imagery, NAVOCEANO Technical Note 3700-65-77 (1977) (Unpublished manuscript).

Haralick, R.M., K. Shanmugam, and I. Dinstein, Textural Features for Image Classification, IEEE Transactions on Systems, Man, and Cybernetics, Vol. SMC-3, No. 6 (1973).

Hayes, K.C., XAP Users' Manual, University of Maryland Computer Science Center Technical Report 348, College Park, Maryland (1975).

Khedouri, E., W. Gemmill, and M. Shank, Jr., Statistical Summary of Oceanic Fronts and Water Masses in the Western North Atlantic, U.S. Naval Oceanographic Office, Reference Publication No. 9 (1976).

Waters , M.P., III, and S.R. Baig, Sea Surface Temperature Gradient Analysis from Digital Meteorological Data, Presented at Joint Conference on Satellite Applications to Marine Operations, New Orleans, LA, November 1977.

Oceanographic products of the Japan Meteorological Agency

Masao Hanzawa
Marine Department, J.M.A.

1. Introduction

In Japan, oceangraphic products on real time and semi-real time basis are prepared by several governmental organizations. Among the institutes the Japan Meteorological Agency has continued to provide the oceanographic products in the western North Pacific related to the IGOSS.

In the present paper the author intends to review the oceanographic products of the Japan Meteorological Agency. The products are summarized in Table, which contains not only the papameters of the products but also the characteristics of the products such as area, periodicity, method of analysis and dissemination procedures. They are the sea surface temperature chats, anomaly chart of sea surface temperature, subsurface temperature chart, sea surface current chart, sea ice chart for analysis and wind waves charts for analysis and forecast.

2. Details of the products

(1) Sea surface temperature

Since 1946 the analysis of sea surface temperature has been carried out every ten days and monthly in the area bounded by latitude 10°N to 53°N and longitude 110°E to 180°. The data bases of sea surface temperature products are ships' reports, 27 coastal and island stations' reports, data from the 4 ocean data bouys, BT reports, ART reports from airplaines and IR data obtained with the G.M.S. (Geostationary Meteorological Satellite). The amount of archived data except the IR data from the G.M.S. are about 30,000 per month. The density of data is high around Japan and along the main routes of ships. On the other hand, it is very sparse in the equatorial waters and in the Yellow Sea.

The sea surface temperature given in tenth of degrees centigrade are transformed on the form of punch card. The quality control of the data is made against the climatological values and the previous analysis and they are averaged in each one degree Lat/Long square for ten days by computer. The averaged sea surface temperature is plotted on the chart by X-Y plotter accompanied with number of data in each square. Isotherms are drawn with one degree intervals. IR data from the G.M.S. is also taken into consideration to draw the isotherms. An example of the product for ten day mean sea surface temperature is given in Figure 1.

The monthly mean product is made by the almost same procedure. In the monthly analysis the grid point values of sea surface temperature at one degree Lat/Long intervals estimated from the ten days analysis are processed instead of the observed data. In this analysis, the objective technique is employed to prepare the sea surface temperature chart by interpolating the grid point values spatially. The anomaly chart and month-to-month difference field are also made the objective method. The monthly products are important for the studies of

climatology in addition to the other purposes.

Since April 1978, the grid point values in each one degree Lat/Long mesh averaged for ten days are derived from IR measurment with the G.M.S., which is a meteorological satellite located at 140°E above the equator. Coverage of the IR measurements from the satellite is enclosed by latitude 50°N to 49°S and longtude 90°E to 170°W. The observations from the satellite is carried out every six hours. Those data are also taken into consideration for drawing the ten days analysis as previously mentioned. It is to be noted that importance of the data from the G.M.S. is increasing in the analysis. The expansion of the analysis area to the South Pacific is in the planning stage by full use of the IR data.

(2) Sea surface current and subsurface temperature

The anlyses of sea surface current and subsurface temperature at the depth of 100 m are prepared in the waters adjacent to Japan ranging from 24°N to 46°N (Lat.) and from 121°E to 158°E (Long.). The data sources of subsurface temperature are mainly the reports of BT observations and those of sea surface current are GEK (Geomagnetic Electric Kinetgraph) observations. In Japan observations of sea surface current with GEK are commonly made as well as subsurface temperature measurements with BT. The Japan Meteorological Agency has extensively collected those data in the western North Pacific on real time and semi-real time.

About 4,000 BATHY Reports are received in 1978 around Japan in the framework of the IGOSS. Large amount of data are reported by the domestic codes and mail. The amount of data archived by the Japan Meteorological Agency for each month are about 1,000. It is estimated that the amount of BT observations in those waters reach about 1,500 in each month and about 70 % of them are used in the analysis of subsurface temperatures in the Japan Meteorological Agency.

The data of those parameters are punched on data processing cards for every day basis. They are averaged in each 10 X 15 minutes square every month and the reduced values are plotted on the charts by computer. Then, the chart of subsurface temperature with contours of each one degree intervals is prepared manually.

(3) Sea ice

In winter season, the Okhotsk Sea is covered with sea ice and information concerning with sea ice are essential and important for the operation of ships and for fishing. The Japan Meteorological Agency has been collecting sea ice information from airplanes, the meteorological satellites NOAA/GMS and the coastal stations. The analysis is made twice a week from December through May manually. Figure 2 is an example of sea ice analysis, which contains not only the information of sea ice but also that of sea surface temperature in open waters.

(4) Wind waves

The analysis of wind waves and swell is produced in every day based upon the ships' and coastal stations' reports for 00Z in the western North Pacific. The Japan Meteorological Agency also prepares the 24 hour forecast of sea condition every day by using the spectral model adding modification to purely numerical products considering of the analysis of actual sea conditions.

(5) Long range forecast of sea surface temperature

The Japan Meteorological Agency provides a long range forecast of sea surface temperature conditions in the seas adjacent to Japan. The forecast is

prepared in March for the coming summer based on various statistical and other methods. It is issued in plain language.

3. Dissemination of the products

The products prepared by the Japan Meteorological Agency are broadcasted by the meteorological radio facsimile. The schedules, frequencies and details on the broadcasts can be obtained from the standard WMO publication (WMO/OHN No. 9 T.P. Volume C). The products excep for sea ice and sea condition are also available by mail. For the dissemination of sea surface temperature, anomaly of sea surface temperature, sea surface current and subsurface temperature analyses the Ten Day Marine Report is published every ten days.

Table. Oceanographic products of Japan Meteorological Agency

(a) Analysis

Parameter	Area	Periodicity	Method	Map	Service
Sea surface temperature	The western North Pacific (10 - 53°N, 110 - 180°E)	10 days	Manual/numerical	Mercator	Mail/Fax.
Sea surface temperature	The western North Pacific (10 - 53°N, 110 - 180°E)	Monthly	Manual/numerical	Mercator	Mail/Fax.
Anomaly of S.S.T.	The western North Pacific (10 - 53°N, 110 - 180°E)	Monthly	Numerical	Mercator	Mail
Subsurface temprature	The seas adjacent to Japan (24 - 46°N, 121 - 158°E)	Monthly	Manual	Mercator	Mail/Fax.
Sea surface current	The seas adjacent to Japan (24 - 46°N, 121 - 158°E)	Monthly	Manual	Mercator	Mail/Fax.
Sea ice	The Okhotsk Sea (see Figure 2)	Twice/week	Manual	Polar St.	Fax.
Wind waves	The western North Pacific (see Figure 3)	Daily	Manual	Polar St.	Fax.

(b) Forecast

Parameter	Area	Periodicity	Method	Map	Service
Wind waves	The western North Pacific	Daily	Numerical/manual	Polar St.	Fax.

Captions of Figures

Figure 1. An example of sea surface temperature analysis of the JMA (The Ten Day Marine Report of the Japan Meteorological Agency).

Figure 2. An example of sea ice analysis in the Okhotsk Sea of the JMA.

Figure 3. An example of wind-waves analysis (in the upper) and forecast (in the lower) of the JMA.

気象庁 全国海況旬報　No. 1146

THE TEN-DAY MARINE REPORT　*Japan Meteorological Agency*

53年 8月上旬 平均海面水温

Aug. 1～10 1978 *Mean Sea-Surface Temperature* (℃)

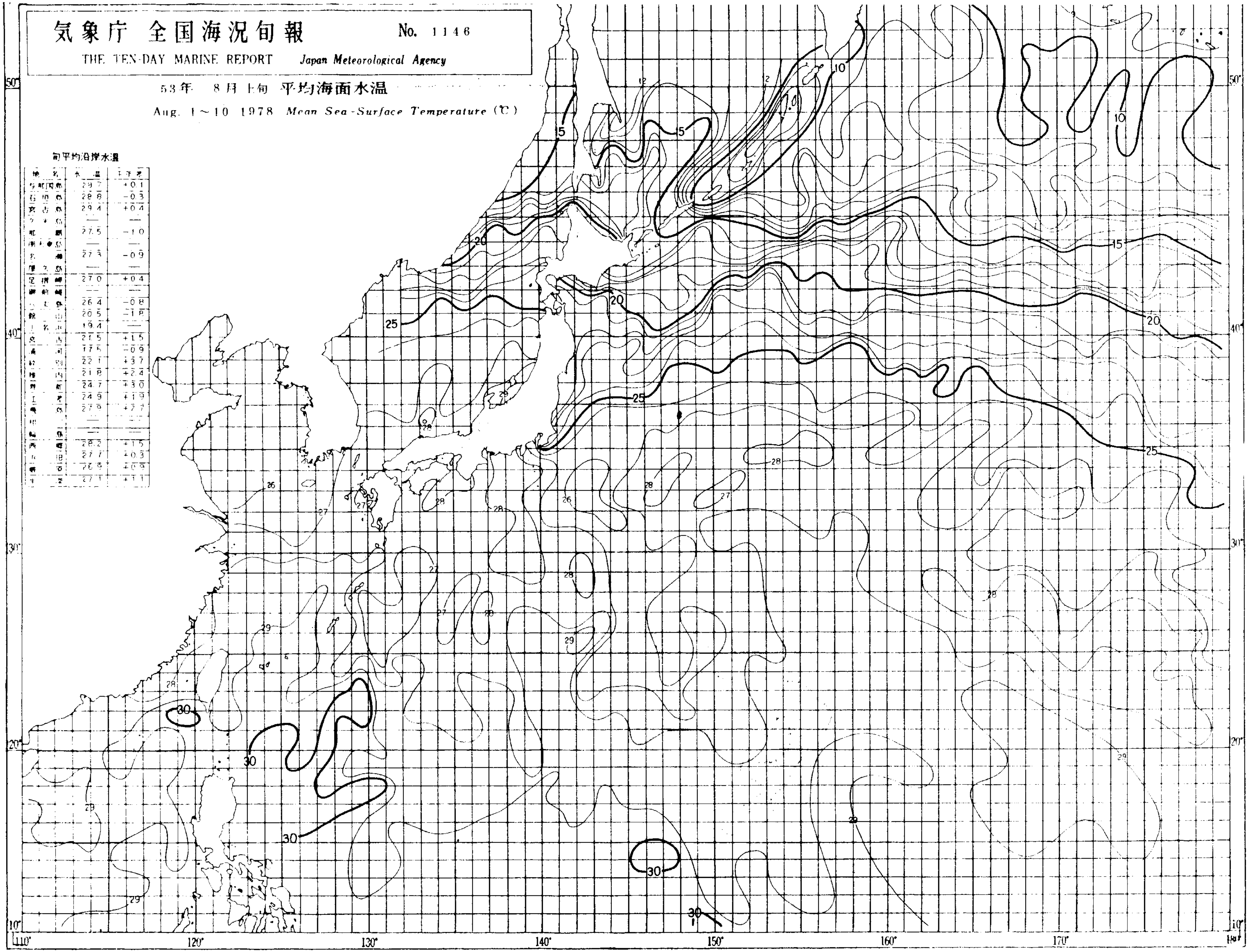

旬平均沿岸水温

地名	水温	平年差
与那国島	29.7	+0.1
石垣島	28.8	−0.3
宮古島	29.4	+0.4
久米島	—	—
那覇	27.5	−1.0
南大東島	—	—
名瀬	27.3	−0.9
屋久島	—	—
足摺岬	27.0	+0.4
[illegible]	—	—
八丈島	26.4	−0.8
館山	20.5	−1.8
小名浜	19.4	—
宮古	21.5	+1.5
浦河	17.5	−0.9
釧路	22.1	+3.7
稚内	21.8	+2.4
[illegible]	24.7	+3.0
[illegible]	24.9	+1.9
[illegible]	27.9	+7.7
[illegible]	—	—
輪島	—	—
西郷	28.2	+1.5
浜田	27.7	+0.3
[illegible]	26.9	+0.9
[illegible]	27.1	+1.1

Figure 1

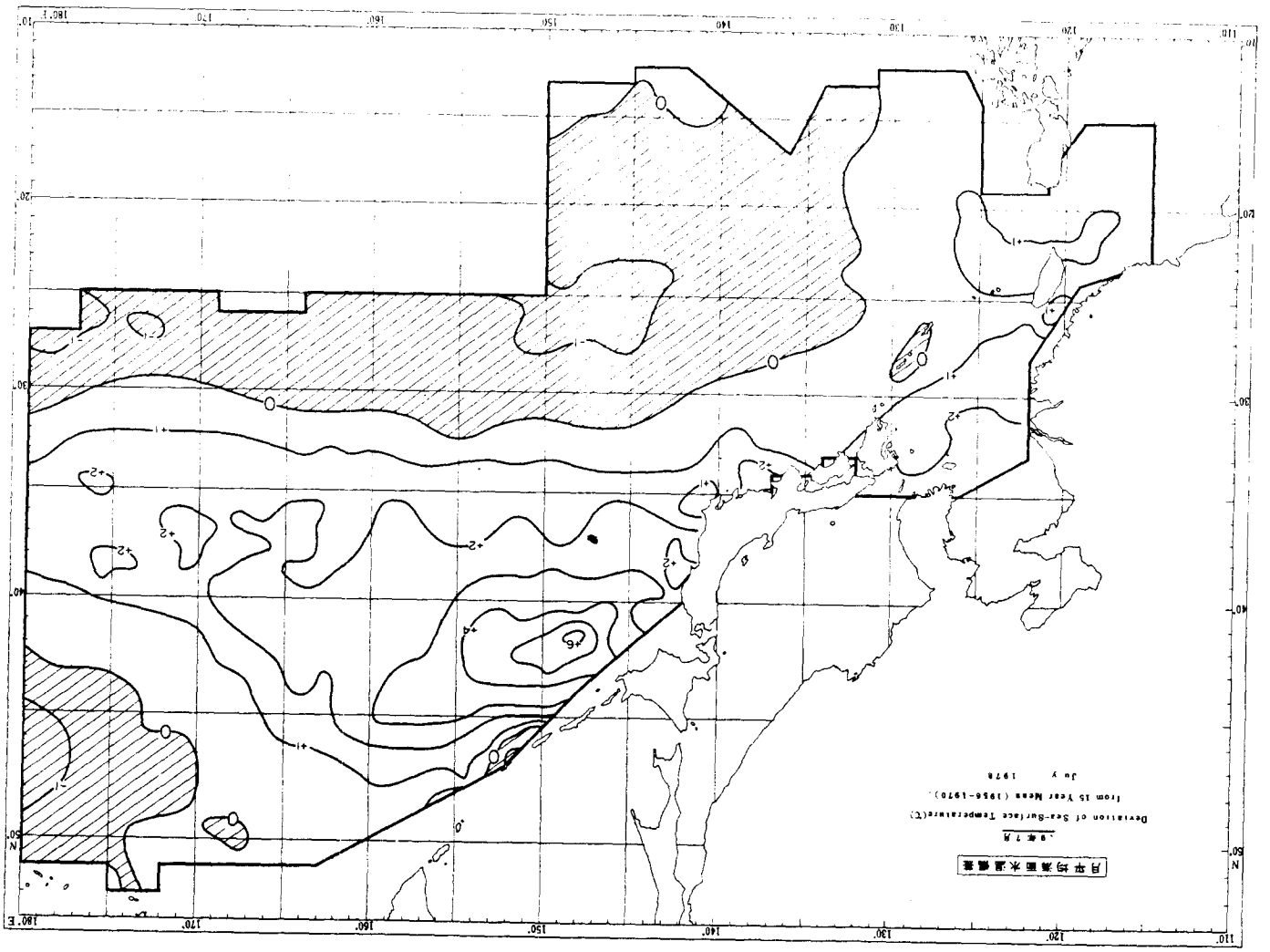
月平均海面水温偏差
Deviation of Sea-Surface Temperature(℃)
from 15 Year Means (1956-1970).
July 1978

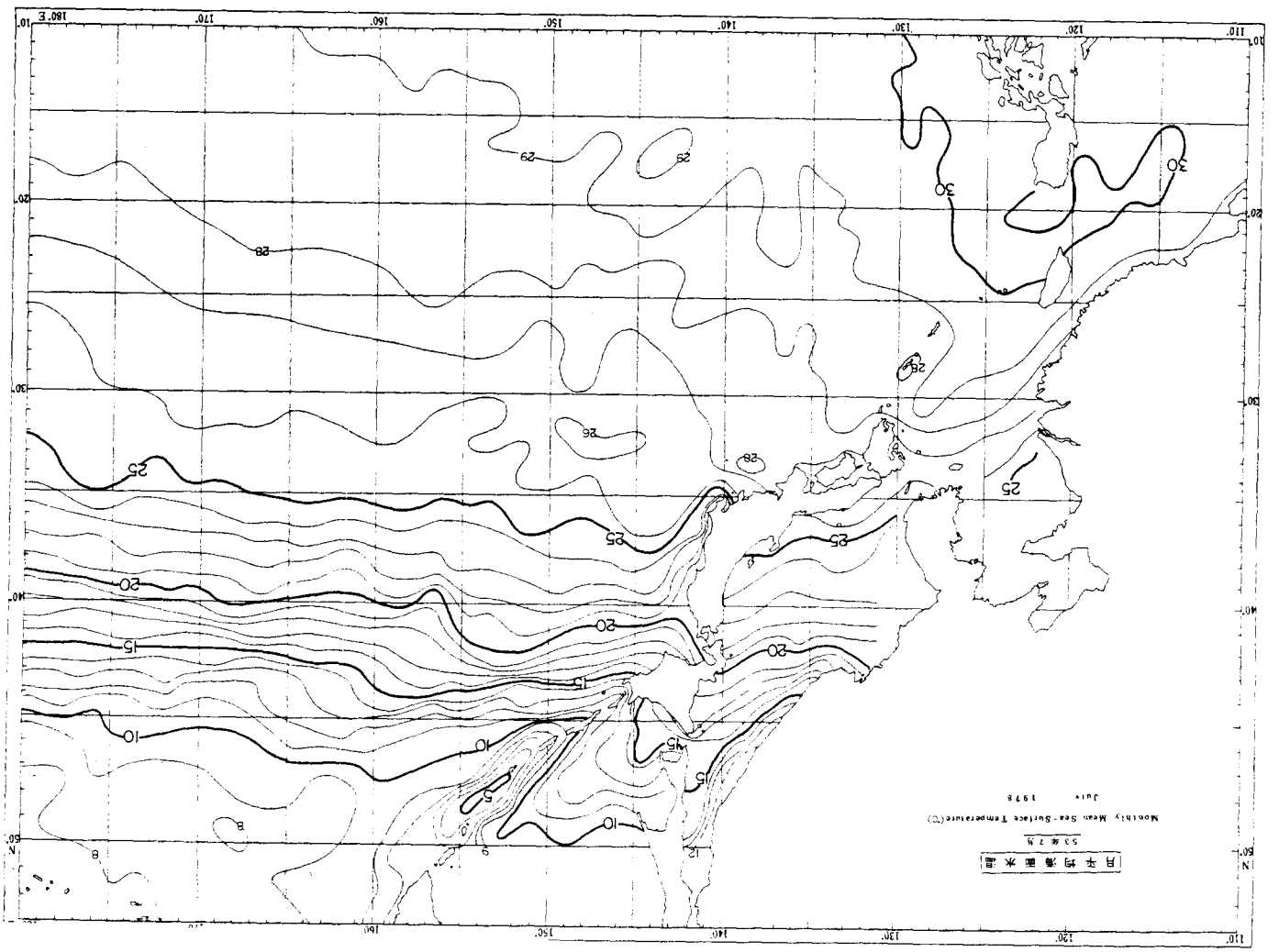
月平均海面水温
Monthly Mean Sea-Surface Temperature(℃)
July 1978

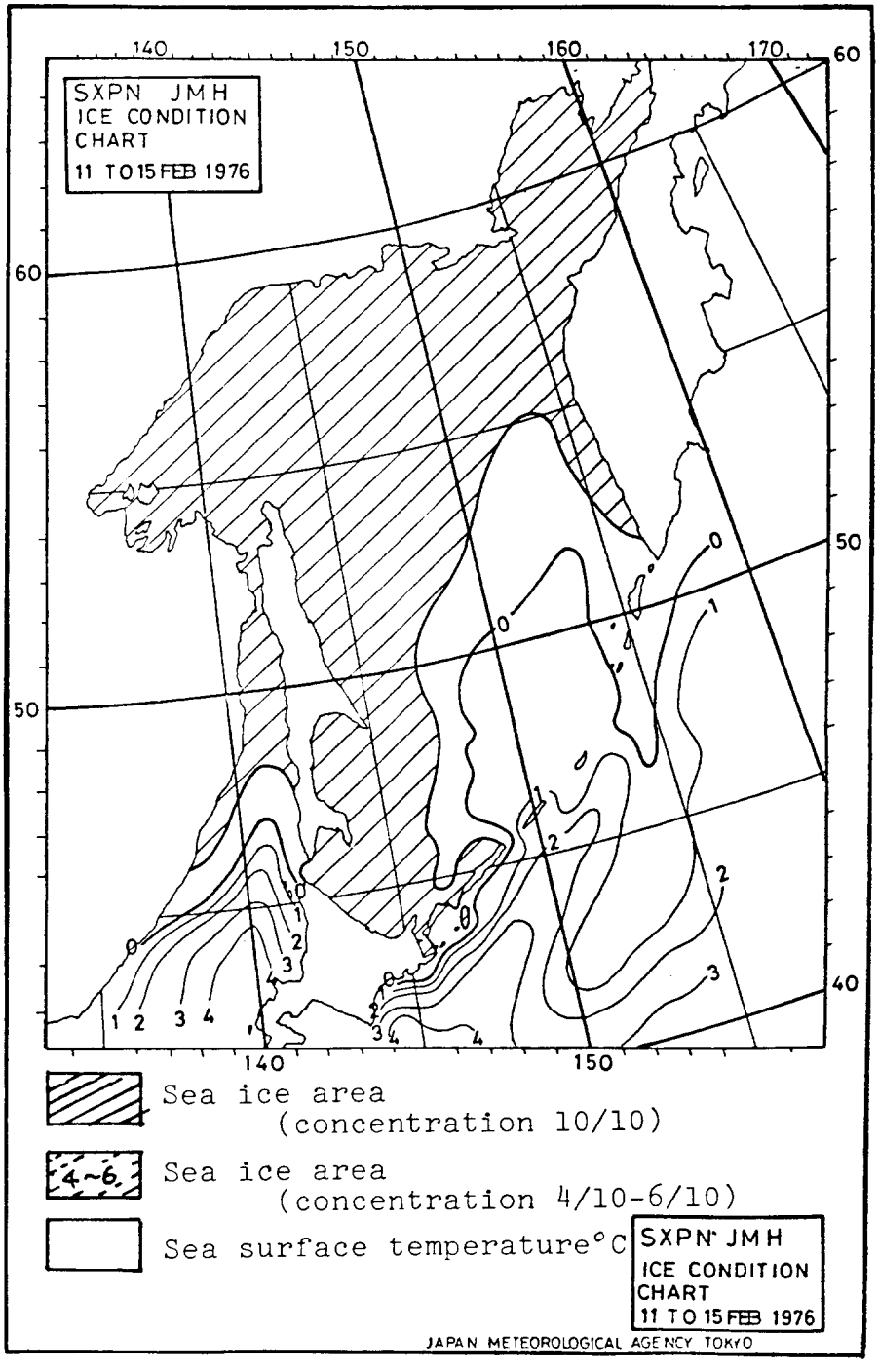
SXPN JMH
ICE CONDITION
CHART
11 TO 15 FEB 1976
140
150
160
170
60
50
40
Sea ice area
(concentration 10/10)
4~6
Sea ice area
(concentration 4/10-6/10)
Sea surface temperature°C
SXPN JMH
ICE CONDITION
CHART
11 TO 15 FEB 1976
JAPAN METEOROLOGICAL AGENCY TOKYO

Figure. 2

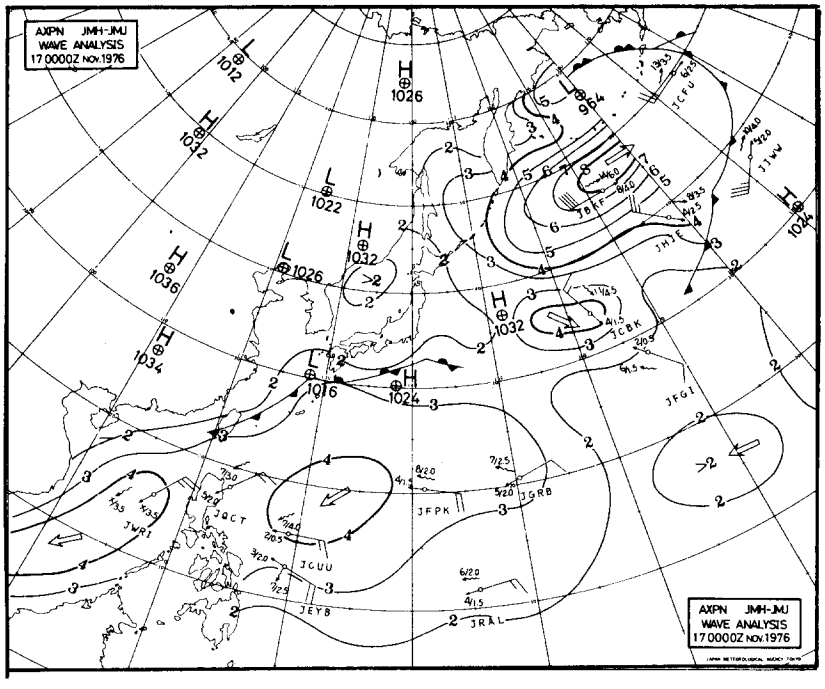
AXPN JMH-JMJ
WAVE ANALYSIS
170000Z NOV.1976
AXPN JMH-JMJ
WAVE ANALYSIS
170000Z NOV.1976

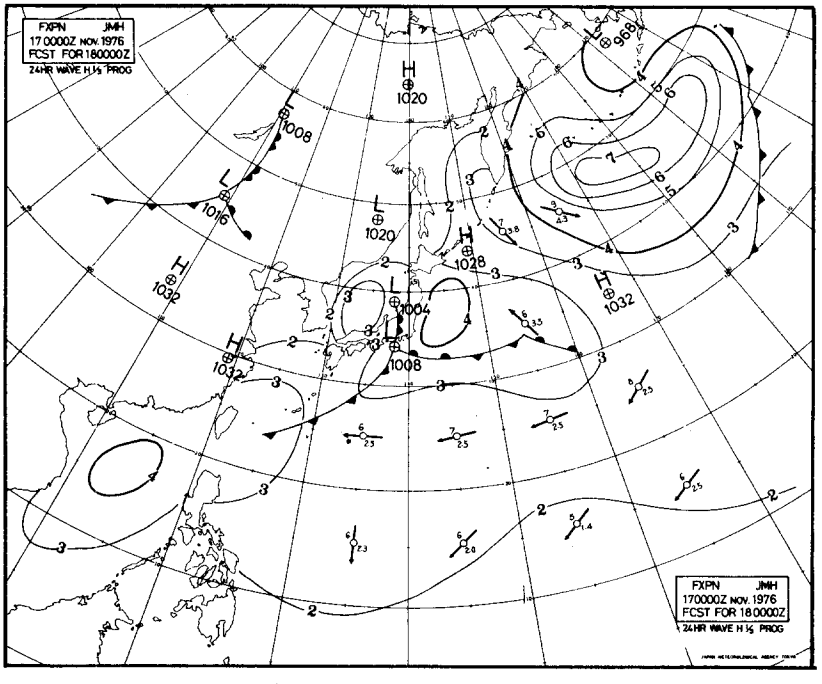
FXPN JMH
170000Z NOV. 1976
FCST FOR 180000Z
24HR WAVE H1/3 PROG
FXPN JMH
170000Z NOV. 1976
FCST FOR 180000Z
24HR WAVE H1/3 PROG

Figure 3

Preparation of sea-surface temperature charts based on the data from the GMS

Masao Hanzawa
Marine Department, J.M.A.

1. Introduction

Since April, 1978, the Japan Meteorological Agency has been operating the Geostationary Meteorological Satellite (GMS) System, which is in the equatorial and geosynchronous orbit at 140°E. The GMS was launched in July, 1977 for one of five geosynchronous meteorological satellites distributed over the equator for main facet of GARP satellites network of FGGE. The GMS carries one imager of the Visible/Infrared Spin Scan Radiometer (VISSR), a Space Environmental Monitor (SEM) System to provide data on environment of space and a Data Collection System. The principal specification of the VISSR is summarized in Table in addition to those of the GOES and the METEOSAT. In the present paper the author intends to introduce the procedure for extraction of sea surface temperature from Infrared Images of the GMS.

2. Extraction of sea surface temperature

The observations of the VISSR from the GMS are usually made every 3 hours, 8 times in each day. IR data are digitized with sampling rate of 0.048 m rad., and intensity is digitized for 8 bits. Among those observations, 6 hourly (03, 09, 15, 21 Z) IR data are used to compute sea surface temperature of the day for each 1° Lat/Long mesh area. Seas covered in the analysis are ranging from 50°N to 49°S in latitude and from 90°E to 170°W in longitude, respectively; namely, the western Pacific and the east part of the Indian Ocean.

From the VISSR Original Data File, the 6 hourly IR digital data are converted to the equivalent black temperature (Tbb) by the calibration table of the Infrared Radiometer. The Tbb vs. frequency histogram for each 1° Lat/Long mesh is constructed for each day. One histogram is constructed by about 8,000 samples near the sub-satellite point, that is, about 2,000 samples are obtained in each observation. This histogram.can be regarded as a Gaussian Distribution in the area where no clouds obscure the sea surface. In such case it is easy to determine the sea surface temperature representative of 1° Lat/Long mesh by finding the peak of the histogram. Generally speaking, clouds give disturbance on the pattern of the Gaussian Distribution in its cold side of Tbb. To eliminate the effects of clouds and determine the sea surface temperature which represents the square, the Japan Meteorological Agency has employed the method developed by Leese et al. In this method the $\overline{Tbb}$ that represents the mesh area is given as follows;

$$\overline{Tbb}=\frac{1}{2}\,\frac{(T_3^2-T_1^2)\cdot \ln F_1/F_2-(T_1^2-T_2^2)\cdot \ln F_3/F_1}{(T_3-T_1)\cdot \ln F_1/F_2-(T_1-T_2)\cdot \ln F_3/F_1},$$

where F_1, F_2 and F_3 are frequencies at T_1, T_2 and T_3, respectively.

In our processing, the three classes of Tbb are selected in the determination of $\overline{Tbb}$ around the maximum slope of the histogram in its warm side. In the area where the total amount of clouds exceeds the limit no determination of $\overline{Tbb}$ is made.

Then, the correction on emissivity is applied for the obtained $\overline{Tbb}$ of the day. This process contains nadir angle and water vapour corrections. Those corrections are essential to obtain the absolute values of sea surface temperature from IR Images. Unfortunately, the GMS does not carry a Vertical Temperature Profile Radiometer (VTPR), it is impossible to estimate the actual contents of water vapour in the atmosphere along the optical path. In our analysis the monthly climatological values of water vapour contents prepared for the grid points at 500 km intervals are used for the correction instead of the data from a VTPR. An empirical function defined as follow is introduced for the correction.

$$\Delta T=(a_1\sec^2\theta+a_2\sec\theta+a_3)[(1-A(Tbb))(a_4-a_5\cdot\ell n\|a_6-Tbb\|)+A(Tbb)(a_7w+a_8w^2)] ,$$

where $A(Tbb)=a_9\cdot[(a_{10}-Tbb)^2+a_9]^{-1}$,
w; content of water vapour
θ; nadir angle and
$\|x\|$; x for $x\geqq 1$, 1 for $x<1$.

The coefficients from a_1 to a_{10} were determined by comparing the water vapour contents measured by aerological observations around Japan and the ground truth of sea surface temperature reported from ships. This comparison was carried out for about two months in winter before they started the operational service of the GMS. The function for correction was finally given as follows;

$$\Delta T=\sec\theta\cdot[0.189w\times\frac{1400}{(310-Tbb)^2+1400}+4(1-\frac{1400}{(310-Tbb)^2+1400})] ,$$

where Tbb is given in °k and w is given in m/m.

After 10 days accumulation, the quality control of data is performed by comparing them with other nearby data (temperature gradient in space), previous values and the climatological values. Time Composite Method is employed to get the sea surface temperature of the 10 days representative of 1° Lat/Long area for the quality controlled data.

The final data are disseminated to foreign countries via GTS from JMA's ADESS by the code of FM-86 VI. The isoline chart for 10 days is also prepared from the grid point data by the objective method and contours are labelled in °C with one degree intervals. Figure shows an example of the products derived from the IR of the GMS.

3. Applications of the products and others

The 10 days sea surface temperature obtained from the IR Images of the

GMS is fully taken into consideration to prepare the Ten Day Marine Report of the JMA. The Report was originally analysed based on sea surface temperature reported from ships. The importance of the data derived from the GMS is increasing in the preparation of the Report.

The accuracy of the sea surface temperature from the GMS is not so sufficient in using as absolute values, that is, in some places there exsit 2°C difference in temperature between sea truth and the data from the GMS. However, it is still usefull in determining the direction of the isoline in the analysis in the regions where ships' reports are sparse. The extensive efforts have been continued to improve the accuracy of the sea surface temprature derived from the GMS, especially in the correction on emissivity. The sea areas for the analysis of the Ten Day Marine Report are limited in the western North Pacific and it planned to expand to the South Pacific by complete use of the IR data from the GMS.

A fine mesh analysis of sea surface temperature from the IR Images of the GMS for each 1/4° Lat/Long mesh area for each 5 days is under development. The objective area of the analysis is in the western North Pacific and the products will be profitable for monitoring the Kuroshio and the Oyashio.

Table VISSR Characteristics

			GMS (Japan)	GOES (U.S.)	METEOSAT (Europe)
Scan System	East-West		Spin Scan - 100 r.p.m.		
	North-South		Scan Mirror		Scan Telescope
	Direction		North→South		South→North
			West←→East		East→West
	No. of steps		2500	1820	2500
	Frame time (minute)		25	18.2	25
IFOV	(m rad.)	IR	0.14	0.25	0.14
		VIS	0.035	0.025	0.07
Resolution (km)*		IR	5	9	5
		VIS	1.25	0.9	2.5
Wave length (μm)		IR	10.5-12.5	10.5-12.5	10.5-12.5
		VIS	0.55-0.75	0.55-0.75	0.55-0.75
		WV	-	-	5.7-1.0
Detector		IR	Hg Cd Te	Hg Cd Te	Hg Cd Te
		VIS	PMT	PMT	Si P Diode
		WV	-	-	Hg Cd Te
No. of Scan lines		IR	2500	1820	2500
		VIS	10000	14560	5000
		WV	-	-	2500

* at Sub-satellite point

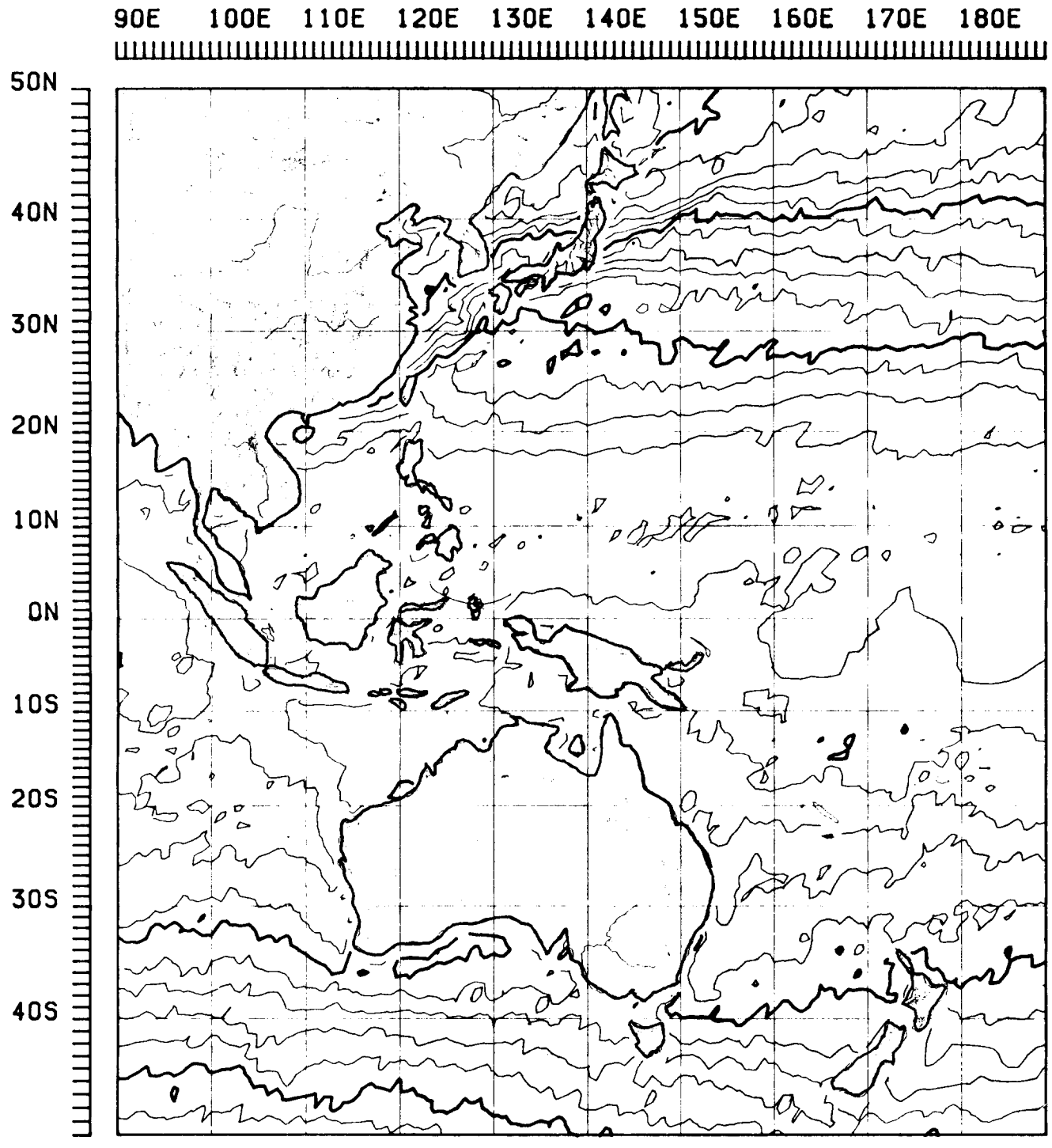

Figure An example of 10 days sea surface temperature chart.

DATA PROCESSING SYSTEM FOR SUMMER MONEX

J.U. Hingorani, R.K. Bansal, B.N. Dewan*
&
R.K. Datta

INDIA METEOROLOGICAL DEPARTMENT

Abstract:-

This paper describes a data processing package to meet the data processing requirements of Summer Monex Data Centre, Delhi. Provision has been made to process BATHY and TASEC reports, besides other meteorological reports which this centre will undertake for Summer Monex.

This package consists of three main modules which carry out the following functions:

1. TELECOMMUNICATION QUALITY CONTROL CHECKS :

Telecommunication computer system at RTH, New Delhi checks the format of header, abbreviated heading and end of the bulletin. This module checks the format of individual reports in a bulletin. Attempts are made to adjust the grouping of characters in a report to a standard format, failing which the report or the specific group of the report is suitably flagged and printed for manual intervention. Whereever alterations are made by the program, the raw data (initial version) is stored on a separate file on disk for possible reference during decoding.

2. DATA DECODING FUNCTIONS :

The reports which pass the telecommunication quality control checks are decoded for individual coded elements. Internal consistency checks on the different elements in a report are applied. In the event of suspected errors the concerned elements are flagged.

3. METEOROLOGICAL QUALITY CONTROL :

After the decoding operation, this module applies space and time consistency checks to provide input data for machine analysis.

The first two modules of the package are being written in Assembler Language of the IBM 360/44 system, and the last one in FORTRAN IV.

- -

* National data centre Pune-INDIA.

DATA PROCESSING SYSTEM FOR SUMMER MONEX (MONSOON EXPERIMENT)

PART - I

Introduction:-

One of the major aims of Monex is to collect and prepare a very rigorous data base for future scientific research on the various aspects of monsoon circulation.

Almost all the Meteorological Services of the world are actively participating in this venture under the aegis of W.M.O and ICSU with India Meteorological Service playing a pivotal role.

International Monex Management Centre (IMMC), New Delhi therefore took over the responsibility to develop a data processing system which could meet the basic needs of Summer Monex. The system is planned to be quite flexible for being used also for operational data processing of R.M.C New Delhi.

New Delhi is a Regional telecommunication Hub(RTH) on the Global telecommunication system (GTS) of W.M.O. All the meteorological messages are exchanged through this system in an internationally accepted code. The exchange of data at RTH New Delhi is carried on through a hot stand bye DS 714 Switching system. Interface of this system with processing computer IBM 360/44 is possible through three different modes, viz i). Physically transferring to processing computer the history tape converted into EBCDIC (Extended binary coded decimal interchange code) through hot stand bye switching system. ii) Conversion of history tape written in ASCII (American Standard Code II) using supervisory program to EBCDIC at the processing computer, and iii) Paper tape punched through switching system (this was developed initially for restricted use and is no longer in use at present).

The operations are envisaged through Ist and 2nd mode.

The purpose of this article is to provide a detailed documentation on the DPPM (Data processing package for Summer Monex). This is rather necessary as a package of this magnitude gets extremely formidable to maintain, not to speak by others, even by those who have written the programs without proper documentation.

This note which forms part I of the complete system describes the logic and philosophy of the package dealing with i) telecommunication checks ii) organization of messages into standard formats iii) decoding of the data in general acceptable form iv) organizing different files for data depending upon the type of date and time and v) providing procedure for human intervention for repairing the data which could not be managed by the machine.

The second part of the DPPM which is being given in a separate note describes the scheme giving internal consistency

checks for surface observations and vertical/horizontal consistency checks for upper observation. This part also describes the logic of preparation of data in FGGE prescribed format.

2. General philosophy of the system:

The philosophy behind devising the DPPM has been that it should endeavour only to repair/check more frequently occurring mistakes and allow human intervention to take care of mistakes of isolated nature. This is to ensure that the package does not get unnecessarily unwieldy. Normally, while planning such a package one could theoretically think of infinite number and type of errors which observer can unconsciously commit while taking the observation and decoding it into standard format for final transmission.

Further for real time processing, the DPPM need not be geared for checking such inconsistencies which are not of much significance for providing quick-look data set (QLDS) and Level II-a data set. All the other minute checks can be incorporated for the preparation of Level II-b data set.

It was also kept in mind that as for as the good data is concerned it should go through without getting into any sort of programming loop. Expectation is that such type of error free messages which will go through without any significant processing will be of the order of 60 - 70% of the total traffic. DPPM has to take care of rest of the messages. Our present expectation is not more than 5 to 10% of the messages would be of the type which may escape the error recovery routines of DPPM.

As the saying goes, a program may not carry out the logic exactly in the form in which the programmer wanted it to do. To take care of such eventuality and to see that finally the data which goes for archival is neat and clean, all the data which at any stage is corrected by the program, is tabulated, if so desired, alongwith the unprocessed version for quick examination by an experienced meteorological assistant.

Also care is being taken that such of the meteorological messages which are not being processed at present are stored in a separate file. These may be processed in future by a separate routine or processed manually.

Another important point which weighed upon us while planning the package was the availability of limited time. The main load was thus divided into three experts, who had the necessary experience in Assembly language programming. Most of the subsystems of part I of the package have been written in Assembly language. It was however found convenient to write part II of the package in a high level language (Fortran IV).

3. Type of errors:-

3.1.1 Structure of a Meteorological Message:

A typical Meteorological message received through G.T.S consists of 4 main parts viz;(i) Starting line (ii) An abbreviated

heading, which provides information on the type of messages, routing schedule, date and time group (iii) The text of the message in a standard format and (iv) The end of the message sequence. Each segment has a unique transmission format.

3.1.1.1 Starting line:-

This part of the messages has the following format.

<< ≡ ↓ ZCZC →↑ nnn (→CLLLL) → → → → →

where ZCZC is header group for meteorological message, details of which are given in appendix ,nnn is transmission sequence number in 3 digits and CLLLLis classification and identification group. Symbols <,≡,↓,↑and →stand for carriage return, line field, letter shift figure shift and blank space respectivaly. This part of the message is processed at RTH New Delhi Switching system and only correct starting line is passed on to the processing system. Thus DPPM takes for granted that starting line is in standard format and no check is thus provided.

3.1.1.2 Abbreviated heading. The next segment in the sequence is the abbreviated heading which has the following format

<< ≡↓ TTAA↑ ii →↓ CCCC →↑ YYGGgg (→↓ BBB)

where TT is the data designator and AA, the geographical designator. The details of TT are given in the appendix, ii is the number used to differentiate two or more bulletins, CCCC the four-letter international location indicator for the station which originates/compiles the bulletin. In the next groupYY represents the day of the month and GGgg represents time of origin in GMT. The last group BBB in the abbreviated heading represents 3 letter indicators, RTD/COR/AMD which means that what follows would refer to retard/correction to report or amendments to previously processed information.

3.1.1.3. Text message:

The text of the message starts with the indicator $M_iM_iM_jM_j$ which indicates the type of message to follow. A typical synoptic surface message is

$M_iM_iM_jM_j$ YYGG IIiii Nddff VVwwW $N_hC_LhC_MC_H$ $T_dT_dJ_aJ_pJ_p$
($6P_oP_oP_oP_o$) (7RRJJ) ($8N_hCh_sh_s$) ($9S_pS_pS_pS_p$)

Except the first two groups which indicate type of message and date and time of observation are of 4 characters each, all the other groups which give information on the various meteorological parameters are of 5 characters each.

Various types of messages accepted for processing are listed in the table 1.

Text of the message is not checked by telecommunication system and is passed to the processing system as received. Special emphasis is required for processing this part of the bulletin which contains all the desired meteorological information.

3.1.1.4 End of message sequence:
This segment has the following format and in most cases checked by the telecommunication system.

↓<< = = = = NNNN ↑↑↑↑↑

3.1. 2 Transmission errors
As already written, each type of message has a unique international transmission format but lot of errors creep in during transmission which could be caused by varied reasons, such as human errors, machine faults etc.

From the statistics received from various RTHS, following types of discrepancies between W.M.O Standard telecommunication formats and those received there have been observed.

i) There are two carriage returns (CR) followed by two line feeds (LF) or CR,CR,LF followed by another CR CR LF

ii) Additional L F

iii) Single CR followed by LF

iv) None or mutilated message indicator group

v) $M_iM_iM_jM_j$ followed by two spaces instead of one

vi) ? or V instead of = sign

vii) Special characters written in a numeric group

viii) Transmission of upper case characters instead of lower case characters.

ix) Missing = sign after the end of a message.

x) Call sign in upper air ship before message indicator.

Besides the above type of transmission errors, in some regions, if operator while passing a message, realizes that a mistake has been committed, he does the correction by introduction of characters EEE and repeating the group by a corrected version.

For Example:

a) TTAA 58001 42369 99999 12009 18004 00114 ///// /////
850 EEE 85450 05439 28519 ---------- =

b) TTAA 58001 42369 99999 12009 18004 00114 ///// /////
85053 EEE 85450 05439 28519 ---------- =

c) TTAA 58001 42369 99999 12009 18004 00114 11111 11111
85050 05439 28519 70 ----------EEE =
TTAA 58001 42369 99999 12009 18004 00114 11111 11111
85450 05439 28519 ---------- =

In the first example operator realizes his mistake immediately after entering third character of 9th group. This he rectifies by introducing EEE to indicate the error in the preceding group, the correct group is further repeated.

In the second example the error was detected after entering 9th group in complete and in the third example the error was detected after complete message was entered.

The DPPM takes care of such type of mistakes. It has also been observed that while entering EEE, the operator instead of following standard paractice enters characters Esand spaces in various combinations. We have provided all type of checks.

Similarly in certain cases the message indicator group is missing or mutilated; The provision is kept to insert this by considering previous line of the bulletin.

In case a new bullitin is started without end of sequence 'NNNN', DPPM also provides the facility to insert this.

3.1.3 Error in grouping

According to the standard WMO format, various groups in the text message consist generally of 5 characters separated by one blank, and the organization of groups with identifier characters if any, is defined in a unique manner. General experience is that good percentage of messages received on G.T.S fail to follow the standard format and if not corrected, create confusion in decoding the text of the message. The errors in this respect have been found to be of the following type.

i) Two groups may not have a blank separator.

ii) Two groups may be separated by a special character instead of blank separater.

iii) Group(s) may not consist of standard number of characters

iv) Alpha characters in a group of numeric characters.

v) A group or a part of group may be repeated without use of error indicator EEE.

vi) Missing of one or more groups.

vii) Mutilation of identifier character.

DPPM has to provide facility to detect and correct most of these errors. Whenever correction is not possible the message is printed separately under mutilated messages for human intervention.

3.1.4 NIL/MISDA messages:

Each meteorological message has fixed schedule of transmission depending upon the time and type of observation. If the message is not received within that time a NIL message is transmitted. Although these type of messages are standard and not part of errors, but DPPM provides a check for such messages and also for MISDA messages for their exclusion from the final list.

4. Data processing package-DPPM

The broad features of the part I of DPPM are described in Fig.1A,1B.This broadly carries out the following important functions;

i) Checks/Corrects/flags various telecommunication errors in the text of message.

ii) Adjusts/reformats in standard groups of 4 or 5 characters as required in a particular format. Fills missing groups or characters and deletes superfluous groups/characters.

iii) Decodes the message into standard acceptable format.

iv) Organises data files/subfiles depending upon type and time of the message. Matches with station in directory and fills geographical parameters of observing station.

v) Provides procedure for human intervention.

In the following we disscuss the details of the logic of various Subsystems of DPPM.

4.1 Identification of message:-

The data from input history tape written in any one of the forms mentioned under introduction is read record by record, each record consisting of 720 bytes. Byte by byte search is made for a valid message identifier listed in table I. In case of mutilation or disturbed combinations, the attempt is made though error correcting routine to correct the identifier group by reference to the abbreviated heading. In case the search is unsuccessful, the record is printed out for human checking.

4.2 Check for EEE's,"ERCHECK"

As illustrated under section (3.1.2) in a certain region especially over Indian subcontinent, characters EEE are utilized to indicate mistake in the preceding part of group, complete group or full message depending upon the location of characters EEE.

In order to take care of such eventuality, each new byte of the following message indicator is checked for the presence of character E. The standard form to indicate correction is to put three Es immediately after the mistaken group or part of the group. If more than one group has been entered wrongly, the procedure is to put three Es followed by = sign and then repeat the whole message.

But unfortunately, the messages have been observed to contain all type of variations from the standerd procedures. We had to make a compromise and provide for a limited number of checks so that most of the messages could be corrected without spoiling correct messages. For example DPPM provides correction for the following salient combinations.

i) A part of group or full group followed by two to four Es, character Es being together or separated by spaces in different forms. Messages like 583 EEE 58341, or 58240 EEE 58340 or 58240 EE 58341 or 582 EEEE 58341 etc.

ii) More than one group entered wrongly and the last group consist of Es followed by = sign.

The routine may not be able to correct the message if operator tried to indicate error in more than one group by Es without following it by = sign.

4.3 Special character check,'SPCHAR'

'SPCHAR' is a routine which is called after a group is cleared of EEE check. This is to ascertain the location of CR, LF etc. and ignore them except to use these for specific indicator group/location of the message. This routine also removes special characters out of groups consisting of numerics except solidi (/) which is retained.

This segment also converts alpha/special characters to there numeric equivalents, if it is suspected that lower case characters have been introduced instead of upper case characters(numerics).

4.4. Adjustment of group of five 'CHKFIVE'

This routine checks and adjusts the various groups into groups of 5 characters which is the standard format. As mentioned earlier under 3.1.2 because of operator's mistake or other reasons, a number of groups have characters other than 5. It is found to occur under following conditions:

i) Two or more groups may get merged without a blank separater.

ii) A few characters of second group may get merged with the first group, thus making one group with numer greater than 5 and the other group with less than 5.

iii) Instead of blank separator, there is a special character between two groups.

iv) Special or convertible alpha characters within a group of numerics.

This routine proceeds by checking the number and type of character within two blanks. Special characters are removed, convertible characters are converted to numerics and then branching takes to three different sections depending upon if the number of character is five, less then five or more than five.

If number is five,the search and checking is started for the next group. If it is less than 5, check is made if by combining the next group, it is possible to complete the group, otherwise this group is completed by appropriate number of solidi.

In case number of characters in a group be more than 5, (provision has been made to accommodate 12 characters) and no special character, the group is broken up into groups of 5 characters if any character found superfluous by consideration of next group, these are dropped. For example if the first group contains 7 characters and second group 5 valid numeric character additional two characters of the first group are dropped.

As already mentioned elsewhere, whenever any changes are made in data through DPPM, the original data is preserved and the corrected data is flagged to indicate that DPPM has made some changes.

4.5 Sorting of upper air data 'UASORT'

After a complete message is checked for possible telecommunication and other errors as discussed above, upper air data is passed through routine UASORT to ensure bringing in the various groups in proper sequence as specified by W.M.O format. Depending upon the message identifier, the block index of the station or the coordinates of the observing ship station are stored in the output area. Next groups are sorted according to specific code and their group indicators. By proper sorting it is possible to identifiy missing groups, superfluous groups and suitable corrections made . The logic takes note of required identification characters in specific group.

After ascertaining block index of the observing (or call sign and its coordinates if ship station) station and time group, the routine checks for the first level indicator. Depending upon the type of observation the program expects a fixed number of groups to carry information for one level, eg for TEMP message, there should be normally two to three groups.

To provide uniform information for subsequent decode routine all the messages are restructured to carry groups for every level, as required in the standard code.

After the routine successfully finds the indicator for the first reported level say L, it checks if the 4th group contains the next level (L+1), the program accepts 2nd and 3rd groups to represent temperature and wind groups for level L. In case 4th group be not next level, this group is checked for duplication of the present level (L) or presence of the level L + 2. Depending upon the results of comparison, the scan proceeds. In case none of the above conditions is satisfied, 3rd and 2nd groups are checked if these refer to level L + 1 or L, additional group of 5 solidi or erasing of Ist group takes place. With the successful execution of this routine, each level is ensured to have requisite groups:

Following two examples illustrate the working of the routine.

4.5.1. Missing of groups:

```
TTAA  57231  91958  99019  22465  08026  00165  21056  08020
85541  70152  08869  13008  50587  03364  15014 ---------- =
```

In the above message after message indicator TTAA, time group 57231 and station block/index 91958, the next six groups (3 each level) refer to surface and 1000 mb level. 7th group has a valid indicator representing height of 850 mb. The program in its normal scan, checks the 10th group for identifier 70 (representing 700 mb) but that group is 13008, which has neither identifier for 500 mb nor for 850 mb. The scan is therefore made for previous groups (9th and 8th). It encounters indicator for 700 mb in 8th group. Thus routine detects that level 850 mb has two missing groups which are inserted by slashes.

Further message again goes through the normal scan and finally reconstituted message looks like.

```
TTAA 57231 91958  99019  22456  08026  00165  21056  08020 85541 /////
/////  70152  08869  13008  50587  03364  15014 -------------
```

4.5.2 Superfluous group:

```
TTAA  57231 91958  99003  22456  08026  00165  21056  08020 85541 1102
10026  70152  08869  13008  70152  07669  18008  50587  03364
15014 -----  -----  -----  -------
```

In this message the process goes smoothly till 700 mb level. But as soon as the scan skips 3 groups it instead of finding indicator group for 500 mb or 300 mb, it finds again indicator for 700 mb. This is a signal to indicate that the complete level has been repeated. The message therefore gets reconstituted in the following form.

```
TTAA  57231 91958  99003  22465  08026  00165  21056 08020
85541 11020  10026  70152  07669  18008  50587  03364  15014 -------
```

It may be noted that the limitation of the procedure is if one of the wind/Temperature group contains first two characters which match the valid indicator group, problem could arise.

Although working for above example appear to be simple, but lot of kitchen work goes into to bring out the clean messages.

4.6 DECODE ROUTINE

4.6.1 UPPER AIR DATA:-

This routine decodes the messages into a standard form giving various parameter such as height/pressure, temperature wind speed and direction etc for various levels and puts them at standard location on a disk file.

The routine scans for identifier characters for the first group of thelevel and then computes the various elements from the following two groups. This scanning proceeds on till ' = ' sign is encountered.

Each element is provided an additional byte of storage on the disk for providing information on the quality of the observed elements.

Various Sections of the upper air message like TTAA,TTBB, TTCC,TTDD or PPAA, PPBB ----- etc are also merged and duplicate messages ignored. It is assumed that the latest report is the better report. The complete ascent is stored in a record of 1080 bytes in Data Set name DCDUAD. This routine also takes care of the messages which were reconstituted by the previous. routines and provides an input for subsequent routine to print out the raw data and decoded data side by side for their quick scrutiny. Corrections/changes if necessary could be carried out by a routine 'HUMANM' This routine also provides a gross checks on temperature, wind speed and direction. These checks are to ansure that TT is not greater than 50^{o} C, wind direction is not greater than 360 and wind speed is not greater than 300 kt. Missing parameters are denoted by X'99' byte on the disk.

4.6.2 Synoptic surface/ship decode:

The decoding procedure for synoptic data is very similar to one discussed for upper air data, except that no check for duplicate messages is made here, which job is performed through a separate routine.

The complete information relating to the each parameter is stored in the disk at DCDSYP area with each record of 360 bytes. One byte is provided for each parameter to indicats its quality. Missing parameters are denoted again byX'99'on the disk.

Although the description of both the above routines is very brief, but it may be mentioned that these segments have to take care of all the codes and their intricacies for their proper information retrieval. These routines consist of over three thousand assembly level instructions.

4.7 File structuring and inserting of geographical parameters. 'DATASORT'

After all the routines mentioned earlier have been processed, we have all the data on disk in following six files.

i) DCDUAD - This file contains all upper air data, decoded in a standard form. Since no sorting of Data and time etc is done, it may contain data belonging to various times of observations also. It does not contain geographical parameters of the stations.

ii) DCDSYP - This file contains all synoptic surface/ship data decoded in a standard form.
It may contain duplicats messages as well as messages belonging to various date and time observations.

iii) DBATHY - This file contains all the BATHY/TESAC data decoded in a standard form, each record being 360 bytes.

iv) RAWSYP - This file contains all unprocessed data pertaining to the synoptic surface/ship data which were reconstituted by any one of the check routines. Such messages after decoding are also entered here. This is required for printing for human intervention. Each record is of 360 bytes

V) RAWUAD - This file contains the same information for upper air as RAWSYP for surface. Each record consists of 1080 bytes.

vi) SPLDTA - This file contains copy of all data which may be required at some stage but is not being processed at present.

DATASORT routine breaks up files DCDUAD and DCDSYP into two saparate files each referring to current and old data. These files are.

i) UADNEW - This file contains all the upper air data of the current date. This file is further split up into 4 subfiles, each subfile pertaining to synoptic observation 00,06,12,18 G.M.T The organization is such that all data which refers to time 2100 of the previous day to 0259 of today goes into subfile pertaining to data of 00 G.M.T, thus keeping the subfile time at centre , such that

$$HH - 0300 \leqslant \text{TIME OF SUBFILE (HH)} < HH + 0300$$

ii) UADOLD - This file has the same structure as the UADNEW, but has data which refers to previous date.

iii) SYPNEW: This file contains all the synoptic/surface data of the current date. The file is further split into 8 subfiles each subfile containing data for each synoptic observation centred around 00,03,06,09,12,15,18,21 hours. For checking which subfile a particular message will be placed depends upon

$$HH - 0130 \leqslant \text{TIME OF SUBFILE (HH)} < HH + 0130$$

iv) SYPOLD: This file contains all thesynoptic/surface data of the previous date in the same form as in SYPNEW.

Besides organizing the data into various files/subfiles depending upon the type and time of observation this routine'DATA SORT' also performs the following important tasks.

a) It matches the stations with the station directory andprovides geographical parameters like latitude/longitude and elevation of the station. If a particular processed station isnot available in the directory, but is within the Monex area (by block index comparison) the station is stored with geographical parameters as X'9999'.

b) The routine also checks and removes duplicate stations, taking that the recent report is a better report.

c) It provides the option to copy data from SYPOLD/UADOLD to the magnetic tape and data from files SYPNEW/UADNEW to SYPOLD/UADOLD. Additional files may be established if data older than 24 hours is also received on G.T.S.

4.8 Printing out routine 'PTM'

This segment which partly forms part of Decode routine and partly separate segment, is mainly designed to print out flagged data both in decoded and unprocessed form.

Data in special area is also printed out, if desired so that experienced Meteorological Assistants could quickly scan the printed data and salvage maximum data which could be restored through the routine 'HUMANM',

4.9 Human Intervention 'HUMANM'

The previous routine prints out the flagged messages as well as the messages which are found to be doubtful during various consistency checks (to be discussed in part II). This would be scanned by experienced meteorological assistants. The purpose will be two fold, firstly it will ensure that the package is working in the way it was expected and secondally it would provide opportunity to salvage such of the isolated type of messages which were left out by DPPM.

This routine which is to be run immediately after rest of the processing is over but before transferring the data to the magnetic tape, provides a scheme to correct the paremeters found wrong in a message on the disk.

5. Conclusions..

This note describes the various facets of the DPPM (Data processing package for Summer Monex) devised for processing data electronically during field phase of Summer Monex. The main philosophy in devising this system has been to make best use of vast processing power of the computer conipared to man and excellence of human ingenuity. It is impossible to provide for all type of checks but attempts have been made to provide correcting measures, for general type of transmission and operator's errors.

Our expactations are that man-machine mix will provide a very good hybrid data processing system.

The system needs continuous monitoring and updating, thus it demands not a static but a very dynamic monitoring by the data processing experts.

6. Acknowledgement

We are grafeful to Dr. P.K.Das for his encouregements and facilities provided for the development of this package.

We are also grateful for various Scientists from India Meteorological Department and U.S.Monex project for useful discussions we had with them. Specially we would like to thank Mr.Z.E.Shaikh, Mr. T.K. Ray, Dr. H.S.Bedi, Mr. Roy Jenne and Mr. Dennis Joseph.

We are grateful to Mr. N.K. Shukla for preparation of the manuscript.

BRIEF DETAIL ON MESSAGES HANDLED BY DPPM (Data processing package for summer Monex) TABLE 1

	HEADER	DESCRIPTION	REMARKS
A.	SURFACE SYNOPTIC DATA		
1.	SYNOP	SURFACE OBSERVATIONS FROM LAND STATIONS	PROCESSED/DECODED
2.	SYNOP (AUTOMATIC)	AUTOMATIC LAND STATIONS DATA	PROCESSED/NOT DECODED
3.	SHIP	SYNOPTIC SURFACE OBSERVATIONS FROM SEA-STATIONS	PROCESSED/DECODED
4.	SHIP (ABBREVIATED)	SYNOPTIC SURFACE OBSERVATIONS (ABBREVIATED FORM)	PROCESSED/DECODED
5.	SHRED	SYNOPTIC SURFACE OBSERVATIONS (REDUCED FORM)	PROCESSED/DECODED
6.	SPESH	SPECIAL WEATHER REPORT	PROCESSED/DECODED
7.	METAR/SPECI	AVIATION ROUTINE WEATHER REPORT	NOT PROCESSED
B.	UPPER AIR DATA		
1.	PILOT	UPPER WIND REPORT FROM LAND STATION	PROCESSED/DECODED
2.	PILOT SHIP	UPPER WIND REPORT FROM SEA-STATION	PROCESSED/DECODED
3.	TEMP	UPPER LEVEL PRESSURE, TEMPERATURE, HUMIDITY, AND WIND FROM A LAND STATION	PROCESSED/DECODED
4.	TEMPSHIP	SAME AS PILOT BUT FROM A SEA-STATION	PROCESSED/DECODED
5.	ROCOB ROCOB SHIP	ROCKETSO-NDE OBSERVATION (TEMP, WIND, AND AIR DENSITY FROM A LAND STATION/SEA-STATION	PROCESSED/NOT DECODED
6.	CODAR	AIR-CRAFT UPPER-AIR REPORT (OTHER THAN RECONNAISSANCE AIRCRAFT)	PROCESSED
7.	RECCO (UNCODED)	AIRCRAFT UPPER AIR REPORT (FROM RECONNAISSANCE AIRCRAFT)	NOT PROCESSED

HEADER	DESCRIPTION	REMARKS
8. AIREP	AIRCRAFT UPPER AIR REPORT (FROM COMMERCIAL AIRCRAFT)	NOT PROCESSED
C. RADAR DATA		
1. RADOB	GROUND RADAR WEATHER OBSERVATIONS FROM LAND/ SEA STATION	PROCESSED/NOT DECODED
D. SATELLITE DATA		
1. SAREB	SYNOPTIC INTERPRETATION OF SATELLITE CLOUD DATA FROM LAND/SEA STATION	NOT PROCESSED
2. SATEM	REPORT OF SATELLITE REMOTE U.A SOUNDINGS OF PRESSURE, TEMP & HUMIDITY	NOT PROCESSED
3. SARAD	REPORT OF SATELLITE CLEAR RADIANCE OBSERVATIONS	NOT PROCESSED
4. SATOB	REPORT OF SATELLITE OBSERVATIONS OF WIND, SURFACE TEMP,CLOUD,HUMIDITY AND RADIATION	NOT PROCESSED
E. OCEANOGRAPHIC DATA		
1. BATHY	BATHYTHERMOGRAPH OBSERVATIONS	PROCESSED/DECODED
2. TESAC	TEMPERATURE,SALINITY AND CURRENT REPORT FROM A SEA-STATION	PROCESSED/DECODED
F. SPECIAL GARP DATA		
1. TEMP DROP	UPPER LEVEL PRESSURE,TEMP,HUMIDITY AND WIND REPORT FROM DROPSONDES	PROCESSED/DECODED
2. COLBA	UPPER AIR REPORT FROM CONSTANT LEVEL BALLON	PROCESSED/DECODED
3. DRIBU	DRIFTING BUOY OBSERVATION	PROCESSED/DECODED

(SHUKLA)

APPENDIX

	HEADER	IDENTIFICATION	Mi Mi Mj Mj	AREA IN WHICH KEPT
A.	SURFACE SYNOPTIC DATA			
1.	SYNOP	SI/SN/SM/SX	M M X X	PRCSYP/DCDSYP
2.	SYNOP (AUTOMATIC)	SI/SN/SM/SX	A A X X	PRCSYP/DCDSYP
3.	SHIP	SI/SN/SM/SX	N N X X	PRCSYP/DCDSYP
4.	SHIP (ABBREVIATED)	SI/SN/SM/SX	N N X X	PRCSYP/DCDSYP
5.	SHRED	SI/SN/SM/SX	N N X X	PRCSYP/DCDSYP
6.	SPESH	SP	SPESH	PRCSYP/DCDSYP
7.	METAR/SPECI	SA	METAR	SPLDATA
B.	UPPER AIR DATA			
1.	PILOT	UP/UG/UI	PPAA,PPBB,PPCC,PPDD	PRCUAD/DCDUAD
2.	PILOT SHIP	UH/UQ/UY	QQAA,QQBB,QQCC,QQDD	PRCUAD/DCDIAD
3.	TEMP	US/UK/UM	TTAA,TTBB,TTCC,TTDD	PRCUAD/DCDUAD
4.	TEMPSHIP	UL/UE/UF	UUAA,UUBB,UUCC,UUDD	PRCUAD/DCDUAD
5.	ROCOB ROCOB SHIP	UN	RRXX/SSXX	SPLDATA
6.	CODAR	UT	LLXX	SPLDATA
7.	RECCO (UNCODED)	UR	-	SPLDATA
8.	AIREP	UA	-	SPLDATA
C.	RADAR DATA			
1.	RADOB	SD,SB,SC	FFAA/GGAA FFBB/GGBB	SPLDATA

HEADER	IDENTIFICATION	Mi Mi Mj Mj	AREA IN WHICH KEPT
D. SATELLITE DATA			
1. SAREB	TC	CCAA/DDAA CCBB/DDBB	SPLDATA
2. SATEM	TU	VVAA,VVBB,VVCC,VVDD	SPLDATA
3. SARAD	TR	WWXX	SPLDATA
4. SATOB	TS	YYXX	SPLDATA
E. OCEANOGRAPHIC DATA			
1. BATHY	SO	JJXX	DTESAC/DBATHY
2. TESAC	SO	KKXX	DTESAC/DBATHY
F. SPECIAL GARP DATA			
1. TEMP DROP	UZ	XXAA.XXBB,XXCC XXDD	PRCUAD/DCDUAD
2. COLBA	UC	IIXX	PRCSYP/DCDSYP
3. DRIBU	SS	ZZXX	DTESAC/DBATHY

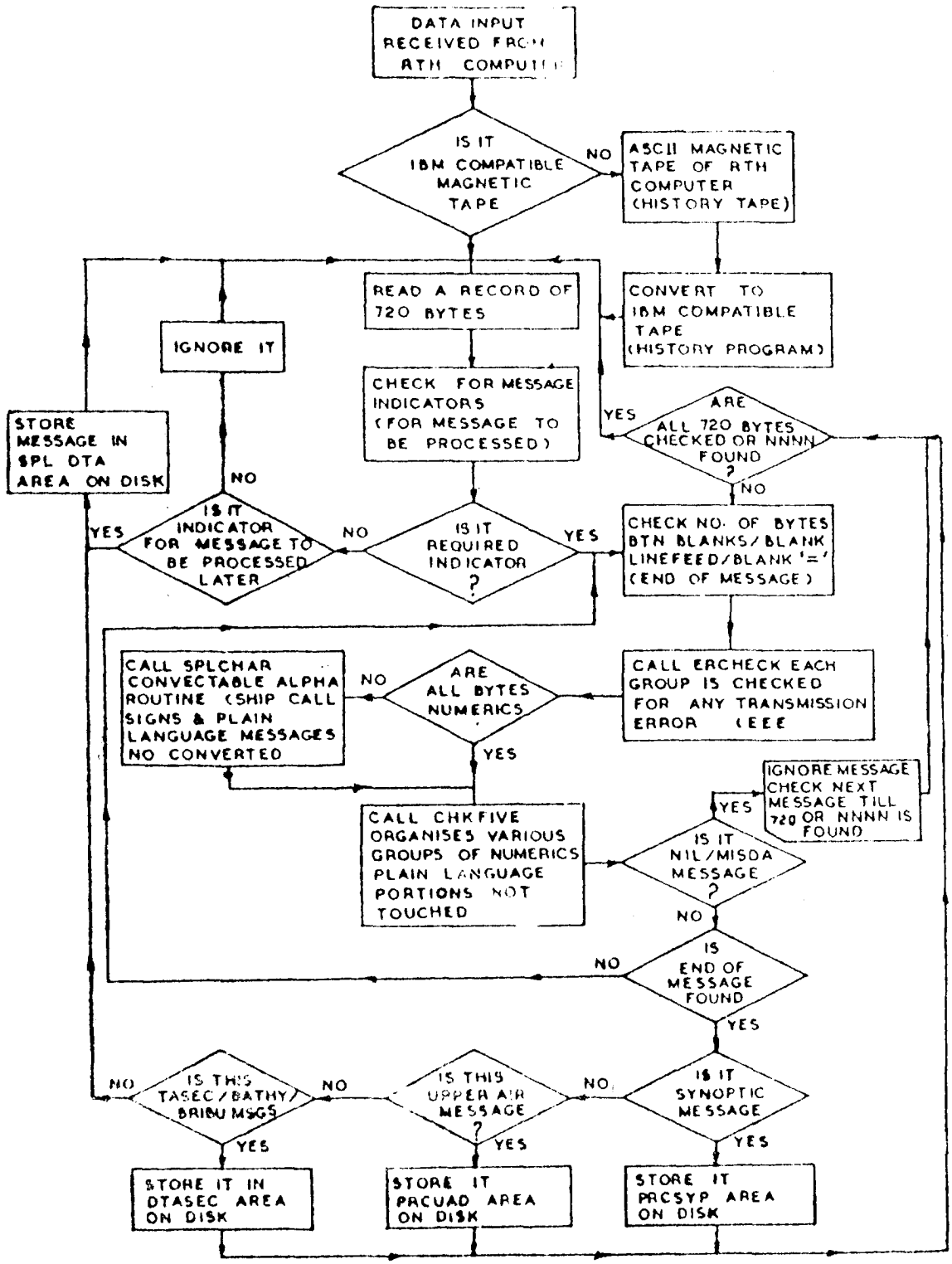
DATA INPUT RECEIVED FROM RTH COMPUTER
IS IT IBM COMPATIBLE MAGNETIC TAPE
NO
ASCII MAGNETIC TAPE OF RTH COMPUTER (HISTORY TAPE)
CONVERT TO IBM COMPATIBLE TAPE (HISTORY PROGRAM)
READ A RECORD OF 720 BYTES
IGNORE IT
CHECK FOR MESSAGE INDICATORS (FOR MESSAGE TO BE PROCESSED)
ARE ALL 720 BYTES CHECKED OR NNNN FOUND ?
YES
NO
STORE MESSAGE IN SPL DTA AREA ON DISK
NO
IS IT INDICATOR FOR MESSAGE TO BE PROCESSED LATER
YES
NO
IS IT REQUIRED INDICATOR ?
YES
CHECK NO. OF BYTES BTN BLANKS/BLANK LINEFEED/BLANK '=' (END OF MESSAGE)
CALL SPLCHAR CONVECTABLE ALPHA ROUTINE (SHIP CALL SIGNS & PLAIN LANGUAGE MESSAGES NO CONVERTED
NO
ARE ALL BYTES NUMERICS
YES
CALL ERCHECK EACH GROUP IS CHECKED FOR ANY TRANSMISSION ERROR (EEE
IGNORE MESSAGE CHECK NEXT MESSAGE TILL 720 OR NNNN IS FOUND
YES
CALL CHKFIVE ORGANISES VARIOUS GROUPS OF NUMERICS PLAIN LANGUAGE PORTIONS NOT TOUCHED
IS IT NIL/MISDA MESSAGE ?
NO
NO
IS END OF MESSAGE FOUND
YES
NO
IS THIS TASEC/BATHY/ BRIBU MSGS
NO
IS THIS UPPER AIR MESSAGE ?
NO
IS IT SYNOPTIC MESSAGE
YES
YES
YES
STORE IT IN DTASEC AREA ON DISK
STORE IT PRCUAD AREA ON DISK
STORE IT PRCSYP AREA ON DISK

Fig - 1 A

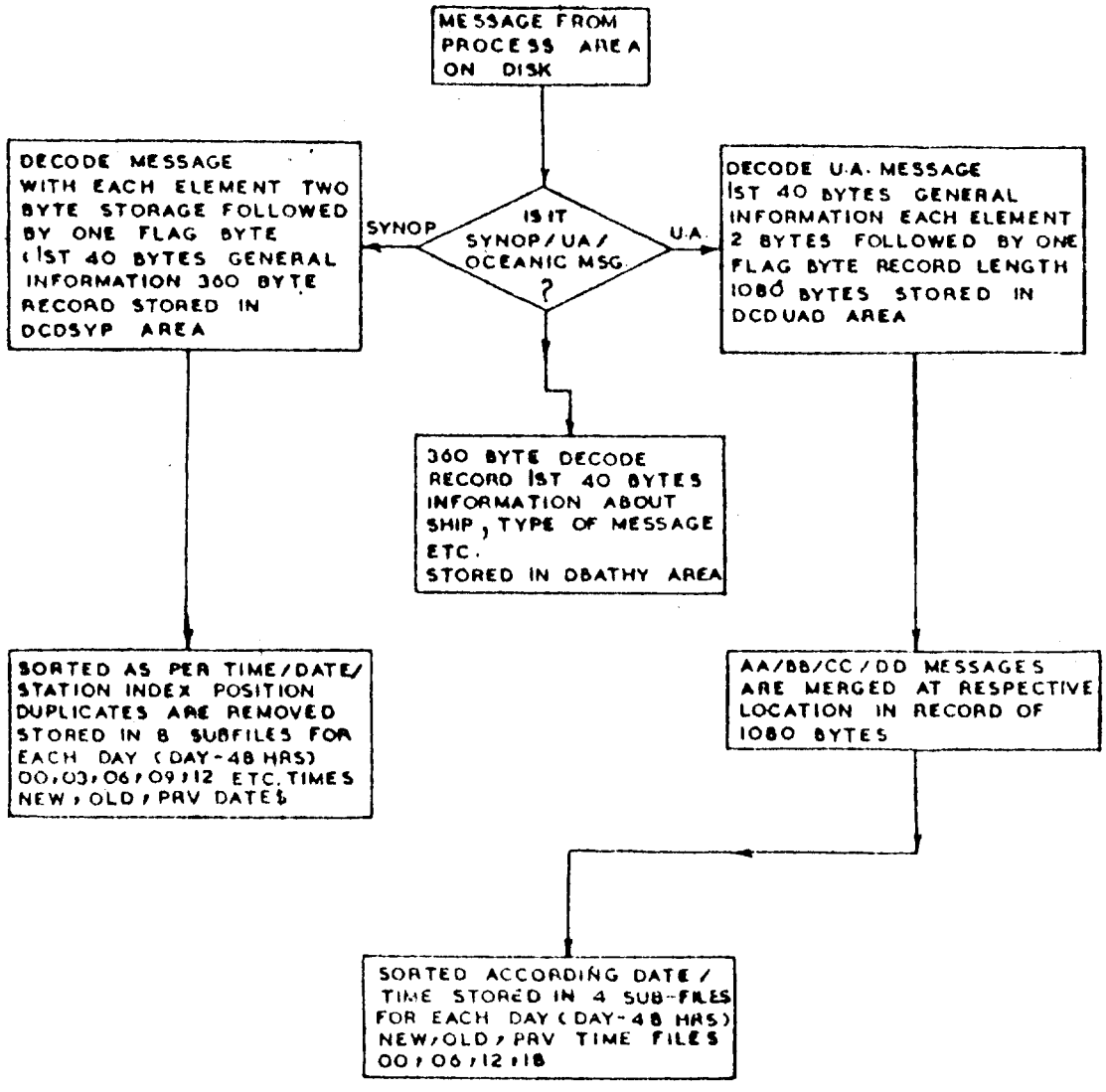
MESSAGE FROM PROCESS AREA ON DISK
IS IT SYNOP/UA/ OCEANIC MSG ?
SYNOP
U.A.
DECODE MESSAGE WITH EACH ELEMENT TWO BYTE STORAGE FOLLOWED BY ONE FLAG BYTE (1ST 40 BYTES GENERAL INFORMATION 360 BYTE RECORD STORED IN DCDSYP AREA
DECODE U.A. MESSAGE 1ST 40 BYTES GENERAL INFORMATION EACH ELEMENT 2 BYTES FOLLOWED BY ONE FLAG BYTE RECORD LENGTH 1080 BYTES STORED IN DCDUAD AREA
360 BYTE DECODE RECORD 1ST 40 BYTES INFORMATION ABOUT SHIP, TYPE OF MESSAGE ETC. STORED IN DBATHY AREA
SORTED AS PER TIME/DATE/ STATION INDEX POSITION DUPLICATES ARE REMOVED STORED IN 8 SUBFILES FOR EACH DAY (DAY-48 HRS) 00,03,06,09,12 ETC. TIMES NEW, OLD, PRV DATES
AA/BB/CC/DD MESSAGES ARE MERGED AT RESPECTIVE LOCATION IN RECORD OF 1080 BYTES
SORTED ACCORDING DATE/ TIME STORED IN 4 SUB-FILES FOR EACH DAY (DAY-48 HRS) NEW/OLD/PRV TIME FILES 00, 06, 12, 18

Fig - 1 B

Critical review and analysis of the statistical summaries concerning the operational data exchange of BATHY and TESAC Reports for 1972 - 1978

by

Klaus Huber

Deutsches Hydrographisches Institut

Abstract

For the planning of future international co-operation within the framework of IGOSS, it is primarily necessary to give an account of how well the "IGOSS" system has functioned to date. One way of doing it is to make "measurements" of the data exchange, and to evaluate these according to their uniform common factors.

Since 1972, the nations taking part in IGOSS have compiled, monthly and every half year, statistical data concerning the data exchange. In the last few years, these statistics have been processed and published several times by groups of experts (the last occasion was in August, 1977). The hitherto existing material was once again critically processed and supplemented by newly received statistical material. A summary of the information used is attached. (In some cases not all existing material was at the author's disposal, especially the statistics for the second half of 1978 was not yet completely available).

The data material will be discussed according to the following criteria:

1) Temporal development of DATA-INPUT

2) Temporal development of DATA-OUTPUT

3) Geographical distribution of IGOSS data and contribution of permanent stations (OWS, buoys)

4) Data exchange through the GTS (Monitoring)

1 Temporal development of DATA-INPUT

At the third meeting of the governmental experts on the BATHY/TESAC Programme (Geneva, March 1976) the input of IGOSS data was defined as follows:

Input of the GTS Centre = total amount of BATHY REPORTS (respectively TESAC/BATHY) received via coastal radio stations and entered into the GTS by a GTS Centre.

Not all participating Member States who have obviously entered IGOSS data have also prepared statistics. So, input informattion from EMNI (Oslo) is lacking, and only incomplete information from ESWI (Norrköping) is available. In both cases the data which have been received in Hamburg from these two GTS Centres were counted as Input of EMNI and ESWI. In analogy, there was no special information for the input of EGRR (Bracknell) until 1976. (EGRR enters all IGOSS reports of the Ocean Weather Stations (OWS) "L" and "R"). Therefore we counted as input of EGRR all OWS-Reports which have

Concerning the output, two facts cause difficulties in some cases :

a) Not in all countries the GTS-Centre involved in the data exchange is identical with the IGOSS NOC which prepares the statistics; this leads occasionally to some confusion within the statistics concerning the definition of input and output.

b) Concerning the counting of output the multiply transmitted reports lead so some difficulties, especially if numbers are to be compared.

There are two types of multiply transmitted data :

Firstly: Totally identical reports (measured data + identifiers) are simply received twice (or several times);

Secondly: Reports are identical in the measured data (Position, Time, Physical Values), but the identifiers (ship call sign and/or GTS call sign) have been changed.

One example for the second type of duplications are the data from Ocean Weather Ship "P". These data were exchanged
by KWBC with the ship call sign CGDN or CGDR
and by CYPF with the ship call sign C 7 P.

According to our experience the portions of multiply transmitted data can be in the order of 10 % of the total amount of data and not all IGOSS-NOCs handle the data in the same manner.

To arrive at comparable figures, the monthly output (BATHY + TESAC + BUOY) was added to the monthly input according to the statistics of the IGOSS NOCs. These monthly sums have been smoothed analogously to the input data and are presented in Figures 3 and 4 together with the total monthly input (BATHY + TESAC + BUOY). Fig. 3 shows the sum of input + output of the IGOSS NOCs Paris, Washington, Tokyo and Hamburg. In Fig. 4 the corresponding numbers of the IGOSS NOCs Moscow, Halifax and Northwood are represented. As a summary the annual figures of the output of the different NOCs are listed in Table II.

The Figures show that the total input and the sum (input + output) are consistent. Normally, the sum lies below the total input curve for all NOCs and it follows the variation of this curve. Since 1976 the sum (input + output) for nearly all NOCs is considerably below the total input. This means that a great deal of data got lost (about 27 % since 1976), according to the statistics of Paris, Washington, Tokyo, Hamburg, Northwood and Halifax. This is not the case for NOC Moscow (see Fig. 4). It seems to be that the main loss of data occurs between GTS-Centre

Moscow (RUMS) and GTS-Centre Offenbach (FDZW). A much more detailed investigation on this aspect will be given in Chapter 4. In 1974 the input + output for NOC Hamburg is above the total input. During GATE (summer 1974) many BATHY and TESAC data have been exchanged via Dakar, but from Dakar no input statistice were available; therefore, the Dakar input was not taken into account in the total input.

3 Geographical distribution of IGOSS data and contribution of permanent stations (OWS, buoys)

Plots for the geographical distribution of BATHY- and TESAC-Reports have been published by the NOCs Washington and Hamburg since 1972 and later, likewise by the NOCs Paris and Tokyo.

To characterize the present status the semi-annual plots for the first 6 months of 1978 of three NOCs have been analyzed. Fig. 5 shows, as an example, the geographical distribution of all BATHY-, TESAC- and BUOY-Reports, which have been received at the NOC Hamburg from Januar until June, 1978.

The data are by no means statistically distributed. There are distinct peaks at the stations of the Ocean Weather Ships "M", "L", "C" and "R" and at the BUOY stations "EB 03", "EB 20" and "EB 21" which can be seen from Fig. 6. The data from these permanent stations contribute to a high extent to the total data base. According to the statistics of the NOC Hamburg, 45 % of the data (January - June 1978) came from the above mentioned permanent stations. Moreover, a high percentage of date lie along lines, which allows the production of temperature (salinity) sections.

The BATHY/TESAC data are mainly restricted to the northern hemispere, which can be seen from Fig. 5 and Fig. 7. Fig. 7 shows a generalized picture of the geographical distribution. Basis for this picture were the above mentioned semi-annual plots. A 10^{o} square was hatched, if there was at least 1 report in one of the 3 semi-annual plots. The counting of the semi-annual geographical distribution led to the result, presented in Table III. They all show mainly the same result. To give a more realistic picture Fig. 8 shows the actual numbers in 10^{o} squares for the distribution, presented in Fig. 5.

4 Data exchange through the GTS (Monitoring)

To monitor the data exchange through the GTS one needs labeled information and an evaluation according to these labels. Both implications are met in our case, therefore a special evaluation of the statistics allows a subsequent monitoring of the data exchange via the GTS.

The reports are normally transmitted as bulletins. The header of each bulletin bears the call sign of the GTS-Centre

been received in Northwood from EGRR. But there is still a discrepancy between EGRR input and the amount of data which other NOCs received from EGRR (see Fig. 13). According to the statistics almost all NOCs got more data than EGRR entered into the GTS.

For presentation of the data the monthly values were smoothed (running mean over 3 values with the weights 0.25, 0.50, 0.25) to weaken the very strong monthly variation of the data. Fig. 1 and Fig. 2 show the result, Table I gives a summary of the annual input of the different GTS Centres.

Fig. 1 shows the smoothed monthly input (according to the statistics), since 1972, split up into input of BATHY, TESAC- and BUOY-data. The area between two curves is a measure for the amount of data considered. (Current data are until now not available).

Fig. 2 shows the total input (BATHY + TESAC + BUOY) which was entered into the GTS by different GTS Centres. The statistics of the Member States mostly indicate only one GTS Centre for the input, but in reality several subordinated Centres are involved. In Fig. 2 the main Centres are represented with the subordinated Centre in brackets.

The curves show an annual variation; during the winter months, the number of reports decreases. Since the BATHY/TESAC Project has entered into the operational phase, the total number of reports increased substantially, especially due to the TESAC- and BUOY-data. Likewise, international experiments like GATE or POLYMODE contribute to the data base.

Fig. 2 shows clearly that the main input comes from the GTS-Centres Washington (KWBC) and Moscow (RUMS). Nevertheless, Fig. 2 gives an imcomplete picture of the input of different nations, because France, for example, feeds its Ocean Weather Ship data through Bracknell (EGRR) into the GTS and many reports of Soviet ships have been entered through Washington (KWBC) during POLYMODE.

2 Temporal development of DATA-OUTPUT

At the third meeting of the governmental experts in the BATHY/TESAC Programme (Genova, March 1976) the output of IGOSS data was defined as follows:

Output at an IGOSS NOC = total amount of BATHY REPORTS (respectively TESAC/BUOY) received via GTS by an IGOSS NOC.

through which the reports have been inserted into the GTS. In general these bulletins are forwarded without changing the header-information, but obviously, not in all cases. The output in the statistics prepared by Member States is split up according to the GTS call signs.

Another kind of labeled information are the BUOY data, these data are exclusively inserted by KWBC and/or PANC and they are counted especially in the statistics.

For an investigation of the routing of the IGOSS reports we compared:

a) the input by KWBC with the output of KWBC+KNMA+KNMF+KNMN+PANC

b) the input of BUOY data with the output of BUOY data,

c) the input by RUMS with the output of RUMS+RUHB+RUNW,

d) the input by RJTD with the output of RJTD+RJHB,

e) the input by EGRR with the output of EGRR

at different NOCs.

The result is presented in Fig. 9 to Fig. 16. The author is not in a position to interprete the results in detail; to do this he needs much more information on how the statistics are prepared at the individual NOCs (How wrong a report must be to be rejected by a computer programme ? To what extent have duplications been considered, etc. ?) Nevertheless, some general conclusions can be made concerning the data flow:

Fig. 9 and Fig. 10 show the input - given by KWBC - against the associated output at the NOCs Moscow, Halifax, Northwood, Tokyo, Paris and Hamburg. Since 1976 nearly all NOCs received a high percentage of the KWBC Input. This can be seen especially from Fig. 12, which compares the Buoy input and output of Buoy data at the NOCs Moscow, Paris, Toky and Hamburg.

Fig. 11 shows a quite different situation; it compares the input by RUMS with the associated output at NOCs Tokyo, Northwood, Paris, Hamburg and Washington. All NOCs received only a small part of the RUMS input. A special break-down was observed in January and February, 1978.

Fig. 13 shows the input and output of EGRR. All NOCs received much more than announced by EGRR.

Looking to the input of RJTD (see Fig. 14) the output curve in Moscow and Washington follows nearly exactly the input curve. But the output in Hamburg is only a small portion of the RJTD input.

Fig. 15 and Fig. 16 give a comprehensive summary of the results given in Figs. 9 to 14 in respect to the routing of BATHY and TESAC reports via the GTS. The Figures show the input of three GTS-Centres (KWBC, RUMS and RJTD) and the proper output at different NOCs for 1977 and 1978 (first six months).

It can be clearly seen that a high percentage of the KWBC input is received at all NOCs, but only a part of the RUMS input (1977 about 50 % and 1978 about 30 %) reaches the other NOCs. Concerning the input at RJTD, the NOCs Moscow and Washington receive nearly all data, but the NOC Hamburg receives less than 40 %.

Final remarks

The present investigation could not deal with all details. A thorough discussion, only, with the originators of the statistics used could shed more light on these details. Therefore, the implications of this paper have been based on a sufficient amount of data. In any way, properties in the data exchange have been pinpointed so that future enterprises of this kind can profit from it.

Literature

1. Monthly statistical evaluation sheets
from Argentina
Canada
Federal Republic of Germany
France
Japan
Union of Soviet Socialist Republics
United Kingdom
United Stats of America

2. Semi-annual statistics
from Federal Republic of Germany
France
Japan
United States of America

3. Programme information circular No. 6
March 1973

4. Programme information circular No. 8
November 1974

5. Programme information circular No. 11
May 1976

6. Programme information circular No. 12
December 1977

YEAR	CYPF CWHF other (Canada)	EDZW DWHA (FRG)	EGRR (UK)	ENMI (Norway)	ESWI (Sweden)	LFPW (France)	KWBC KNMA KNMF KNMN PANC (USA)	RJTD RJHB (Japan)	RUMS RUHB RUNW (USSR)	SABM (Argentina)	TOTAL
1972	2092	112	752	660			2472		1446		7534
1973	100	860	2406	557	149		7714	111	6183		18080
1974	*	578	*	*	*	*	*	*	*	*	14216
1975		355	1674	1066	258		8605		6724	309	18991
1976	2177	590	862		265	104	17892	347	11352	240	33829
1977	2029	629	1177		222	33	18124	2442	13726	132	38514
1978	2888	1573	1481		228	651	18962	2069	19870	323	48045

* detailed information not available

Table I: Input (Bathy + Tesac + Buoy) per year by different GTS-Centres according to the Statistics

YEAR	Halifax Canada	Paris France	Hamburg Fed.Rep. Germany	Tokyo Japan	Northwood UK	Washington USA	Moscow USSR
1972	3788		5803	4820	2701	5862	978
1973	763		9022			6807	5364
1974	*	*	11811	*	*	*	*
1975			14341		9724	6373	5391
1976	*	25126	23702	20173	15707	8418	3688
1977	22783	29612	27773	22105	15044	12314	22851
1978	16282	33861	26970	22299	25513	13852	27116

* detailed information not available

Table II: Output (Bathy + Tesac + Buoy) per year from different IGOSS NOCs resp. WOCs

Source of data	NOC* Paris	NOC Washington	NOC Hamburg
North Pacific, North of 20°N	58 % (46 %)	57 %	51 % (29 %)
North Atlantic, North of 20°N	34 % (38 %)	34 %	40 % (48 %)
Equatorial belt, 20°N - 20°S	5 % (9 %)	5 %	5 % (16 %)
Mediterreanean	1 % (2 %)	2 %	3 % (5 %)
South Pacific South of 20°S	1 % (2 %)	1 %	1 % (1 %)
South Atlantic South of 20°S	1 % (2 %)	1 %	1 % (1 %)

Table III: Geographical distribution of BATHY-, TESAC- and BUOY Data for Jan. - June 1978.

In ( ) the aequivalent figures for July - Dec. 1978.

*Figures from NOC Paris are given for BATHY reports only.

revised Figures 1 and 2

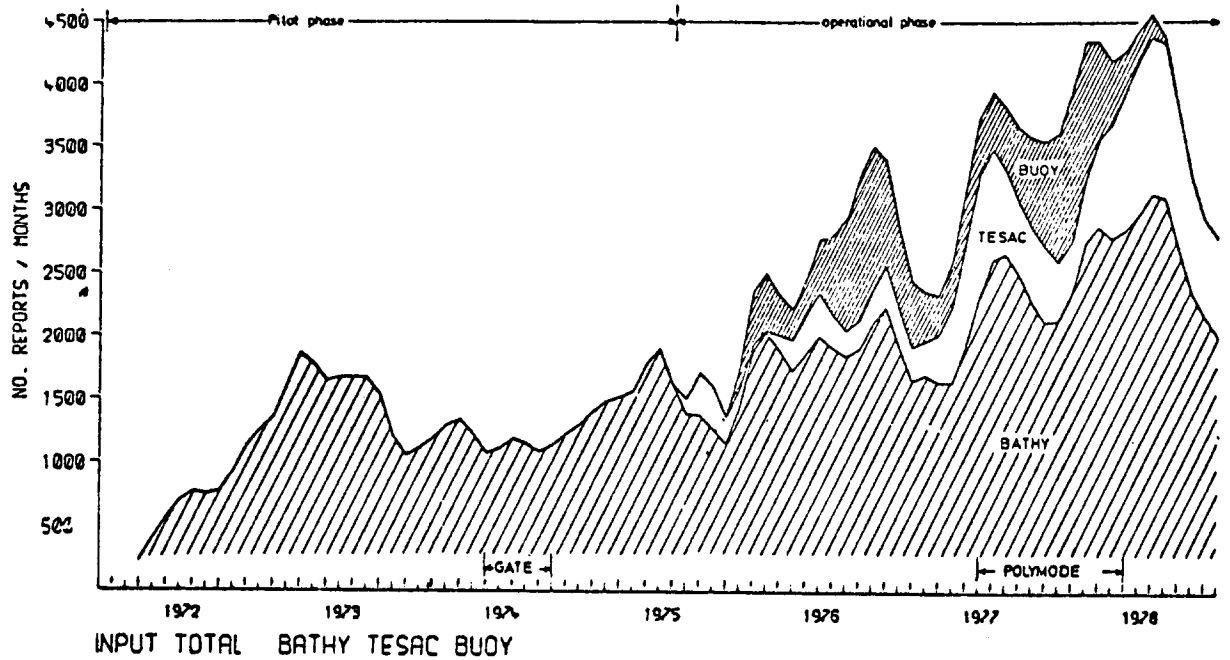

Fig. 1

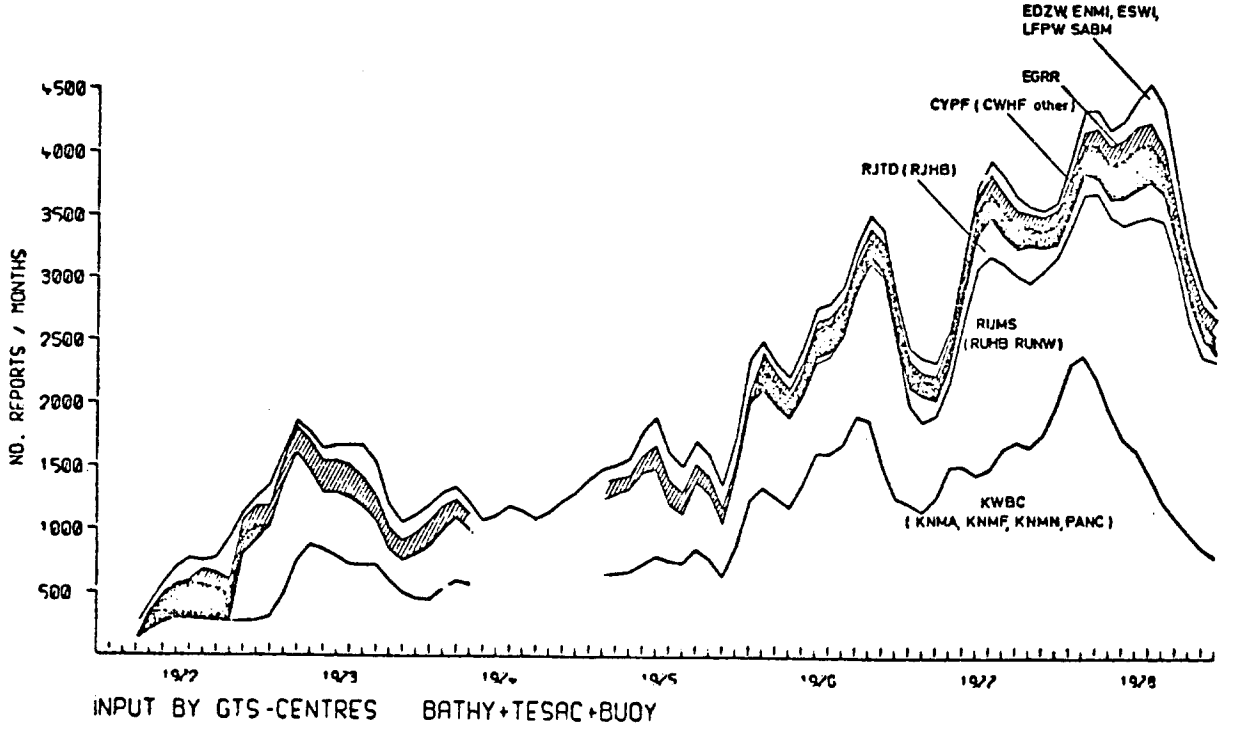

Fig. 2

revised Figures 3 and 4

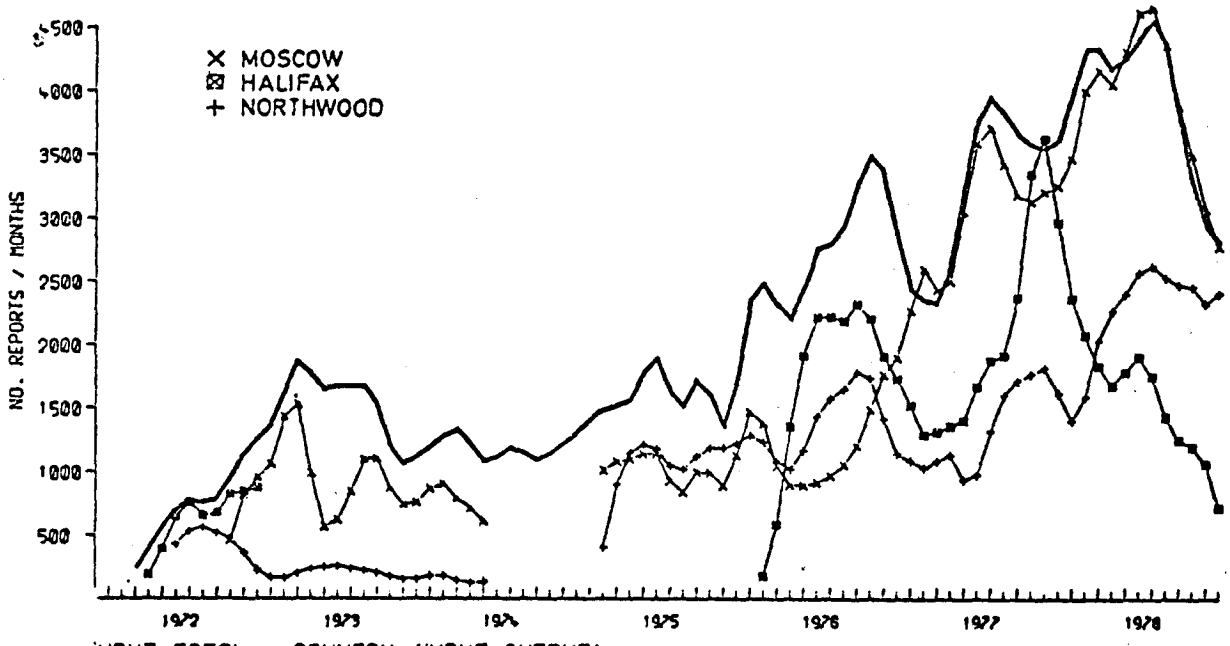

Fig. 4

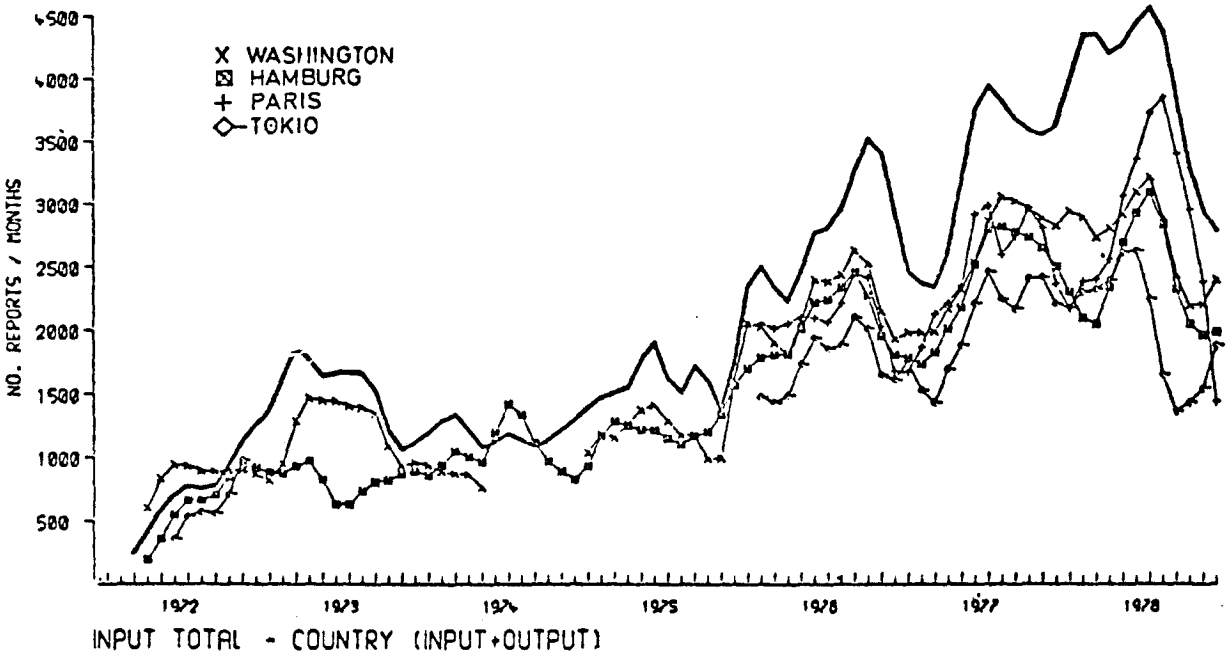

Fig. 3

additional information

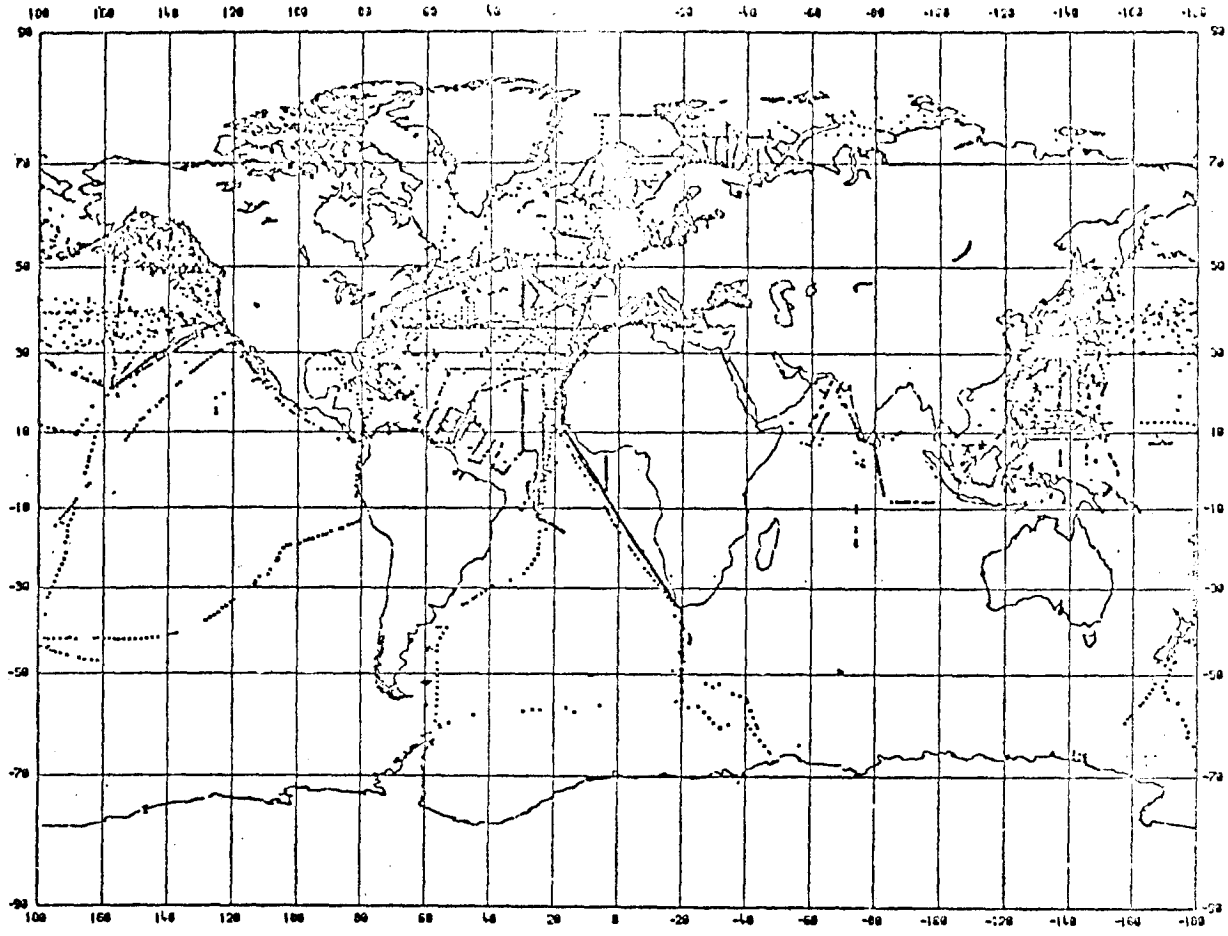

DHI, H A M B U R G, FRG

GEOGRAPHICAL DISTRIBUTION OF BATHY-,TESAC reports received at the Deutsches Hydrographisches Institut from July to December 1978

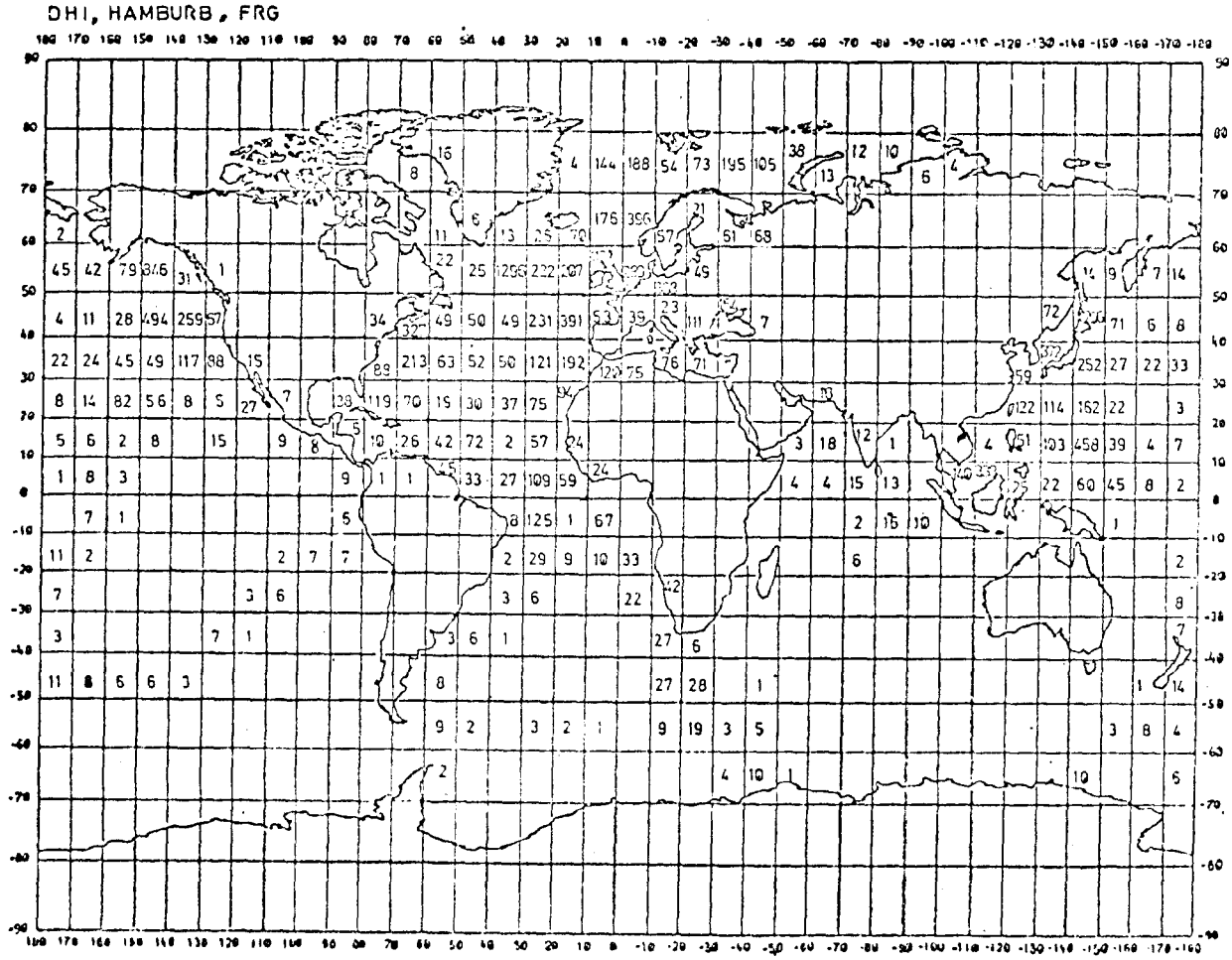

GEOGRAPHICAL DISTRIBUTION OF BATHY-,TESAC reports received at the Deutsches Hydrographisches Institut from July to December 1978

additional information

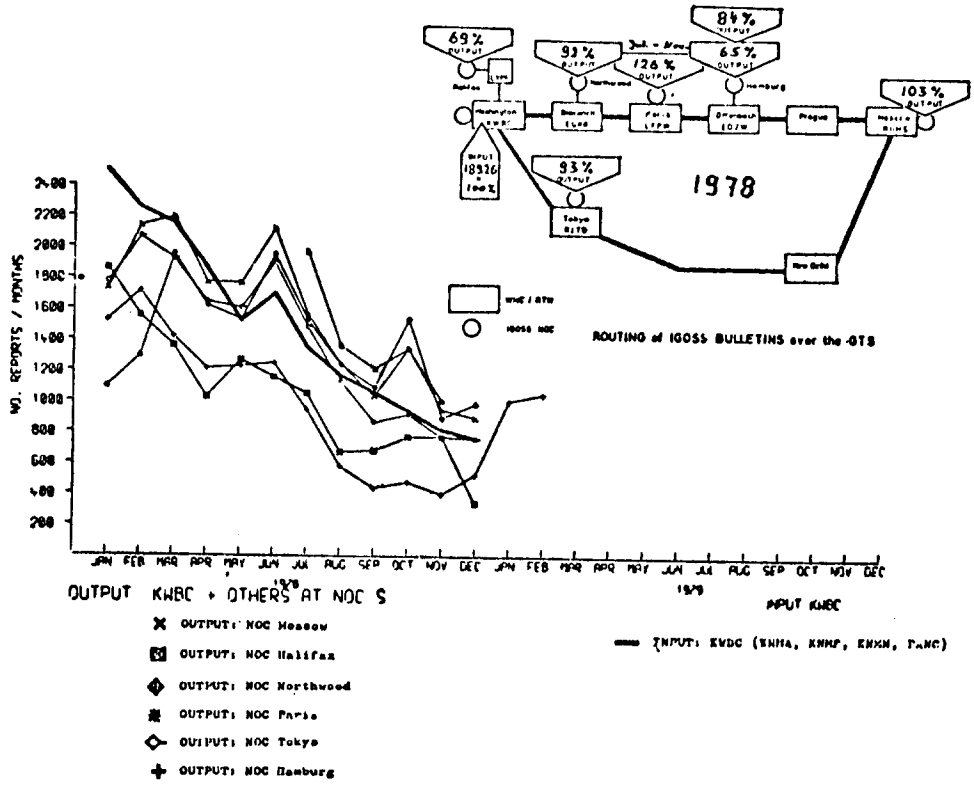

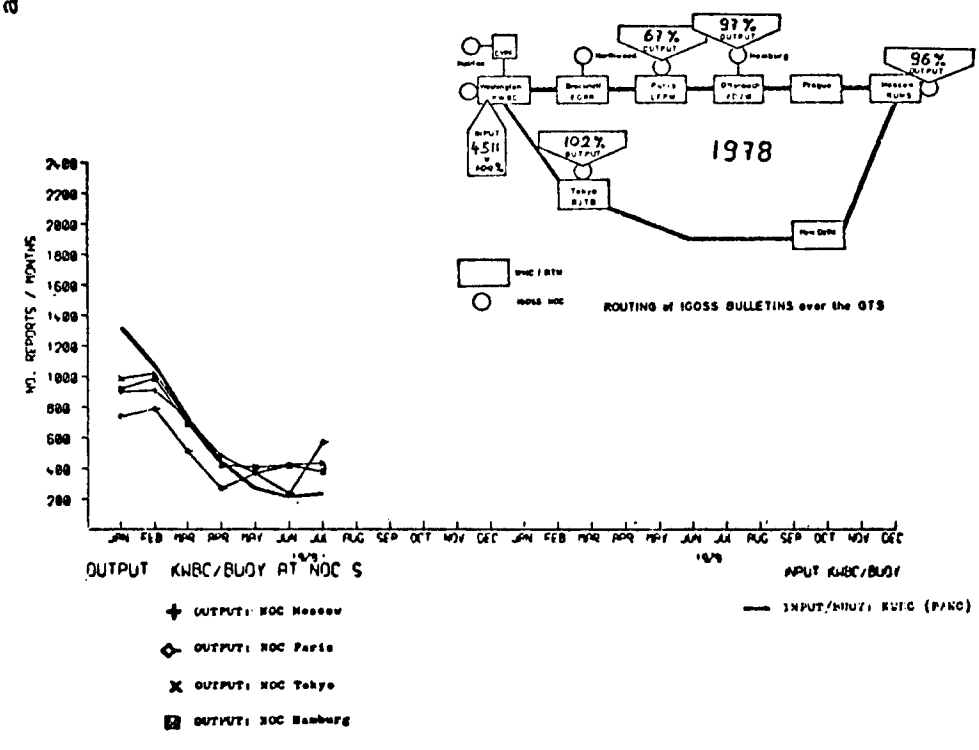

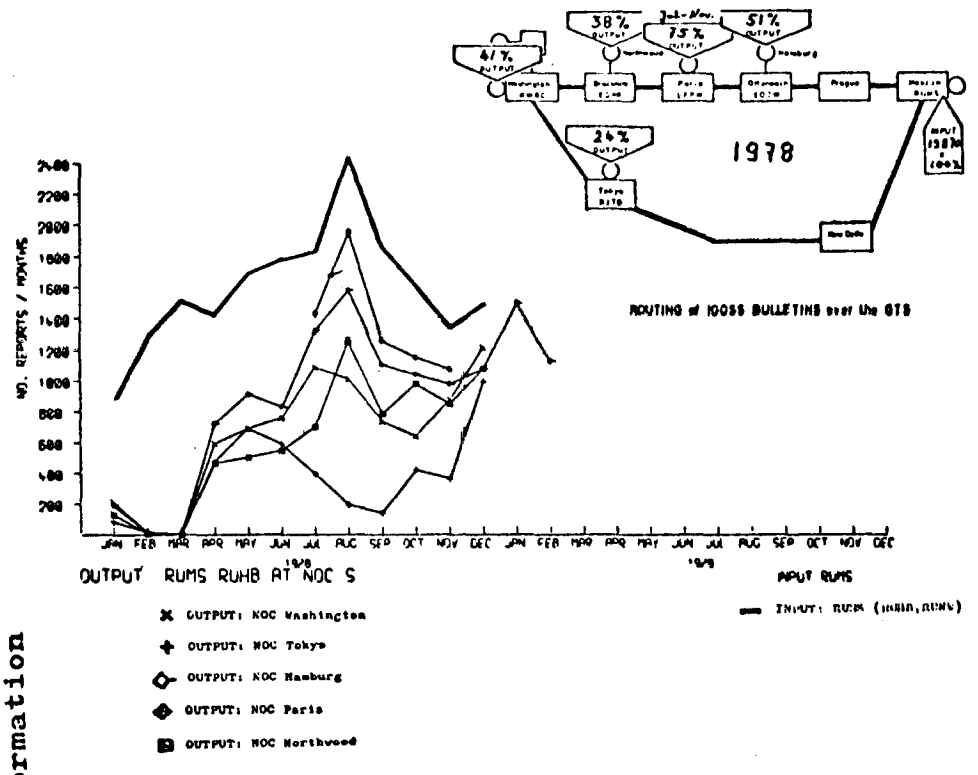

additional information

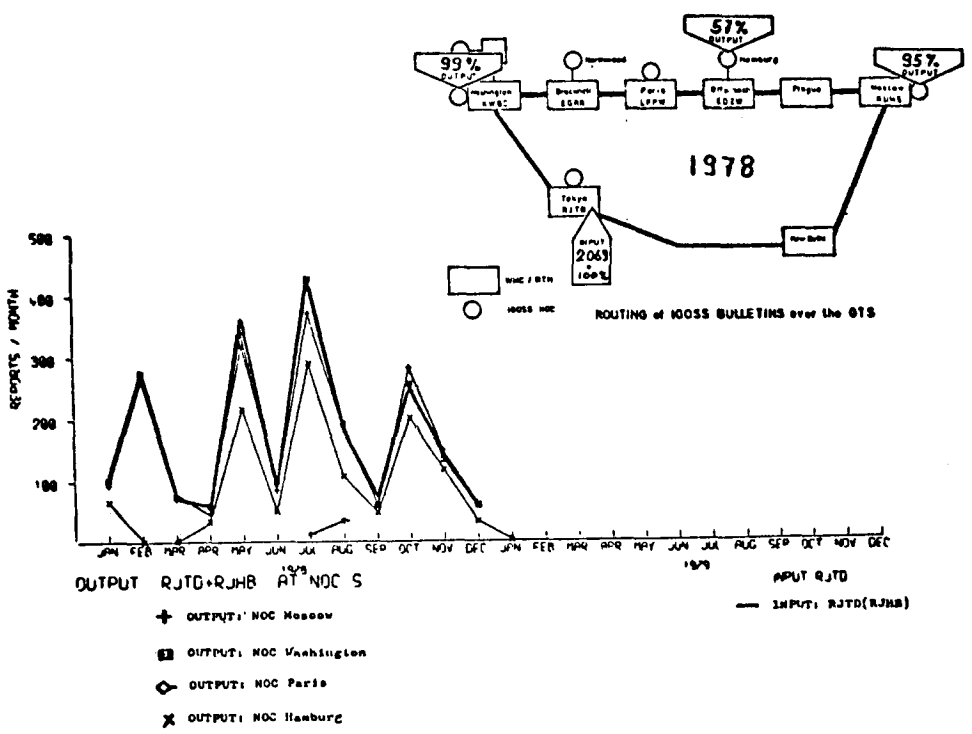

Fig. 19

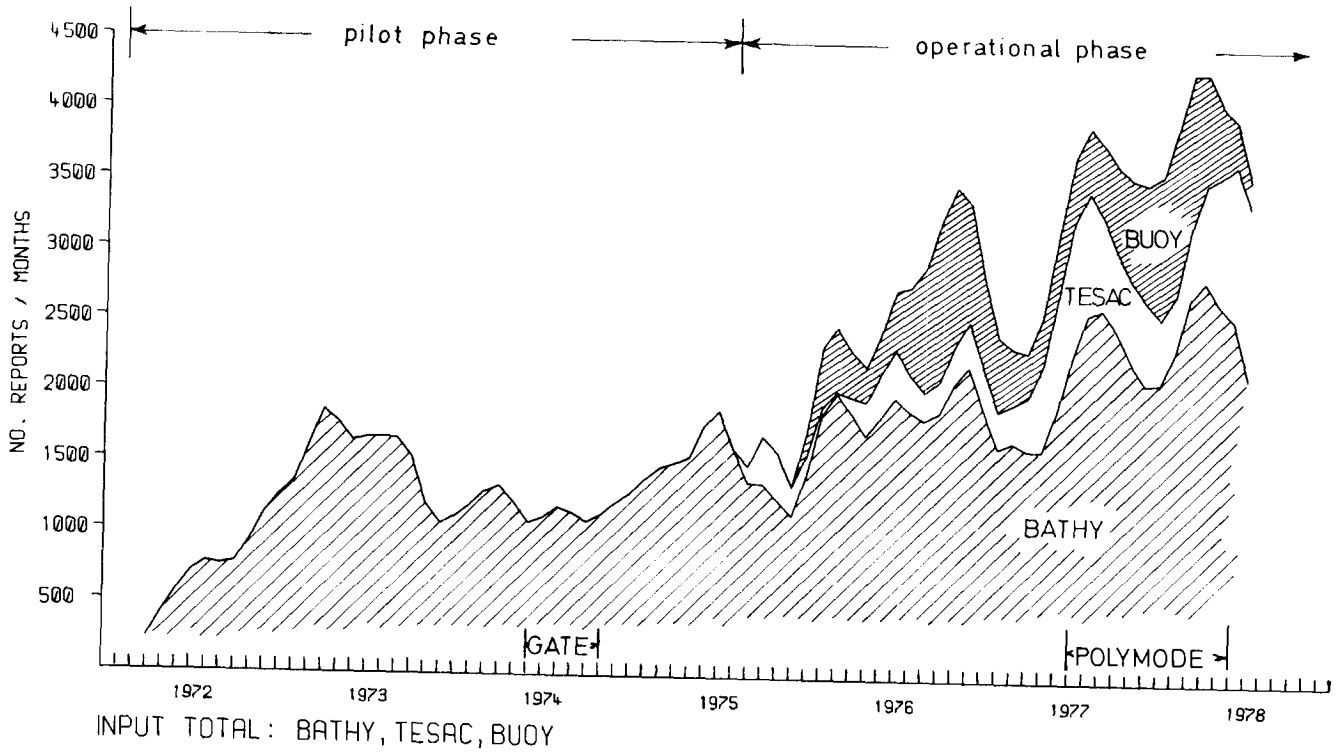
pilot phase
operational phase
NO. REPORTS / MONTHS
4500
4000
3500
3000
2500
2000
1500
1000
500
BUOY
TESAC
BATHY
GATE
POLYMODE
1972
1973
1974
1975
1976
1977
1978
INPUT TOTAL: BATHY, TESAC, BUOY

Fig. 1

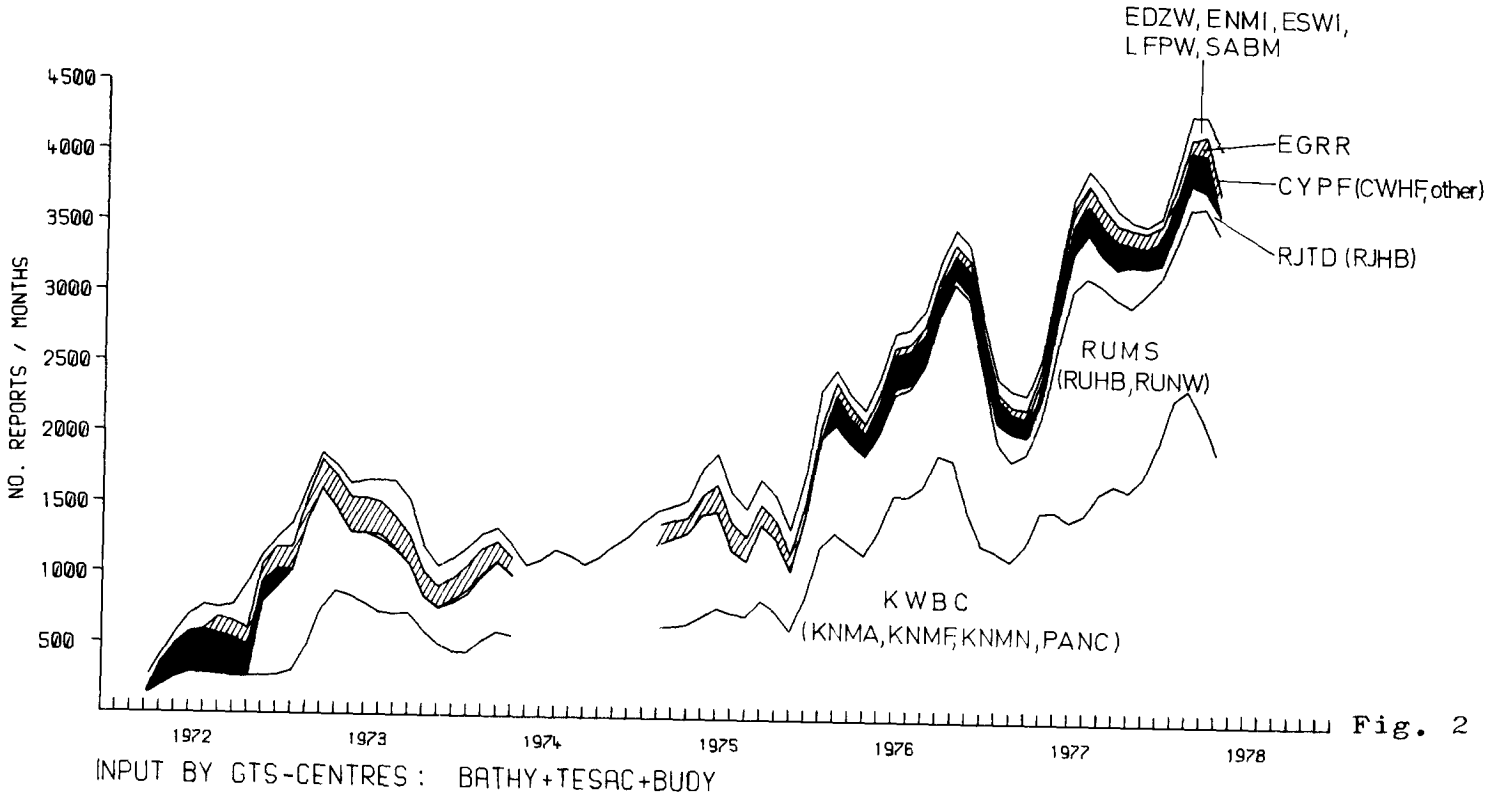
EDZW, ENMI, ESWI,
LFPW, SABM
EGRR
CYPF (CWHF, other)
RJTD (RJHB)
RUMS
(RUHB, RUNW)
KWBC
(KNMA, KNMF, KNMN, PANC)
NO. REPORTS / MONTHS
4500
4000
3500
3000
2500
2000
1500
1000
500
1972
1973
1974
1975
1976
1977
1978
INPUT BY GTS-CENTRES: BATHY+TESAC+BUOY

Fig. 2

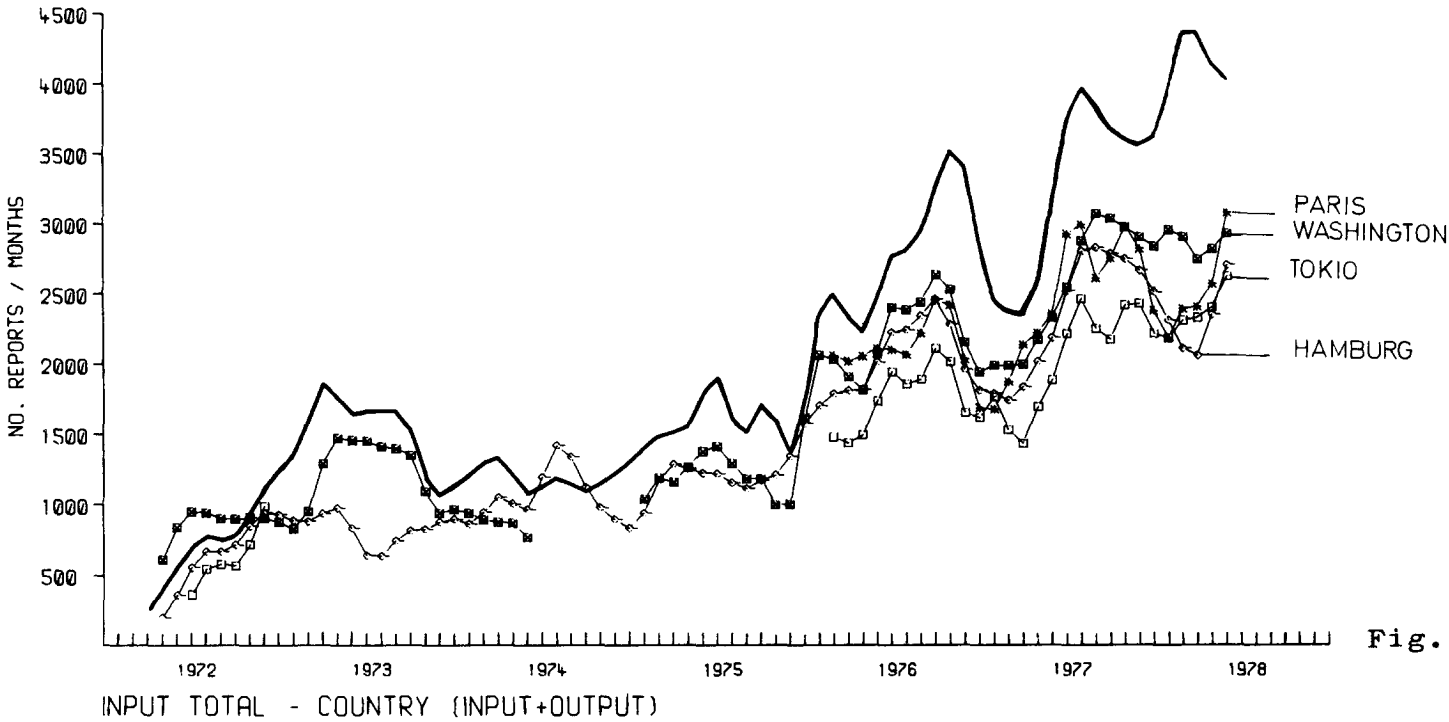
4500
4000
3500
3000
2500
2000
1500
1000
500
NO. REPORTS / MONTHS
PARIS
WASHINGTON
TOKIO
HAMBURG
1972
1973
1974
1975
1976
1977
1978
INPUT TOTAL - COUNTRY (INPUT+OUTPUT)

Fig.

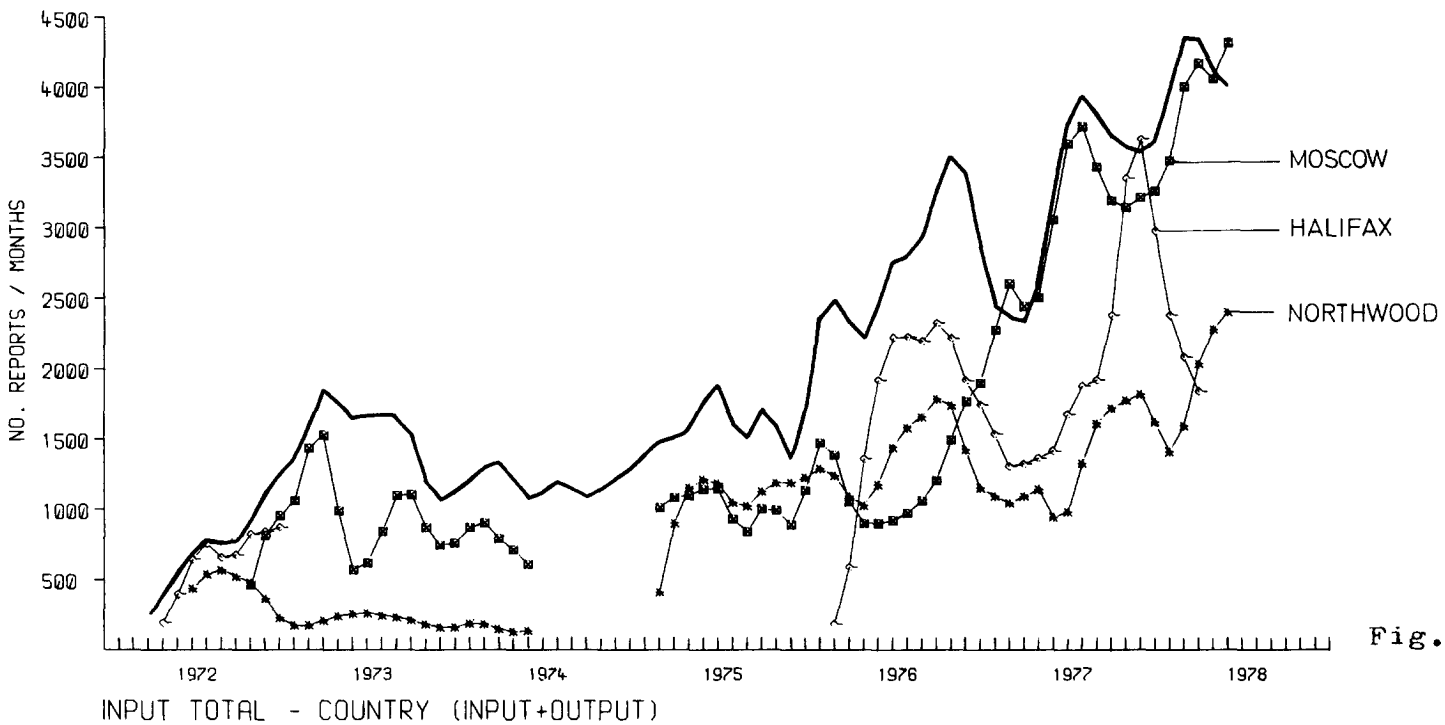
4500
4000
3500
3000
2500
2000
1500
1000
500
NO. REPORTS / MONTHS
MOSCOW
HALIFAX
NORTHWOOD
1972
1973
1974
1975
1976
1977
1978
INPUT TOTAL - COUNTRY (INPUT+OUTPUT)

Fig.

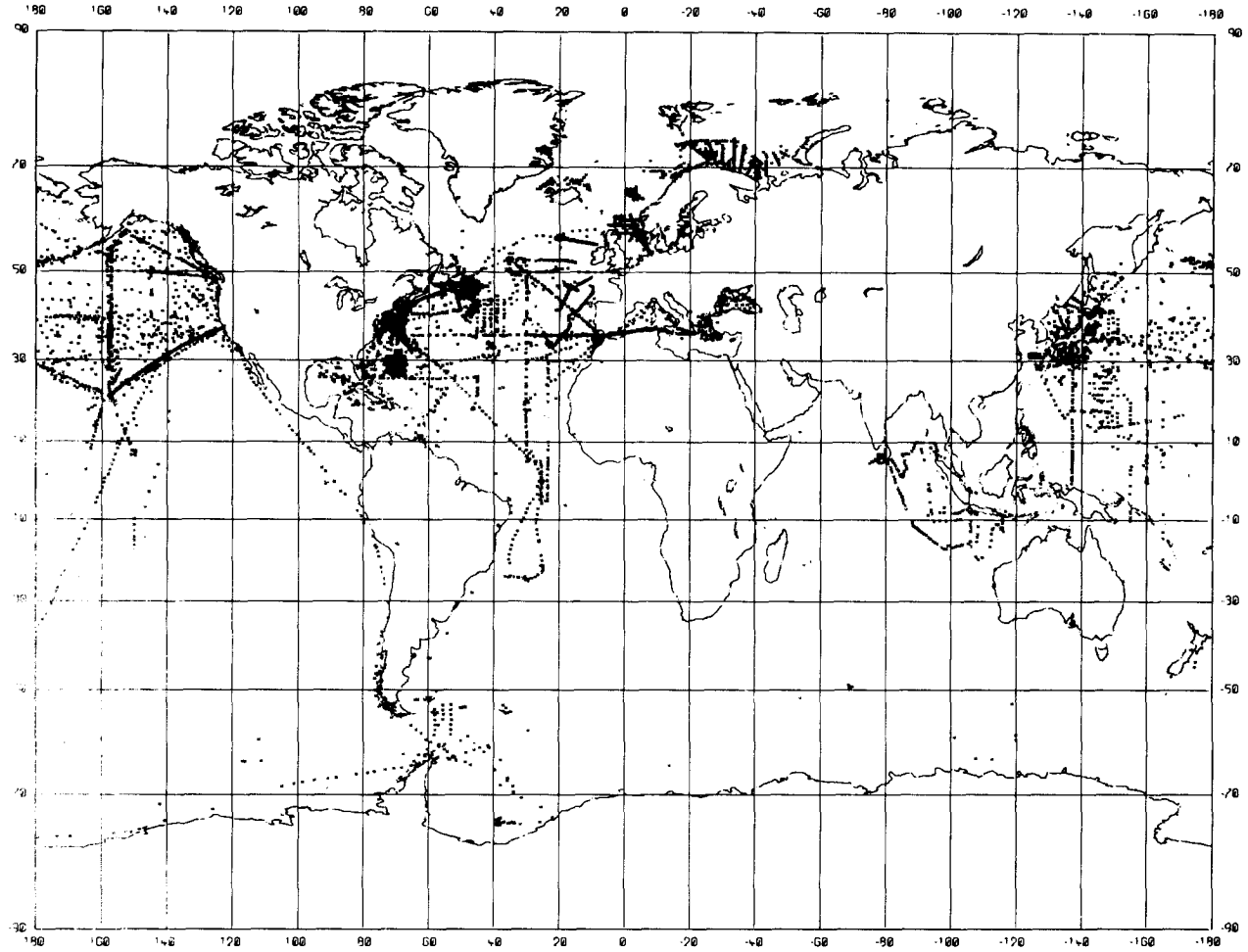

DHI, H A M B U R G, FRG

GEOGRAPHICAL DISTRIBUTION OF BATHY-, TESAC-AND BUOY-REPORTS FROM JANUARY TO JUNE 1978

Fig. 5

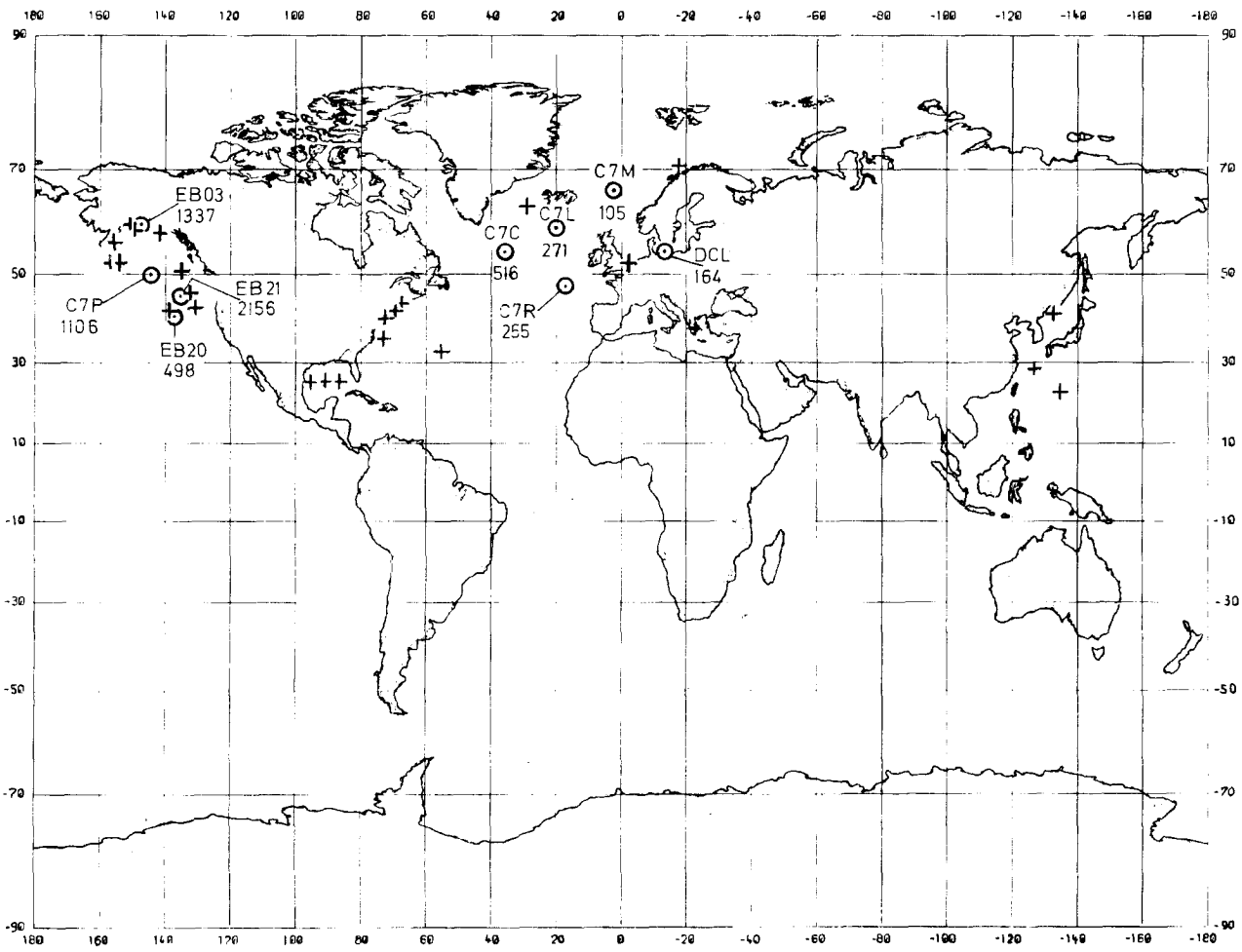

Fig. 6

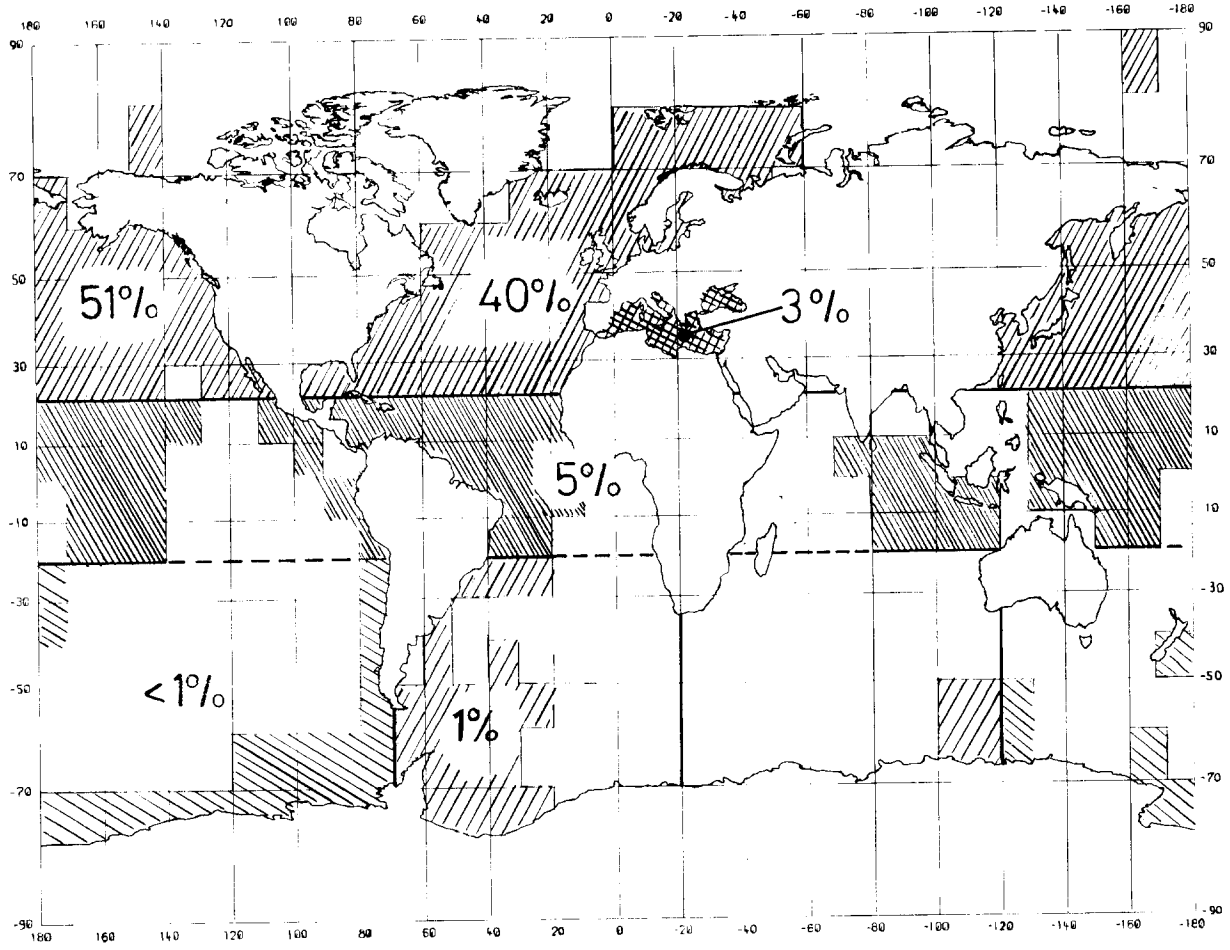

Fig. 7

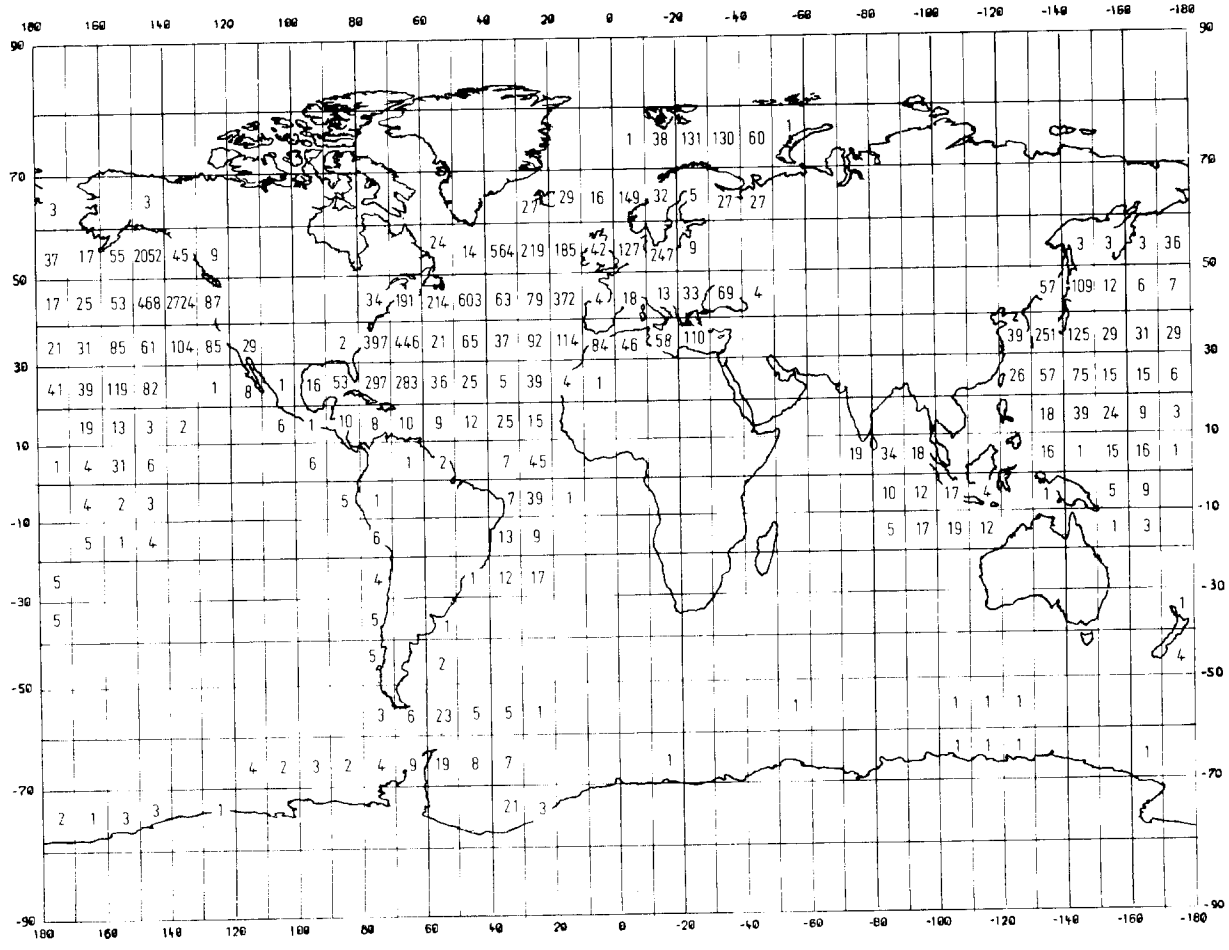

Geographical distribution of BATHY/TESAC reports received at the Deutsches Hydrographisches Institut from January to June 1978

Fig. 8

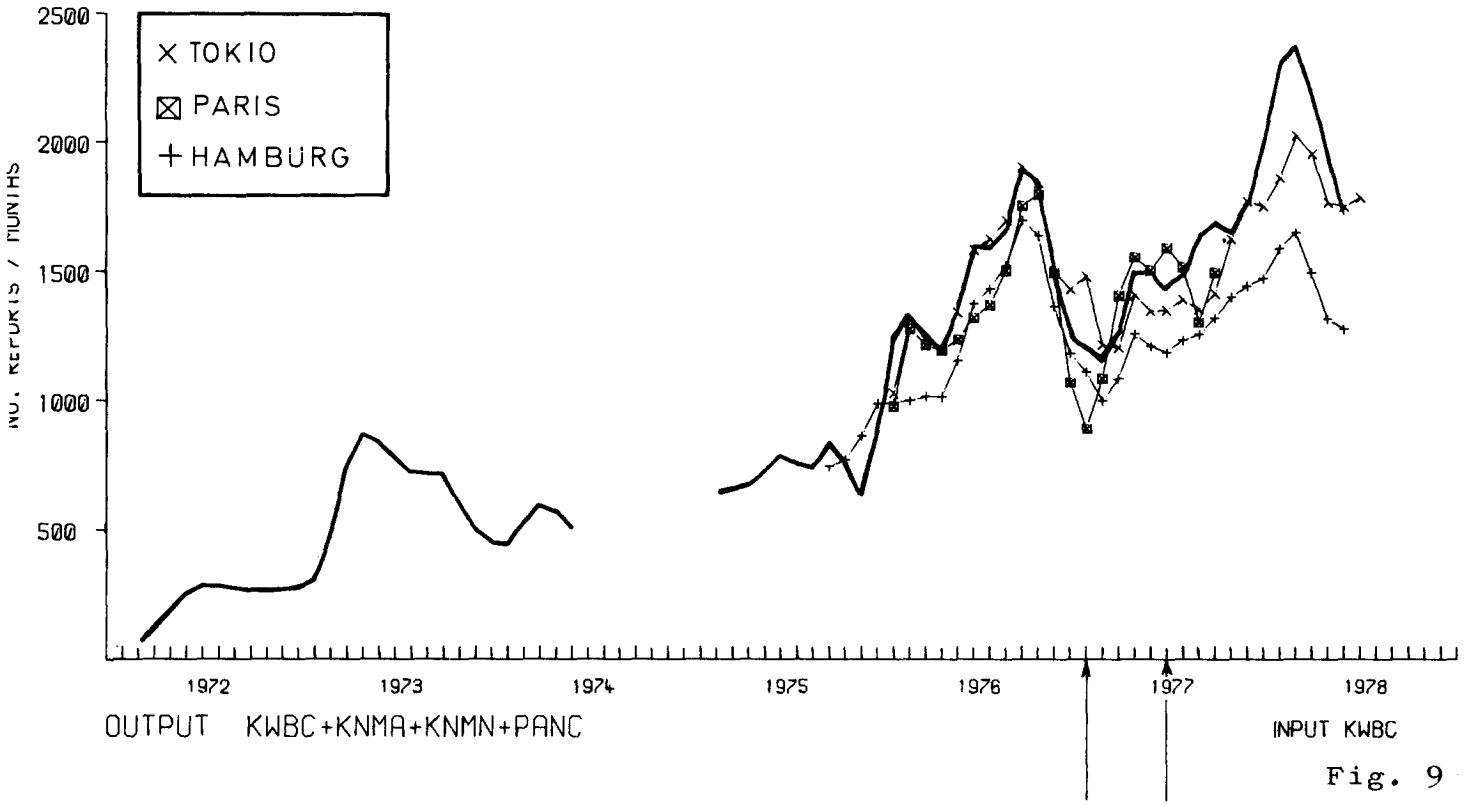
2500
2000
1500
1000
500
X TOKIO
PARIS
+ HAMBURG
1972
1973
1974
1975
1976
1977
1978
OUTPUT KWBC+KNMA+KNMN+PANC
INPUT KWBC

Fig. 9

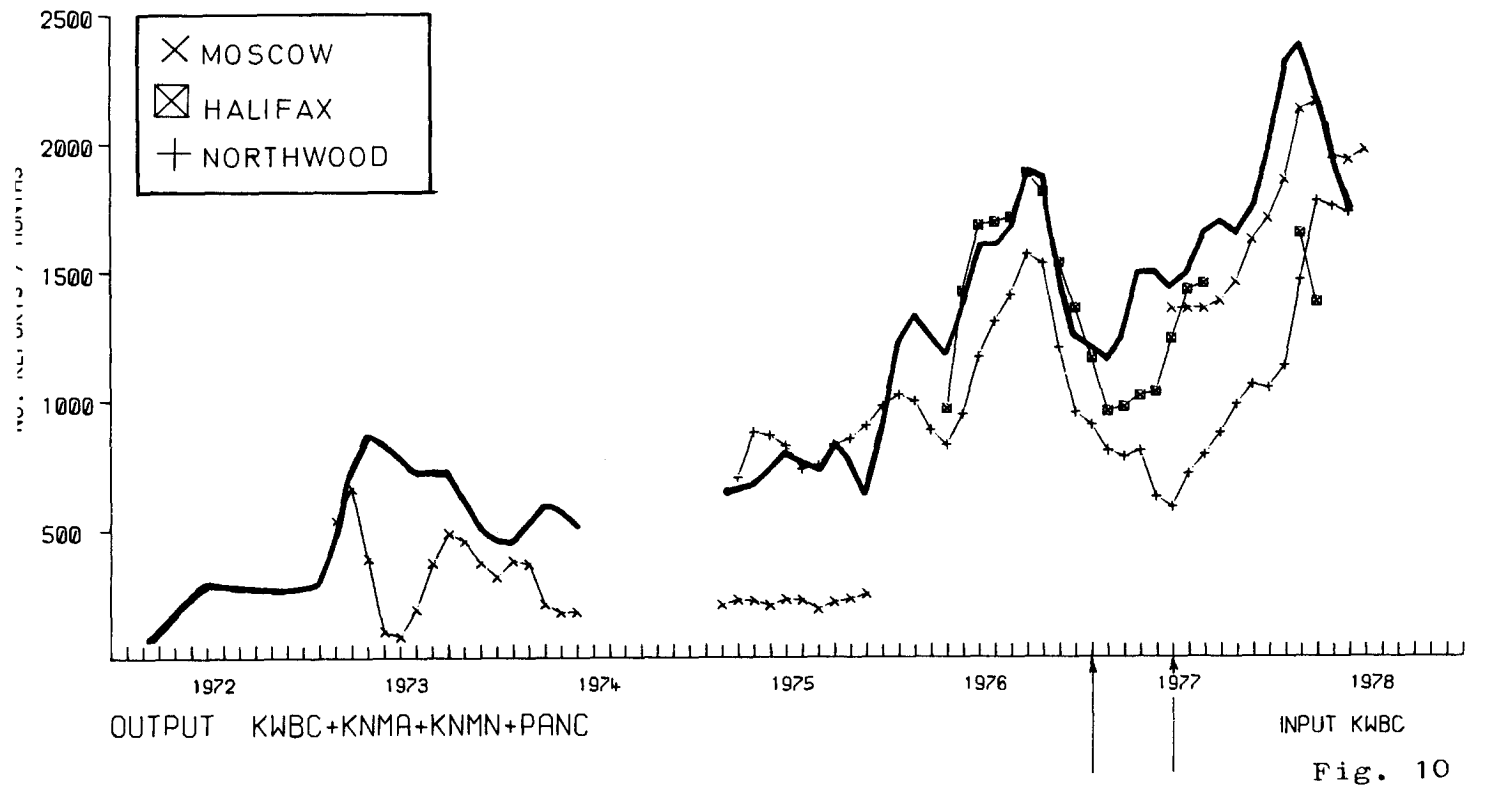
2500
2000
1500
1000
500
X MOSCOW
HALIFAX
+ NORTHWOOD
1972
1973
1974
1975
1976
1977
1978
OUTPUT KWBC+KNMA+KNMN+PANC
INPUT KWBC

Fig. 10

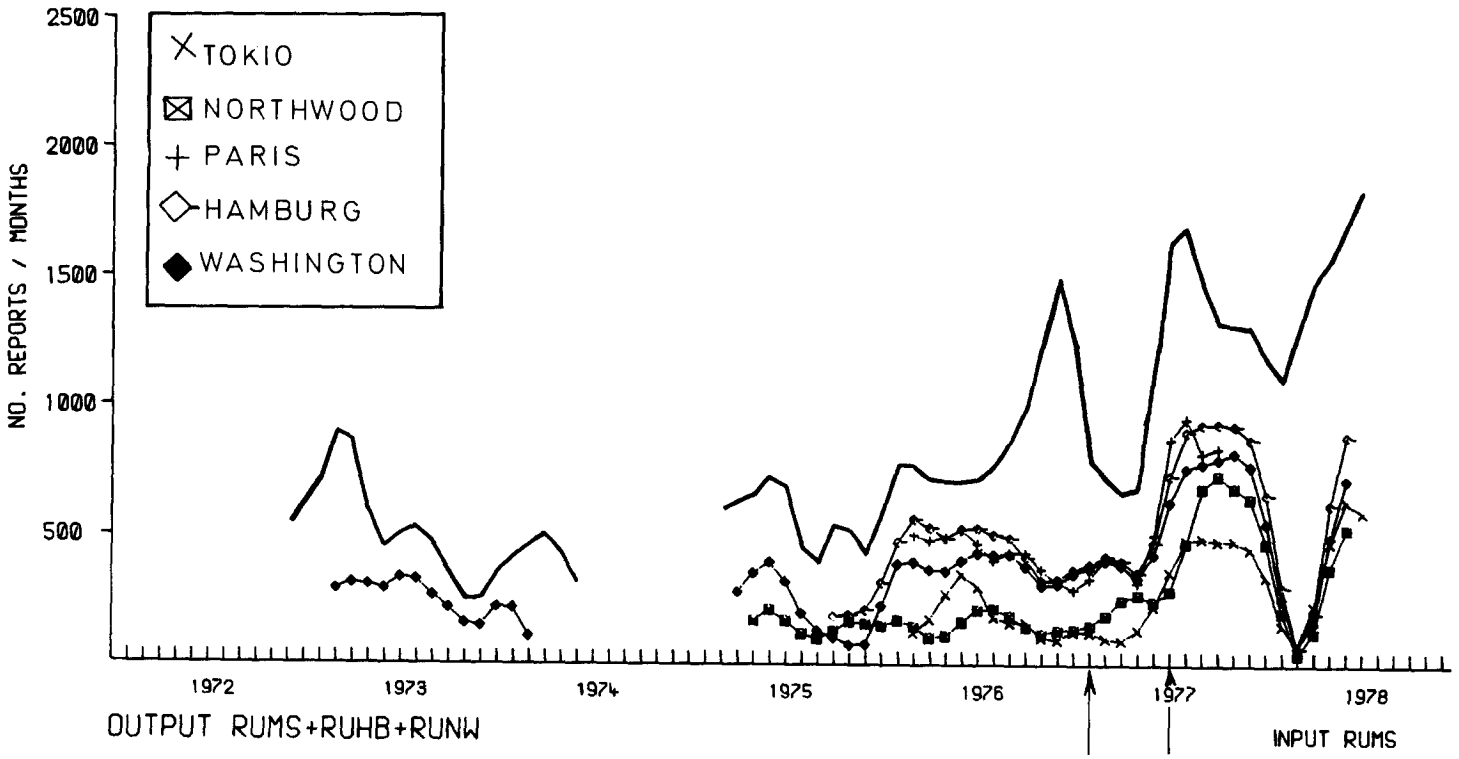
TOKIO
NORTHWOOD
PARIS
HAMBURG
WASHINGTON
NO. REPORTS / MONTHS
2500
2000
1500
1000
500
1972
1973
1974
1975
1976
1977
1978
OUTPUT RUMS+RUHB+RUNW
INPUT RUMS

Fig. 11

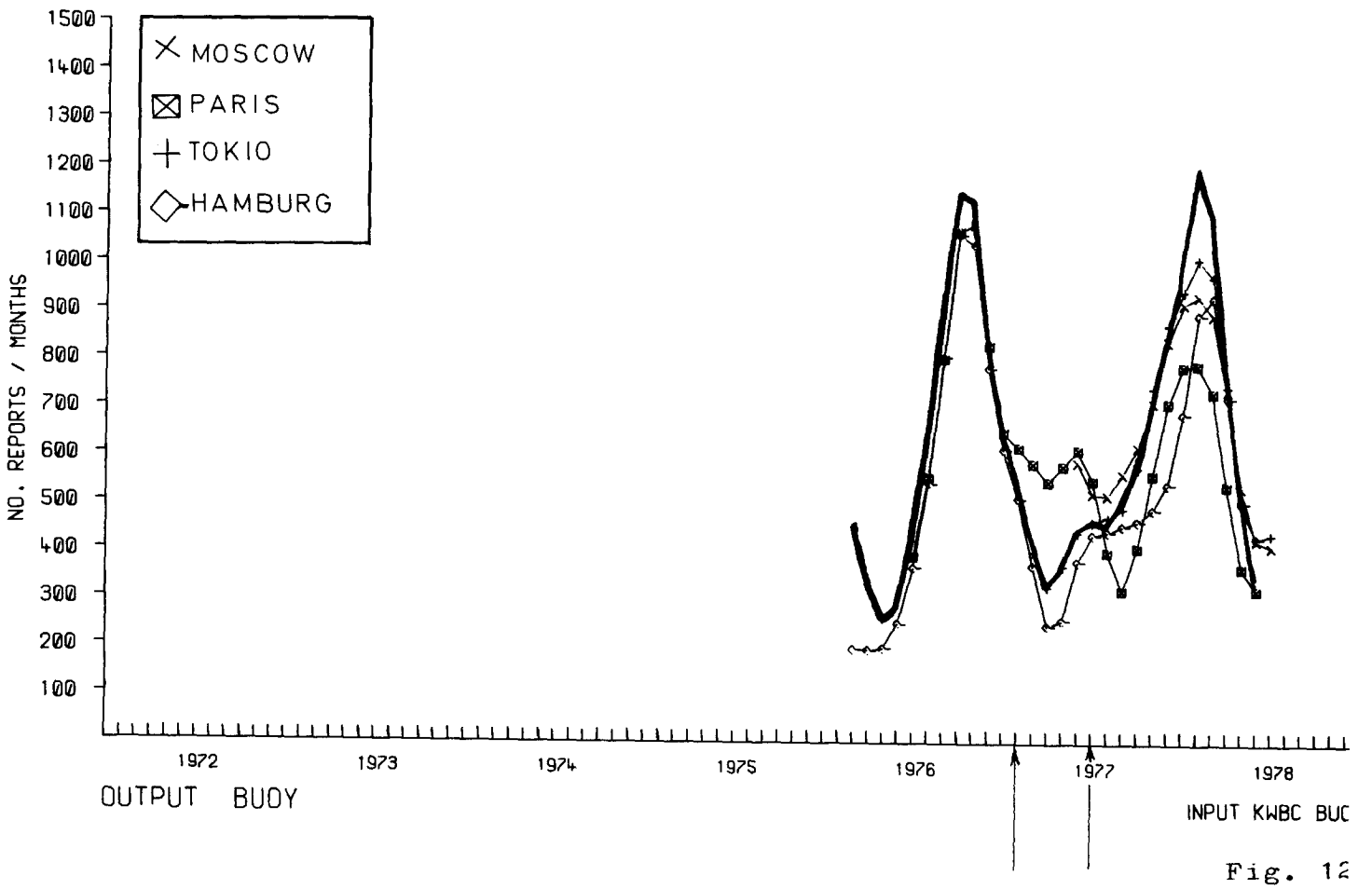
MOSCOW
PARIS
TOKIO
HAMBURG
NO. REPORTS / MONTHS
1500
1400
1300
1200
1100
1000
900
800
700
600
500
400
300
200
100
1972
1973
1974
1975
1976
1977
1978
OUTPUT BUOY
INPUT KWBC BUC

Fig. 12

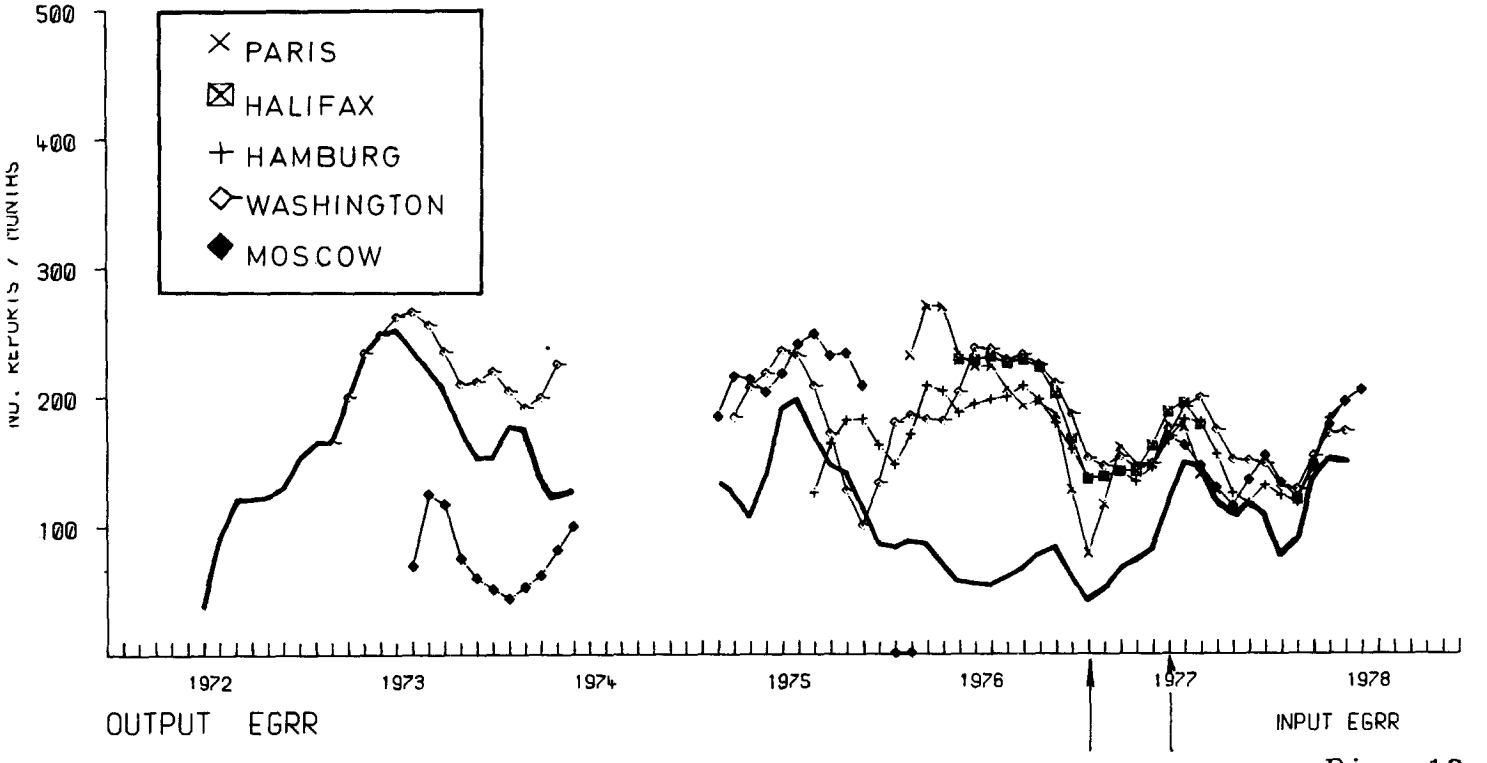
500
400
300
200
100
PARIS
HALIFAX
HAMBURG
WASHINGTON
MOSCOW
1972
1973
1974
1975
1976
1977
1978
OUTPUT EGRR
INPUT EGRR

Fig. 13

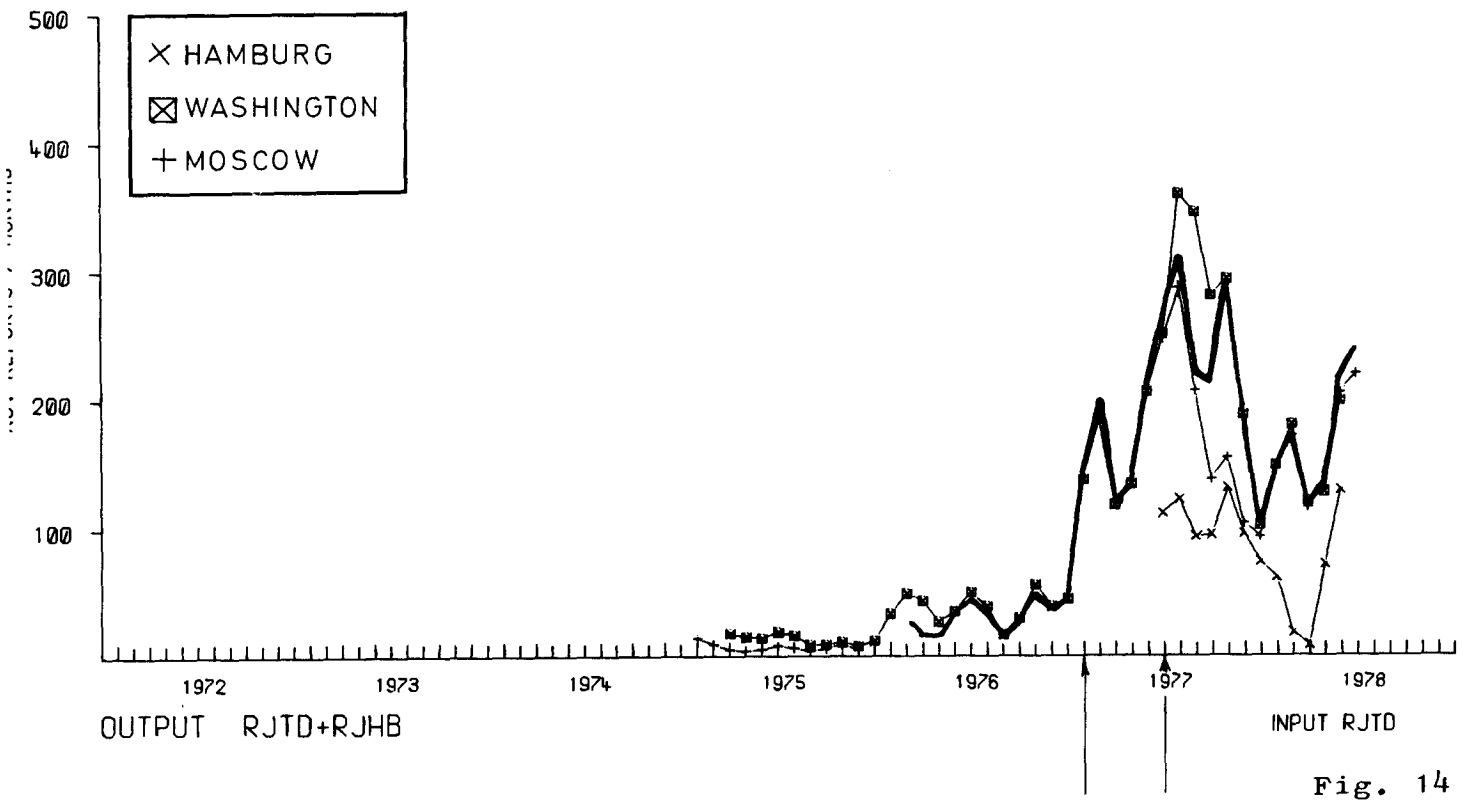
500
400
300
200
100
HAMBURG
WASHINGTON
MOSCOW
1972
1973
1974
1975
1976
1977
1978
OUTPUT RJTD+RJHB
INPUT RJTD

Fig. 14

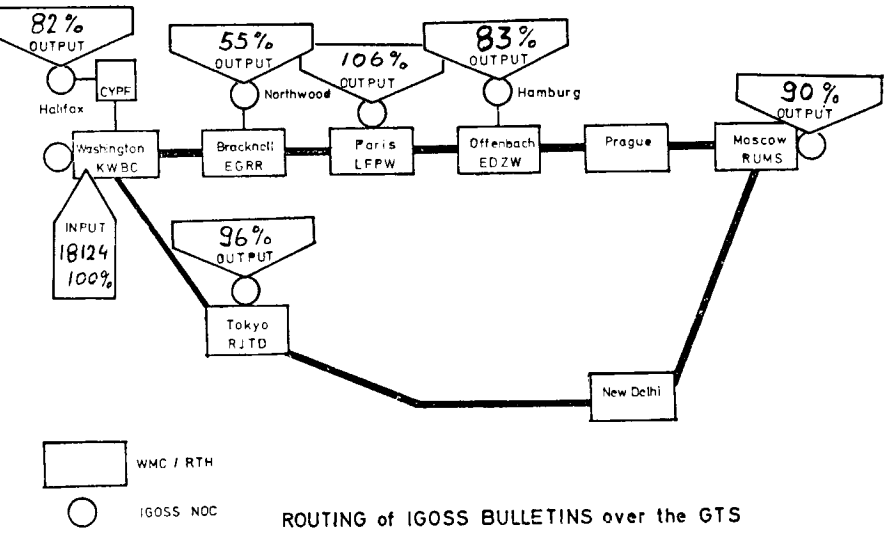

ROUTING of IGOSS BULLETINS over the GTS

INPUT KWBC (Bathy+Tesac) 1977

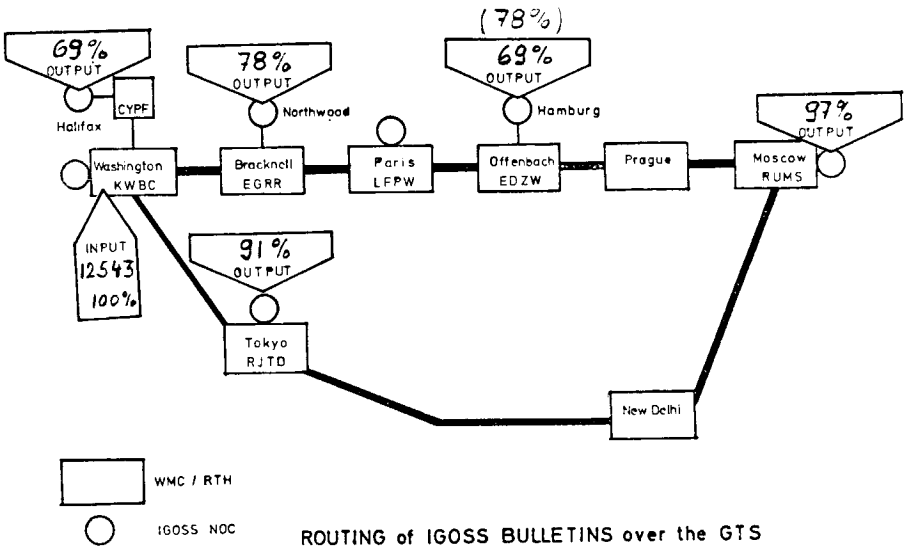

ROUTING of IGOSS BULLETINS over the GTS

INPUT KWBC (Bathy+Tesac) 1978 (Jan.-June)

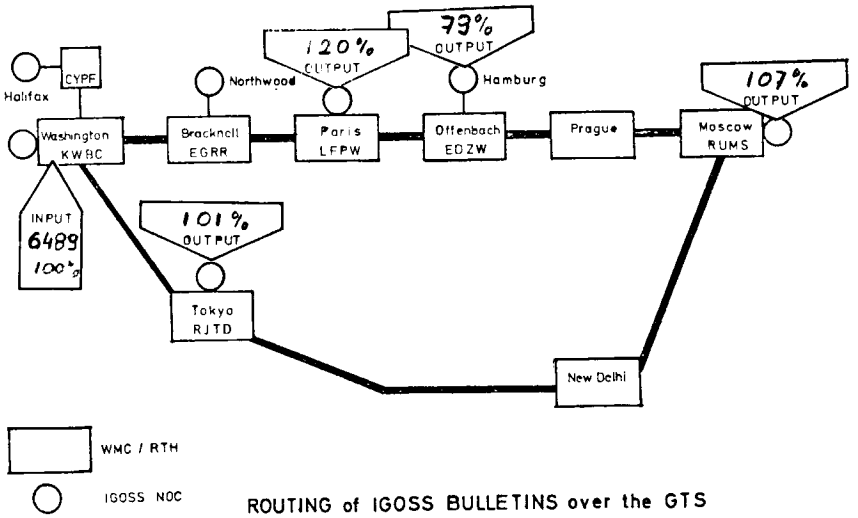

ROUTING of IGOSS BULLETINS over the GTS

INPUT KWBC (Buoy) 1977

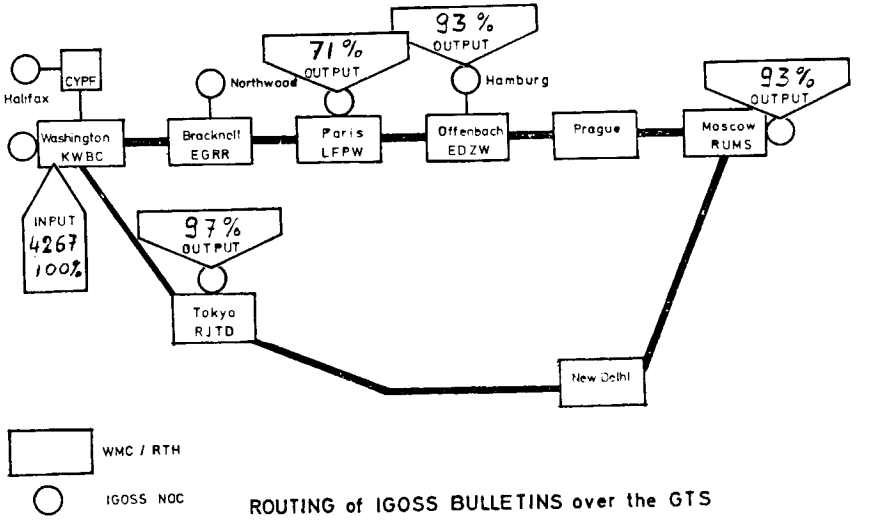

ROUTING of IGOSS BULLETINS over the GTS

INPUT KWBC (Buoy) 1978 (Jan.-June)

Fig. 15

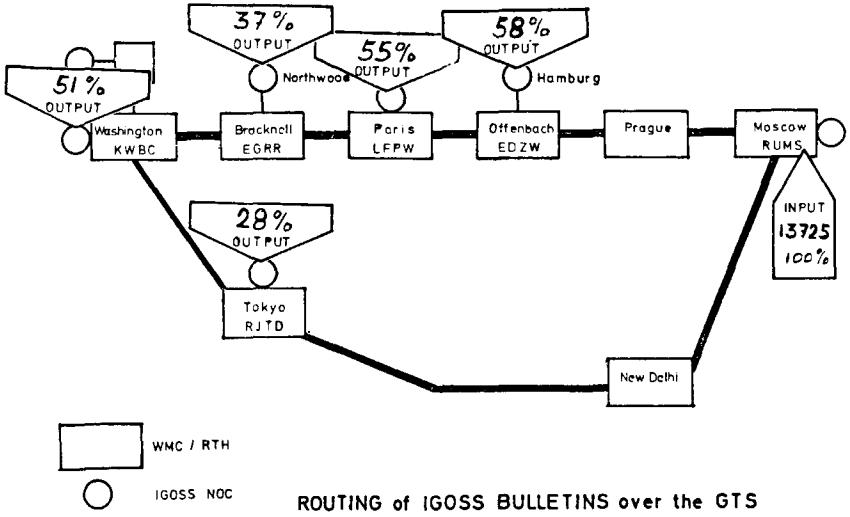

ROUTING of IGOSS BULLETINS over the GTS

INPUT RUMS (Bathy+Tesac) 1977

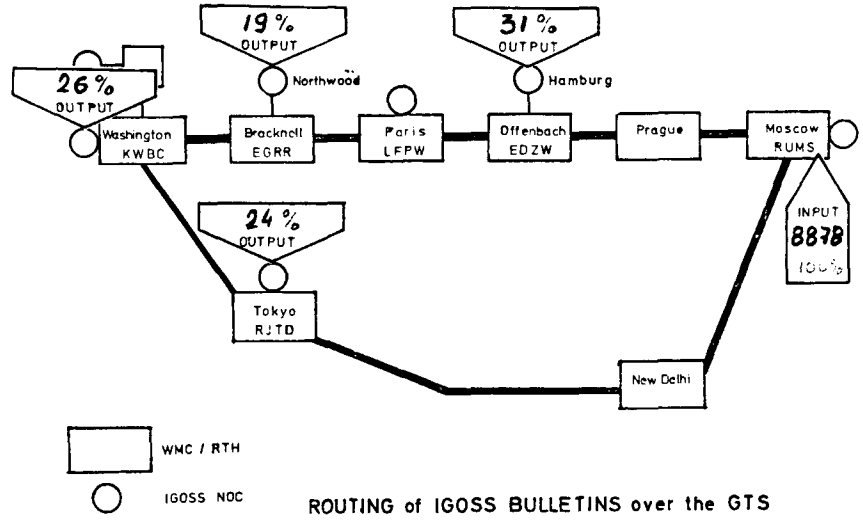

ROUTING of IGOSS BULLETINS over the GTS

INPUT RUMS (Bathy + Tesac) 1978 (Jan.-June)

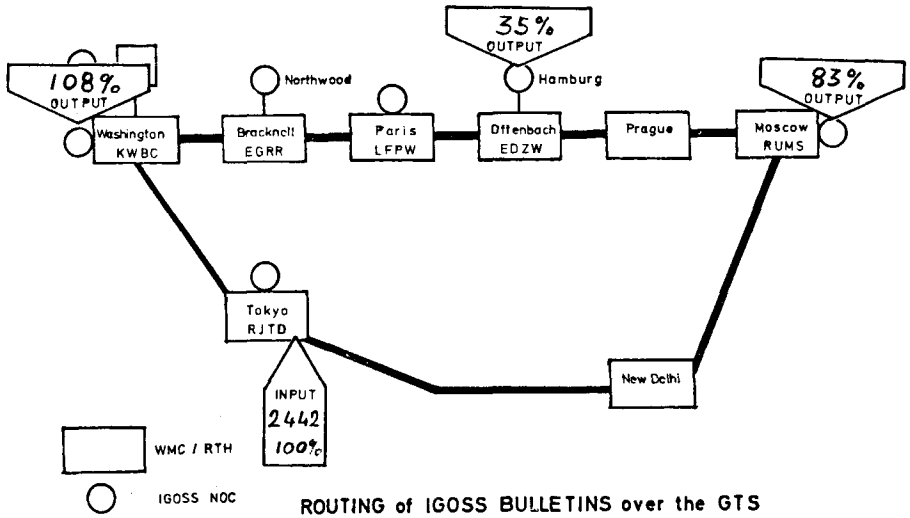

ROUTING of IGOSS BULLETINS over the GTS

INPUT RJTD (Bathy) 1977

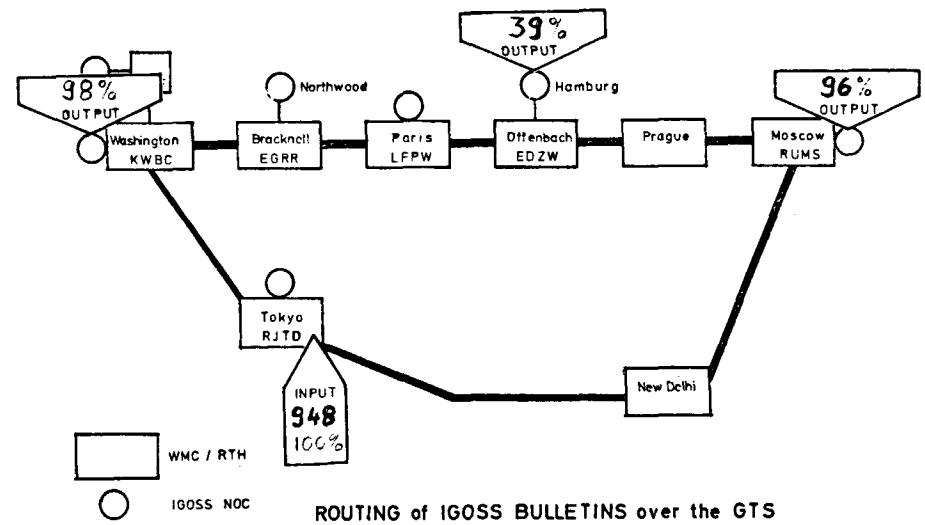

ROUTING of IGOSS BULLETINS over the GTS

INPUT RJTD (Bathy) 1978 (Jan.-June)

Fig. 16

Quality control procedures applied to IGOSS data at the Specialized Oceanographic Data Centre, FRG

by

Klaus Huber

Deutsches Hydrographisches Institut

Summary

It is desirable that quality control be internationally agreed, and this paper is intended to be a contribution towards that aim.

During FGGE the Deutsches Hydrographisches Institut (DHI) acts as a Specialized Oceanographic Data Centre, which means that the BATHY and TESAC reports exchanged through the GTS are collected, controlled, archived, and passed on to an FGGE Level IIb data centre.

The quality control procedures which are used with these data are briefly described, and information is provided concerning the frequency of certain errors, with particular attention to the FGGE build-up year 1978.

1 General remarks, definition and sources of errors

Before discussing the error statistics, and before explaining our quality control procedures, some general remarks have to be made concerning the origin and the judgement of erroneous reports. In this respect the following summary shows the path of a report from his origin on board a ship until the desk o the computer of a user. The table also indicates the possible errors which may occur at the different stages.

Stages	Handling	Possible Errors
Observing Platform	Measurement of T,S,D Date, Position.	Physical errors due to instrument failure.
	Encoding of a report.	Encoding errors concerning the format. Encoding errors concerning the measured values.
	Radio transmission	Misreading and subsequent transmission of wrong data. Transmission errors via radio.
Coastal Radio Station	Accepting of reports and forwarding to national GTS-Centres.	Misinterpretation of data by men or telex equipment and subsequent transmission of wrong data.
National GTS Centres	Compiling of reports to bulletins.	Multiple transmitting of reports.
	Adding of headings.	Encoding errors,concerning the format of the header.
	Changing of storage medium	Transmission errors.
G T S	Transmission	Transmission errors.
	Sorting our of reports due to erroneous headings due to priority of message	Data loss.
User	Accepting of bulletins Changing of storage medium	Transmission errors.

Looking through this table, three main types of errors can be distinguished with regard to their origin :

1 Physical errors

2 Coding errors

3 Transmitting errors

Physical errors arise from incorrect instruments and become visible in correct temperature, salinity, depths, time and position. Today, oceanographic instruments are often very sophisticated and it is difficult to find persons who are both technically skilled and oceanographically experienced to judge an oceanographic measurement in respect to a possible error. Looking to the origion of a physical errror, this type of error originates on board a platform.

Coding errors are primarily caused by men, in case they do not encode a measurement according to the rules or in case they insert a wrong value. The latter shows that coding errors become visible as physical errors. Coding errors in this sense occur at two stations of a report, at the observing platform and at a national GTS centre.

Transmission errors appear always during a transmission of data from one place to another, or if the data changes from one storage medium to another, or because of a misunderstanding between two persons. This type of errors come into existence at all stages in a path of a report. At least two persons handle the data: Between ship and coastal station the radio officer on beoard and at the shore station; or in case the data are transmitted by telex, they change the storage medium. The same will occur, maybe several times, before the data enter into the GTS, even at the last station of a report, when the data are fed in to a computer of a user, there is a possibility for transmisssion errors.

Normally, a transmission error looks like a coding error or a physical error. Both, coding errors and transmission errors very often garble a report in such a way that a computer programme is not able to interprete it correctly.

2 Error statistics

An error statistic can be made up from different point of views. First from the point of view of an expert for data transmission. He would try to count the errors according to the above mentioned three categories. On the other hand a statistic can be made up from the point of view of an expert, who intends to prepare products from the data. He does not care if an obviously wrong temperature has been caused by an instrument failure or a coding or transmission error, respectively. He distinguishes between "usable" and "unusable" reports.

A typical example is the following: An erroneous or missing "ship call sign" (caused by a coding error) makes a report not unusable, but still the "ship call sign" is necessary for a correct position control, as it will be explained later. On the other hand, he would count all multiply transmitted data as "unusable".

In this context I will look at all problems under discussion from the point of view of an expert who wishes to prepare products. Therefore the following different types of errors are defined in respect to the statistics which will be presented. In this definition, the origin of an error is not attended to , only the kind h o w it offers itself to a processor is taken into account.

Typ		Definition
1.	Coding errors	
1.1	Format errors	Within a report the formats are not kept (except concerning the "ship call sign")
1.2	Errors in "ship call sign"	In an otherwise correctly formated report the "ship call sign" is wrong or missing
2.	Physical errors	
2.1	T/S/D errors	Temperature, Salinity, Depth: wrong
2.2	Time errors	Date (year, month, day) : wrong
2.3	Position errors	Latitude, longitude : wrong
3.	Multiply transmitting	The same report (in respect to date, position and temperature, salinity, depth) is transmitted several times.

During 1978 (FGGE build-up year) we investigated how frequently the above defined different types of errors appeared; the result is shown in Table 1 and Figures 1 to 3.

Before going into details I have to point out that only such bulletins which passed the GTS centres arrived at the DHI. That means, bulletins which were sorted out by a GTS centre, due to a failure within the bulletin header, are not included in this statistic.

Concerning coding errors, Fig. 1 shows that up to 22 % of the monthly exchanged IGOSS reports contain format- and ship-call-sign-errors. The steady increase from January to the middle of the year 1978 may be explained by the fact that we learned to detect coding errors during the time under consideration. Principally, there is no check possible against the

original data, because these data are not available to the user. This means that these reports would be unusable if they cannot be corrected. Fortunately, a high percentage (according to our experience about 90 %) of reports containing format errors, can be easily corrected. But this correction implicated a visual inspection and an individual manual handling of the data. It is for example not difficult to insert a missing 88888-group. Some other examples will be given later in Chapter 3. These corrections are of cause subjective and will in some cases produce an error of the physical-error-type.

Moreover, the coding errors do not determine the amount of unusable reports. From a point of view of a product-producer it is essential to know how many reports are transmitted and how many of them contain physically erroneous information.

Concerning multiply transmitted reports: Figure 2 shows the monthly distribution in percentage of the duplications. These figures are less certain than the respective figures for the coding- or physical-errors because duplicates have been sorted out manually at the time when the data have been fed in to the computer. As it will be explained later (Chapter 3) we have to distinguish between different types of duplications: On the one hand, there are the fully identical reports which have been transmitted twice and on the other hand, those reports which run through the GTS under a different name. An example for the latter ones are the reports from the buoy EB 03 and the Ocean Weather Station PAPA. Nearly all reports from EB 03 were received through the GTS centre KWBC and PANC and we got nearly all reports from PAPA as reports from the ships C7P and CGDN/CGBR. As the reports from fixed stations contribute to a high extent to the total number of reports this leads to a high percentage of duplicates. Fig. 2 shows that up to 20 % of all reports have been transmitted twice.

Finally the statistics concerning the physical errors will be discussed. These are errors which are related to the measured values which are temperature, salinity, depth, time and position. It is on principle not possible to identify these errors definitely, because of the lack of the original data. But with some simple checks - e.g. a check against temperature/salinity limits; a check against spikes and et cetera - a lot of obviously erroneous data can be discovered. These checks will be described in Chapter 3. Using these simple checks, one will find a lower limit for physically erroneous reports. In preparing actual products like horizontal maps, time series or sections, many more erroneous reports will be found. Fig. 3 shows that 12 % to 20 % of the monthly transmitted reports contain physical errors in position, date or temperature /salinity/depth. The highest proportion is due to errors in temperature/salinity/depth, which range between 9 % and 15 %. Looking at all physical errors, about 1/3 to 1/2 can be repaired, so that a measurement will be almost "correct". For example, nearly all position errors can be corrected, because only correctable posion errors will be discovered, the same is also true of time errors. Time errors

are normally restricted to errors in month and year and can exactly be corrected. Temperature/salinity errors are mostly spikes, which can be replaced by the most likely value. Examples will be given in Chapter 3.

The presented statistics on coding and physical errors allow an estimate on the amount of unusable reports. Taking into account the 10 % of irrepairable format errors (annual mean 1.2 %) and about 1/2 of the temperature/salinity/depth-errors (mean over the year: 5.4 %), the total amount of unusable reports will be in the order to 7 %.

Two conclusions can be drawn out of the above presented statistics:

1 The proportion of erroneous reports, (talking about coding errors and/or physical errors) is too high that erroneous reports can simply be neglected.

2 The quality control procedures have to be carried out in two stages. In each stage a visual inspection must be applied.

Concerning the second conclusion: The reports must - above all - be checked for coding errors, especially format errors. This should be done before feeding them in to the computer. Reports which do not pass this quality control, have to be printed in order that a subsequent correction by hand may be carried out. Only a small portion of format errors can be corrected automatically.

Secondly, after storage, the reports have to be controlled for physical validity. This can be done using more or less sophisticated quality checks. A report which does not pass a quality check, must be printed, because a decision about a correction can be done only in comparing the erroneous report with other reports from the same ship at the same time. To use the automatically applied correction is rarely possible only in a few cases. In this context the word "correction" should also mean that a possibly erroneous value is simply marked by a quality control mark.

In the DHI control procedures were developed to meet these goals acting as a Specialized Oceanographic Data Centre for FGGE. These quality control procedures will be described briefly.

3 Quality control procedures applied in the Specialized Oceanographic Data Centre, FRG

In the following a brief description is given of the principal procedure. Details are outlined in ;Quality control procedures", issue II, prepared by the Specialized Oceanographic Data Centre, FRG.

Fig. 4 shows a diagram of IGOSS data handling especially with regard to the quality control. The data are supplied on papertape and are transferred onto a disc by means of a computer programme which also performs checks for coding errors. There are also some physical checks. These checks are done primarily to detect coding errors. If a report does not pass at least one check, the report will be printed in its original version. In addition, there is a code number, which indicates which check has not passed. Reports which have not passed the check will not be transferred onto the disc. The following checks for coding errors are applied:

a) ship call sign missing or not in ship call sign list;

b) 5 character groups;

c) α - character in numerical group;

d) / in time group;

e) 88888 resp. 77777 group;

f) 2-3-4 sequence in TESAC;

g) quadrant (equal 1, 3, 5, 7);

h) year, month, day, hour in usual limits;

i) month, day $<$ month,day of inserting by a GTS centre;

j) month, year not older than 2 months;

k) position in usual limits;

l) temperature, salinity in limits;

m) depth,increasing values

The effect of these checks can easily be explained by an example. Fig. 5 shows a printout of 4 examples of erroneous reports at the stage of feeding them in to the computer. The first line of each example gives:

- the date on which the report was offered to the DHI computer
- the date on which the report was entered into the GTS
- the call sign of the GTS centre
- the ship call sign
- the code numbers (1 - 15), which indicate the check not passed.

Example 1

Code No. 5 indicates "incorrect 5 character group"
Code No. 18 indicates "depth not increasing"

Error: Indicator group 999.. consists of 6 characters
Correction: Replacing 990904 by 99904

Example 2

Code No. 4 indicates that the "report is older than 2 months"
Code No. 15 indicates "temperature not within given limits"

Error: Year of report is 1973 instead of 1978. Within the temperature group probably one "9" was taken from the following group.
Correction : Replacing the 3 by 8
Replacing the 639 by 063

Example 3

Code No. 18 indicates "depth not increasing"
Error: Indicator group 999.. is missing
Correction : Inserting of 99901

Example 4

Code No. 16 indicates "no correct 2-3-4 sequence"

Error: one temperature and one depth indicator is not correct
Correction : Replacing 4 by 3
and 3 by 2

After the reports have been accepted formally by the computer, i.e. that a physical value could be attached to each figure sequence, a second check for physical validity will be applied.

First of all the duplicated will be eliminated. There are two types of duplicates :

a) reports which are uniform in
Time, Position, Ship call sign, GTS call sign, Measurement

b) reports which are only partly uniform

b. 1) Time, Position, GTS call sign, Measurement

b. 2) Time, Position, Measurement

b, 3) Time, Position

b. 4) Time, Ship call sign

Reports which are completely uniform (type a) will be eliminated automatically, except one.

Those reports which are partly uniform (type b.1) - b.4)) are printed and the processor decides how to proceed.

Fig. 6 shows a printout with two examples of partly uniform reports.

Examples 1a resp. 1b

Two reports, uniform, exept in GTS call sign.
One was entered by KNMF, the other one by KWBC.
One of them will be ignored.

Example 2a resp. 2b

Two reports seemed to be made by the same ship at the same time, but at different positions. A comparison with other reports from the same ship makes it very likely that the date of one of them is erroneous and the date should read 10 instead of 9.

This last example makes it very clear that a visual inspection is necessary to detect as many erroneous reports as possible.

The pysical check of the data follows the elimination of duplicates. The following checks are carried out:

a) Depth

a.1 depth monotonously increasing

a.2 depth within certain limits

b) Temperature

b.1 temperature in certain limits

b.2 spikes control

c) Salinity

c.1 salinity in certain limits

c.2 spikes control

c) Density (in case of TESAC)

d.1 density in certain limits

d.2 density monotonously increasing with allowed tolerance

e) Position

The position of a given ship is checked. Consecutive position must be reached within the given time difference assuming a given mean ship's speed.

In case a report passes the checks, the controlmark "1" will be added.

In case a report does not pass one of the above checks, the report is printed and the processor decides how to proceed. He may correct a value or simply add a quality control mark with the following meaning:

Quality control mark

"2" value found to be suspect during quality control check

"3" value found to be erroneous during quality control check

"4" observed value was changed, most likely value was entered

The handling of erroneous reports with physical errors will be explained, showing two examples in Figs. 7 and 8.

Fig. 7 gives two examples for spikes, which are the most frequent errors. In the first example the temperature is obviously wrong but a correction is uncertain, therefore the erroneous value stands as it is ond only a quality control mark No. 3 is added. In example 2 the temperature at 100 metres is obviously wrong, the reason for this error is possibly a misreading. In this case the value is replaced by a most likely value which reads 23.03°C instead of 33.03°C, and the quality control mark 4 is added.

Fig. 8 gives an example how quality control with regard to the position is handled. Reports of one vessel have been arranged in a consecutive order. As the velocity is calculated from the difference of position and time, the mark "POS" is attached to the printout of header information of the report, if this calculated velocity exceeds a given average speed (in our case: 17 nm/h). The processor decides if a correction is opportune or not. In the example shown in Fig. 8 four corrections concerning the position seem to be necessary. The reason for these errors were probably coding errors or at least in one case a misreading, so to speak a transmission error.

4 Final remarks

Above results are the essence of our experience with working up the IGOSS data during the last year 1978. I am convinced that other centres dispose of many more experiences in this respect. It seems to me, that the time is approaching when we should exchange our experiences gained on quality control and on the operational handling of oceanographic data. In this sense the presented paper should be understood.

Month	Total No. of usable reports without multiply transmitted reports	Multiply transmitted reports % *	Coding errors % *		Physical errors % *		
			Format errors	Call sign errors	Error in T/S/D	Error in Date/Time	Error in Position
1	2	3	4	5	6	7	8
Jan.	2191	18	4.2	1.0	5.3	1.6	0.2
Feb.	2203	14	6.7	1.9	11.6	2.3	
March	1816	20	9.8	1.0	9.2	1.9	0.3
April	2377	15	11.2	2.0	9.2	2.1	1.0
May	2797	13	11.9	1.6	8.7	2.6	1.5
June	2797	15	15.3	3.3	12.7	2.3	1.9
July	3303	12	11.7	3.2	9.3	1.0	1.8
Aug.	2966	10	14.8	6.1	9.6	1.0	2.0
Sept.	2107	11	14.6	6.0	15.6	2.7	1.7
Oct.	2117	9	16.5	6.2	12.1	1.9	1.3
Nov.	1879	10	12.3	5.3	11.4	1.5	2.0
Dec.	1991	8	17.5	6.0	16.7	2.3	1.6
	28544	13	12.2	3.6	10.8	1.9	1.3

Table 1

* All % Figures are related to the Figures given in column 2.

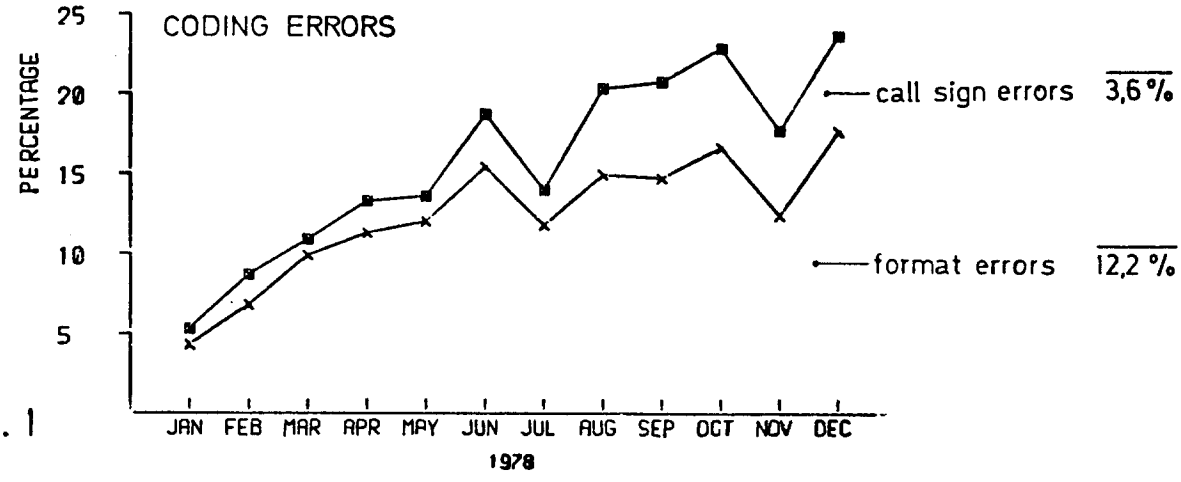

Fig. 1

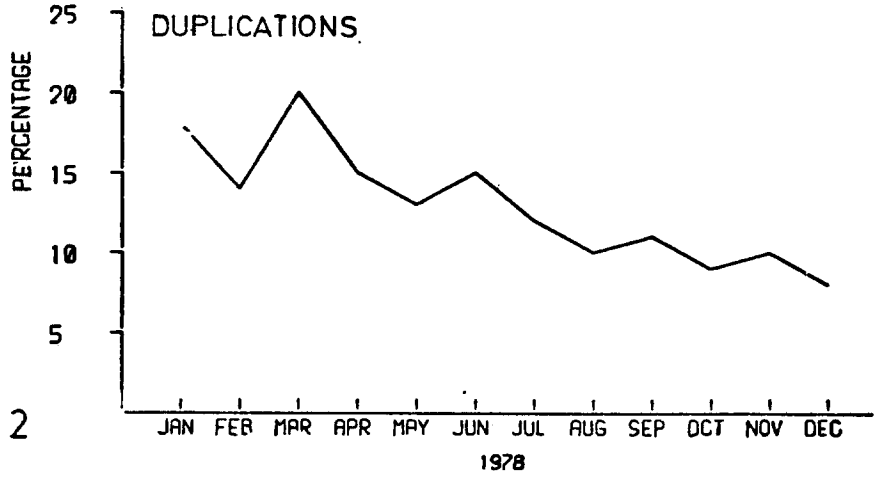

Fig. 2

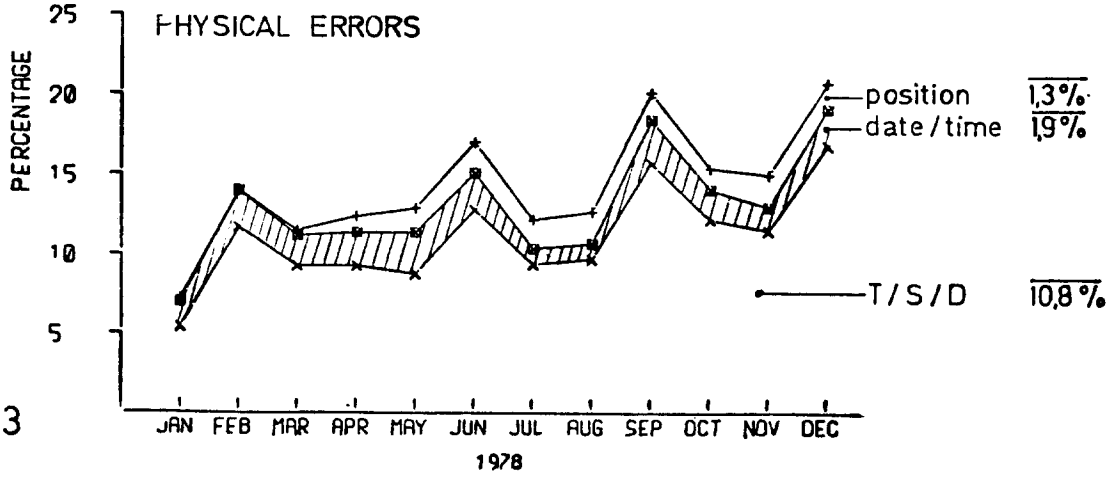

Fig. 3

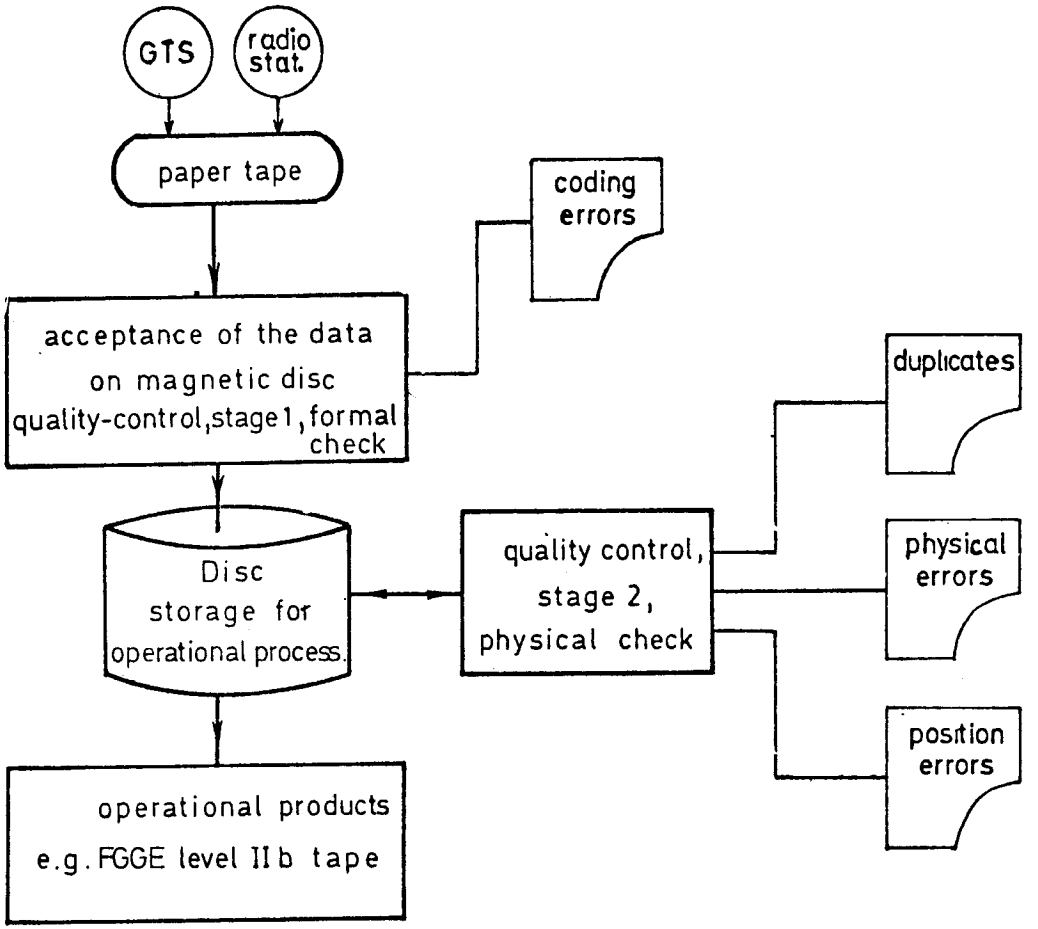

Fig.4 Scheme for data flow and data process, especially in regard to quality control.

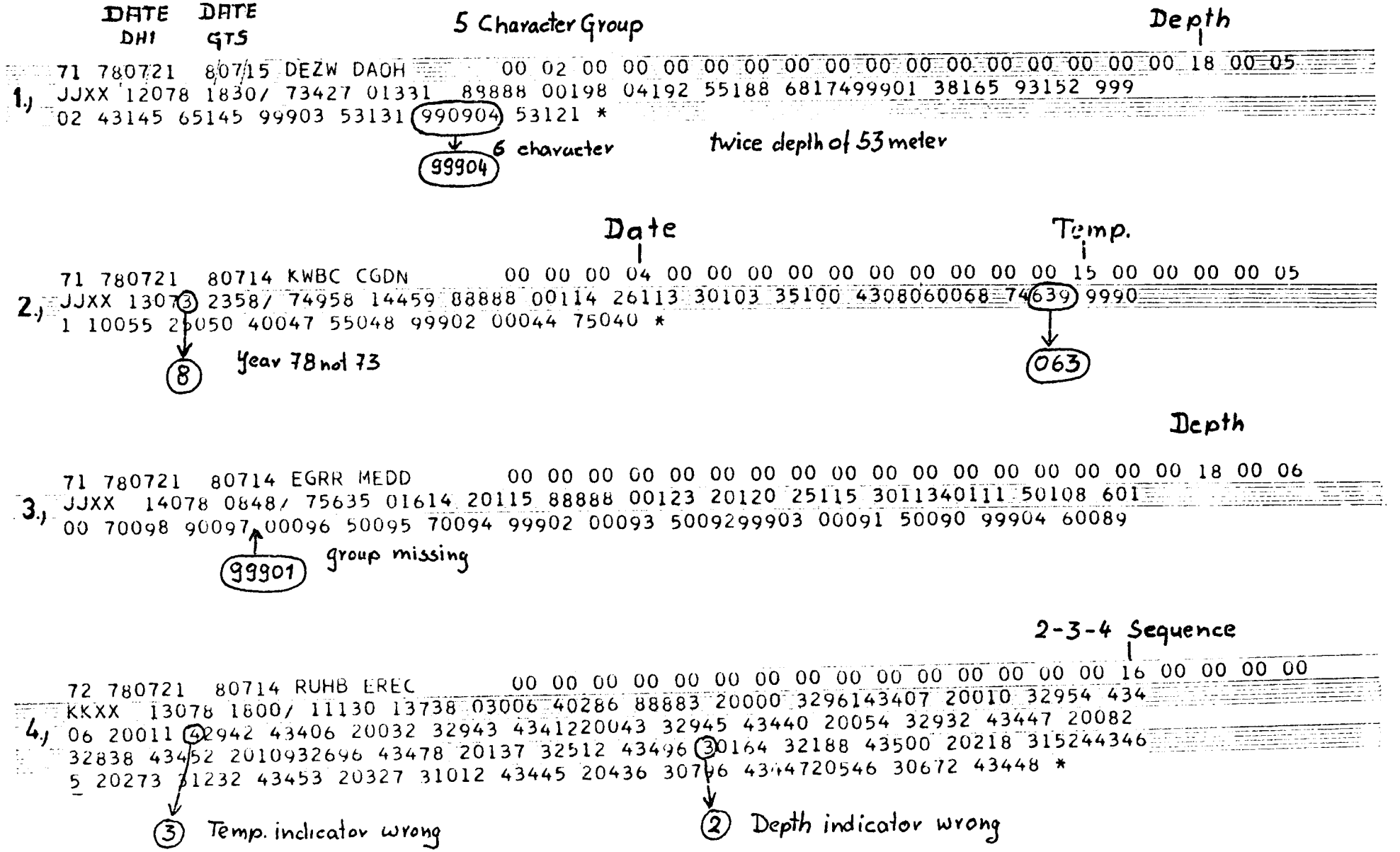
DATE DHI
DATE GTS
5 Character Group
Depth
71 780721 80715 DEZW DAOH 00 02 00 00 00 00 00 00 00 00 00 00 00 00 00 00 18 00 05
1.) JJXX 12078 1830/ 73427 01331 88888 00198 04192 55188 6817499901 38165 93152 999
02 43145 65145 99903 53131 990904 53121 *
6 character
99904
twice depth of 53 meter
Date
Temp.
71 780721 80714 KWBC CGDN 00 00 00 04 00 00 00 00 00 00 00 00 00 00 15 00 00 00 00 05
2.) JJXX 13073 2358/ 74958 14459 88888 00114 26113 30103 35100 4308060068 74639 9990
1 10055 25050 40047 55048 99902 00044 75040 *
8
Year 78 not 73
063
Depth
71 780721 80714 EGRR MEDD 00 00 00 00 00 00 00 00 00 00 00 00 00 00 00 00 00 18 00 06
3.) JJXX 14078 0848/ 75635 01614 20115 88888 00123 20120 25115 3011340111 50108 601
00 70098 90097 00096 50095 70094 99902 00093 5009299903 00091 50090 99904 60089
99901
group missing
2-3-4 Sequence
72 780721 80714 RUHB EREC 00 00 00 00 00 00 00 00 00 00 00 00 00 00 00 16 00 00 00 00
KKXX 13078 1800/ 11130 13738 03006 40286 88883 20000 3296143407 20010 32954 434
4.) 06 20011 42942 43406 20032 32943 4341220043 32945 43440 20054 32932 43447 20082
32838 43452 2010932696 43478 20137 32512 43496 30164 32188 43500 20218 315244346
5 20273 31232 43453 20327 31012 43445 20436 30796 4344720546 30672 43448 *
3
Temp. indicator wrong
2
Depth indicator wrong

Fig. 5

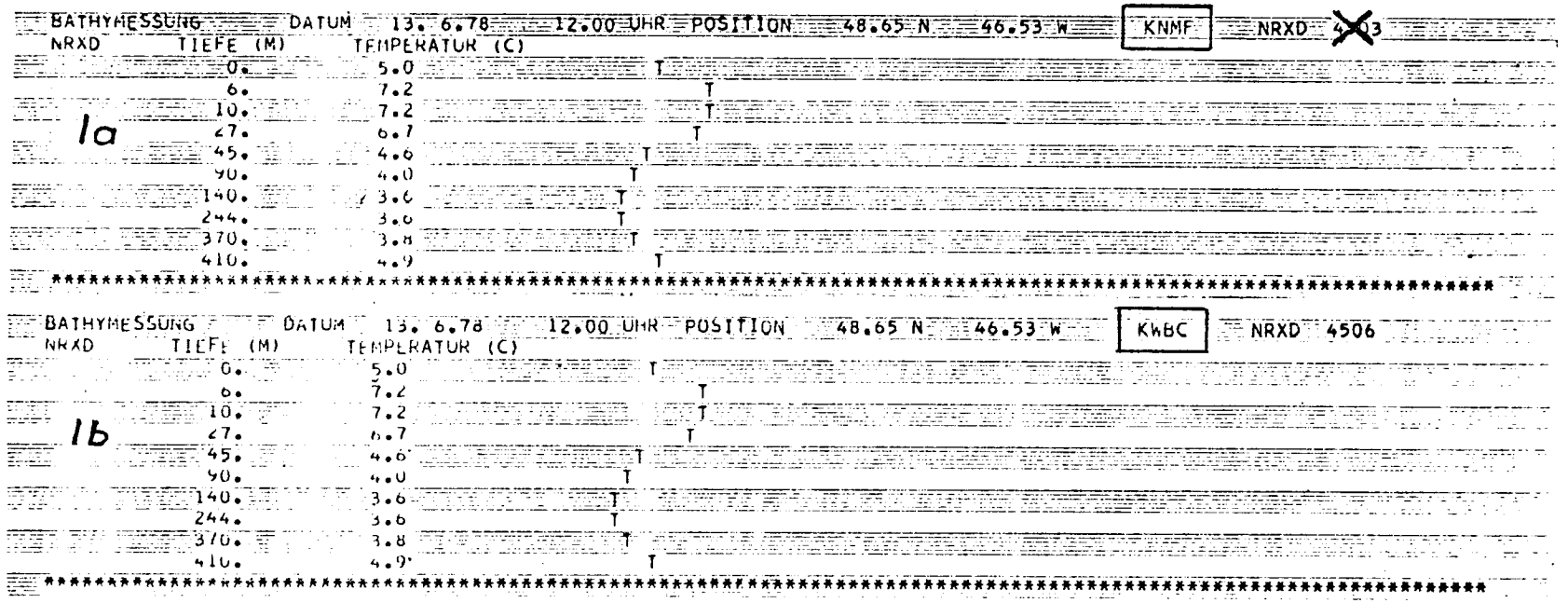

Same report transmitted by KNMF and KWBC

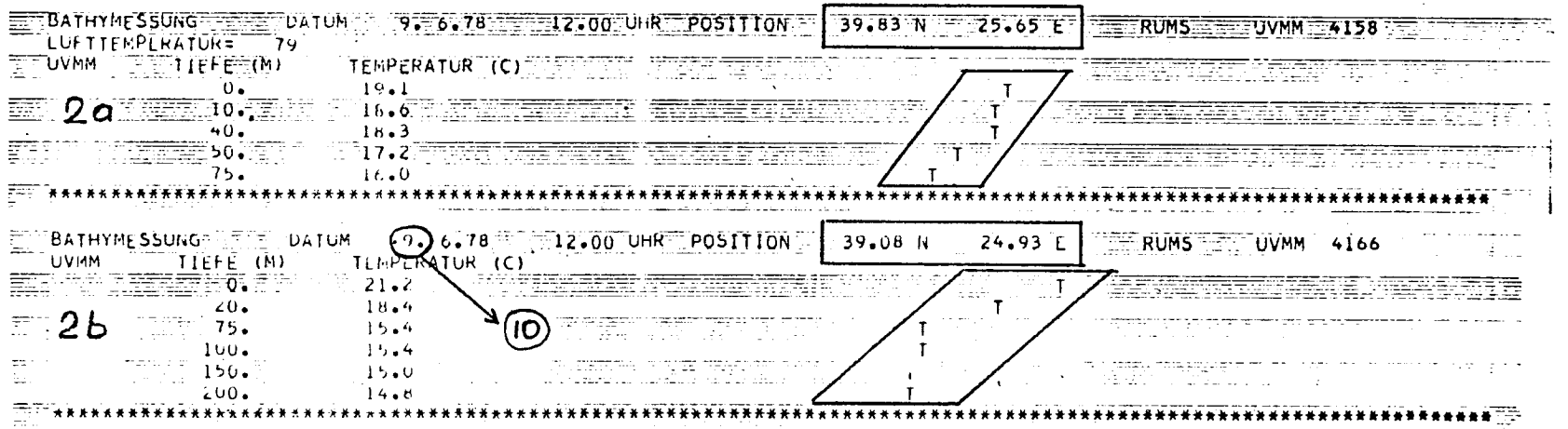

At the same time at two different positions
Comparison with other reports from UVMM leads to the correction of day

Fig. 6

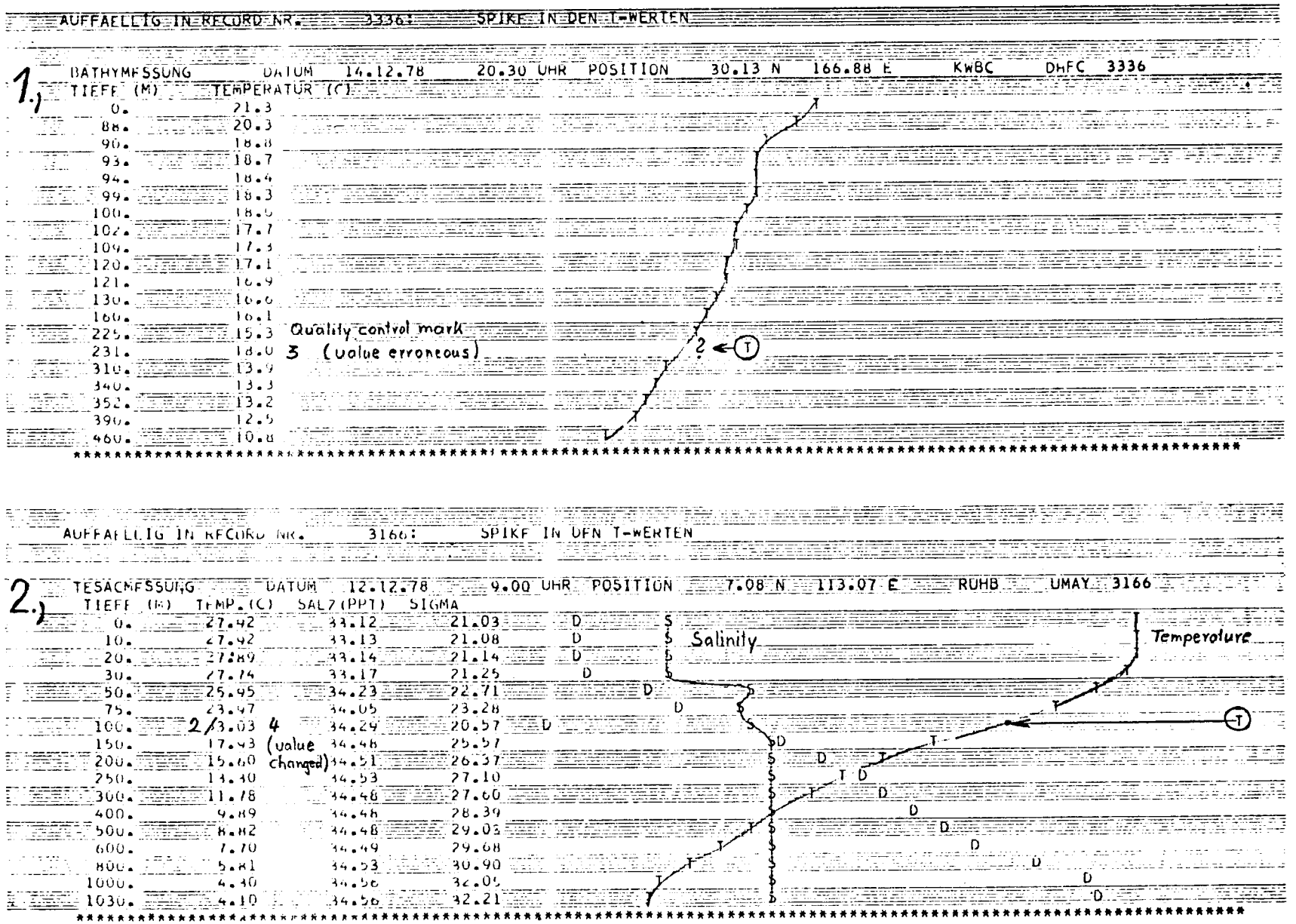
AUFFAELLIG IN RECORD NR. 3336: SPIKE IN DEN T-WERTEN
1.)
BATHYMESSUNG DATUM 14.12.78 20.30 UHR POSITION 30.13 N 166.88 E KWBC DHFC 3336
TIEFE (M) TEMPERATUR (C)
0. 21.3
88. 20.3
90. 18.8
93. 18.7
94. 18.4
99. 18.3
100. 18.0
102. 17.7
109. 17.3
120. 17.1
121. 16.9
130. 16.6
160. 16.1
225. 15.3
231. 15.0
310. 13.9
340. 13.3
352. 13.2
390. 12.5
460. 10.8
Quality control mark
3 (value erroneous)
2
T
AUFFAELLIG IN RECORD NR. 3166: SPIKE IN DEN T-WERTEN
2.)
TESACMESSUNG DATUM 12.12.78 9.00 UHR POSITION 7.08 N 113.07 E RUHB UMAY 3166
TIEFE (M) TEMP.(C) SALZ(PPT) SIGMA
0. 27.42 33.12 21.03 D
10. 27.42 33.13 21.08 D
20. 27.39 33.14 21.14 D
30. 27.24 33.17 21.25 D
50. 25.45 34.23 22.71 D
75. 23.47 34.05 23.28 D
100. 21.03 34.29 20.57 D
150. 17.43 34.46 25.57
200. 15.60 34.51 26.37
250. 14.30 34.53 27.10
300. 11.78 34.48 27.60
400. 9.89 34.48 28.39
500. 8.82 34.48 29.03
600. 7.70 34.49 29.68
800. 5.81 34.53 30.90
1000. 4.30 34.56 32.05
1030. 4.10 34.56 32.21
2
4
(value changed)
Salinity
Temperature
T
D
S

Fig.7

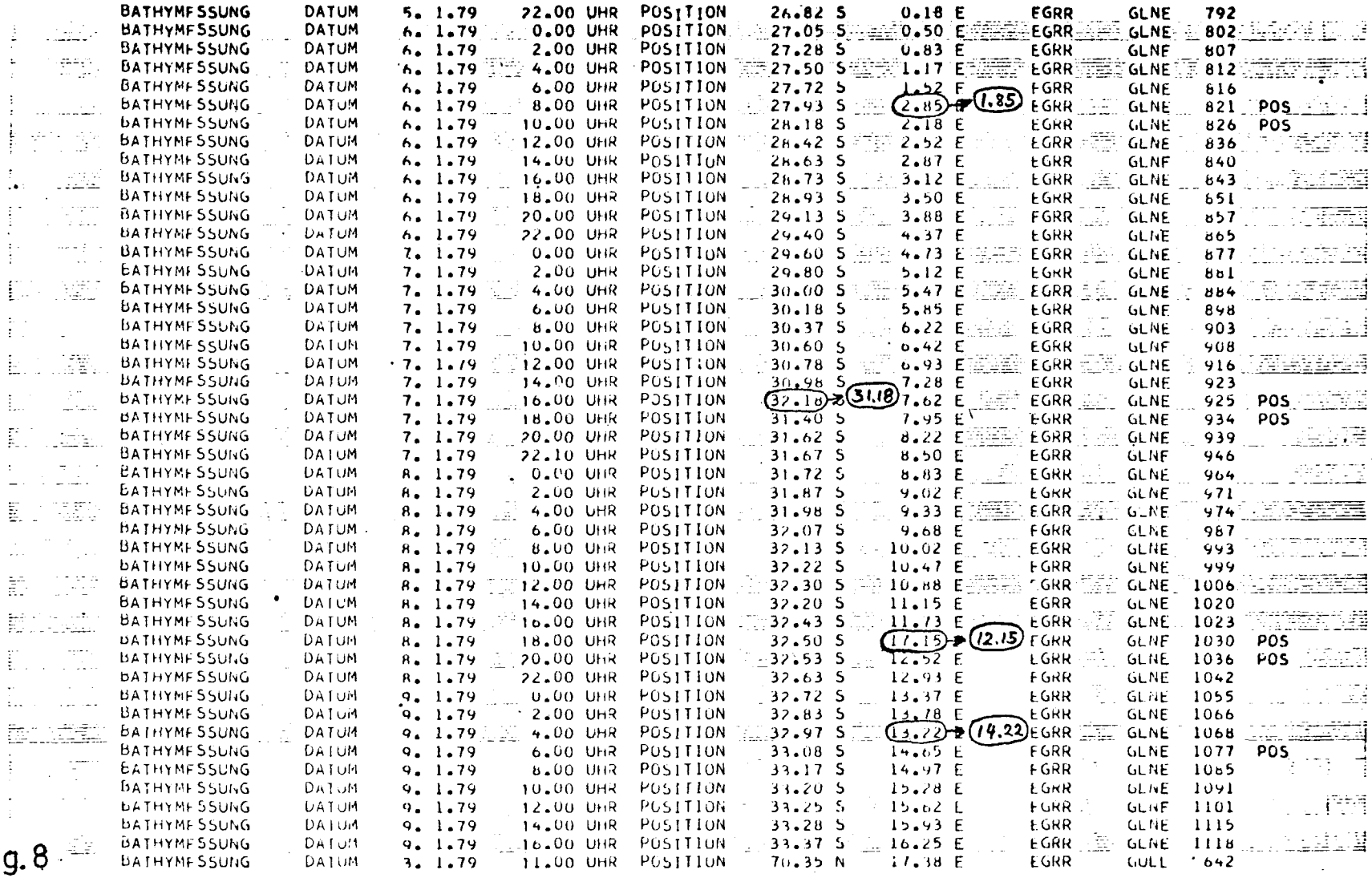

BATHYMESSUNG	DATUM	5. 1.79	22.00 UHR	POSITION	26.82 S	0.18 E	EGRR	GLNE	792			
BATHYMESSUNG	DATUM	6. 1.79	0.00 UHR	POSITION	27.05 S	0.50 E	EGRR	GLNE	802			
BATHYMESSUNG	DATUM	6. 1.79	2.00 UHR	POSITION	27.28 S	0.83 E	EGRR	GLNE	807			
BATHYMESSUNG	DATUM	6. 1.79	4.00 UHR	POSITION	27.50 S	1.17 E	EGRR	GLNE	812			
BATHYMESSUNG	DATUM	6. 1.79	6.00 UHR	POSITION	27.72 S	1.52 E	EGRR	GLNE	816			
BATHYMESSUNG	DATUM	6. 1.79	8.00 UHR	POSITION	27.93 S	2.85 → 1.85 E	EGRR	GLNE	821	POS		
BATHYMESSUNG	DATUM	6. 1.79	10.00 UHR	POSITION	28.18 S	2.18 E	EGRR	GLNE	826	POS		
BATHYMESSUNG	DATUM	6. 1.79	12.00 UHR	POSITION	28.42 S	2.52 E	EGRR	GLNE	836			
BATHYMESSUNG	DATUM	6. 1.79	14.00 UHR	POSITION	28.63 S	2.87 E	EGRR	GLNE	840			
BATHYMESSUNG	DATUM	6. 1.79	16.00 UHR	POSITION	28.73 S	3.12 E	EGRR	GLNE	843			
BATHYMESSUNG	DATUM	6. 1.79	18.00 UHR	POSITION	28.93 S	3.50 E	EGRR	GLNE	851			
BATHYMESSUNG	DATUM	6. 1.79	20.00 UHR	POSITION	29.13 S	3.88 E	EGRR	GLNE	857			
BATHYMESSUNG	DATUM	6. 1.79	22.00 UHR	POSITION	29.40 S	4.37 E	EGRR	GLNE	865			
BATHYMESSUNG	DATUM	7. 1.79	0.00 UHR	POSITION	29.60 S	4.73 E	EGRR	GLNE	877			
BATHYMESSUNG	DATUM	7. 1.79	2.00 UHR	POSITION	29.80 S	5.12 E	EGRR	GLNE	881			
BATHYMESSUNG	DATUM	7. 1.79	4.00 UHR	POSITION	30.00 S	5.47 E	EGRR	GLNE	884			
BATHYMESSUNG	DATUM	7. 1.79	6.00 UHR	POSITION	30.18 S	5.85 E	EGRR	GLNE	898			
BATHYMESSUNG	DATUM	7. 1.79	8.00 UHR	POSITION	30.37 S	6.22 E	EGRR	GLNE	903			
BATHYMESSUNG	DATUM	7. 1.79	10.00 UHR	POSITION	30.60 S	6.42 E	EGRR	GLNE	908			
BATHYMESSUNG	DATUM	7. 1.79	12.00 UHR	POSITION	30.78 S	6.93 E	EGRR	GLNE	916			
BATHYMESSUNG	DATUM	7. 1.79	14.00 UHR	POSITION	30.98 S	7.28 E	EGRR	GLNE	923			
BATHYMESSUNG	DATUM	7. 1.79	16.00 UHR	POSITION	32.18 → 31.18	7.62 E	EGRR	GLNE	925	POS		
BATHYMESSUNG	DATUM	7. 1.79	18.00 UHR	POSITION	31.40 S	7.95 E	EGRR	GLNE	934	POS		
BATHYMESSUNG	DATUM	7. 1.79	20.00 UHR	POSITION	31.62 S	8.22 E	EGRR	GLNE	939			
BATHYMESSUNG	DATUM	7. 1.79	22.10 UHR	POSITION	31.67 S	8.50 E	EGRR	GLNE	946			
BATHYMESSUNG	DATUM	8. 1.79	0.00 UHR	POSITION	31.72 S	8.83 E	EGRR	GLNE	964			
BATHYMESSUNG	DATUM	8. 1.79	2.00 UHR	POSITION	31.87 S	9.02 E	EGRR	GLNE	971			
BATHYMESSUNG	DATUM	8. 1.79	4.00 UHR	POSITION	31.98 S	9.33 E	EGRR	GLNE	974			
BATHYMESSUNG	DATUM	8. 1.79	6.00 UHR	POSITION	32.07 S	9.68 E	EGRR	GLNE	987			
BATHYMESSUNG	DATUM	8. 1.79	8.00 UHR	POSITION	32.13 S	10.02 E	EGRR	GLNE	993			
BATHYMESSUNG	DATUM	8. 1.79	10.00 UHR	POSITION	32.22 S	10.47 E	EGRR	GLNE	999			
BATHYMESSUNG	DATUM	8. 1.79	12.00 UHR	POSITION	32.30 S	10.88 E	EGRR	GLNE	1006			
BATHYMESSUNG	DATUM	8. 1.79	14.00 UHR	POSITION	32.20 S	11.15 E	EGRR	GLNE	1020			
BATHYMESSUNG	DATUM	8. 1.79	16.00 UHR	POSITION	32.43 S	11.73 E	EGRR	GLNE	1023			
BATHYMESSUNG	DATUM	8. 1.79	18.00 UHR	POSITION	32.50 S	17.15 → 12.15 E	EGRR	GLNE	1030	POS		
BATHYMESSUNG	DATUM	8. 1.79	20.00 UHR	POSITION	32.53 S	12.52 E	EGRR	GLNE	1036	POS		
BATHYMESSUNG	DATUM	8. 1.79	22.00 UHR	POSITION	32.63 S	12.93 E	EGRR	GLNE	1042			
BATHYMESSUNG	DATUM	9. 1.79	0.00 UHR	POSITION	32.72 S	13.37 E	EGRR	GLNE	1055			
BATHYMESSUNG	DATUM	9. 1.79	2.00 UHR	POSITION	32.83 S	13.78 E	EGRR	GLNE	1066			
BATHYMESSUNG	DATUM	9. 1.79	4.00 UHR	POSITION	32.97 S	13.22 → 14.22 E	EGRR	GLNE	1068			
BATHYMESSUNG	DATUM	9. 1.79	6.00 UHR	POSITION	33.08 S	14.65 E	EGRR	GLNE	1077	POS		
BATHYMESSUNG	DATUM	9. 1.79	8.00 UHR	POSITION	33.17 S	14.97 E	EGRR	GLNE	1085			
BATHYMESSUNG	DATUM	9. 1.79	10.00 UHR	POSITION	33.20 S	15.28 E	EGRR	GLNE	1091			
BATHYMESSUNG	DATUM	9. 1.79	12.00 UHR	POSITION	33.25 S	15.62 E	EGRR	GLNE	1101			
BATHYMESSUNG	DATUM	9. 1.79	14.00 UHR	POSITION	33.28 S	15.93 E	EGRR	GLNE	1115			
BATHYMESSUNG	DATUM	9. 1.79	16.00 UHR	POSITION	33.37 S	16.25 E	EGRR	GLNE	1118			
BATHYMESSUNG	DATUM	3. 1.79	11.00 UHR	POSITION	70.35 N	17.38 E	EGRR	GULL	642			

Fig. 8

NUMERICAL ANALYSIS OF TEMPERATURE AND SURFACE CURRENT FIELDS IN THE NORTH ATLANTIC WITH ACCOUNT OF THE UPPER MIXED LAYER

by

V.P. Kochergin, V.I. Klimok, V.A. Sukhorukov, A.V. Shcherbakov
(USSR)

One of the important problems of present-day oceanography is the objective of constructing a mathematical model (and its numerical realization) of the baroclinic ocean dynamics which would be able to describe fundamental mechanisms of large-scale oceanic circulations, would make it possible to evaluate the quantitative contribution of different factors during the process of formation of main macro-circulation systems and would permit the exploration of the role of the oceanic active layer.

Let us consider the prognostic model of large-scale circulations with account of baroclinic effects and bottom relief. The set of equations of motion, continuity and diffusion of density is following:

$$\frac{\partial u}{\partial t} + \ell v = -\frac{g}{a\sin\theta}\left(\frac{\partial \zeta}{\partial \lambda} + \frac{1}{\rho_0}\frac{\partial}{\partial \lambda}\int_0^z \rho\, dz\right) + \frac{\partial}{\partial z} K \frac{\partial u}{\partial z} + \frac{\mu}{a^2}\Delta u; \qquad (1)$$

$$\frac{\partial v}{\partial t} - \ell u = -\frac{g}{a}\left(\frac{\partial \zeta}{\partial \theta} + \frac{1}{\rho_0}\frac{\partial}{\partial \theta}\int_0^z \rho\, dz\right) + \frac{\partial}{\partial z} K \frac{\partial v}{\partial z} + \frac{\mu}{a^2}\Delta v; \qquad (2)$$

$$\frac{\partial w}{\partial z} + \frac{1}{a\sin\theta}\left(\frac{\partial u}{\partial \lambda} + \frac{\partial}{\partial \theta} v \sin\theta\right) = 0; \qquad (3)$$

$$\frac{\partial \rho}{\partial t} + \frac{u}{a\sin\theta}\frac{\partial \rho}{\partial \lambda} + \frac{v}{a}\frac{\partial \rho}{\partial \theta} + w\frac{\partial \rho}{\partial z} = \frac{\partial}{\partial z} K_\rho \frac{\partial \rho}{\partial z} + \frac{A_e}{a^2}\Delta \rho. \qquad (4)$$

The boundary conditions will be written below when discussing the results from solution of specific problems.

Symbols are conventional: U, V, W are velocity components along axes of the spherical coordinate system; $\theta = \pi/2 - \varphi$, φ is the geographical latitude; λ is the longitude; ρ_0, ρ is the mean value and anomaly of sea water density respectively; ζ is the datum water level of the ocean surface; a, ω is the radius and angular velocity of Earth rotation; g is the gravitational acceleration;

$\ell = 2\omega \cos\theta$ - the Coriolis parameter.

In investigation of the wind effect upon formation of large-scale density fields non-stationary terms have been omitted in equations of motion (1)-(2). Boundary conditions are the following:

$$
\begin{aligned}
&z=0: \quad K\frac{\partial u}{\partial z} = -\frac{\tau_\lambda}{\rho_0}, \quad K\frac{\partial v}{\partial z} = -\frac{\tau_\theta}{\rho_0}, \quad w=0, \quad K_\rho \frac{\partial \rho}{\partial z} = Q;\\
&z=H_1: \quad K_\rho \frac{\partial \rho}{\partial z} = 0;\\
&z=H: \quad u=v=w=0;\\
&\text{на } \Gamma_T: \quad A_e \frac{\partial \rho}{\partial n} = 0, \quad u=v=0;\\
&\text{на } \Gamma_n: \quad \rho = \rho^*(\lambda,\theta,z), \quad u=v=0;\\
&t=0: \quad \rho = \rho^{**}(\theta,z).
\end{aligned}
\tag{5}
$$

Here K_ρ, A_e are vertical and horizontal eddy diffusion coefficients (assumed to be constant); K, μ are coefficients of vertical and horizontal turbulent exchange of impulse (also assumed to be constant); $\tau_\lambda, \tau_\theta$ is friction stress on the ocean surface along axes λ, θ; $\Gamma = \Gamma_T \cup \Gamma_n$ is the lateral oceanic surface; n is the direction of the normal to the boundary Γ. H is the ocean bottom relief. In depth the ocean is divided into two layers. In the upper layer $0 \le z \le H_1$ equations (1)-(4) are solved; in the lower layer $H_1 \le z \le H$ we consider that $\rho(\lambda,\theta,z) = \rho(\lambda,\theta,H_1)$.

The general scheme of solving the problem (1)-(5) is following. The equation (4) is linearized at the $[t, t+\Delta t]$ time interval. Considering as known ρ^0, u^0, v^0, w^0 at the previous time interval t we solve the linearized equation (4) relatively ρ in the time moment $t+\Delta t$. Further, from equations (1)-(3) velocity vector components and the integral stream function are being determined using formulas of the diagnostic method, and the next time step is made. In so doing, terms which describe the lateral exchange by momentum in equations (1), (2) are referred to the preceding time moment. The computation process proceeds up to the determination of the density field.

In solving the equation of diffusion and density transport the method of telescoping is used for the equation of the integral stream function.

Calculations are performed for the North Atlantic zone 12.5° - 52.5°N with a horizontal resolution of 2.5°. In the vertical line a new variable $h = (z+q)^p$, $(p=0{,}47, q=10^2 cm)$ is introduced with respect to which a uniform grid is constructed. In the Z variable it corresponds to levels: 0, 35, 126, 277, 490, 768, 1110, 1522, 2000 m. Density values at liquid boundaries Γ_{ne} and the wind friction stress are taken from observational data of the winter season. Calculations have been performed in the following values of parameters: $\rho_0 = 1 g/cm^3$; $g = 980 cm/sec^2$; $\omega = 0.73 \cdot 10^{-3}$ 1/sec; $\mu = 10^7 cm^2/sec$; $a = 6.48 \cdot 10^8 cm$; $K = 10^2 cm^2/sec$; $K_\rho = 1 cm^2/sec$; $A_\theta = 10^7 cm^2/sec$.

Let us dwell on results from three numerical experiments. In all calculations the initial density distribution and values of physical parameters are the same.

In the first version the flow Q and the wind friction stress $\tau_\lambda, \tau_\varphi$ are the sources of motion.

As a whole, calculated density fields are in a satisfactory qualitative conformity with observational data. In the 0-126 m surface layer an actual density distribution has been obtained with isopycnals directed from the south-east toward the north-west. At middle levels in the depth of the 277-1110 m layer a local subtropical density minimum has been formed, a local maximum is recorded at the 2000 m depth in middle latitudes.

In the second version currents in the ocean were caused by the Q flow while $\tau_\lambda = \tau_\varphi = 0$. At the upper calculation levels the derived density field distribution is qualitatively similar to the preceding version; the local density minimum disappeared at 277-1110 m levels.

In the third experiment, where the wind effect was taken into account and the flow Q=0, the calculated density fields coincided practically with the results of the first experiment.

It should be noted that in the above three experiments one more motion force existed - the meridional density gradient governed by the difference of given density values on the northern and southern "liquid" boundaries and the corresponding to it the initial zonal density field. In the above three versions the surface distribution of density was obtained the same and this resulted from the impact of the same meridional density gradient which is of maximum value

just in the surface layer.

Presented results from calculations permit to formulate a conclusion that the wind affects essentially the formation of the subtropical density minimum and linked with it the anticyclonic circulation in the subtropics. Besides this, these calculations are of pure methodical nature, as approval of the method for the sequence of nested grids in solution of a rather complicated problem with given density flows on ocean boundaries at a rather crude space grid aimed at further dissemination of this numerical scheme for calculation of the global oceanic circulation.

Let us turn to the discussion of the results from modelling the seasonal variability of the surface turbulent oceanic layer.

For finding the coefficient of the vertical turbulent exchange the Obukhov's formula is used in combination with the Prandtl mixing path concept.

We consider that coefficients of vertical turbulent exchange of impulse K and diffusion K_ρ are equal, $K_\rho = K$. The eddy viscosity coefficient K is being determined from the formula:

$$K = (0.05h)^2 \sqrt{\left(\frac{\partial u}{\partial z}\right)^2 + \left(\frac{\partial v}{\partial z}\right)^2 - \frac{g}{\rho_0}\frac{\partial \rho}{\partial z}}\,. \qquad (6)$$

Boundary conditions for the set of equations (1)-(4) in which $\int u = 0$ and $\mathfrak{I} = \frac{1}{g\rho_0} p_a - \frac{1}{\rho_0}\int_0^H \rho\, dz$ are the following:

$$z=0:\ K\frac{\partial u}{\partial z} = -\frac{\tau_\lambda(t)}{\rho_0},\quad K\frac{\partial v}{\partial z} = -\frac{\tau_\theta(t)}{\rho_0},\quad w=0,\quad \rho=\rho^0(t,\lambda,\theta);$$
$$z=H_1:\ \frac{\partial u}{\partial z} = \frac{\partial v}{\partial z} = 0,\quad K_\rho\frac{\partial \rho}{\partial z} = 0. \qquad (7)$$

at coastal boundaries, which are considered to be vertical, density values are given $\rho|_\Gamma = \rho_\Gamma(t,\lambda,\theta,z)$

In presented versions of calculation $A_e = 10^8 \text{cm}^2/\text{sec}$; $K \geqslant 0.1\ cm^2/c$, $K_\rho \geqslant K_0 = \min K_\rho = 10\ cm^2/c$.

The method of nested grids has been used to remove the limitation for the minimum value of the vertical turbulent exchange coefficient which appears in previous calculations.

The set of equations (1)-(4), (6) with boundary conditions (7): for density taken from observations for the summer and winter seasons with a sinusoidal interpolation between seasons

and wind stress taken from Halleman's tables for four seasons with a linear interpolation between them was solved numerically for the North Atlantic area 10-65°N and 10-80°W with a horizontal resolution of 5°. 40 calculation levels have been used in the vertical. Steady-state solutions for winter and summer seasons and a non-stationary solution of the seasonal variability resulted from the numerical integration.

In Fig. 2 stationary solutions (the depth of the turbulent layer) are given for two seasons.

The solution for the summer season is being characterized by the set up of the stable density stratification in the whole oceanic area while the local value of wind stress is mainly responsible for the depth of the surface turbulent layer.

Periodical solutions, obtained with a time step equal to 10-day periods, served as initial data for the problem of seasonal variability. Calculations of the seasonal course are performed with a time step equal to 12 hours.

In accordance with data on heat balance of the North Atlantic the solution indicates qualitatively correctly on certain features of loss and supply of heat of the ocean surface resulting from the effect of oceanic currents (is characterized by the sign of the magnitude of $K_s \frac{\partial s}{\partial z}\Big|_{z=0}$).

An essential difference occurs between stationary and non-stationary solutions and, first of all, in the depth of the turbulent layer (see Figs 2,3). In a non-stationary problem the thickness of the turbulent layer during the summer season is markedly less while in the winter season noticeably more. This difference is governed by the distribution of vertical density gradients which is a key factor in finding the base of the turbulent layer in accordance with the formula (5).

The decrease of the minimum value of the vertical turbulent exchange coefficient K_o from 10 to 1; 0.1 cm^2/sec cause an essential rearrangement of density flows at the ocean surface in a non-stationary problem, in particular, when K_o=1-0.1cm^2/sec during the spring-summer period areas of unstable stratification appear at the surface. This fact emphasizes the important role of the magnitude of the vertical exchange coefficient in a deep ocean.

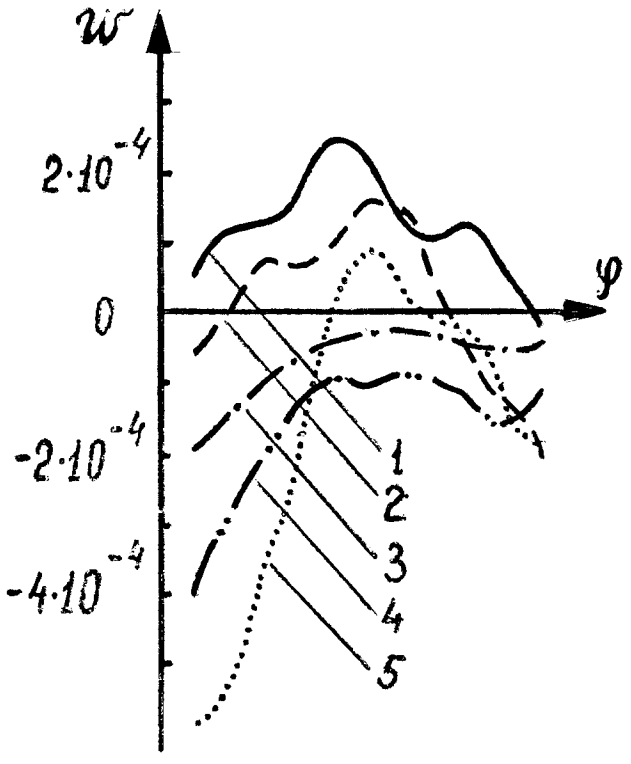

Figure 1 - Vertical velocity W along the meridian 65°, W as the function of latitude φ at the depth 126 m and 490 m.

1. Wind component W and so on;
2. W at depth 126 m, $\tau_\lambda \neq 0$, $\tau_\theta \neq 0$, $Q \neq 0$;
3. W at depth 126 m, $\tau_\lambda = \tau_\theta = 0$, $Q \neq 0$;
4. W at depth 490 m, $\tau_\lambda \neq 0$, $\tau_\theta \neq 0$, $Q \neq 0$;
5. W at depth 490 m, $\tau_\lambda = \tau_\theta = 0$, $Q \neq 0$.

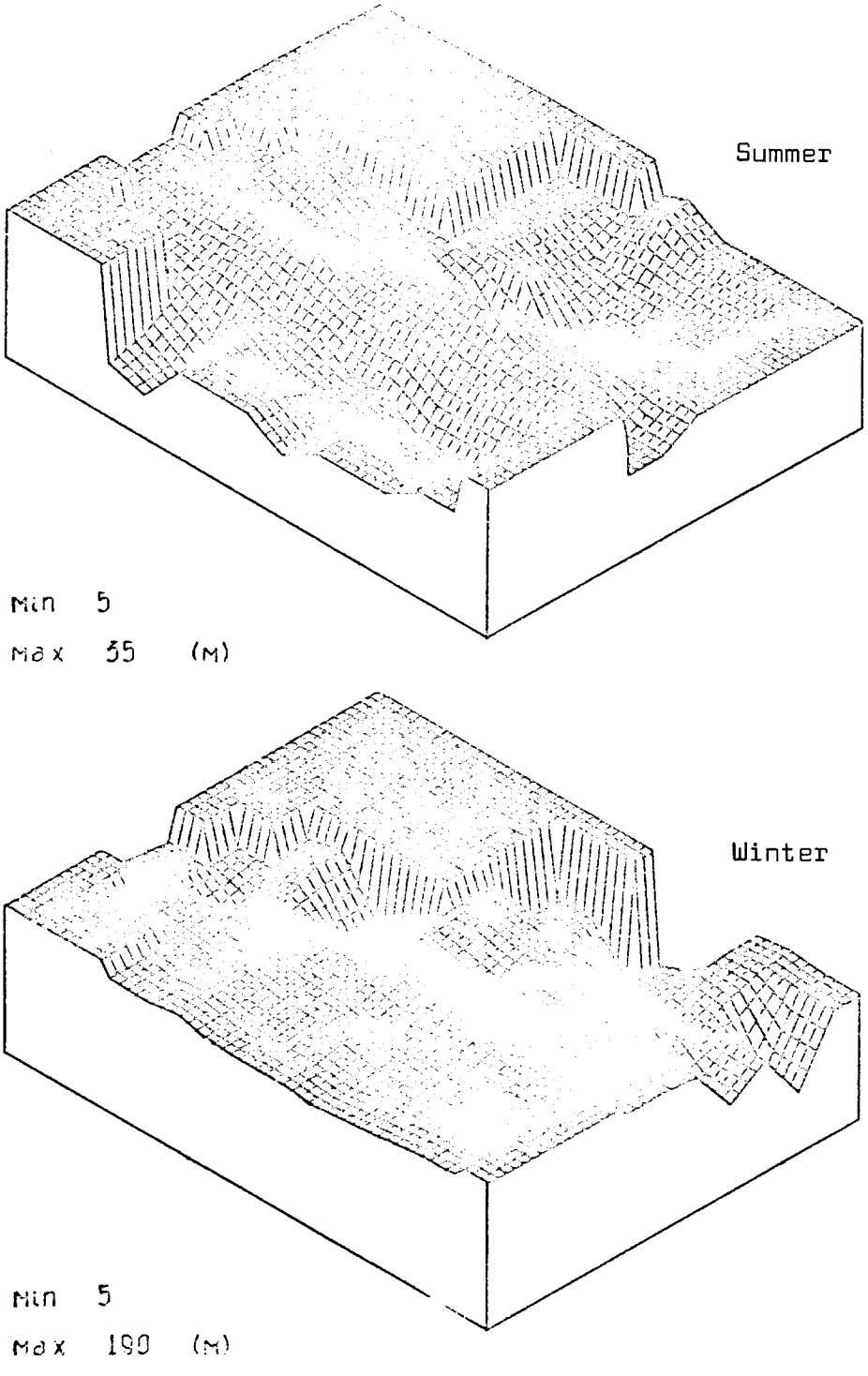

Figure 2 - Depth of the surface turbulent layer (stationary)

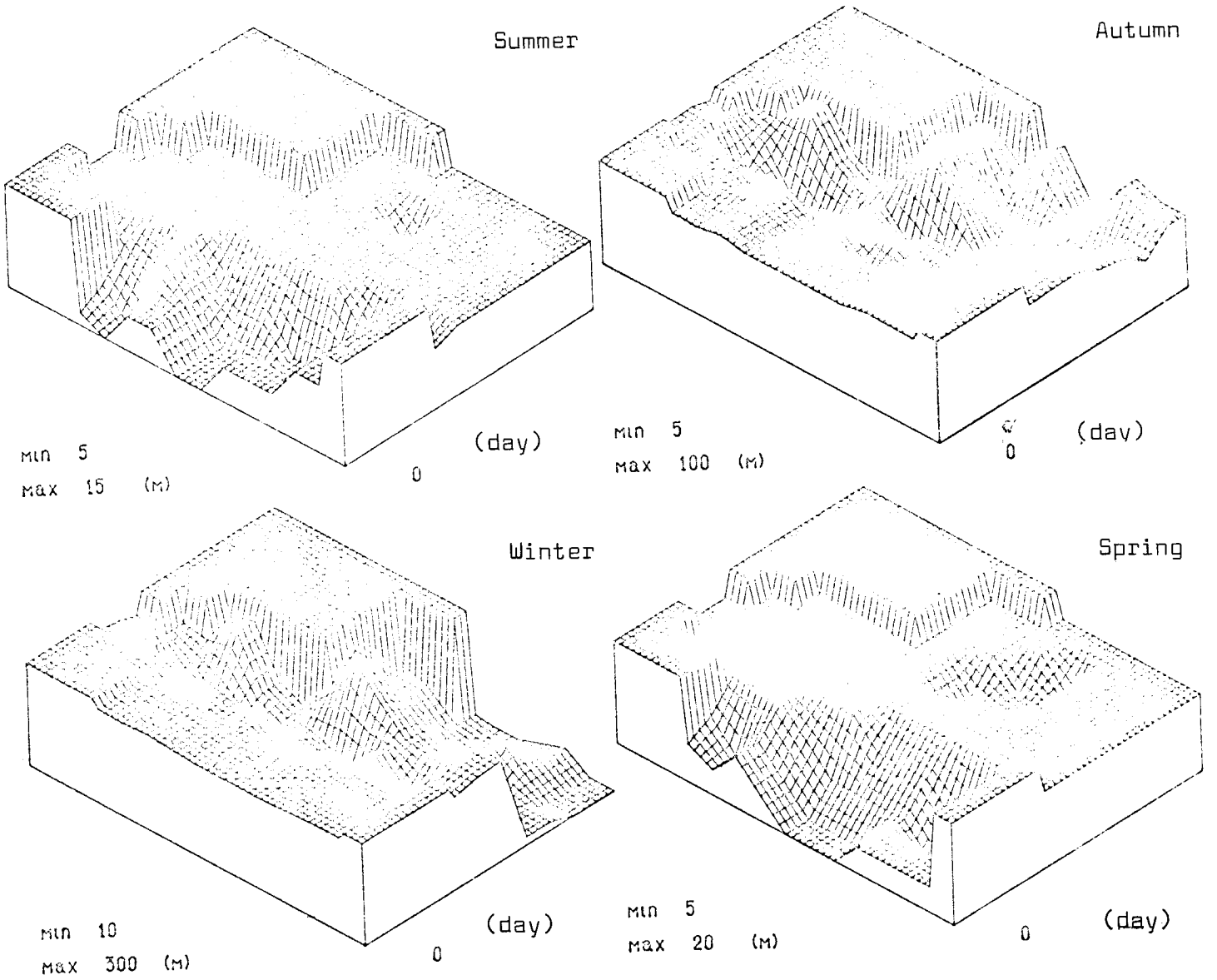

Figure 3 - The depth of the surface turbulent layer (seasonal trend)

NDBO F-325

DATA FLOW AND APPLICATIONS OF U.S. DEEP OCEAN MOORED AND DRIFTING DATA BUOYS

SEMINAR OF OCEANOGRAPHIC SERVICES

MOSCOW, U.S.S.R.

APRIL 2-11, 1979

DR. JERRY C. McCALL
DIRECTOR, NOAA DATA BUOY OFFICE

U.S. DEPARTMENT OF COMMERCE

National Oceanic and Atmospheric Administration

Office of Ocean Engineering

NOAA DATA BUOY OFFICE

NSTL Station, MS 39529

April 1979

BACKGROUND

Since June 1972, NDBO has deployed environmental reporting data buoys in various gulf and ocean regions to provide synoptic data for weather reports and for scientific data archives. As of April 1, 1979, 21 moored buoys were reporting environmental data on a routine basis. In addition, NDBO has 50 drifting buoys being deployed by both ships and aircraft for the U.S. commitment to the buoy portion of the Global Weather Experiment Program. The first of two special observing periods to be conducted during this worldwide experiment was completed during January-February 1979. A large complement of approximately 200 free drifters was deployed during the 1975-1976 period in support of various global atmospheric research programs. Finally, NDBO has developed and deployed several special classes of buoys which will be addressed in more detail further on.

The present complement of buoy data acquisition and telemetry electronics was determined by a series of hardware evolutions, which in turn were brought about by our continued quest for the most accurate and reliable equipment that technology could offer at realistic costs. The evolution of the data buoy hardware, together with the availability of microprocessor technology and suitable communication satellites, has permitted a fully automated, reliable approach for the acquisition of remote marine environmental data on a synoptic basis in all weather conditions. These conditions encompass a wide range of sea states, from smooth seas to severe disturbances. In addition, the measurement and reporting of environmental data is accomplished on remote ocean platforms which are relatively inaccessible for maintenance and therefore require a high degree of equipment and data link reliability.

SOURCES OF DATA

The environmental data acquired by NDBO are derived from both moored and drifting buoys. Several types of payloads and buoy hulls are currently being maintained and operated by NDBO. Figure 1 shows the moored buoy deployment locations as of April 1979. The buoys continuously acquire and telemeter synoptic environmental data in near real time to the weather forecasting community, including the National Weather Service (NWS). These data, along with other environmental data, are used for engineering evaluation and analysis, and are provided monthly to the National Oceanographic Data Center (NODC) and the National Climatic Center (NCC) for archival purposes.

MOORED BUOY PAYLOADS

Background

The first-generation NDBO payloads were developed to meet both R&D and data product delivery requirements. These payloads were designated the Engineering Evaluation Phase (EEP) payloads, and were placed on 12-meter discus hull buoys with 100-ton displacement, for evaluation of advanced state-of-the-art sensors and buoy components. Deployment of six of the EEP buoys began in June 1972. Our definition of payload refers to the buoy

instrumentation, which includes on-board sensors, data processing, communications, and the power source.

A companion development to the EEP units were the Phase I payloads, which were designated for simple, less flexible data acquisition requirements and which were originally placed on small 1.7-meter diameter drifting buoys. Deployment of Phase I payloads began in January 1973.

Current Deployment Scenario

Four types of moored buoy payloads are currently being maintained and operated by NDBO: the Prototype Environmental Buoy (PEB) payload, the Phase I and Phase II payloads, and a newly developed General Purpose Buoy Payload (GSBP). Of the payloads currently deployed, eight are PEBs, two are Phase I payloads, five are Phase II payloads, and six are GSBPs.

Prototype Environmental Buoy (PEB) Payload - The PEB design was based on concepts proven during initial NDBO programs. Although originally tailored to meet the needs of the weather community, its measurement capability was expanded to include surface wave data and subsurface water temperatures down to 300 meters.

Figures 2 and 3 display 10- and 12-meter diameter hulls, respectively. Both types of hull support PEB payloads. Meteorological sensors are located on the mast at the 10-meter level. Measured values are telemetered via satellite link to shore every 3 hours in a self-initiated, internally programmed mode. For special needs (e.g., during abnormal weather disturbances), the on-board weather data acquisition and reporting sequence changes to hourly operation by command from shore. Present and previous data frames can also be acquired on demand via radio link. The on-board data acquisition and timing is controlled by a special-purpose, stored-program computer. Batteries provide the power required for up to 3 years of continuous buoy operation.

This payload is equipped with a dual HF/UHF communications system. Redundant rf links were implemented to ensure a reliable and orderly transition from HF to UHF satellite communications. Conversion to UHF communications is nearly complete, and will allow us to take advantage of this more reliable mode of communications. Eight 10- and 12-meter diameter hulls equipped with PEB payloads are currently in service in deep ocean areas, including the Gulf of Alaska, North Pacific, and Atlantic Ocean. All PEBs are being modified to incorporate a microprocessor system to replace the stored-program minicomputer. The PEB microprocessor system is comprised of two RCA 1802 microprocessors. A 2K memory microprocessor provides the communications and timing function, while a 1K memory microprocessor provides the data processor function.

Phase I and Phase II Payloads - The Phase II payload program is an outgrowth of the Phase I payloads for small buoy systems that were developed in the 1972-1973 time period. These earlier buoys were configured as spheres and as horizontal and vertical cylinders, with typical diameters ranging between 1.4 and 1.7 meters. None of the small buoy systems achieved significant success with regard to survivability and operability in the open sea; however, the data acquisition payloads were quite reliable.

The Phase II payloads are second-generation payloads that are presently integrated in existing 6-meter boat-shaped hulls, NOMADs, shown in Figure 4. (The NOMAD hulls were developed in earlier U.S. Navy programs.) Phase II payloads are also installed on the larger discus hulls. The Phase II payload provides meteorological environmental parameters and surface wave data. The on-board data processing and rf data link are very similar to that of the PEB payload, employing nonprogrammable hardware and both HF and UHF satellite communications. However, the Phase II payloads are being upgraded to an all-UHF configuration. Five Phase II payloads are in service in both deep ocean and continental shelf areas. Two buoys are still using the earlier Phase I payloads. However, the buoys will, within 6 months, be replaced with the General Service Buoy Payload described below.

General Service Buoy Payload (GSBPs) - The first 15-unit production run of this advanced payload class has just been completed. Six GSBPs are now in service on-board one 5-meter discus, three NOMADs, and two 10-meter hulls. Ten additional payloads will be in service by the spring of 1979, along the continental shelf, in the Great Lakes, and in the deep ocean areas.

The GSBP system design draws extensively upon proven hardware and systems. For example, the entire meteorological sensor suite is identical to that used in the Phase II payload. In addition, data input ports are provided for future sensor additions, including a wave measurement system and a multi-element temperature measurement system. Buoy communications consists of a UHF-satellite transceiver with 40-watt output power, and associated electronics similar to that used on Phase II and PEB payloads.

The GSBP relies entirely on a UHF-satellite communications relay link, which eliminates the need for the large antennas required for previous HF systems. The GSBP features a program-controlled microprocessor instead of the nonprogrammable special-purpose computers employed on earlier payloads. This element, the Intel 8080 microprocessor, acquires sensor data and digitally processes and formats the data. This microprocessor has a 3K core memory.

Future Moored Buoy Activities - A new program is being initiated in the Great Lakes. The loss of the Great Lakes ore carrier EDMOND FITZGERALD in November 1975 prompted an intensive investigation of weather forecasting in this area. Several deficiencies in the program were found which led to the decision to deploy and operate a series of data buoys in this area. Two buoys are planned for 1979 and the remainder in 1980 and 1981. Each buoy will be equipped with a meteorological sensor suite and a wave measurement system.

DRIFTING BUOYS

Unlike moored buoys, whose primary purpose is to report synoptic data to weather forecasting groups, drifting buoys provide information to the scientific community, usually for nonsynoptic purposes. Occasionally, there is a need for near-real-time receipt of data (e.g., the use of a buoy to track oil spills, as was done in the case of the ARGO MERCHANT, which broke up on the Georges Bank off New England in December 1977). Generally, drifting buoys are used for various scientific investigations, including such

projects as arctic ice dynamics, Lagrangian ocean current measurements, and large-scale experiments such as the Global Weather Experiment. These buoys are deployed worldwide.

Ice Drifting Buoys - The ice drifting buoys monitor environmental conditions in the deep polar regions to further the understanding of the dynamics and the thermodynamic interaction between arctic ice and the environment. These buoys are usually equipped with pressure and temperature sensors, and use a UHF orbiting satellite relay data link for telemetry and position fixing. The daily changes in position provide the measurement of ice movements needed to assess the ice dynamics. Figure 5 shows an air-deployable ice buoy.

Lagrangian Drifting Buoys - The primary purpose of this buoy type is to achieve Lagrangian tracking of water parcels, while simultaneously measuring basic meteorological parameters. Tracking is enhanced by the use of a drogue which couples the surface buoy to a particular water layer depth. The drogue also reduces the wind drift of the buoy. The meteorological sensor suite generally measures air pressure and sea surface temperature. Future instrumentation may include wind speed and air temperature.

Communications and position fixing depend upon the operation of a UHF transmitter on the buoy, which sends data to a specialized electronics package on board a polar-orbiting satellite. The satellite in turn relays the data to a ground station. Relative motion between the satellite and buoy produces a Doppler effect on the frequency of the rf link. This frequency shift is processed along with the satellite orbital track to derive buoy position. Our experience with position-fixing accuracy has been found to be well within 5 km rms.

Global Weather Experiment Participation - NDBO is currently participating in the Global Weather Experiment, which is being conducted from December 1, 1978, through November 30, 1979. We have developed a TIROS Meteorological Drifting (TMD) buoy for this application.

The TMD buoy is a small, free-drifting buoy which measures barometric pressure and sea-surface temperature in the open-ocean environment. The buoy also monitors its internal temperature and battery voltage. In operational use during the Global Weather Experiment, the TMDs are acquiring data on a continuous basis and transmitting via a UHF radio-frequency up-link to the TIROS-N satellite. Approximately two up-link transmission sequences of 10 minutes' duration can be expected to reach the satellite with high accuracy each day.

Figure 6 shows the design configuration of the TMD buoys. The mechanical characteristics are as follows:

Overall length	3.05 m (10 feet)
Maximum diameter	68.6 cm (27 inches)
Spar diameter	20.3 cm (8 inches)
Deployed weight	92.7 kg (294 pounds)
Total buoyancy	228.6 kg (503 pounds)

Fifty TMD buoys will be deployed by ship in remote areas of the Southern Ocean from Peru to New Zealand during the Global Weather Experiment. Since reseeding of the buoy network by ship would be difficult, NDBO has developed the capability to make deployments from long-range high-altitude aircraft. In this effort, air-drop tests were conducted at the National Parachute Test Range at El Centro, California. Four buoys were made available for the test, and the U.S. Air Force provided C-141 aircraft support. The buoys were mounted on wooden pallets and gravity launched from an altitude of 610 meters into the Salton Sea, California. This altitude was chosen because of precision navigation problems with high-altitude low-speed drops, but it was sufficient for air-drop certification purposes at higher altitudes. A 6.7-meter cruciform parachute was attached to each buoy and opened by static line. The water entry speed with this parachute was about 9 meters per second. The TMD buoys had previously undergone free-fall tests from 12.2 meters, which corresponds to a water entry speed of about 15 meters per second. Both test series were successful, and the buoys were certified by the Air Force for deployment by both C-130 and C-141 aircraft from altitudes of 150 to 6100 meters and maximum drop speeds of 155 knots.

Another series of drops from 610 meters was made 50 miles at sea off of Norfolk, Virginia. Both the buoys and buoy instrumentation performed flawlessly during and after all testing. Figure 7 shows a TMD buoy dropping into the water with an open parachute.

Future Activity for Drifting Buoys - New missions for drifting buoys are in the research and development process, and will include the following:

- Fully develop the air-drop capability for meteorological and oceanographic buoys to include subsurface temperature and Lagrangian measurements.
- Further develop the capability and utility of the numerical buoy model.
- Develop and test drogue configurations designed to improve buoy dynamics and Lagrangian performance, including the development of an air-dropped drogue configuration.

CUSTOM-DESIGNED BUOY PAYLOADS

Supplementing our standard moored and drifting buoy payloads are several types of custom-designed payloads required for experimental and dedicated applications. Major custom-designed payloads which will be addressed are the Ocean Thermal Energy Conversion (OTEC) buoy, the Ocean Platform Environmental Monitoring System (OPEMS), a Waverider buoy, and a Subsurface Temperature Monitoring (Tz) buoy.

Ocean Thermal Energy Conversion (OTEC) Buoy - Many of us are pursuing ocean energy sources, and OTEC is one of the projects being investigated. Although the basic concept is simple enough (i.e., deriving electrical energy from thermogradients in the ocean), the OTEC mechanization is not only complex, but also must be highly efficient in order to make the concept viable. It should be pointed out that, unless the selected OTEC basic

elements lie within a critical range of physical and biochemical performance characteristics, the entire concept cannot operate productively.

The object of the OTEC buoy is to provide an in situ platform for determining heat transfer coefficients and their derivatives on various samples of OTEC heat exchanger ocean-flow tubing. Heat transfer coefficients are degraded by in situ biofouling corrosion and scaling. To measure these changes, NDBO was tasked by the Department of Energy to provide a 12-meter discus buoy instrumented to acquire biofouling and corrosion data on various samples of OTEC heat exchanger tubing. In addition, the OTEC buoy was instrumented to acquire water quality data on near surface seawater. To satisfy the data requirements applicable to the OTEC experiments, instrumented hardware was installed on the buoy. For OTEC, control of the data processing and control systems is through a modified Phase II payload. HF rather than UHF satellite communications is used to enable virtually unlimited command control directly between the OTEC buoy and the NSTL base station. UHF satellite communications was not deemed suitable for this application because of the high-capacity rf traffic required.

NDBO's first OTEC buoy was deployed in the Gulf of Mexico in mid-March 1978. The platform was instrumented to perform three heat transfer experiments to determine the fouling factor in aluminum and titanium samples. The fouling factor target value was specified at 0.0005 over a 90-day period. The achieved factor after a 7-week period was 0.0002.

By early June, the OTEC platform had experienced a number of problems which required retrieval of the buoy for refurbishment. The refurbishment effort incorporated features to enhance buoy reliability and to increase the scope of the experiments. The pumping system was modified to operate the experiments on the pressure side rather than the suction side of the pumps. Redundant pumps were incorporated to enhance reliability. In addition, an improved 23-meter suction hose system incorporating separators was implemented to help reduce interference with the buoy mooring chain.

The scope of the experiments was increased by the addition of a fourth heat transfer monitor which now enables monitoring aluminum, titanium, copper/nickel, and stainless steel sample tubes. An experiment to test the effect of flow on the aluminum tube exterior surface was also added. Finally, a corrosion and biofouling sampling system for each sample under test was incorporated. From the previous OTEC deployment, we were able to recover many varieties of living organisms which were sent to marine laboratories for analysis. In order to keep up with the increased power demands brought about by the additional scope of experimentation, more powerful diesel engines were substituted for the original ones.

On December 2, 1978, the refurbished buoy was redeployed in the Gulf of Mexico. Approximately 16 frames of heat transfer monitor experimental data are being acquired weekly by the HF data transmission system. This is in addition to corrosion, biofouling, meteorological, and status data which is being acquired routinely on a daily basis.

Figure 8 shows the OTEC buoy configuration.

Waverider Buoy - NDBO has successfully instrumented a small Waverider buoy capable of transmitting wave covariance data via UHF satellite communications. The Waverider hull is about 1 meter in diameter, and was selected because of its proven record for obtaining wave measurements. Existing Waverider inertial sensors and a double integrator are used to sense vertical acceleration and resultant displacement. A wave data analyzer generates a covariance function from the inertially derived time series displacements. The covariances are formatted into a number of discrete computer words (approximately 150) and transmitted to shoreside processing facilities via UHF satellite self-initiated transmissions. At the shoreside processing site, the covariances are converted to displacement spectral densities by Fourier transformations. Integration of the spectra produces the moments from which the wave height and period are calculated. This system has produced spectra in the range of 0.5 Hz, with a 0.01 Hz resolution; significant wave heights beyond 3 meters were also computed from the spectra.

Two improved versions of the Waverider buoy are now under procurement, with the possibility of additional buoys being procured for deployment in support of other projects such as the Wave Climate Program. In summary, by providing a capability for accurate buoy-based measurement of ocean waves, users such as the National Weather Service, the U.S. Navy, marine shipping interests, and offshore operators can receive near-real-time wave spectral data.

Figure 9 shows a Waverider hull.

Ocean Platform Environmental Monitoring System (OPEMS) - In order to provide a strategic oil reserve, our government will be storing large quantities of oil in salt domes. The OPEMS was developed to monitor and control the orderly displacement of brine from major salt domes while these domes are being filled with oil.

The OPEMS sensors and satellite communications systems were essentially in hand prior to development; however, the OPEMS electronics package is a new design. This design incorporates a solar cell and battery for virtually unlimited power supply life. The design also features a solid-state recording device for elimination of risks associated with tape transport units. Finally, the OPEMS has a built-in test-readout printer for on-site verification of performance. The OPEMS has been deployed on an oil rig off the Texas coast since September 1977. To date, the system has performed well with a report success rate of approximately 90 percent.

A second-generation OPEMS has recently been designed and installed, replacing the previous system at the site off the Texas coast. This system incorporates several enhancement features including redundant wind sensors, an improved barometric pressure sensor, addition of a conductivity sensor, increased solid-state storage from 8K bytes to 30K bytes, and an improved Geostationary Operational Environmental Satellite (GOES) transmit terminal. Figure 10 shows the OPEMS operating off the existing platform in Texas. Future effort will be directed to improvement of materials and instruments, to reduce the high rate of marine biofouling and to seek materials and devices for implanting instruments in the warm coastal waters which will allow longer periods between service visits.

Subsurface Ocean Temperature Monitoring (Tz) Buoy - NDBO equipped a 5-meter discus buoy with a multiple thermistor transducer sensor system and a mooring attachment loop system. This buoy was deployed in the Gulf of Mexico in December 1978 as an R&D effort, to measure and transmit gradients of ocean temperature at specific depths between 2 and approximately 300 meters. The data acquisition system consists of a thermistor string connected to an electronics package which converts each analog thermistor voltage into a digital word. The array of digital words, representing temperatures at each discrete depth, is then periodically transmitted via the GOES satellite to a shore-based data collection receiver. The Tz buoy is required to operate unattended for 12 months of continuous service.

This buoy is outfitted with 12 thermistors and 2 pressure transducers in accordance with the drawing shown in Figure 11. Six mooring attachment loops were incorporated to minimize adverse effects of buoy rotation and other buoy motions. This is the latest in a series of attempts to attach a Tz line to the mooring line of a large buoy. A combination mooring line/Tz line has had modest success on small buoys, but has not yet been demonstrated on a large buoy. This remains a problem area.

BUOY HARDWARE

Sensors

Figure 12 presents an overview of the sensor requirements of the three different NDBO payloads - moored, drifting, and custom-designed. These sensors can conveniently be grouped into two major categories: meteorological and oceanographic.

Meteorological Sensors - I will treat the subject of meteorological sensors briefly via the meteorological sensor matrix shown in Figure 13. From these sensors, we are able to prepare our standard meteorological data message, coded into the conventional World Meteorological Organization format WMO FM-24V.

Subsurface Ocean Sensors - The development of subsurface ocean sensors was perhaps one of our most ambitious and difficult undertakings. An early result of this effort was the delivery of several inductively coupled ocean sensors capable of being attached to a combination mooring line/data line. Each sensor was packaged within a cylindrical pressure housing with hemispherical end caps, and each contained individual oceanographic transducers and secondary power cells. The total package was 52 centimeters long by 32 centimeters in diameter.

In June 1975, NDBO deployed a 12-meter discus hull buoy in the Gulf of Mexico. In addition to the standard meteorological instrumentation, five inductively coupled ocean sensors attached to a mooring line/data line were included on this buoy. The ocean sensor packages were installed at depths of 50, 100, 200, 350, and 500 meters, to measure conductivity, temperature, pressure, and current direction. The 50- and 100-meter packages were additionally equipped with transducers to measure current velocity.

The buoy was retrieved in late January 1976. Extensive damage was noted on the mooring line/data line at the oceanographic sensor package attachment points. The extent of the damage was such that complete separation of the packages would have occurred in a matter of weeks. It was also found that the internal batteries of the ocean sensor packages would neither accept nor retain a charge. In reviewing the results of this experiment, the following conclusions were drawn:

- The inductive coupling concept appears to be a valid technique for transmission of information.
- The NDBO-configured ocean sensor system is not operationally feasible, due to its high degree of complexity.
- Reliable measurement of current velocity and direction cannot be obtained from a surface moored buoy, due to motion of the mooring line and the blockage from both the sensor and mooring line.

In view of the limitations associated with the ocean sensor package, NDBO sought alternative solutions. During the past 3 years, we have supported the development of systems capable of providing oceanographic current velocity data. This effort has in turn led to the development of improved current meters capable of enduring in the environment for reasonable lengths of time up to 1 year. Based on previous experience that current meters with moving parts were inherently incapable of long-term reliability in the ocean environment, we have pursued further development of electromagnetic and accoustic current meters.

Figure 14 shows a Marsh-McBirney electromagnetic probe current meter during installation for preliminary at-sea testing on an offshore tower. Two Marsh-McBirney units were recovered following a short deployment period and found to be operating satisfactorily. Following close-in at-sea testing on the tower, the current meter will be deployed on a subsurface mooring array and coupled to an acoustic telemetry unit to transmit data and status to the surface in real time for relay through a geostationary satellite link to shore. The current meter contains a microprocessor integral to the unit housing, to preprocess the current data before transfer to the acoustic telemetry unit for transmission to the surface.

Figure 15 shows a Neil Brown acoustic probe current meter being installed for preliminary testing. Two such meters were recently retrieved from an offshore tower following 4 months of operation in 20 meters of water. Although satisfactory performance is indicated from analyses performed to date on the current meter data records, insufficient analysis precludes judgment at this time on the degree of technical performance.

The Neil Brown design also includes an interface to an acoustic telemetry link for real-time reporting of data and hardware status. These units also record the data and status on an internal tape cassette. Pending verification of good performance, each unit will be attached on a subsurface mooring array and will be interfaced with an acoustic telemetry system for long-term at-sea testing. A test period of approximately 1 year is planned to evaluate the reliability of the current meters under operational conditions.

A major development paralleling the current meter activity is the acoustic telemetry link. The first system has been designed with variable design features to aid in system refinement. The telemetry system can vary key parameters such as bit rate and symbol duration to determine the correct combination required to combat channel fading and multipath. The system is designed to operate in the 15 to 25 KHz frequency band, using frequency hopping techniques and employing frequency shift keying modulation (FSK) with single and a multi-tone capability. The acoustic telemetry system is designed for a range of 1 nautical mile.

During 1979, a complete system test will be run for 1 year. It will consist of up to four current meters mounted in a subsurface buoy array, a surface buoy reporting data to shore, and the acoustic telemetry link relaying data from the current meters to the surface buoy. This test will be conducted on the continental shelf in the Gulf of Mexico at a depth of approximately 200 meters. In addition, we will test our acoustic telemetry link separately in deep water for other oceanographic research applications.

Wave and Wave Spectra Data Sensors - In the area of wave data, NDBO systems have evolved from simple systems providing only wave height and period to microprocessor systems providing wave spectral outputs. The first wave measurement system was essentially a buoy motion measurement system mounted within the buoy hull. The measurement device was enclosed in a gyrostabilized platform from which acceleration and pitch and roll angles were derived. Problems with the stabilized platform led to a strapped-down system. The strapped-down system consumed considerably less power and was quite reliable, but faltered when it came to producing high-quality data.

Although an improved version of the strapped-down system was under development, the requirement for spectral data as well as wave height and period let to the parallel development of two other systems. One of these systems, the digital wave data analyzer, produces spectra using time series inputs to generate a covariance function on board a buoy microprocessor. At the shore processing site, the covariances are converted to displacement spectral density by performing the Fourier transform on the covariance function. Integration of the spectra produces the moments from which the wave height and period are calculated. This system produces data of excellent quality. The other wave measurement system resulted from a requirement for a system that could generate coarse spectral density and reasonable wave height and period data on board a platform without a sophisticated processor. In this system, time series inputs are derived from a strapped-down single-axis accelerometer. Twelve frequency-sensitive analog filter circuits receive the time series inputs, after which each output is squared and smoothed. At the shore station, the data are processed with a matrix to generate a spectrum for acceleration, velocity, displacement, and estimates of the average value of the displacement spectral density in the bandpass of each of the 12 analog channels.

The analog wave spectrum analyzer systems are currently installed on the PEB payloads. By the end of this year, they will be replaced by digital wave analyzers. Phase II payloads already have digital wave analyzers on board. The GSBPs will be augmented with digital wave analyzers by the end of this year.

The next area is the development of wave directional spectra. Recent demands by various government agencies for directional spectra have prompted NDBO to pursue this development vigorously. An experimental system has been developed and tested that will provide directional spectra in 15-degree directional increments. The experimental system calculates auto- and cross-covariances of heave acceleration and wave slope in two orthogonal directions for a number of time displacements. Similar to the routine for nondirectional spectra, these functions are transmitted to shore where the spectra are constructed via the Fourier transform. The output data is three-dimensional and includes displacement spectral density, frequency, and direction.

In the future, NDBO plans to prepare specifications for an operational Directional Wave Data Analyzer (DWDA) to function with existing and future payloads. Continued development using the 12-meter experimental buoy will take place during 1979, including upgrading the system software, calibrating its directional wave measurement system, and distributing directional data to selected users for evaluation on a trial basis.

DATA FLOW

Data Requirements - There are two general categories of data requirements for NDBO programs. The first requirement comes from various weather forecasting groups, including the National Weather Service (NWS), needing real-time or near-real-time data. The NDBO weather message is approximately 10 seconds long when transmitted at a 75 bit per second rate, and includes air pressure and temperature, wind speed and direction, sea surface temperature, and wave data. NDBO buoys are deployed in the Atlantic Ocean, Gulf of Mexico, North Pacific, Gulf of Alaska, and Great Lakes. These diverse geographic locations require over-the-horizon data links.

The second requirement is governed by the needs of the scientific community. These applications generally do not require the real-time feature of the first type, although processed data occasionally is desired in a matter of hours. An important example of user applications would be oceanographers, who have for many years mapped ocean currents through Lagrangian tracking techniques. The oceanographers are interested in obtaining position fixes from drifters that follow ocean currents. The length of the position-fixing message is about 1 second. These messages contain about four to eight 8-bit words. Another example of scientific users would be investigators concerned with wave data. The U.S. Navy Fleet Numerical Weather Central (FNWC) currently utilizes NDBO's wave spectral data from moored buoys as calibration points for their formulation of prediction models used to forecast sea states for the entire northern hemisphere. Shippers in the Great Lakes and North Pacific are keenly interested in wave data for safety and optimum ship routing. The length of the spectral wave data message is approximately 40 seconds and contains approximately 150 sixteen-bit words. There are other important applications of buoys for scientific uses, including oil spill tracking and the worldwide Global Weather Experiment discussed previously.

Data System Implementation - Since program inception, the long-range plans for accomplishing environmental data reporting called for the utilization of

satellite telemetry links. Initially, these plans had to be held in abeyance because suitable cooperative satellites did not exist in 1972, nor had international frequency allocations been assigned for the collection of environmental data on the ocean surface via satellite relay. Due to these limitations, initially and up to 1978, NDBO employed high-frequency over-the-horizon communications to satisfy the data link requirements. However, since the launch of the first two Geostationary Operational Environmental Satellites (GOES) in May 1974 and February 1975, respectively, NDBO has tested buoy-satellite link hardware on the ground and on board ocean platforms. Simultaneously, we have worked very closely with allied U. S. government agencies, including the National Environmental Satellite Service (NESS), the National Meteorological Center (NMC), and the National Weather Service (NWS), to implement a timely, reliable system from data acquisition to data dissemination.

As indicated previously, data flow was initially carried out via HF telemetry links. Judicious implementation of equipment on board the data buoys and at the shore receiving sites has provided NDBO with a consistent delivery of synoptic data to NWS from all platforms on station (well above 90 percent). Since we have just concluded our successful transition from HF to UHF satellite data link, I will not address HF data flow, but will limit my discussion to UHF satellite data flow for both moored and drifting buoys.

GOES System for Moored Buoys - The GOES satellite is operated by NOAA's Environmental Satellite Service (NOAA/NESS) and is the first of a series of international meteorological satellites. GOES satellites were launched in May 1974, February 1975, October 1975, June 1977, and the spring of 1978. The current operational configuration comprises the GOES satellites designated GOES-3 and GOES-2, and provides the coverage and elevation patterns shown in Figure 16. The elevation contours define the buoy-to-satellite pointing angles with respect to eAch satellite. With the current configuration, realistic coverage exists from approximately the Greenwich Meridian westward out to 150^{o}E longitude, or better than one-half earth coverage.

The GOES contains the necessary communications hardware to serve as a stationary relay for environmental instrumentation on board ships and buoys, and on land-based stations. It is this feature, together with the shared satellite concept, that makes GOES ideally suited for NDBO's remote on-board data acquisition and telemetry function. The data collection relay function is only one of several major functions associated with GOES. Other GOES capabilities include an earth's surface and clous cover camera, a weather facsimile for cloud cover picture transmission, and a space environmental monitoring system to measure particle trajectory and energy content near the satellite.

System Data Flow and Timing for Moored Buoys - Figure 17 shows a comprehensive data flow and timing diagram for NDBO moored buoys. Data from moored buoys are transmitted, in sequence, to either the east or west GOES satellite, depending upon elevation angle geometry. In general, all satellite transmissions are aimed at achieving the highest buoy-to-satellite elevation angle, to minimize the effect of sea-multipath during periods of buoy motion. A secondary criterion in selecting either the east or west GOES is for achieving a balance of traffic load. These two criteria have resulted

in an overall system wherein our buoys located in the North Atlantic region use the east GOES and our buoys in the Pacific region and Gulf of Mexico use the west GOES.

On-board data acquisition begins 20 minutes before the synoptic hours (i.e., 0000, 0300, 0600, ..., GMT). From 9 minutes before the synoptic hour, until nearly 20 minutes after the hour, all buoys transmit their environmental data, each buoy at a programmed time slot to either the east or west GOES. Each buoy is provided an opportunity to report via a self-initiate, automatically pre-timed mode. The primary objective at the NMC dissemination center is to place synoptic data on-line to NWS by 20 minutes after the synoptic hour. In the event the self-timed report is either missed or fails to meet minimum data quality criteria, the message is automatically requested again, during the 20- to 40-minute period following the synoptic hour. In general, three interrogations are programmed in the attempt for a satisfactory message reply. If the message cannot be acquired by 40 minutes following the synoptic hour, the message is disseminated the following hour. During periods of heightened environmental conditions or disturbances, buoys can be interrogated to provide data in either near real time or in the same sequence during the synoptic hour, while providing data hourly as opposed to every 3 hours.

Data Processing - Following the transmission of data from the buoy to the satellite, the data is immediately relayed from the satellite to a NESS Command and Data Acquisition (CDA) station at Wallops Island, Virginia. At the CDA, the data is received, detected, identified, and checked for quality with regard to parity and proper message heading and termination. From the CDA, the data are transmitted over a 9600 baud landline to the NESS World Weather Building at Suitland, Maryland. Here the data are placed in dissemination queues for simultaneous transmission to NMC and NDBO data processing facilities.

At NMC, the data are further processed and scaled into engineering units. Data quality refinements are implemented utilizing boundary value limits and time rate-of-change limits. Similar analyses and processing are done at NDBO with a view toward changing on-board acquisition modes via interrogation commands. Landline communications between NDBO and NMC computers is maintained to ensure that final data dissemination is limited to valid data.

Data Base Systems - NDBO maintains both information and archival data base systems. The information data base serves to provide the necessary integrity for the buoy processing programs at both NMC and NDBO. The data base program is established at NDBO and maintains a disc storage file there. Via computer-to-computer wireline transfer, NDBO maintains and updates the disc data base at NMC.

We also maintain archival data base systems from which 7- and 9-track magnetic tapes are generated. Once a month, tapes are sent to the National Climatic Center (NCC) and the National Oceanographic Data Center (NODC) for archival and meteorological and oceanographic data base analyses.

Data Formatting and Dissemination - The United States, similar to other nations, has deployed environmental data buoys to provide reliable, periodic

weather information from remote ocean areas. Buoy instrumentation provides measurement capabilities which exceed the accuracies achieved with shipboard observation systems. For this reason, NDBO has recently changed its meteorological dissemination format and is now using a new code which allows us to reflect the accuracy and resolution of our on-board instrumentation and shore processing.

The new weather code is sponsored by the World Meteorological Organization (WMO). The code will be implemented by all cooperating nations for disseminating reports derived from their own automated marine weather stations. The full name of the code as listed in the WMO Manual on Codes is "FM 24-V SHIP - Report of synoptic surface observation from a sea station."

We have generated our own unique code with regard to the dissemination of spectral wave data. Every 3 hours, on the synoptic hour, and at accelerated intervals during abnormal disturbances, values of power spectral density of vertical displacement at specified frequency intervals are disseminated by NMC. Both the WMO Code FM 24-V message and our own code spectral wave data are disseminated directly by NMC. The coded formats are generated by the NMC computer and placed into switching directories for dissemination to the NWS user community.

Data Flow for Drifting Buoys - Figure 18 shows the data flow for the TIROS drifting buoys. The major acquisition, processing, and dissemination function parallels those described for our moored buoy systems. The main difference between the two systems is that the drifting buoys cannot provide synoptic data, but rather provide data approximately every 6 hours depending upon buoy latitude. The TIROS-6 data orbiting satellite successfully launched in October 1978 collects drifting buoy sensor data and determines buoy position by measuring the frequency shift of the buoy transmission during the time the buoy is in view of the satellite. All the data are collected at the CDA stations in Gilmore, Alaska, and Wallops Island, Virginia. The received and detected data are then sent to the spacecraft operational control center in Suitland, Maryland, for preliminary processing. All the data are then transmitted to the Centre National d'Etudes Spatiales (CNES), an agency of the French Government in Toulouse, France, where it is processed and disseminated worldwide. Special formats for each class of drifting buoys have been prepared and are contained in this workshop manual.

CONCLUSION

I would like to highlight some of NDBO's major accomplishments. In the area of buoy systems, we have initiated and refined environmental moored buoy data relay using GOES and NESS/NDBO data processing and dissemination facilities. This achievement enabled us to acquire and disseminate well over 2500 synoptic weather messages per buoy in 1978 from a complement of approximately 15 buoys. In addition to weather messages, approximately 25,000 wave spectra reports were disseminated in 1978 from 10 buoys equipped with wave measurement systems.

The data quality requirements and achievements associated with our moored buoy program is shown in Figure 19. We believe our ability to deliver high-quality data from various remote and often hostile ocean areas

on a reliable basis, has provided major impacts in the following areas of WMO activities:

- Improved weather forecasting
- Enhancement of climate monitoring program
- Assistance to energy source assessment problems
- Augmented ocean monitoring studies.

Our drifting buoy program has furnished 50 buoys comprising the entire U.S. commitment to the buoy portion of the Global Weather Experiment. Each buoy has been designed to include an air-drop deployment capability and a sensor data link compatible with the TIROS satellite. Results from the Global Weather Experiment will increase our understanding of the entire global ocean/atmosphere interaction system. Systematic knowledge about the behavior of this global system will enable numerical weather prediction for periods extending beyond just a few days, with increased reliability and accuracy.

Our activities in advanced deployment areas have also flourished during the past year. These activities included development of directional wave spectra systems, buoy motion packages, subsurface current measurement instrumentation, acoustic data links, profiling and discrete level ocean temperature measurement systems, advanced meteorological sensors, and an on-site meteorological sensor test and evaluation facility.

Finally, we have developed remote data acquisition and telemetry operational systems for custom applications. Perhaps the major undertaking in this category was development and implementation of two unique laboratory-supported biofouling and corrosion field experiments in the Gulf of Mexico in support of our Department of Energy's Ocean Thermal Energy Conversion (OTEC) Project. Another custom system designed and established by NDBO was the Ocean Platform Environmental Monitoring System (OPEMS) for brine discharge activity for the Strategic Oil Reserve Program.

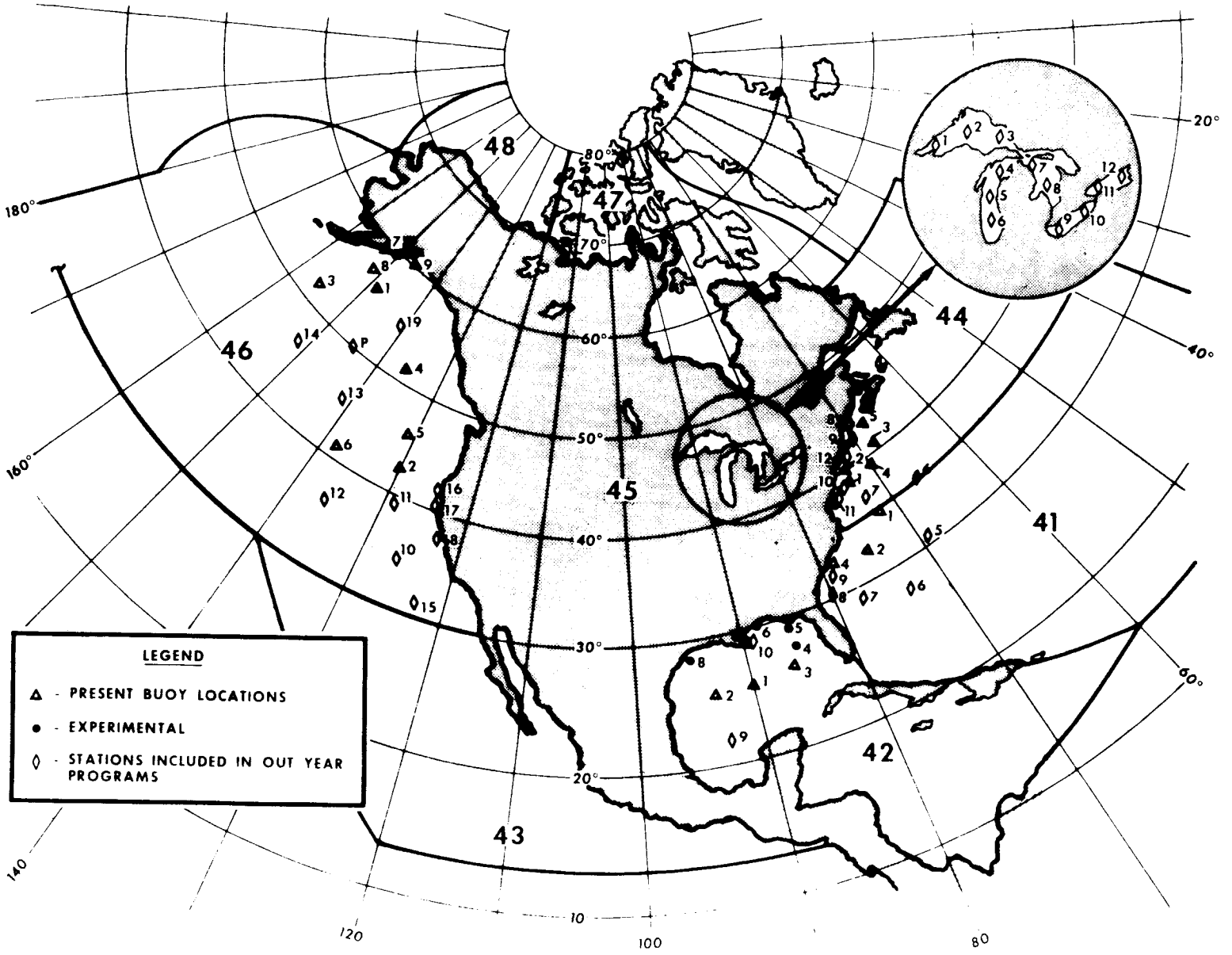

Figure 1. MOORED BUOY DEPLOYMENT LOCATIONS

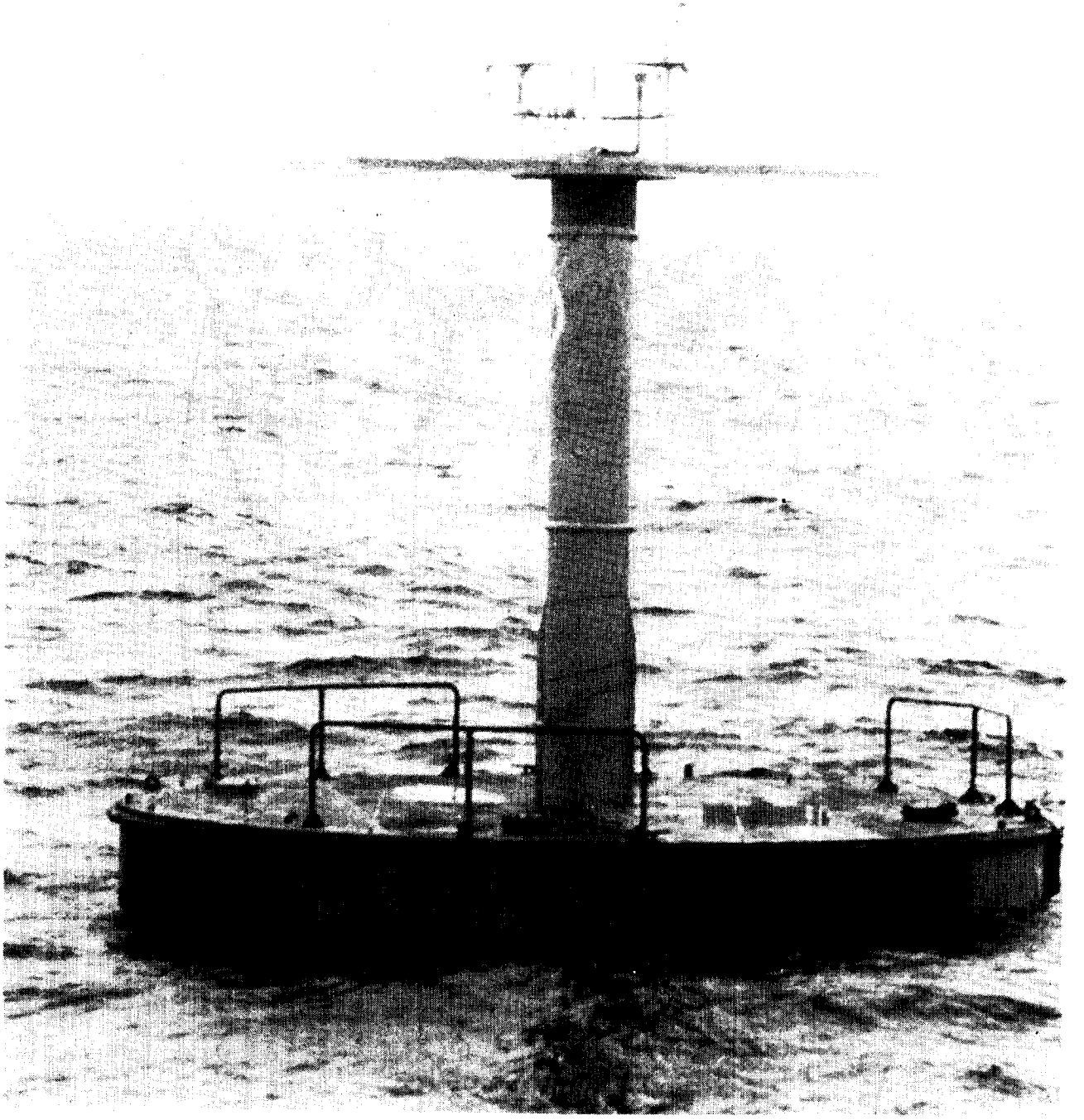

Figure 2. 10-METER DISCUS HULL BUOY

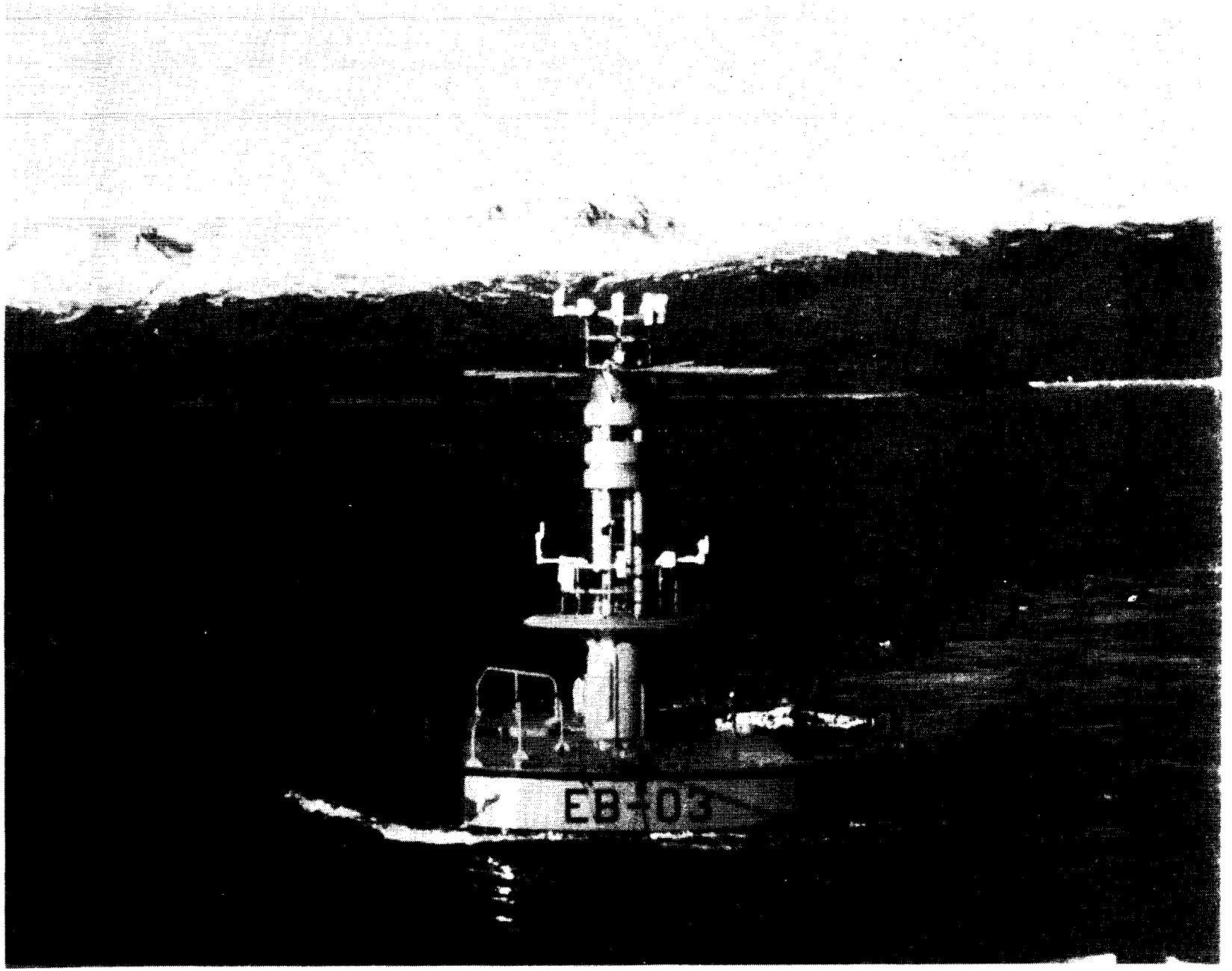

Figure 3. 12-METER DISCUS HULL BUOY

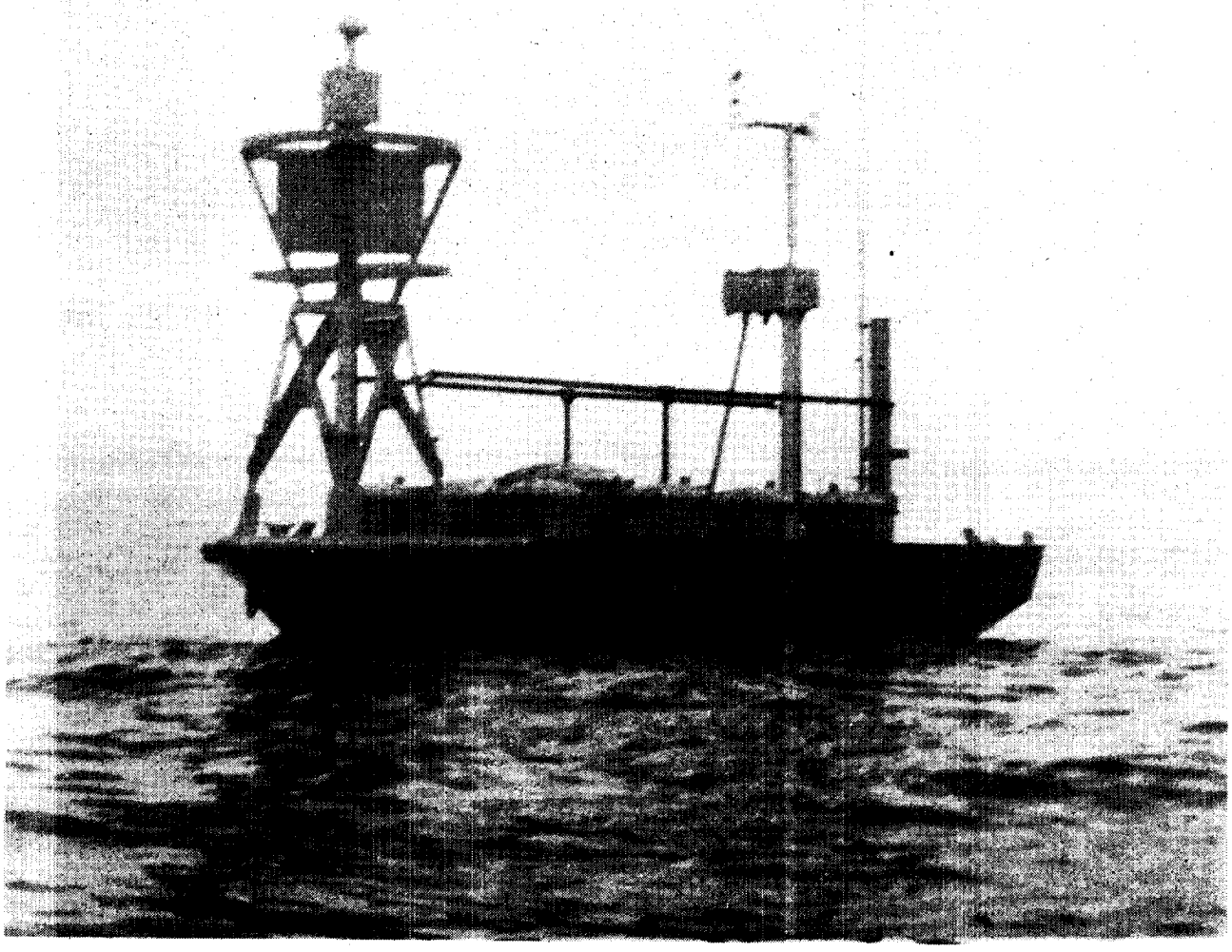

Figure 4. NOMAD BUOY

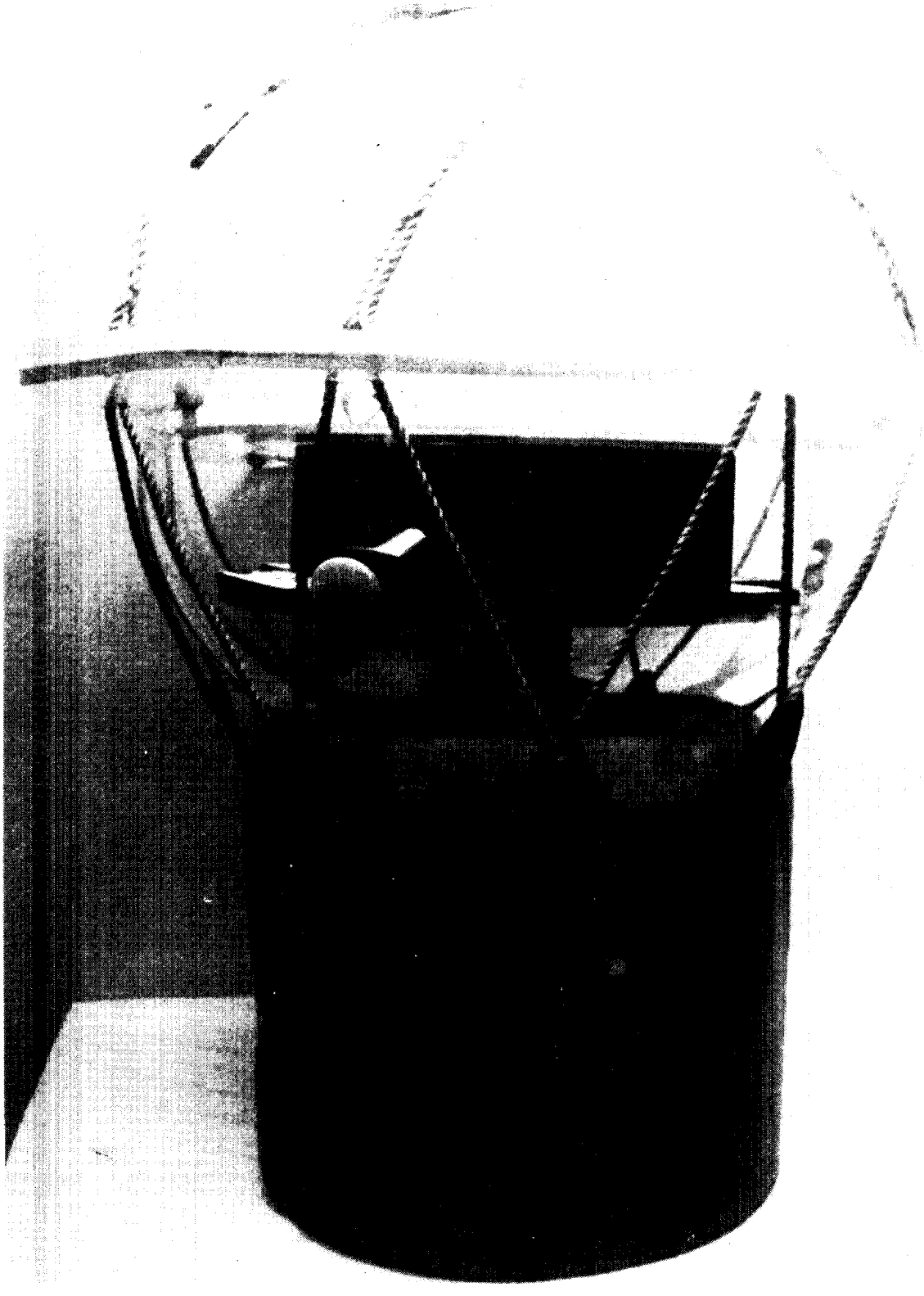

Figure 5. ICE BUOY

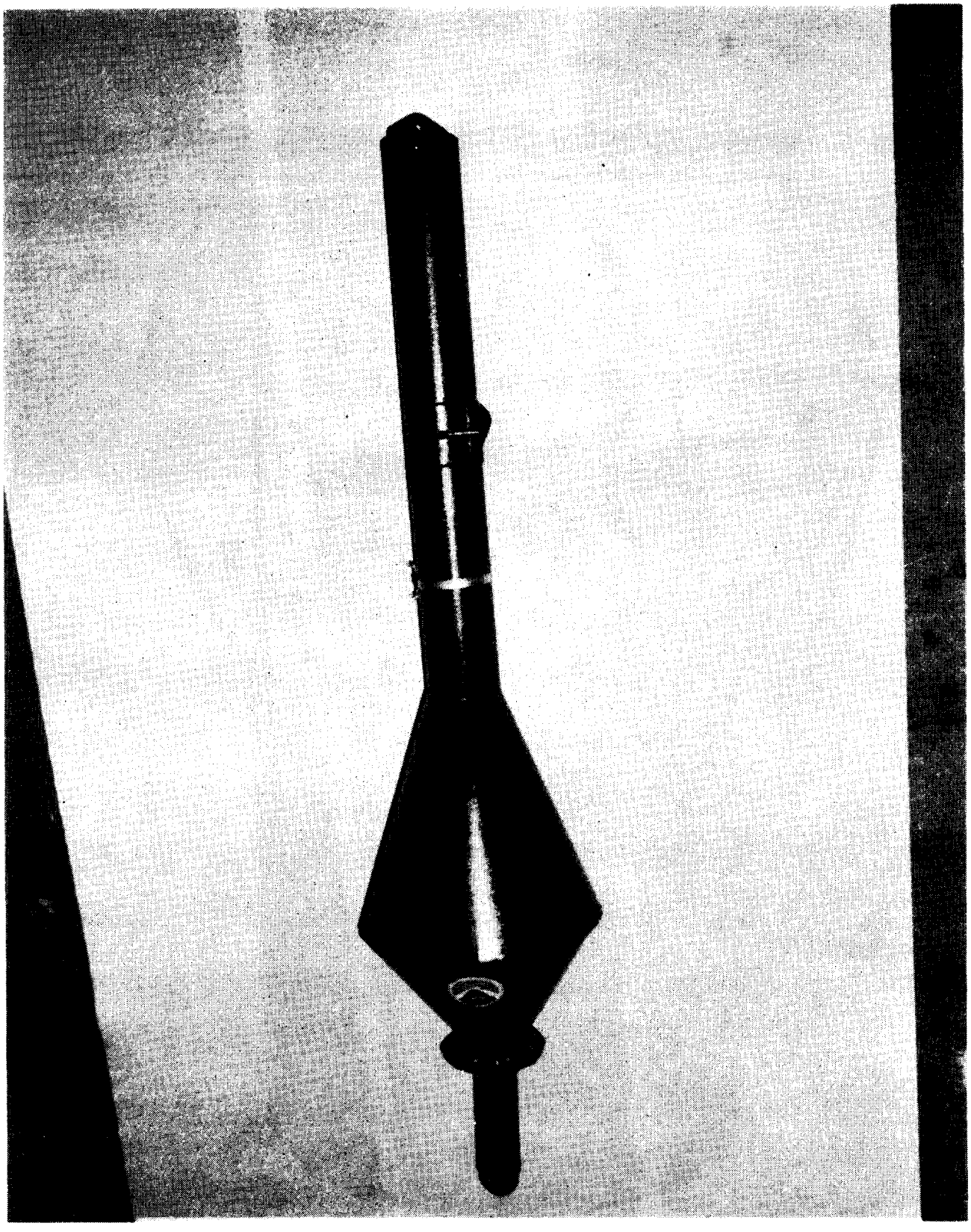

Figure 6. TMD BUOY

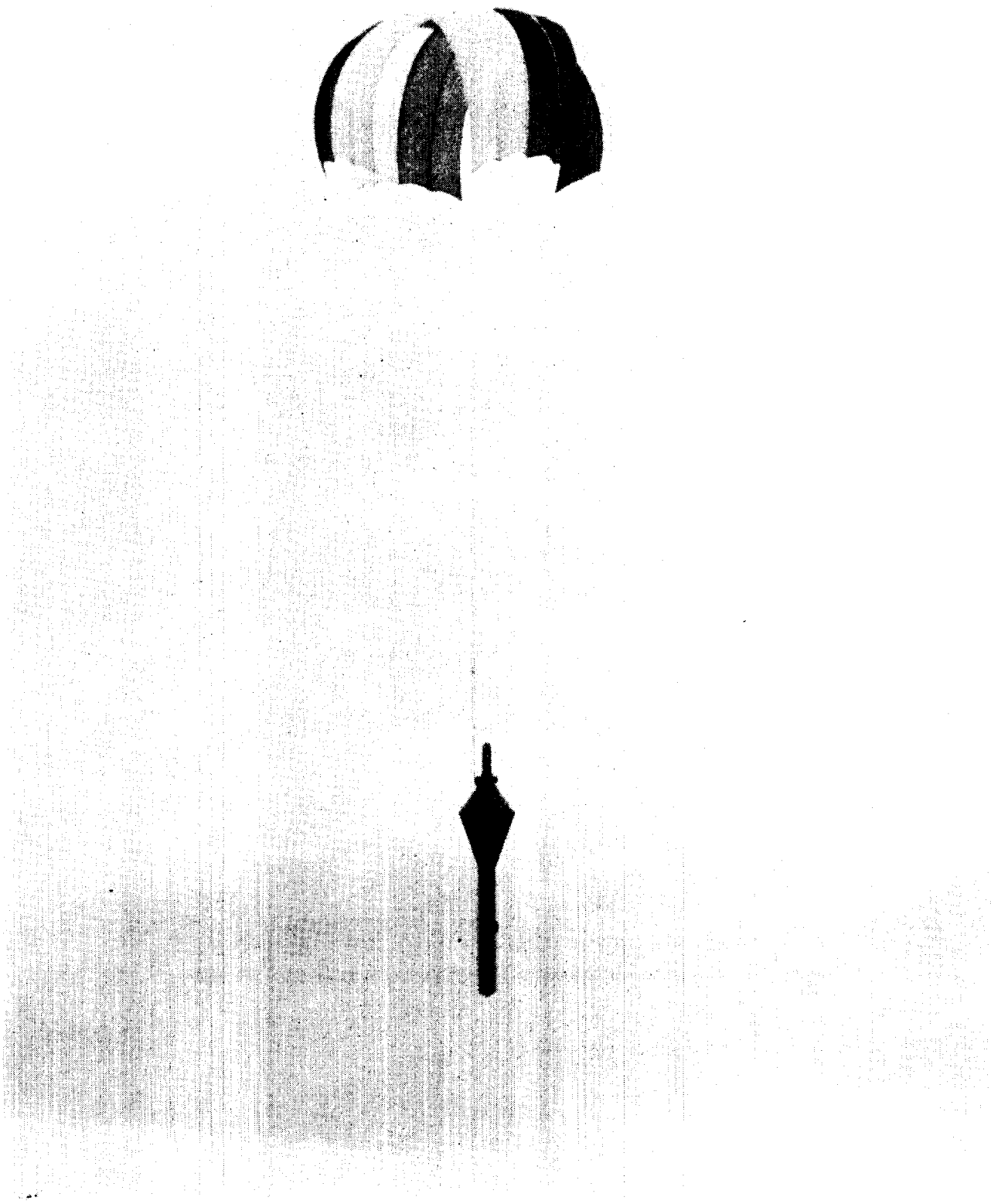

Figure 7. TMD DROPPING VIA PARACHUTE

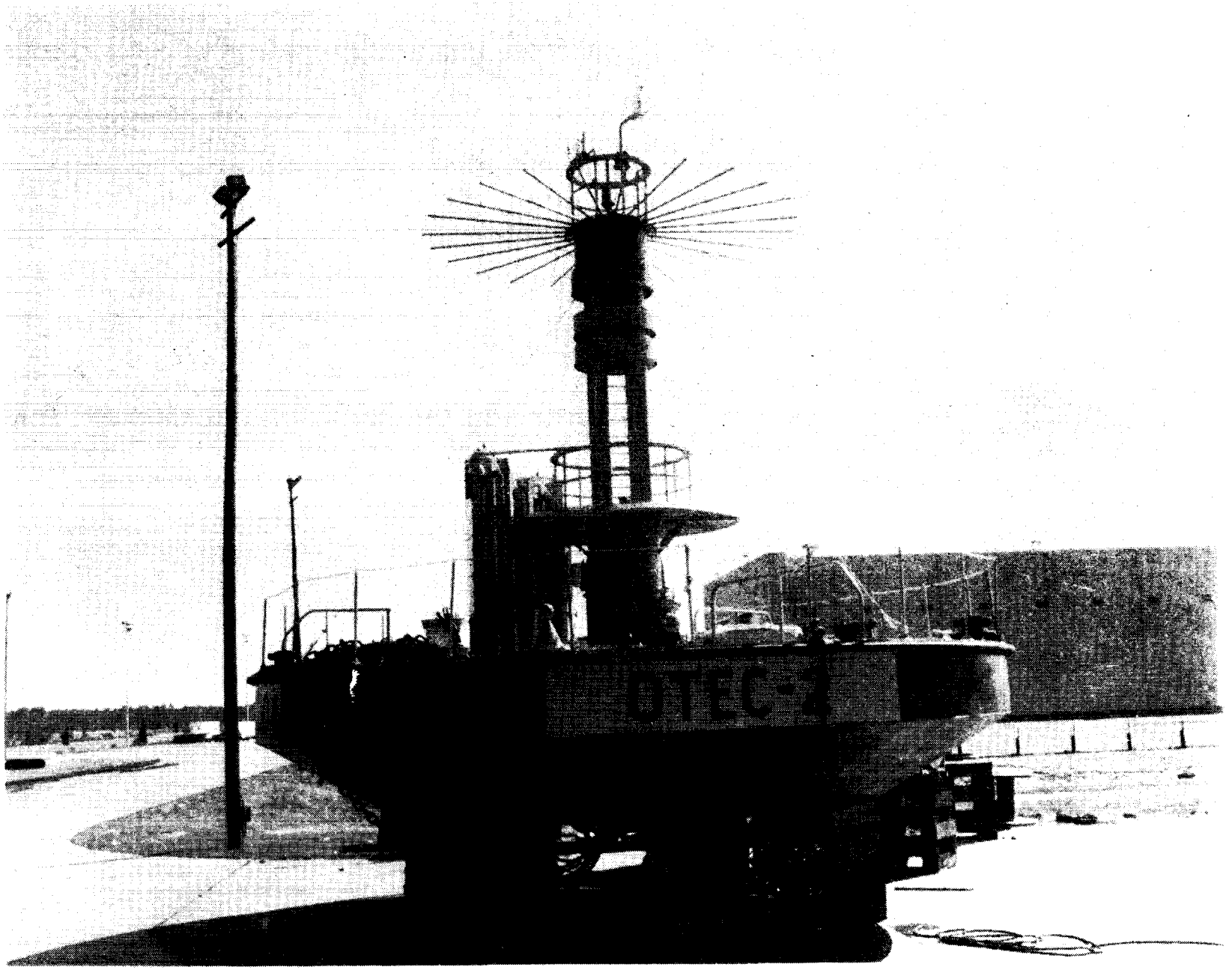

Figure 8. OTEC BUOY

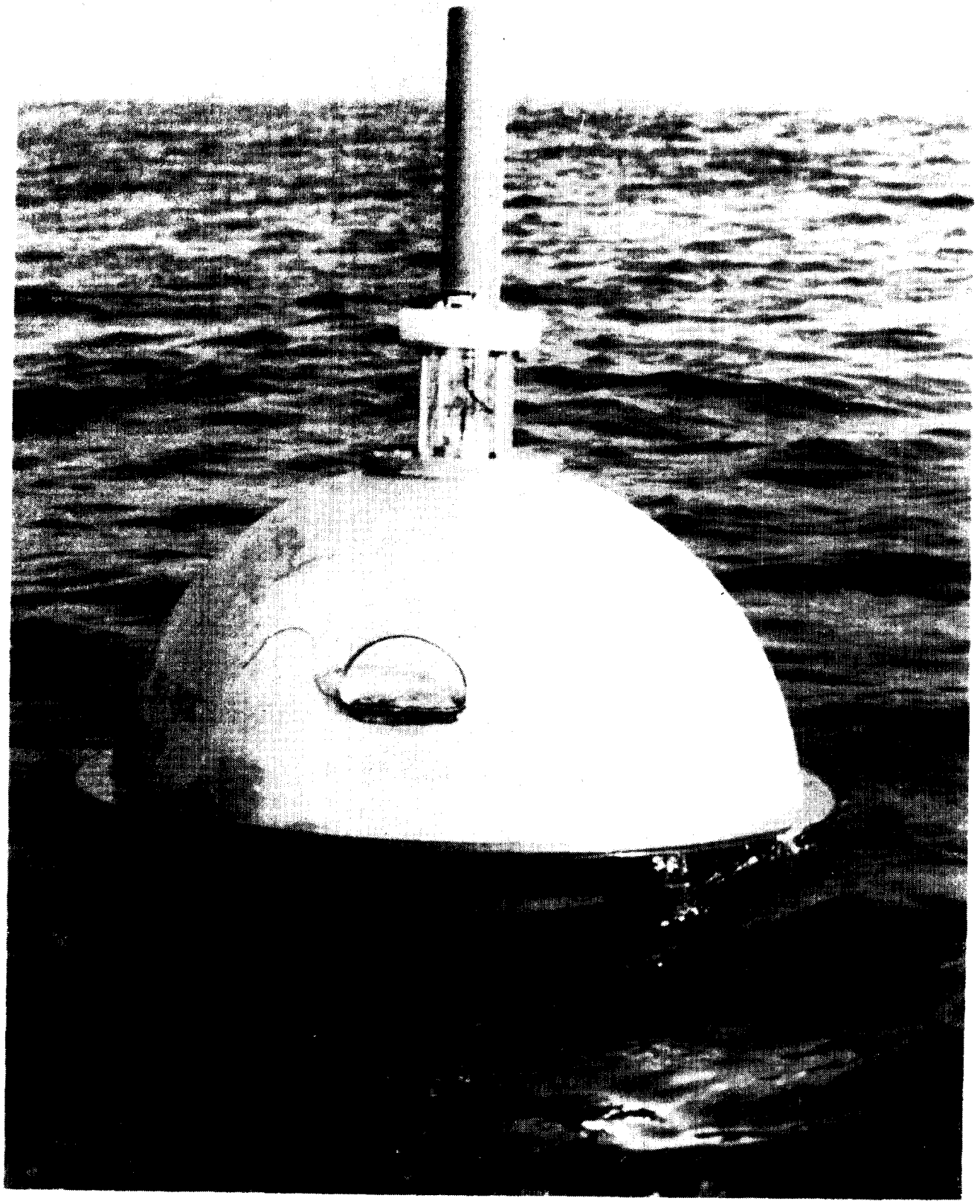

Figure 9. WAVERIDER HULL

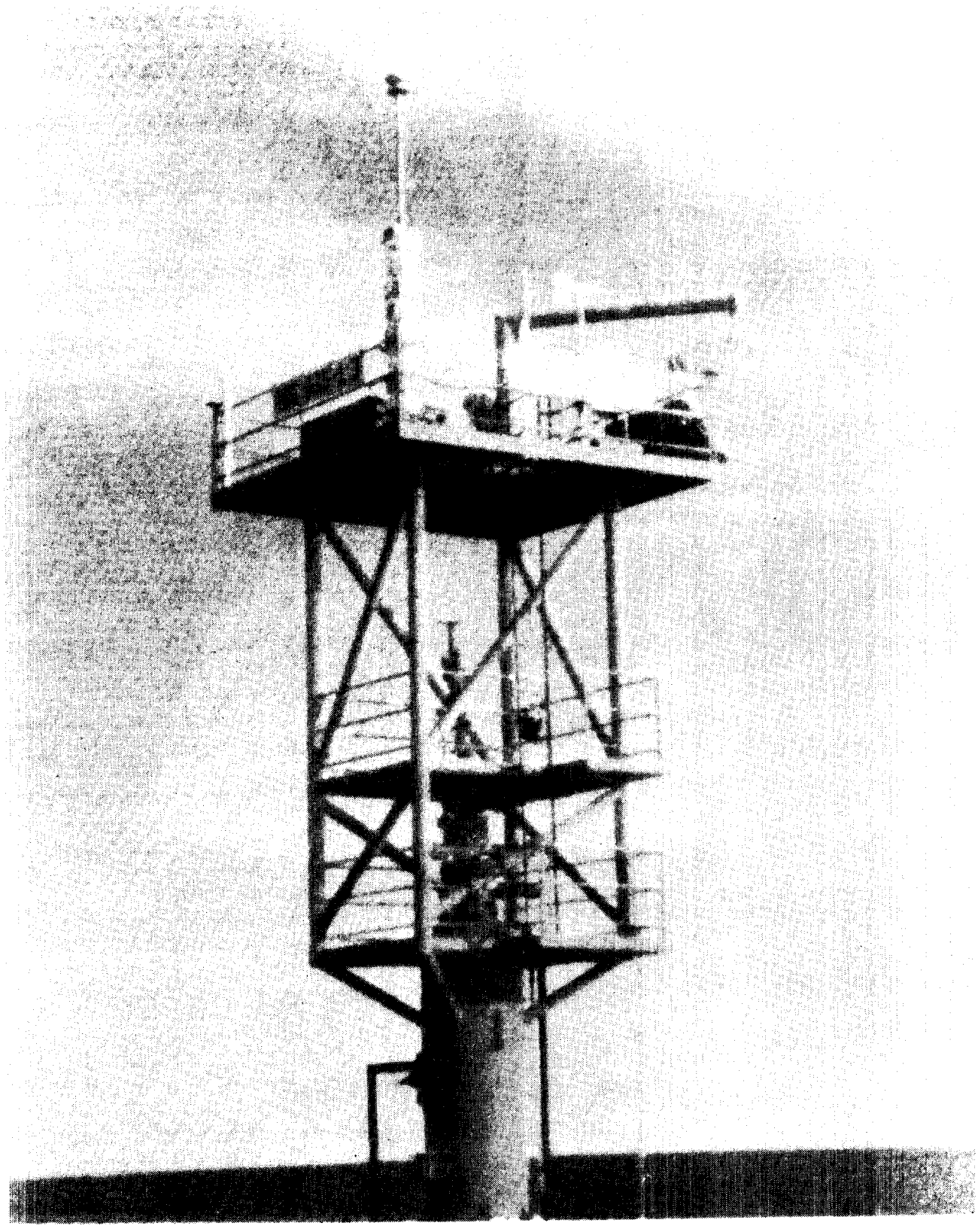

Figure 10. OPEMS PLATFORM

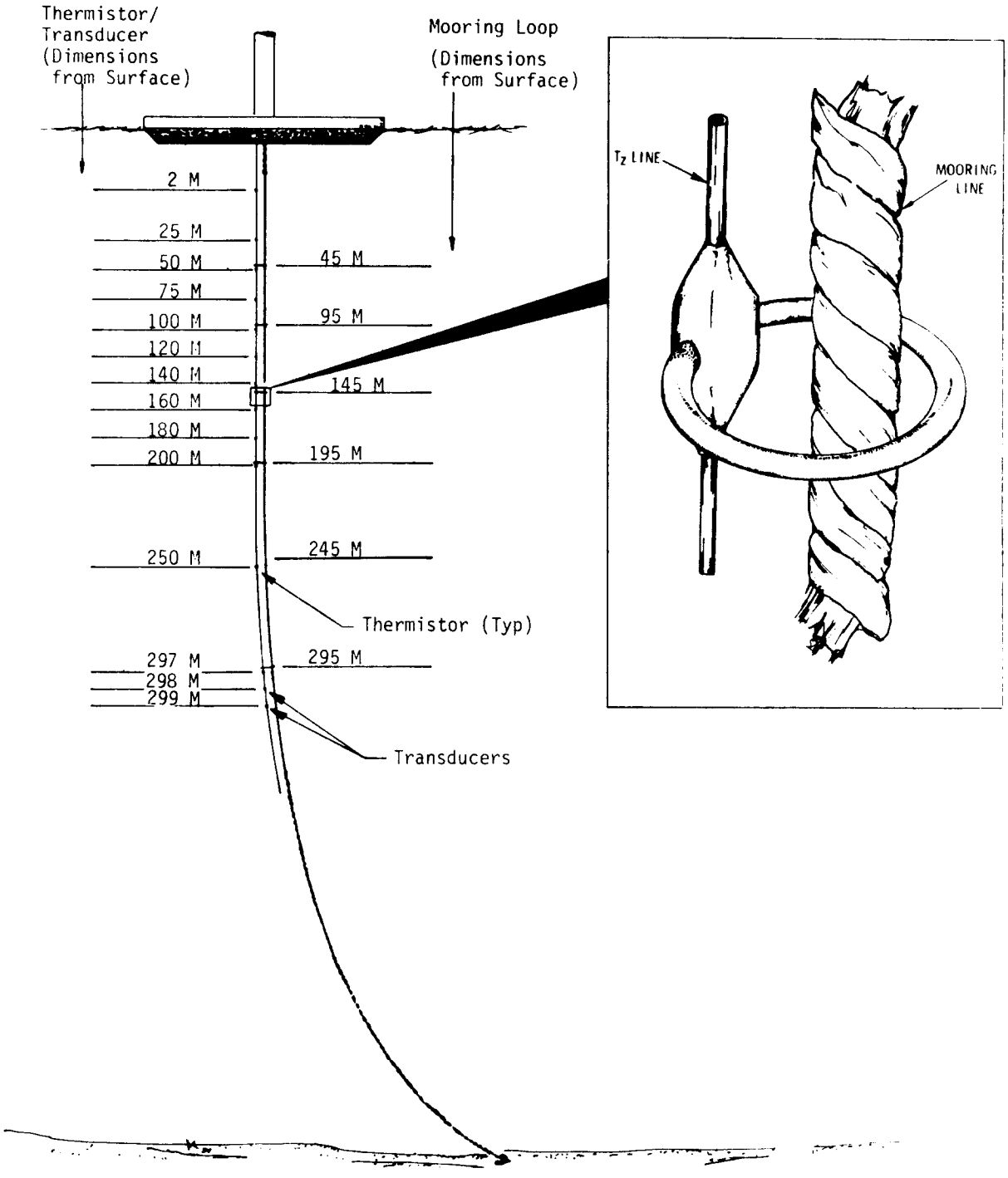

Figure 11. Tz BUOY

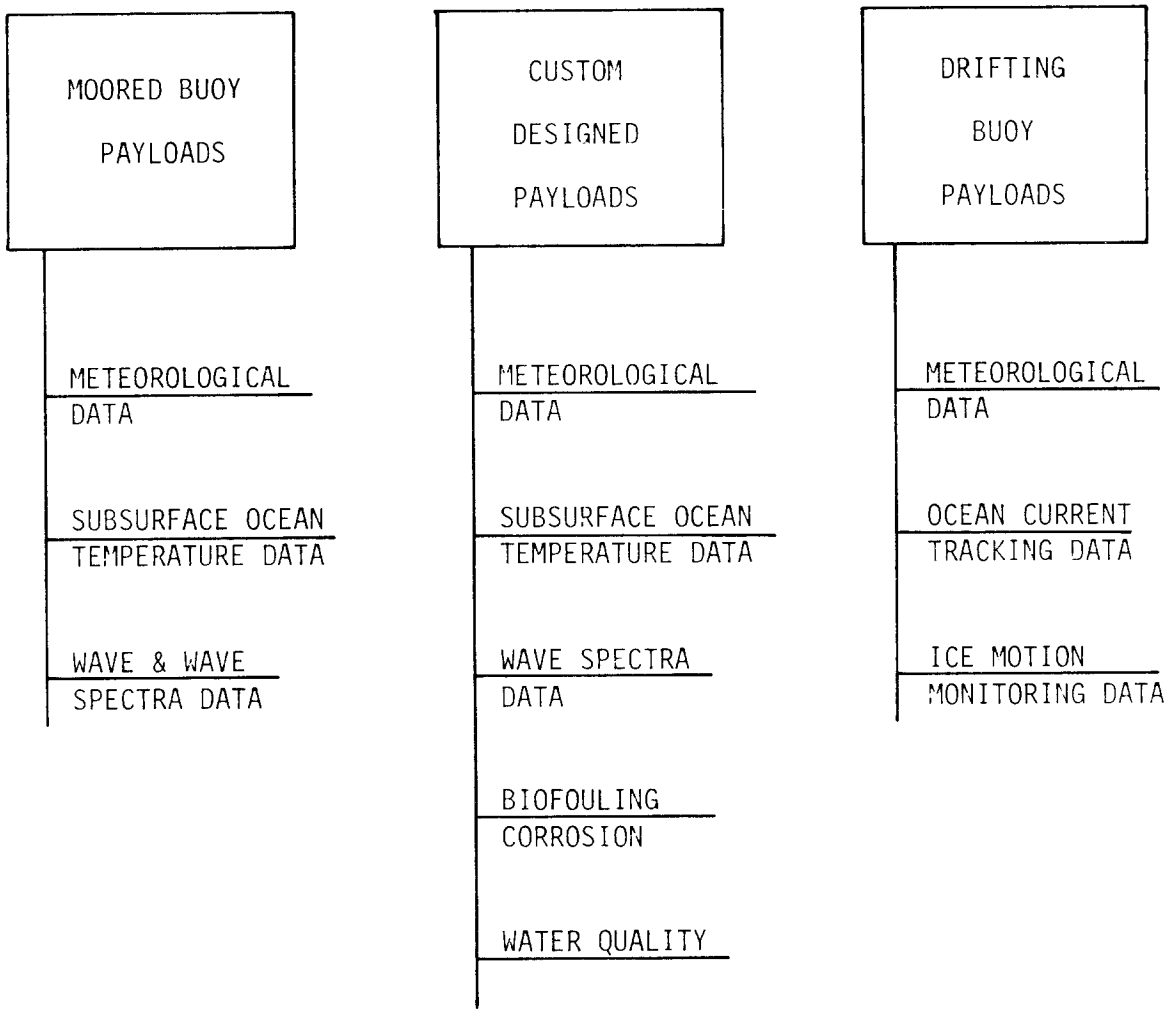

Figure 12. PAYLOADS VERSUS SENSOR REQUIREMENTS

STATUS

STATE-OF-THE-ART SENSORS IN USE:

BENDIX PROPELLER-VANE ANEMOMETER MAURO MARINE ROTATING COMPASS	WIND SPEED & DIRECTION
J-TEC VA-300/VA-320 ANEMOMETER MAGNAVOX FLUX-GATE COMPASS	WIND SPEED & DIRECTION
ROSEMOUNT 1201 BAROMETER	AIR PRESSURE
ROSEMOUNT PLATINUM WIRE	AIR TEMPERATURE
YELLOW SPRING INSTRUMENT THERMISTOR	OCEAN SURFACE TEMPERATURE

ACTIVITY

- EXTEND OPERATIONAL LIFE OF PRESENT SENSORS
- IMPROVE MEASUREMENT ACCURACY OF PRESENT SENSORS
- IMPROVE AT-SEA SENSOR REPLACEMENT TECHNIQUES
- TEST RUGGED SENSORS FOR EXTREME ENVIRONMENT
- TEST SENSORS FOR NEW MEASUREMENT REQUIREMENTS (HUMIDITY, PRECIPITATION, SOLAR RADIATION)

Figure 13. METEOROLOGICAL SENSORS

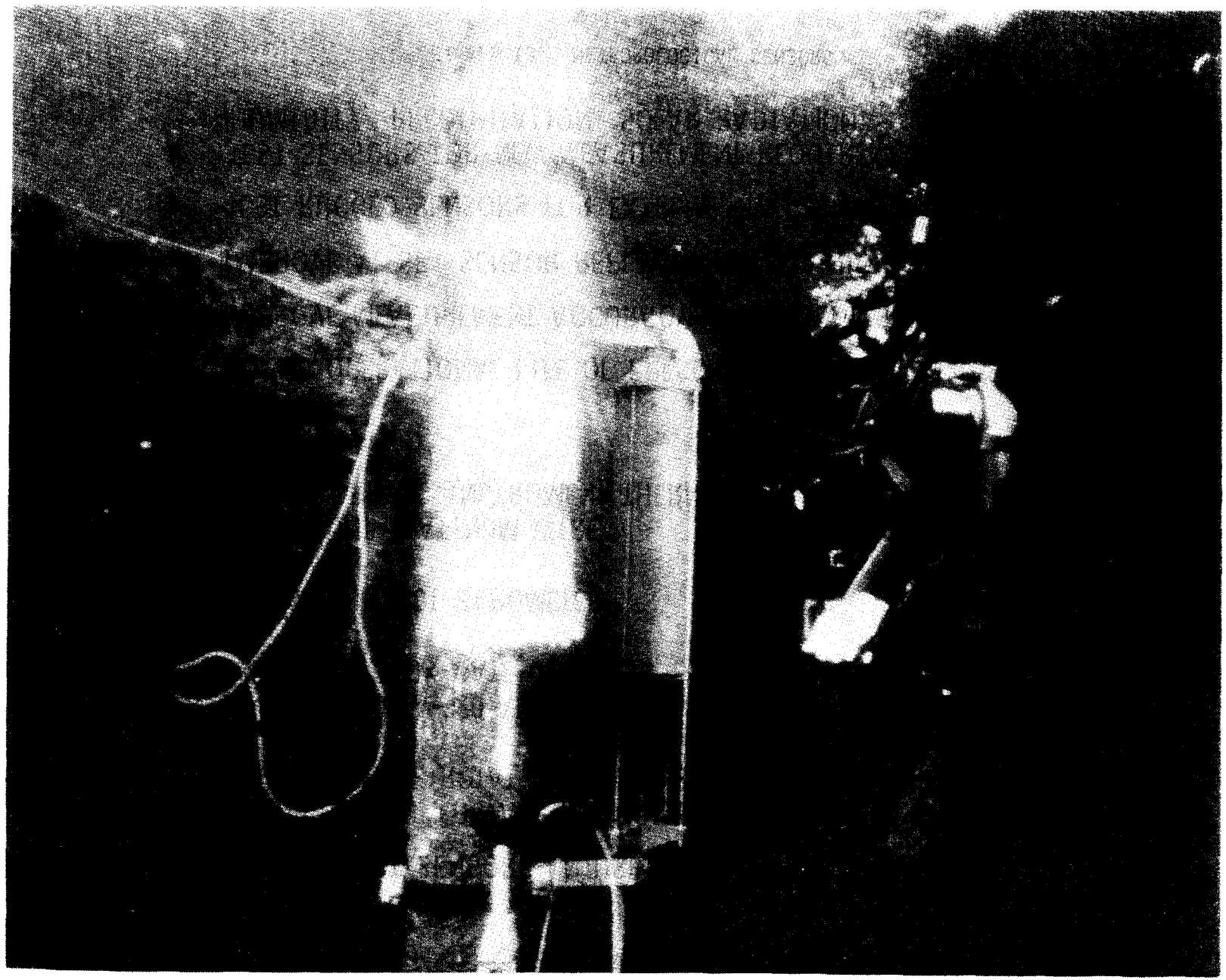

Figure 14. MARSH-McBIRNEY CURRENT METER

Figure 15. NEIL BROWN ACOUSTIC PROBE

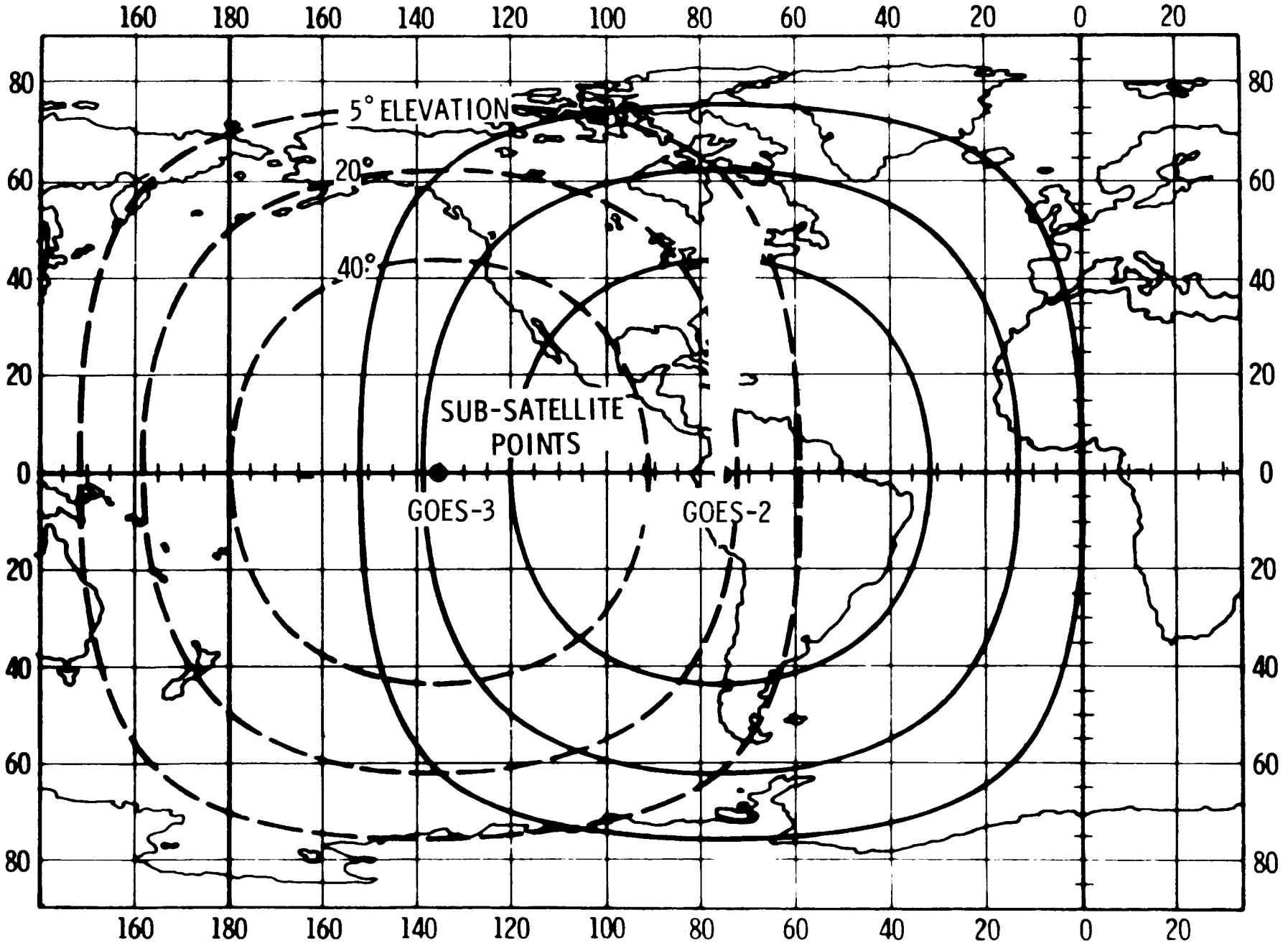

Figure 16. GOES Coverage and Elevation Pattern

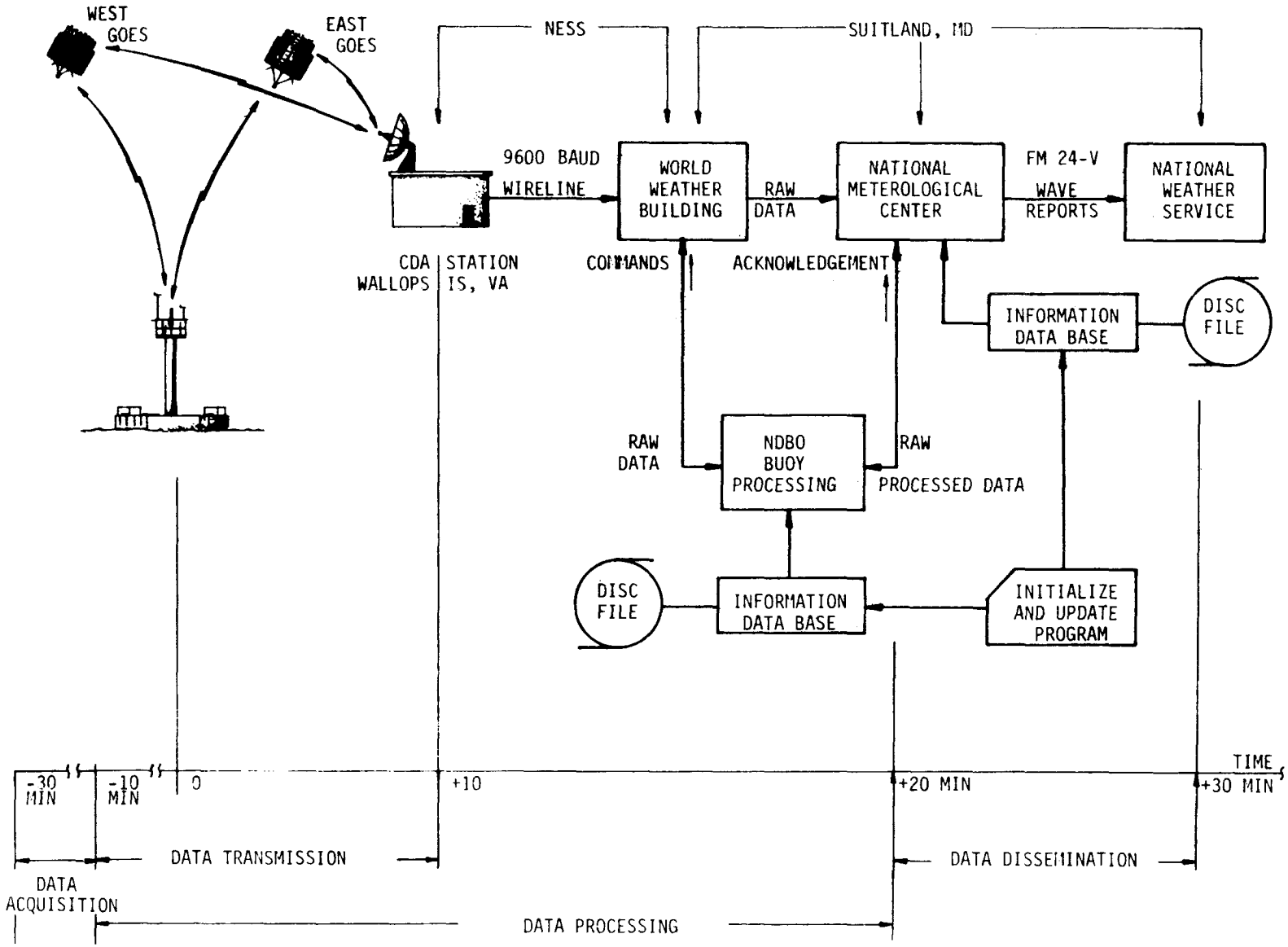

Figure 17. DATA FLOW AND TIMING FOR MOORED BUOYS

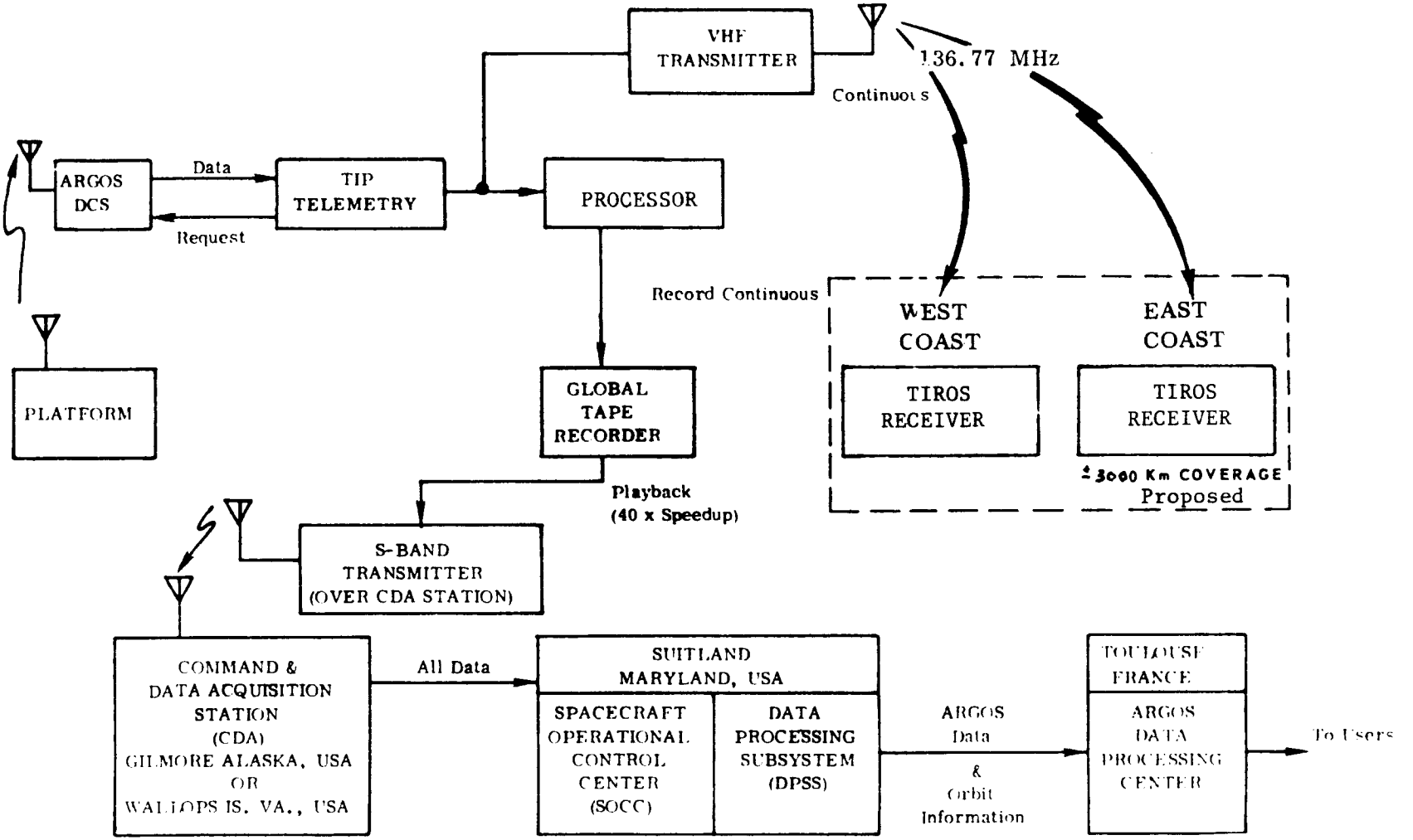

Figure 18. DATA FLOW FOR DRIFTING BUOYS

.BUOY MTBF

1972-75	1977
36 days	150 days
4 buoys	15 buoys

.DATA QUANTITY

1972-75	1977
2200 MSG per buoy	2550 MSG per buoy

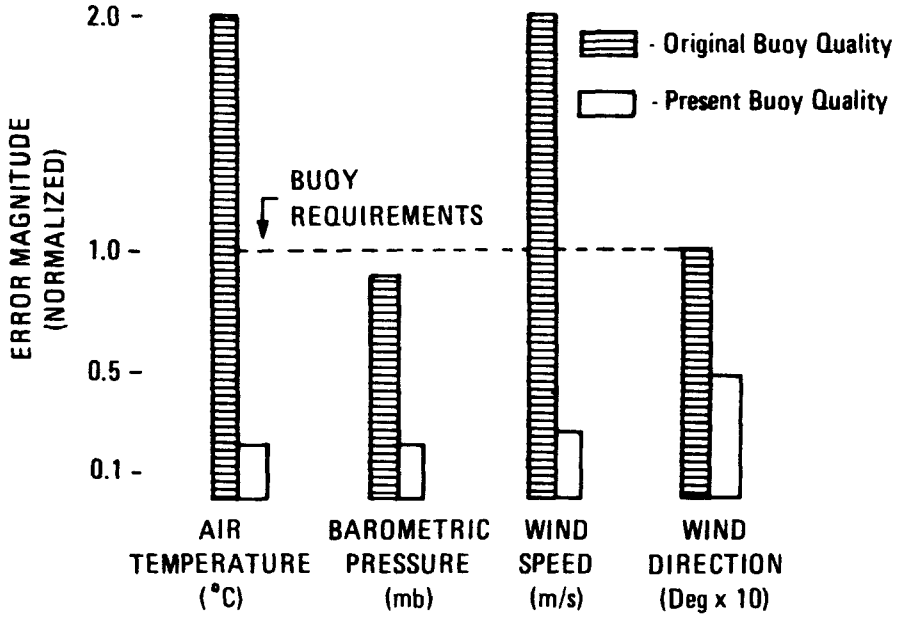

Figure 19. BUOY DATA QUALITY REQUIREMENTS

A NUMERICAL MODEL OF CALCULATION OF THERMODYNAMIC CHARACTERISTICS OF THE WORLD OCEAN

by
G.I. Marchuk, V.B. Zalesny, V.I. Kuzin

Methods and results of numerical modelling of large-scale dynamics of the World Ocean are presented. Principles of a unite approach to creation of the numerical model of global oceanic circulation are described, and some examples demonstrating the numerical methods are considered.

Assume that the World Ocean basin is presented in the form of a multiply connected region D limited by cylindrical lateral surfaces σ_n, water surfaces $z=\zeta(\lambda,\theta,t)$ - and bottom relief $H=H(\lambda,\theta)$.

Consider the set of equations of ocean hydrodynamics within the spherical co-ordinates (λ,θ,H), where λ is the longitude, $\theta=\varphi+\frac{\pi}{2}$, φ is the latitude, z is a co-ordinate directed along the Earth's radius toward the centre with the beginning of reading at the undisturbed ocean surface. The set of equations consists of two equations for horizontal components of velocity vector in linear approximation, equations of hydrostatics, continuity, heat and salt diffusion and sea state.

The system has the following form

$$\begin{aligned}
&\frac{\partial u}{\partial t} - lv = -\frac{m}{\rho_0}\frac{\partial p}{\partial \lambda} + \frac{\partial}{\partial z}\nu\frac{\partial u}{\partial z} + F_\lambda ,\\
&\frac{\partial v}{\partial t} + lu = -\frac{n}{\rho_0}\frac{\partial p}{\partial \theta} + \frac{\partial}{\partial z}\nu\frac{\partial v}{\partial z} + F_\theta ,\\
&\frac{\partial p}{\partial z} = g\rho ;\\
&m\left[\frac{\partial u}{\partial \lambda} + n\frac{\partial}{\partial \theta}\left(\frac{v}{m}\right)\right] + \frac{\partial w}{\partial z} = 0
\end{aligned} \qquad (1)$$

$$\frac{\partial T}{\partial t} + mu\frac{\partial T}{\partial \lambda} + nv\frac{\partial T}{\partial \theta} + w\frac{\partial T}{\partial z} = \frac{\partial}{\partial z}\nu_T\frac{\partial T}{\partial z} + \mu_T\Delta T,$$

$$\frac{\partial S}{\partial t} + mu\frac{\partial S}{\partial \lambda} + nv\frac{\partial S}{\partial \theta} + w\frac{\partial S}{\partial z} = \frac{\partial}{\partial z}\nu_S\frac{\partial S}{\partial z} + \mu_S\Delta S,$$

$$\rho = f(T, S)$$

In set of equations (1) u, v, w are the components of velocity vector $\vec{u}$, $l = -2\omega\cos\theta$ is the Coriolis parametr, ρ is the density, p is the pressure, S is the salinity (in S%), T is the temperature, ρ_c is the mean density of sea water, r is the mean Earth's radius,

$$m = \frac{1}{r\sin\theta}, \quad n = \frac{1}{r}, \quad \Delta = m^2\frac{\partial^2}{\partial\lambda^2} + mn\frac{\partial}{\partial\theta}\sin\theta\frac{\partial}{\partial\theta}$$

is Laplasian on the sphere, F_λ, F_θ are some functions which parameterize the influence of dissipation forces

$$F_\lambda = \mu\Delta u, \quad F_\theta = \mu\Delta v$$

Below are given the boundary conditions

$$\nu\frac{\partial u}{\partial z} = -\frac{\tau_1}{\rho_c}, \quad \nu\frac{\partial v}{\partial z} = -\frac{\tau_2}{\rho_c}, \quad w = 0 \qquad \text{with } z = 0 \qquad (2)$$

$$T = T_c, \quad S = S_c$$

$$\nu\frac{\partial u}{\partial z} = -R\int_0^H u\,dz, \quad \nu\frac{\partial v}{\partial z} = -R\int_0^H v\,dz \qquad \text{with } z = H \qquad (3)$$

$$w = \frac{dH}{dt}, \quad \nu_T\frac{\partial T}{\partial n} = 0, \quad \nu_S\frac{\partial S}{\partial n} = 0$$

$$u=v=0, \quad \alpha_T \frac{\partial T}{\partial n} + \beta_T T = 0, \quad \alpha_S \frac{\partial S}{\partial n} + \beta_S S = G_S \text{ at } \tilde{\sigma}_n \qquad (4)$$

Initiary conditions are as follows.

$$u=u^\circ, \; v=v^\circ, \; T=T^\circ, \; S=S^\circ \qquad t=0 \qquad (5)$$

Since the motivated application of the splitting method is possible only for evolutional sets of equations, let us transform respectively the initial problem (1)-(5).

Introduce the following substitution of variables

$$z=Hz', \quad \lambda=L_1\lambda', \quad \theta=L_2\theta', \quad w=\tilde{w}+mz'\left(\frac{\partial H}{\partial \lambda'}u+ \right.$$
$$\left. +n\frac{\partial H}{\partial \theta}\frac{v}{m}\right), \quad uH=\tilde{u}, \quad vH=\tilde{v}$$

which transforms D into the unite cube with a plane base. Then reduce the problem to the evolutional form. For this purpose let us use the following representation of the unknown functions.

$$\tilde{u}=\bar{u}+u', \quad \tilde{v}=\bar{v}+v', \quad \bar{a}=\int_0^1 a\,dz$$

As a result, we will get a system of differential equations for the integral stream function and a system of equations as regards to deviations from the mean in the vertical components of vector of velocity, temperature and salinity

$$-\frac{\partial}{\partial t}\left(\frac{\partial}{\partial \theta}B\frac{\partial \varphi}{\partial \theta}+\frac{\partial}{\partial \lambda}A\frac{\partial \varphi}{\partial \lambda}\right)-\frac{\partial}{\partial \theta}C\frac{\partial \varphi}{\partial \lambda}+\frac{\partial}{\partial \lambda}C\frac{\partial \varphi}{\partial \theta}- \qquad (6)$$

$$-\frac{\partial}{\partial \theta}BR\frac{\partial \varphi}{\partial \theta}-\frac{\partial}{\partial \lambda}AR\frac{\partial \varphi}{\partial \lambda}+A_M\varphi=\frac{\partial f_2}{\partial \lambda}-\frac{\partial f_1}{\partial \theta}$$

$$\frac{\partial u'}{\partial t} - \ell v' = -\frac{mgH}{\rho_0}\left(I_1 - \int_0^1 I_1\, dz\right) + \frac{MH}{H_0}\Delta u' + \frac{\partial}{\partial z}\nu\frac{\partial u'}{\partial z} + R\bar{u} - \frac{\tau_1}{\rho_0},$$

$$\frac{\partial v'}{\partial t} + \ell u' = -\frac{ngH}{\rho_0}\left(I_2 - \int_0^1 I_2\, dz\right) + \frac{MH}{H_0}\Delta v' + \frac{\partial}{\partial z}\nu\frac{\partial v'}{\partial z} + R\bar{v} - \frac{\tau_2}{\rho_0}; \qquad (7)$$

$$H\frac{\partial T}{\partial t} + m(\bar{u}+u')\frac{\partial T}{\partial \lambda} + n(\bar{v}+v')\frac{\partial T}{\partial \theta} + w\frac{\partial T}{\partial z} = \frac{\partial}{\partial z}\nu_T\frac{\partial T}{\partial z} + \mu_T D T,$$

$$H\frac{\partial S}{\partial t} + m(\bar{u}+u')\frac{\partial S}{\partial \lambda} + n(\bar{v}+v')\frac{\partial S}{\partial \theta} + w\frac{\partial S}{\partial z} = \frac{\partial}{\partial z}\nu_S\frac{\partial S}{\partial z} + \mu_S\Delta S, \qquad (8)$$

where $\bar{u} = \frac{\partial \varphi}{\partial \theta}$, $\bar{v} = -\frac{m}{n}\frac{\partial \varphi}{\partial \lambda}$

$$I_1 = \int_0^z \frac{\partial \rho}{\partial \lambda}\, dz - \frac{1}{H}\frac{\partial H}{\partial \lambda} z\rho; \quad I_2 = \int_0^z \frac{\partial \rho}{\partial \theta}\, dz - \frac{1}{H}\frac{\partial H}{\partial \theta} z\rho$$

$$\rho = \rho(T, S)$$

$$w = \int_z^1 m\left[\frac{\partial u'}{\partial \lambda} + n\frac{\partial}{\partial \theta}\left(\frac{v'}{m}\right)\right] dz$$

$$A = \frac{m}{nH}, \quad B = \frac{n}{mH}, \quad C = \frac{\ell}{H}$$

A_M is the biharmonic operator on the sphere;

D is the diffusion operator with accounting of the substitution of the variables.

Note that the horizontal diffusion operator of the moment of momentum is simplified in the following manner.

$$H\Delta u' = \frac{H}{H_0}\left(m^2\frac{\partial^2 u' H}{\partial \lambda^2} + mn\frac{\partial}{\partial \theta}\sin\theta\frac{\partial u' H}{\partial \theta}\right)$$

$$H_0 = \iint_{D_0} H(\lambda, \theta)\, d\Omega \Big/ \iint_{D_0} d\Omega$$

is the mean depth of the ocean.

Formulate the boundary value problem for the integral stream function.

Note that the solution of the equation for the stream function often presents some interest of its own since it describes the means with respect to the transport of water masses to the World Ocean area and may serve as an object of diagnostic calculations of the current field from the density field and wind stress.

Left-hand side of equation (6) depends on the direction of wind on the ocean surface (τ_1, τ_2), and for the variable bottom relief it will also be the density function. Let us consider it known. Assume then that the influence of the operator of horizontal turbulent exchange can be neglected and consider that $A_M \varphi = 0$.

Seek the solution of (6) in the area $[0,t] \times D_0$, where D_0 is the projection of area D on the plane $z = 0$. It ia non-single-linked. Let D_0 be limited by contours $\Gamma_0, \Gamma_1, \ldots, \Gamma_N$ with Γ_0 being external. In such a case, the boundary and initial conditions for (6) are respectively

$$\varphi|_{\Gamma_0} = 0, \quad \varphi|_{\Gamma_i} = \Phi_i(t), \quad (i = \overline{1,N}) \tag{9}$$

$$\varphi = \varphi_0 \qquad \text{with} \quad t = 0. \tag{10}$$

Note that values of φ on contours $\Gamma_1, \ldots, \Gamma_N$ are being determined with the aid of certain functional relations which are natural, from the viewpoint of variation, additional boundary conditions on $\Gamma_1, \ldots, \Gamma_N$.

To take this fact into account is necessary for correct formulation of discrete approximations of problems (6), (9) and (10).

Formulate the variational setting of the problem. Call the function $\bar{\varphi}(t) \in \tilde{W}_2^1$ satisfying the following intergo-differential equation

$$\frac{\partial}{\partial t}\left(\iint_{D_0}\left(A\frac{\partial\bar{\varphi}}{\partial\lambda}\frac{\partial\omega}{\partial\lambda}+B\frac{\partial\bar{\varphi}}{\partial\theta}\frac{\partial\omega}{\partial\theta}\right)dD_0\right)+\iint_{D_0}\left(AR\frac{\partial\bar{\varphi}}{\partial\lambda}\frac{\partial\omega}{\partial\lambda}+\right. \tag{11}$$

$$\left.+BR\frac{\partial\bar{\varphi}}{\partial\theta}\frac{\partial\omega}{\partial\theta}+C\frac{\partial\bar{\varphi}}{\partial\lambda}\frac{\partial\omega}{\partial\theta}-C\frac{\partial\bar{\varphi}}{\partial\theta}\frac{\partial\omega}{\partial\lambda}\right)dD_0=\iint\left(f_1\frac{\partial\omega}{\partial\theta}-f_2\frac{\partial\omega}{\partial\lambda}\right)dD_0$$

the generalized solution (6), (9) and (10).

Here $\tilde{W}_2^1$ is the space of functions equal to zero on summarized with square together with their first derivatives and depending on t on $\Gamma_1, \ldots, \Gamma_N$.

Integral relation (11) generates the boundary problem with initial data (6)-(8) with additional conditions

$$\frac{d}{dt}\int_{\Gamma_i}\frac{R}{H}\frac{\partial\bar{\varphi}}{\partial n}d\Gamma_i + \int_{\Gamma_i}\left(\frac{R}{H}\frac{\partial\bar{\varphi}}{\partial n} + c\frac{\partial\bar{\varphi}}{\partial s} + f_s\right)d\Gamma_i = 0 \qquad (12)$$

We use two possible dicretizations of the variational problem (11)-(12), i.e. the method of finite differences and finite elements.

Figs. 1-2 present results of calculation of the integral stream function of the World Ocean by two methods. Wind stress over surface in the winter season (for the Northern Hemisphere) was taken as an information about the driving force. Calculations were made on 5° grid; parameter R was taken equal to 10^{-5}.

Consider some basic moment in the solution of the set of equations (7), (8) in regard to derivations. Assume that motion equations are somehow resolved in regard to the values u', v' as functions of the density gradients.

Then substituting these functions as well as the values of velocity components $\bar{u}$ and $\bar{v}$, averaged in vertical in the equations for temperature and salinity, get two basic equations which are to be resolved.

Describe two methods of the solution of the above equations which differ both in the discretization of space operators and the scheme of integration with respect to time. Since these equations have the same form in regard to temperature and salinity, we will carry description for one equation with regard to function Φ which can assume values of any of these functions.

The equation under investigation may be written in the following form

$$H\frac{\partial \Phi}{\partial t} + m\left[\tilde{u}(\varphi)+u'\right]\frac{\partial \Phi}{\partial \lambda} + n\left[\tilde{v}(\varphi)+v'\right]\frac{\partial \Phi}{\partial \theta} + \tag{13}$$

$$+ m\int_z^1 \left[\frac{\partial u'}{\partial \lambda} + n\frac{\partial}{\partial \theta}\left(\frac{v'}{m}\right)\right] dz \frac{\partial \Phi}{\partial z} = \mu \Delta \Phi + \frac{\partial}{\partial z}\nu \frac{\partial \Phi}{\partial z}$$

with boundary conditions

with $z=0$: $\Phi=\Phi_0$

with $z=H$: $\frac{\partial \Phi}{\partial z}=0$ (14)

on σ : $\alpha\frac{\partial \Phi}{\partial n}+\beta\Phi=0$

and initial conditions $\Phi=\Phi_0$ with $t=0$ (15)

The form of equation (11) is initial for carrying the first version of splitting. Splitting is performed with respect to co-ordinates using two-cycle rearrangement of operator in the scheme.

On the interval $t_{j-1} \le t \le t_j$ the scheme has the form

$$\frac{\partial \Phi_1}{\partial t} + \frac{1}{2}L_\lambda^{j-1}\Phi_1 = 0 \qquad \Phi_1(t_{j-1}) = \Phi(t_{j-1}) \tag{16}$$

$$\frac{\partial \Phi_2}{\partial t} + \frac{1}{2}L_\theta^{j-1}\Phi_2 = 0 \qquad \Phi_2(t_{j-1}) = \Phi_1(t_j)$$

$$\frac{\partial \Phi_3}{\partial t} + L_z^{j-1}\Phi_3 = 0 \qquad \Phi_3(t_{j-1}) = \Phi_2(t_j)$$

$$\frac{\partial \Phi_4}{\partial t} + \frac{1}{2}L_\theta^{j-1}\Phi_4 = 0 \qquad \Phi_4(t_{j-1}) = \Phi_3(t_j)$$

$$\frac{\partial \Phi_5}{\partial t} + \frac{1}{2}L_\lambda^{j-1}\Phi_5 = 0 \qquad \Phi_5(t_{j-1}) = \Phi_4(t_j)$$

The following symbols are used here

$$L^{j}_{\lambda}\Phi = \left[\frac{1}{2}m(\bar{u}+u')\frac{\partial\Phi}{\partial\lambda} + \frac{1}{2}\frac{\partial}{\partial\lambda}\left[(\bar{u}+u')\Phi\right] + \mu m^{2}\frac{\partial^{2}\Phi}{\partial\lambda^{2}}\right]\frac{1}{H}, \qquad (17)$$

$$L^{j}_{\theta}\Phi = \left[\frac{1}{2}n(\bar{v}+v')\frac{\partial\Phi}{\partial\theta} + \frac{1}{2}\frac{\partial}{\partial\theta}\left[(\bar{v}+v')\Phi\right] + \mu m n\frac{\partial}{\partial\theta}\sin\theta\frac{\partial\Phi}{\partial\theta}\right]\frac{1}{H}$$

$$L_{z}\Phi = \left[\left(\int_{z}^{1} m\left[\frac{\partial u'}{\partial\lambda} + \kappa\frac{\partial}{\partial\theta}\left(\frac{v'}{m}\right)\right]dz\right)\frac{\partial\Phi}{\partial z} + \frac{\partial}{\partial z}\nu\frac{\partial\Phi}{\partial z}\right]\frac{1}{H}$$

Operators (17) are approximated by the finite difference relations based on the schemes suggested by Marchuk and permitting to preserve in the the finite-difference representation the analogues of certain integral invariants inherent to the differential model.

Each problem of set (17) is integrate with respect to time on the elementary interval $t_{j-1} \leq t \leq t_{j}$ using Krank-Nicolson's scheme.

The second method of solution is based on equation (13) in the transformed form. Solving motion equations (7) as regard to functions u', v' in the explicit form and using repsentation of $\bar{u}, \bar{v}$ via the stream function, equation (13) may be transformed into the following form

$$\frac{\partial\Phi}{\partial t} + m\left[\left(\frac{\partial}{\partial\lambda}\Gamma_{1}\frac{\partial\Phi}{\partial\theta} - \frac{\partial}{\partial\theta}\Gamma_{1}\frac{\partial\Phi}{\partial\lambda}\right) + \left(\frac{\partial}{\partial z}\Gamma_{2}\frac{\partial\Phi}{\partial z} - \frac{\partial}{\partial\lambda}\Gamma_{2}\frac{\partial\Phi}{\partial z}\right) + \right. \qquad (18)$$

$$\left. + \left(\frac{\partial}{\partial\theta}\Gamma_{1}\frac{\partial\Phi}{\partial z} - \frac{\partial}{\partial z}\Gamma_{1}\frac{\partial\Phi}{\partial\theta}\right)\right] - \frac{\partial}{\partial\lambda}\Gamma_{4}\frac{\partial\Phi}{\partial\lambda} - m\frac{\partial}{\partial\theta}\Gamma_{5}\frac{\partial\Phi}{\partial\theta} - \frac{\partial}{\partial z}\Gamma_{6}\frac{\partial\Phi}{\partial z} = 0$$

The form of coefficients Γ_{i} depends on the concrete form of motion equation which are used in this model.

Write coefficients for the simplest case when the ocean depth is constant. Then the terms of time and vertical diffusion are thrown away from motion equations, and the horizontal diffusion is replaced by the linear friction with a coefficient.

Then expressions for deviations u', v' will assume the form

$$u' = \frac{m}{\rho_0 (R_1^2 + \ell^2)} \left[- \frac{R_1 m}{n} \frac{\partial \eta}{\partial \lambda} - \ell \frac{\partial \eta}{\partial \theta} \right]$$

$$v' = \frac{n}{\rho_0 (R_1^2 + \ell^2)} \left[\frac{\ell m}{n} \frac{\partial \eta}{\partial \lambda} - R_1 \frac{\partial \eta}{\partial \theta} \right]$$

where $\eta = \left(\int_0^z \rho dz - \int_0^1 dz \int_0^z \rho dz \right) H$

In this case coefficients Γ_i have the form

$$\Gamma_1 = n \left[\frac{\varphi}{nH} + \frac{\ell \eta}{\rho_0 (R_1^2 + \ell^2)} \right]$$

$$\Gamma_2 = \frac{n R_1}{\rho_0 (\ell^2 + R_1^2)} \frac{\partial}{\partial \lambda} H \int_z^1 \eta dz - \frac{H}{\rho_0} \frac{\partial}{\partial \theta} \left(\frac{\ell}{R_1^2 + \ell^2} \right) H \int_z^1 \eta dz$$

$$\Gamma_3 = \frac{R_1 n^2}{m \rho_0 (R_1^2 + \ell^2)} \frac{\partial}{\partial \theta} H \int_z^1 \eta dz$$

$$\Gamma_4 = \mu m^2$$

$$\Gamma_5 = \frac{\mu n^4}{m^2}$$

$$\Gamma_6 = \gamma$$

For the solution of equation (18) a two-cycle splitting scheme analogous in form to scheme (16) is used. This scheme differs from scheme (16) by the fact that operators Λ_λ^{j-1}, Λ_θ^{j-1}, Λ_z^{j-1} are replaced by operators $m \Lambda_{\lambda,\theta}^{j-1}$, $m \Lambda_{\lambda,z}^{j-1}$, $m \Lambda_{\theta,z}^{j-1}$ respectively.

The latter are plane elliptical operators on the sections parallel to co-ordinate planes (λ, θ), (λ, z), (θ, z) respectively and has the form

$$\Lambda_{\lambda,\theta}^{j-1} \Phi = \frac{\partial}{\partial \lambda} \Gamma_1^{j-1} \frac{\partial \Phi}{\partial \theta} - \frac{\partial}{\partial \theta} \Gamma_1^{j-1} \frac{\partial \Phi}{\partial \lambda} - \frac{1}{2} \frac{\partial}{\partial \lambda} \frac{\Gamma_4}{m} \frac{\partial \Phi}{\partial \lambda} - \frac{1}{2} \frac{\partial}{\partial \theta} \Gamma_5 \frac{\partial \Phi}{\partial \theta}$$

$$\Lambda_{\lambda,z}^{j-1} \Phi = \frac{\partial}{\partial z} \Gamma_2^{j-1} \frac{\partial \Phi}{\partial \lambda} - \frac{\partial}{\partial \lambda} \Gamma_2^{j-1} \frac{\partial \Phi}{\partial z} - \frac{1}{2} \frac{\partial}{\partial \lambda} \frac{\Gamma_4}{m} \frac{\partial \Phi}{\partial \lambda} - \frac{1}{2} \frac{\partial}{\partial z} \frac{\Gamma_6}{m} \frac{\partial \Phi}{\partial z}$$

$$\Lambda_{\theta,z}^{j-1} \Phi = \frac{\partial}{\partial z} \Gamma_3^{j-1} \frac{\partial \Phi}{\partial z} - \frac{\partial}{\partial z} \Gamma_3^{j-1} \frac{\partial \Phi}{\partial \theta} - \frac{1}{2} \frac{\partial}{\partial \theta} \Gamma_5 \frac{\partial \Phi}{\partial \theta} - \frac{1}{2} \frac{\partial}{\partial z} \frac{\Gamma_6}{m} \frac{\partial \Phi}{\partial z}$$

Plane problems obtained at each step of splitting are approximated with the aid of the finite-elements method on the sections parallel to co-ordinate planes. Then each of the obtained finite-difference operators is splitted into three one-dimensional operators and additional splitting of each equation of the scheme into elementary steps is made.
At each step one of the three one-dimensional operators takes part.
Two of them are acting in the co-ordinate directions and one acts in the diagonal direction which conforms with triangulation carried out in the dicretization of equation (18) using the finite-elements method.

In such a manner we obtain two numerical realizations of the model of global circulation in the World Ocean having conservative properties of the second order with respect to time. The operators inversion at each time step was provided by the factorization method.

A numerical experiment related to the calculation of mean climatic characteristics in the World cean was carried out using the above model. The model included the set of equations (7) and (8) and equation (6) for the stream function. The finite-elements method was used for solution of (6) and the finite-differences method was used for solution of system (7), (8). On the ocean surface the mean climatic temperature was given for the winter of the Northern Hemisphere,on the lateral cylindric surface Neiman conditions were set. At the initial time moment, the temperature was equal to zero, and calculation of heat "diffusion" for the period of 110 years was carried. Further, the solution obtained was taken as initial approximation for the solution of the full problem (7), (8) but in the absence of wind stress over the surface. Figures present the calculations of temperature and salinity at the depth of 100 and 450 m obtained at the final stage of computations.

ICEBERG DRIFT PREDICTION BY THE INTERNATIONAL ICE PATROL

DAVID G. MOUNTAIN

Abstract

As a U.S. Coast Guard mission the International Ice Patrol produces forecasts of sea ice and iceberg locations in the western North Atlantic Ocean to warn ships at sea of ice danger. This information is transmitted by radio facsimile twice daily during the ice season. The forecasts are accomplished by first sighting the icebergs visually from aircraft and then predicting their drift between observations, often over periods of two or more weeks. The iceberg drift prediction requires the use of forecasted surface winds and forecasted near surface currents, making it a second level product.

A new system developed for iceberg drift prediction uses prognosis wind data supplied every twelve hours by the U.S. Naval Fleet Numerical Weather Central. The near surface currents are than forecasted using the sum of a geostrophic and wind-driven current. The geostrophic component is determined from conductivity/temperature/depth (CTD) surveys in the van of the icebergs. The data are processed real-time at sea to yield dynamic height values and surface geostrophic currents, which are sent by radio message to Commander, International Ice Patrol. If no recent surveys are available, an historical average data file is used. The wind-driven component in four layers is calculated by solution of a time-dependent Ekman equation forced by the local wind history. Using these inputs, the iceberg drift is predicted by solving differential equations which balance the iceberg acceleration with the water drag, the wind drag, and the Coriolis acceleration.

Improved methods of iceberg detection and drift prediction represent both increased safety for lives at sea and economic benefit for commercial users of the product. Techniques being considered and tested for future operational use, including remote sensing and the tracking of buoys by satellite are discussed.

Introduction

The icebergs encountered in the North Atlantic Ocean originate primarily from the calving of glaciers along the west coast of Greenland and travel around the Labrador Sea under the influence of the wind and currents (Fig. 1). The Labrador Current carries the ice southward along the eastern edge of the Grand Banks of Newfoundland, where it becomes a danger to ships transiting the North Atlantic Ocean. The period of ice danger usually extends from March through early July, with a yearly average of about 300 icebergs drifting south of 48°N.

The International Ice Patrol (IIP) forecasts the locations of icebergs and sea ice in the western North Atlantic Ocean during the spring of each year. An ice bulletin containing these locations is broadcast every twelve hours for the information of ships transiting the area. The ice warning service was created by the first International Conference on the Safety of Life at Sea after the sinking of the R.M.S. Titanic in April 1912. The United States undertook the management of the service, with funding provided by the signatory nations on a pro rated basis proportional to the shipping tonnage of each nation transiting the region. Since 1914 the U.S. Coast Guard has operated the Ice Patrol without loss of life due to unreported ice outside of the reported limits of ice danger.

The iceberg position forecasts are accomplished by visually observing the icebergs from aircraft and predicting their drift between observations. The persistance of fog in the Grand Banks region often prevents the visual observation of ice for periods of two or more weeks, and as a result drift predictions often must be made over long periods of time. The accuracy of the ice bulletins, therefore, depends largely upon the accuracy of the drift prediction scheme used.

The Iceberg Drift Model

Predicting the drift of an iceberg can be approached by two methods. Empirical relationships can be established between contributions to the iceberg velocity and the respective forces acting on the ice [e.g. Budinger, 1960; Dempster, 1974]. The results of the relationships are added vectorially to yield the net movement of the iceberg. This approach is well suited for operational use because of its simplicity, but suffers in accuracy by attempting to combine complex dynamic processes into individual parameters and by neglecting the time dependence often inherent in the problem.

The second approach to drift prediction is through a dynamical analysis with the forces acting on the iceberg being expressed as differential equations of motion [e.g. Wolford, 1973]. This allows the complex physics of the problem to be addressed in a mathematically rigorous form. The method, however, can be difficult to adapt to an operational system since to solve the equations can require prohibitive computer time and the form of the equations may require input information not avaliable on a real-time basis.

To obtain accurate drift predictions within the constraints imposed by an operational system. IIP has chosen the dynamical approach to the problem with the inclusion of empirical parameters to simplify certain complex relations. For the model chosen by IIP the form of the forces in the equations of motion is compatible with avaliable real-time information sources and a time efficient method of solution is used. The forces included in the drift model are the Coriolis force, the wind drag, the water drag, and a gravitational component due to the sloping sea surface. Wave forces on the iceberg are neglected. The form of each force used in the model is discussed below.

1. Coriolis Force - The Coriolis force is a pseudoforce acting on a moving body due to the rotation of the earth. It acts perpendicular (to the right in the northern hemisphere) to the line of motion and is proportional in magnitude to the speed of the iceberg:

$$\text{Coriolis Force} = fV_i$$

where

V_i = the iceberg speed
$f = 2\omega \sin\theta$
ω = the rotation rate of the earth
θ = the latitude

2. Wind Drag - The wind or air drag on the iceberg acts in the direction of the wind and is expressed as:

$$\text{Wind Drag} = \tfrac{1}{2}\rho_a CD_a A_a W^2$$

where

CD_a = the air drag coefficient
A_a = the above water cross sectional area of the iceberg
W = the wind speed
ρ_a = the density of air

Only the form drag is considered and the velocity of the iceberg is assumed small compared to the wind velocity.

3. Water Drag - The water drag on the iceberg is nearly always the most important forcing term and is also the most difficult to evaluate realistically. The water drag is expressed in vector form as

$$\text{Water Drag} = \tfrac{1}{2}\rho_w CD_w A_w |\vec{V}_w - \vec{V}_i| (\vec{V}_w - \vec{V}_i)$$

where

CD_w = the water drag coefficient
A_w = the submerged cross sectional area of the iceberg
$\vec{V}_i$ = the iceberg velocity
$\vec{V}_w$ = the water velocity
ρ_w = the water density

As with the wind only the form drag is considered, but here the velocity of the iceberg is not considered small. The drag depends upon the relative velocity of the ice with respect to the water.

The true water velocity varies with time and depth. To obtain the actual water drag the expression above should be integrated over the submerged portion of the iceberg. To approximate this procedure the water column is divided into four layers. The water velocity in each layer is determined as described below and then the water drag in each layer is calculated. The results are summed to yield the total water drag on the iceberg, as shown schematically in figure 2. The water velocity is considered to be the sum of a mean value, constant in time and depth, and of a time and depth dependent component. The latter is assumed to be driven solely by the local wind and is derived from a solution to a time dependent Ekman force balance. For a piecewise-constant wind forcing [i.e. 12 hourly wind values] a rigorous and efficient solution to the time-dependent Ekman equation is obtained by operating on the wind stress history with rotation and decay coefficients derived by Mountain and Mooney (1979). The average value of the time-dependent Ekman current in each of the four layers is determined in the model using a 96 hour history of the local wind.

Calculating the water drag in layers allows different sizes of icebergs to be considered. Small icebergs lie in the surface water layer which is greatly affected by the local wind, while larger icebergs have much of their cross sectional area below the influence of the local wind-driven currents.

4. Gravitational Force - The gravitational force is the component of gravity acting parallel to the sloping sea surface, or equivalently, the pressure gradient force due to the sloping sea surface. The sea surface slope is assumed to be the slope associated with the local geostrophic current. The gravitational force exactly balances the Coriolis force that would result from movement with the geostrophic current, and thus, is expressed as:

$$\text{Gravitational Force} = -fV_g$$

where V_g is the local mean or geostrophic current. Inclusion of this term allows for the equilibrium drift of an iceberg with the mean current in the absence of wind.

With the forces described above, the equations of motion for the drift of an iceberg in component form are:

$$\frac{dx}{dt} = U$$

$$\frac{dy}{dt} = V$$

$$\frac{dU}{dt} = fV - fV_g + [\tfrac{1}{2}\rho_a C D_a A_a W^2 \sin\phi + \sum_{i=1}^{4} \tfrac{1}{2}\rho_w C D_w A_i (E_i - U) S_i]/M$$

$$\frac{dV}{dt} = -fU + fU_g + [\tfrac{1}{2}\rho_a C D_a A_a W^2 \cos\phi + \sum_{i=1}^{4} \tfrac{1}{2}\rho_w C D_w A_i (N_i - V) S_i]/M$$

where

x,y	=	east, north components of position
U,V	=	east, north components of iceberg velocity
U_g, V_g	=	east, north components of mean or geostrophic water velocity
U_{E_i}, V_{E_i}	=	east, north components of Ekman current in ith layer
E_i	=	$U_g + U_{E_i}$ the east component of total water current in the ith layer
N_i	=	$V_g + V_{E_i}$ the north component of total water current in the ith layer
S_i	=	$[(E_i - U)^2 + (N_i - V)^2]^{1/2}$ the speed of the iceberg relative to the water in the ith layer.
A_i	=	iceberg cross sectional area in the ith layer
M	=	iceberg mass
ϕ	=	wind direction

This set of four equations is now just an initial value problem and is solved by a fourth order Runge-Kutta technique. Given the initial location of the iceberg, the equations are stepped forward in time to yield predicted positions. The convergence of the solution is tested by comparing the results after a single time step Δt with that after two steps of $\frac{1}{2}\Delta t$. The step length used is varied to insure that the comparison is within a preset error limit, while also keeping the time step as large as possible and thus provide an efficient solution. The maximum step allowed is one hour.

Inputs to the Model

In solving the equations of motion given above, certain information is needed

1. Iceberg Observation - The first inputs required by the model are the iceberg locations and size. Observations are made visually from HC-130 aircraft which are stationed in St. John's , Newfoundland during the ice season. When weather conditions reduce visibility, radar is used to locate targets, and the aircraft then diverts from its trackline to fly over and identify the target. The positions and size of the iceberg are sent by radio message to the Commander, International Ice Patrol (CIIP). Fog often prevents all observations for extended periods of time.

2. Wind Data - To forecast the drift of icebergs the model requires forecast wind data to calculate the wind drag. Also a time history of the wind is needed to estimate the wind driven current. The U.S. Navy Fleet Numerical Weather Central supplies wind data in the ice patrol area on a one degree latitude by two degree longitude grid every twelve hours. Both the most recent analysis wind information and a twelve hour forecast or prognosis are provided. A file is maintained of the analysis wind data and the most recent prognosis information, with the latter being replaced by analysis values when they become available.

3. Mean Current Data - For over thirty years U.S. Coast Guard vessels have measured oceanographic parameters (temperature and salinity) in the area through which the icebergs were likely to drift. Originally obtained with Nansen bottles, the data are now collected by Conductivity, Temperature, Depth (CTD) instruments and are processed real-time at sea to yield surface geostrophic current values which are sent by radio message to CIIP. The data obtained since 1934 have been compiled to yield a mean surface current field for the area (Scobie and Schultz, 1976) (Fig. 3).

A second source of real-time current information is derived from the tracking of BTT (buoy transmit terminals) buoys by the Nimbis 6 and Tiros 14 satellites. The buoys, with window shade drouges attached, have been used since 1976 to measure the core velocity of the Labrador Current, which is generally underestimated in the mean current field mentioned above. The U.S. Coast Guard has a satellite receiving unit to insure the real-time reception and avaliability of this information.

The average surface geostrophic currents (Scobie and Schultz, 1976) are kept on file on a 20 minute latitude by 20 minute longitude grid for use as the mean current in the model. These values are assumed constant with depth over the draft of the iceberg. The average file is updated with the most recent real-time information available, either CTD survey or BTT drift.

4. Iceberg Characteristics - The cross sectional area and mass data needed in the model cannot be obtained for each iceberg. Instead observations made over a number of years (Robe and Farmer, 1978; Robe, 1978) have been used to establish seven classes of icebergs which could be distinguished from aircraft. The average areal and mass characteristics for each class are shown in Table 1 (Robe, Personal Communication).

A value of 1.5 is used for both the air and the water drag coefficients, regardless of the size or shape of the iceberg.

Tests of the Model

The drift model described above was tested during the 1978 ice patrol season to estimate its accuracy. Predicted drifts generated by the model were compared with observed positions for two large icebergs that were resighted a number of times and for a BTT buoy that was tracked by satellite.

TABLE 1

ICEBERG CHARACTERISTICS

Non Tabular Icebergs

Size	Mass (10^6kg)	Dry Area (M^2)	Wet Area (M^2) Per Depth Layer			
			0-20M	20-50M	50-100M	100-120M
Growler	.45	10	80	0	0	0
Small	75	230	780	820	0	0
Medium	900	910	1800	1900	2700	0
Large	5500	2000	3500	3750	5300	1400
Tabular Icebergs						
Small	245	650	1900	2600	0	0
Medium	2170	2700	4400	5900	8700	0
Large	8235	5200	7200	9700	14400	5000

The BTT buoy was deployed in the Labrador Current on 13 April 1978 and drifted southward along the eastern edge of the Grand Banks. The drift was predicted using size characteristics of the buoy, although the mass was artifically increased to allow an operationally compatible time step in the model. Also the wind drag on the buoy was ignored since the above water portion of the buoy lies below the normal wave height. The predicted drift compares favorably with the observed drift track (Fig. 4). The drift error defined as the distance between the predicted and observed positions (Fig. 5) is generally less than 35 km and is as low as 6 km after twelve days and 260 km of drift. Some aspects of the observed drift cannot be accounted for by our present knowledge of the currents in the area, particularly the east-west movement on 25-27 May. As a result the model overdrifted the buoy to the south during this time and the error increased at the end of the comparison period.

A large tabular iceberg was sighted six times over a twenty-five day period at approximately five day intervals. By predicting the drift from each observation to the final position, a number of drifts of different durations (5 of 5 days, 4 of 10 days, 3 of 15 days, 2 of 20 days, and 1 of 25 days) were generated for comparison with the observations. The average error for each drift duration (Fig. 6) was 90-150 km, while the average length of drift increased from 90 to 500 km. The twenty- five day predicted drift is compared to the observed positions in figure 7. The initial observations indicated that the iceberg moved to the northwest over the six day period 9-15 May, which was opposite to the predicted drift direction and represents the worst case situation encountered in the testing.* The movement suggests that significant variations in the current field may exist that are not able to be included as inputs to the model with our present knowledge. More representative predicted drifts were obtained for drifts starting on 20 May and 25 May (Figure 8).

The last operational test of the model was the drift of a large pinnacle iceberg followed for six days by the USCGC EVERGREEN. The predicted drift was in error by 57 km after the sixth day, which is comparable to the results for the large tabular iceberg discussed above.

The error in the predicted drifts, although perhaps large initially, remains relatively constant for drifts of up to three weeks durations. Expressed in a different manner, the error per day of drift for the two icebergs discussed above decreased from 17 km per day for five day drifts to 6 km per day for the twenty five day drift. The primary cause of the error is believed to be inaccuracies in the inputs, particularly the currents, and not in the physics of the model itself. While some short term features of the drift were missed, the long term or general trend was more faithfully represented.

---

* The northwest movement of the iceberg is contrary to most previously observed drifts in this area. The possibility exists that the 19 May position was incorrect. If it were excluded from the analysis the drift errors in figure 6 would be 55-90 km.

Future efforts will be directed toward obtaining better real-time current information to supply to the drift model and more importantly, toward obtaining an all weather iceberg location and identification system. Improved methods of iceberg detection and iceberg drift forecasting represent both increased safety for lives at sea and econonic benefit to the users of the IIP service.

Acknowledgment

Discussions with R. Q. Robe proved helpful in the formulation of the drift model. The assistance of G. Mangun in adapting the model to the IIP operational system is greatfully acknowledged. K. Mooney and R. Hayes made constructive comments on an earlier version of the manuscript. Ms. E. Simms is thanked for her careful typing of the manuscript.

Future Operations

A primary area for improvement in the iceberg drift prediction scheme presented above is in the current field supplied to the model. Through increased use of BTT buoys IIP plans to obtain better real-time current information in critical areas. In an effort to improve its current prediction capabilities, IIP has also undertaken a program to make long term direct measurement of the currents in the area, to better understand their variability.

Ultimately IIP desires to reduce its dependence on long term drift predictions by obtaining an all weather iceberg location and identification capability. A Side Looking Airborne Radar with a Radar Image Processor (SLAR-RIP), an operational system designed in cooperation with the NASA Lewis Research Center, has been used by the U.S. Coast Guard to monitor ice conditions in the Great Lakes to aid in ship routing. The SLAR-RIP system, currently being tested for use on Ice Patrol, could provide repeated coverage of the Ice Patrol area about every five days regardless of visibility conditions (Marthaler and Heighway, 1978).

A second system being tested by IIP is the tracking of icebergs by satellite using instrument packages similar to the BTT buoys discussed above. The method has been used successfully to track large icebergs in the Labrador Sea for periods of up to six months (Robe, personal communication). For smaller icebergs an ice dart is being tested to allow attachment of the electronics package to the iceberg from an aircraft. This iceberg tagging system could provide continuous monitoring of particular icebergs with no drift prediction being required.

Conclusions

The International Ice Patrol has developed a model which forecasts the drift of icebergs by solving differential equations expressing the forces acting on the iceberg. The accuracy of the drift model is believed to be limited primarily by the accuracy of the avaliable real-time input information.

REFERENCES

Budinger, T. E. 1960. Wind effect on icebergs. Unpublished manuscript of the International Ice Patrol.

Dempster, R. T. 1974. The measurement and modeling of iceberg drift. IEEE International Conference on Engineering in the Ocean Environment, Halifax, Nova Scotia, August 21-23, 1974, pp. 125-129.

Marthaler, J. G. and J. E. Heighway 1978. Radar image processing of real aperture SLAR data for the detection and identification of iceberg and ship targets. Fifth Canadian Symposium on Remote Sensing, Victoria, B. C., 28-31 August 1978.

Robe, R. Q. 1978. Physical properties of icebergs-height to draft ratios. Report of the International Ice Patrol Service in the North Atlantic Ocean - Season of 1975, CG-188-30, 1978, pp. 70-77.

Robe, R. Q. and L. D. Farmer 1978. Physical properties of icebergs - total mass determination. Report of the International Ice Patrol Service in the North Atlantic Ocean - Season of 1975, CG-188-30, 1978, pp. 61-69.

Scobie, R. W. and R. H. Schultz 1976. Oceanography of the Grand Banks Region of Newfoundland, March 1971-December 1972, CG-373-70, 298 pp.

Wolford, T. C. 1973. Iceberg Drift. A dissertation submitted to Catholic University of America as partial fulfillment of the requirements for the degree of Ph.D., 265 pp.

LIST OF FIGURES

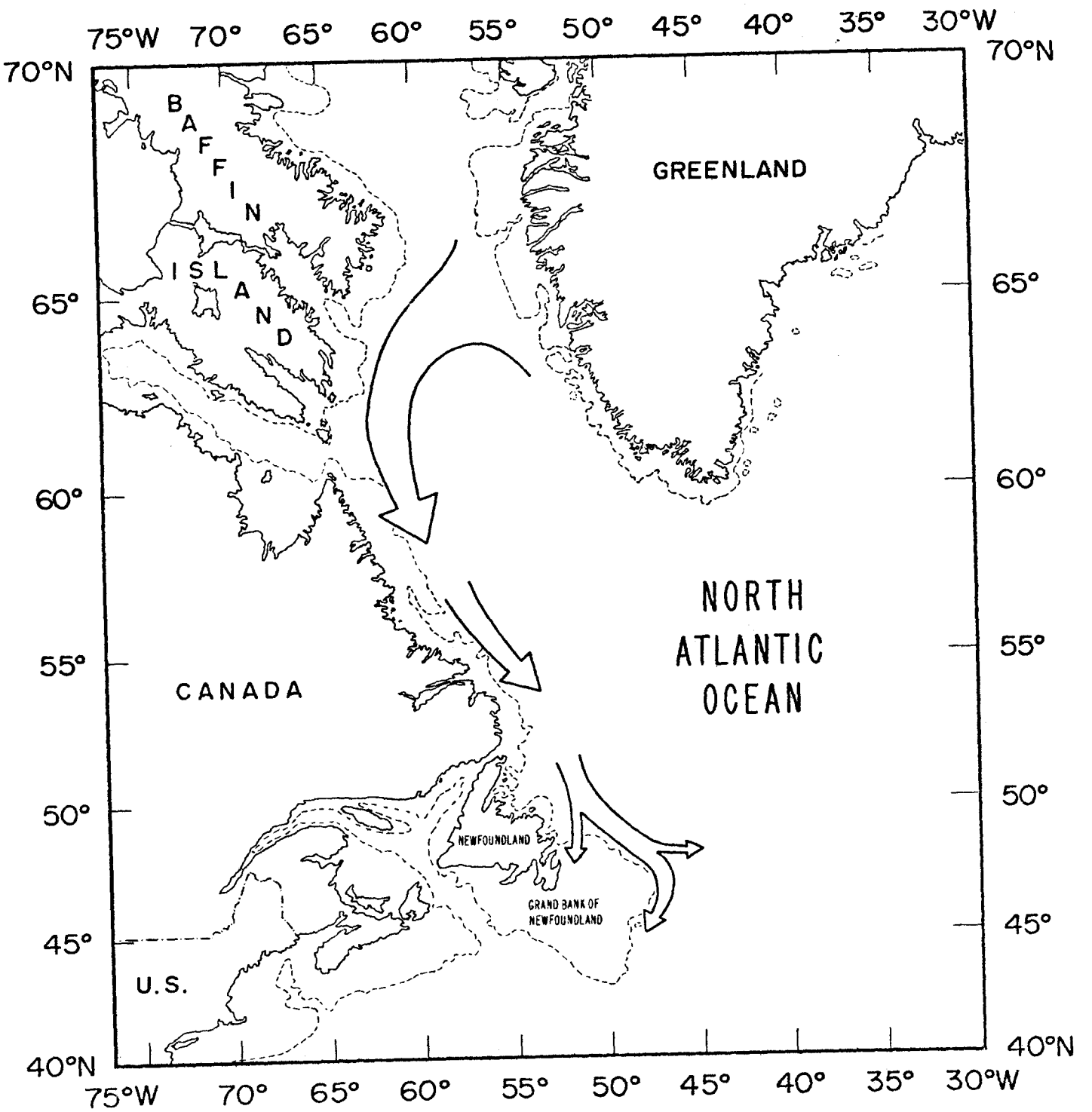
75°W
70°
65°
60°
55°
50°
45°
40°
35°
30°W
70°N
65°
60°
55°
50°
45°
40°N
BAFFIN ISLAND
GREENLAND
CANADA
NORTH ATLANTIC OCEAN
NEWFOUNDLAND
GRAND BANK OF NEWFOUNDLAND
U.S.

Figure 1

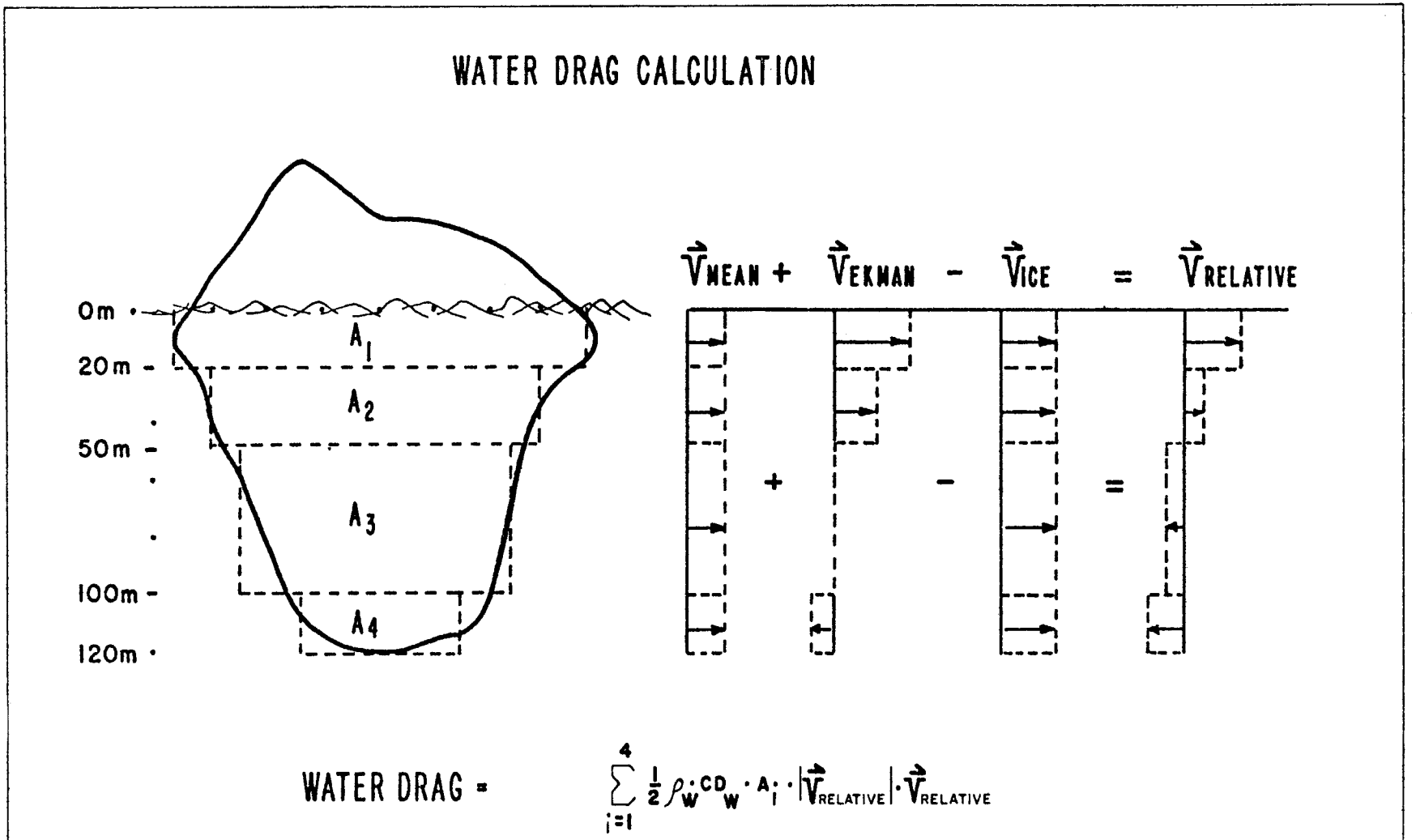
WATER DRAG CALCULATION
0m
20m
50m
100m
120m
A1
A2
A3
A4
V MEAN + V EKMAN - V ICE = V RELATIVE
WATER DRAG = Σ (i=1 to 4) ½ ρW CDW · Ai · |V RELATIVE| · V RELATIVE

Figure 2

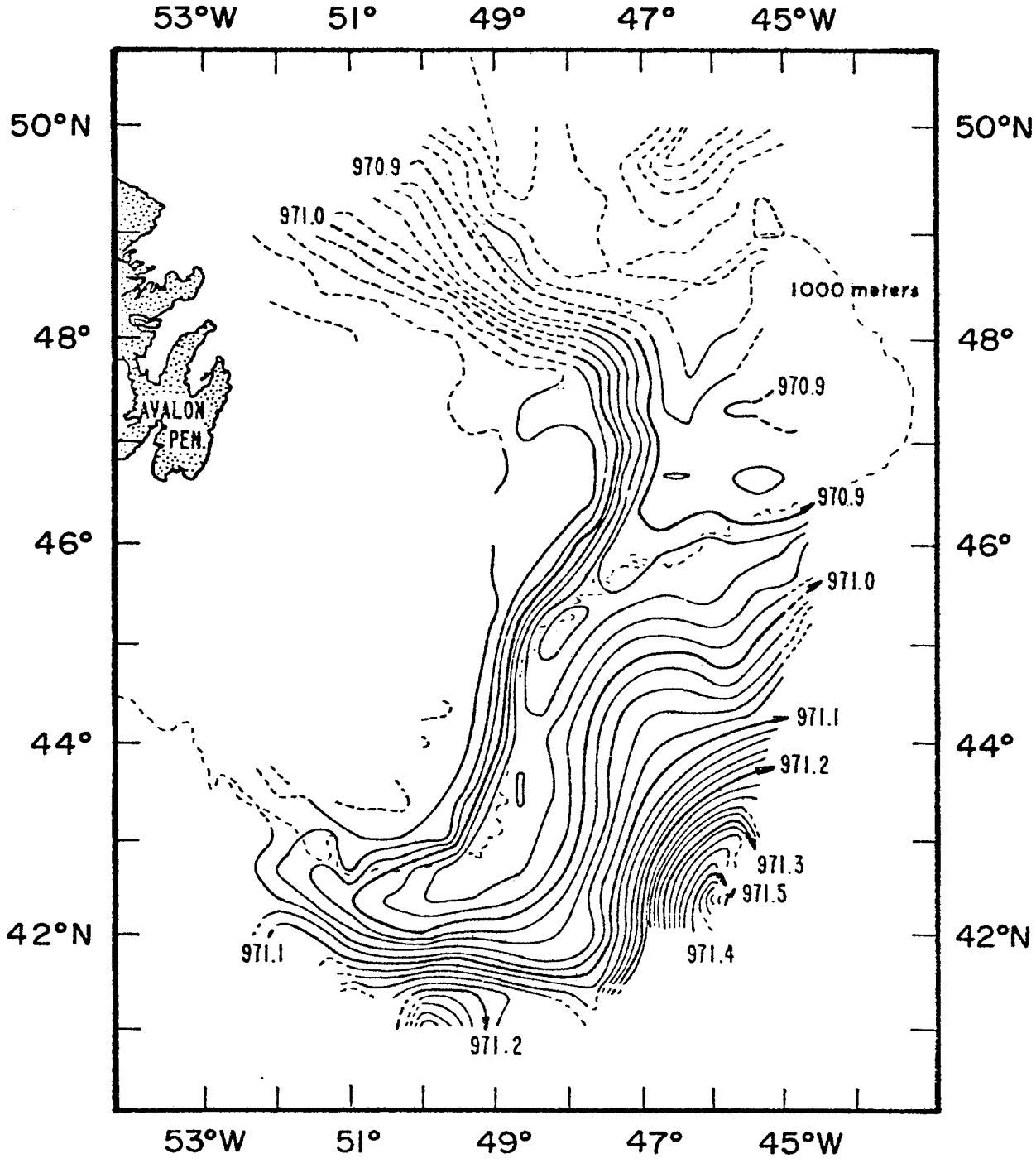
53°W
51°
49°
47°
45°W
50°N
48°
46°
44°
42°N
970.9
971.0
1000 meters
970.9
970.9
971.0
971.1
971.2
971.3
971.5
971.4
971.1
971.2
AVALON PEN.

Figure 3

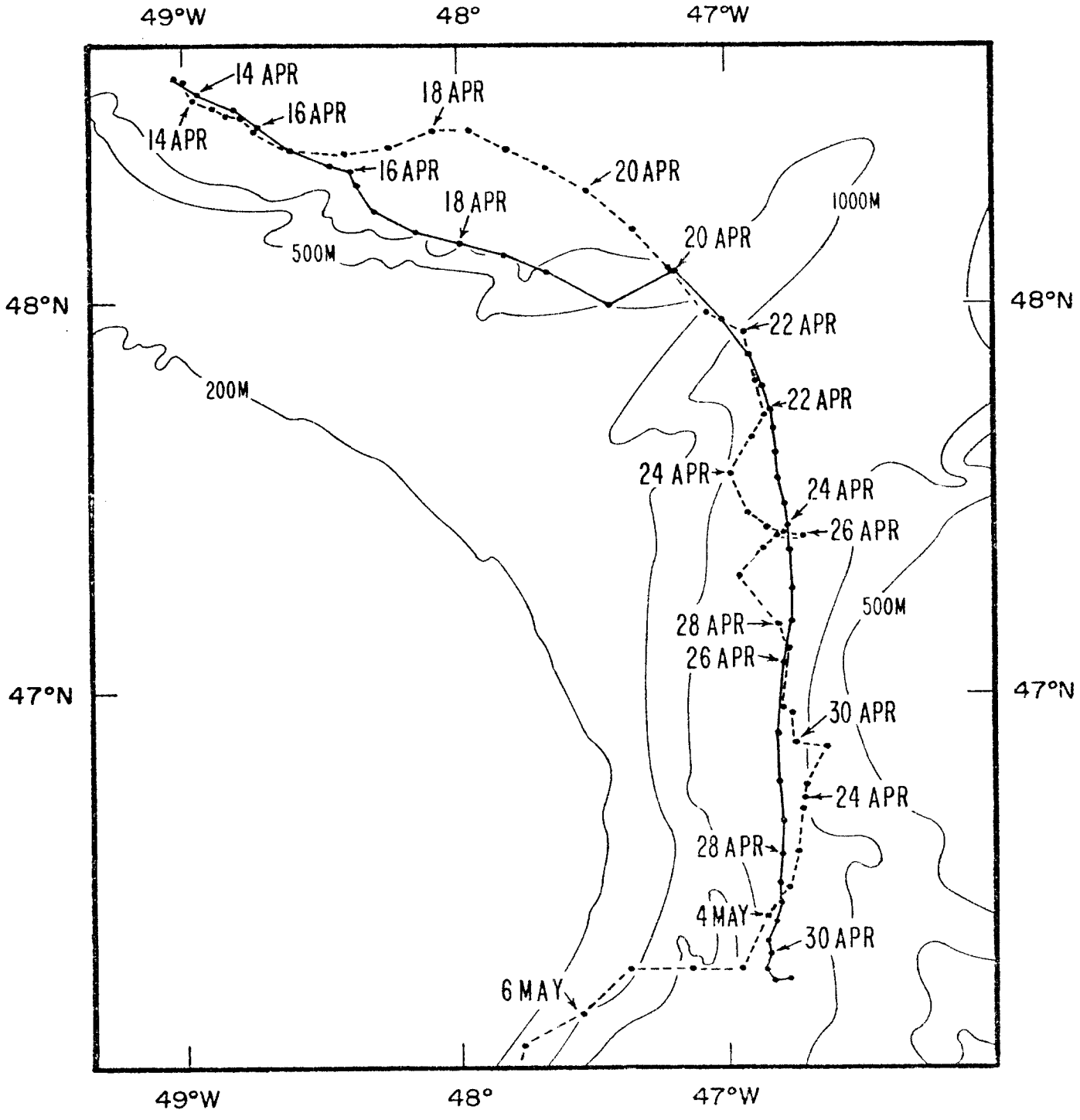
49°W
48°
47°W
48°N
47°N
14 APR
14 APR
16 APR
16 APR
18 APR
18 APR
20 APR
20 APR
22 APR
22 APR
24 APR
24 APR
26 APR
26 APR
28 APR
28 APR
30 APR
30 APR
24 APR
4 MAY
6 MAY
1000M
500M
500M
200M

Figure 4

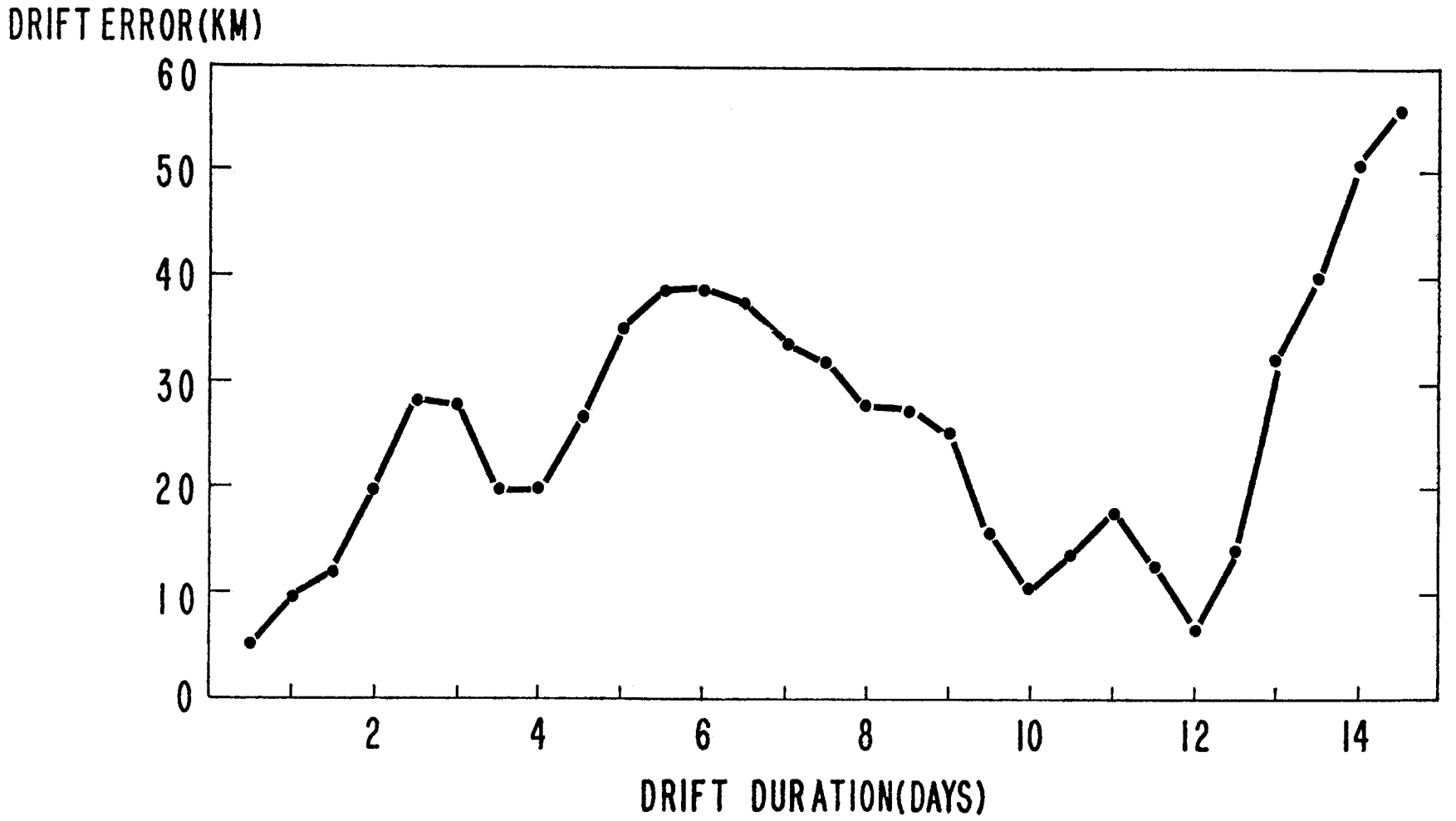
DRIFT ERROR(KM)
60
50
40
30
20
10
0
2
4
6
8
10
12
14
DRIFT DURATION(DAYS)

Figure 5

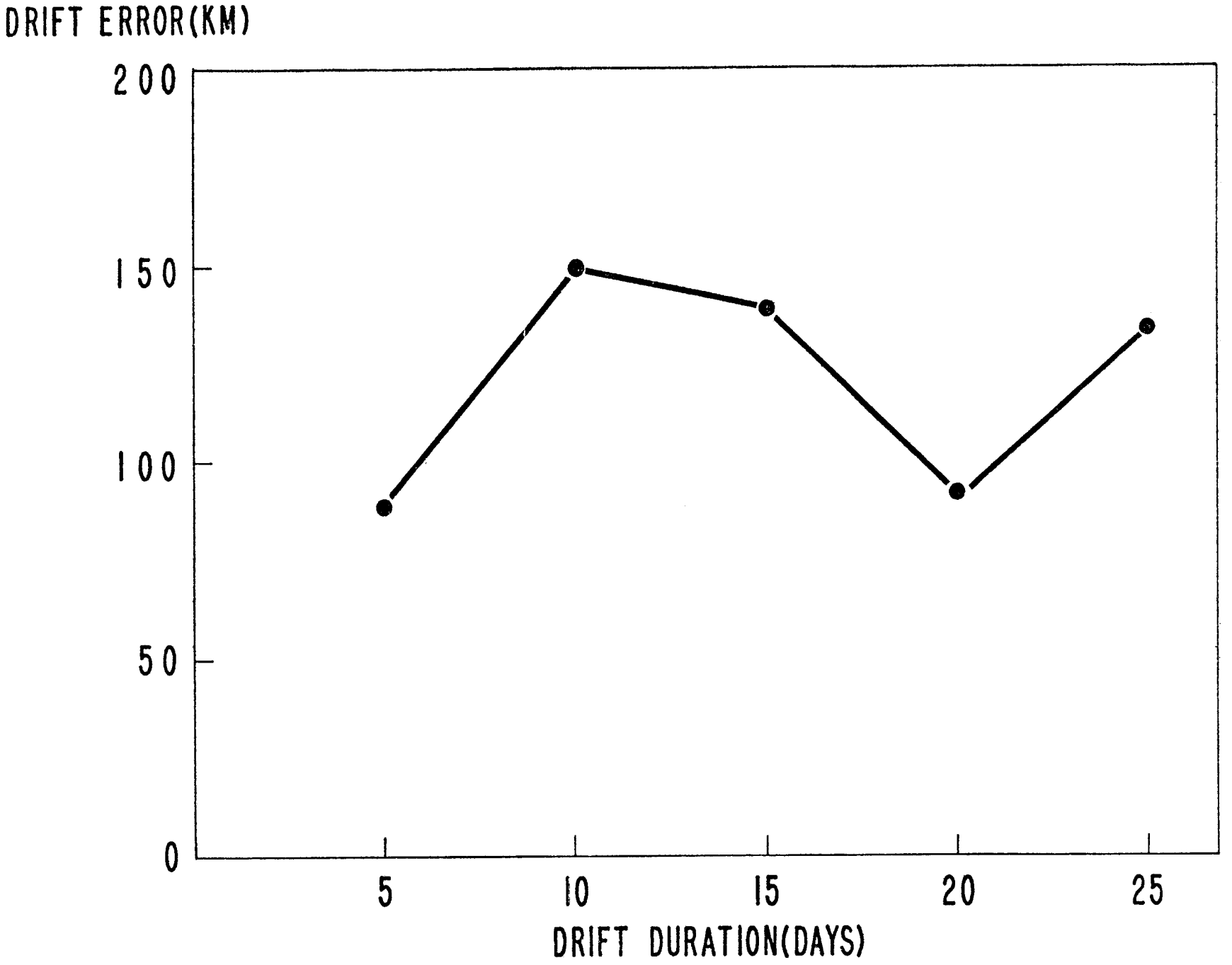
DRIFT ERROR(KM)
200
150
100
50
0
5
10
15
20
25
DRIFT DURATION(DAYS)

Figure 6

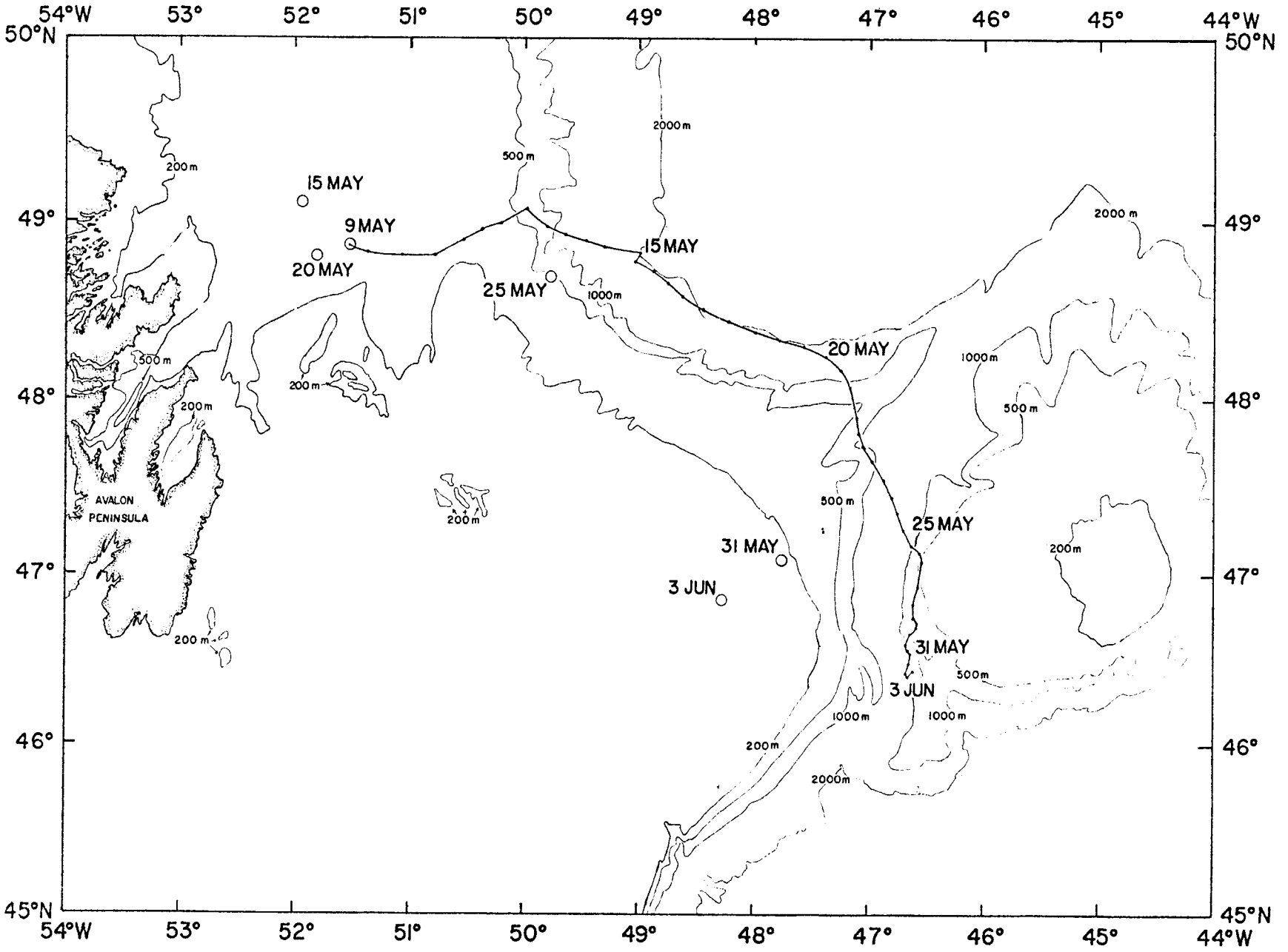
54°W
53°
52°
51°
50°
49°
48°
47°
46°
45°
44°W
50°N
49°
48°
47°
46°
45°N
15 MAY
9 MAY
20 MAY
25 MAY
15 MAY
20 MAY
25 MAY
31 MAY
3 JUN
31 MAY
3 JUN
AVALON
PENINSULA
200 m
500 m
1000 m
2000 m

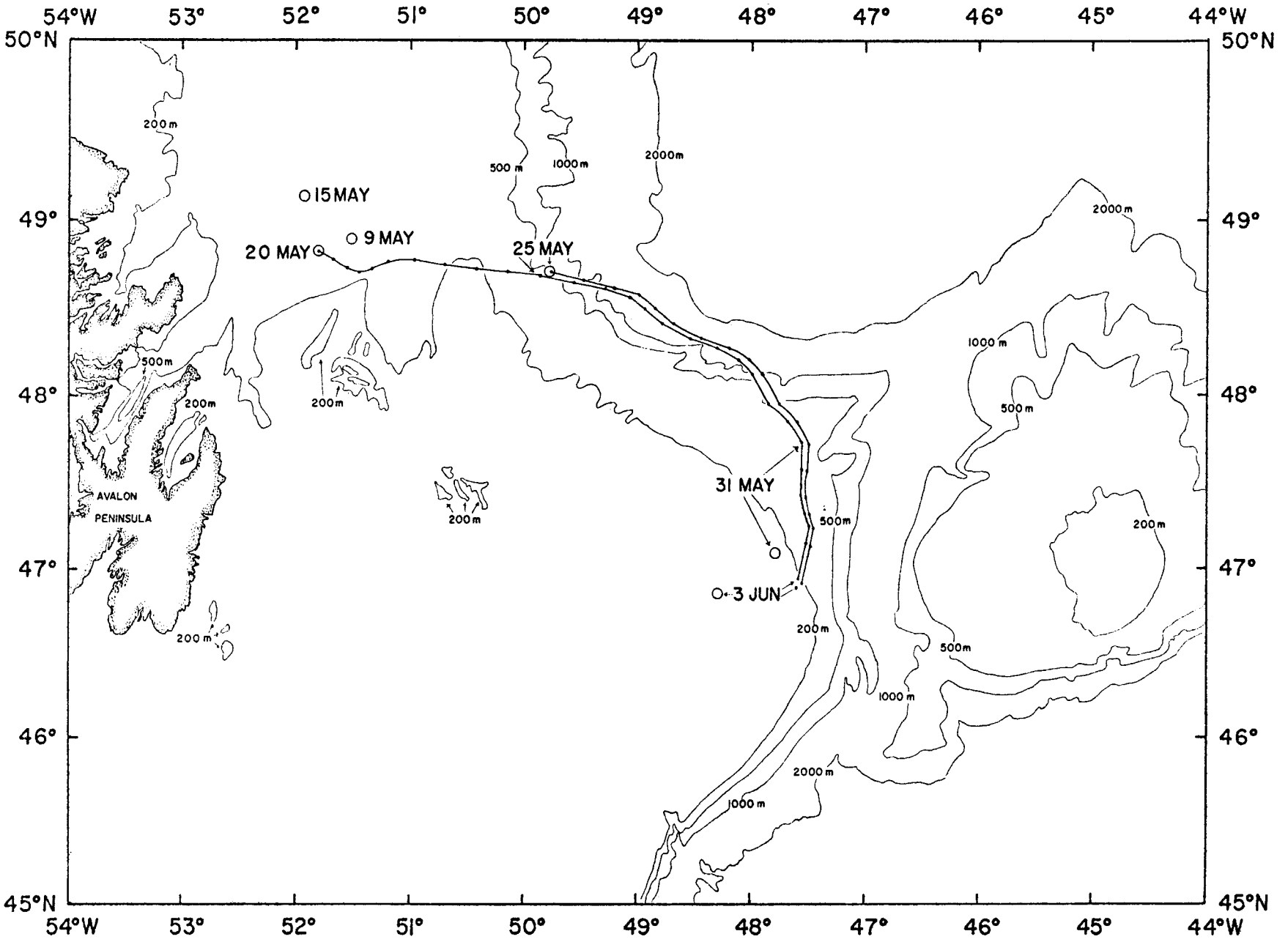
54°W
53°
52°
51°
50°
49°
48°
47°
46°
45°
44°W
50°N
49°
48°
47°
46°
45°N
15 MAY
9 MAY
20 MAY
25 MAY
31 MAY
3 JUN
AVALON
PENINSULA
200m
500m
1000m
2000m

Figure 8

ON-LINE USE OF INFRA-RED DATA FROM THE GEOSTATIONARY SATELLITE "METEOSAT" FOR BOTH SCIENTIFIC AND INDUSTRIAL PURPOSES

J.A.H. NOEL*

* Physicist oceanographer, ORSTOM, France
(In charge of numerical data processing at the teledetection office)

SUMMARY

The high repetitivity and global view of geostationary satellites make it possible to set up simple systems for utilization and to operate in real time.

The transfer of information to the user presupposes the existence of a system for the processing of information.

THE GEOSTATIONARY SATELLITES PROGRAMME

The Global Atmospheric Research Programme (GARP) has undertaken to set up five geostationary satellites with a view to permanent observation of the terrestrial sphere.

These satellites, situated 36,000 km from the earth, have their orbits in the equatorial plane and appear immobile in relation to the earth.

The European satellite "METEOSAT", launched on 23 November 1977, is situated on the meridian 0°. It allows of observation particularly suited to the African continent and the near Atlantic.

Particulars concerning "METEOSAT"

The satellite is equipped with a radiometer by means of which the globe can be sounded every 30 minutes. These data, received at Odenwald-Darmstadt, are processed prior to dissemination.

Three types of detector are available on the satellite:

- visible channel 0.4 - 1.1 µm,
- thermic infra-red channel 10 - 12.5 µm,
- water steam channel 5.7 - 7 µm.

The field of vision is 2.5 km for the visible channel and 5 km for the other two channels.

The image given by the visible channel has a definition of 5000 lines of 5000 dots, that given by the infra-red one a definition of 2500 lines of 2500 dots.

As a result of the high quality of the data and the remarkable stability of the satellite, applications in real time can be envisaged without onerous processing or heavy infrastructures.

Scientific applications

The first scientific application was the drawing up of temperature maps for the Atlantic zone.

For this purpose the very high repetitivity of the data and their relative stability were used.

With simple algorithms by means of which constant infra-red data can be extracted on a number of views spaced in time, a plausible proposition concerning temperature distribution in the ocean can be drawn up. Controlled temperature data have to be used for such maps.

Since April 1978 changes in the surface temperature off the coasts of Senegal and Mauritania have been followed on a weekly basis. As a result we have a more exact knowledge of these changes and their effects on exploitable species.

Since November 1978 infra-red data have been used on a daily basis in the Gulf of Guinea zone. A system of transmission enables fishing flotillas to use the information in real time.

During the months of July and August 1978 recordings were stepped up so that the data collected could be used as a source of extrapolation of environment parameters for the CIPREA project.

Projects for utilization of the terrestrial zone are scheduled to start at the beginning of 1978. They involve the use of high repetitivity of data, making it possible to follow day-by-day temperature changes in a zone. A number of sites were selected in the Sahel zone and the study of the daily and seasonal temperature cycles should make possible a new approach to the humidity problems of these zones.

Industrial and economic applications

The industrial and economic applications of "METEOSAT" are all dependent on the existence of both a system for the transfer of processed information and a system for the utilization of that information.

The case of aid for fishing is the most characteristic of such needs, for this is an organized industrial sector capable of making direct use of the information product.

Our better knowledge of the climatic seasons in the African tropical zone as a result of "METEOSAT" should enable us to make more accurate economic estimates in regard to both resource potentials and development operations:

- information on the opening of seasons,
- information on the I.F.C.2
- estimates of hydrological resources.

SURFACE TRAJECTORY MODEL FOR CONTINENTAL SHELF WATERS*

by

J. E. Overland
J. A. Galt

National Oceanic and Atmospheric Administration
Environmental Research Laboratories
Pacific Marine Environmental Laboratory
Seattle, Washington 98105

ABSTRACT. A comprehensive surface trajectory model has been developed for the northeastern Gulf of Alaska continental shelf that includes three elements: surface wind drift, barotropic currents (wind driven), and baroclinic currents (density driven). To provide regional winds, previous synoptic climatologies were specialized for the segment in proximity to the high coastal mountains. Currents are provided by a finite-element diagnostic shelf circulation model, which assumes that currents are a combination of geostrophic and Ekman flows as modified by bathymetry. The diagnostic model is decomposed into density-driven and wind-driven components. A set of barotropic current patterns were developed to correspond to each one of the weather types of the synoptic climatology. In a trajectory scenario, a sequence of weather types are selected from synoptic weather charts, the magnitude of the pattern is scaled by a single anemometer record, and the density fields are provided by recent hydrographic surveys. Dispersion of trajectories in the Gulf of Alaska is quite large and bimodal. Temporal variation of the wind plays an important role as well as the spatial variation of the relative magnitude of wind-driven and density-driven drift.

1. Introduction

The Northeast Gulf of Alaska (NEGOA) area is situated in the northern bight of the Gulf of Alaska, with the present area of interest centered on the continental shelf between Yakutat and Montague Island (Fig. 1). The shelf topography is quite complex with many small- and intermediate-scale features (5-50 km). On a large scale, the shelf is relatively narrow east of Kayak Island and comparatively broad west of that point. The shelf break, as indicated by the 100-fathom contour, is irregular and gives the shelf domain a very complex shape. The coastal morphology is dominated by mountains, and the weather patterns and coastal winds show evidence of significant orographic influence. For many years this region saw very few sytematic oceanographic studies, but with the advent of potential offshore gas and oil development a series of studies was initiated. These have included the repeated mapping of state variables with CTD or STD cruises, moored current-meter deployments, Lagrangian drifter studies, installation of bottom-mounted pressure gages, coastal meteorological studies, and the placement of large weather buoys within the study area.

*Contribution No. from the NOAA/ERL Pacific Environmental Laboratory

Early studies have shown the relationship of the NEGOA area to the larger scale current of the Gulf of Alaska (Favorite, et al. 1976). More detailed studies of the shelf circulation proper were presented by Galt and Royer (1975) and Royer (1978). The relationship between the bottom pressure distribution across the shelf off Icy Bay and the local currents has been investigated by Hayes and Schumacher (1976) and by Hayes (1979). The Lagrangian current measurements from drogue studies have been described by Royer, et al. (1978). In addition to these recent oceanographic studies, the regional meteorology has also come under scrutiny. The coastal region has been investigated by Reynolds, et al. (1978) with particular attention being directed towards the description of the nearshore wind regime. Starting with earlier work by Sorkina (1963) and Putnins (1966), Overland and Hiester (1979) extended the climatology for the Gulf of Alaska with weather typing studies concentrating on the definition of a set of inclusive patterns for the synoptic scale pressure field and their relationship to the regional wind fields.

A great deal of new information has become available about the NEGOA region within the last few years, and it now possible to qualitatively describe many of the features of the general flow. In addition a number of dynamic processes have been identified and in some cases can be quantitatively documented. The off-shelf region is under the continuing influence of the general Gulf Alaska circulation, and its baroclinic signature is clearly evident over the continental slope and shelf break. Coastal runoff and precipitation also induce baroclinic fields that are clearly seen to influence the near shore region over the shelf. Over the shelf proper, the regional winds set up a barotropic response with a much shorter adjustment period than is evident in the internal density field and in the resulting density-driven currents. In all cases, the irregular bathymetry appears to have a significant effect by channeling the flow.

The object of this study is to synthesize available meteorological and hydrographic data by means of a diagnostic current model and a comprehensive trajectory model.

2. Wind Fields

Among the processes that control the movement and spreading of spilled oil, a major component is the wind. The wind generates a local surface wind drift, which advects any floating pollutants. In addition the local wind transfers momentum to floating oil indirectly through wave and stress interactions. Although neither one of these local wind effects is completely understood, the net movement of the oil can be reasonably parameterized in terms of the wind. The wind also enters the trajectory problem through the regional forcing of shelf circulation; the wind blowing across the shelf sets up the sea-surface slope, creating a pressure gradient that drives the flow. To fulfill these requirements for both regional wind patterns and detailed local wind vectors, a regional meteorological synoptic climatology was developed for NEGOA (Overland and Hiester, 1979).

Six subjectively derived weather types have been established for the Northeast Gulf of Alaska (NEGOA)-Kodiak Island region, which are subdivided into thirteen subtypes. These six patterns were derived from combining and

modifying patterns from two previous studies by Sorkina (1963) and Putnins (1966), subjective analysis of fall 1977-summer 1978 sea-level pressure charts from the National Meteorological Center, and post modification of patterns based upon daily typing of candidate patterns. Post analysis indicated the necessity of including subtypes. Subtypes contain the same general distribution of features and meteorological basis as a type but represent slight variations in locations of features, which cause changes in the orientation of the geostrophic wind at the central location of the NEGOA coastline.

The six types represented by thirteen subtype patterns are summarized by Table 1. Figure 2 shows a sample pressure pattern for type 1.0.

Small scale local wind patterns have been investigated by concentrating on the processes that modify the larger scale synoptic patterns in the planetary boundary layer and in coastal regions. Included in these studies were the results of one-and two-dimensional boundary layer models, as well as the results of observational studies of coastal winds (Reynolds, et al., 1978). The final wind patterns chosen to represent the NEGOA region are based on the studies. Figure 3 shows the local wind pattern that corresponds to the synoptic pattern type 1.0.

3. Shelf Current Model

In this section the linear decomposition of the diagnostic model equations are briefly reviewed, and the relationship of these component flows to the input data and assumptions is outlined. A more detailed description of the linear aspects of model formulation and the rationale for this partitioning are presented by Galt and Watabayashi (1978).

The basic governing equation for the diagnostic model describes the dependent variable, the surface elevation, as follows:

$$N_2\nabla^2\xi - J(\xi,d) + N_1N_2\nabla^2\alpha - N_1J(\alpha,d) - k\cdot\nabla\chi\tau = 0 \qquad (1)$$

where

ξ = surface elevation

d = depth

α = the integral of the density from the bottom to the surface

$k\cdot\nabla\chi\tau$ = curl of the surface wind stress

N_1 = stratification parameter

N_2 = bottom friction parameter

All of the terms in this vorticity equation are scaled and nondimensional. The first term represents the vorticity stretching caused by the barotropic mode, depth-independent flow created by pressure forces of variations in the surface elevation driving a bottom Ekman layer. The second term represents the interaction of the barotropic flow with the bottom and describes the vorticity stretching caused by the flow crossing isobaths. The third term represents vorticity stretching of the baroclinic mode, evaluated at the bottom. This flow, created by the pressure forces of the internal mass distribution, drives a bottom Ekman layer. The forth term represents the vorticity induced by the joint baroclinic and bathymetric interaction and is seen to relate to the stretching caused by the baroclinic component of the flow crossing isobaths. The last term is the curl of the wind stress, or the vorticity added by the wind.

As the system is linear, a decomposition of solutions is possible. The following two problems can be considered:

$$N_2\nabla^2\xi_1 - J(\xi_1,d) - k\cdot\nabla\chi\tau = 0 \tag{2}$$

and

$$N_2\nabla^2\xi_2 - J(\xi_2,d) + (N_1N_2\nabla^2\alpha - N_1J(\alpha,d)) = 0 \tag{3}$$

The total solution is the sum of these two component solutions, i.e.,

$$\xi = \xi_1 + \xi_2 \tag{4}$$

We refer to the problem defined by the first of these equations as the wind set-up component and to the problem defined by the second equation as the density-driven component.

Regarding first the wind set-up component of the flow, we define appropriate boundary conditions and apply the finite element solution technique described by Watabayashi and Galt (1978). To develop these boundary conditions for the NEGOA area, we make a number of assumptions.

As a point of departure the curl of the wind stress is considered negligible for the region. This is done for two reasons: first, the actual data available on regional wind stress curl on this scale is practically nil (Bakun, 1973); and second, the direct local set-up of the cross-shelf sea-surface slope by along-shore winds is the dominant wind forcing. To parameterize the relationship between the wind and the cross-shelf component of the sea-surface slope, we hypothesize a bathystrophic balance. A bathystrophic balance assumes that the along-shore component of the wind stress is locally balanced by the along-shore component of the water stress and that the normal component of the sea-surface gradient is in geostrophic balance with the along-shore current. Such a response has been suggested for other areas in the past (Beardsley and Butnman, 1974). In specific studies of the NEGOA area, Hayes

(1979) suggested that such a linear cross-shelf hinge profile accounts for a major segment of the variance observed in the bottom-pressure measurements. For a more detailed discussion, refer to Galt and Watabayashi (1978).

The question of where to apply the hinge profiles to drive the wind set-up response of the model requires careful consideration. Obviously the wind acts as a continuum along the coastline, and at any coastal boundary point we could impose a uniform slope through a line of stations leading away from the shore. Solving the model with this single imposed hinge profile will give the regional response to forcing at this location. To combine a number of these is straightforward, since it is possible to consider any single hinge profile as the Green's function response to an imposed bathystrophic profile.

For example, suppose that

$$R(x, y, S_0)$$

is the model response to a unit amplitude hinge imposed on the coastline at point S_0, and that

$$W(S)$$

is the distribution of alongshore wind specified along the coastline, with S representing distance along the coast. Then the total wind set-up response is the superposition

$$\xi_1(x, y) = \int_{\text{coast}} C\, R(x, y, S) \quad W(s)\, ^2\cos(\phi_s)ds \tag{6}$$

where C is the constant relating wind speed to hinge amplitude.

For the present NEGOA study, the numerical approximation to this integral formulation will be made with six simple hinge modes, each of which is seen to influence specific segments of the shelf domain. Figure 4 shows the barotropic response to hinge No. 1. The relative magnitude of the hinges are determined for each synoptic weather type. Figure 5 shows the composite currents for weather type 1.0.

It should be pointed out that the Green's function formulation outlined here does not result in a composite pattern that has a uniform cross-shelf profile everywhere. Instead each cross-shelf profile is influenced by its neighbors, taking into account alongshore variations in the wind, bathymetry, and model dynamics.

A final point to consider with the wind set-up response is that alternate strategies are possible for determining the relative hinge weights in the composite patterns. For example, if sea-surface elevations were available at n locations along the coast, the Green's function integral could easily be inverted to solve for the coefficients associated with n independent hinge modes, whose composite would satisfy the observed coastal distribution, consistent with the model dynamics.

It is now possible to consider the second partition of the diagnostic mode, the density-driven response. This is represented by Equation (3), in which it can be seen that the density distribution acts as forcing through two terms: the baroclinic bottom Ekman layer, and the joint baroclinic-bathymetric interaction. Both of these can be seen to induce vorticity to the barotropic flow either through cross-isobath flow or through stretching of the water column. This ξ_2 component of the sea-surface displacement (a barotropic mode) is required; in fact any given density-driven flow will in general result in some stretching of the water column through these bottom interactions. In the presence of this stretching, some barotropic adjustment is required to satisfy model dynamic constraints, even in the absence of wind set-up or forcing.

An examination of Equation (3) shows that

$$\xi_2 + N_1\alpha^* = \text{constant} \tag{6}$$

is a solution for the interior of the domain, where α^* is the pressure deviation defined for any region as

$$\alpha(x, y, z) = \alpha'(z) + \alpha^*(x, y) \tag{7}$$

The solution given by (7) has a number of characteristics of interest. Galt and Watabayashi (1978) have shown that this solution corresponds to a minimum potential energy of the sea-surface distribution ξ_2 that is consistent with the model dynamics over an extended open shelf domain. This minimum barotropic mode forced by the density field signifies physically that for an unforced region, with a fixed density distribution, one would expect the sea surface to relax, or set-down, as much as possible, consistent with the dynamic vorticity constraints. It can also be seen that (3) yields a solution that gives a terrain following level of no motion because the baroclinic and barotropic flow cancel out at the bottom over the entire domain. This, then is a natural extension of the level of no motion concepts that are routinely applied in deep water off of the shelf. The minimum potential energy barotropic mode can also be seen to represent the minimum bathymetric interaction mode. It should also be noted that (7) is the only possible inviscid solution to Equation (3), and that as such it is the only possible unforced, steady state solution that could be expected. Figure 6 shows the baroclinic currents for density data from July 1974.

4. Trajectories

In physical terms, the trajectory model is composed of several FORTRAN programs and a variety of data sets that depict the spatial and temporal variability of the wind and current. The main trajectory program calculates the boundary location of an oil spill given wind and current time series, wind and current patterns, and starting date and locations. The output from this program is converted to graphical plots of the trajectories. An auxiliary output is also available which can be used to generate stick plots of the wind and current time series as seen at the wind and current stations and at the simulated spill.

Figure 7 shows the method used to synthesize the local wind velocity. The surface-wind fields from the climatology were utilized to provide the relative magnitude and the direction of the local wind. The absolute magnitude of the local wind was obtained by scaling the field with an anemometer station. The factor formed from the ratio of this scaling was then applied to the wind velocity throughout the region. Thus, if the wind field showed a wind velocity of 12 m s^{-1} to the NW at the spill coordinate, and if the nominal wind speed at the anemometer location was 10 m s^{-1} whereas the observed wind was 5 m s^{-1} averaged over twelve hours, the wind field would be scaled by (5 ÷ 10), resulting in a modeled wind of 6 m s^{-1} to the NW at the location of the spill.

Hourly perturbations were then added to the scaled wind-field velocity to simulate the higher frequency changes. These perturbations were calculated by first determining the differences between the hourly time series velocity and the scaled wind-field velocity at the anemometer location. This perturbation was then resolved into components lying along and normal to the vector of the wind field velocity. These components were then scaled by the ratio of the wind field speed at the spill position and the wind field speed at the anemometer. Finally, the perturbations were added in the along and normal direction relative to the local wind velocity at the spill. Thus in the example above a perturbation of 1 m s^{-1} lying to the left perpendicular of the wind-field velocity at the anemometer station would be scaled by (12 ÷ 10) and added to the local velocity in the left perpendicular direction. In this case, the direction of the perturbation is towards the SW since the field velocity was to the NW, and the amplitude is 1.2 m s^{-1}.

Releases are simulated at a rate of one per day during July 1974. Sample trajectories from site 6 are shown in Figure 8 and show a wide scatter, but appear to fall into several classes. The majority appear to be trapped in the gyre circulation west of Kayak Island and eventually end off the west coast of Kayak Island and along the Copper River delta. A second class moves west north of Middleton Island and then northwest towards Hinchinbrook Island. One trajectory diverges from the pattern and is seen to move east for about three days, eventually going ashore halfway to Icy Bay. Drifter data was not available for July 1974 although drifters in July 1975 (Fig. 9) show similar features as the model trajectories.

ACKNOWLEDGEMENTS

R. J. Stewart and C. H. Pease developed the trajectory algorithms. Glen Watabayashi and Thomas Hiester contributed to the diagnostic modeling and synoptic climatology. The major fraction of the support for this project was provided by the Outer Continental Shelf Environment Assessment Project (OCSEAP). This paper is a contribution to the Marine Services Program at the Pacific Marine Environmental Laboratory.

TABLE 1

Type	Description	Sorkina Type	Putnins Type	Dominant Season
I	Low in Gulf of Alaska	4c	A', A_1, G, H	Winter
II	Aleutian Low	5b	A, C, E, A_c	Winter, Spring, Fall
III	High pressure in Alaskan Interior	6a	D, B, D	Winter
IV	Low pressure center over Central Alaska	1a	A'', A_3, F	Summer
V	Pacific Anticyclone	1b, 5a	A''', A_2, E', E_1'	Summer
VI	Stagnating low off of Queen Charlotte Islands	7a	D', E'', E_1, F_1	Spring, Fall

REFERENCES

Bakun, A., 1973, Coastal upwelling indices: West coast of North America NOAA Tech. Report, NMFS SSRF - 671, 103 pp.

Beardsley, Robert C. and Bradford Butman, 1974, Circulation on the New England continental shelf: Response to strong winter storms, Geophy. Res. Letters 1 (4), 181-184.

Favorite, F., A. J. Dodimeand and K. Nasu, 1976, Oceanography of the Subartic Pacific region, 1960-71 Bull. Int. N. Pac. Fish. Comm., 33, 187 pp.

Galt, J. A., and Glen Watabayashi, The linear decomposition of a diagnostic shelf circulation model and discussion of alternate boundary condition formulations, 1979 Unpublished manuscript.

Hansen, D. V., 1977, Lagrangian surface currents, Annual report to the Outer Continental Shelf Environmental Assessment Program, NOAA, ERL, Boulder, CO.

Hayes, S. P., 1979, Variability of currents and bottom pressure across the continental shelf in the Northeast Gulf of Alaska, Journal Phy. Oc. (in press).

Hayes, S. P. and J. D. Schumacher, 1976, Description of wind, current and bottom pressure variations on the continental shelf in the Northeast Gulf of Alaska, from February to May, 1975. JGR 81 (36), 6411-6419.

Overland, J. E. and Thomas R. Hiester, A Synoptic Climatology for Surface Winds Along the Southern Coast of Alaska, 1979 Unpublished manuscript.

Putnins, P., 1966, The sequence of baric pressure patterns over Alaska. Studies on the meteorology of Alaska 1st Interim Report, Washington D. C., Environmental Data Service, ESSA, 57 pp.

Reynolds, R. M., T. R. Hiester and S. A. Macklin, Coastal Meteorology of the Gulf of Alaska, Icy Bay to Yakutat Bay, 1979 Unpublished manuscript.

Royer, T. C., 1975, Seasonal variations of waters in the northern Gulf of Alaska, DSR 22, 403-416.

Royer, T. C., 1978, On the effect of precipitation and runoff on coastal circulation in the Gulf of Alaska, J. P. O. (in press).

Royer, T. C., Donald V. Hansen and David J. Pashinski, Coastal flow in the Gulf of Alaska as observed by dynamic topography and drogued drift buoys, 1979 Unpublished manuscript.

Sorkina, A. I., 1963, Tipy atmosfernoi tsirkuliatsii, Israel Program for Scientific Translations, Jersalem, 247 pp.

Watabayashi, G. and J. A. Galt, 1978, A finite element solution technique for a diagnostic shelf circulation model, 1979 Unpublished manuscript.

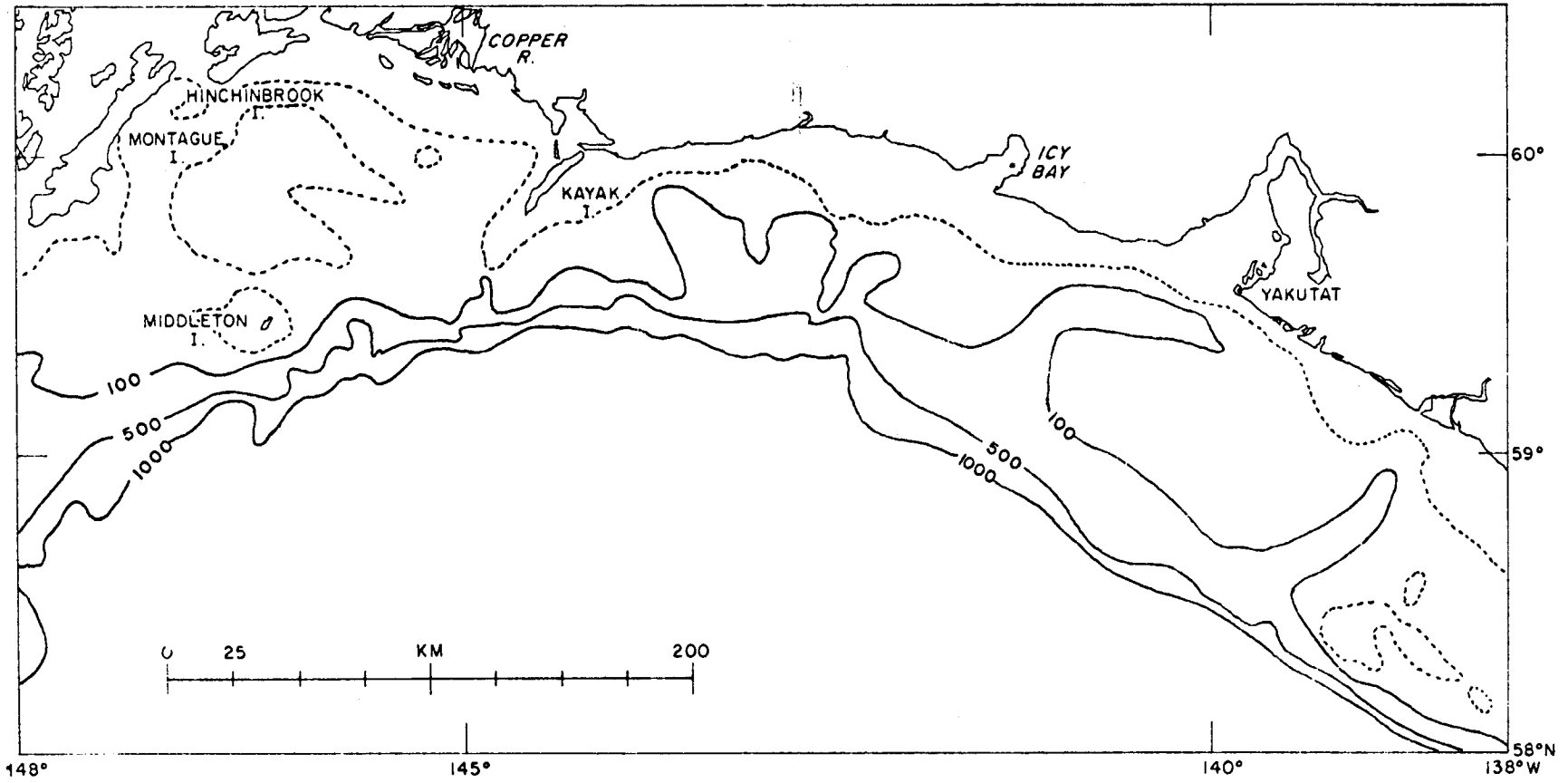

Figure 1: Northeast Gulf of Alaska study area. Depth contours shown in fathoms. Dotted contour represents 50 fathom curve.

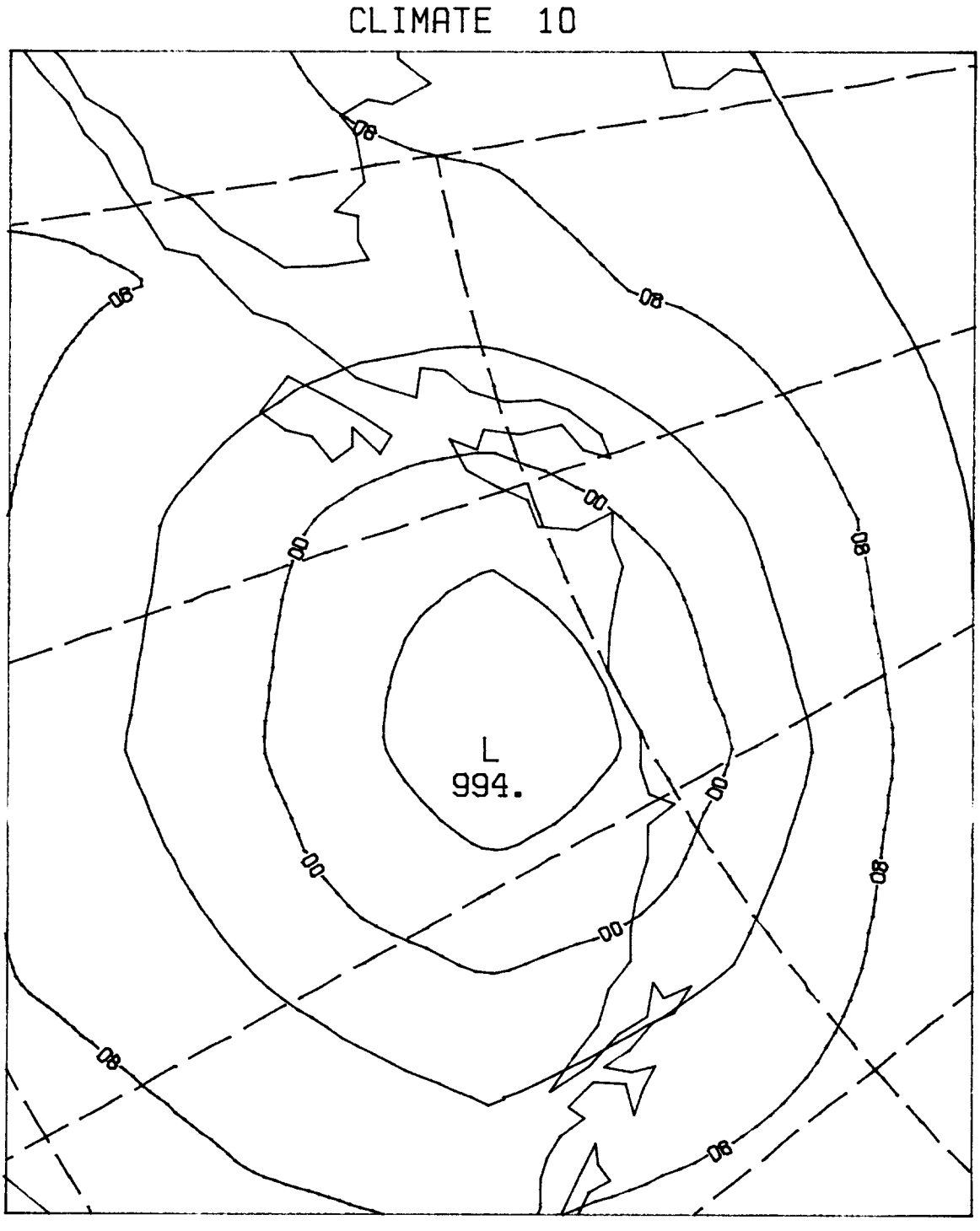

Figure 2: Subjective synoptic pattern type 1.0, low pressure centered south of the Alaskan coastline.

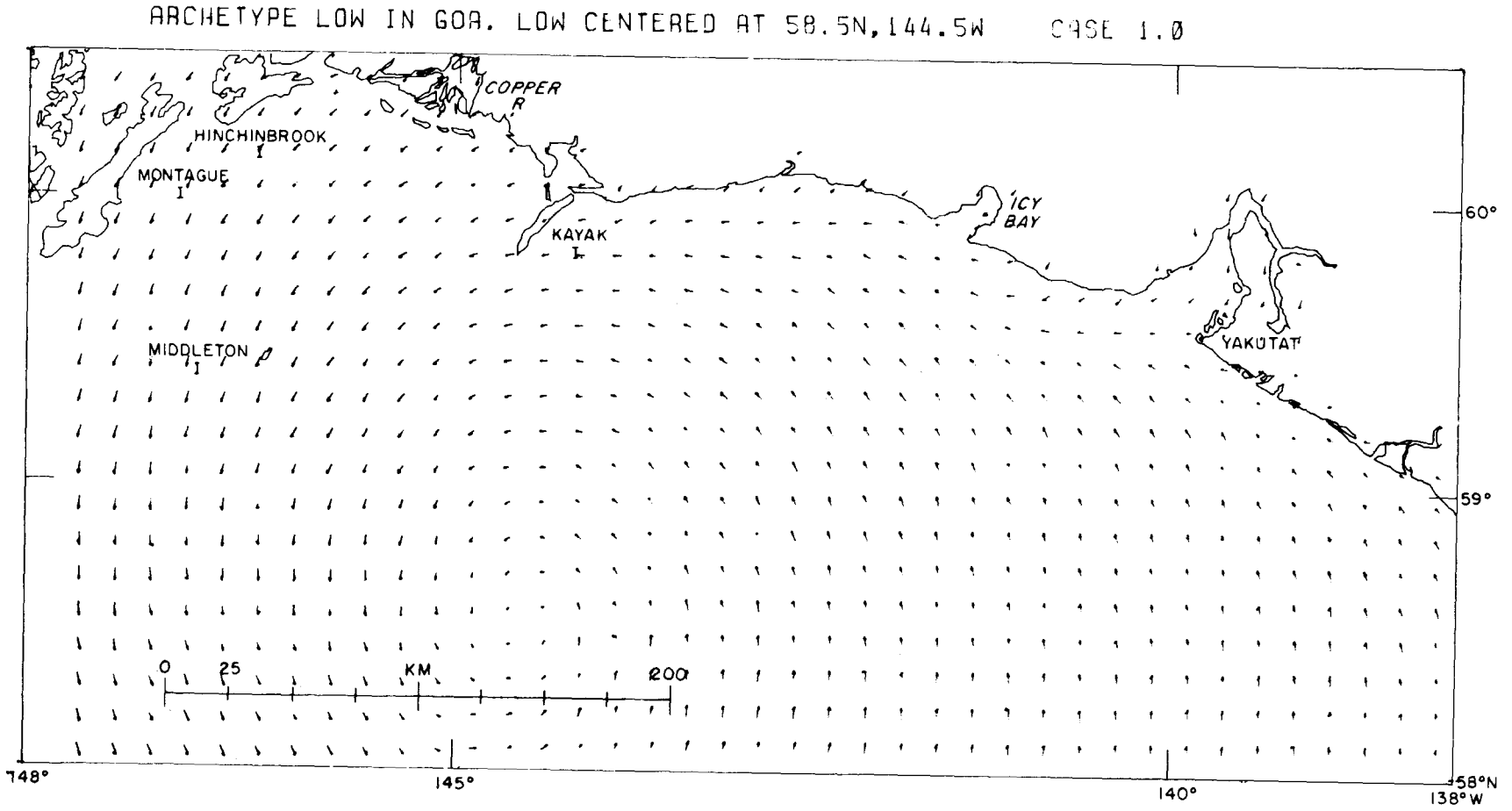

Figure 3: Local wind fields for synoptic weather type 1.0.

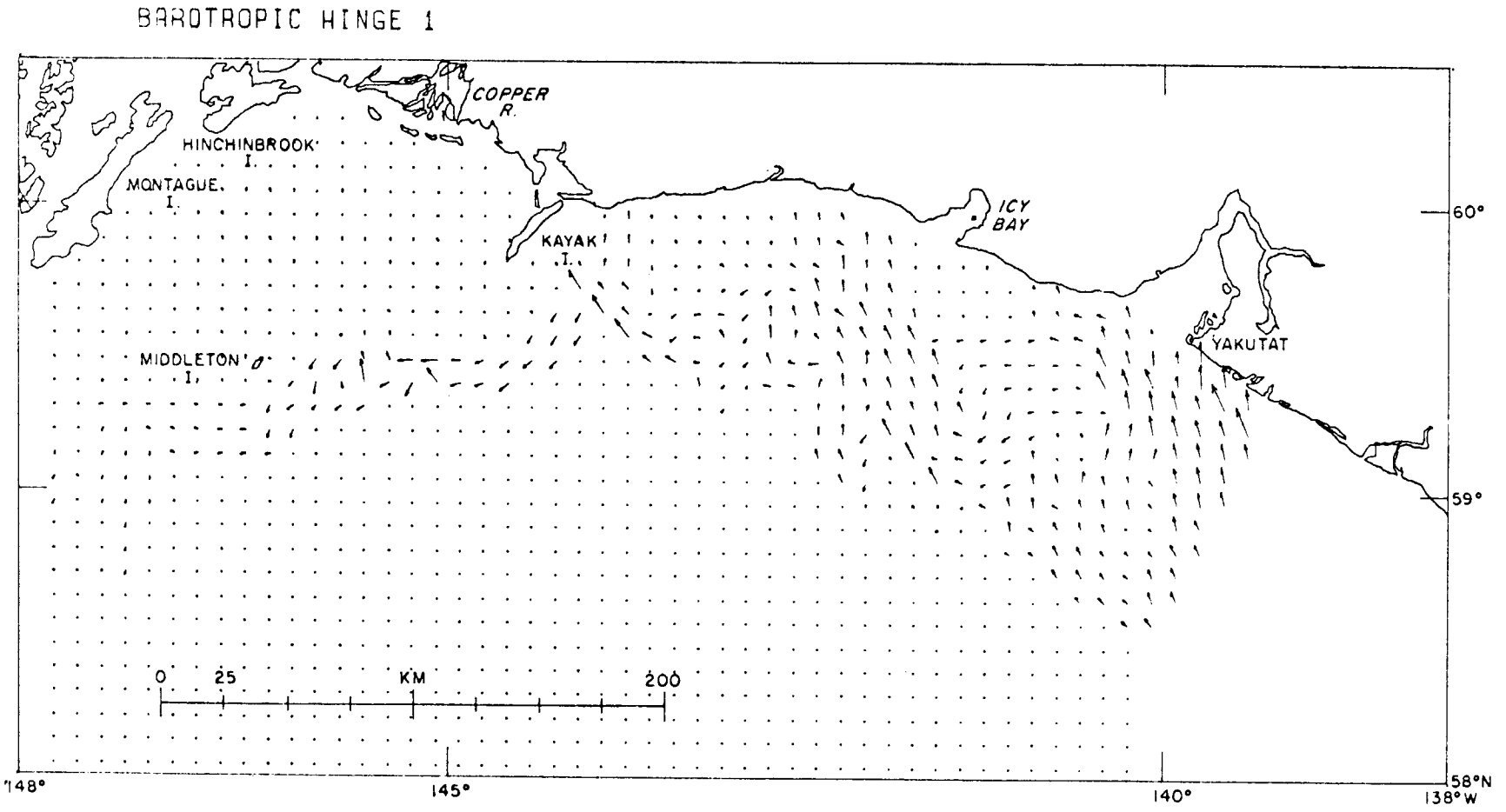

Figure 4: Bathystrophic wind set-up, or hinge mode one (Yakutat).

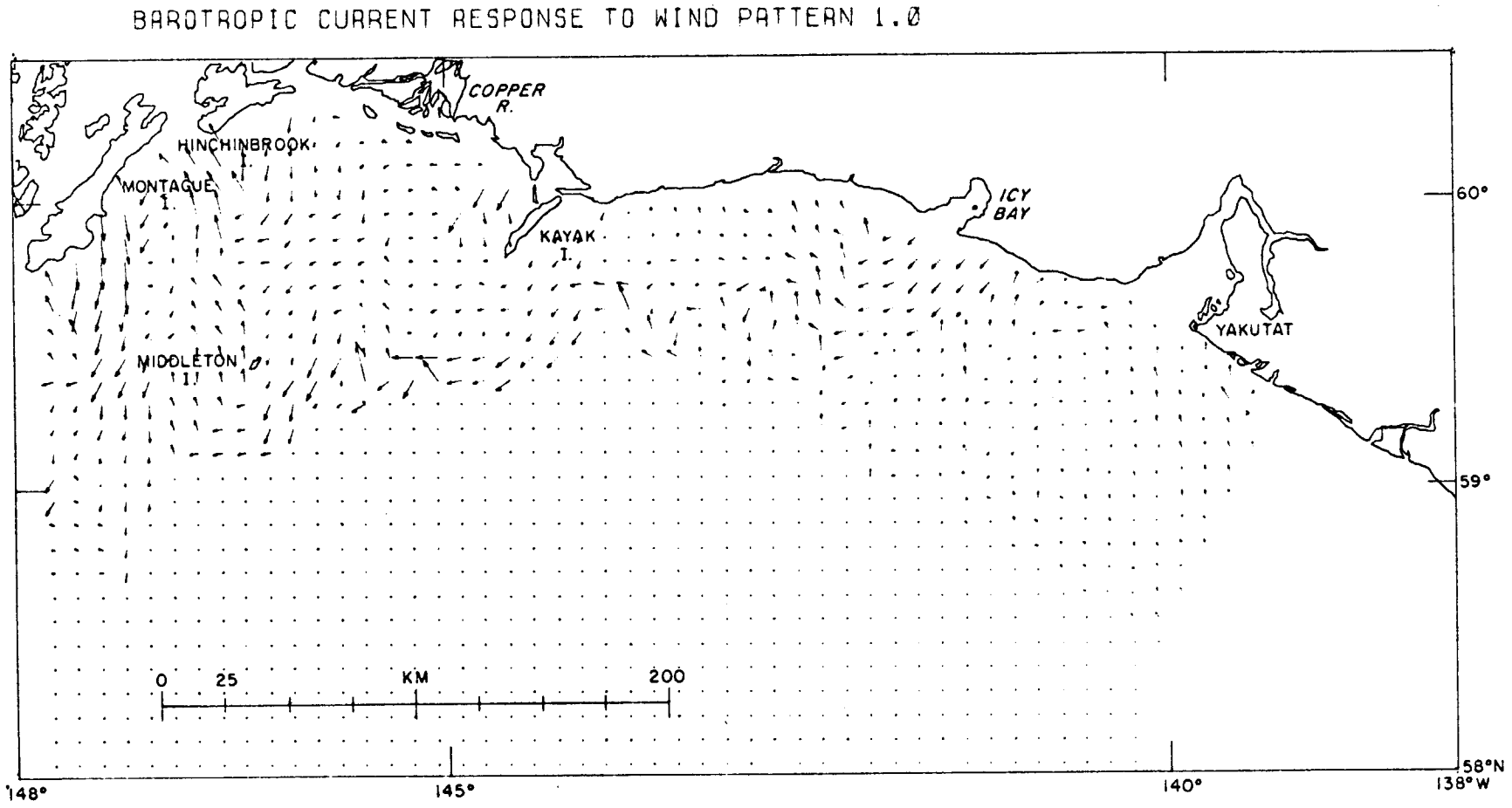

Figure 5: Composite wind set-up response for Northeast Gulf of Alaska weather type 1.0.

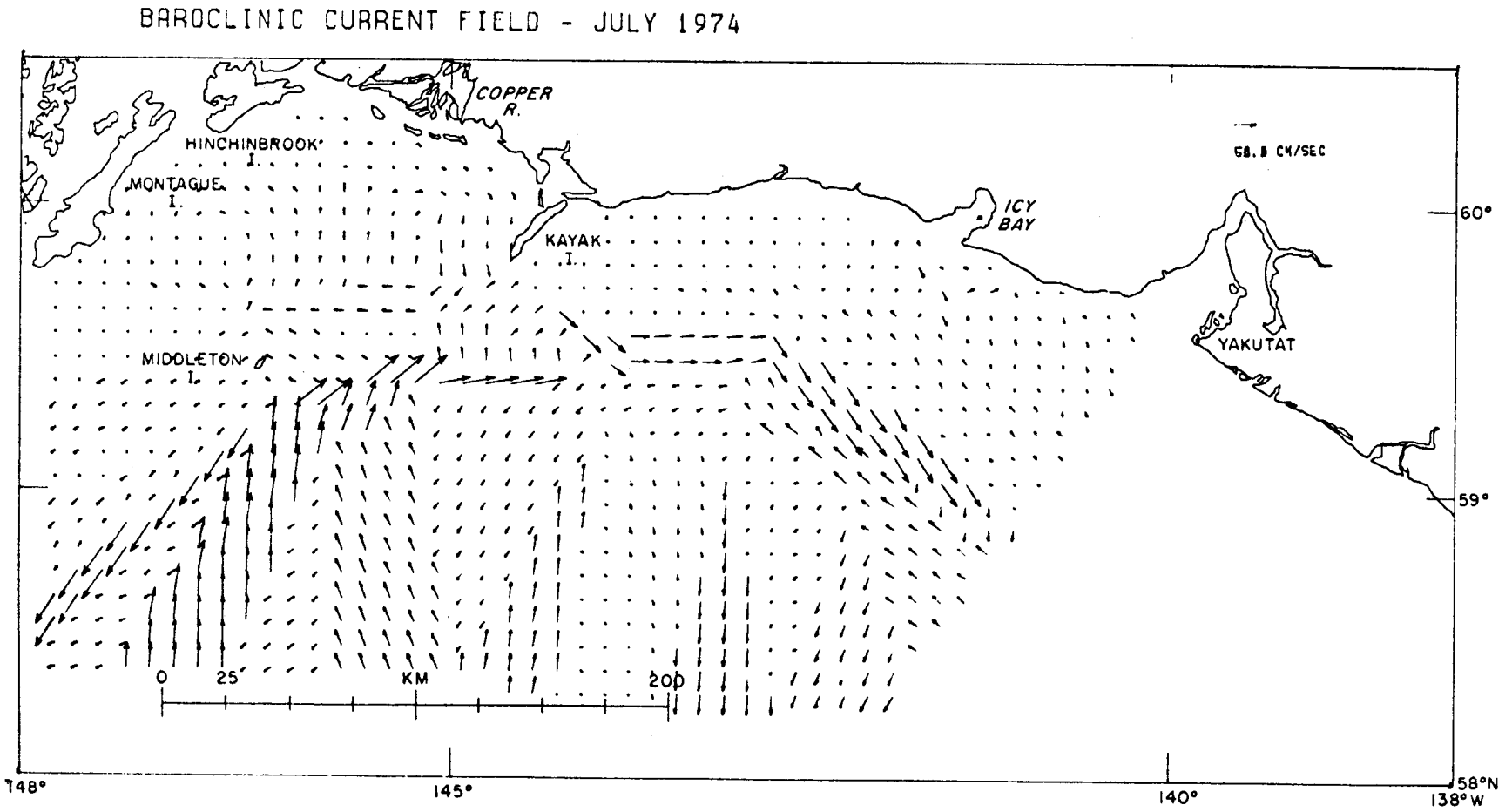

Figure 6: Density driven response currents for the Northeast Gulf of Alaska from data collected in July 1974.

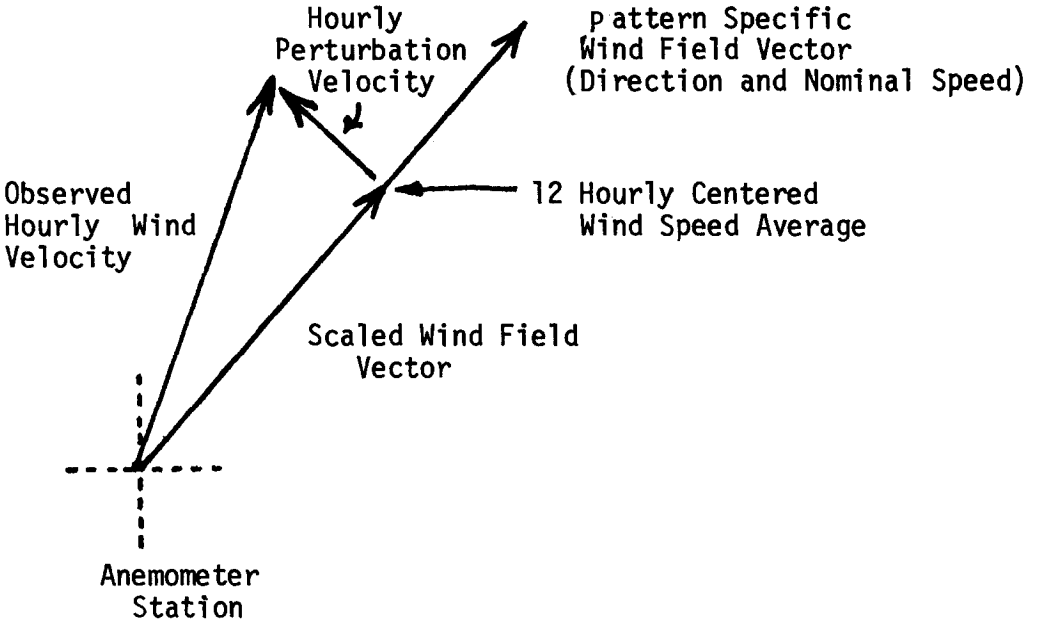

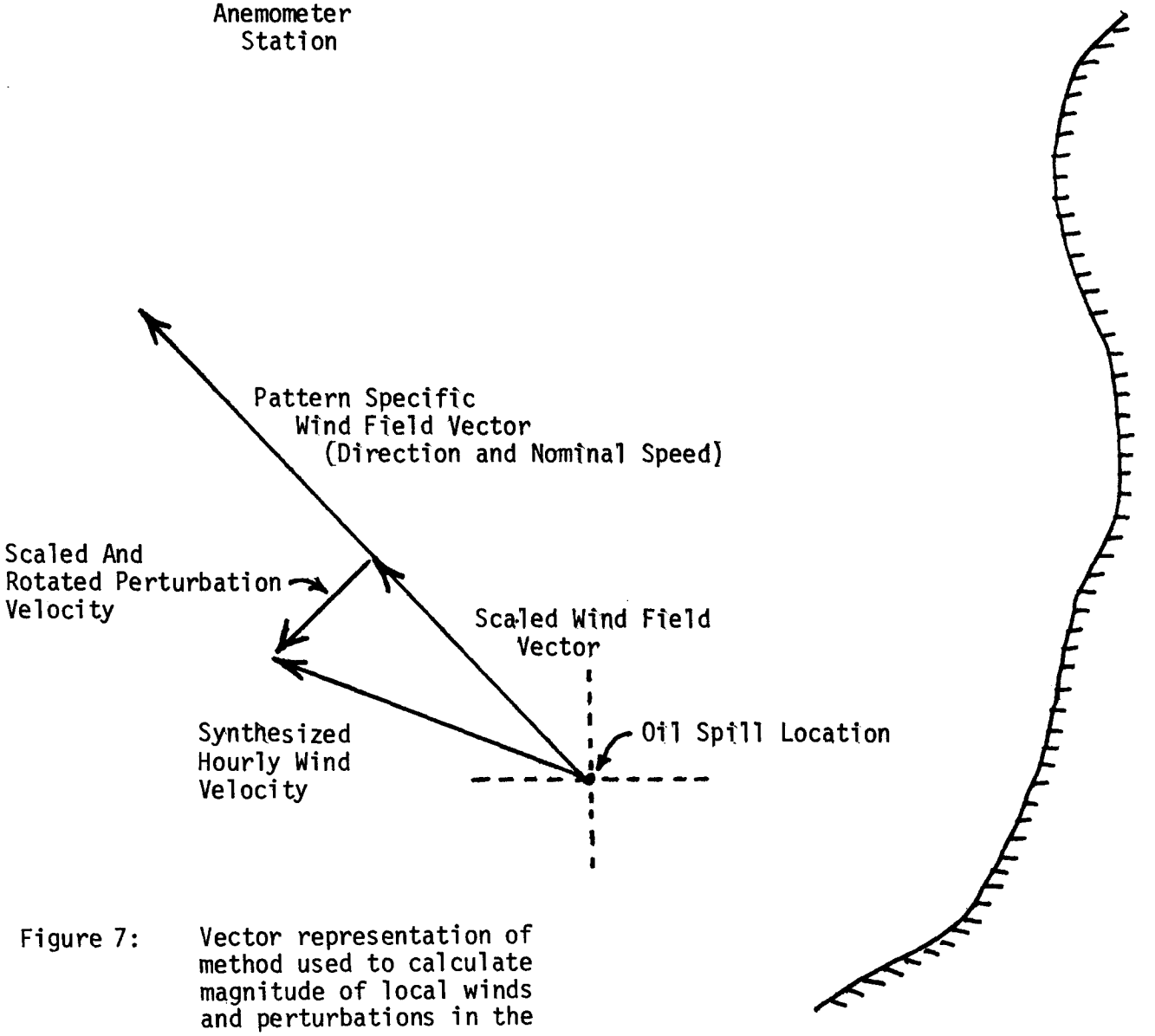

Figure 7: Vector representation of method used to calculate magnitude of local winds and perturbations in the wind field.

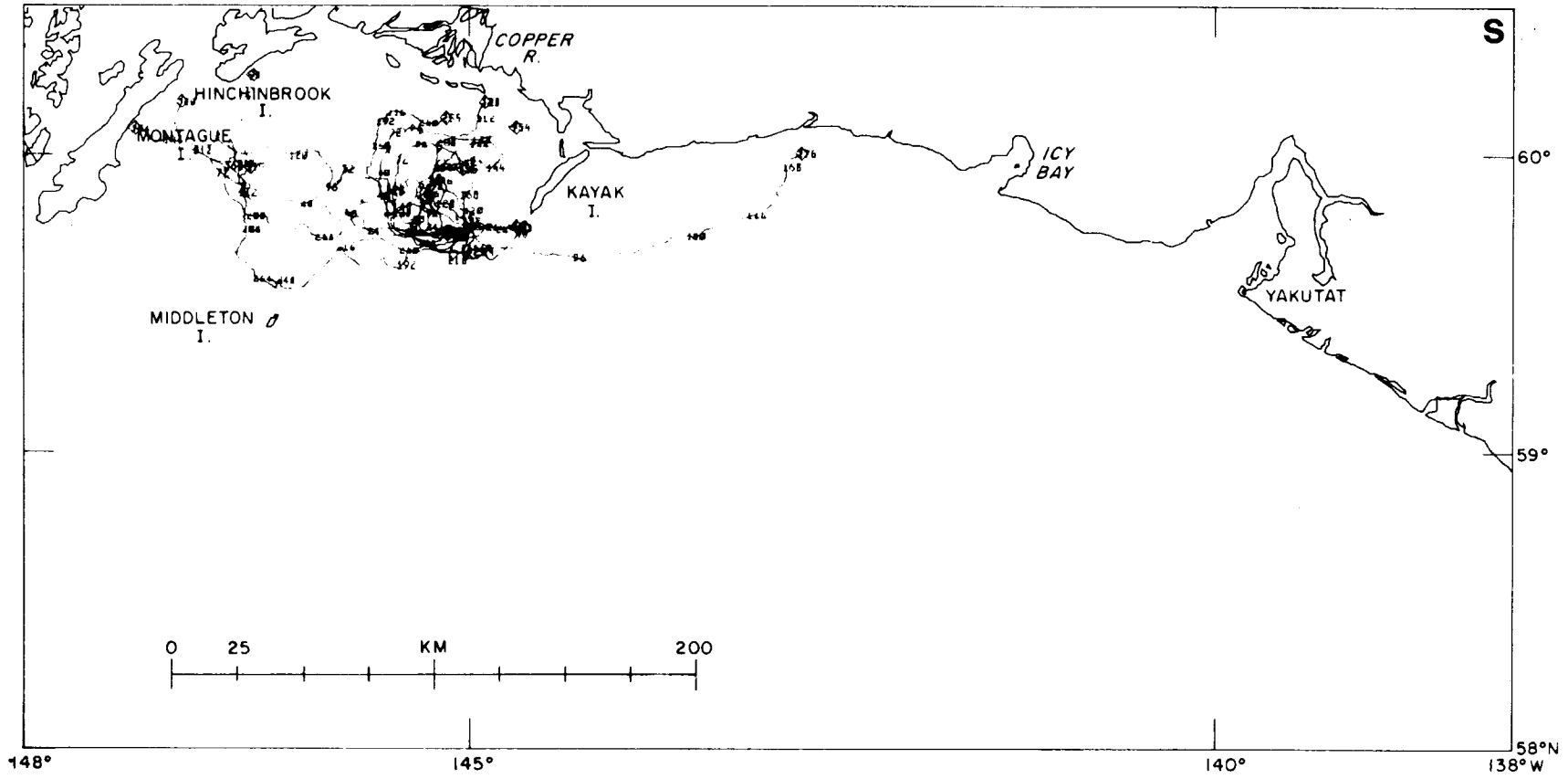

Figure 8: Summer trajectories released from site six.

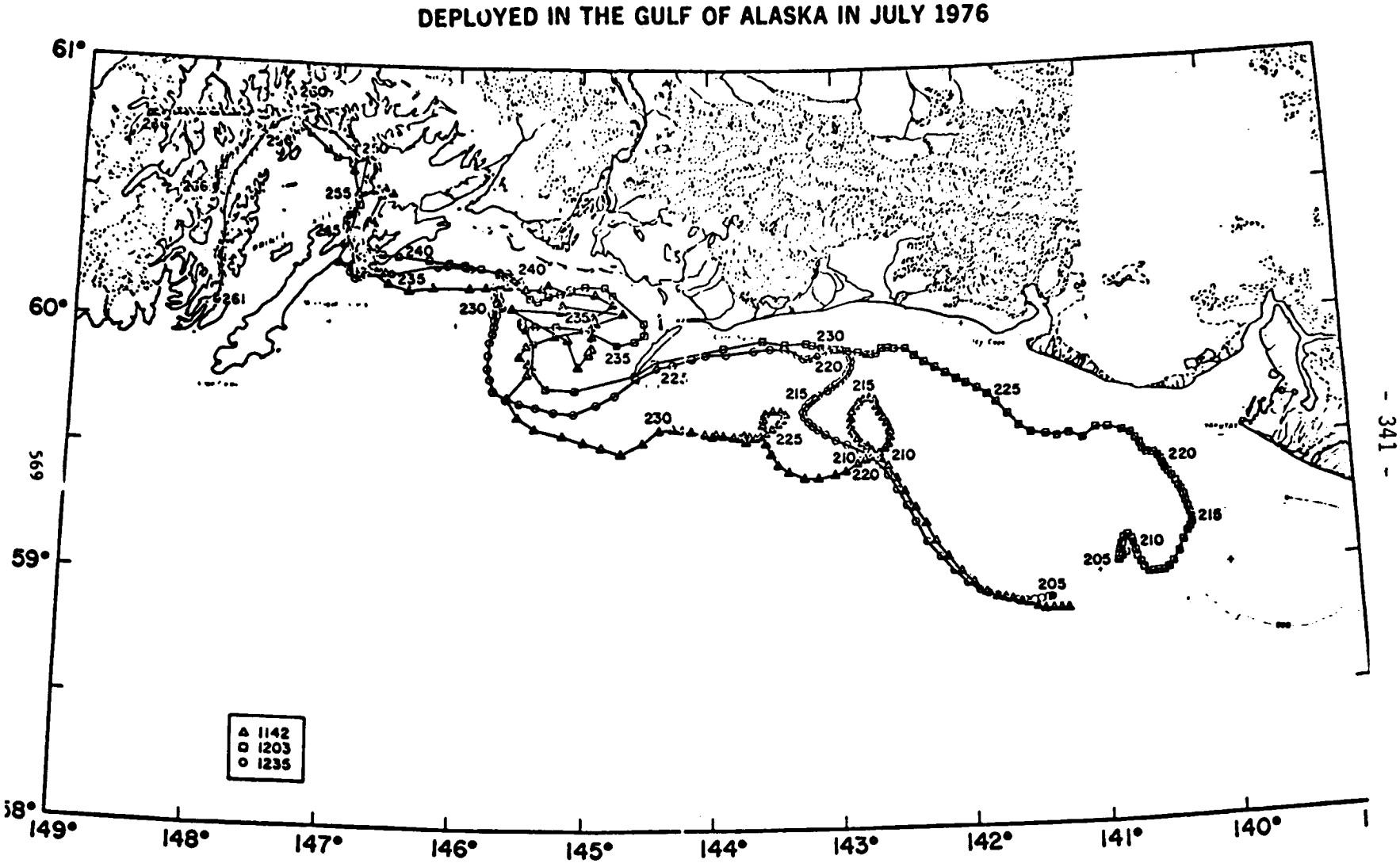

Figure 9: Drifter Trajectories NEGOA July 1976

THE REQUIREMENT FOR HYDROMETEOROLOGICAL SERVICES TO FISHERIES AIMED AT IMPROVING THE EFFECTIVENESS OF THEIR UTILIZATION

(V. PALKIN, V. CHUDOV, K.P. VASILIEV) *

The versatile production activities of the important branch of the USSR national economy - the fishing industry, its coastal enterprises and the numerous fishing transport as well as scientific-search fleet is impossible without accurately organized, permanently improving hydrometeorological services.

The conditions which were created for fisheries in the World Ocean posed a number of problems and requirements for reconstruction of the operations of the fishing industry as well as the scientific-search fleet aimed at studies and assimilation of new fishing areas of the World Ocean.

The effectiveness of fleet operations under new conditions calls for, amongst others, to solve the problem of permanent improving methods and forms of hydrometeorological services.

For the implementation of significant objectives posed by the fishing industry heavy emphasis is placed on:

a) the estimation of biological resources of the Southern Ocean (south of 40°S up to the antarctic ice edge) aimed at expansion of fisheries in these regions;

b) expansion of research activities in ice-free areas of the World Ocean;

c) continuation of investigations of raw material resources of continental slopes, in the first place, down to 1500-2000 m depths in the Pacific and Atlantic;

d) wide introduction of new fisheries instruments into the fishing fleet.

The fishing industry fleet of the USSR continues to develop and replenish by new, above all, large-capacity vessels. The middle- and small-capacity fleet for fisheries in coastal areas and internal water bodies is being developed as well.

---

* USSR Ministry of Fisheries and the Hydrometeorological Centre of the USSR

Such development of the fishing fleet, the fisheries as a whole, poses additional tasks in hydrometeorological services to their activities both for ensuring the safety of navigation and fisheries and for rising the effectiveness of fisheries activities.

In parallel with technical measures, rising the quality of hydrometeorological services to fisheries as well as to operations of scientific-search vessels and ships of coastal fisheries becomes of growing importance.

Hydrometeorological services to the fleet of the USSR Ministry for Fisheries is organized by the USSR State Committee for Hydrometeorology and Control of the Natural Environment (Goskomgidromet) in conformity with the General Agreement. This Agreement is specified by local agreements between the Goskomgidromet and local fisheries authorities taking into account local features and "Plan-schemes of hydrometeorological services" coordinated with user's organizations.

The Hydrometeorological Service, as a whole, its Hydrometeorological Centre, weather bureaus, hydrometeorological bureaus, hydrometeorological observatories, weather ships, operational hydrometeorological (synoptic) groups are of great assistance to the fisheries fleet operating in remote areas of the World Ocean in severe hydrometeorological conditions, are assisting in fulfilling the plan of fish and marine products catch as well as in ensuring the safety of navigation.

An example: the recently issued "Measures for ensuring safety of navigation of ships of the Antarctic scientific-search fisheries expedition" have been developed jointly with the Goskomgidromet.

Realization of these measures is the responsibility of the Ukrainian Administration of the Hydrometeorological Service, the Far East Research Hydrometeorological Institute, the Weather Bureau of the Antarctic Molodezhnaya station which compile weather forecasts and storm warnings for ship navigation areas, provides ice condition information.

Problems have been solved concerning organization of hydro-

meteorological services to fisheries expeditions operating in the Scotia Sea in the South Atlantic as well as in the Central Atlantic.

Weather and ice conditions forecasts,compiled by bodies of the Goskomgidromet,are of great significance for fisheries in the Labrador region in wintertime under severe hydrometeorological and ice conditions.

The existing system of hydrometeorological services to ships of the fisheries fleet is mainly adequate for the fishing industry. This system provides broadcasts of weather forecasts, storm warnings, ice and other hydrometeorological information, facsimile weather and sea state charts.

Secondment of experts of the Hydrometeorological Service, as a part of operational groups in the fishing regions, is of great effectiveness. This kind of hydrometeorological services became widespread in our country. From our viewpoint, it is fully justified.

For the working of such operational groups aboard of large-capacity ships special synoptic deck-cabins are equipped where necessary facsimile and radioteletype apparatus are installed.

Much work is done for equipping of the fleet with facsimile apparatus. At present, more than 1000 ships are equipped with such instruments.

As it is known, ice accretion on ships is a dangerous phenomenon for fishing ships operating in wintertime in high and middle latitudes. This phenomenon caused damage to a number of ships of various countries due to loss of stability.

The USSR Ministry for Fisheries had carried out much work for introduction of organizing and technical measures directed to solution of that problem.

Great assistance in solving the above problem is given to the Ministry for Fisheries by workers of the Goskomgidromet.

They have studied the hydrometeorological conditions responsible for ice accretion on different types of fishery vessels, the ice distrubution onto various parts of ships in icing, the physical and chemical properties of ice, the degree of being splashed of vessels by sea water and other factors.

At present time, methods are developed of forecasting ice accretion on ships in basic sea and oceanic areas of fishing.

The weather routeing of ships when going to the fishing areas and returning home carried out by the Goskomgidromet bodies is an essential assistance in rising the effectiveness of using the fisheries fleet.

The weather routeing of towings of nonautomotive floating facilities, floating docks, repair ships as well as middle-capacity fishery vessels, often at large distances, for example, from the Black Sea to the Far East, gives a great assistance to the fisheries branch of the national economy.

From our viewpoint, there are still some shortcomings in hydrometeorological services to fisheries:

a) a number of cases is marked when the skill of weather forecasts and storm warnings is inadequate due to overestimation of the expected wind force; this causes loss of fishing time by vessels;

b) forecasts and warnings on the ice accretion on ships are often compiled not in the conformity with the existing Manual, i.e. the intensity of expected icing is not given;

c) the number of radio stations which transmit facsimile weather and sea state charts for fisheries is inadequate;

d) the number of radio stations which transmit weather forecasts and storm warnings for fishing areas on a round-the-clock basis is inadequate; the power of operating stations is small;

e) ice conditions reconnaissance data are inadequate and, in a number of cases, unavailable for separate fishing areas;

f) the number of deep sea hydrological observations in oceanic fishing areas is inadequate.

From our point of view, the following improvements are necessary in hydrometeorological services to the fisheries fleet operating in sea and ocean fishing areas:

a) it is rationally to continue and expand hydrometeorological services to fisheries expeditions by secondment of experts of the Hydrometeorological Service as a part of operational hydrometeorological groups on board the ship;

b) it is expediently to increase the number of radio stations which transmit facsimile weather and sea state charts for fishing areas as well as weather forecasts and storm warnings for ships on a round-the-clock basis;

c) the problem is to be solved on the production of a portable receiving facsimile apparatus for installation aboard of middle- and small-capacity ships;

d) deep-sea observations in ocean fishing areas, first of all, down to 1500-2000 m depths are to be increased appreciably. Observations available are inadequate for the assimilation of these depths;

e) ice observations from aircraft in remote fishing areas are of great significance for successful fisheries and safety of the fleet during wintertime;

f) hydrometeorological manuals should be further developed and introduced for use in the fisheries fleet;

g) those research and methodical works should be intensified which are oriented to improving weather forecasts and storm warning skill. Particular attention should be placed to forecasting ice accretion on ships and other hazardous and disastrous hydrometeorological phenomena;

h) with respect to a number of fishing areas, particularly for the South Kuril fishing area, there is a need for sea-surface temperature forecasts of the adjacent portion of the Sea of Okhotsk and North-West Pacific;

i) for compiling facsimile sea-surface temperature charts not only ship information is to be used but aircraft and satellite information as well;

k) the problem is to be solved on the equipping of all ships making hydrometeorological observations with automatic meteorological stations;

l) measures are to be taken for the expansion and improvement of the ship weather routeing and weather forecasting techniques;

m) the hydrometeorological services to the fleet operating south of 40°S (near-Antarctic waters) call for further improvement.

The development of the following techniques is necessary:

a) forecasting the ice edge in the North-West Atlantic for the autumn-winter months not less than 2 months in advance;

b) forecasting the ice edge in the Barents Sea for the period November-February;

c) manuals are to be issued on the hydrometeorological and ice regimes for the area of South Georgia and Orkney Islands;

d) the problem is to be solved on the allocation of additional frequencies (in some cases, the change of allocated frequencies) for rising the stability of facsimile charts reception as well as allocation of a common frequency for receiving hydrometeorological and navigational messages.

We hope that the solution of problems posed will promote rising the effectiveness of utilization of our fisheries fleet.

OCEANOGRAPHIC INFORMATION IN SUPPORT OF SCIENTIFIC STUDIES

by

prof. M.A. Petrosyants

Director, Hydrometeorological Centre
of the USSR

(Moscow)

The influence of the ocean on our life cannot be overestimated. It can be observed not only ashore but in the interior of continents and thousands kilometres from coasts the ocean affects the human activities. First of all, it is the vast impact of the ocean on climate and weather of our planet.

Recent meteorological studies show that changes in large-scale weather patterns over periods of weeks to many years are closely related to changes in the temperature distribution of the water layers near the surface of the sea. Because the sea behaves more sluggishly than the air, these observations indicate that improvements in long-range weather forecasting can be made through studies of the large-scale interactions between the oceans and the atmosphere. The present accuracy of long-range forecasting is low, but if it could be improved, great economic benefits would follow; for example, in planting and harvesting crops, in planning seasonal fuel transportation and storage, in the timing of building and road construction, and in flood and drought protection.

The atmosphere in which we live and the ocean of water beneath us are interlocked components of a great heat engine. The engine works to transport heat energy from low latitudes to high latitudes, where it is radiated into space. Much of the energy of the air - about one third - enters it through the condensation of water vapour evaporated from the sea surface. A large part of the remainder is transferred as sensible heat from the warm sea to cooler air. Evaporation and heating do not take place uniformly over the ocean nor are they uniform at any given latitude. They are high where the cloud cover is small and in those regions where the difference in temperature between the sea and the air is greatest.

The areas of maximum temperature difference between the surface ocean waters and the air shift in location and vary in intensity with time. Similarly, the regions where storms are born and the paths of storm travel appear to change with variations in water temperature near the sea surface. Because of its high heat capacity and massive inertia, the ocean can change only slowly with time. The persistence of weather patterns over periods of weeks to years may result, in part, from this sluggishness of the ocean.

The hope of improved long-range weather forecasting depends on our learning how to predict changes in persistent weather patterns. In so far as these patterns depend on patterns in the sea, it is clear that in order to gain greater understanding of the mechanisms of change we need to understand the large-scale interactions between the sea and the air.

Recent work has shown that anomalies in atmospheric circulation result in anomalies of ocean surface temperature. For example, with increasing winds of cold origin there is an increased transfer of sensible and latent heat from the ocean to the atmosphere and an increased stirring of the upper layers of the stratified sea. Both these processes result in a lowering of the sea surface temperatures. The restoring processes by which the sea surface temperature return to their"average value" come from a slow strengthening of the poleward-moving ocean currents near the sea surface. One unsolved problem is to determine the character and find the rate of the changes in the ocean density distribution that cause these poleward currents.

The large-scale interactions between the sea and the air need to be studied co-operatively by oceanographers and meteorologists. Time series of measurements at many points in the upper water layers need to be combined with continuous maps of cloud cover, winds,and atmospheric temperature distributions over the oceans. Many of these atmospheric measurements will come from weather satellites, but the measurements of the ocean waters will probably require the establishment of a network of buoys.

To attain the practical objective of improved long-range weather forecasts will require both meteorological and oceanographic research. The requirement has already been recognized. Responsibility

for the application of new knowledge to the problems of weather forecasting must, of course, rest primarily with the meteorologists, and in May 1967 the World Meteorological Organization presented and approved for implementation, a plan of World Weather Watch, covering the oceans as well as the land, to improve and extend the network of observing stations, and to carry out large-scale research. Complementary to this plan is the Intergovernmental Oceanographic Commission's recommendation of a year later to institute an Integrated Global Ocean Station System, the immediate purpose of which is to provide more extensive, timely,and synchronous information on the state of the world oceans as a whole, and the processes therein with a view to their prediction, the plan to be operated closely with that of the World Weather Watch.

Forecasting, however, is not, in and of itself, the only economic objective of modern atmospheric and oceanographic research. There is reason to hope that some aspects of weather and oceanic phenomena can be controlled, or at least anticipated sufficiently for safeguarding or ameliorative measures to be taken. The murderously destructive tropical storms, called hurricanes in the Atlantic and typhoons in the Western Pacific, are born and have their embrionic growth over the ocean. It is not impossible that these storms can be aborted in their early stages if a means can be found to prevent anomalously large transfers of heat energy and water vapour from the sea to the air in the regions of hurricane formation.

There are other natural disasters, i.e. disasters originating in natural causes, which might well be modified or limited, and in some cases even prevented, by improved scientific knowledge of the processes - the initiation and build-up - of atmospheric and oceanic forces, especially in their more severe manifestations.

In coming years, we shall need a greater degree of co-operation not only among marine scientists of different countries, but among different kinds of scientists - oceanographers, meteorologists, engineers, mathematicians, many kinds of biologists, geophysicists, astronomers, in fact all scientists who are concerned with the earth and the solar system as they are and have been.

RELIABILITY OF IGOSS BATHYTHERMOGRAPH (BT) DATA

by Irving Perlroth

Introduction

The U. S. National Oceanographic Data Center (US NODC) serves as a functional Responsible National Oceanographic Data Center (RNODC) and accessions IGOSS BATHY and TESAC data in GTS FM63 and 64 format from METRO Washington. The data are converted by the RNODC into the standard IGOSS SYNDARC archive format. Data services and analyses are performed from the OCEAN SYNDARC files. The purpose of this paper is to compare data in the IGOSS BATHY SYNDARC file at the RNODC with high resolution archived X-BT data in the US NODC.

A substantial volume of X-BT data accessioned at the US NODC is in analog strip chart form. These data originate from national and international activities. The digitization of the XBT analog is basically a two-fold process. The first stage is a prescreening of the strip chart for legibility and structure, which may indicate possible probe failure. The second stage is the actual digitization of the trace by use of an analog-digital recorder.

At the time of digitization the station identifying information is entered onto tape. The digitization is accomplished with a hand-guided stylus. The data are then passed through a series of logic edit and environmental quality control programs which flag such errors as: positional information, date-time consistency, ship speed, depths less than 0 or greater than 1,930 meters, temperatures less than -4°C or greater than 35°C, etc. A more comprehensive description of detailed quality control procedures will be discussed in the Environmental Quality Control Analyses section of this paper.

Data Sources

The data files used were obtained from the U. S. RNODC. The BATHY OCEAN SYNDARC file was initially provided by the U. S. National Meteorological Center (NMC) of the National Weather Service, Washington, D. C. in GTS message format. A total of 80,000 messages derived BATHY data are now on file at NODC. The US NODC archived data were used as the standard in the comparison with the SYNDARC data.

The BATHY OCEAN SYNDARC file used for the comparison of specific data points was comprised of only U. S. IGOSS-designated ships, because their analog strip charts-were available for digitization by the US NODC. Data analyzed were for the period 1974 to 1976. The data evaluated are from the following ships: FAIRWEATHER, DAVID STAR JORDAN, GLOMAR CHALLENGE, TANEY, DUANE, OCEANOGRAPHER, BIBB, EVERGREEN and CAMPBELL. The IGOSS BATHY SYNDARC file analyzed was originally transmitted via the World Weather Watch Global Telecommunications System (GTS). These data were

subjected to an initial analyses for transmission garble, completeness of message, etc. Duplicate observations (30-40%) were eliminated during conversion to SYNDARC format, but no other environmental or scientific quality control was applied. Some of the shipboard data were also available in the initial IGOSS BATHY log form. In addition, listings of BATHY SYNDARC data were screened by the author for gross error for the years of 1973 to 1976. Approximately 4,700 observations were reviewed which comprised data from various IGOSS participating countries and platforms.

Statistical analyses of the absolute mean percent error between the SYNDARC data points and the corresponding NODC archive data were computed. In general, the number of data points for the NODC archive observations exceeded those received through the BATHY SYNDARC file.

Data Analyses

IGOSS SYNDARC and US ship data were matched using the following criteria: ship name, date, time and position. Plots of observations from both files are represented in figures 1 to 7. Data from the BATHY SYNDARC file encoded at significant data points on shipboard from a XBT strip chart were plotted. The identical observation (the same XBT strip chart) digitized at the US NODC was also plotted on the same graph. Temperatures of BATHY SYNDARC depths were compared to temperatures at the same depths on the NODC digitized curve. Each BATHY SYNDARC XBT is represented by a solid line while each identical NODC archival X-BT observation is represented by a dashed line. Approximately 30 observational plots were used to determine temperature differences at the IGOSS encoded levels. Temperature differences can be attributed to a number of factors, transposition and transmission being just a few. The IGOSS curve shown in figure 1 (long dashed to solid curve), for example, indicates a surface temperature of 16.5°C. This is 0.7°C higher than the NODC high resolution surface temperature (short dashed). A check of the shipboard log for this observation shows an encoded surface temperature of 15.6°C which is only 0.2°C lower than US RNODC curve. Apparently a transposition error of the initial log value of 15.6°C to 16.5°C occurred between ship and processing center.

The 0.2°C temperature difference may be attributed to a correction factor applied to the NODC digitized data. This was necessary because the initial shipboard strip chart calibration line was at 16.5°C. The standard calibration line should be at 16.7°C to allow the strip chart to be interpreted properly in the relationship between temperature and depth. A series of equations in the US NODC program library are utilized to permit a computer correction when an anomaly from the standard calibration occurs.

Figure 2 shows a temperature difference of 1.1°C at the 65 meter level. This apparently is an error in the interpretation of the analog charts on shipboard. Except for these anomalies the basic thermal structure in figures 1 and 2 are consistent.

Figure 3 and 4 show a remarkable correlation between IGOSS SYNDARC data and the US NODC data. Temperature differences at all SYNDARC levels do not differ more than 0.2°C. This represents accurate encoded data, considering the complex thermal structure exhibited. The strong negative vertical gradients superimposed by a number of positive gradients are well represented by the BATHY encoded message. This is characterized at the 73 and 96 meter levels, where accuracies to within 0.1°C and depths to within 1 meter identified these features. This correlation is very impressive.

An error in the surface encoded data of 1.2°C in the SYNDARC observation in figure 5 is noteworthy. The representation of the remainder of the thermal structure agree quite well with the NODC digitized data.

Figure 6 depicts a noteworthy thermal pattern in a mid-summer trace. The BATHY encoded data deviated from the NODC data between the 99 to 450 meter levels. This deviation probably can be attributed to the fact that SYNDARC reported a reading at 99 meters and 450 meters. The US NODC recorded 15 significant data points between these two levels. This may be common for GTS FM63 data messages, where attempts may have been made to reduce the number of significant data points far below acceptable levels of detail. The thermal slope below the 99 meter level in the SYNDARC message represents a true picture of the curve.

A more significant error occurred in figure 7. The surface temperature difference of 4.1°C is noteworthy, and at the 13 meter level, the SYNDARC temperature difference exceeded the NODC by 6.5°C. It is difficult to account for this deviation. The initial IGOSS BATHY logs were not available to verify the encoded message. The two curves line up at approximately the 30 meter level through the 460 level, with no temperature deviations exceeding 0.2°C.

In the total of 30 observational comparisons, only 2 exhibited excessive temperature differences and these occurred at or near the surface levels. The basic thermal structure patterns between GTS message (shipboard encoded data) and the high resolution digitized data showed remarkable consistency.

A statistical representation of the significant BATHY SYNDARC data points as compared to the NODC digitization data points is presented by the computation of the absolute mean percentage error. This is represented by:

$(\frac{1}{n} \sum di/TI)\ 100$ = mean percent error

TI = NODC temperature at BATHY SYNDARC levels

di = temperature difference between BATHY SYNDARC and NODC at SYNDARC levels

A total of 274 data points were compared and evaluated. The average absolute mean percent error at the SYNDARC data points was 3.72 percent. This is a significantly low mean percentage error. A frequency distribution of temperature differences is presented in figure 8.

Approximately 80 percent of the encoded SYNDARC data points fell within the class interval of ± 0.3°C, while 89 percent fell within the class interval of ± 0.5°C. Approximately 6 percent of the shipboard encoded BATHY data points fell in the class interval which exceeds ± 1.0°C.

The frequency distribution of temperature differences (figure 8) appears to be skewed from a normal distribution. A possible explanation for this skewed distribution may be attributed to the frequency distribution of calibration lines, shown in figure 9. Approximately 83 percent of the observations exhibited a calibrated line value less than the standard of 16.7°C.

A review of the 4,700 observations from the RNODC BATHY SYNDARC files covering the years 1973 to 1976, which include data from various countries and ships, were screened for gross error. A high degree of accuracy was noted. Only 3.3 percent of the BATHY messages showed the presence of a significant error (usually confined to a single value) which would affect the thermal structure. Transposition of numerical digits in temperature and transmission induced negative signs appear to be the most common errors noted.

Environmental Quality Control Analyses

During the past year the US NODC has developed automated computer models of historic bathythermograph data (digitized to high resolution) for each 1° square and month using the total available X-BT data archives. These models incorporate the mean environmental computations of:

(1) Sea surface temperature as reported at zero meters.

(2) Depth of significant gradient. The significant gradient is defined as that portion of the profile in which the gradient is at least -0.03°C per meter and which contains the greatest total temperature change. Depth of the top of this segment is called depth of significant gradient.

(3) Gradient magnitude. Total temperature change divided by total depth change of the significant gradient defined above.

(4) Depth of three isotherms. The depth of each isotherm is found by linear interpolation between inflection points. Isotherms are chosen according to geographic region.

(5) Depth of positive gradient. Depth of the top of the shallowest positive temperature change.

Average values of each parameter are based on historical X-BT data, except that historical mechanical BT data are used in computing 2, 3 and 5. Contemporary X-BT digital data are passed through appropriate models for evaluation. Deviations from the historic mean conditions are computed and listed during the edit routines in the processing stage. These environmental edits provide a measure of assessment of the real time data as compared to that of historic data.

In this study, only GTS message data in the approximate location of ship Hotel in the Atlantic were evaluated against the historical models. Table 1 compares some SYNDARC observations to a number of the parameters identified. The comparisons were made by visual inspection with the model computations.

An analyses of the computations show that the basic GTS BATHY message thermal structure presented agrees favorably with the historic model.

Conclusions

An attempt has been made to relate certain small samples of GTS reported BATHY message data stored in SYNDARC format at the US RNODC as part of its IGOSS archives to the same data subsequently processed from the original X-BT strip charts by the US NODC for the basic archives. Although some significant errors were noted, the overall accuracy of the BATHY messages appears to be noteworthy. Except for some major transposition errors, the depiction of the ocean thermal patterns by the GTS BATHY message appears to be consistent with the high resolution digitized data.

It is also surprising that a gross error of only 3 percent is noted from a sample of over 4,700 observations, considering the multiplicity of ships, the variety of shore receiving stations, and the number of countries participating.

Ship	Model # Obs.	Model SST	SYNDARC SST	Model Gradient Depth	SYNDARC Gradient Depth	Model Depth of 13°C	SYNDARC Depth of 13°C
DUANE 3806N 7108W (Figure 1)	90	14.4°C	15.5°C	155m	110m	146m	158m
BIBB 3802N 7052W (Figure 2)	100	20.0°C	18.6°C	76m	65m	158m	150m
BIBB 3806N 7106W (Figure 3)	119	19.6°C	18.9°C	61m	48m	150m	150m
BIBB 3804N 7002W (Figure 4)	100	20.0°C	22.2°C	76m	47m	158m	195m
TANEY 3800N 7100W (Figure 6)	280	26.1°C	26.2°C	22m	20m	137m	90m

Table 1 - A Comparison of the SYNDARC BATHY Messages with NODC Historical Model Derived from High Resolution High Volume Data Archives

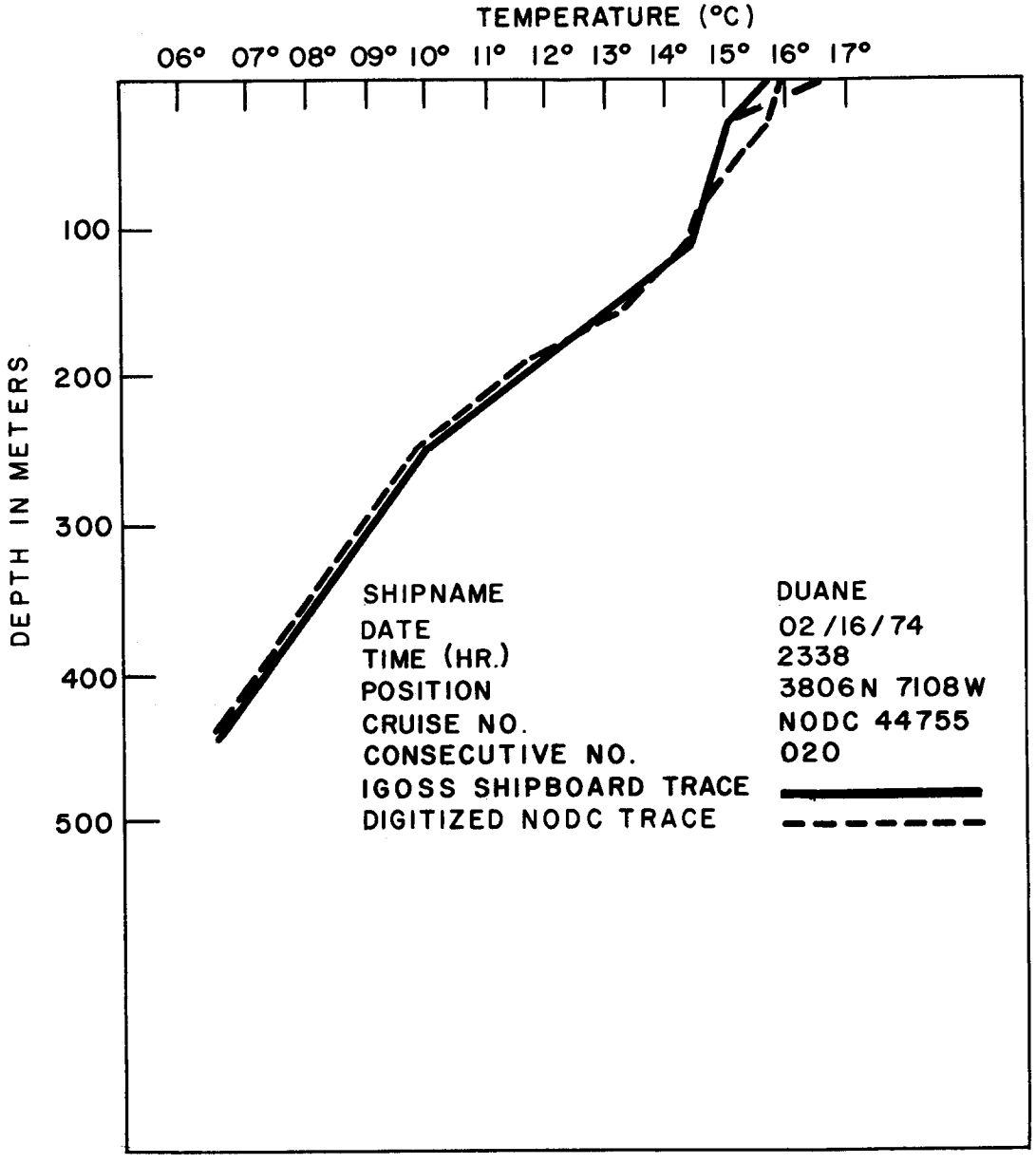
TEMPERATURE (°C)
06° 07° 08° 09° 10° 11° 12° 13° 14° 15° 16° 17°
DEPTH IN METERS
100
200
300
400
500
SHIPNAME DUANE
DATE 02/16/74
TIME (HR.) 2338
POSITION 3806N 7108W
CRUISE NO. NODC 44755
CONSECUTIVE NO. 020
IGOSS SHIPBOARD TRACE
DIGITIZED NODC TRACE

FIGURE (1)

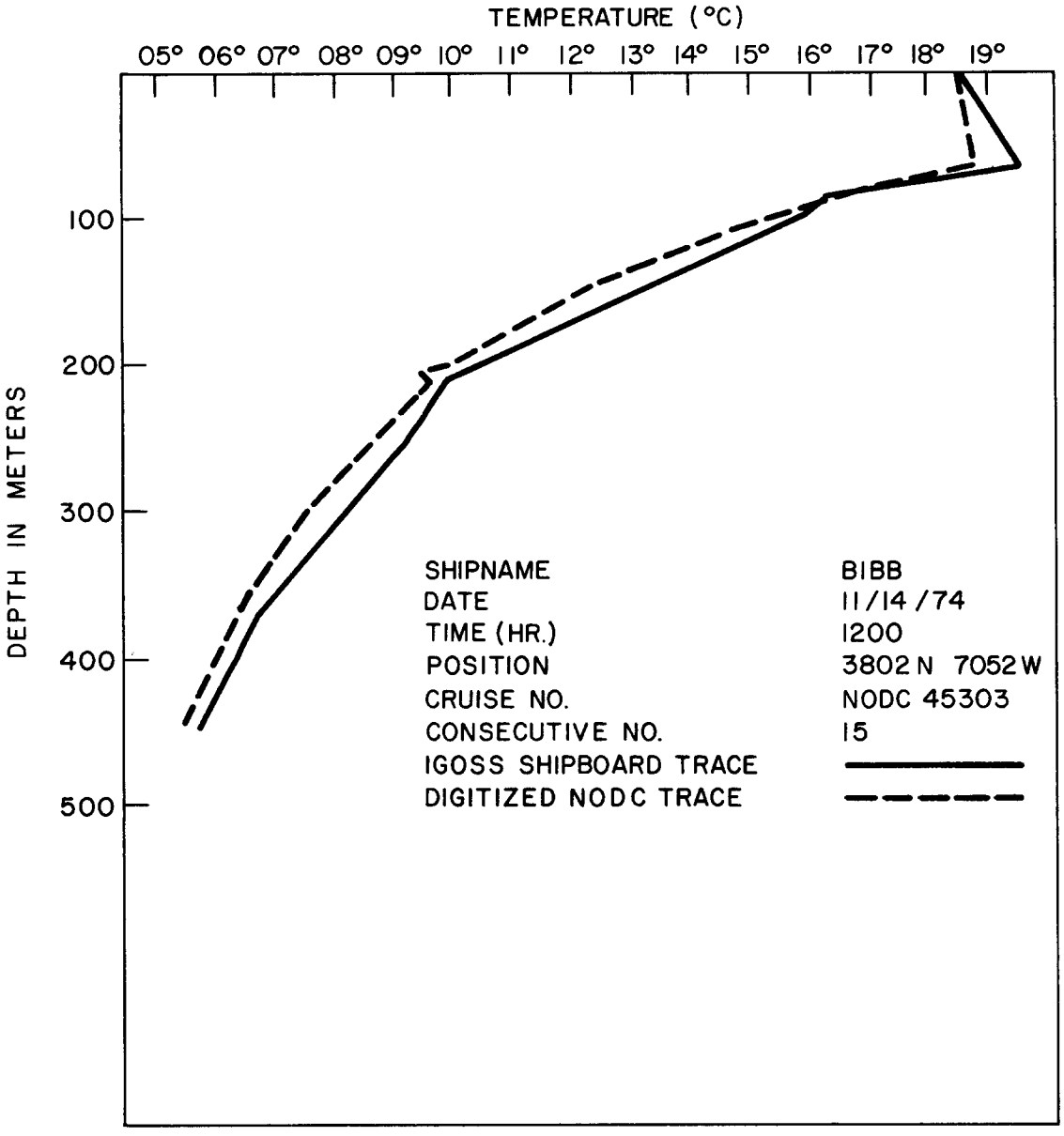
TEMPERATURE (°C)
05° 06° 07° 08° 09° 10° 11° 12° 13° 14° 15° 16° 17° 18° 19°
DEPTH IN METERS
100
200
300
400
500
SHIPNAME BIBB
DATE 11/14/74
TIME (HR.) 1200
POSITION 3802 N 7052 W
CRUISE NO. NODC 45303
CONSECUTIVE NO. 15
IGOSS SHIPBOARD TRACE
DIGITIZED NODC TRACE

FIGURE (2)

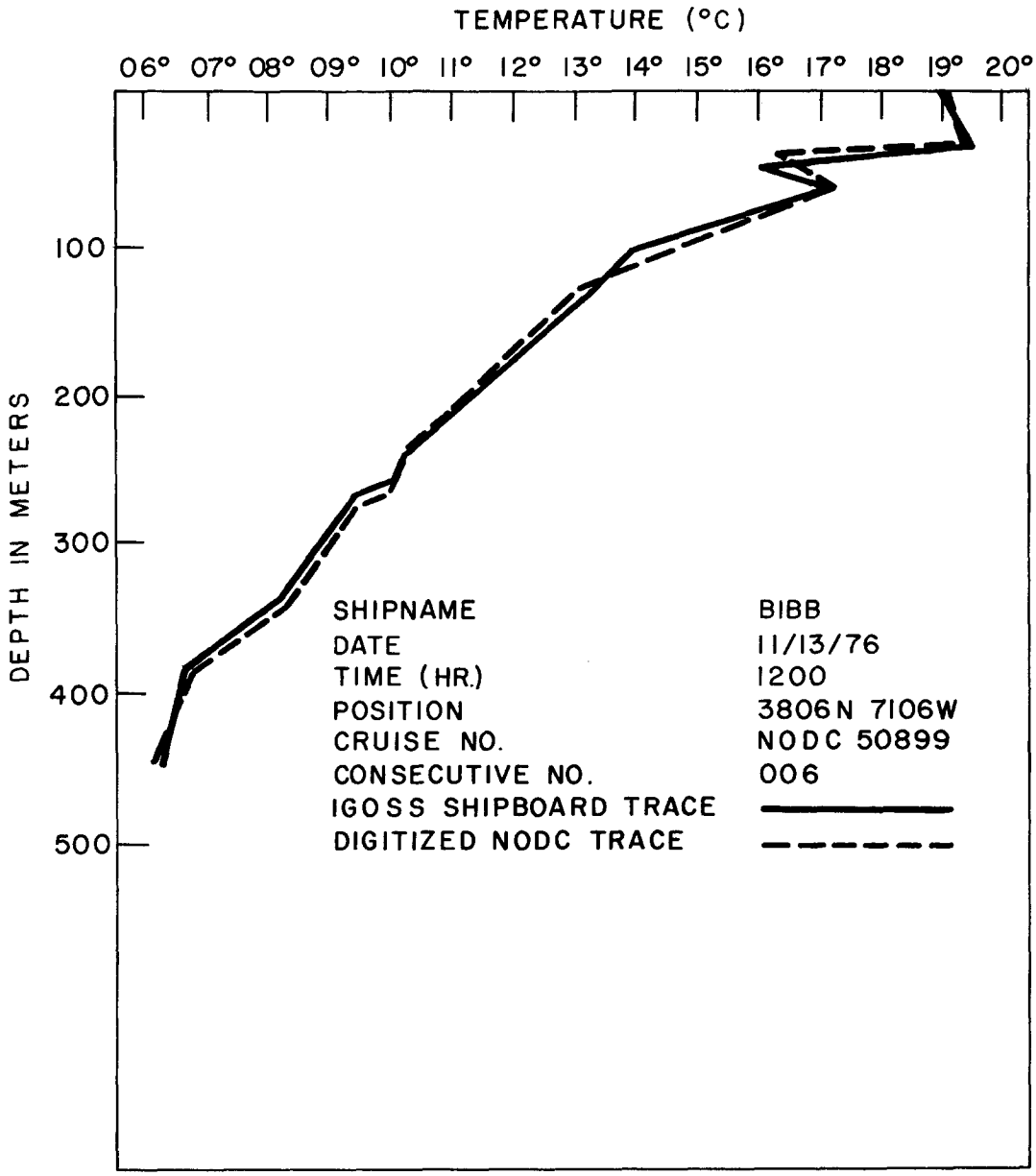
TEMPERATURE (°C)
06° 07° 08° 09° 10° 11° 12° 13° 14° 15° 16° 17° 18° 19° 20°
DEPTH IN METERS
100
200
300
400
500
SHIPNAME BIBB
DATE 11/13/76
TIME (HR.) 1200
POSITION 3806N 7106W
CRUISE NO. NODC 50899
CONSECUTIVE NO. 006
IGOSS SHIPBOARD TRACE
DIGITIZED NODC TRACE

FIGURE (3)

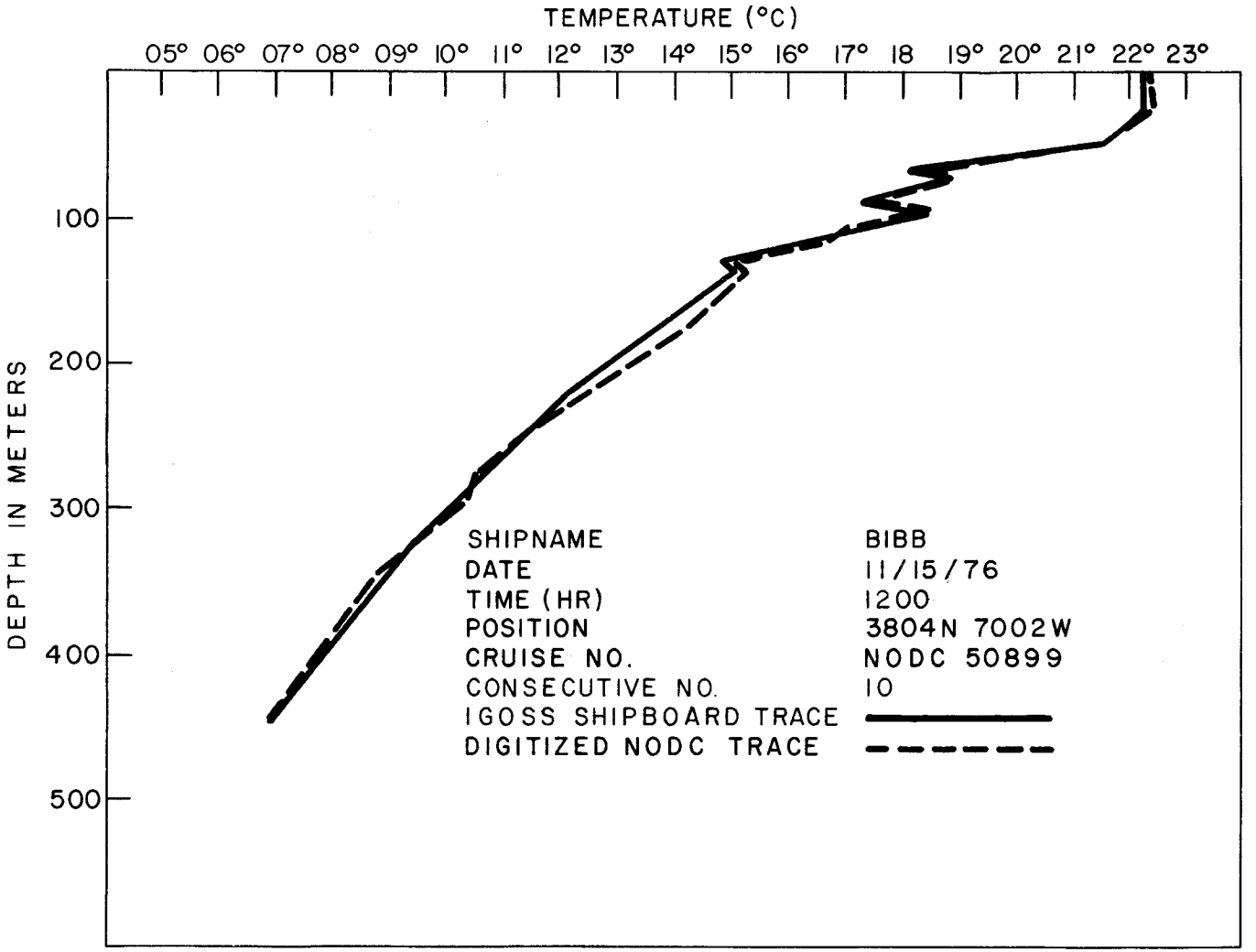
TEMPERATURE (°C)
05° 06° 07° 08° 09° 10° 11° 12° 13° 14° 15° 16° 17° 18 19° 20° 21° 22° 23°
DEPTH IN METERS
100
200
300
400
500
SHIPNAME BIBB
DATE 11/15/76
TIME (HR) 1200
POSITION 3804N 7002W
CRUISE NO. NODC 50899
CONSECUTIVE NO. 10
IGOSS SHIPBOARD TRACE
DIGITIZED NODC TRACE

FIGURE (4)

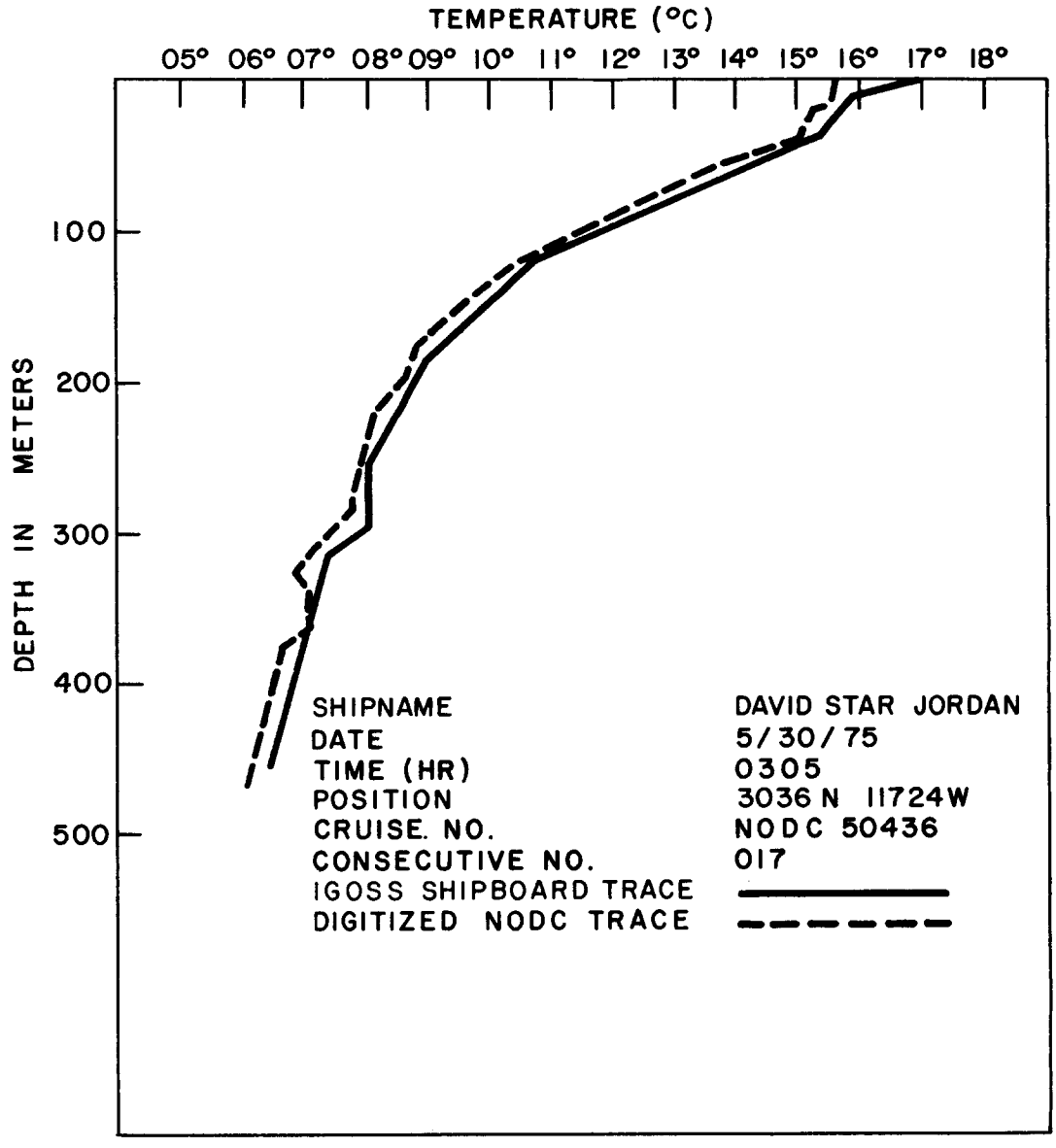
TEMPERATURE (°C)
05° 06° 07° 08° 09° 10° 11° 12° 13° 14° 15° 16° 17° 18°
DEPTH IN METERS
100
200
300
400
500
SHIPNAME
DATE
TIME (HR)
POSITION
CRUISE. NO.
CONSECUTIVE NO.
IGOSS SHIPBOARD TRACE
DIGITIZED NODC TRACE
DAVID STAR JORDAN
5/30/75
0305
3036 N 11724W
NODC 50436
017

FIGURE (5)

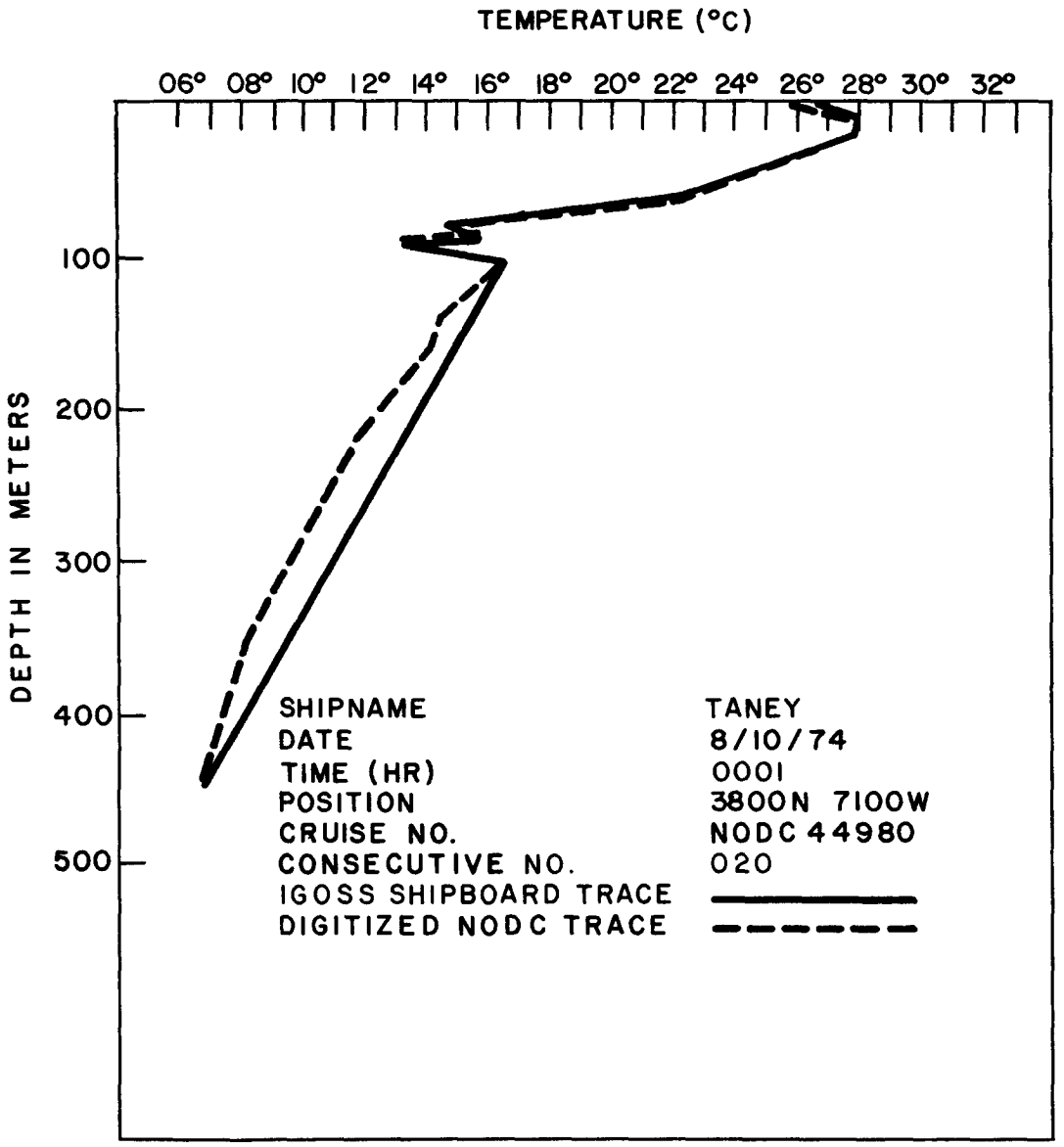
TEMPERATURE (°C)
06° 08° 10° 12° 14° 16° 18° 20° 22° 24° 26° 28° 30° 32°
DEPTH IN METERS
100
200
300
400
500
SHIPNAME TANEY
DATE 8/10/74
TIME (HR) 0001
POSITION 3800N 7100W
CRUISE NO. NODC 44980
CONSECUTIVE NO. 020
IGOSS SHIPBOARD TRACE
DIGITIZED NODC TRACE

FIGURE (6)

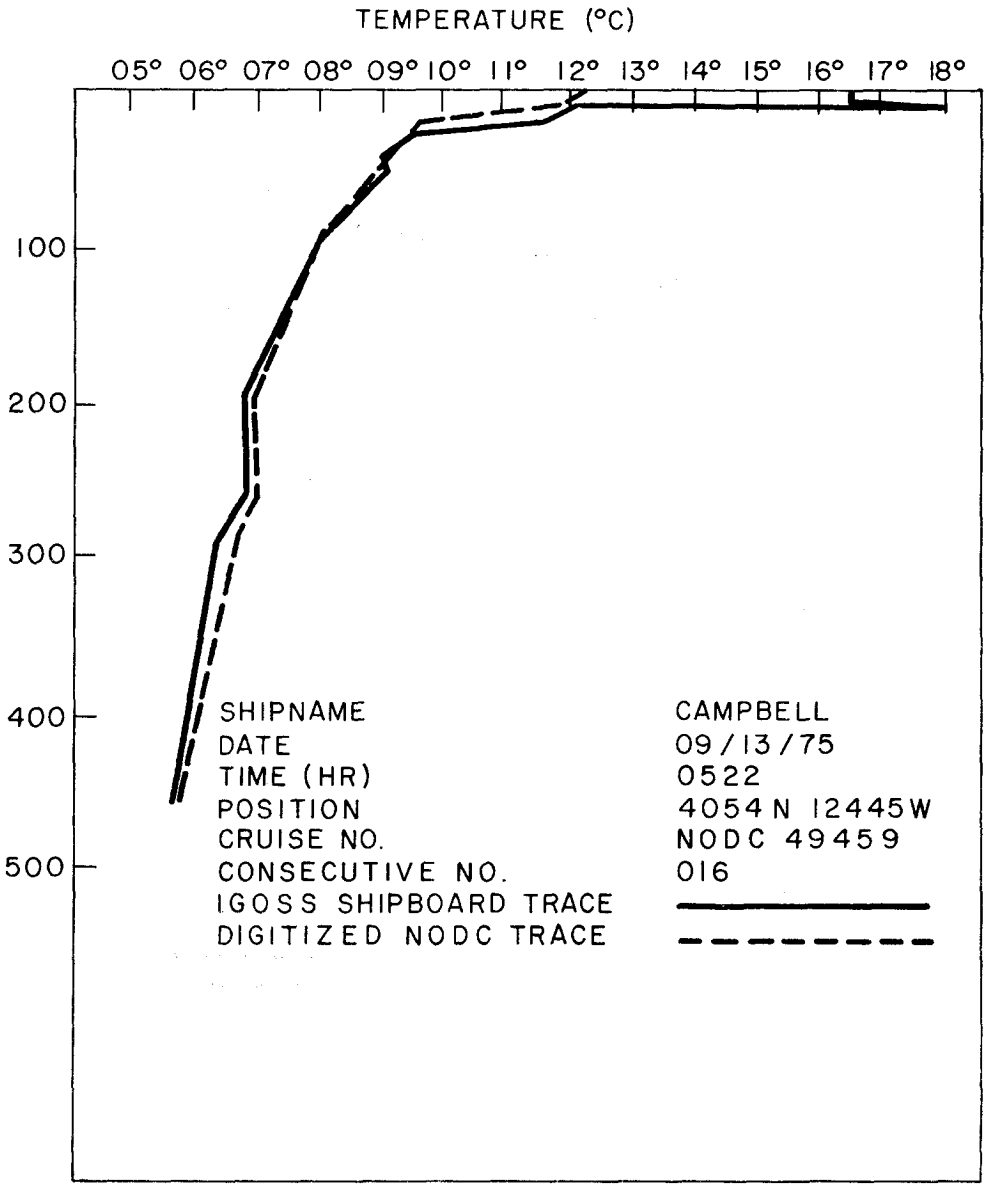
TEMPERATURE (°C)
05° 06° 07° 08° 09° 10° 11° 12° 13° 14° 15° 16° 17° 18°
100
200
300
400
500
SHIPNAME CAMPBELL
DATE 09/13/75
TIME (HR) 0522
POSITION 4054N 12445W
CRUISE NO. NODC 49459
CONSECUTIVE NO. 016
IGOSS SHIPBOARD TRACE
DIGITIZED NODC TRACE

FIGURE (7)

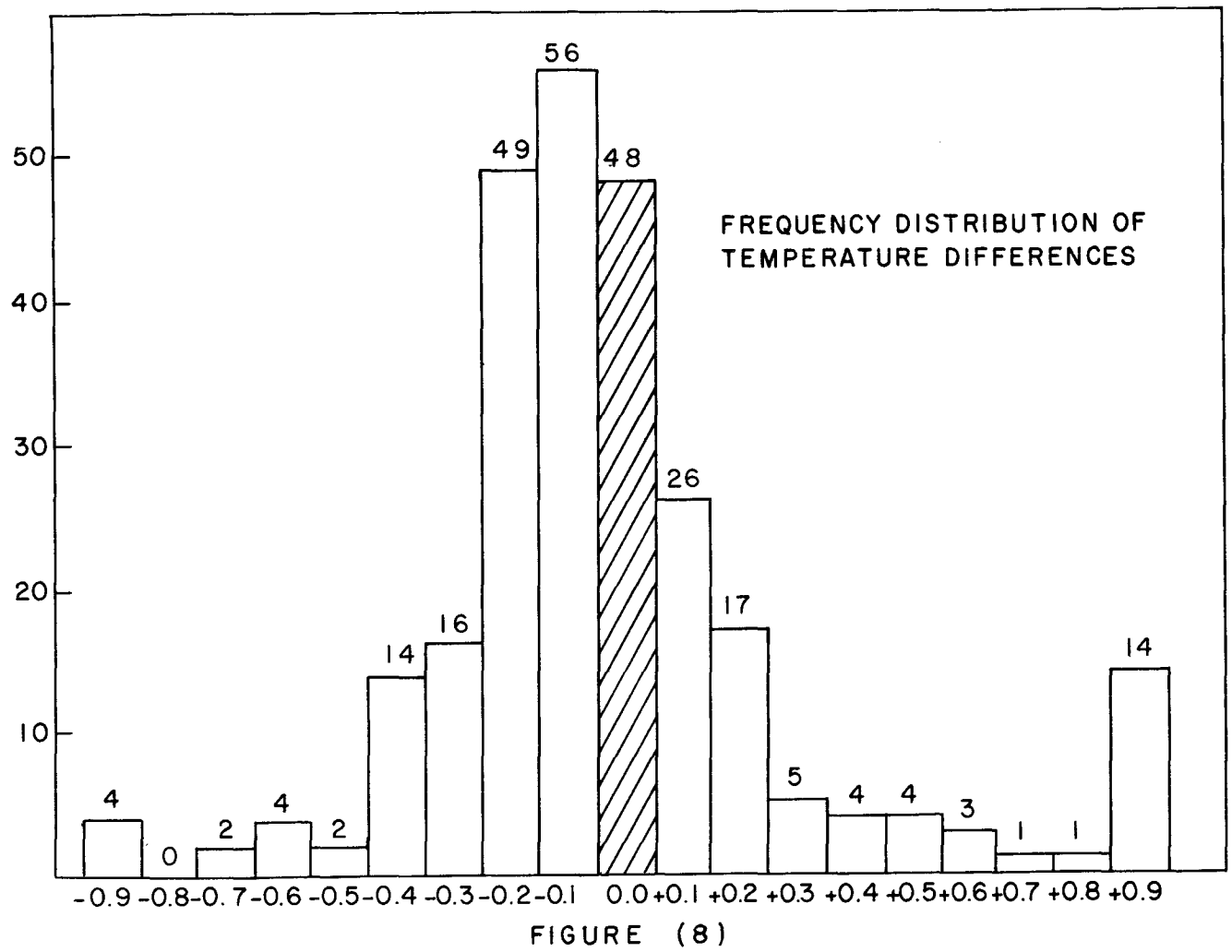
FREQUENCY DISTRIBUTION OF
TEMPERATURE DIFFERENCES
50
40
30
20
10
4
0
2
4
2
14
16
49
56
48
26
17
5
4
4
3
1
1
14
-0.9 -0.8 -0.7 -0.6 -0.5 -0.4 -0.3 -0.2 -0.1 0.0 +0.1 +0.2 +0.3 +0.4 +0.5 +0.6 +0.7 +0.8 +0.9

FIGURE (8)

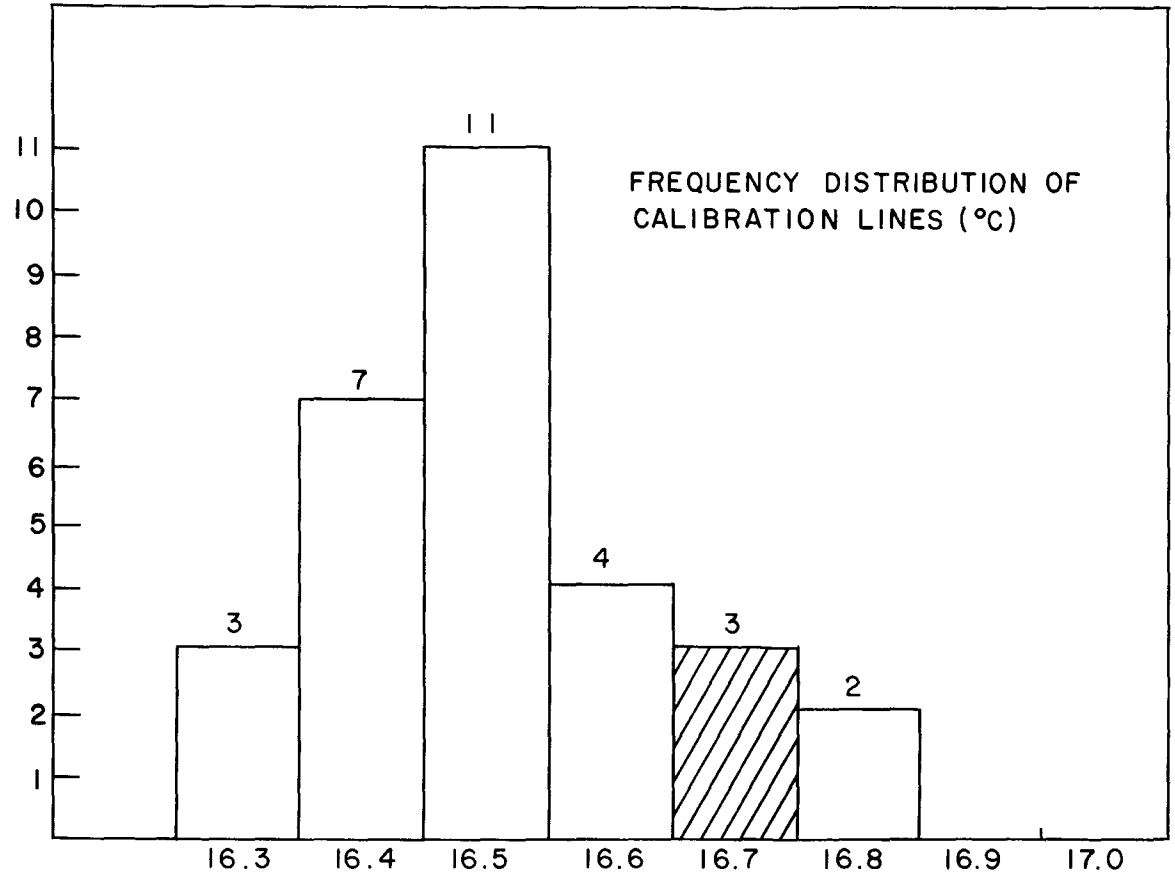
FREQUENCY DISTRIBUTION OF
CALIBRATION LINES (°C)
11
10
9
8
7
6
5
4
3
2
1
3
7
11
4
3
2
16.3
16.4
16.5
16.6
16.7
16.8
16.9
17.0

FIGURE (9)

NOAA/NESS OPERATIONAL SATELLITE OCEANOGRAPHIC PRODUCTS

William G. Pichel, Franklin E. Kniskern, Robert L. Brower

U.S. Department of Commerce
National Oceanic and Atmospheric Administration
National Environmental Satellite Service
Washington, D.C. 20233

1. INTRODUCTION

One of the most dramatic recent technological contributions increasing our knowledge of oceanographic processes has been the development of infrared remote sensing instrumentation. These instruments, when mounted aboard earth orbiting satellites, have made possible the derivation of products which have opened a new era in oceanography. The capability demonstrated by satellite systems to monitor the ocean-surface thermal environment was here-to-fore impractical, if not impossible, to achieve by more conventional means. From their vantage point in space, infrared sensing instruments can monitor all oceanic regions of the earth several times per day. They make possible the detailed study of temporal changes in the surface thermal structure indicative of dynamic processes such as current movements, eddies, upwelling, and thermal advection.

The National Environmental Satellite Service (NESS) of the National Oceanic and Atmospheric Administration (NOAA) has responsibility for the development and routine production of oceanographic products from environmental satellite sensors. Satellite oceanographic instrumentation and derived products are described herein to illustrate the existing capabilities of satellite systems to provide technological support in oceanography.

2. EVOLUTION OF SATELLITE OCEANOGRAPHIC INSTRUMENTATION

2.1 ITOS

The first generation of operational environmental satellites began with the launch of TIROS-1 on April 1, 1960. The first operational satellite to yield globally-useful oceanographic data was the Improved TIROS Operational Satellite (ITOS-D), launched in October, 1972. Three additional ITOS satellites were launched in this second-generation series. Each of the ITOS-series spacecraft was placed into a sun-synchronous 1450 km orbit, and carried three primary earth-oriented, environmental sensors (Schwalb, 1972).

(1) The Scanning Radiometer (SR) sensed energy in both the visible and infrared portions of the spectrum with a resolution of 4 km and 7.5 km, respectively. Although the SR was designed primarily for meteorological imaging, SR data were also used on a daily basis to measure sea surface temperatures for the global ocean.

(2) The Vertical Temperature Profile Radiometer (VTPR) was used to measure the vertical temperature structure of the atmosphere and to obtain

atmospheric attenuation corrections for the SR measurements.

(3) The Very High Resolution Radiometer (VHRR) was sensitive to energy in the visible spectrum and the infrared (IR) window with a resolution of 0.9 km in both channels. However, data coverage was limited to approximately 3600 km of the readout stations located at Wallops Island, Virginia, Gilmore Creek, Alaska, and Redwood City, California. VHRR data from limited areas outside the range of these readout stations were recorded aboard the spacecraft and played back when the satellite passed over either Wallops Island or Gilmore.

2.2 TIROS-N

The prototype of the third-generation polar-orbiting system, TIROS-N, was launched October 13, 1978, with the second spacecraft of the series, NOAA-A, scheduled for launch in the Spring of 1979. The initial TIROS-N spacecraft was launched into an afternoon orbit, crossing the equator, ascending, at 1500 local time. It is in a near-polar, sun-synchronous orbit at an average altitude of 870 km (Hussey, 1977).

Two TIROS-N instruments are relevant to the derivation of oceanographic products: (1) The Advanced Very High Resolution Radiometer (AVHRR), and (2) The High Resolution Infrared Radiation Sounder (HIRS/2).

The AVHRR instrument senses radiation in four spectral regions (i.e. channels). There are two visible channels (0.55 - 0.90 μm and 0.725 - 1.10 μm) and two IR channels (3.55 - 3.93 μm and 10.5 - 11.5 μm). A planned change in the instrument design will add a fifth channel in the 11.5 - 12.5 μm region. Data from the AVHRR instrument are available from the satellite in four operational modes. The first is direct readout of visible and infrared data at 4 km resolution to ground stations of the Automatic Picture Transmission (APT) class, worldwide. The second mode is direct readout of all spectral channels at 1.1 km resolution to ground stations of the High Resolution Picture Transmission (HRPT) class, worldwide. The third mode is the global on-board recording of 4 km resolution data from all spectral channels, known as Global Area Coverage (GAC), and the fourth mode is the on-board recording of data of all spectral channels from selected portions of each orbit at 1.1 km resolution, known as Local Area Coverage (LAC).

The HIRS/2 is an atmospheric sounding instrument which measures radiation in 20 separate spectral regions of the visible, intermediate IR, and far IR. At the subsatellite point, the resolution is 17.4 km (Schwalb, 1978). Vertical atmospheric-temperature profiles and calculations of atmospheric water vapor content are the principal products derived from the HIRS/2 data. In addition, data from a number of HIRS/2 channels are used in discriminent functions for cloud detection and in regression equations for atmospheric attenuation correction in the calculation of sea surface temperatures.

2.3 GOES

The Synchronous Meteorological Satellite (SMS), or as it is presently called, the Geostationary Operational Environmental Satellite (GOES), adds the temporal dimension to oceanographic monitoring. Using the satellite's continuous-viewing capability, near-real time dynamic surface thermal processes can be observed (Miller, et al., 1977). The first geostationary satellite (SMS-1) was launched in May, 1974. Since that time, SMS-2 and three GOES satellites have been launched into a geostationary altitude of approximately 36,000 km. Two geostationary satellites are maintained in an operational posture at all times, an east satellite located at 75° West longitude and a west satellite located at 135° West longitude. All GOES satellites carry the Visible and Infrared Spin Scan Radiometer (VISSR) which provides continuous day and night imaging (pictures every half hour) of the Western Hemisphere between the 60° latitude lines. The visible sensors respond to energy in the 0.55 to 0.75 μm range with a resolution of 1 km. The IR channel senses energy in the 10.5 to 12.5 μm wavelength region with a resolution of 7.5 km.

3. CURRENT PRODUCTS

The number of oceanographic products derived from satellite data has grown rapidly during the past five years. These products are available in a variety of spacial and temporal resolutions. Products are derived using both qualitative and quantitative processes and are made available to the international community in the form of digital data and hard-copy displays.

Products which have been based on ITOS instrument data are currently being replaced by products derived from TIROS-N data. Unfortunately, all TIROS-N products are not available for presentation at the time of this writing. The examples used to illustrate the high-resolution oceanographic products have been derived from VHRR data only.

3.1 GULF STREAM ANALYSIS

Figure 1 is a VHRR infrared image of the western North Atlantic Ocean and shows the Gulf Stream as it meanders northeastward from the Carolina coast. A large warm eddy is also visible about 400 km southeast of Cape Cod. In the VHRR infrared imagery, the dark shades represent warm temperatures, and the white or light gray areas, colder temperatures. Figure 2 is an example of the Gulf Stream analysis produced by NOAA/NESS. This analysis is a weekly composite chart depicting the Gulf Stream, oceanic fronts, and eddies in the western North Atlantic Ocean (Kniskern and Thompson, 1975). This particular analysis was produced manually, using an overlay grid, from the satellite image in Figure 1. Shelf, slope, and Gulf Stream water are outlined along with warm and cold eddies. This product is used by fishermen to determine fishing grounds along oceanic fronts, by the United States Coast Guard for search and rescue missions, and by merchant vessels for optimum routing. The Gulf Stream analysis was originated in 1973 and is disseminated over the United States National Facsimile (NAFAX) and the United States National Marine Facsimile (NAMFAX). Once the TIROS-N

high-resolution data base becomes available, sea surface temperature values will be included for the various water masses depicted in this product.

3.2 GULF STREAM WALL BULLETIN

The Gulf Stream Wall Bulletin is a frontal analysis transmitted via message encoded in alphanumeric format. It gives the location of the west and north wall of the Gulf Stream from Florida to Cape Hatteras and thence eastward to approximately 60°W. The same VHRR infrared imagery used to prepare the Gulf Stream Analysis is utilized for the Gulf Stream Bulletin. Tankers and ships transiting the coastal waters of the western Atlantic are the primary users of this bulletin. Considerable time is saved by navigating in the Gulf Stream (with the current) when northbound, and by avoiding it when southbound. The bulletin, first transmitted in 1975, is now updated three times a week, but broadcast twice daily by the United States Coast Guard.

3.3 ALASKAN ICE ANALYSIS

The Alaskan Ice Analysis (first produced in 1973), is a weekly composite depiction of ice conditions, observed from VHRR satellite data, of the Bering, Chukchi, and Beaufort Seas. Figure 3 is a VHRR visible-channel image from March 17, 1976, showing the extent of the ice pack in the Chukchi and Bering Seas. Since the visible detector senses the amount of reflected radiation, the ice and frozen land appear white or light gray while the sea appears black.

Figure 4 is an example of an Alaskan ice analysis which is disseminated over NAFAX and NAMFAX weekly. Using the data from satellite imagery such as Figure 3, a weekly composite analysis is made. Parameters analyzed include the ice edge, ice concentration, openings and leads in the ice, and an estimation of the ice thickness. The 1 km imagery allows the detection of individual ice floes and an accurate assessment of the ice edge. These ice analyses are employed by the ice forecaster to provide forecasts and ship routes to vessels transiting the ice pack in the seas surrounding Alaska. Fishermen utilize the analyses, as there is an intensive fishery along the ice edge in the Bering Sea. Researchers also use the analyses as input for their ice models. Satellite-derived ice data for other areas in the Northern Hemisphere including Baffin Bay, the Greenland Sea, the Labrador Sea and the Barents Sea are processed regularly along with imagery for the Weddell and Ross Seas in the Southern Hemisphere. IR imagery specially enhanced for cold temperatures are used during the "Polar Night" in both hemispheres.

3.4 GREAT LAKES ICE ANALYSIS

The high-resolution VHRR and VISSR sensors also allow the monitoring of ice in small bodies of water, such as the fresh water ice in the Great Lakes. Figure 5 is a VHRR visible-channel ice image from February 7, 1977, showing the Great Lakes with considerable ice cover. Only a small lead in Lake Erie keeps this lake from being completely ice covered. Figure 6 is the corresponding Great Lakes Ice Analysis utilizing the imagery from Figure 5. The three

main ice parameters analyzed from the imagery are ice concentration, fast ice, and leads. The Great Lakes Ice Analysis commenced in January, 1974 and has been produced twice weekly each ice season (January through April), to aid the United States National Weather Service (NWS) in its goal of keeping the Great Lakes open for navigation the entire winter. Close surveillance, which the satellite imagery helps provide, is the only practical way to achieve this goal.

3.5 GREAT LAKES SURFACE TEMPERATURE ANALYSIS

The Great Lakes Surface Temperature Analysis was first produced in August, 1975. This analysis was developed to test the accuracy of the VHRR IR sensors and as a prototype for high-resolution numerical sea surface temperature charts which will be produced from TIROS-N data. A real-time knowledge of the lake surface temperatures will facilitate the accurate prediction of weather conditions for the Great Lakes region.

The analysis is produced from VHRR IR digital data upon which a temperature extraction and formatting program has been run. The temperature output is then transferred to a base map (figure 7) by an optical device known as a Zoom Transfer Scope. The chart is then hand adjusted for accuracy and continuity. An empirical relationship to correct for atmospheric attenuation in the IR spectral band is calculated for each analysis. Presently, a more refined atmospheric attenuation correction program is being tested to correct for atmospheric thermal inversions which can cause a surface temperature error of several degrees Celsius. The analysis is produced on cloudless days when the lakes are ice free and depicts surface temperatures with 2° C contours. Figure 8 is an example of the finalized surface-water analysis of Lake Ontario for June 3, 1976, and is the product which is disseminated to the customer by mail.

3.6 GLOBAL SEA SURFACE TEMPERATURE OBSERVATIONS

Sea surface temperatures were derived from ITOS-series SR and VTPR data beginning December, 1972. These temperatures were calculated from arrays of data approximately 100 km on a side. Now, satellite-derived observations of SST are produced daily from TIROS-N AVHRR and HIRS/2 data using an improved version of the fully-automated Global Operational Sea Surface Temperature Computation (GOSSTCOMP) procedure. These satellite-derived temperatures, representative of approximately 50 km square areas, are calculated for all oceanic regions of the world. They are derived from target arrays of the GAC 4 km resolution AVHRR infrared data using a statistical technique described by Crosby and Glasser (1978). HIRS/2 data temporally and spacially coincident with the AVHRR data are employed in a procedure developed by Walton (1977) to select those targets which are cloud-free. Corrections for atmospheric attenuation are then calculated with regression algorithms (discussed in Legekis et al. 1976). The TIROS-N GOSSTCOMP procedure is an evolutionary extension and refinement of the computational algorithms used to process SST from the ITOS SR and VTPR data. Although differing substantially in specific details, the basic approach to the problem is similar to that described in Brower et al. (1976) and Walton

(1976). New techniques are under development which take advantage of the synergistic information available in simultaneous processing of data from the available channels of the AVHRR (Yates, 1977).

A total of 30,000 to 40,000 SST measurements a day are derived by the improved GOSSTCOMP procedure (three to four times the number obtained from ITOS data), and are made available on a near-real-time basis. These measurements are usually obtained within 8 hours of satellite data transmission to the ground stations. Observations derived during the most current 7 days are accessible by computer terminal. Observations older than a week are archived on magnetic tape and made available to climatic and oceanographic researchers by the Environmental Data Information Service (EDIS). The satellite observations augment ship observations in the analysis of the SST fields produced by the NWS and the U.S. Navy's Fleet Numerical Weather Center. Selected observations are also transmitted twice daily by teletype on the Global Telecommunications System (GTS) formatted in the SATOB Code.

3.7 SEA SURFACE TEMPERATURE ANALYZED FIELDS

The 50 km satellite SST observations are routinely used to produce analyzed fields of SST with a procedure called the Objective Analysis Technique. The technique currently employed to analyze these data is essentially the same procedure used with ITOS data and described by Brower et al. (1976) and Kalinowski et al. (1977). Although the analysis procedure has not changed significantly, the end products are quite different. ITOS temperatures were analyzed to produce a single global polar-stereographic field. Now, with TIROS-N data, four different types of fields are being produced:

(1) A 100 km field, the primary field, contains gridpoints at all 1° latitude-longitude intersections between 70° S and 70° N for all longitudes. This field is updated daily using satellite data processed during the previous 24 hours.

(2) A 500 km field is also created daily with the same geographic coverage as the 100 km field, but with gridpoints at every 5° latitude-longitude intersection.

(3) Three meso-scale 50 km analyzed fields cover the U.S. 200-mile Conservation and Management Zone with gridpoints at every 1/2° latitude-longitude intersection. These analyses cover the Atlantic coast, Pacific coast, and the waters between Hawaii and Alaska. The 50 km fields are produced weekly using satellite temperatures from the preceeding seven days.

(4) A global 250 km monthly-mean field is also produced. For this field, all satellite temperature observations from the past month are averaged to form a monthly-mean SST for each 2 1/2° latitude-longitude quadrangle.

The current analyzed fields are resident and available for direct access on computer disk storage. They can be displayed by remote terminal, as

illustrated in Figure 9. The fields are also archived on magnetic tape at convenient time intervals for retrospective applications. Hard-copy field displays are widely distributed. These are isotherm contour maps produced from the 100 km (Figure 10) and 50 km (Figure 11) fields. Created and distributed once per week by mail, these maps are available for all oceanic regions of the globe. In addition, isotherm and observation-density contour maps of the monthly-mean fields are produced each month for climatic applications. Two photographic field displays are generated for use principally in product quality assessment (Figures 12 and 13). Also, GTS transmission of sectors of the 100 km field is possible with grid temperatures formatted in the WMO grid code.

Satellite SST analyzed fields are currently used for many applications. Remote-terminal displays such as Figure 9 are utilized by the National Hurricane Center in Miami, Florida, for monitoring conditions conducive to hurricane formation and intensification. The National Marine Fisheries Service in LaJolla, California, refers to the satellite analyzed fields in preparing information useful to the Pacific tuna fleet. Isotherm contour maps are distributed internationally to research centers, oceanographic and meteorological services, universities, corporations, and private individuals. These maps have been used in weather forecasting, physical and biological oceanographic research, and climatology.

4. REFERENCES

Brower, Robert L., Gohrband, Hilda S., Pichel, William G., Signore, T.L., and Walton, C. 1976: Satellite derived sea-surface temperatures from NOAA Spacecraft, NOAA Technical Memorandum, NESS 78, NOAA/NESS, U.S. Department of Commerce, Washington, D.C., 74 pp.

Crosby, David S. and Glasser, Kenneth S., 1978: Radiance estimates for truncated observations, Journal of Applied Meteorology, Vol. 17, No. 11, November, 1978, 1712-1715.

Hussey, W.J., 1977: The TIROS-N Orbiting Environmental Satellite System, NOAA/NESS, U.S. Department of Commerce, Washington, D.C., 28 pp.

Kalinowski, J. Keith, Signore, Theodore L., Pichel, William G., Walton, Charles C., Brower, Robert L., Brown, Stanley R., and Bennekamper, Kenneth G., 1977: Present and future operational NOAA satellite oceanographic products: an introduction, Proceedings of the Eleventh International Symposium on Remote Sensing of Environment, April 25-29, 1977, Ann Arbor, Michigan, 625-633.

Kniskern, F.E., Thompson, B.J., 1975: Some oceanographic service products derived from satellite data, 63rd Statutory meeting on the International Council for the Exploration of the Sea, Montreal, Canada, 20 September - 3 October, 1975, (unpublished paper), 25 pp.

Legekis, Richard, Signore, Theodore, Tarpley, Dan, and Walton, Charles, 1976: Recommended "day one" TIROS-N SST retrieval techniques, NESS internal memorandum, (unpublished), NOAA/NESS, Washington, D.C., September 13, 1976, 19 pp.

Miller, Donald B., Waters, M.P., Tarpley, I.D., Green, R.N., and Dismacheck, D.C., 1977: Potential applications of digital visible, and infrared data from geostationary environmental satellites, Proceedings of the Eleventh International Symposium on Remote Sensing of Environment, April 25-29, 1977, Ann Arbor, Michigan, 10 pp.

Schwalb, Arthur, 1972: Modified version of the Improved TIROS Operational Satellite (ITOS D-G), NOAA Technical Memorandum, NESS 35, NOAA/NESS, U.S. Department of Commerce, Washington, D.C., 48 pp.

Schwalb, Arthur, 1978: The TIROS-N/NOAA-A - G satellite series, NOAA Technical Memorandum, NESS 95, NOAA/NESS, U.S. Department of Commerce, Washington, D.C., 75 pp.

Walton, Charles C., Brower, Robert L., Signore, T.L., 1976: Satellite derived sea surface temperatures by multi-channel regression, Proceedings of the Symposium of Meteorological Observations from Space: Their Contribution to the First GARP Global Experiment, June 8 - 10, 1976, Boulder, Colorado, 155 - 159.

Walton, Charles C., 1977: Recognition of clear sounder radiances with disriminent functions, NESS internal memorandum (unpublished), NOAA/NESS, Washington, D.C., February 10, 1977, 23 pp.

Yates, Harold W., 1977: Recommended method for "AVHRR Only" sea surface temperature computations, NESS internal memorandum, (unpublished), NOAA/NESS, Washington, D.C., June 24, 1977, 4 pp.

Figure 1 - NOAA-4 VHRR IR image of water structure off the eastern coast of the United States, May 28, 1976.

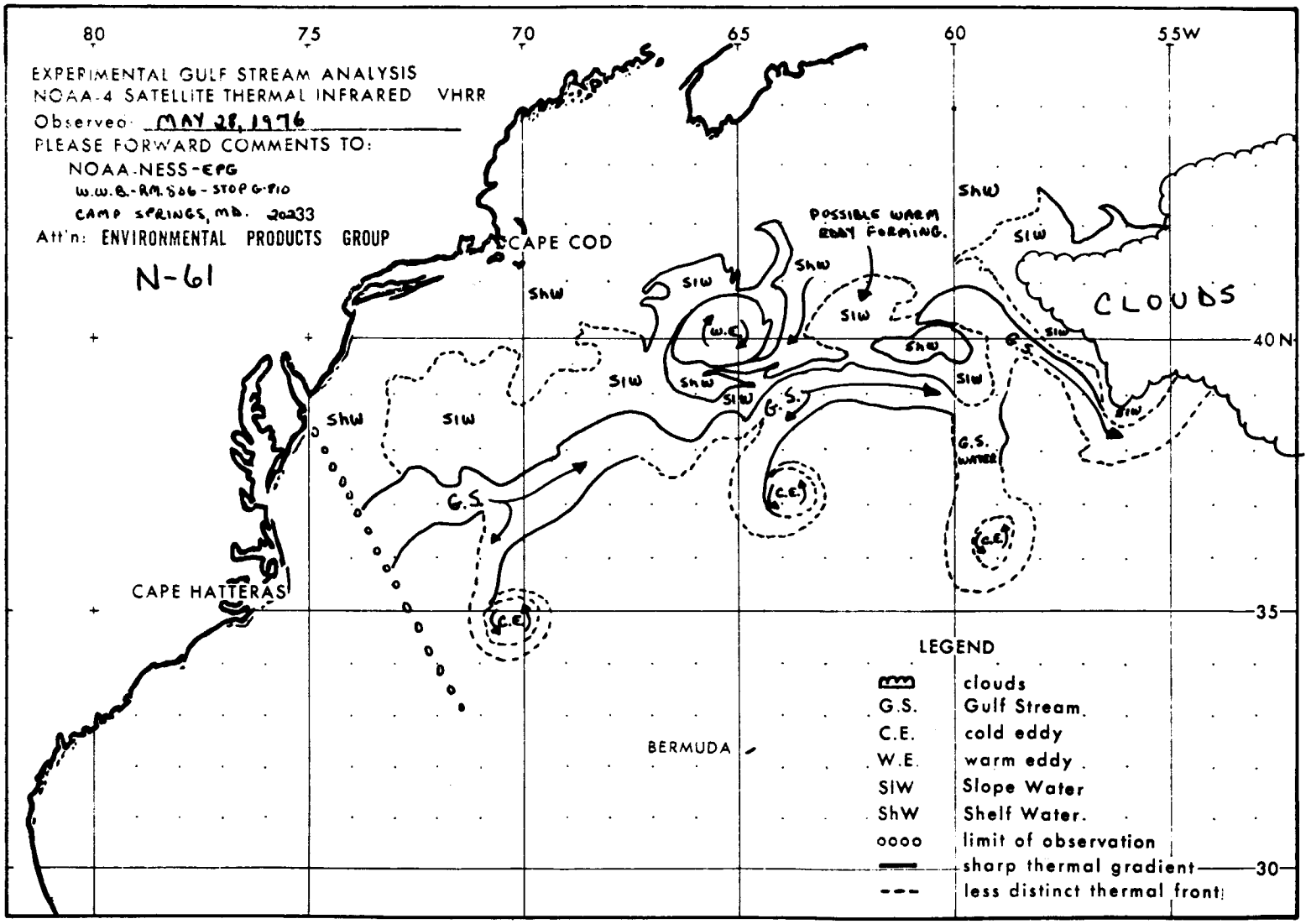

Figure 2 - Gulf Stream Analysis corresponding to Figure 1.

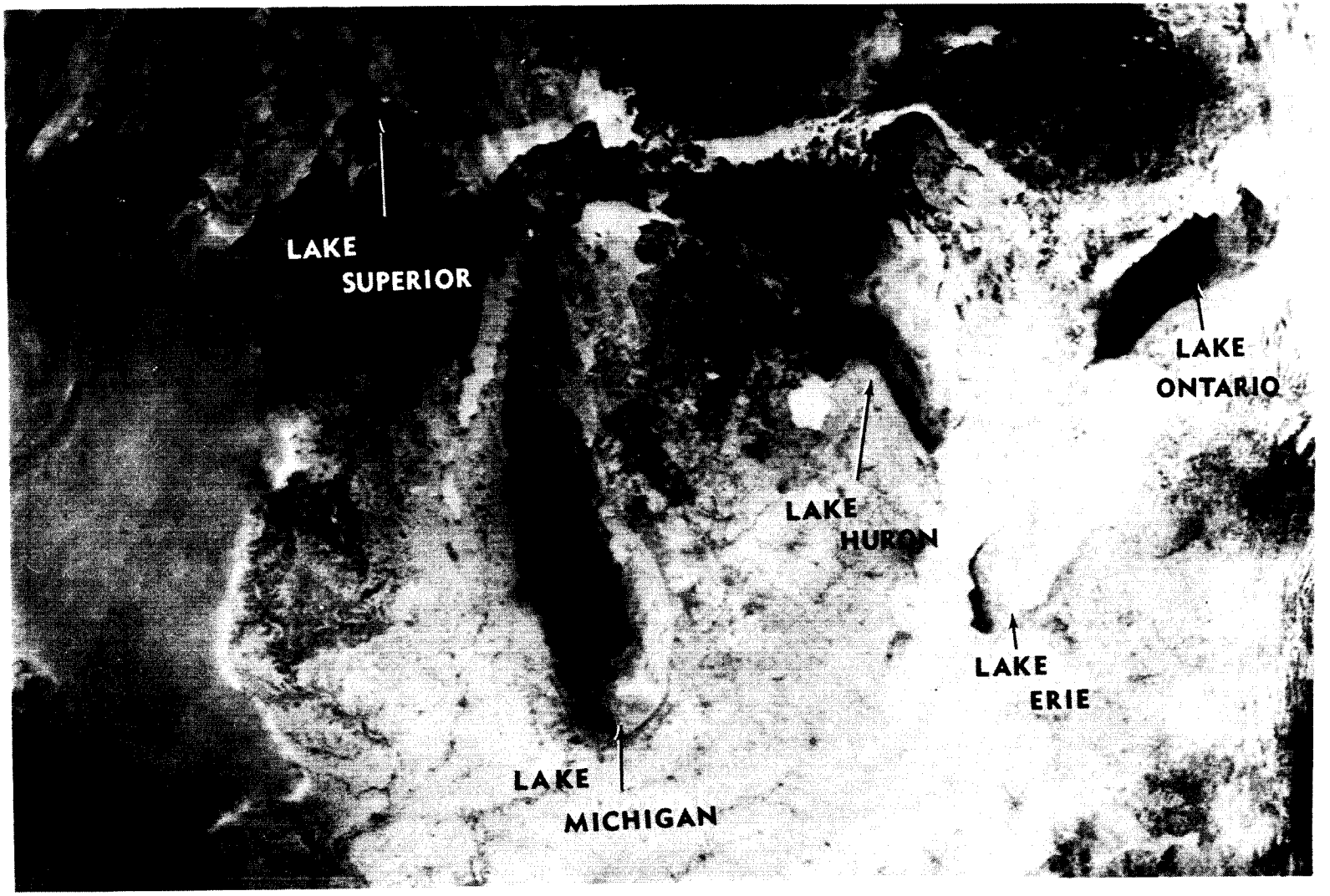

Figure 5 - NOAA-5 VHRR Visible image of ice conditions in the Great Lakes, February 7, 1977.

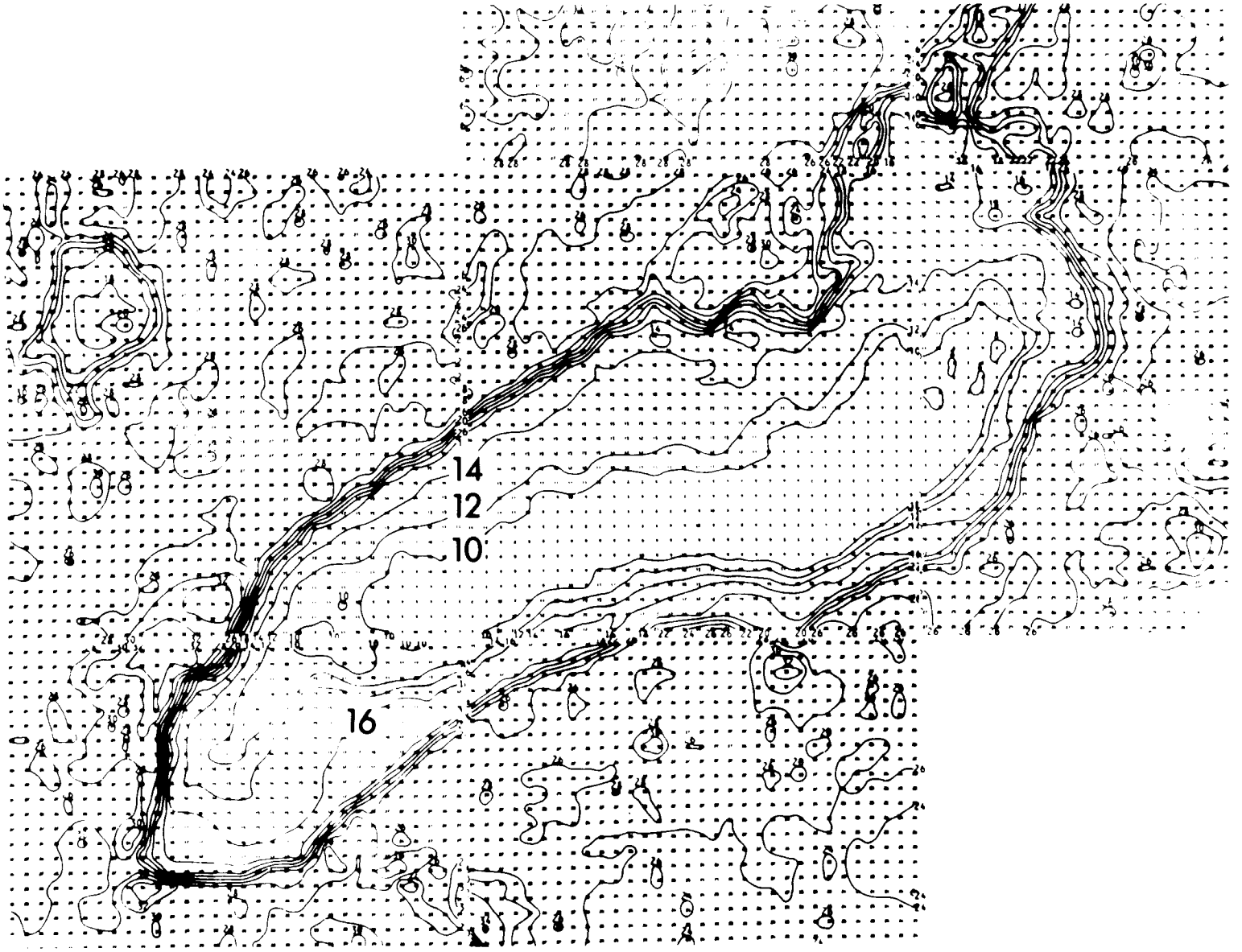

Figure 7 - Computerized Lake Ontario Water Temperature Analysis from NOAA-4 VHRR data, June 3, 1976.

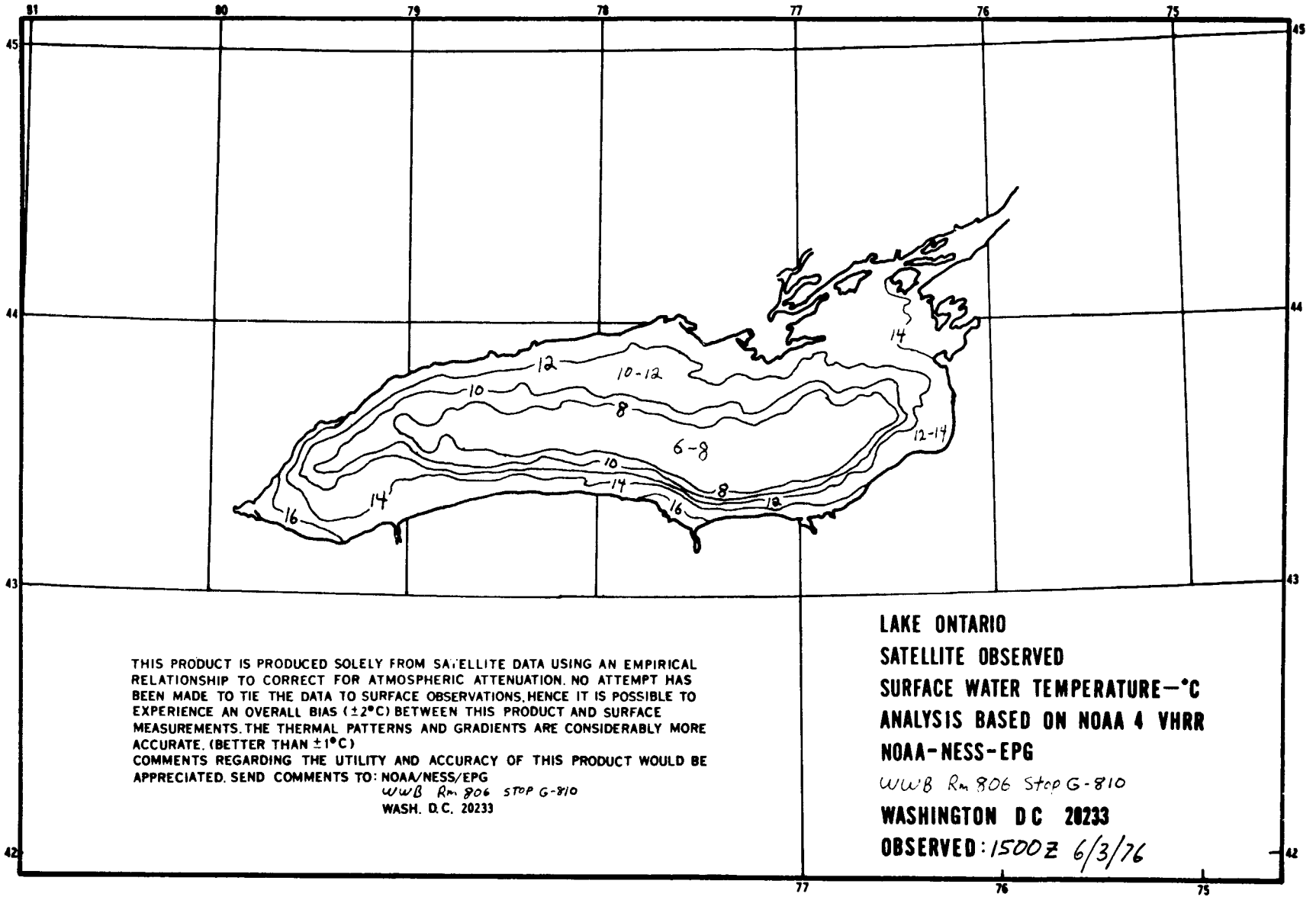

Figure 8 - Finalized Surface Water Temperature Analysis corresponding to Figure 7.

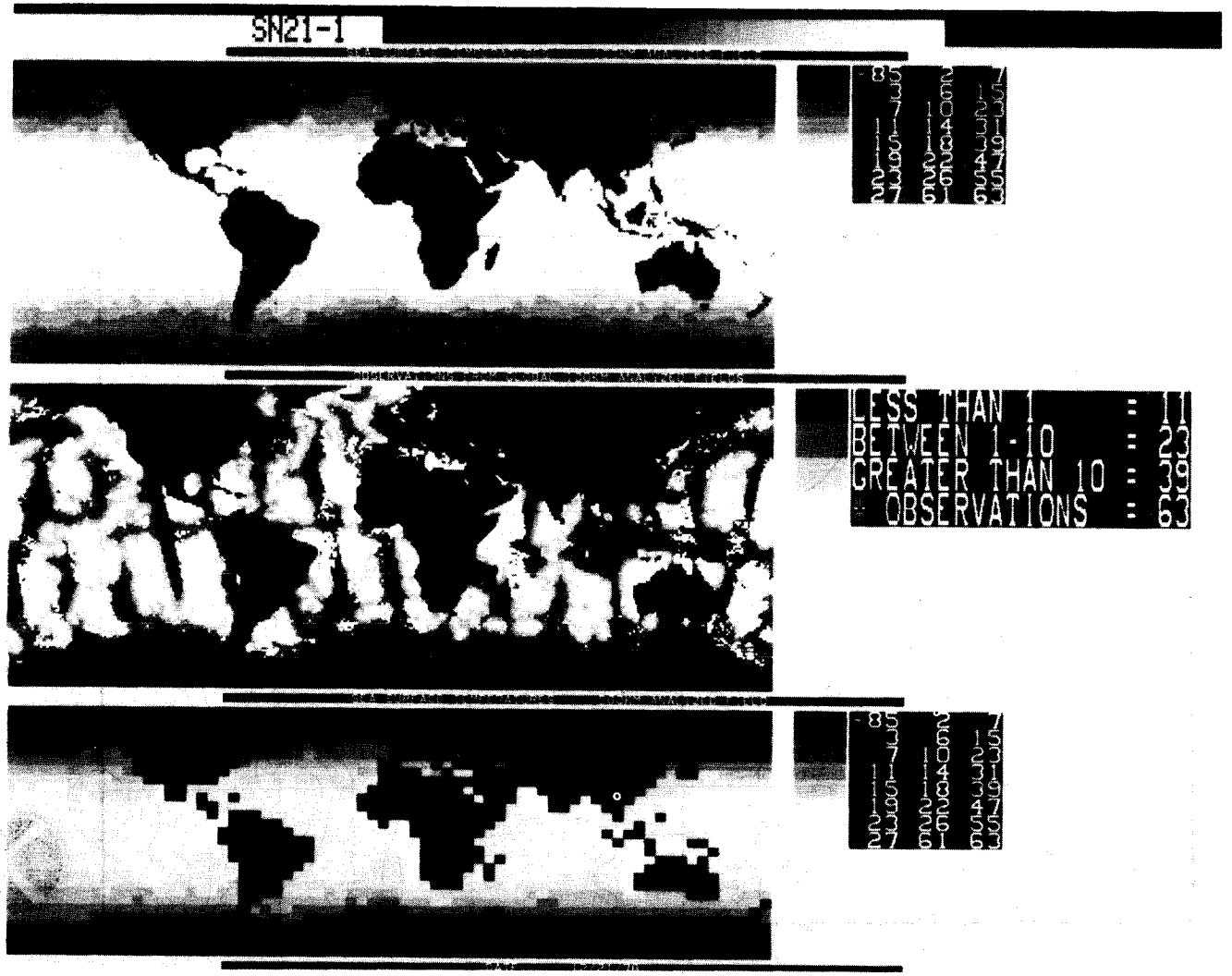

Figure 12 - Photographic display of the 100 km and 500 km analyzed fields. The top display of the 100 km field shows surface temperature in gray shades. The gray wedge to the right indicates the temperature range (e.g. 27°C to 61°C for the white region) and the gray value (e.g. 63 is white). The middle display shows the distribution of observations. White squares show observation location; gray shades indicate observation density. Surface temperatures in the 500 km field are depicted in the bottom display.

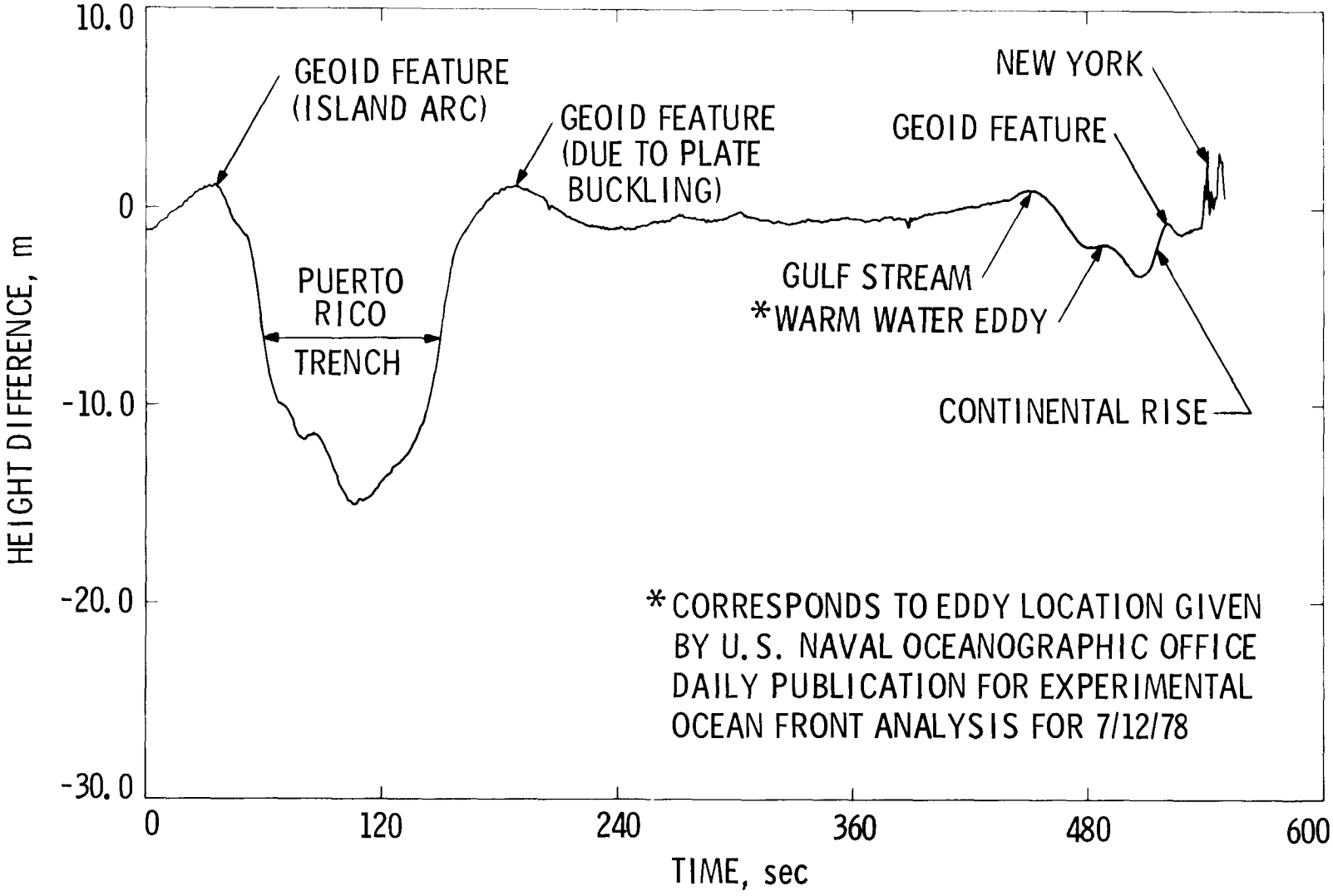

Figure 4. Difference of Seasat Altimeter Sea Surface Height and GEM 10B Geoid for North Atlantic Pass (7/10/78, Rev 191)

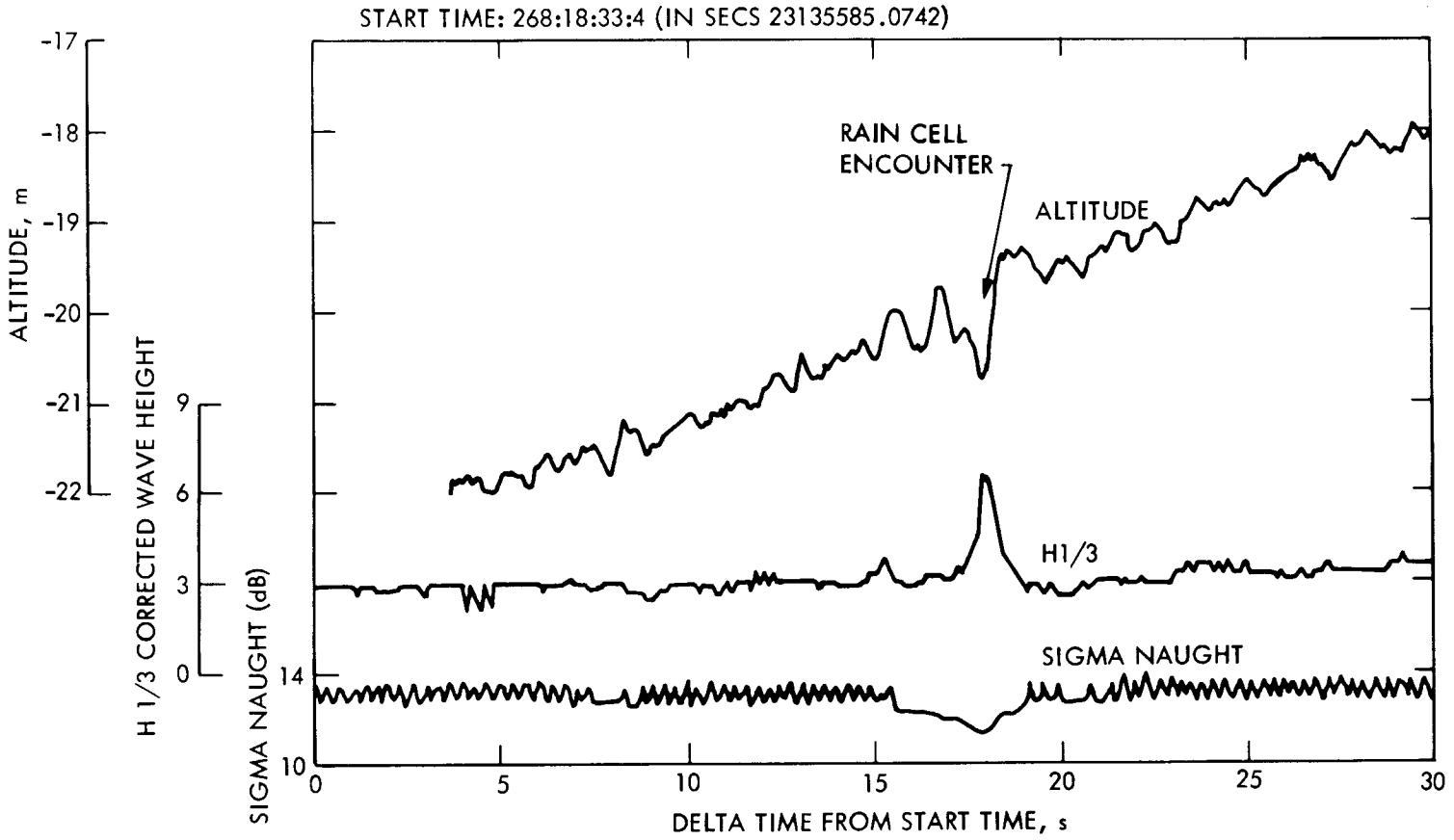

Figure 6. Response of Altimeter h, $H_{1/3}$, and σ_o to Rain Cell on Rev 1298.

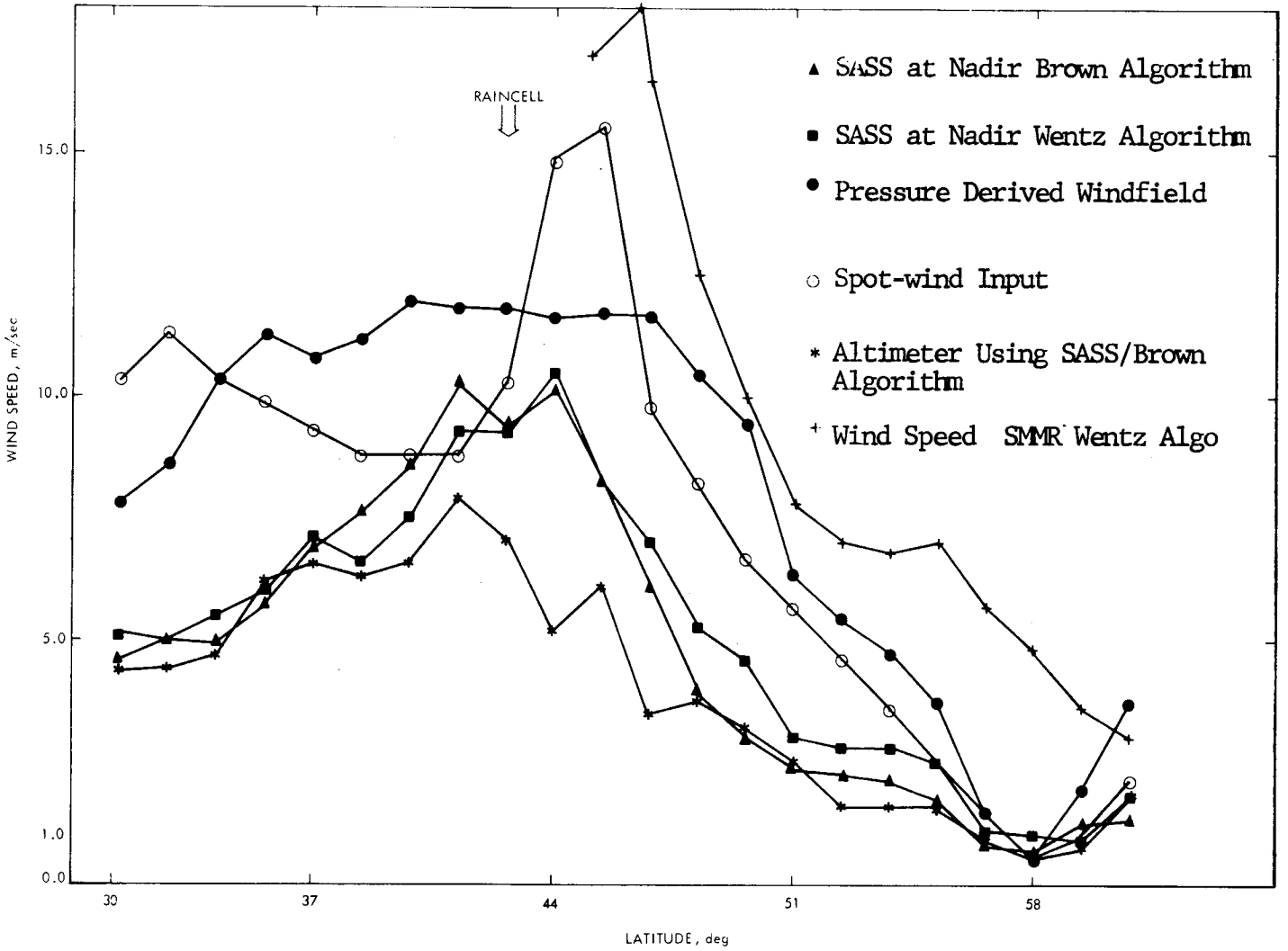

Figure 9. Wind Speed Comparisons (Rev 1298): SASS at Nadir Using Brown Algorithm; SASS at Nadir Using Wentz Algorithm; Pressure Derived Windfield; Spot-wind Input; Altimeter Using SASS (Brown) Algorithm; and SMMR Ground-track Wind Speed Using Wentz Algorithm.

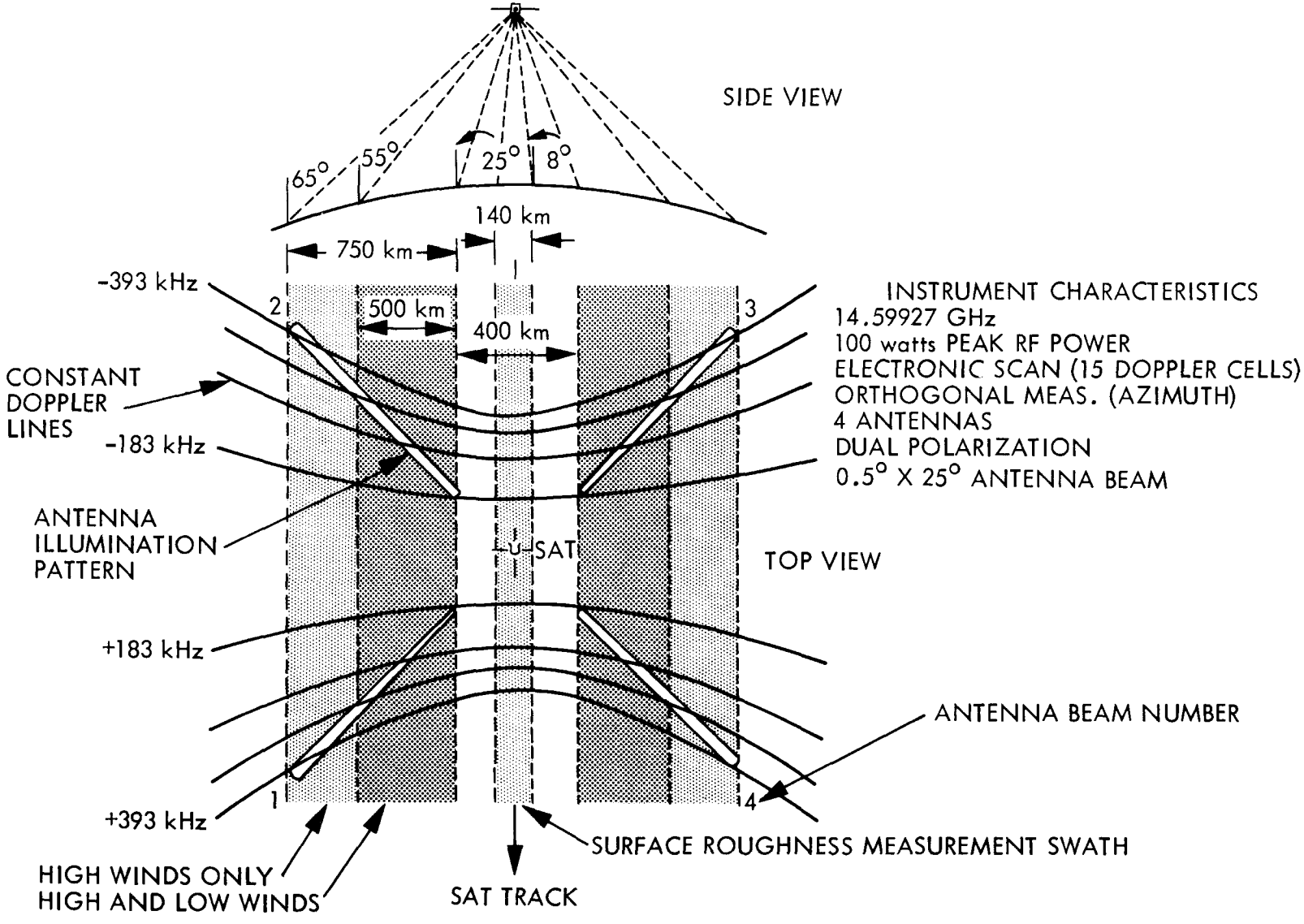

Figure 10. Geometry and Characteristics of SASS

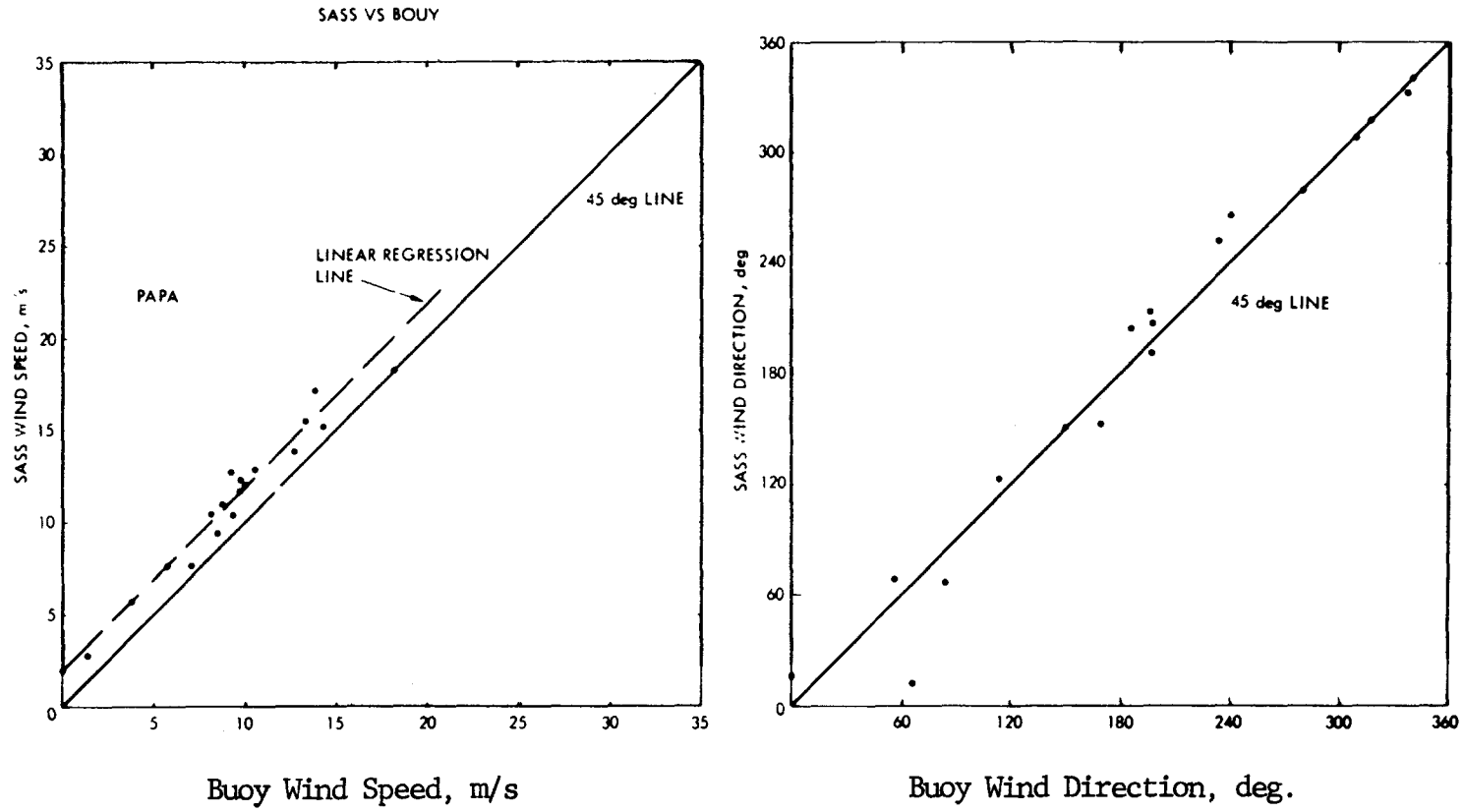

Figure 13. Comparison of SASS Derived Winds to Buoy Winds.

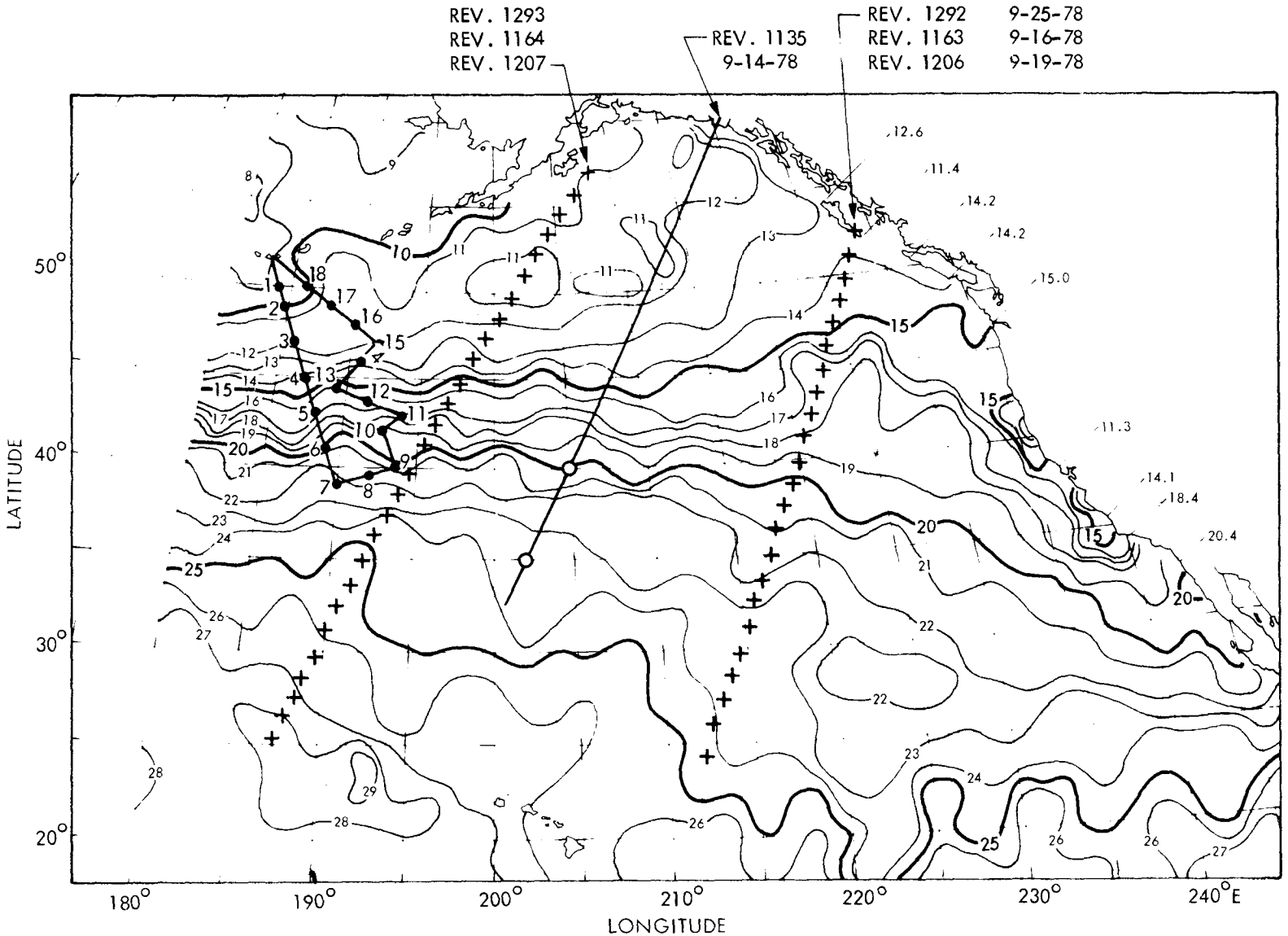

Figure 15. National Marine Fisheries Service (NMFS) analysis of sea surface temperature for September 1978. SMMR swath center tracks are superimposed for data used in this intercomparison report. In upper left is aircraft track and station numbers of higher quality air expendable bathy thermograph data used to verify NMFS analysis.

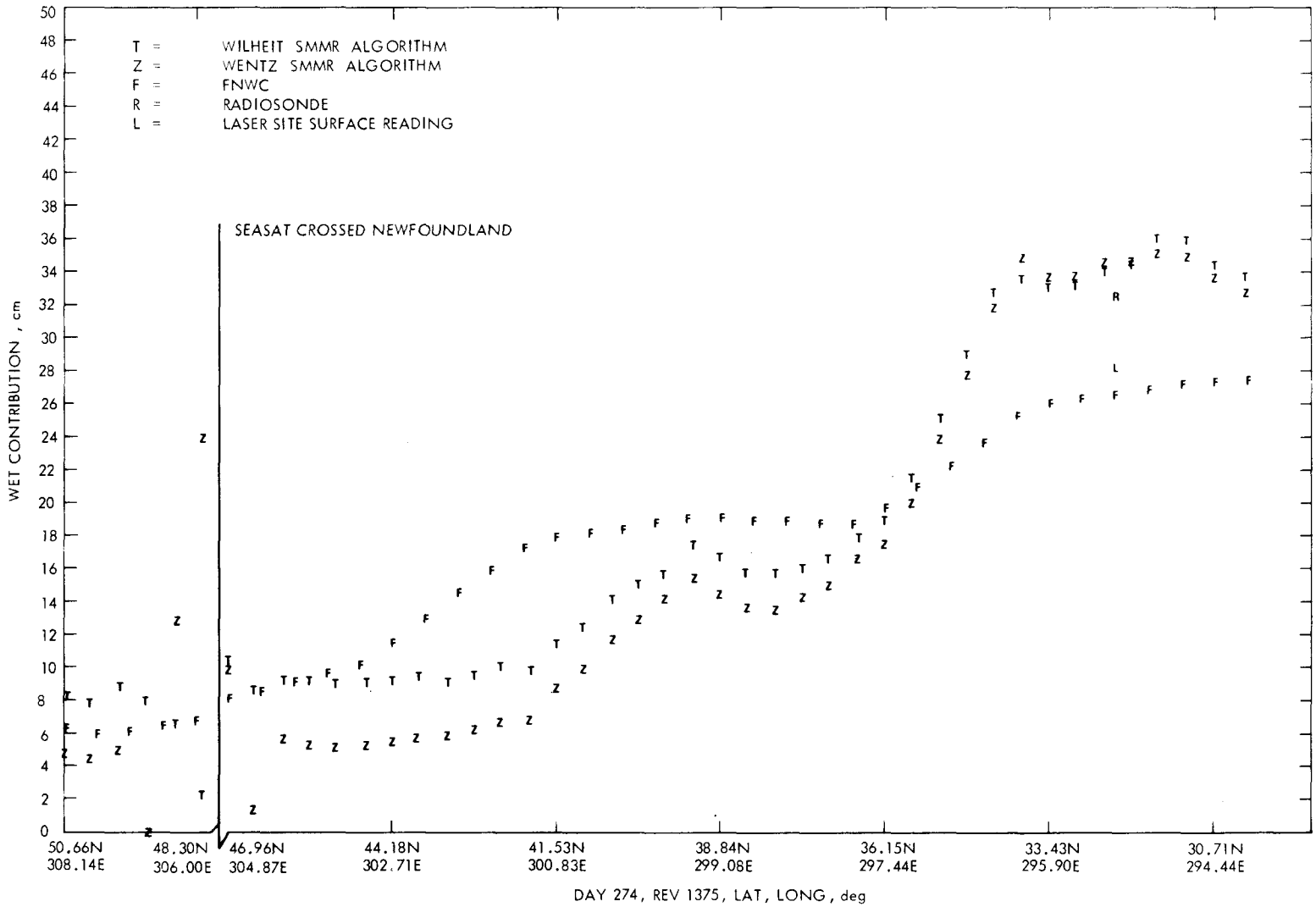

Figure 18. Comparison of altimeter path length correction determined from SMMR data by T and W algorithms with FNWC estimates.

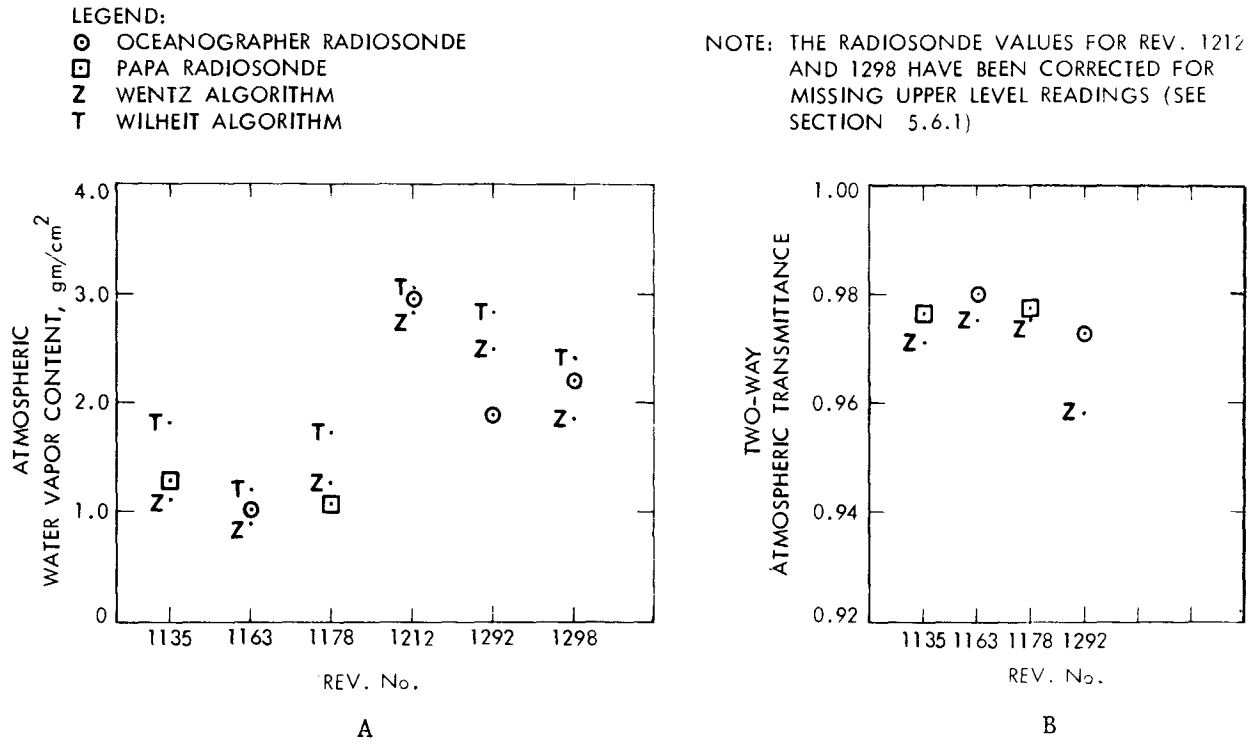

Figure 19. Comparison of integrated atmospheric water vapor obtained from radiosonde ascents (see text) with the SMMR/CV values obtained by Wilheit and Wentz's algorithms. Note: The radiosonde values for Revs 1212 and 1298 have been corrected for missing upper level readings.

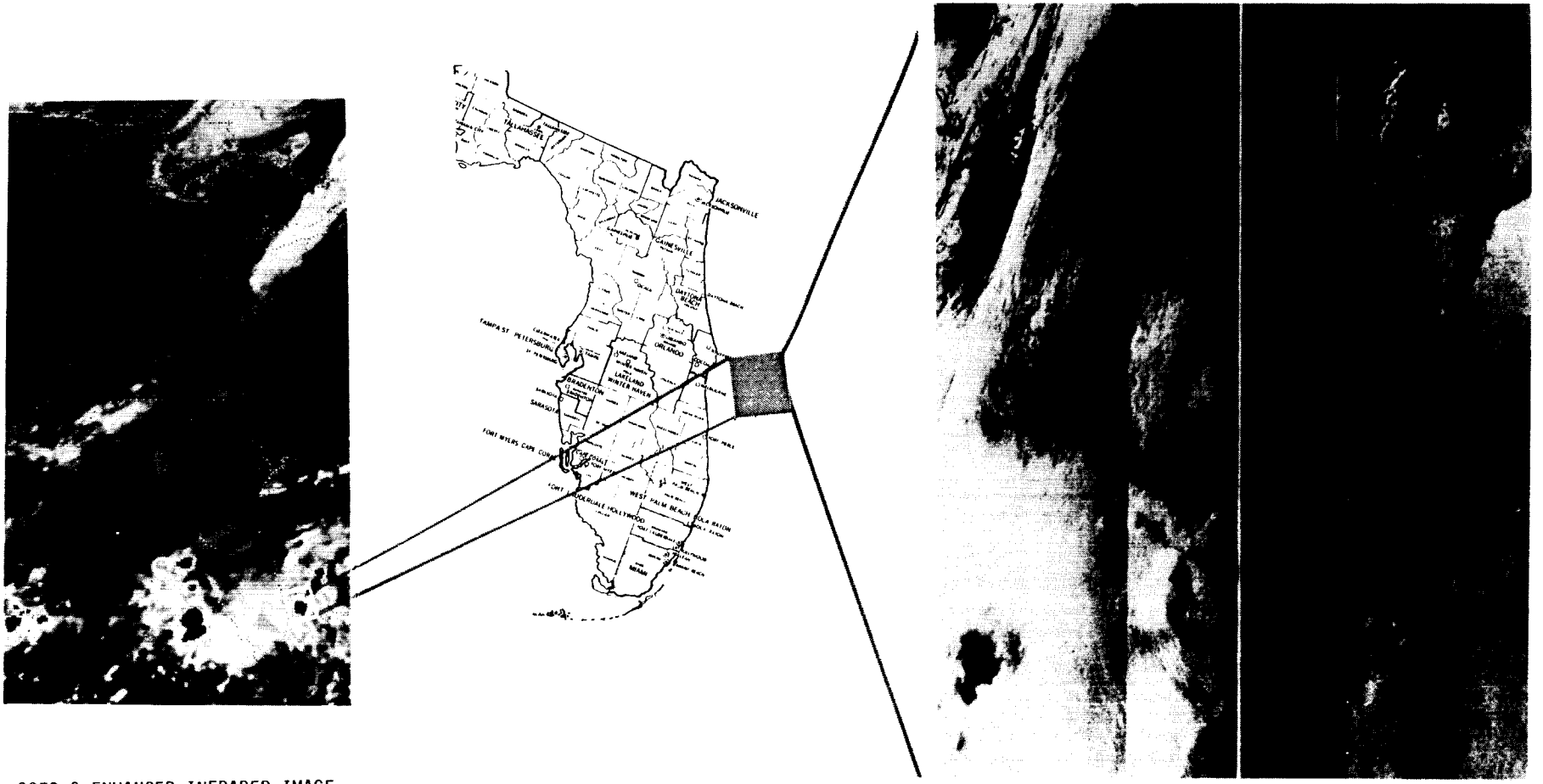

GOES 2 ENHANCED INFRARED IMAGE
0600 EDT-JULY 8, 1978

SEASAT SYNTHETIC APERTURE RADAR IMAGE
0604 EDT-July 8, 1978

Figure 29a. COMPARISON OF GOES 2 IMAGE WITH THE SEASAT IMAGE SHOWING THE ABILITY OF THE SEASAT MICROWAVE INSTRUMENT TO PENETRATE CLOUD COVER. THE GOES 2 IMAGE SHOWS THE DESIGNATED AREA COVERED BY CLOUDS. SEASAT SHOWS OCEAN SURFACE FEATURES SUCH AS GULF STREAM MOTION (UPPER LEFT) AND SURFACE ROUGHNESS (LOWER LEFT) DUE TO RAIN SHOWERS. THE BLACK AREAS WITHIN WHITE AREAS ARE RAIN SQUALLS.

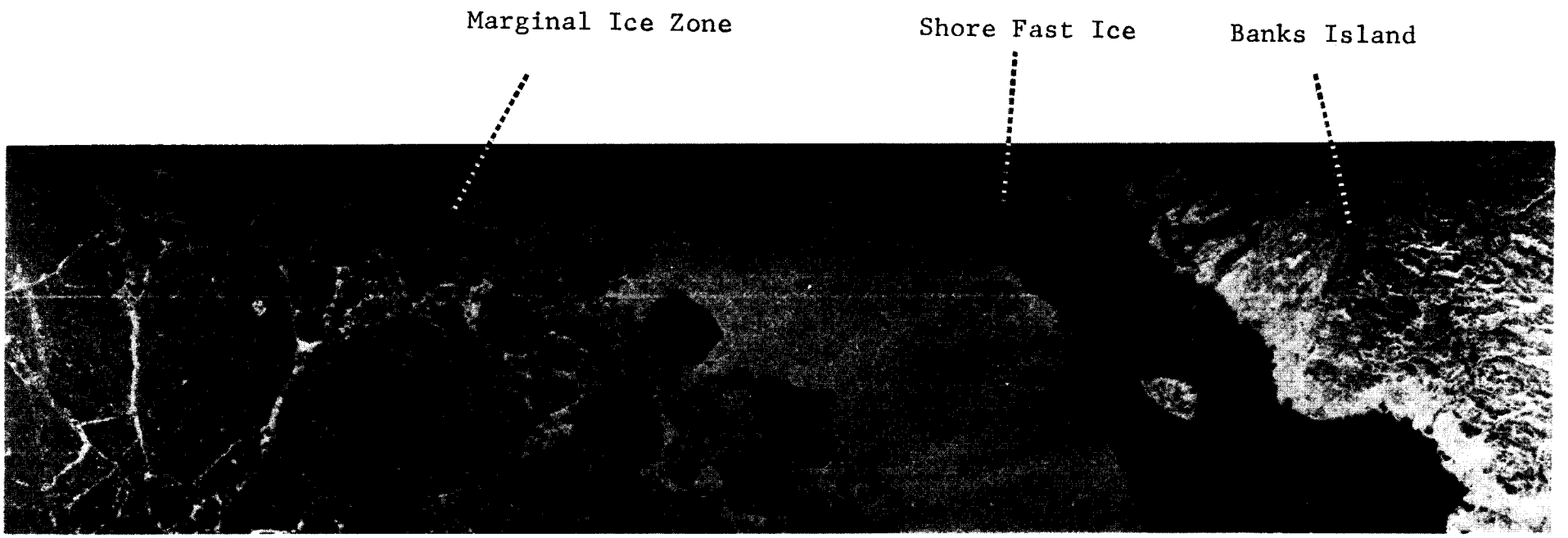

Figure 30. The Synthetic Aperture Radar (SAR) Image of Banks Island, Canada, And Various Types of Sea Ice on July 11, 1978.

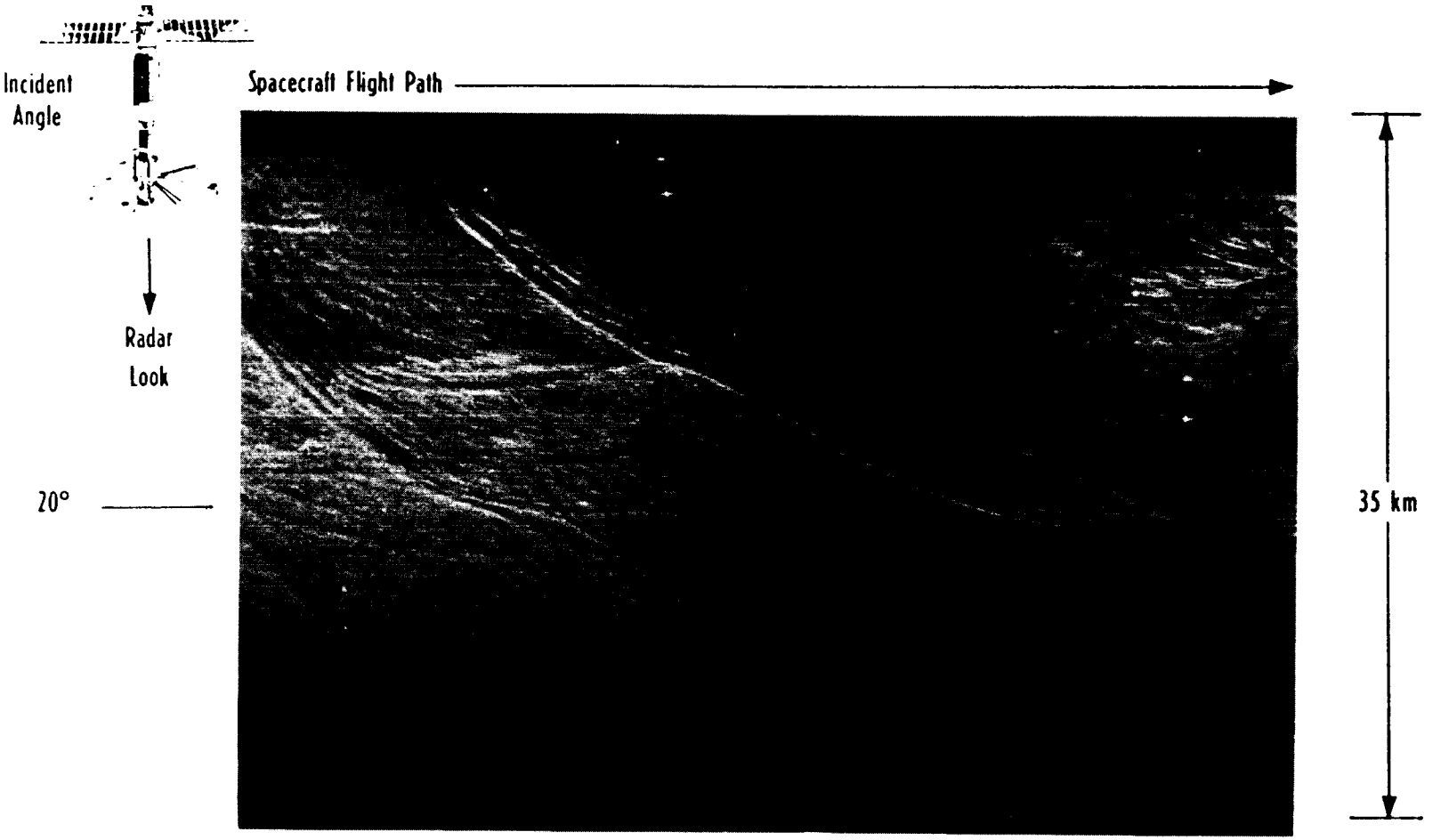

Figure 31. SAR Images of Hudson Canyon Area off the U.S. East Coast (Rev 1232; September 21, 1978).

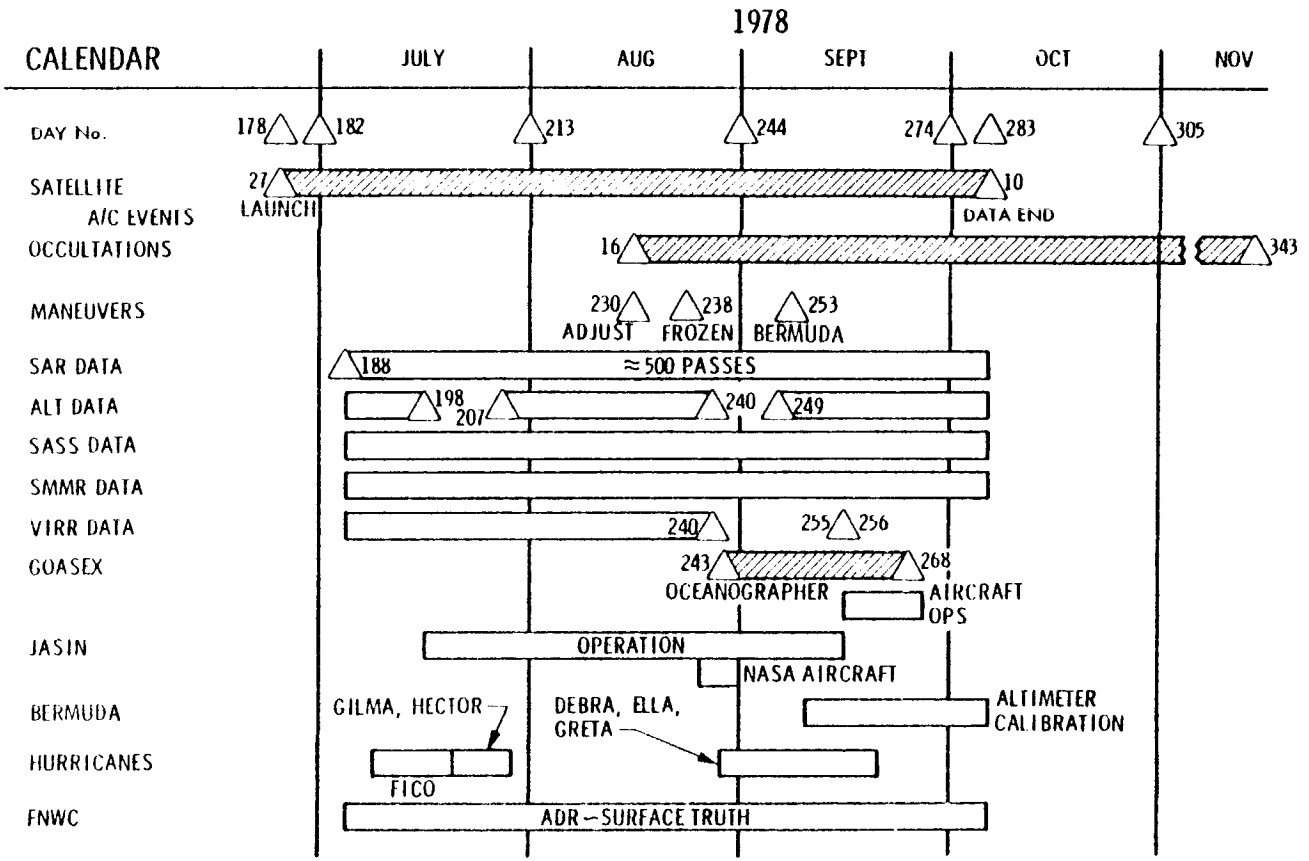

Figure 32. Seasat Mission Profile Showing Days of Data Collection.

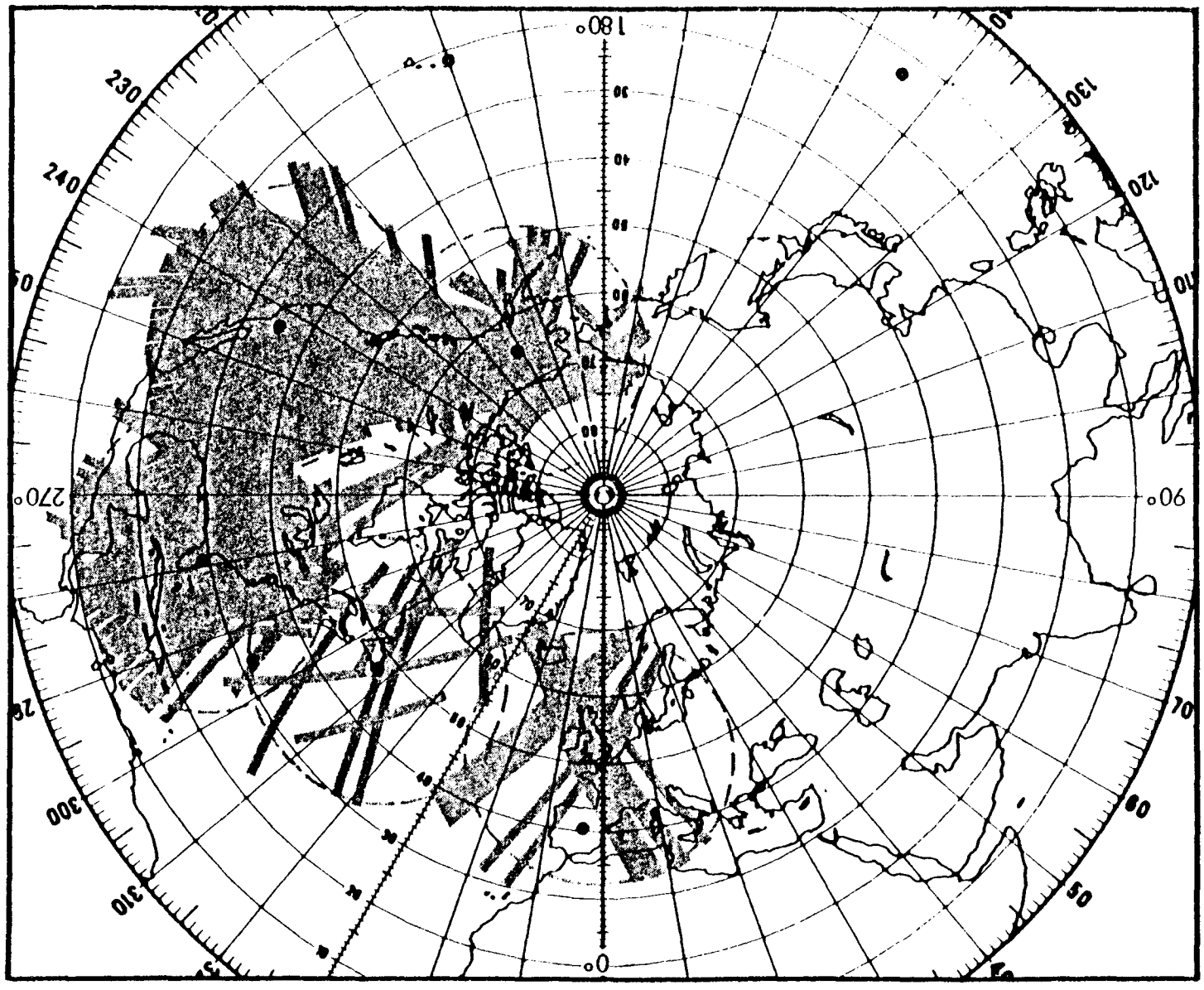

Figure 33. Seasat SAR Data 33 Collection Coverage from July 3rd to October 10th, 1978 (Revs 107-1502).

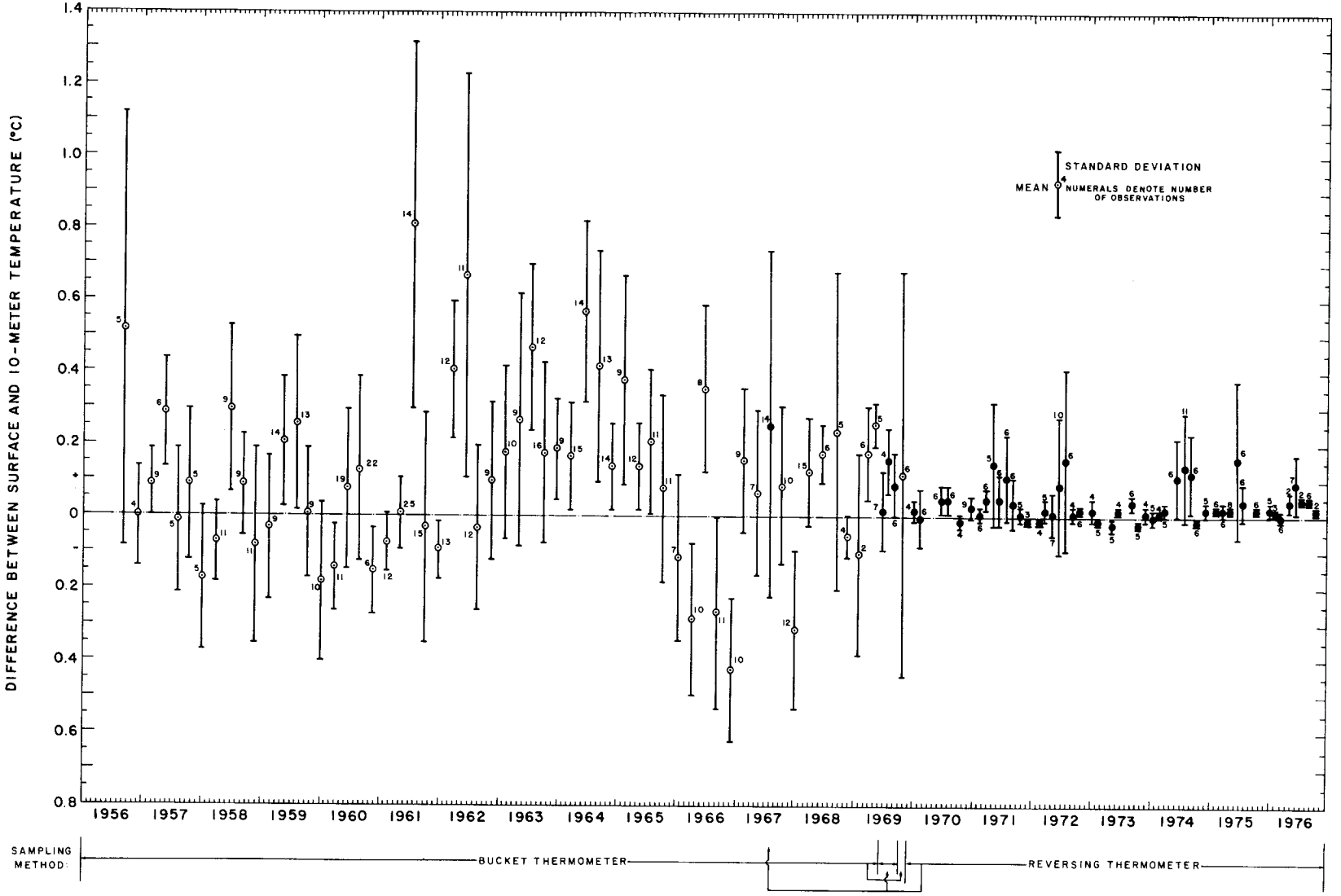

Fig. 1 Cruise mean differences between surface and 10-m temperatures (°C), and the associated standard deviations, for each cruise at Station"P" during the period 1956-1976. The methods used to determine the surface temperatures are also indicated. The closed circles represent surface temperatures measured with reversing thermometers. The 10-m temperatures were measured with one or two reversing thermometers. Two thermometers were utilized after mid-May 1969.

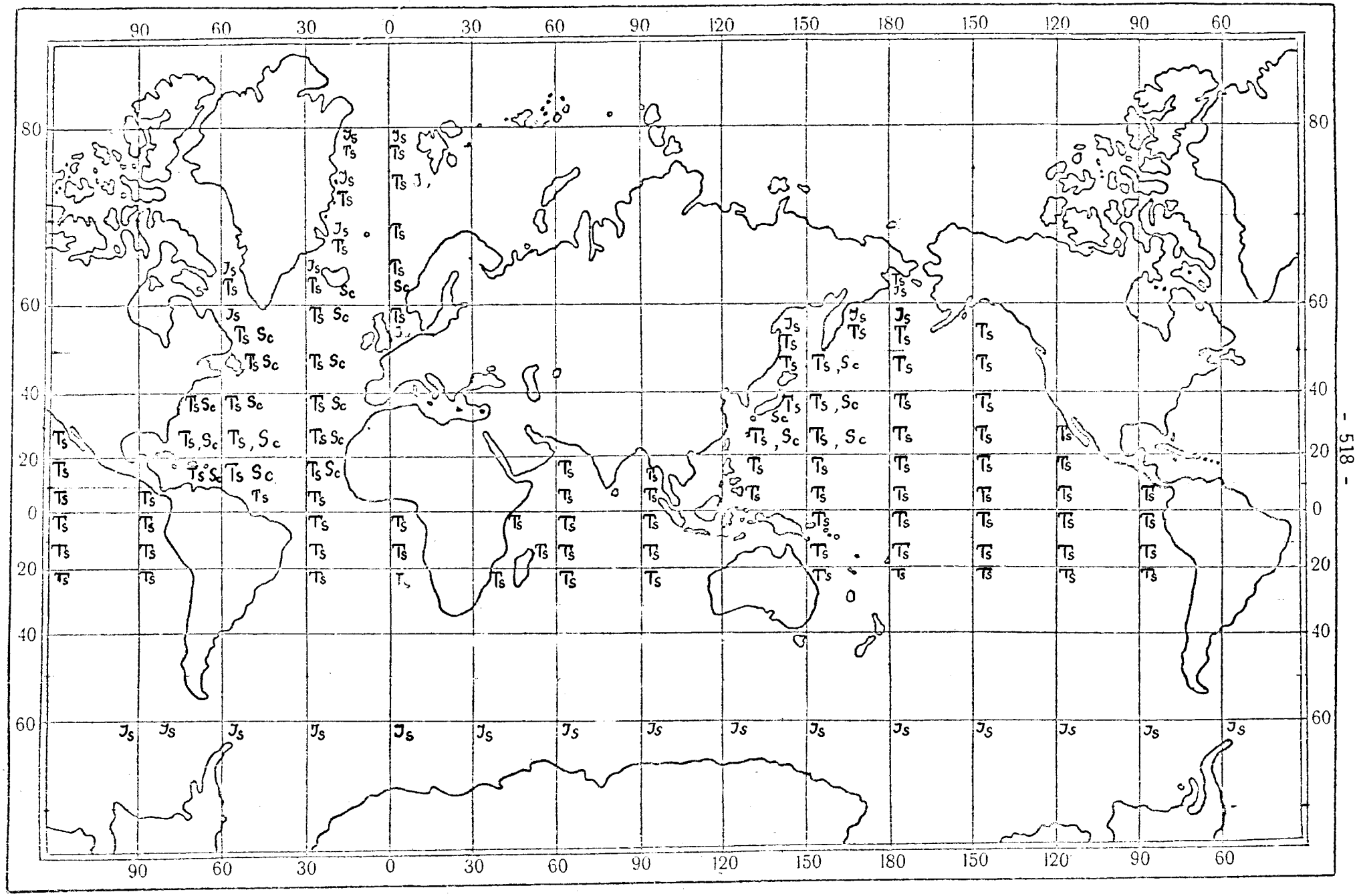

Figure 1 - (T_S - surface temperature; S_C - sea conditions; J_S - ice conditions)

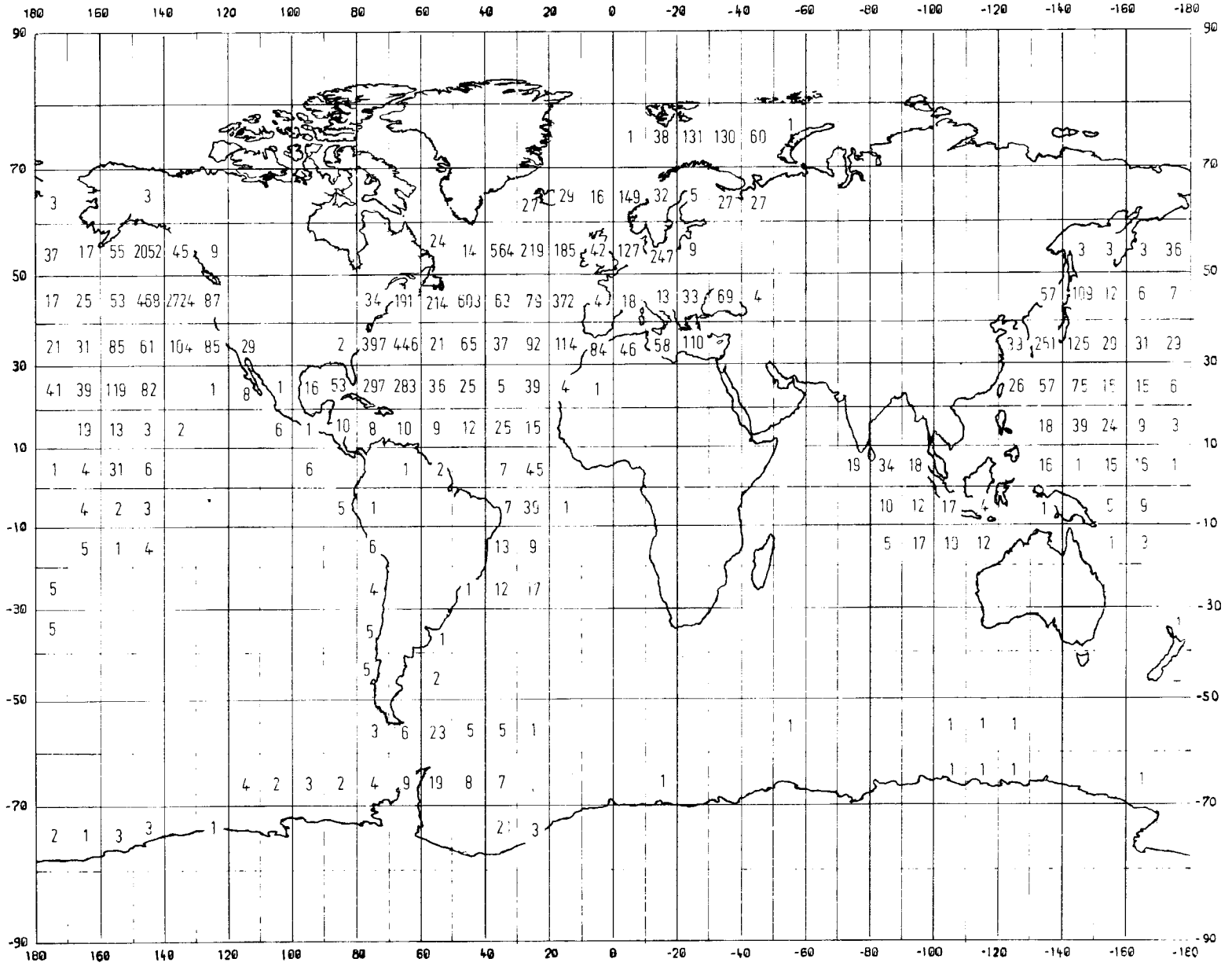

Geographical distribution of BATHY/TESAC reports received at the Deutsches Hydrographisches Institut from January to June 1978

Fig.1

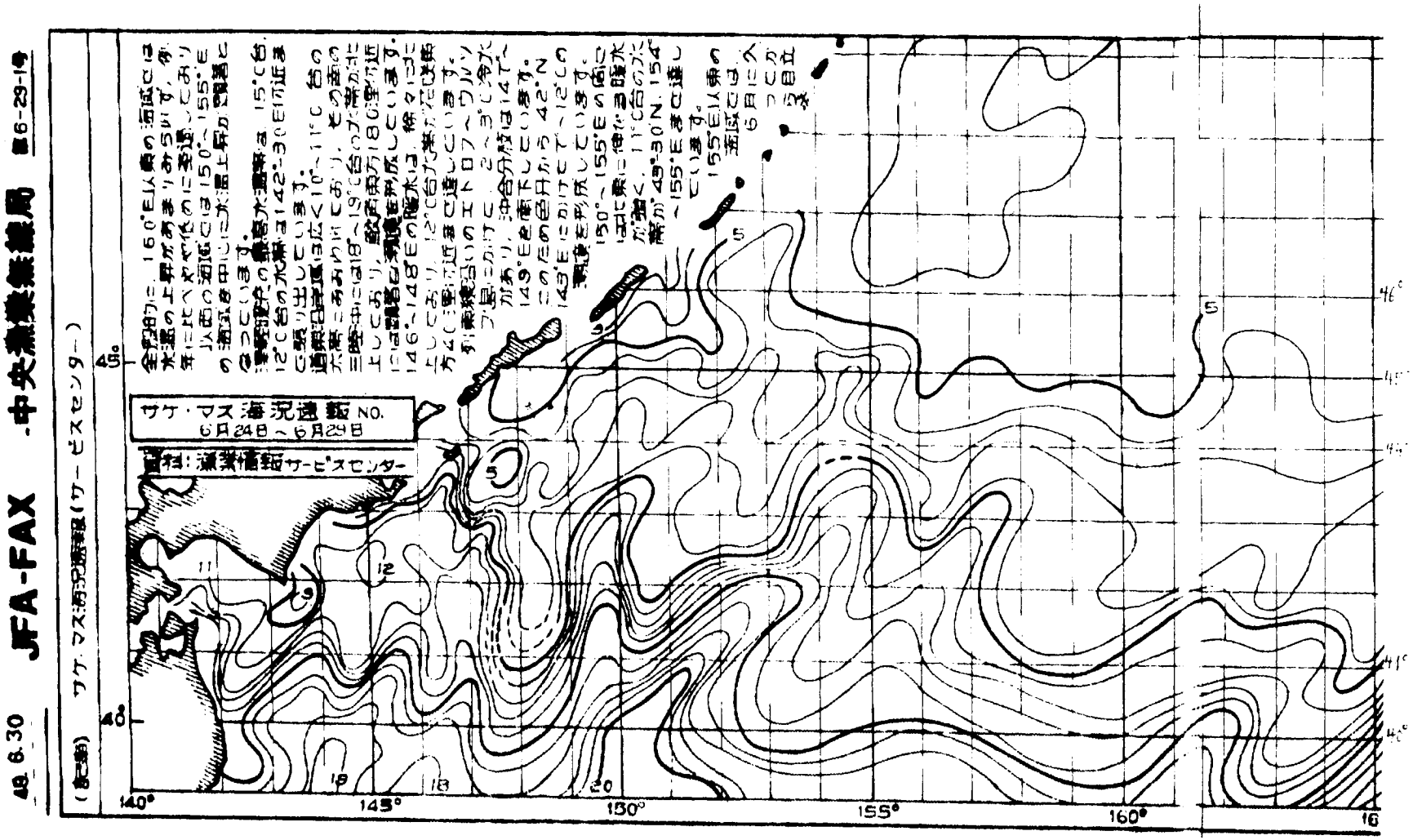

Figure 4: MAP C, Western North Pacific Ocean (Excerpt only: the original map covers the area from 140° to 180°E; for translation of Japanese text see Annex I)

Fig.4

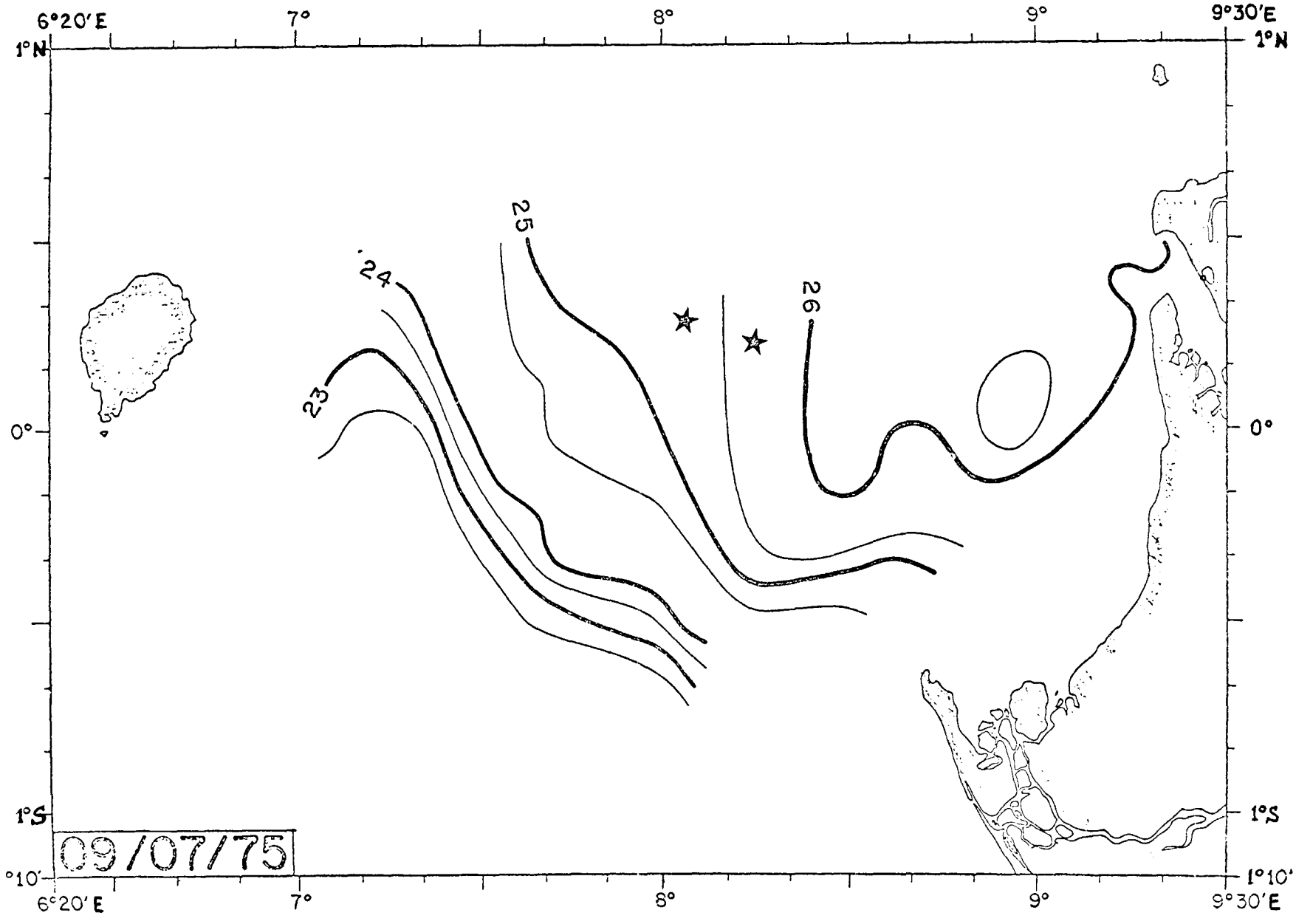

Figure 1: Sea surface temperature map for the Gulf of Guinea, 9 July 1975
(* = location of tuna fleet)

Fig.5

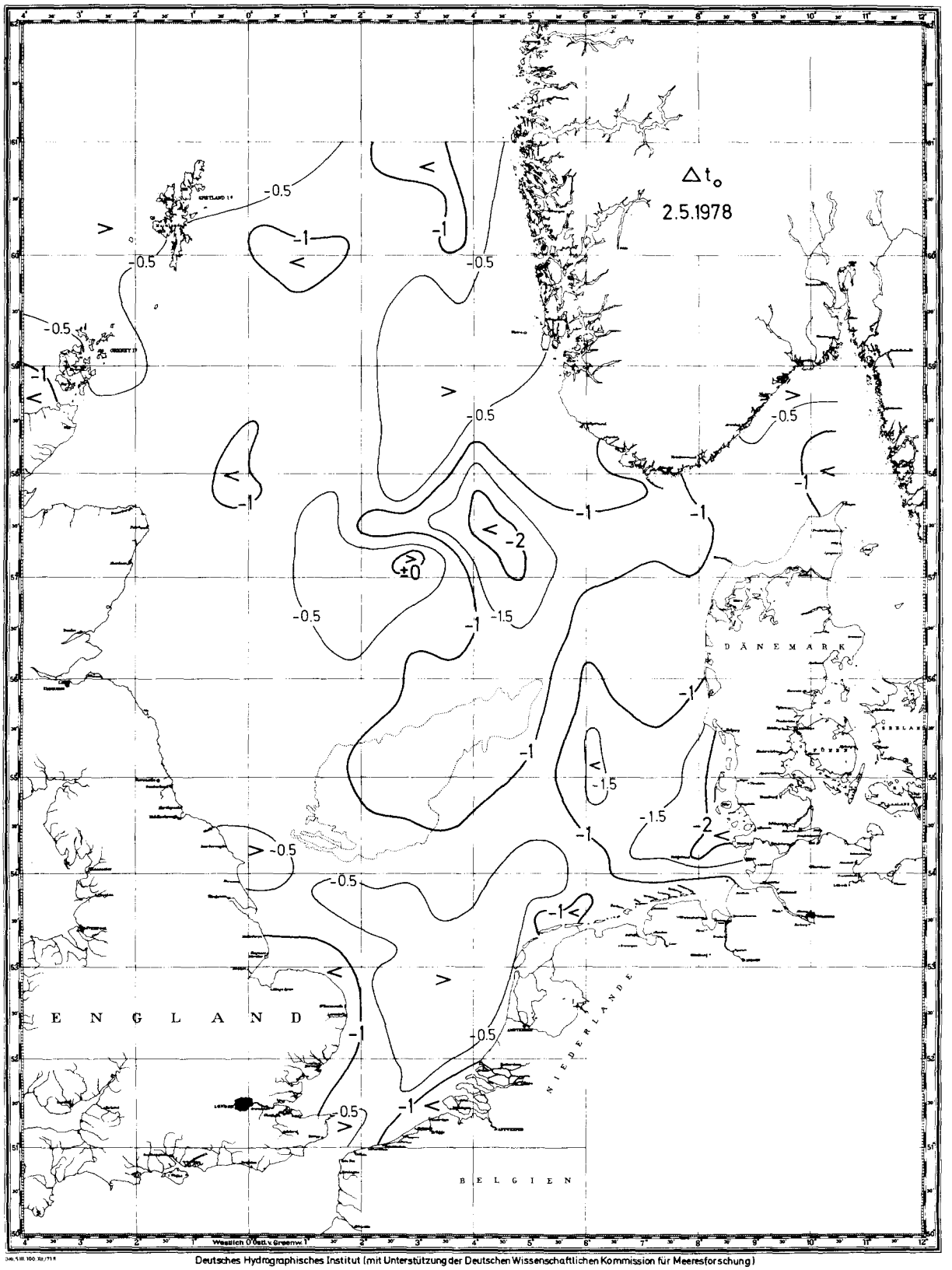

Fig.8 SST Anomalies North Sea

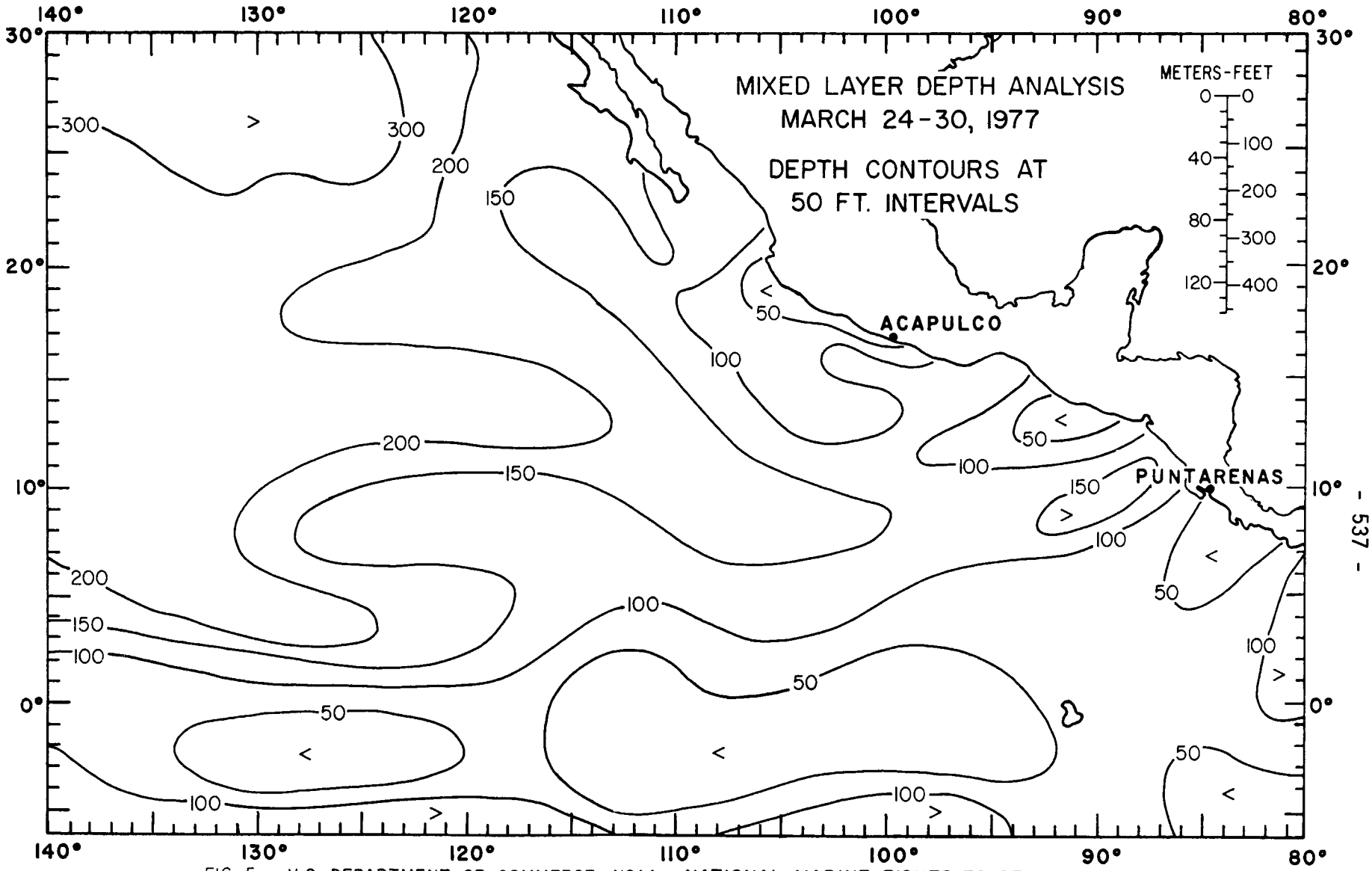

FIG. 5 : U.S. DEPARTMENT OF COMMERCE, NOAA NATIONAL MARINE FISHERIES SERVICE, FOC La Jolla, Calif.

Fig.9

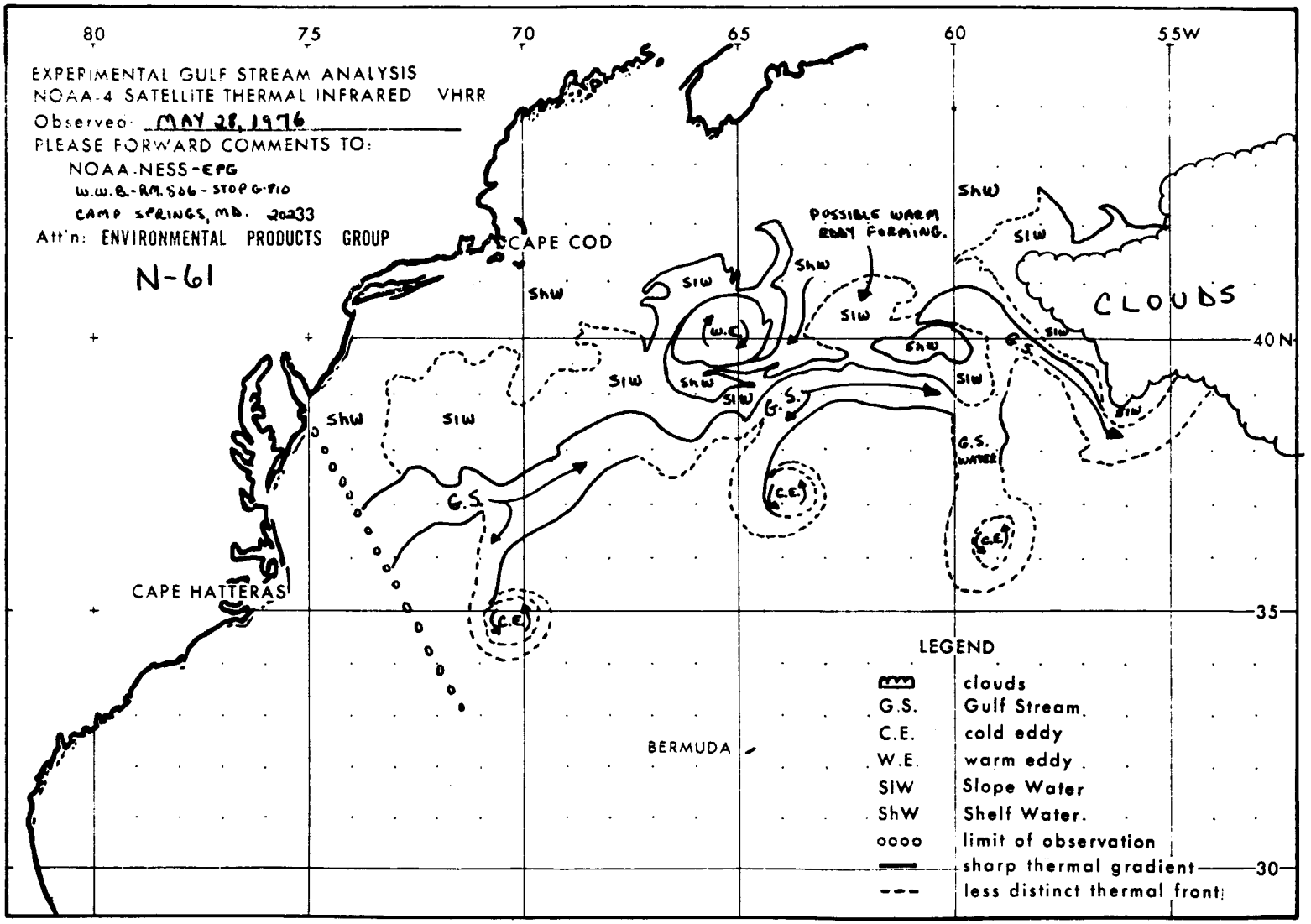

Figure 2 - Gulf Stream Analysis corresponding to Figure 1.

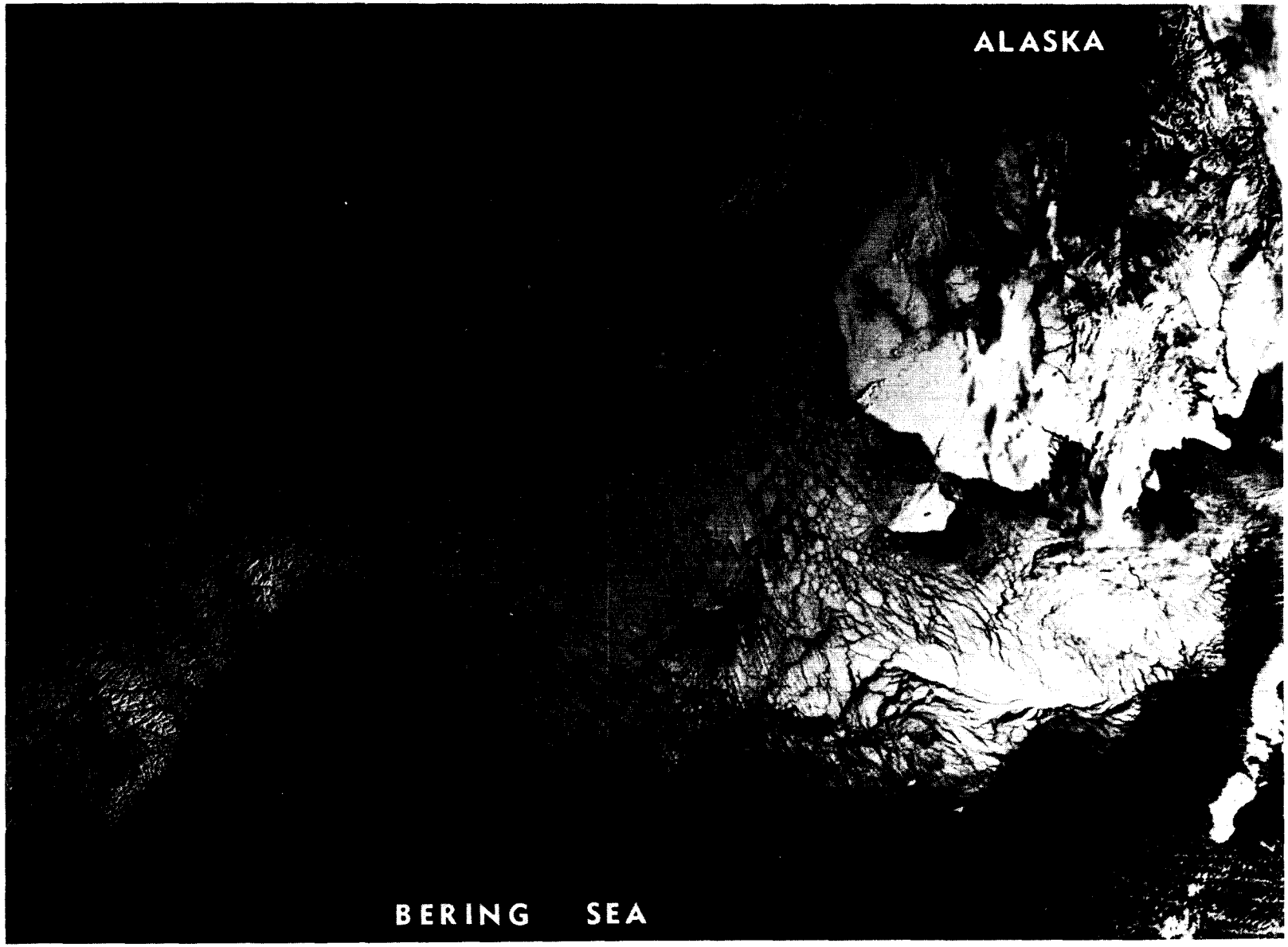

Figure 3 - NOAA-4 VHRR Visible image of sea ice in the Alaskan seas, March 17, 1976.

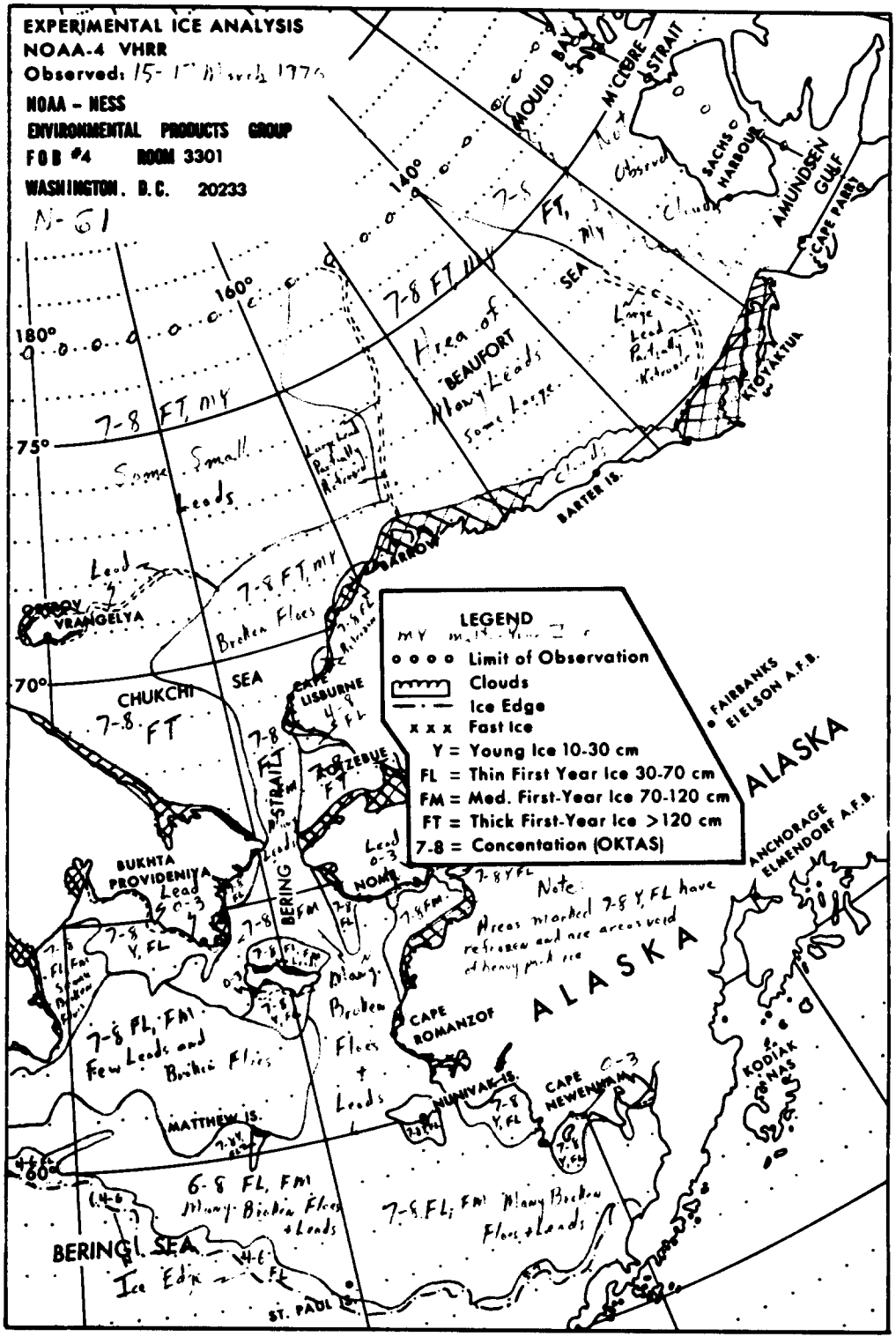

Figure 4 - Alaskan Ice Analysis corresponding to Figure 3.

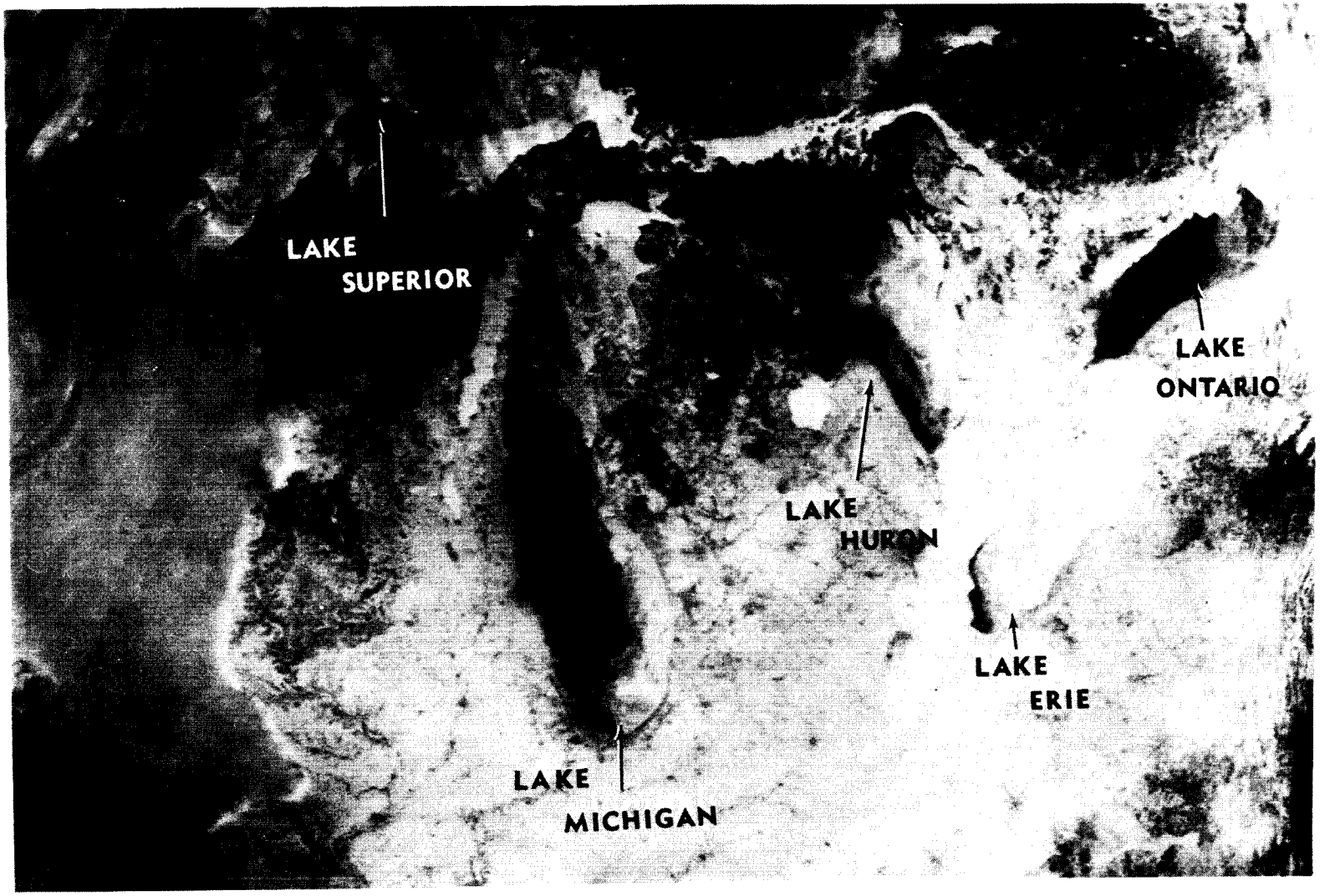

Figure 5 - NOAA-5 VHRR Visible image of ice conditions in the Great Lakes, February 7, 1977.

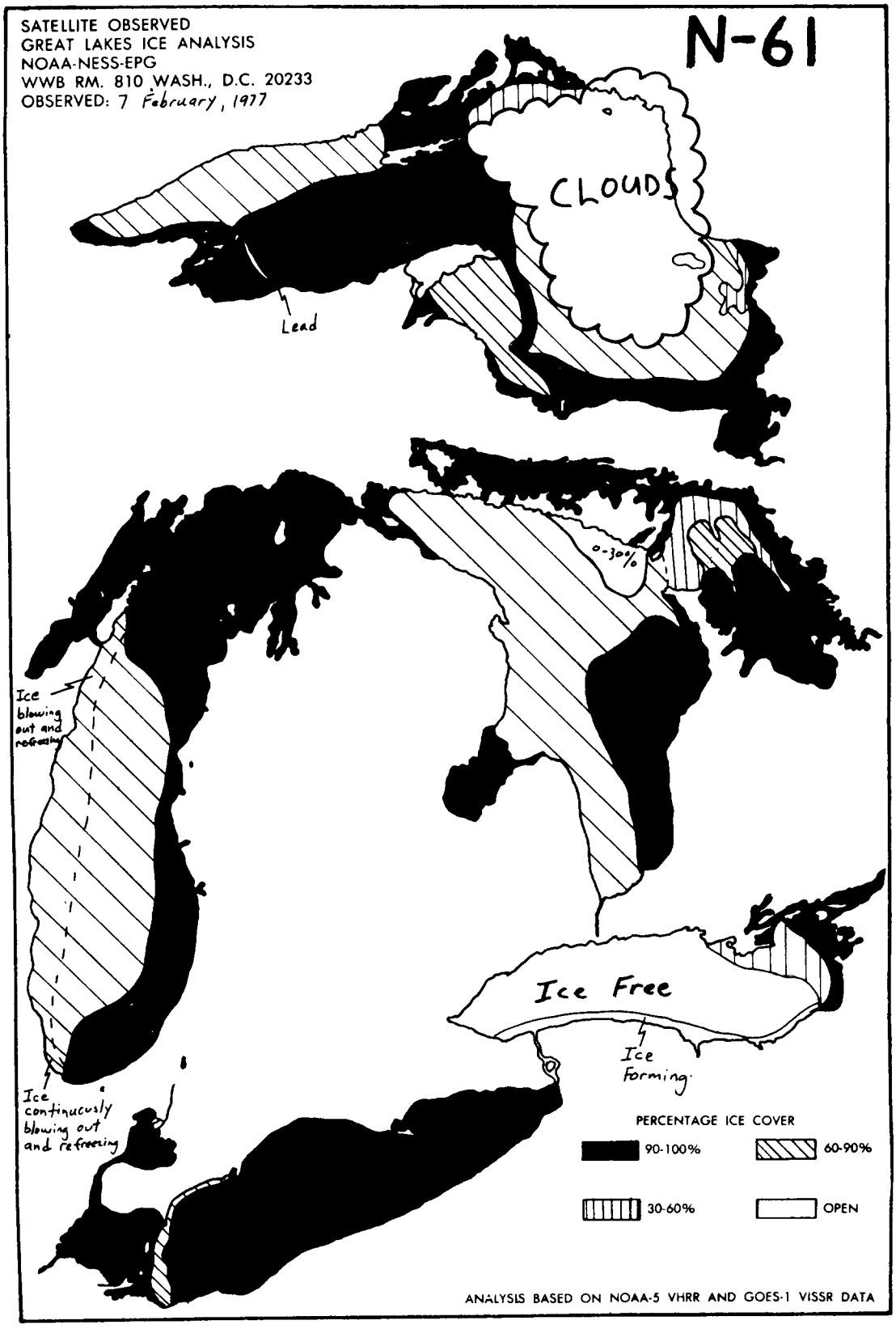

Figure 6 - Great Lakes Ice Analysis corresponding to Figure 5.

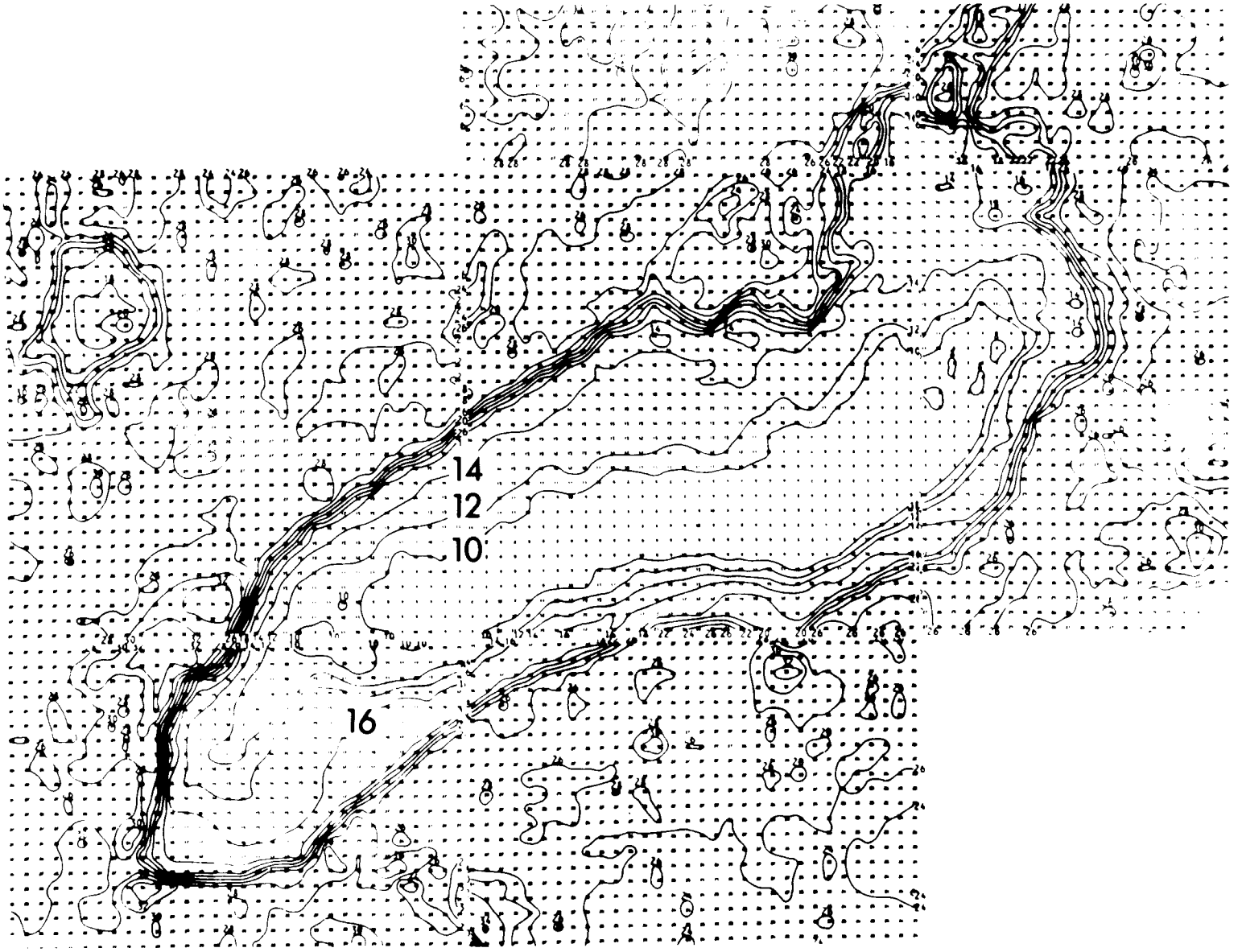

Figure 7 - Computerized Lake Ontario Water Temperature Analysis from NOAA-4 VHRR data, June 3, 1976.

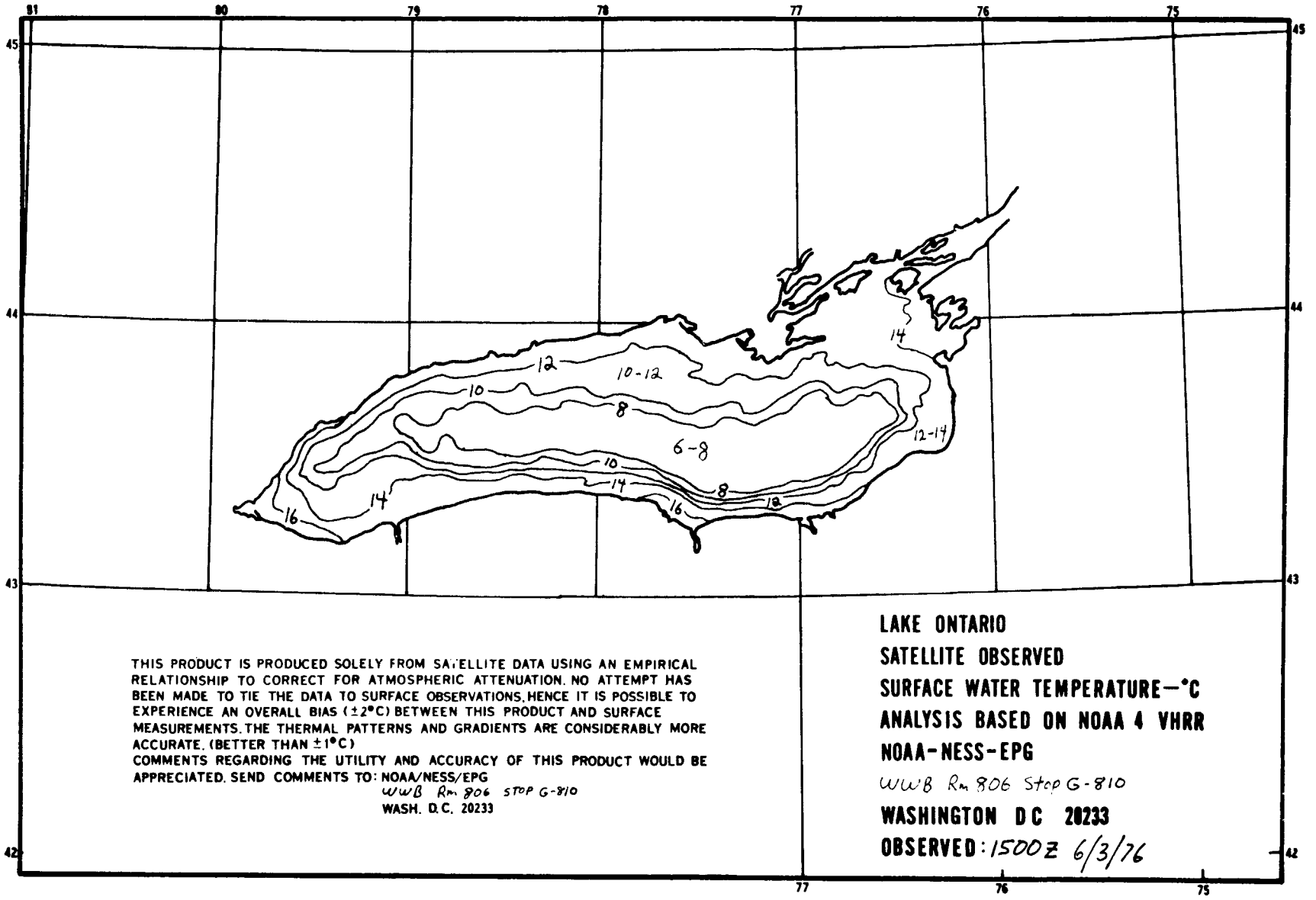

Figure 8 - Finalized Surface Water Temperature Analysis corresponding to Figure 7.

GOSSTCOMP SEA SURFACE TEMPERATURES

LONGITUDE WEST OF GREENWICH IN TENTHS OF DEGREES

LATITUDE IN TENTHS OF DEGREES

	900	880	860	840	820	800	780	760	740	720
340	** **	** **	** **	** **	** **	** **	** **	+2 241	+2 236	+2 233	+2 232	+2 229	+1 225	+1 216
330	** **	** **	** **	** **	** **	** **	+1 226	+1 221	+1 229	+1 230	+2 232	+1 228	+1 221	+1 216
320	** **	** **	** **	** **	** **	+1 251	+1 230	+1 224	+1 232	+1 229	+2 229	+1 225	+1 218	+1 216
310	** **	** **	** **	** **	** **	+1 242	+1 245	+1 242	+1 238	+1 236	+1 229	+1 227	+1 223	+1 222	+1 220
300	** **	+1 231	+1 230	+1 228	+1 227	** **	** **	** **	+1 240	+1 244	+1 244	+1 241	+1 239	+2 229	+1 228	+1 225	+1 225	+1 223
290	+1 236	+1 235	+1 233	+1 230	+1 228	+1 228	+1 227	** **	** **	** **	+1 251	+1 241	+1 247	+1 241	+2 232	+2 232	+1 230	+1 229	+1 229
280	+1 237	+1 237	+1 236	+1 234	+1 231	+1 232	+1 233	+1 237	** **	** **	+1 251	+1 249	+1 245	+2 238	+2 235	+2 234	+1 233	+1 232	+1 234
270	+1 239	+1 238	+1 238	+1 238	+1 237	+1 239	+1 238	+1 240	** **	** **	+4 253	+3 250	+3 246	+3 237	+2 236	+2 237	+1 237	+1 237	+1 239
260	+1 239	+1 240	+1 243	+1 245	+1 249	+1 249	+1 246	+1 242	+1 248	** **	+4 258	+3 256	+3 252	+3 238	+2 239	+2 239	+2 241	+1 245	+1 248
250	+1 241	+1 245	+1 251	+1 255	+1 255	+1 253	+1 249	+1 245	+1 247	+1 242	+1 240	+1 240	+1 251	+3 240	+2 241	+2 243	+2 246	+1 249	+1 253
240	+1 245	+1 250	+1 256	+1 258	+1 258	+1 256	+1 252	+1 248	+1 247	+1 243	+1 241	+1 245	+1 252	+3 252	+3 245	+2 248	+2 251	+1 255	+1 254
230	+1 246	+1 248	+1 253	+1 257	+1 262	+1 263	+1 256	** **	** **	** **	+3 263	+3 260	+3 260	+3 257	+3 247	+2 254	+2 256	+1 256	+1 255
220	+1 245	+1 246	+1 250	+1 255	+1 268	+1 269	** **	** **	** **	** **	** **	** **	** **	+3 262	+3 258	+2 259	+2 260	+1 258	+1 256
210	** **	** **	** **	** **	+1 272	+1 270	+1 269	+1 267	+1 266	+1 265	+1 261	+1 260	** **	** **	** **	+3 262	+2 262	+1 259	+1 257
200	** **	** **	** **	+1 268	+1 270	+1 270	+1 269	+1 267	+1 266	+1 266	+1 264	+1 261	+1 261	** **	** **	** **	+ 266	** **	** **
190	** **	** **	** **	+1 267	+1 268	+1 269	+1 268	+1 267	+1 266	+1 266	+B 264	+B 263	+A 263	+A 258	+A 258	+A 258	+A 258	** **	** **
180	** **	** **	+1 264	+1 265	+1 267	+1 267	+1 267	+C 267	+D 266	+E 265	+F 265	+G 266	+G 266	+G 265	+E 262	+B 258	+A 257	+A 259	** **
	900	880	860	840	820	800	780	760	740	720

LOCATION OF TEMPERATURE WITH REFERENCE TO LAT LONG GRID

+5 -AGE OF TEMPERATURE IN DAYS,IF BLANK OVER 9 DAYS.
IF LETTERED 1 DAY OLD,WHERE THE NUMBER OF OBSERVATIONS USED IN ANALYSYS AT POINT IS GIVEN IN LETTER CODE, A IS 1-4 OBS,B IS 5-8...ETC
145-TEMPERATURE IN DEGREESX10 CENTIGRADE
(RIGHT JUSTIFIED)

LAND IS SIGNIFIED BY ASTERISKS

Figure 9 - Computer terminal display of 100 km analyzed SST field for 12/22/78. Depicted are the waters surrounding Cuba and the state of Florida.

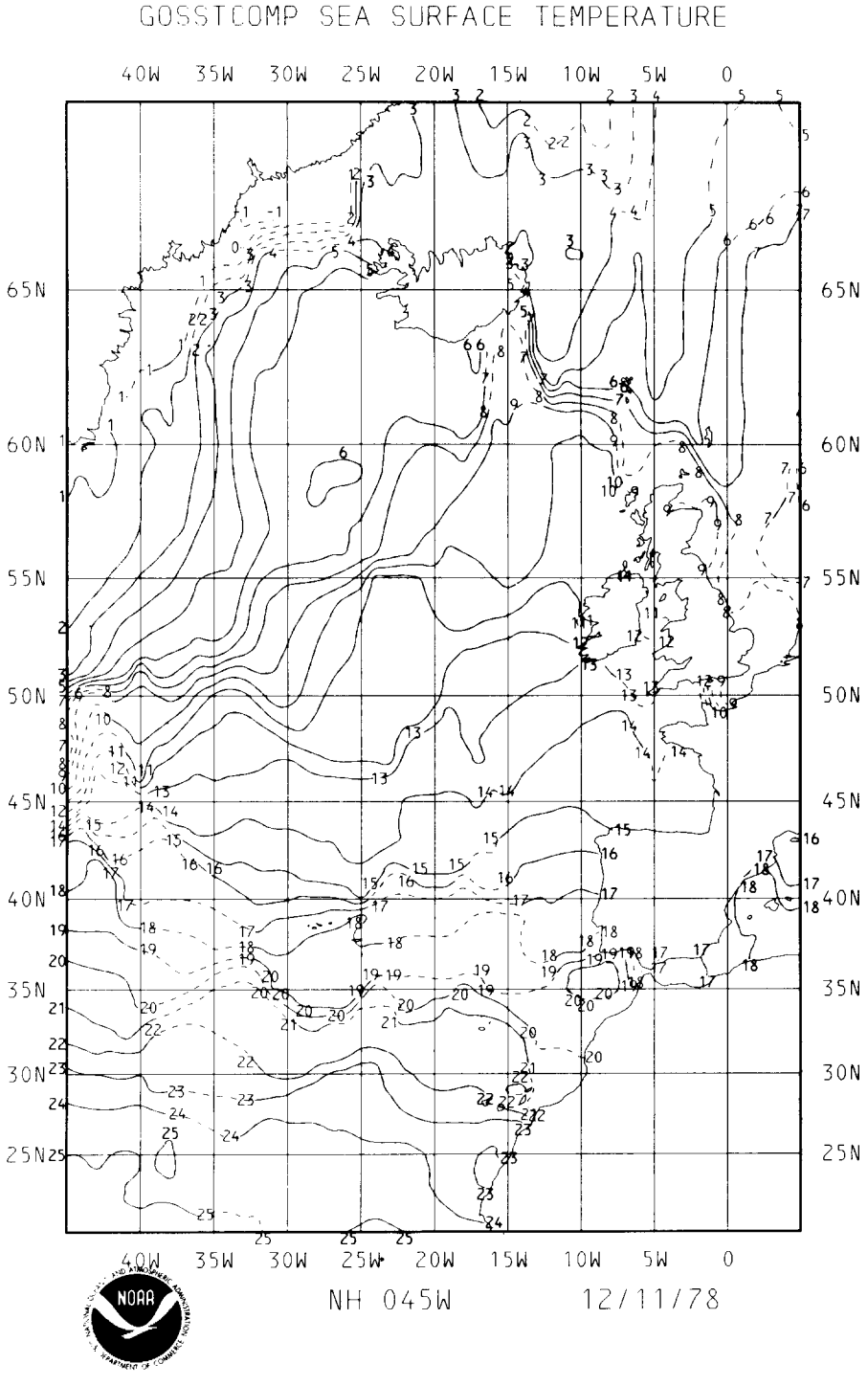

Figure 10 - Isotherm contour map of the eastern North Atlantic Ocean derived from the 100 km analyzed SST field. Isotherm labels are in Celsius. Dashed isotherms indicate regions with no satellite coverage for at least three days.

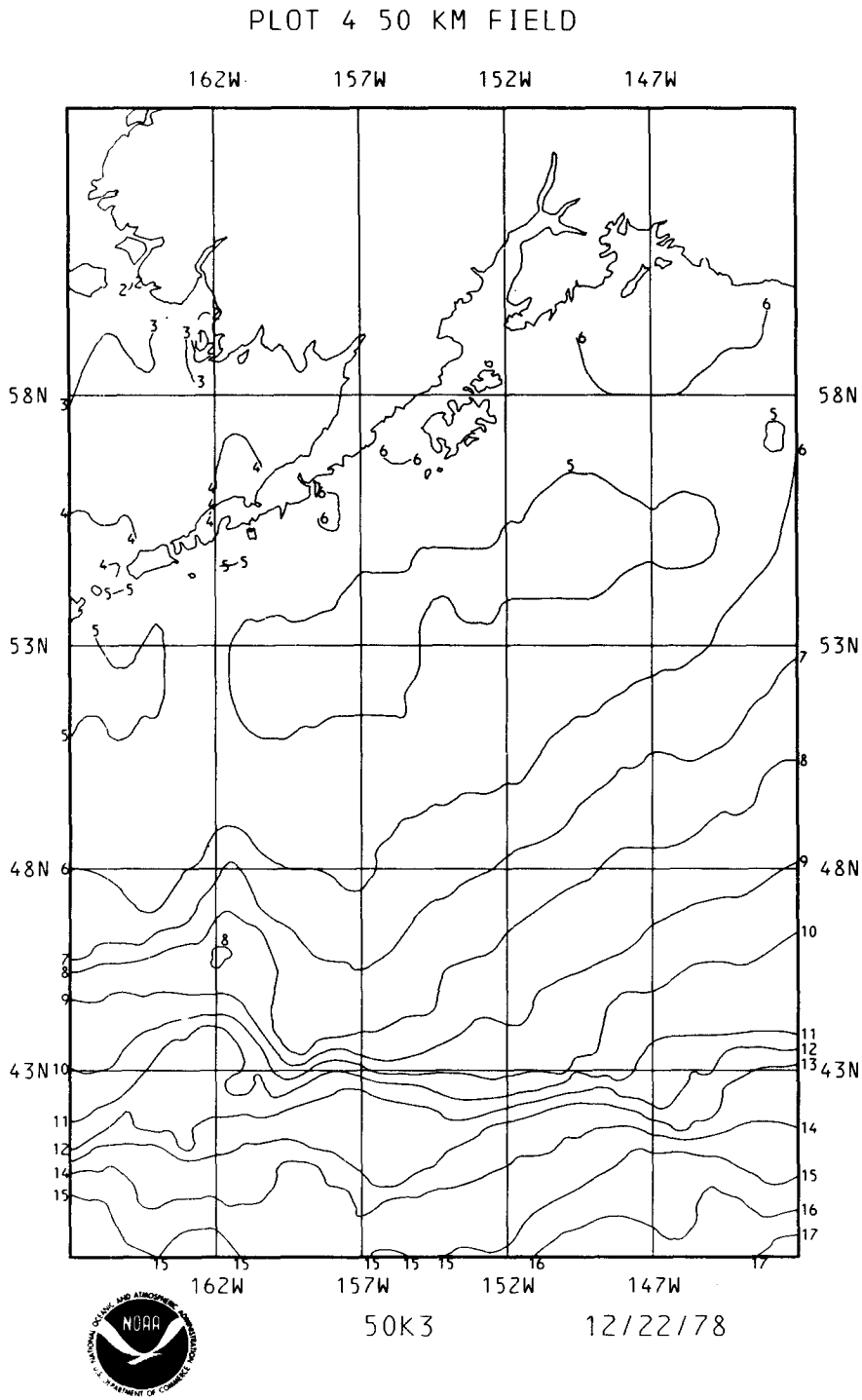

Figure 11 - Isotherm contour map of the North Pacific, south of Alaska, derived from one of the 50 km analyzed SST fields. Isotherm labels are in Celsius.

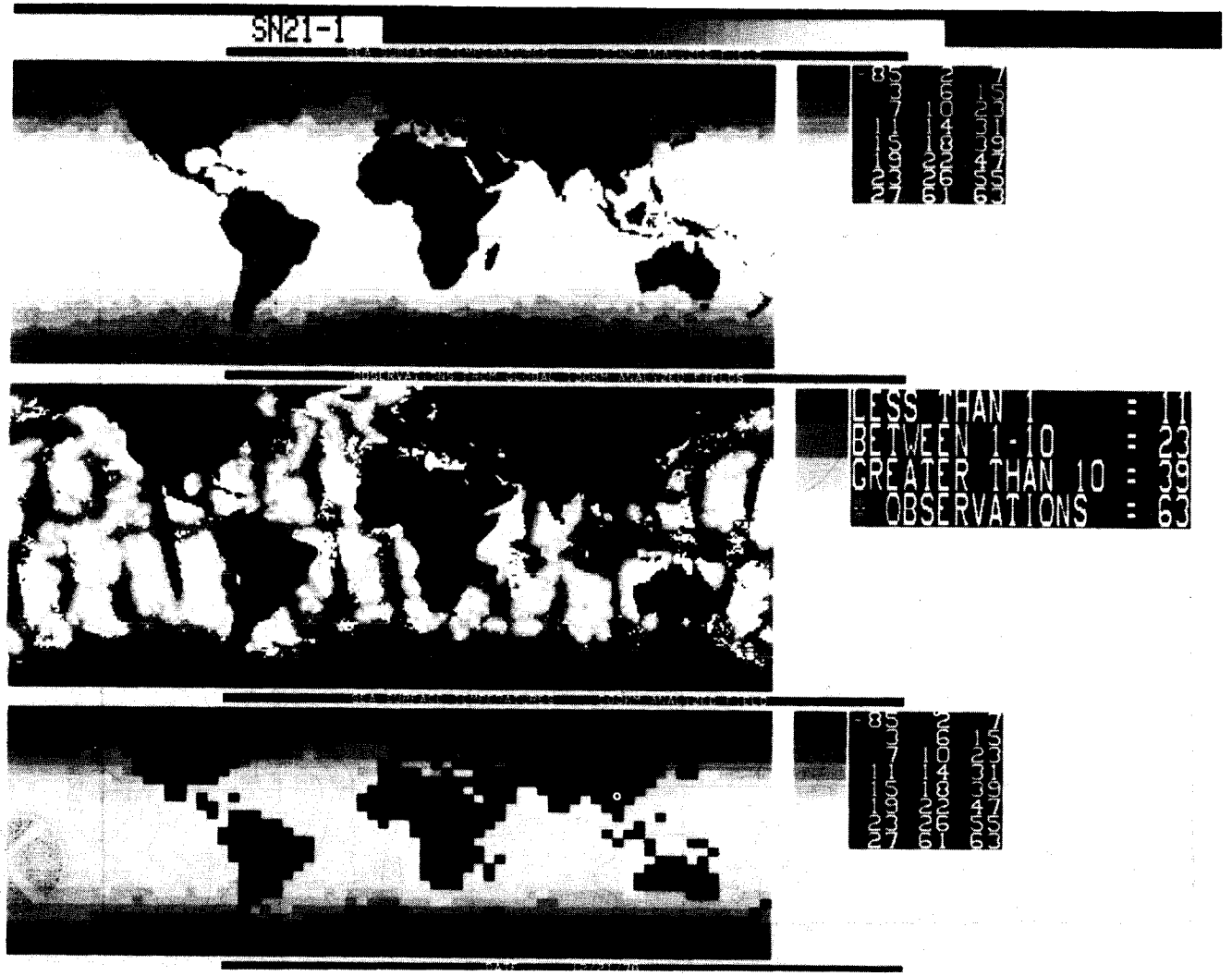

Figure 12 - Photographic display of the 100 km and 500 km analyzed fields. The top display of the 100 km field shows surface temperature in gray shades. The gray wedge to the right indicates the temperature range (e.g. 27°C to 61°C for the white region) and the gray value (e.g. 63 is white). The middle display shows the distribution of observations. White squares show observation location; gray shades indicate observation density. Surface temperatures in the 500 km field are depicted in the bottom display.

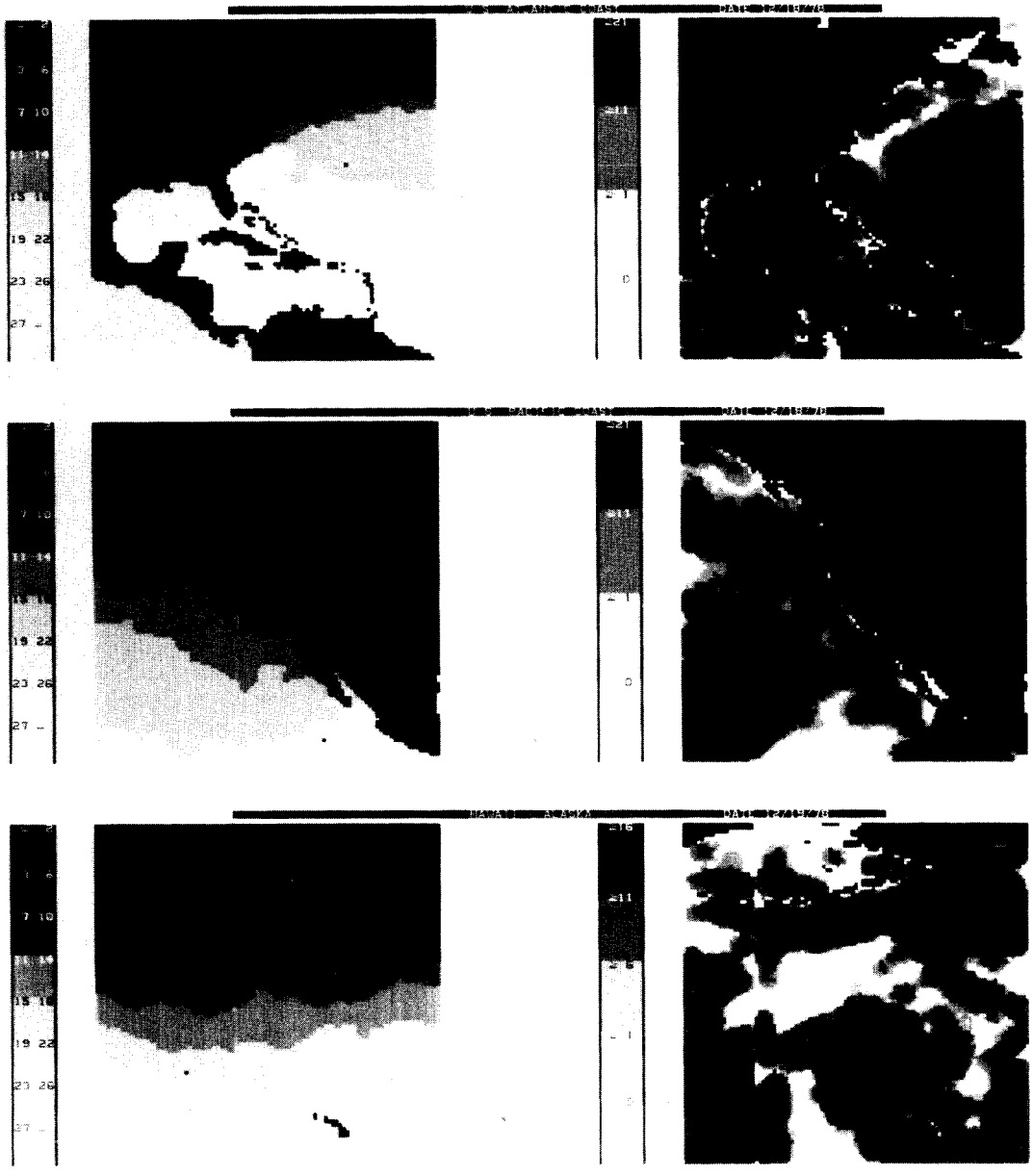

Figure 13 - Photographic display of the three 50 km analyzed fields. The left display shows surface temperature in gray shades. Temperature ranges are given on the left in Celsius. The right display shows observation density for the week prior to the analysis date. The number of observations depicted by each gray shade is given to the left.

AUTOMATIC WAVE FORECAST FOR THE SOUTH ATLANTIC OCEAN

Omar R. Rivero - Carlos E. Ereño

ABSTRACT.

In this work a study on the application for the South Atlantic Ocean of a diagnosis and forecast model of the state of the sea is carried out, based on the Method of Spectral Densities Nº 5 which was developed in the Marine Meteorology of France.

With the same, the diagnosis of the state of the sea for deep waters is accom - plished by means of an IBM 360/50 computer, taking into account the wind force at each point of a grid formed by a network of points equally spaced. The method also allows by introducing the values of the wind field which result from the forecasted surface map, to obtain the automatic forecast of the state of the sea.

Operative implementation of the model was attained from January 1974. At present radiotelegraphy and facsimile emissions are carried out with the products obtained from the same.

After a year of experiences and through comparison with observations carried out on board Argentine Navy oceanographic ships as well as on other vessels, it was possible to establish empirical corrections which allowed outstretching the results of the deep water model up to 20 fathoms.

The daily diagnosis is automatically recorded and its results are statistically compiled. It is hoped that the said information may contribute to the knowledge of mean parameters of the state of the sea.

By means of instruments mounted on board a petroleum prospecting platform, observations of wave parameters have recently been made with a minimum subjectiveness. Comparison with values diagnosed by the model will provide enough elements for considering, in data to be initially introduced, not only wind direction and force but some other representative factors of the effects on the boundary layer.

1. INTRODUCTION.

A study of Method Nº 5 of Spectral Densities for the forecast of the state of the sea, which is used operationally since 1965 in the Marine Meteorology of France has been carried out. With the same it is possible to forecast, by means of a computer, the state of the sea for deep waters as a function of the geostrophic wind for each point of a grid. Besides, by introducing the same values which result from the forecasted meteorological surface chart, the method allows the automatic forecast of the state of the sea. Nevertheless, due to present limitations which are a consequence of the lack of sea data, forecasts are still realized non automatically, on the basis of the corresponding diagnosis.

The comparison of values obtained by the model with observations carried out on shipboard has allowed the establishment of empirical corrections, making it possible to extend the results to shallower waters of the Argentine atlantic coast.

By means of the automatic record of the model's issues some statistics of height and period of significant waves have been obtained and determined their seasonal variation.

2. THE MODEL.

The model's basis for calculation are the following:

It is considered that sea waves are generated by a superposition of a great number of sinusoidal wave trains of which the periods and propagation direction are different.

The following assumptions are made:

a) Each wave train propagates independently of the others in its own direction at a group speed which depends of the period of the waves.

b) The amplitude of a given component is the function of wind speed.

c) Sixteen azimuth values increasing clockwise, with their origin in the geogra - phical North, are taken. Speeds up to 85 knots are considered; it is supposed that speeds less than 10 knots do not affect the state of the sea and that speeds greater than 85 knots produce a similar effect to that of the latter value. Wind speed values are introduced at 5 knots intervals.

d) The spectrum considered is formed by 6 bands of 3 seconds for a spectral interval of 2, 5 to 20, 5 seconds. Thus, the sea state in each point is described by 76 spectral and angular components.

With these hypothesis is used the following work equation:

$$\frac{dq}{\partial q} = \Gamma\left[W, |\theta - \omega|, T\right] = \frac{Aq}{T^4} mo - \vec{V}(T,\theta) \cdot \nabla q(T,\theta)$$

where:

$\Gamma[W, |\theta-\omega|, T] = P(T,W) \times S(\theta - \omega)$: increase term

$\frac{Aq}{T^4} mo$: damping term

$\vec{V}(T,\theta) \cdot \nabla q(T,\theta)$: propagation term

q : spectral-angular density

W : surface wind in knots

T, S : period of a component in seconds

θ, φ : azimuth of a component

ω : azimuth of surface wind

mo : $\sum_T \sum_\theta q\,T,\theta$

Γ : spectral-angular increase

P : spectral increase

$S(\theta-\omega)$: funcion of angular dispersion, so that

$$\int_{-\pi/2}^{\pi/2} S(\theta-\omega)\, d(\theta-\omega) = 1$$

$|\theta - \omega|$: absolute value of angle $\theta - \omega$

$\vec{V}(T,\Theta)$: g roup speed of component (T, Θ)

$$V(T,\Theta) = \frac{gT}{4\pi}$$

A : damping empirical coefficient

Consequently, the said treatment implies taking into account three different phases: propagation, increase and damping.

Propagation is punctual and displaces in its own direction each spectral-angular density with the theoretical speed for its period; increase is a function of speed and direction of wind; and damping is a function of the winds contrary to wave development. The conjunction of these three effects is considered as a proper objective representation of the state of the sea.

The grid used (figure 1) covers with a net of points spaced 90 nautical miles, an area comprised between the atlantic coast and the following extreme points: a) 25°00' S, 25°00' W; b) 55°00' S, 12°30' W; c) 56°30' S, 72°30' W.

In order to obtain the corresponding charts, the accumulation of spectral-angular densities in each node of the grid is carried out by means of a computer. Time interval for the introduction of data is of three hours and, if not imposed, these are automatically introduced by the model. For practical reasons the imposition is carried out at intervals of 12 hours, though it would be desirable to do it at intervals of 6 hours.

This consideration in fact, means that for the 12 Z diagnosis, data of 23 Z are repeated during the six subsequent hours and data of 12 Z, during the six former hours. If at a given moment in that lapse the synoptic situation decidedly changes, the procedure can be modified.

As to the period in which the process is developed, it must be taken into account that the same cannot be indefinite, as analysis errors make it convenient to start again with the sea at zero in case they acquire considerable magnitude. It must be remarked that the mentioned errors, at any point, do not only affect the same but the rest of them.

Data input is obtained measuring, for each point of the grid, the distance in mm. between isobars and the orientation of the same. These values are introduced in the computer by means of an IBM 2740 terminal. As an issue of the computer is obtained the geostrophic wind and finally the state of the sea for each point. This is shown in figure 2 where, besides, lines of equal wave heights have been drawn. Figure 3 shows the code form for the issue of the automatic forecast.

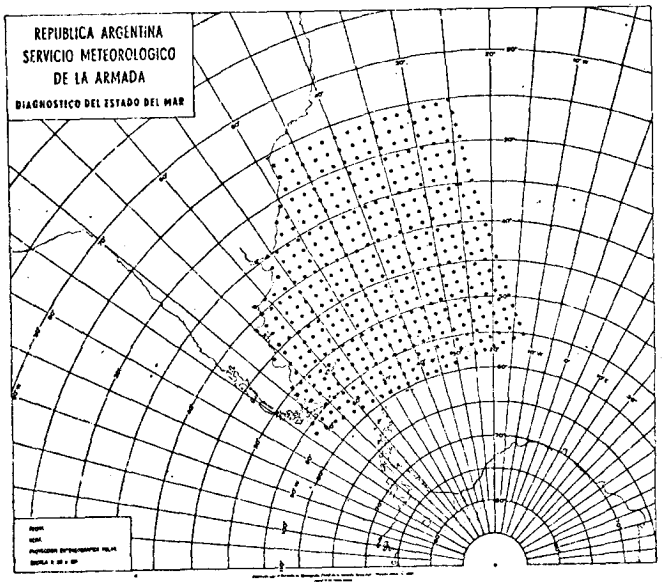

Figure 1.- Grid used in the model.

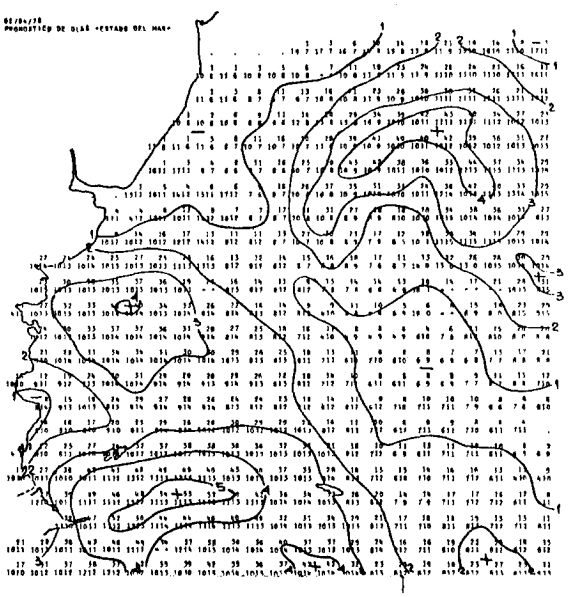

Figure 2.- Example of model issue where lines of equal wave height were drawn.

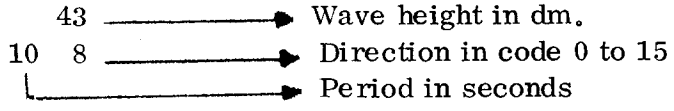

DIRECTION CODE

350) 360) 010) 0	080) 090) 100) 4	170) 180) 190) 8	260) 270) 280) 12
020) 030) 1	110) 120) 5	200) 210) 9	290) 300) 13
040) 050) 2	130) 140) 6	220) 230) 10	310) 320) 14
060) 070) 3	150) 160) 7	240) 250) 11	330) 340) 15

Figure 3.- Issue of the automatic diagnosis or forecast for each point of the grid.

3. EXPERIENCES CARRIED OUT.

Taking advantage of the cruise of the oceanographic vessel ARA "GOYENA" which took place on July 1973 and of observations of the state of the sea expressly carried out during the same by technical experts, the results obtained were compared in three different ways. The first one placing sea height at zero each 24 hours, this is to say, effacing from the memory all entries prior to the 2300 Z chart of the previous day. The second one accumulating data during 72 hours previous to the diagnosis, as was first considered in the model application. Finally, in the third one, the information was first introduced on a given day at 2300 Z, carrying out the experience for 20 days, up to the end.

After the study, it was concluded that the first method was the most convenient. This conclusion was afterwards supported all through the time the model was used.

It was also noted that real height data were somewhat lower than the values calculated by the model; it was estimated that this difference could be corrected by intro -

ducing some empirical modifications to the same.

With the purpose of going on with the study, advantage was taken of a new oceanographic cruise of the ARA "GOYENA" (summer 1973/74), and other ships which provided reliable observations were chosen as well.

With the data obtained, a new comparison between results and observations was carried out, taking besides into account the influence of the decrease in depth.

After the analysis, it was first thought as convenient to carry out a continuous reduction of heights calculated in deep waters zones and to extend the results to zones of minor depths. The latter was also considered feasible with a constant but variable correction by zones, according to their depth.

The isobaths of 20, 50 and 100 fathoms were considered as convenient boundaries of shallow waters, with a special indication that for depths lower than 20 fathoms or in estuaries, gulfs or very closed bays, the model was not valid.

The following correction percentages for wave heights were estimated at first sight for each of the mentioned zones.

ZONE	DEPTHS (fathoms)	%
I	20 to 50	30
II	50 to 100	25
III	to 100	20

The said modifications were provisionally introduced in operative manner from April 1974. Afterwards a regression curve between the heights given by the model and those observed for each zone was calculated with the method of minimum squares, assuming a linear relation.

The straight lines are shown in figure 4, where the correlation obtained in each zone is displayed.

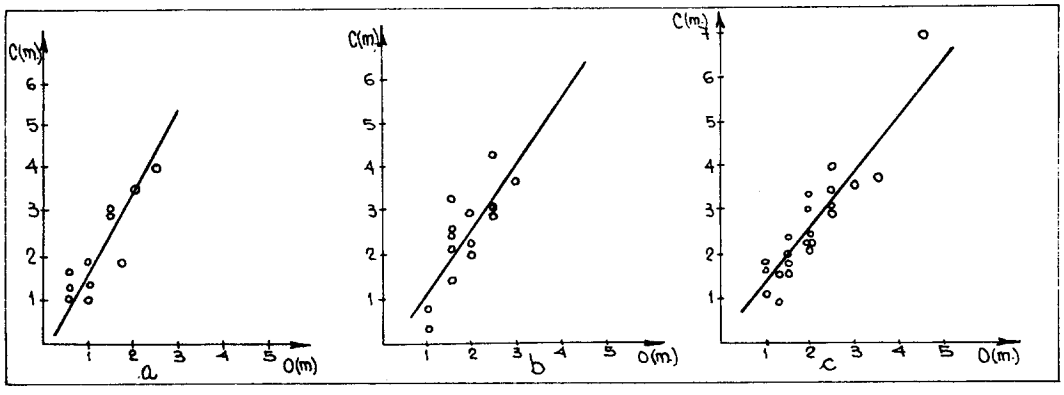

Figure 4.- Heights calculated by the model (c) versus heights observed (o) for zones of depths: a) between 20 and 50 fathoms; b) between 50 and 100 fathoms and c) greater than 100 fathoms.

The slopes show the existing relation between the mentioned variables and determine the corrections to be made. They are the following:

ZONE	DEPTHS (fathoms)	%
I	20 to 50	39
II	50 to 100	32
III	to 100	28

With the purpose of backing this conclusion, particularly the assumption of constant corrections by zones, an analysis of the correlation between variables for the three cases considered was carried out.

The results were:

ZONE	CORRELATION COEFFICIENTS
I	0, 74
II	0, 95
III	0, 93

From these it appears that the assumed linear relation between the observed heights and the calculated heights is correct. In zones II and III a linear and quite satisfactory correlation coefficient has been found. In zone I it can be considered quite acceptable, as in shallower waters a greater irregularity in wave height is anticipated.

It was then believed that to take the values obtained from the slopes of the regression straight lines for making corrections was justified. Nevertheless, between these values and those previously estimated there was only a difference smaller than 10 % of the total wave height. This is generally less than the error in observations of the state of the sea. In spite of this, the necessary arrangements were carried out so as to obtain results according to the corrections detailed before.

At last, by means of a wave recorder on board a petroleum exploring platform located 100 nautical miles from the coast at 40° S, it was possible to obtain for the first time a series of continuous observations of the state of the sea. Comparisons between observations and diagnosis obtained with the model make it possible to conclude that significant errors, due to lack of data in the oceanic zone considered, were not greater than 25% of the diagnosis obtained.

At present a facsimile chart is issued daily with the diagnosis of the state of the sea (figure 5). On another hand an emission by radiotelegraphy of the state of the sea and its forecast is carried out for the zones shown in figure 6.

4. STATISTICAL RESULTS.

Daily diagnosis are automatically recorded and their results have been statistically compiled so as to determine some mean parameters of the state of the sea.

For the areas considered in the preparation of forecasts (figure 6), the frequency distribution of height and period of the significant wave shown in figure 7 have been calculated. In the same figure are shown height values ($\overline{H}$) and mean periods ($\overline{T}$) with

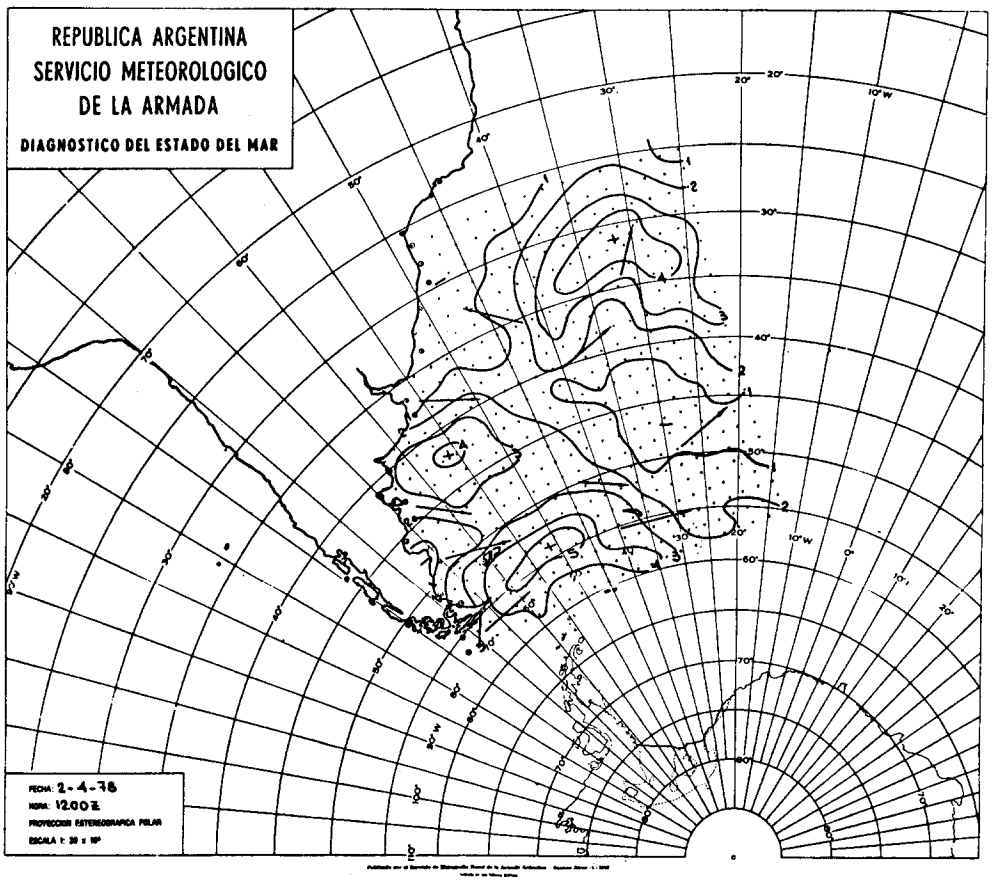

Figure 5.- Example of a facsimile chart with the diagnosis of the state of the sea.

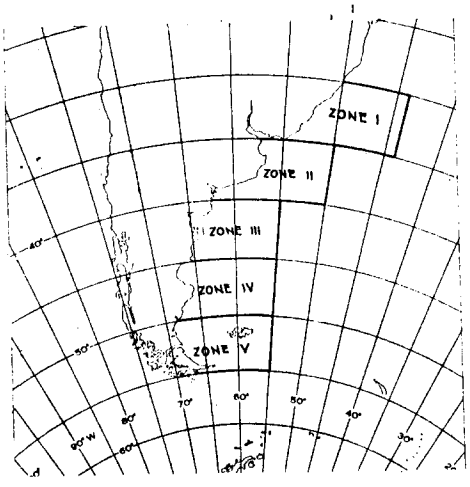

Figure 6.- Zones for which a forecast of the state of the sea is issued.

their corresponding standard deviations Σ_H and Σ_T .

The total number of observations considered, N, arises from taking into account data forecasted for all the points of the grid corresponding to each zone. When heights are lower than 0,1 dm. and/or periods shorter than 4 s., it has been considered a calm sea.

The distribution of heights shows a definite positive assimetry while heights increase with latitude.

Periods show a very similar distribution for the five zones with a mean value which ranges from 7,5 to 8 s.

Finally in figures 8, 9 and 10, values of wave heights for seasonal periods according to criteria expressed by Van Loon (reference 6) are shown; this is:

Season	Months
Winter	June-July-August-September
Intermediate	April-May-October-November
Summer	December-January-February-March

The correspondence between maximum wave heights over 20 dm. (stripped areas) and areas of greater cyclogenesis density determined in the works of Rivero and Ereño (reference 7) can be verified.

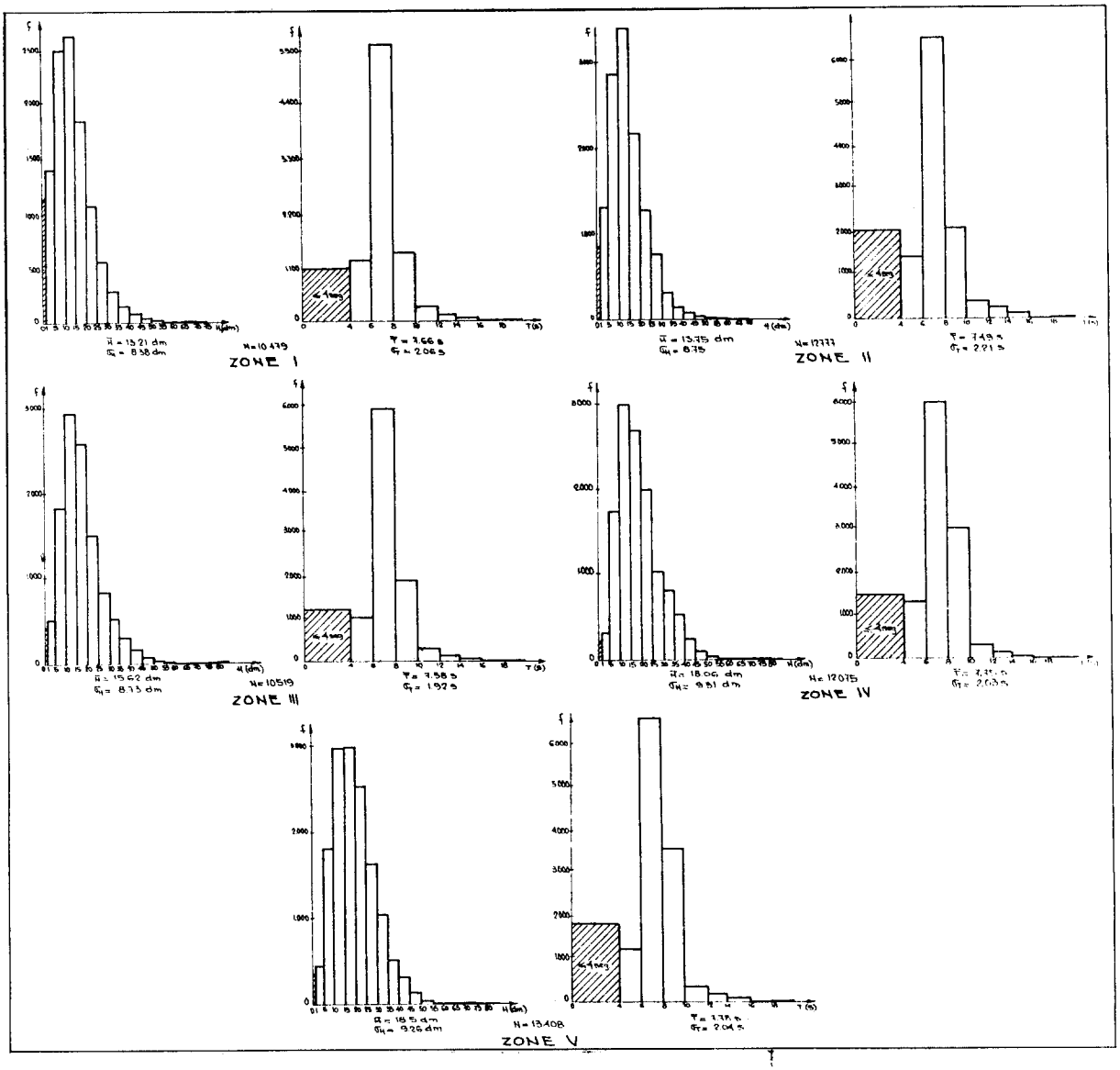

Figure 7.- Wave height and period distribution for the zones shown in figure 6.

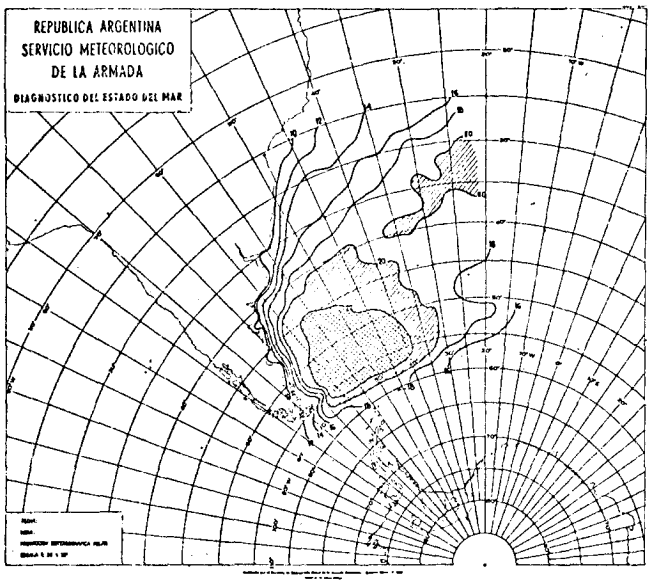

Figure 8.- Wave height in decimeters. Winter.

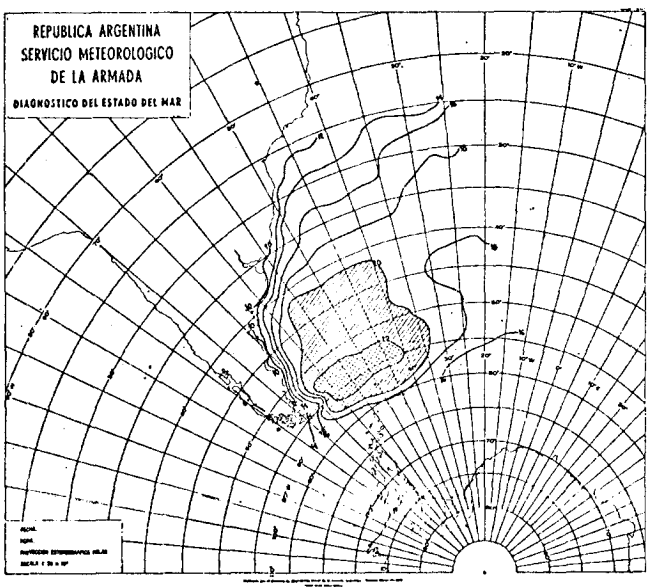

Figure 9.- Wave heights in decimeters. Intermediate season.

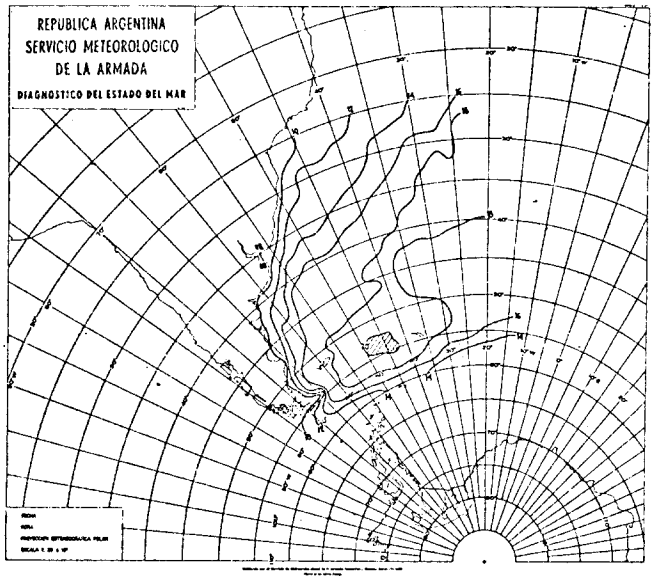

Figure 10.- Wave height in decimeters. Summer.

5. FUTURE OUTLOOK.

a. It is desirable to continue with the accumulation of data of state of the sea diagnosis with a view to obtain larger statistics.

b. To study, when quantity and quality of data make it feasible, the possibility of introducing at first some other factors as for instance the difference of air-sea temperature, following a similar outline to that presented by I. Isozaki and T. Uji. (Ref. 8).

c. To compare the results obtained with those produced by other models resulting from level III b of the International Data Processing Global System of the FGGE and which can be reached through the Garp Argentine Committee. Also, to take maximum advantage of the new data which are expected to be obtained through wave recorders on petroleum platforms and principally those provided by the drifting buoy system of the FGGE.

d. To start the automatic quantitative forecast process already worked out as soon as the first values of charts calculated with numerical procedures can be obtained. It must be taken into account that for attaining this object the mentioned charts must also be drawn with sufficiently dense, exact and extended data.

e. Depending on how much SEASAT information on the state of the sea in the Southern Hemisphere can be obtained in the future, to look for the appropriate way in which the same may contribute to the improvement of the exactness of data introduced in the model.

6. REFERENCES.

(1) Lebel D. and Gelci R.: La prévision numérique de l'état de la mer a l'aide d'un calculateur. Notice d'informations techniques, January 1960.

(2) Devillaz E.: Traitement numérique de l'état de la mer. Notes de l'établissement d'études et de recherches météorologiques, No 179, June 1964.

(3) Fons C.: Prévision de la houle. La méthode des densités spectro-angulaires. Cahiers océanographiques, Vol. XVIII, No 1, January 1966.

(4) Rivero O.R., Lloret M.L.D. and Collini E.A.: Pronóstico automático de olas en el Atlántico sur. Boletín del Servicio de Hidrografía Naval, Vol. X, No 2, 1974.

(5) Rivero O.R., García N.O. and Collini E.A.: Implementación de un pronóstico automático de olas para uso operativo. Boletín del Servicio de Hidrografía Naval, Vol. XI-XII, No 3/1, 1975.

(6) Van Loon H.: A Climatological Study of the Atmospheric Circulation in the Southern Hemisphere during the I.G.Y., Part I, 1 July 1957 31 March 1958. Journal of Applied Meteorology, Vol. 4, No 4, 1965.

(7) Rivero O.R. and Ereño C.E.: Ciclogénesis, movimiento y distribución de depresiones y densidad de pasaje de frentes en océanos australes durante el período abril 1967 a marzo 1972, Meteorológica, Vol. 8/9, 1977/78.

(8) Isozaki I. and Uji T.: Numerical Model of Marine Surface Winds and its Application to the Prediction of Ocean Wind Waves. Papers in Meteorology and Geophysics, Vol. XXV, No 3, 1974.

Observing and Predicting Hurricane Wind and Wave Conditions

by

Duncan Ross

Sea-Air Interaction Laboratory
Atlantic Oceanographic and Meteorological Laboratories
National Oceanic and Atmospheric Administration
Miami, Florida

Introduction

Early attempts to describe the areal distribution of wave conditions in tropical cyclones were based on necessarily arbitrary and unverified assumptions regarding the equivalent fetch and duration as a function of radial distance from the storm's eye and the forward velocity of the storm (cf. Patterson, 1971, and Bretschneider, 1972). Additional complications entered when attempts were made to specify the hurricane wind field which is responsible for the generation of the waves.

Recently, measurements of winds and waves were obtained in hurricane Camille, a Gulf of Mexico storm of September 1969, Ava, an eastern Pacific storm which occurred in June of 1973, and Eloise, a Gulf of Mexico storm (Withee and Johnson, 1975). The Camille data (Patterson, 1974) was obtained by a consortium of oil companies led by the Shell Development Company. The waves were measured by resistance-wire wave staffs mounted on several drilling platforms. The Ava data were obtained by the author by means of a laser altimeter operated from a low-flying aircraft (150 meters) in the rear quadrant of the storm (cf. Ross et al., 1974, and Ross, 1975). The Eloise data set was obtained by an environmental data buoy operated by the National Oceanic and Atmospheric Administration.

A rigorous specification of the wave field within a hurricane (or any other meteorological system) is dependent upon the solution of the energy balance equation

$$\frac{\partial E}{\partial t}(k,x,t) + V \cdot \nabla_x F(k,x,t) = S(k,x,t) \qquad (1)$$

where $F(k,x,t)$ is the wave number energy spectrum as a function of space x, and time t; $V \cdot \nabla_x F$ is the divergence of the energy flux; V is the group velocity of the wave energy, and $S(k,x,t)$ is the source function term and represents the effects of energy input, dissipation, and transfer within the spectrum due to nonlinear interactions. Preliminary estimates of the net source function term $S(k,x,t)$ have been obtained in the JONSWAP experiment (Hasselmann et al., 1973) which proved the importance of nonlinear interactions in the evolution of the spectrum. Another important part of the JONSWAP results was the application of the similarity theory of Kitaigorodskii (1962) to describe the evolution of the total wave energy, E, and peak frequency, f_m, of the spectrum in nondimensional terms as a function of fetch where the local surface wind U_{10} and the gravity constant g are used to obtain the dimensionless parameters.

The experimental results described in the JONSWAP report can be used to estimate S, allowing integration of the energy balance equation to specify the wave field for an arbitrary wind field. This is the approach that has been followed in the development of spectral wave models.

The results of JONSWAP and other similar studies (cf. Ross and Cardone, 1974, Schule et al., 1971, and Barnett and Wilkerson, 1967) suggest that if fetch in the hurricane situation could be specified nondimensionally, a relationship may exist between the dimensionless fetch parameterization and the important shape and scale parameters of the wave spectrum allowing prediction of the wave field without integration of equation (1).

In this paper, the scale and shape parameters of the wave energy spectrum within tropical hurricanes are examined in terms of a fetch implicitly proportional to the radial distance to the storm's eye nondimensionalized by the average surface wind as measured at 10 meters and g.

Specification of the Surface Windspeed

Windspeeds associated with the wave data considered herein were measured by an anemometer which averaged for a period of 15 minutes at an altitude of 10 meters in the case of Eloise and by an inertial navigation system aboard the NOAA aircraft flying at a level of 150 meters in the case of Ava. Since Ava and Camille were virtually identical storms, Camille winds were established based upon an analysis of the Ava wind field using the aircraft data. In addition, 30-minute average surface winds were measured from a drilling platform during Camille and verified the Ava analysis transformation. Unfortunately, the one platform with good measurements of the windspeed was not equipped with a wave staff.

Aircraft winds which were used to perform the Ava analysis were first adjusted to the equivalent surface value using the familiar logarithmic profile for neutral stability and a windspeed-dependent z_0 of the form

$$z_0 = .1525/U_* + 1.468 \times 10^{-5} U_*^2 - 3.71 \times 10^{-3} , \qquad (2)$$

where z_0 is the roughness length, and U_* is the friction velocity. The z_0 relationship is a modification of the formulation of Cardone (1969) using the results of Garratt (1977) according to Cardone (1979). The aircraft winds were averaged for a period of thirty seconds when the aircraft track was cross-wind and for two minutes during downwind tracks. Alternate approaches to specification of the hurricane wind field would be equally appropriate if properly scaled to the average wind as observed at a 10 meter anemometer height.

One such method is that described by Patterson (1971):

$$U = [A + B\rho + C\rho^2 + D\rho^3 + E\rho^4] \times \left\{0.692\,[12.45\,(\Delta P)^{1/2} - 0.575\,Rf] + \frac{V_f}{2}\right\} - \frac{V_f}{2}(1-\cos\theta) \quad (3)$$

where A = 1.2132
B = -0.2326
C = 0.0295
D = -0.0021
E = 0.001
f = Coriolis parameter = .525 sin (latitude)
U = Wind velocity in knots at a height of 10 meters
V_f = Forward velocity of storm in knots
R = Radius to maximum winds in nautical miles
ΔP = Difference between the peripheral atmospheric pressure and the central pressure of the storm in millibars
ρ = Distance from storm's center to point where winds are desired divided by R
θ = Angle between radial perpendicular to track of hurricane and location of desired wind information; 90^0 would be the along-track direction.

The above technique assumes flow parallel to the isobars. Increased accuracy could be obtained by assuming an inflow angle proportional to $\rho^{-.75}$ with a maximum value of 50^0 at R, as observed in hurricane Eloise.

Development of the Model

Hasselmann et al. (1973 and 1976) suggested that for growing seas, the observed spectrum will be of the form

$$E(f) = \alpha g^2 (2\pi)^{-4} f^{-5} \exp\left\{-\frac{5}{4}\left(\frac{f_m}{f}\right)^4 + \ell n\,\gamma \times \exp\left[-\frac{(f-f_m)^2}{2\sigma^2 f_m^2}\right]\right\} \quad (4)$$

$$\text{where } \sigma = \begin{cases} \sigma_a, f \geq f_m \\ \sigma_b, f \leq f_m \end{cases}$$

This function contains both scale and shape parameters. The scale parameters have been found to be interrelated when considered in the dimensionless form according to

$$\alpha = .033\ \nu^{2/3} \tag{5}$$

where $\nu = \frac{f_m U_{10}}{g}$, f_m is the spectral peak frequency, and g the gravity constant. For growing seas the shape parameters σ_a and σ_b were found to scatter considerably about a mean value of about 0.07 while γ, the ratio of the energy at the peak frequency f_m to that derived from the Pierson-Moskowitz (PM) (1964) fully-developed form of the spectrum, was found to have a mean value of 3.3 with little dependence upon ν. It should be noted that equation (4) reduces to the fully-developed PM form for a γ of 1.0.

Least squares fits of the hurricane data set to the spectral form of equation (4) have been determined, and the shape and scale parameters derived. Figures 1-a, b, and c are examples of the quality of the fit (see also

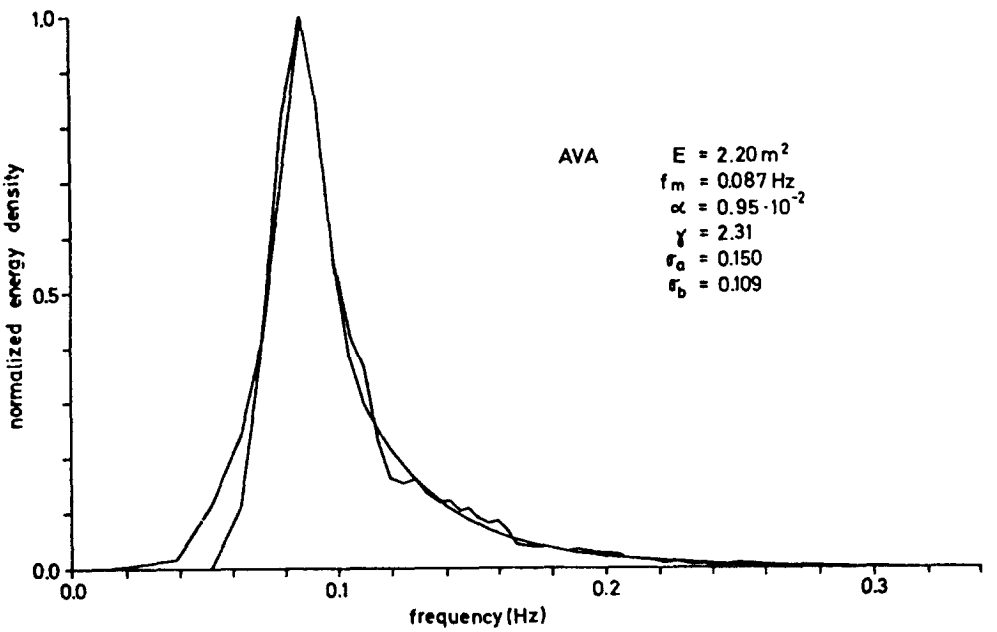

(a)

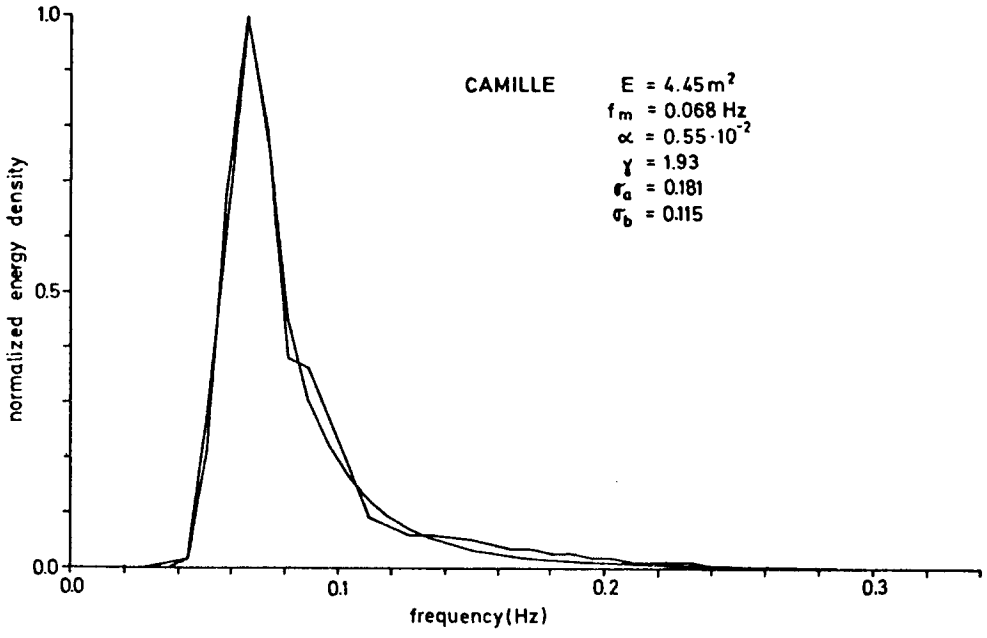

(b)

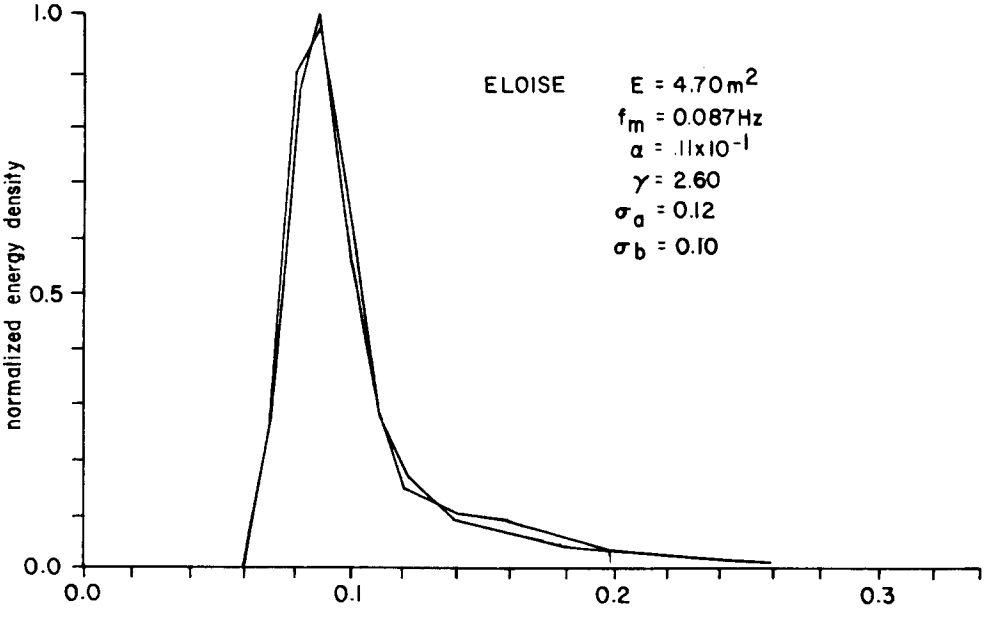

(c)

Figure 1. Examples of spectra and analytical fits for hurricane data sets.

Hasselmann et al., 1976, and Müller, 1976, for a more complete representation of fitted spectra for Ava and Camille). The scale parameters were then nondimensionalized, where appropriate, in the JONSWAP manner and, along with the shape parameters, regressed against the dimensionless radial distance from the eye of the hurricane. Figure 2 presents the dimensionless scale parameters ε and ν versus nondimensional radial distance ξ_r. Also shown are error bars which reflect the maximum error one would encounter with an error in the windspeed specification of ± 5 m/s. It can be seen from Figure 4 that a power law regression well describes the behavior of these parameters and that the scatter can largely be attributed to position and wind field errors. Table I presents the coefficients and exponents of the power law fits of the shape and scale parameters determined from the regression analysis.

Table I

Regression line variables of shape and scale parameters.

$$\nu = .97\ \xi_r^{-.21}$$

$$\varepsilon = 2.25 \times 10^{-5}\ \xi_r^{.45}$$

$$\gamma = 4.7\ \xi_r^{-.13}$$

$$\alpha = .035\ \nu^{.82}$$

Testing the Model

An opportunity to test the model presented itself when hurricane Belle passed directly over NOAA buoys equipped with wind and wave measurement systems. The total energy E was derived from the appropriate regression equation (using a windspeed obtained from a model tuned to the buoy observations) and the significant wave height ($\overline{H}_{1/3} = 4\sqrt{E}$) was calculated from each observation period (cf. Ross and Cardone, 1977). The results, along with $\overline{H}_{1/3}$ calculations from a spectral model (Cardone, Pierson, and Ward, 1976, and Forristall et al., 1978) are shown in Figures 3 and 4. Since the spectral shape parameters are also available from Table I, it is also possible to intercompare observed and predicted spectra. Figure 5 is such an example for hurricane Belle.

Another opportunity to test the model was presented when hurricane Anita developed in the Gulf of Mexico in August of 1977 and passed near the NOAA buoy EB 04. Figure 6 presents forecast values of significant wave height and spectral peak frequency, again from both the spectral and parametric models. It should be noted here that the forecast hurricane track errors were removed prior to construction of the figure since their inclusion would complicate evaluation of the wave models. Figure 7 is an example of the forecast wind

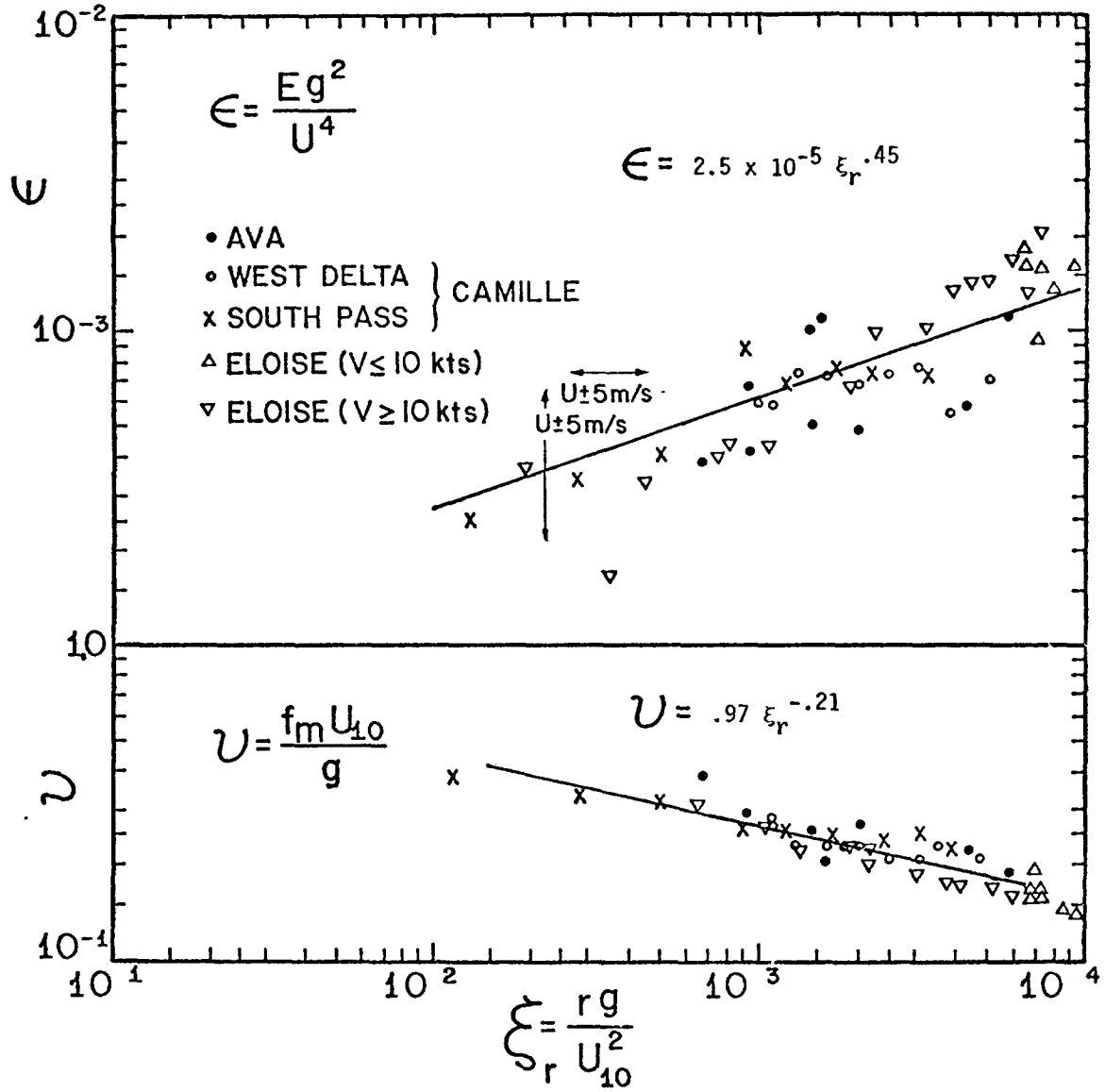

Figure 2. Dimensionless spectral scale parameters as a function of the dimensionless radial distance to the hurricane.

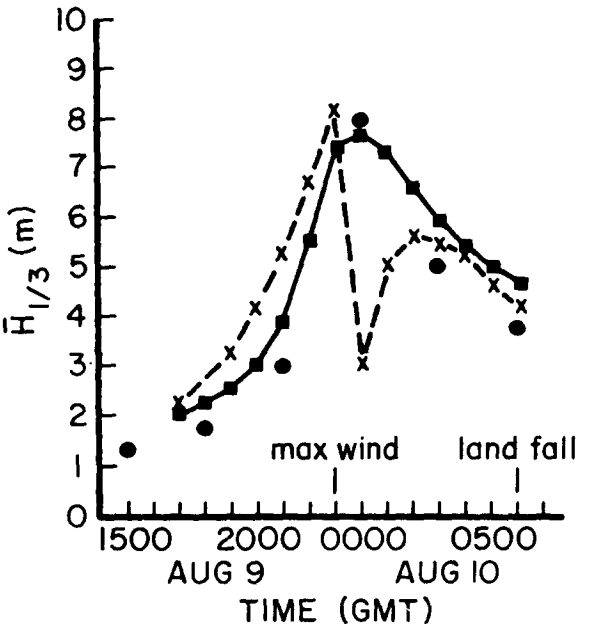

Figure 3. Comparison of measured and hindcast significant wave height at EB 41 during hurricane Belle: ● - measured; X - parametric; ■ - spectral.

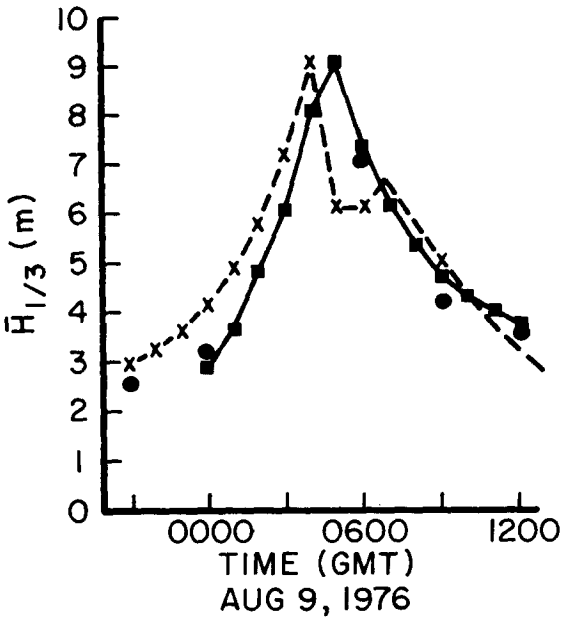

Figure 4. Comparison of measured and hindcast significant wave height at EB 15 during hurricane Belle: ● - measured; X - parametric model; ■ - spectral model.

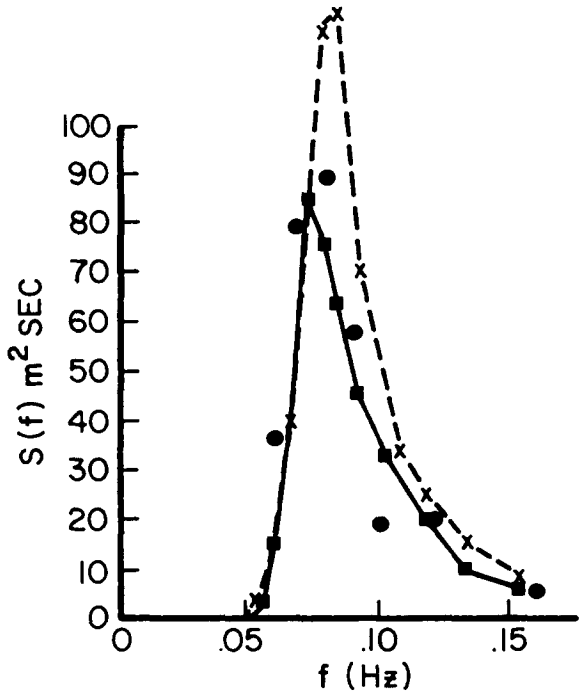

Figure 5. Maximum predicted spectra for hurricane Belle at EB 41: X - parametric model, $\overline{H}_{1/3}$ = 8.2 m; ■ - spectral model $\overline{H}_{1/3}$ = 7.8 m. Also shown is the maximum observed spectrum (●), $\overline{H}_{1/3}$ = 7.8m.

and wave field produced by the model, which is presently being transferred to the NOAA National Hurricane Center computer for operational use.

The important physical characteristics of the storms used in this study along with observed and calculated maximum average winds and significant wave heights are shown in Table II.

Table II

Storm	ΔP (mb)	Radius to Max. Wind (nmi)	V_f (kts)	Observed U Max. (m/s)	Calc. U Max. (m/s)	Max. Obs. $\overline{H}_{1/3}$ (m)	Max. Calc. $\overline{H}_{1/3}$ (m)
Anita	41	20	4	34.0	29.9	6.5	6.7
Ava	100	15	12	—	48.3	—	13.3
Belle	58	12	13	33.0	37.8	7.8	8.54
Camille	105	15	12	51.7	49.4	13.5	13.6
Eloise	41	15	15	35.8	32.8	8.7	7.2

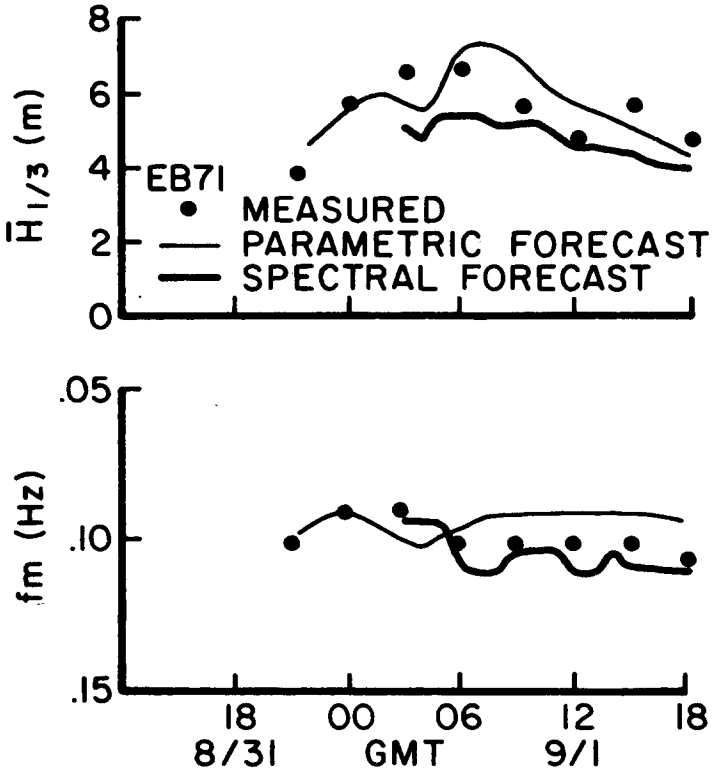

Figure 6. Measured and forecast significant wave height and peak frequency in hurricane Anita at EB 71.

Conclusions

The parametric wave model described here has been found to give accurate specifications of the deep water wave field in tropical cyclones. Its use for forecasting and hindcasting is warranted when detailed knowledge of the directional parameters of the spectrum are not required. Since the model predicts the total energy of the wave field, it is possible to calculate extreme value statistics such as the maximum expected single wave following the work of Longuet-Higgins (1952). Recent work by Forristall (1978) and Bouws (1978), however, suggests that this approach does not strictly hold for determining maximum waves in intermediate or shallow water and that in such situations the ratio of maximum to significant wave height should be reduced by about 10%.

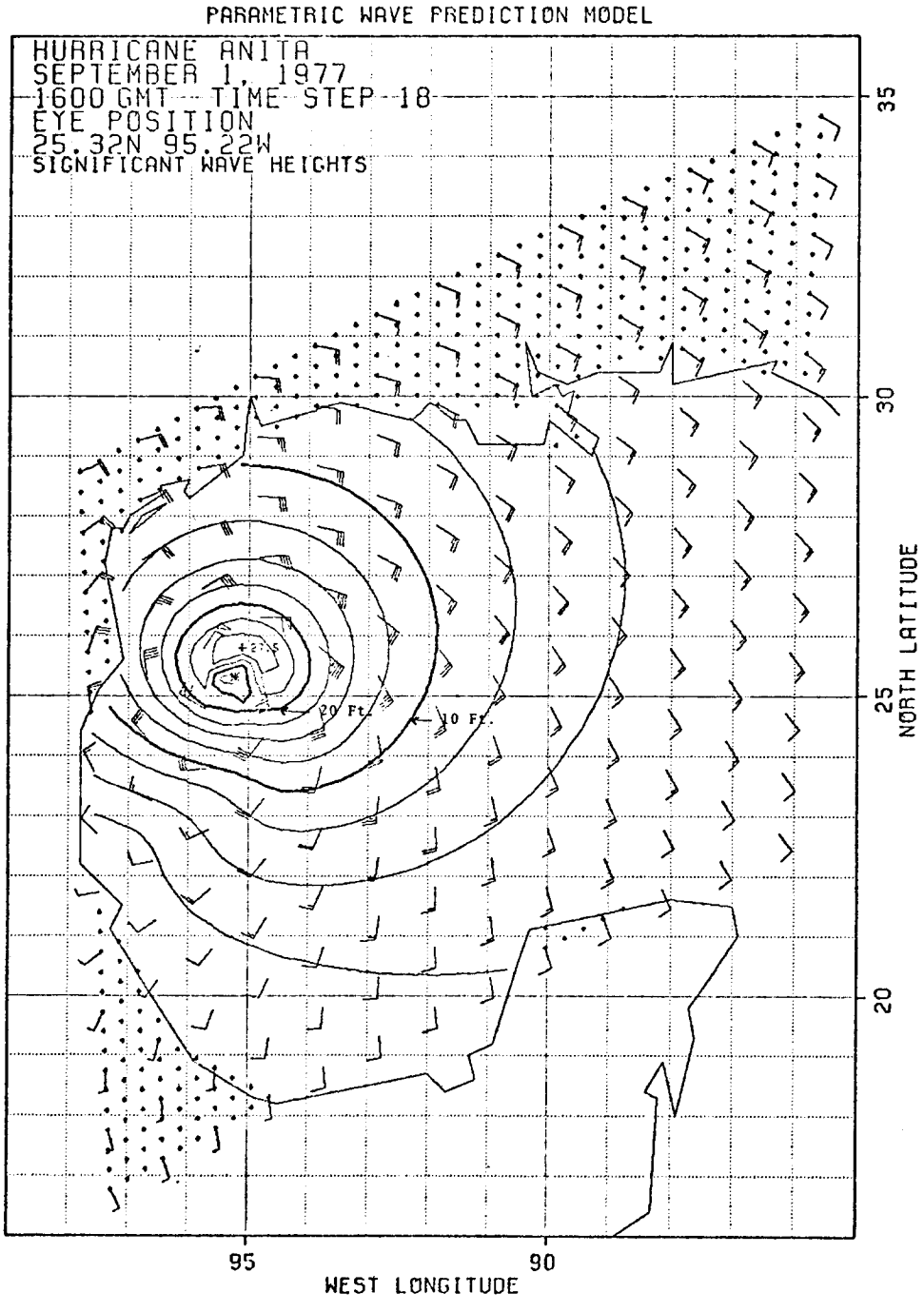

Figure 7. Contour diagram of significant wave height from the parametric wave model. Also shown are wind flags at every third grid point.

References

Barnett, T. P., and J. C. Wilkerson, 1967: On the generation of ocean wind waves as inferred from airborne radar measurements of fetch-limited spectra. J. Marine Res., 25, 292-328.

Bouws, E., 1978: Wind and wave climate in the Netherlands sector of the North Sea between 53° and 54° north latitude. Wetenschappelijk Rapport No. W. R. 78-9, Koninklijk Nederlands Meteorologisch Instituut, De Bilt, Netherlands, 54 pp.

Bretschneider, C. L., 1972: A non-dimensional stationary hurricane wave model. Preprint, 4th Annual Offshore Technology Conference (OTC 1517).

Cardone, V. J., 1969: Specification of the wind field distribution in the marine boundary layer for wave forecasting. Rept. TR 69-1, Geophys. Sci. Lab., New York University.

——, 1979: Personal communication.

——, W. J. Pierson, and E. G. Ward, 1976: Hindcasting the directional spectra of hurricane-generated waves. J. Petrol. Technol., 28, 385-394.

Forristall, G. Z., 1978: On the statistical distribution of wave heights in a storm. J. Phys. Oceanogr., 85, No. C5, 2353-2358.

——, V. J. Cardone, and R. C. Hamilton, 1977: Continental shelf currents in tropical storm Delia: theory and observation. J. Phys. Oceanogr., 7, No. 4, 532-546.

Garratt, J. R., 1977: Review of drag coefficients over oceans and continents. Monthly Weather Review, 105, No. 7, 915-929.

Hasselmann, K., T. P. Barnett, E. Bouws, H. Carlson, D. E. Cartwright, K. Enke, J. A. Ewing, H. Gienapp, D. E. Hasselmann, P. Kruseman, A. Meerburg, P. Müller, D. J. Olbers, K. Richter, W. Sell, and H. Walden, 1973: Measurements of wind-wave growth and swell decay during the Joint North Sea Wave Project (JONSWAP). Deut. Hydrogr. Z., Suppl. A, 8, No. 12.

——, D. B. Ross, P. Müller, and W. Sell, 1976: A parametric wave prediction model. J. Phys. Oceanogr., 6, No. 2, 200-228.

Kitaigorodskii, S. A., 1962: Applications of the theory of similarity to the analysis of wind-generated wave motion as a stochastic process. Izv. Akad. Nauk SSSR, Ser. Geofiz., No. 1, 73-80.

Longuet-Higgins, M. S., 1952: On the statistical distribution of the heights of sea waves. J. Marine Res., 11, No. 3, 245-266.

Müller, P., 1976: Parametrization of one-dimensional wind wave spectra and their dependence on the state of development. Hamburger Geophysikalische Einzelschriften, G. M. L. Wittenborn Sohne, 2 Hamburg 13, 177 pp.

Patterson, M. M., 1972: Hindcasting hurricane waves in the Gulf of Mexico. J. Petrol. Eng., 321-328.

——, 1974: Oceanographic data from Hurricane Camille. Proc. Offshore Technology Conference (OTC 2109).

Pierson, W. J., Jr., and L. Moskowitz, 1964: A proposed spectral form for fully developed wind seas based on the similarity theory of S. A. Kitaigorodskii. J. Geophys. Res., 69, 5181-5190.

Ross, D. B., 1975: A comparison of Skylab S-193 and aircraft views of surface roughness and a look toward Seasat. Proc. NASA Earth Resources Survey Symposium, Houston, Texas, June, 1911-1920.

——, and V. J. Cardone, 1974: Observations of oceanic white caps and their relation to remote measurements of surface wind speed. J. Geophys. Res., 79, 444-452.

——, B. Au, W. Brown, and J. McFadden, 1974: A remote sensing study of Pacific hurricane Ava. Proc. of the Remote Sensing Symposium, Willow Run Laboratories, Ann Arbor, Mich., April, 15-20.

——, and V. Cardone, 1977: A comparison of parametric and spectral hurricane wave prediction products. To be published in the Proc. NATO Symposium on Turbulent Fluxes through the Sea Surface, Wave Dynamics and Prediction, Marseille, France, September. Plenum Publishing Corp., New York, N. Y.

Schule, J. J., L. S. Simpson, and P. S. DeLeonibus, 1971: A study of fetch-limited wave spectra with an airborne laser. J. Geophys. Res., 76, 4160-4171.

Withee, G. W., and A. Johnson, Jr., 1975: Buoy observations during hurricane Eloise. Data Buoy Office, National Oceanic and Atmospheric Administration, Bay St. Louis, Mississippi.

ON SHORT-RANGE HYDRODYNAMIC NUMERICAL PREDICTION OF HYDROLOGICAL ELEMENTS OF THE NORTH ATLANTIC WATERS

by

A.S. Sarkisyan, K.P. Vasiliev, Ye.V. Semyonov, T.S. Allakhverdova
(USSR)

The necessity for creation of hydrodynamic numerical forecasts of hydrological elements of the oceanic active layer, in particular, short-range ones, is obvious. The creation of such a forecast may be reduced to solution of the Caushy problem for the whole three-dimensional forecasting area. At present, this problem cannot be precisely solved because of the lack of adequate operational information on the hydrological regime of the ocean. Nevertheless, attempts of approximate forecasting with assimilation of available information, particularly, climatic data, may prove useful. Finalizing methods for short-range numerical forecasting the hydrological elements of the oceanic active layer is a non-conventional problem. For short-range forecasting, an assumption is made that the total kinetic energy of synoptic space-time scale processes cannot be essentially changed by the dissipation due to short time available. In other words, the quality of the forecast will, in the first place, be determined by the quality of giving the initial state. The calculation process is divided into 3 stages. The first stage consists of storage and processing the available operational information on the sea-surface temperature, near water-surface air layer and atmospheric pressure at the ocean level. Strictly speaking, this information is insufficient for calculations. Initial conditions in the whole three-dimensional volume of the forecasting area are necessary. Therefore, it is clear a priori that assimilation of available information including climatic one, in one or another form, is required. Thus, the forecasting problem is mainly reduced to calculation of the initial state with a maximum possible accuracy, this is the second stage of calculation. The third stage is the forecast proper. At this stage, an essential difficulty is the giving of substance fluxes at the boundaries, in the first place, the heat flux at the ocean surface and water discharges at fluid boundaries of the area.

Let us dwell on the second and third stages of forecasting. The calculation of the oceanic initial state is performed by solving the Dirichlet boundary value problem for heat and salt transfer equation in the whole forecasting area. Posing the problem is following. The distribution of thermohydrodynamic characteristics within the area is calculated in settled values of temperature and salinity at all boundaries and in giving the flux of impulse at the oceanic surface. A basin with arbitrary coastal outlines as well as the bottom relief is located in an arbitrary region of the World Ocean. A portion of boundaries may be liquid. We originate from the following set of equations written in the spherical right-angle coordinate system.

The equation of motion along the horizontal line:

$$\frac{\partial v_\lambda}{\partial t} + \frac{v_\theta}{a}\frac{\partial v_\lambda}{\partial \theta} + \frac{v_\lambda}{a\sin\theta}\frac{\partial v_\lambda}{\partial \lambda} + v_z\frac{\partial v_\lambda}{\partial z} + \frac{v_\theta v_\lambda}{a}\operatorname{ctg}\theta + 2\omega\cos\theta v_\theta = -\frac{1}{a\rho_0\sin\theta}\frac{\partial p}{\partial \lambda} + \frac{\partial}{\partial z}\nu\frac{\partial v_\lambda}{\partial z} + A_L\Delta v_\lambda; \quad (1)$$

$$\frac{\partial v_\theta}{\partial t} + \frac{v_\theta}{a}\frac{\partial v_\theta}{\partial \theta} + \frac{v_\lambda}{a\sin\theta}\frac{\partial v_\theta}{\partial \lambda} + v_z\frac{\partial v_\theta}{\partial z} - \frac{v_\lambda^2}{a}\operatorname{ctg}\theta - 2\omega\cos\theta v_\lambda = -\frac{1}{\rho_0 a}\frac{\partial p}{\partial \theta} + \frac{\partial}{\partial z}\nu\frac{\partial v_\theta}{\partial z} + A_L\Delta v_\theta; \quad (2)$$

The hydrostatic condition is used as an equation of motion in the vertical:

$$\frac{\partial p}{\partial z} = -\rho g. \quad (3)$$

The continuity equation for an incompressible liquid:

$$\frac{\partial v_z}{\partial z} + \frac{1}{\sin\theta\cdot a}\left(\frac{\partial}{\partial \theta}\sin\theta v_\theta + \frac{\partial v_\lambda}{\partial \lambda}\right) = 0. \quad (4)$$

The equation of state:

$$\rho = \rho(T, S). \quad (5)$$

The equation of heat and salt transport:

$$\frac{\partial T}{\partial t} + \frac{v_\lambda}{a\sin\theta}\frac{\partial T}{\partial \lambda} + \frac{v_\theta}{a}\frac{\partial T}{\partial \theta} + v_z\frac{\partial T}{\partial z} = \frac{\partial}{\partial z}\mu\frac{\partial T}{\partial z} + \frac{A_T}{a^2}\Delta T; \quad (6)$$

$$\frac{\partial S}{\partial t} + \frac{v_\lambda}{a \sin\theta}\frac{\partial S}{\partial \lambda} + \frac{v_\theta}{a}\frac{\partial S}{\partial \theta} + v_z\frac{\partial S}{\partial z} = \frac{\partial}{\partial z}\mu\frac{\partial S}{\partial z} + \frac{A_S}{a^2}\Delta S. \qquad (7)$$

Let us set up the following boundary conditions. At the free oceanic surface ($z = -\zeta(\theta, \lambda)$):

$$T = \varphi^1(\theta, \lambda); \qquad (8)$$

$$S = \varphi^2(\theta, \lambda); \qquad (9)$$

$$\rho_0\nu\frac{\partial v_\lambda}{\partial z} = -\tau_\lambda; \quad \rho_0\nu\frac{\partial v_\theta}{\partial z} = -\tau_\theta \qquad (10)$$

$V_z = 0$ (the "rigid cover" condition); (11)

$$p = p_a(\theta, \lambda). \qquad (12)$$

On solid lateral walls:

$$T = \varphi^3(\theta, \lambda, z); \qquad (13)$$

$$S = \varphi^4(\theta, \lambda, z); \qquad (14)$$

$$\frac{\partial v_\lambda}{\partial n} = \frac{\partial v_\theta}{\partial n} = 0 \qquad \text{(the free sliding condition);} \qquad (15)$$

$$(\vec{v}\cdot\vec{n}) = 0 \qquad \text{(the nonflowing condition),} \qquad (15a)$$

here $\vec{n}$ is a normal to the lateral surface.

At liquid lateral boundaries:

$$T = \varphi^5(\theta, \lambda, z); \qquad (16)$$

$$S = \varphi^6(\theta, \lambda, z); \qquad (17)$$

$$\frac{\partial v_\lambda}{\partial n} = \varphi^7(\theta, \lambda, z); \qquad (18)$$

$$\frac{\partial v_\theta}{\partial n} = \varphi^8(\theta, \lambda, z). \qquad (19)$$

At the lower surface $z = -H(\theta, \lambda)$ (in a particular case $H(\theta, \lambda)$ — is the ocean bottom relief)

$$v_\lambda = \varphi^9(\theta, \lambda, -H); \qquad (20)$$

$$v_\theta = \varphi^{10}(\theta, \lambda, -H); \qquad (21)$$

$$\tau_z = \varphi^{11}(\theta, \lambda, -H); \qquad (22)$$

$$T = \varphi^{12}(\theta, \lambda, -H); \qquad (23)$$

$$S = \varphi^{13}(\theta, \lambda, -H). \tag{24}$$

In the case, when $H(\theta, \lambda)$ is the ocean bottom relief, we use the adherence condition: $v_\lambda = v_\theta = v_z = 0.$ (25)

Functions $\varphi^1 - \varphi^{13}$ are considered to be given, φ^1 and P_a we obtain from the operational (daily) information incoming into the Hydrometeorological Centre of the USSR; $\varphi^2 - \varphi^{13}$ are given from climatic data, sometimes, from physical considerations, for instance (25). Water discharges in grid points at liquid boundaries are being determined, at first, from climatic data. The error of the integral discharges along the vertical line at the lateral contour is uniformly distributed over the whole contour.

The utilization of the second kind conditions in the form of:

$$\frac{\partial T}{\partial n} = f^1(\theta, \lambda, z); \quad \frac{\partial S}{\partial n} = f^2(\theta, \lambda, z). \tag{26}$$

instead of (13), (14), (16), (17), (23) and (24) is a very interesting version of calculating the initial state; where f^1 and f^2 may be given, for instance, from climatic data. In this case, for existence of solution of the problem satisfying of following conditions is necessary:

$$\int_{\tilde{\sigma}} \frac{\partial T}{\partial n} d\tilde{\sigma} = 0. \tag{27}$$

$$\int_{\tilde{\sigma}} \frac{\partial S}{\partial n} d\tilde{\sigma} = 0 \tag{28}$$

where $\tilde{\sigma}$ is the total surface of the volume under consideration and $\vec{n}$ is the normal to it at each point.

For finding the coefficient of vertical turbulent exchange Obukhov's formula is applied in combination with the Prandtl mixing path concept. The coefficient of turbulent exchange by impulse we shall assume to be equal to the diffusion coefficient. Its magnitude we shall determine from the formula:

$$K = \mu = \nu = (0.05h)^2 \sqrt{\left(\frac{\partial v_\lambda}{\partial z}\right)^2 + \left(\frac{\partial v_\theta}{\partial z}\right)^2 - \frac{g}{\rho}\frac{\partial \rho}{\partial z}} \tag{29}$$

Posing the problem for the third stage, i.e. forecasting proper, differs from the above by substitution of the boundary condition (8) for the condition in the form:

$$\frac{dT}{dz} = Q(T_a, T_w, h); \tag{30}$$

where Q is a known empirical function, h is the thickness

of the upper quasi-homogeneous layer, T_a is the air temperature in the near-surface air layer.

Empirical relations (30) in that posing is impossible to eliminate, due to the fact that for explicit writing the heat balance components of the oceanic surface the ideal solution of the joint ocean-atmosphere system is necessary, as well as an essentially larger volume of operational hydrometeorological information.

In posing the above (1)-(25), (29-30) problem first numerical experiments have been carried out. The calculation area is the North Atlantic region 25°N - 65°N. The ocean depth is divided into 31 levels; the interval of the difference grid is uniform and equal to 1° along the longitude and latitude. The lower surface is selected 200 m and is constant. At that surface, solving a diagnostic problem (calculation of surface currents from the given density field),climatic velocities of currents are derived from given climatic values of temperature and salinity. The first numerical experiments demonstrate that obtained three-dimensional fields of temperature, salinity and surface currents can be utilized, for the first approximation, as initial conditions for forecasting temperature and surface currents in the active layer of the North Atlantic, which demonstrate the large-scale elements of the North Atlantic water circulation. Velocities of Gulf Stream surface currents attain 1-1.5 knots. Vertical velocities are of the order of 10^{-3}-10^{-4} CGS units. As a whole, one can draw a conclusion that the calculation of water circulation by solving the (1)-(25), (29)-(30) is more preferable as compared to the use of simply climatic or purely drift velocities. The next step is considered to be the substitution of conditions (13), (14), (16), (17), (23) and (24) for conditions of the second kind (26).

SEASAT APPLICATIONS TO OCEANIC MONITORING

John W. Sherman, III

National Oceanic and Atmospheric Administration
National Environmental Satellite Service
Washington, D.C. 20233

INTRODUCTION

The United States through the National Aeronautics and Space Administration (NASA), Jet Propulsion Laboratory (JPL), launched Seasat, the first ocean-dedicated satellite, on June 27, 1978, at 02:12 GMT (Day 178). This research spacecraft carried five sensors onboard the 2290-kg platform operating in an 108° inclination circular orbit 800 km above Earth. Seasat circled the Earth 14 times daily, covering 95 percent of the global ocean area every 36 hours. Data transmitted from five sensors onboard included information on sea surface winds and temperatures, currents, wave heights, internal waves, precipitation, sea ice features, storm surge, ocean topography and characteristics of severe storms at sea.

On October 10, 1978, at about 03:12 GMT (Day 283), a catastrophic failure occurred during Revolution (Rev) Number 1503. The failure was in the satellite's prime power electrical subsystem which resulted in no signals being received from Seasat after 04:08 GMT. All further efforts to make contact with the spacecraft were unsuccessful.

This paper summarizes a portion of the 105-day mission of Seasat, focusing principally on results from a 30-day experiment conducted in the Gulf of Alaska. This experiment, designated as the Gulf of Alaska Seasat Experiment (GOASEX), was the only dedicated sea truth experiment conducted to validate the satellite data. This discussion addresses initial quantiative results from Seasat. Based on early evaluation of these results, there is reason to believe that each sensor has met its design specification.

THE SEASAT SENSORS

The five Seasat instruments included a radar Altimeter, a Seasat-A Scatterometer System (SASS), a Synthetic Aperture Radar (SAR), a Visible and Infrared Radiometer (VIR) and a Scanning Multichannel Microwave Radiometer (SMMR).* These instruments were

*Seasat carried a laser retroreflector and tracking beacons for precise orbit determination but are not discussed here.

discussed by both McCandless (1975) and Sherman (1975). For this reason only a summary of the instruments is given here in order to emphasize early results.

A short pulse (3 nanoseconds) radar Altimeter operating at 13.5 GHz was the first instrument selected for Seasat. Because the sensor looks only at nadir (its swathwidth is between 1.8 and 12 km, depending on sea state),the orbit of Seasat was tailored to support geodesy requirements of the altimeter. Precision of the altimeter measurement is expected to be 10 cm rms (root-mean-square) over seas with a significant wave height from calm to about 20 m. Precise spacecraft tracking is needed for geodesy, currents, and storm surge analyses. Processing of the Altimeter pulse is expected to yield an estimate of significant wave height to ±0.5 m or 10% whichever is larger,over seas from calm to 20 m, as its mission goal.

The SASS is an active microwave instrument that illuminates the sea surface with four-fan shaped beams (two orthogonal beams each 500 km wide on each side of the Seasat groundtrack). The amount of energy returned provides an estimate of sea surface wind magnitude and direction. The transmitted frequency is 14.6 GHz with the returned energy shifted slightly due to doppler effects. The doppler shift aids in establishing a spatial resolution of 50 km over a region from 200 km to 700 km on either side of the spacecraft. As a goal, surface winds were to be determined to ±2 m/s or 10% in magnitude, whichever is greater, and ±20° in direction. With less precision the SASS was expected to measure winds out to 950 km from the spacecraft. The range of winds to be measured was from 3 to 25 m/s.

The VIR is identical to the National Oceanic and Atmospheric Administration (NOAA) series, Scanning Radiometer (SR) sensor, except for modification for orbit altitude change and a digital telemetry down-link tailored for the signals associated with surface phenomena, in addition to clouds. VIR, on Seasat primarily for feature identification, operated with both a visible channel(0.49 to 0.94 μm) providing information on cloud conditions (day only) and a thermal infrared channel (10.5 to 12.5 μm) providing information on surface and cloud temperatures. Temperature sensitivity was expected to be 0.5 K.

The L-band (1.275 GHz) SAR looked to the starboard side of Seasat centered 20° off nadir with a swathwidth of 100 km. The length of the SAR image track was determined by the receive-station-view duration with about 4000 km being the maximum. Spatial resolution of 25 m needed for wave analyses generated a very high data rate so that on-board recording was not used. Data only within view of Rosman (North Carolina), Goldstone (California), Fairbanks (Alaska) within the USA, and Shoecove (Canada) and Oakhangar (England) were collected by SAR. The goal was to measure waves and wave spectra to oceanic wavelength of 50 m or greater

in addition to sea ice features, possible iceberg detection, wave-land interfaces and penetration to the surface through major storms such as hurricanes.

The SMMR sensor operated at frequencies of 6.6, 10.7, 18, 21 and 37 GHz. Spatial resolution ranged from about 100 km at 6.6 GHz to 22 km at 37 GHz. Three primary classes of data obtained from SMMR were: Sea Surface Temperature (SST), sea ice mapping, and surface winds. Liquid water and water vapor were potentially measureable as well and will be used to formulate pathlength and attenuation corrections for the altimeter and SASS, respectively. SST is expected to be ± 2 K, an important first step to determine SST under cloudy conditions. The magnitude of surface winds is expected to be ± 2 m/s or 10%, whichever is greater, from 7 m/s to about 40 to 50 m/s. The Seasat SMMR scanned the starboard side of the spacecraft, aft-viewing, with a constant 42° angle from nadir. The scan angle is from about 0° to 50° from the aft-starboard side resulting in a swathwidth of about 600 km. The 42° angle from nadir resulted in a 49° angle of incidence at the surface due to the earth's curvature. The Seasat SMMR coverage was chosen for maximum overlap with SASS.

Data from the microwave sensors were recorded on-board and telemetered to one of the previously noted receiving stations. The exception was the SAR data, transmitted directly as noted previously. Hence, global coverage is available for four of the five instruments.

SURFACE INFORMATION

Two major sea surface information activities were jointly planned by NASA and NOAA in the United States and the multi-National Joint Air-Sea Interaction Experiment (JASIN). The Gulf of Alaska Seasat Experiment (GOASEX) was specifically dedicated to the early validation of Seasat data. The JASIN program, conducted in the Eastern Atlantic near Scotland (August - September 1978), focused on the marine boundary layer and air-sea energy transfer. This Atlantic data set will provide surface information for the second phase of Seasat validation.

The initial validation of Seasat used the GOASEX surface data set (September, 1978). This activity was planned and conducted by NOAA, including the Pacific Marine Environmental Laboratory (PMEL), the National Environmental Satellite Service (NESS), the Atlantic Oceanographic and Meteorological Laboratory (AOML), the Wave Propagation Laboratory (WPL), and the National Data Buoy Office (NDBO). The principal oceanic research facility deployed during GOASEX was NOAA's Class 1 Research Vessel Oceanographer. The Canadian weather ships Quadra and Vancouver, alternating at Ocean Weather Station PAPA, also obtained special data on satellite over-pass times.

The GOASEX Operating Area is shown in Figure 1. Participating aircraft included the NASA Ames Research Center's CV-990 equipped with an airborne version of the SMMR, the NASA Johnson Space Center's NC-130B with the Seasat underflight scatterometer, the Naval Research Laboratory's RP-3A equipped with meteorological and microwave radiometer instrumentation, and a Canadian CV-580A aircraft carrying the Environmental Research Institute of Michigan's synthetic aperture radar system. A typical aircraft flight track is shown in Figure 2. This experiment was also supported by nine NOAA data buoys moored in the Gulf of Alaska. Selected research vessels from the U.S. Geological Survey and the University of Alaska made special weather observations during satellite overpass of their positions. A very comprehensive data set was collected, corresponding to some 60 satellite overpasses, including more than a dozen SAR passes. An intensive, coordinated study of this data set was conducted in January, 1979, and is the basis for the results reported herein (Born, 1979).

PRELIMINARY RESULTS

Altimeter

Studies with the Seasat radar Altimeter have been divided into three classes of activities. Those concerned with height measurements, those with wave heights, and those with surface wind speeds. Height measurements, thus far, occurred principally in the area of Bermuda, an area used for calibration of the third Geodynamic Experimental Ocean Satellite (GEOS-3) altimeter. The other two studies occurred in conjunction with GOASEX.

An altimeter system noise comparison of performance capabilities of Seasat to GEOS-3 is shown in Figure 3. As GEOS-3 was expected to operate with a rms displacement error of 0.5 to 1.0 m and Seasat was to perform at a level of 10-cm rms, then the Seasat Altimeter system noise must be inherently less. Seasat and GEOS-3 data in Figure 3 (collected at different times and places using different scales for the abscissa), show Seasat Altimeter noise to be significantly less, now measured at around 7-cm rms.

The height measurement, as well as the geodetic and oceanographic features detected, are shown in Figure 4. In this figure, the difference between the GEM 10 B Geoid (a 5^{o} x 5^{o} grid geoid used as a "quick-look" standard of performance) and Seasat Altimeter measurements is given. The ascending pass was Rev 191 (July 10th) and having landfall in the United States around the State of Rhode Island. The actual surface demarcation from the spherical ellipsoid is too small a feature to show in the large grid GEM 10 B geoid but shows about a 15-m difference as measured by Seasat.

Two features of interest are first, the geostrophic current system of the Gulf Stream shows as a slope slightly greater than

1 m in about 240 km (about 30 seconds of orbit travel) with the height difference decreasing in the westward direction. The second feature is perhaps of even greater importance; the slope associated with a warm water eddy is also detected. The location of the Gulf Stream and eddy feature is shown in Figure 5 during the period of overpass.

In order to fully process altimetric data to its maximum precision for ocean surface topography, a number of environmental and measurement errors should be considered as contributors to the error budget. Some of these errors also affect short-arc results shown in Figure 4. In general the following need to be evaluated: topographically trapped waves and currents, with errors on the order of 2 cm; local currents, in which a current of 1 m/s would produce an error of 5 cm; wind set-up in which, for example, a 1.5-m/s wind produces an elevation difference of about 0.01 cm; atmospheric pressure effects wherein the sea surface elevation is effected by about 1 cm/mb, with a resultant error of no more than 1 cm; tidal measurement uncertainty with errors no larger than 1 cm; shelf topographic effects with errors of about 0.2 cm; leveling errors with a maximum discrepancy of 1 cm; tidal wave phase effects (tide gage located different from altimeter pass wherein the tidal wavelength is around 10^3 km) resulting in errors approaching 1 cm. The composite rms error associated with the above sources (specific errors for the Bermuda test site) is 3.5 cm.

Tropospheric refraction can be modelled partially from other data sources or from SMMR. Dry corrections based on a surface algorithm are believed good to about 3 cm. The wet correction can vary greatly and cannot be accommodated by surface values only. It is estimated that SMMR wet correction is good to 2 cm, but wet corrections based on surface values can be in error by as much as 20%.

The implication of the altimetric error analysis is that many environmental indices must be measured with great accuracy if the true altimeter performance is to be determined. Errors in range associated with sea state are such that corrections for sea state imply the measurement of sea state. A rain cell can introduce errors in satellite height and simultaneously a change in significant wave height, $H_{1/3}$, and the nadir backscattering cross-section σ_o. Figure 6 illustrates such a small-scale rain cell, about 10 to 15 km in extent that was undetected until a microscale meteorological analysis was conducted in GOASEX (Rev 1298 at 18^h 33^m 22^s GMT). While such localized events make it difficult to "truth" all Seasat instruments, they illustrate the ultimate potential of such ocean-dedicated sensors.

The measurement of surface wave height was provided by both an on-board processor and a surface algorithm processing. Figure 7 illustrates two $H_{1/3}$ samples collected on Rev 1164 during GOASEX. The asterisk represents data points extrapolated from contour maps at the time of overpass. Both the on-board and surface processing (Fedor, in press) appears to agree relatively well, and in the lower figure of Figure 7 the GEOS-3 altimetric wave height data are shown also. Using data from several passes, and surface information from the FNWC charts, one GEOS-3 crossing, two buoys, Weather Station PAPA, and the Navy's laser profilometer, a comparison has been made of the Seasat algorithm (△) and Fedor algorithm (·). Figure 8 is the result of this intercomparison. The region where the data met the goal requirements for precision of ±50 cm is indicated on the graph by the two dashed lines. The apparent quantization of data points along the ordinate for sea truth is due primarily to reporting in 3, 6, and 9 foot increments of significant wave height.

Energy returned to the radar altimeter is particularly sensitive to ocean wave heights of the same order of magnitude as the microwave energy wavelength. For the altimeter frequency of 13.5 GHz, this corresponds to heights associated with capillary waves. As such, surface wind tends to reduce energy returned to the altimeter as wind speed increases. This is the reverse effect from backscattering off nadir. Figure 9 combines data from several sources including surface data points: SASS at nadir using the Applied Sciences Associates (ASA) algorithm (▲) SASS using the Wentz and Associates, Inc. algorithm (■), pressure derived wind field (●), spot-wind input (0), wind speed from the Altimeter (*), and wind speed from the SMMR (+). The altimetric algorithm (*), due also to ASA, estimates the wind speed at 10 m above sea level. The 10-m wind is approximately 94 percent of the 19.5-m wind used for SASS and SMMR. The altimetric wind speed is about 1 to 2 m/s lower than SASS, a feature consistent with the present altimetric algorithm overestimating the normalized backscattering cross-section. No atmospheric corrections have been made to the Altimeter, SASS, or SMMR wind fields.

Seasat-A Scatterometer System (SASS)

The SASS provides a footprint on the surface of Earth as shown in Figure 10. An asymmetry arises due to spacecraft motion and Earth rotation as illustrated by the geometry. As noted earlier, maximum sensitivity to surface winds occurs between about 200 km to 700 km on either side of the spacecraft. Limited sensitivity exists at nadir (±70 km) and from 700 to 950 km (each side of the groundtrack).

To date, two algorithms are under development, both requiring use of fore and aft antenna beam. This discussion will not compare the two algorithms, only their geophysical results. Both agree well in defining wind direction (subject to a 180° directional ambiguity), and both point up the need to use individual spot reports for surface data, rather than analyzed wind fields for comparison. Figure 11, based on the City University of New York (CUNY) algorithm, illustrates the nature of high resolution wind fields available from SASS. In this particular data set the winds appear to maintain about the same direction with a gradient of the wind from about 2 m/s to 5 m/s over about a distance of 350 km. An even sharper gradient is shown in Figure 12, which if derived from pressure fields, would have required a very high resolution pressure field model to define the surface wind field. Both data sets in these figures are in very good agreement with the surface wind reported by the data buoy or ship in the immediate vicinity of the surface platform.

A more general comparison of SASS data to buoys is shown in Figure 13. No attempt has been made to separate any data which may have been influenced by possible rain attenuation. A linear regression line is plotted for wind speed compared to the NOAA data buoy. The error statistics in Table 1 show a bias of 1.8 to 3 m/s exists between SASS and surface observations, with a standard deviation of 1 to 2.7 m/s. Note that the error statistics compared only to the buoys are within SASS Specifications.

Table 1. Statistics for (SASS - Spot Observations) Wind Speed and Wind Direction

	Wind Speed, m/s					Wind Direction, Deg			
	Mean Error		Standard Deviation of Error		No. of Samples	Mean Error		Standard Deviation of Error	
	V/H	V	V/H	V		V/H	V	V/H	V
Buoy	1.79	1.48	0.9	1.5	22,14	2.33	0.36	16.2	18.6
Ship Known Anem.	3.72		2.44		9	-1.39		17.9	
Ship Unknown Anem.	3.0		2.69		24	3.34		22.92	
Beau-fort	2.11		2.66		30	7.6		16	

While not a part of the GOASEX program, but of importance to this discussion, Seasat made several passes over Hurricane Fico in July, 1978. Figure 14, a visible spectrum image from the NOAA Geostationary Operational Environmental Satellite (GOES), was taken just before a Seasat pass on July 20. The Seasat subtrack is the black dotted line in the image. The SASS-derived surface wind fields are believed to be the first time that synoptic scale oceanic wind velocities have been obtained in a hurricane. In the 450 km SASS swathwidth, the winds are seen to range from about 2 m/s in the doldrums South of Fico, to more than 25 m/s near the hurricane's center. Again, atmospheric corrections have not been made nor has the SASS data been processed at its full 50 km spatial resolution. Winds have been averaged over a $1^{o} \times 1^{o}$ grid, and have probably been underestimated due to the spatial averaging.

Scanning Multichannel Microwave Radiometer (SMMR)

The SMMR operating with dual polarizations at five frequencies from a common antenna has had a major portion of its activities focused on developing the antenna pattern correction algorithm. Until this algorithm is properly defined, all results are given in antenna temperatures rather than brightness temperatures. However, lack of antenna pattern correction principally creates biases or systematic errors in results, rather than random errors. Results discussed here will be in terms of antenna temperatures and will not include cross-polarization errors introduced by antenna scanning. It is believed that results presented here are those that will ultimately be achieved across the entire 600-km swathwidth of the SMMR system. Another possible source of error ignored in this review is Faraday rotation which might be as large as 1.7 K.

The SMMR Sea Surface Temperature (SST) comparison to National Marine Fisheries Service (NMFS) data has been accomplished using the September 1978 SST data set shown in Figure 15. Results of this comparison are shown in Figure 16 and, with exception of consistently lower SMMR surface temperatures (biases of 3 to 5 K), the comparisons are believed good. Standard deviation about the bias is approximately 1.5 K. These data use the Wilheit and Wentz algorithms.

The SMMR wind estimates are shown in Figure 17 for Rev 1298. Of the two algorithms, the "Wentz" algorithm, in this case, appears to provide the most successful surface wind field results. Overall performance of entry algorithms examined in GOASEX is shown in Table 2. Statistics computed are the mean difference or bias (SMMR - surface data), the root mean square difference (RMSD), and the standard deviation of the error about the mean, δ. Surface wind estimates assigned a Category 2 are believed accurate to about ± 2 m/s and Category 1 about ± 3 m/s. Accuracy of the kinematic analysis is related to the quality and proximity of the surface point to the SMMR grid point.

Table 2. Comparison of SMMR-Derived Surface Wind Speed (m/s) Against Surface Truth Field Data from Kinematic Analysis for Revs 1135, 1212, 1292, 1298

		Category 2. Surface Truth Wind Speed (m/s)			
		Inner Edge	Center Scans	Outer Edge	Overall
Wentz Algo	Bias	2.83	1.54	0.46	1.54
	RMSD	4.41	3.22	2.49	3.30
	δ	3.66	2.86	2.61	2.95
	N	7.0	42.0	8.0	57.0
Wilheit Algo	Bias	10.56	7.75	5.31	7.75
	RMSD	10.95	8.02	5.73	8.20
	δ	3.13	2.28	2.29	2.71
	N	7.0	42.0	8.0	57.0
		Category 1. Surface Truth Wind Speed (m/s)			
Wentz Algo	Bias	2.62	2.28	0.78	2.16
	RMSD	4.30	4.18	3.21	4.09
	δ	3.47	3.52	3.20	3.49
	N	27.0	96.0	18.0	141.0
Wilheit Algo	Bias	12.28	8.51	4.58	8.73
	RMSD	12.61	9.07	5.60	9.51
	δ	2.84	3.14	3.21	3.77
	N	27.0	96.0	18.0	141.0

Because the SMMR system is anticipated to support the Altimeter for path length corrections, SMMR algorithms are being evaluated to permit improved altimetric measurements. The initial comparison is shown in Figure 18. Because the path length correction is most strongly influenced by atmospheric water vapor content and rain rate , Figures 19 and 20, respectively, show the initial algorithms performance in measuring these environmental parameters.

Visible and Infrared Radiometer (VIR)

The VIR was not designed as a primary sensor on Seasat, but rather as a supporting instrument to the microwave sensors. The VIR would provide more conventional visible reflectances and thermal infrared emissions from oceanic, coastal, and atmospheric features. These features would aid interpretation of data from other sensors.

However, by using corrections to satellite brightness temperature for atmospheric water vapor, it has been possible to compare (on a pixel-by-pixel basis) the NOAA SST's, as reported by buoys, to the VIR corrected temperatures. Figure 21 shows the results of this comparison. The linear regression correlation coefficient, r=0.84, and the RMSD of 1.7 K represent excellent agreement in view of uncertainty in the atmospheric correction and uncertainity and smoothness of the NOAA field.

Since the VIR was to be used for basic feature identification Figure 22 is the VIR thermal channel of the east coast of the United States acquired on July 7, 1978 (Rev 156, Day 188). The gray scale has been enhanced to improve contrast between warmer water (dark) and colder water (light). Clouds are also shown in which warmer clouds (lower in altitude) can be discriminated from the higher clouds (colder). These images will permit detailed definition of weather patterns through which microwave energy from the other sensors must penetrate.

Seasat Synthetic Aperture Radar (SAR)

The SAR was designed to image ocean wavelengths as short as 50 m. A principal goal was to derive wave spectra for ocean wavelengths between 50-100 m. Other goals include studies of sea and lake ice, icebergs, internal waves, waves in hurricanes, oil spills, and other environmental features such as current boundaries and wave refraction effects.

The methodology for deriving wave spectra using Optical Fourier Transform (OFT) is shown schematically in Figure 23 (after Shuchman 1979). For Rev 1126 the OFT is shown in Figure 24. Analyses of Rev 1126 and other GOASEX passes are shown in Table 3 with specific limitations and constrants on the data. All data results are after Shuchman et. al. (1979).

Table 3. Comparison of Pitch and Roll Buoy Spectra to Seasat SAR Spectra

(Revised 25 January 1979)

Data Source	SEASAT Revolution	Peak Frequency (1/P)	Ocean Wavelength (m)	Direction (T°)
SEASAT SAR	1126 (dominant)	.077	264	114 or 294
	1126 (secondary)	.087	205	84 or 264
	1169	.079	250	88.5 or 268.5
	1255	.093	182	85 or 265
	1269	.093	165	90.5 or 270.5
	1306	Spectra not Discernable		
Pitch and Roll Buoy*	1126**	.078	256	276 or 96
	1169	.078	256	110
	1255	.093	180	86
	1269	.109	127	102
	1306	.078 (dominant)	213	358
		.109	128	100
		.281	20	278

SAR/BUOY COMPARISON

SEASAT Revolution	Wavelength (% Difference)	Direction (Degree Difference)
1126 (dominant)	+3	18°
1169	-2.4	-21.5°
1255	+1.10	-1°
1269	+23***	-11.5°

*Pitch and Roll Buoy data supplied by Mr. Duncan Ross of NOAA/SAIL
**Estimate only at present time
***Pitch and Roll Buoy data acquired 3 hours after SEASAT overflight

A SAR image from Hurricane Fico, which is a sample of about 5 km x 5 km area, is shown in Figure 25 (Rev 251, July 14, 1978). The OFT of this image is shown in Figure 26. Using special OFT filtering (as shown in Figure 27) the waves within Hurricane Fico appear as those shown in Figure 28.

A major advantage of centimeter wavelength electromagnetic energy is its capability to penetrate cloud cover. On July 8. 1978, the GOES-2 (1000 GMT) infrared image, as shown in the left portion of Figure 29-a, indicates a cloud system which masked a portion of central Florida. The SAR pass (Rev 163 at 1004 GMT) on the same day shows about a 90-km wide by 120-km long portion of the Atlantic just off Cape Canaveral, Florida. Figure 29-b is an enlargement of the right portion of Figure 29-a which shows the surface roughened by a squall system occurring at that time. In addition, the effects of precipitation (Ross, 1979) on the surface (dark patches) are prevalent. In the upper left are indications of the current boundaries between the Gulf Stream and the coastal waters. Other features appear to include both surface waves and internal waves.

Two remaining areas of application of SAR data are for observation of sea ice (the untimely demise of Seasat prevented collection of lake ice and iceberg data) and internal waves. Figure 30 is an image of a portion of the Beaufort sea ice pack West of Banks Island, Canada (right portion of image). The region imaged covers an area about 30 km x 120 km, and is Northeast of Alaska, United States, some 800 km inside the Arctic Circle. The image was acquired at very low visibility conditions (Rev 205, around 2:00 a.m. local time on July 11, 1978) when visible imagery would have been difficult. The dark zone adjacent to Banks Island is an area of shore fast ice composed primarily of first-year sea ice, 1 to 2-m thick. Linear pressure ridges are seen within the shore-fast zone, and West (left) of this zone is a shore lead (open water). At the edge of the lead is a marginal ice zone composed of a mixture of open water, and large and small rounded multi-year floes, typically 3 to 4-m thick. Some first-year ice is also present. Further West is the main polar pack, made up of floes up to 20 km in extent, and surrounded by new leads. The very bright areas within the floes indicate intensive surface roughness.

The SAR has demonstrated a consistent ability to image surface manifestations of internal waves. Figure 31, from the Hudson Canyon Area, just off the East Coast of the United States (Shuchman, personal communication), illustrates several forms of internal waves with wavelengths from several hundred meters to several kilometers. These internal waves are occurring at about 100-fathom depth in the vicinity of exploratory offshore drilling platforms (Image is centered at 39° 10'N, 72° 45' W). Surprisingly, these surface effects of internal waves are being imaged more frequently and under a greater variety of wind conditions than anticipated prior to the launch of Seasat.

DATA AVAILABILITY

Seasat operated for about 105 days from Day 178 to Day 283. The five sensors, which were turned on for operation on the 10th day, operated near their maximum potential until the end of the mission. The SASS and SMMR were on continuously for 95 days. The radar Altimeter was interupted twice for nine days each. The SAR acquired data on about 500 passes over the five receiving stations for durations of 2 to 10 minutes each. The VIR scan motor failed on Day 240, so that only 52 days of VIR data were acquired.

Figure 32 summarizes the profile of the mission showing the days when the sensors were operating. As noted earlier, the two primary surface collection periods were covered during the lifetime of Seasat. It is estimated that about 80% of all NASA and NOAA mission objectives can be fulfilled with the existing data set.

The SAR, due to its limited acquisition capability, did not collect data on a global basis, but in a more limited area. The actual coverage of the SAR data set is shown in Figure 33.

The Seasat data is currently in the first phase of validation of results. Once the validation process is completed, Seasat data requests should be directed to:

Mr. Eugene R. Hoppe
Satellite Data Services Division
Environmental Data Service/NCC
World Weather Building, Room 606
Washington, D.C. 20233
U.S.A.

SUMMARY

The four microwave sensors on Seasat have performed well based on the initial algorithms and the GOASEX surface data set. The Seasat Science Steering Group (SSG) met at the Jet Propulsion Laboratory on February 8, 1979, and reviewed the initial analyses of Seasat data. The status report summarized by the SSG is shown in Tables 4 and 5 (Dunne, 1979). The original objective for each geophysical quantity is stated in the left column and the current assessment is in the right column. The VIR was not assessed at this time.

Table 4. SSG Observations on Altimeter and Scatterometer Measurement Objectives Based upon the GOASEX Workshop Review

ALTIMETER (ALT)

Objective	Feb. 8, 1979 SSG Observation
1. Range (height) precision ±10 cm, (1σ, 1 s average).	1. Objective met up to $H_{1/3} \leq 10$ m.
2. Ocean topography solutions on submeter level	2. Submeter topographic features have been observed.
3. $H_{1/3}$ (signiticant wave height) from 1-20 m, ±10% or 0.5 m, whichever is larger.	3. Objective met within specification up to $H_{1/3} < 4$ 1/m. Expected to be met up to 12 m, the highest $H_{1/3}$ observed in the data.
4. σ_o (backscatter coefficient) ±1 dB.	4. Objective met.
5. Precision orbit determination submeter level globally, 10 cm in the calibration zone.	5. Presently no better than 2 1/2 m globally - 50 cm can be reasonably anticipated globally, but calibration zone will not be better than 20 cm.

MICROWAVE SCATTEROMETER (SASS)

1. Wind speed from 4 - > 26 m/s, ±2 m/s or 10% whichever is larger.	1. Objective met for winds 2-15 m/s. Higher winds will be analyzed in storm workshop.
2. Wind direction ±20 deg.	2. Objective met for winds 2 - 15 m/s using external means of ambiguity removal.
3. 50-km resolution, 500 km swath each side of satellite.	3. Objective met.

Table 5. SSG Observations on SAR and SMMR Measurement Objectives Based on the GOASEX Workshop Review

SYNTHETIC APERTURE RADAR (SAR)

Objective	Feb. 8, 1979 SSG Observation
1. 25 x 25 m spatial resolution over 100 km swath.	1. Objective met.
2. Demonstrate capability to measure wavelength and direction.	2. Objectives met for range travelling waves. Minimum wavelength detected was 100 m in GOASEX data, 70 m in Gulf Stream squall. Data required on azimuth travelling waves. Internal waves measured in the range 75 m - 2 km.
3. Provide data for the study of coastal processes.	3. Data acquired, but sparse surface truth may limit interpretability.
4. Ice field/lead charting.	4. Objective met.
5. Iceberg detection.	5. Objective will not be met.
6. Fishing vessel surveillance.	6. Status unknown.
7. Land imaging for geological hydrological and glaciological experiments.	7. Data acquired, but surface truth limited.

SCANNING MULTICHANNEL MICROWAVE RADIOMETER (SMMR)

1. All weather global measurement of sea surface temperature, ±2 K absolute, ±0.5 K relative.	1. Data internally consistent to ∿2 K, but contains biases of several degrees. Relative performance better than 1 1/2 - 2° cannot be demonstrated because of inherent noise in surface truth temperature fields.
2. Wind speed from 7050 m/s, ±2 m/s or 10%, whichever is larger.	2. Objective met for winds < 20 m/s, but yet to be demonstrated in rain.
3. Measurement of integrated atmospheric water vapor and liquid water.	3. Objectives met to ±20% level. Wet tropo correction for ALT to ±2 cm.
4. Measurement of rainfall rate.	4. Rain has been detected in the data, but quantitative comparisons have not been made because of limitations in surface truth data set.

ACKNOWLEDGEMENTS

Seasat has been a major effort involving about a hundred oceanologists, physicists, meteorologists, engineers, space technologists, and program manager. Some key developers of Seasat, such as Frank Williams, NASA, Director of Special Projects; Walter McCandless, NASA Seasat Program Manager; and Eugene Giberson, JPL Seasat Project Manager, have made a dedicated commitment to the oceanic community through their respective Seasat roles and have to other endeavors. Special acknowledgement is made to:

J.R. Apel, Director, Pacific Marine Environmental Laboratory
P.J. Rygh, Manager, Seasat Data Utilization Project
C.A. Yamarone, Manager, Seasat Information Processing
A.J. Spear, Manager, Seasat Data Evaluation
J.A. Dunne, Manager, Seasat Science
G.C. Cleven, Manager, Project Data Processing System
J.W. Brown, Leader, Algorithm Development Facility Implementation
C.J. Klose, Leader, Instrument Data Processing System Implementation
J.W. Wilkerson, NESS Surface Truth Coordinator
G.H. Born, JPL GOASEX Workshop Chairman
D.B. Lame, JPL GOASEX Workshop Coordinator

The five Sensor Experiment Teams were Chaired by P. Teleki, SAR; D. Ross, SMMR; P. McC[illegible]in, VIR; B. Tapley, Altimeter; and W. Pierson, SASS. To these Team Chairmen and their members, and the many participants in the GOASEX Workshop, the author acknowledges both the excellent efforts of these scientists and the privilege of working with them during the Seasat years.

REFERENCES

Born, G., Wilkerson, J., and Lame, D. 1979; "Seasat Gulf of Alaska Workshop Report", Vol. 1 and 2, Preliminary Draft, Jet Propulsion Laboratory, California Institute of Technology, Pasadena, California, February.

Dunne, J.A., 1979, "Minutes of the 18th Seasat Science Steering Group Meeting", Jet Propulsion Laboratory, Pasadena, California, February 8.

Fedor, L.S., Godbey, T.W., Gower, J.F.R., Guptill, R., Hayne, G.S., Rufenach, C.L., and Walsh, E.J. (in press). "Satellite Altimeter Measurements of Sea State - An Algorithm Comparison," J. Geophys. Res.

McCandless, Jr., S.W., 1975; "The U.S. Seasat Program: NASA Element" Proceedings of the Tenth International Symposium on Remote Sensing of Environment, Ann Arbor, Michigan.

Ross, D., 1979; Personal Communication, Atlantic Oceanographic and Meterological Laboratory, February.

Sherman, III, J.W., 1975; "The U.S. Seasat Program: The NOAA Element", Proceedings of the Tenth International Symposium on Remote Sensing of Environment, Ann Arbor, Michigan.

Shuchman, R.A., Dwyer, J.C., Gonzalez, F., Ross, D., Davis, C.F., 1979; "Preliminary GOASEX Wave Analysis", Environmental Research Institute of Michigan, Report 138600-1-X, NOAA/NESS Contract M0-A01-78-00-4339, January.

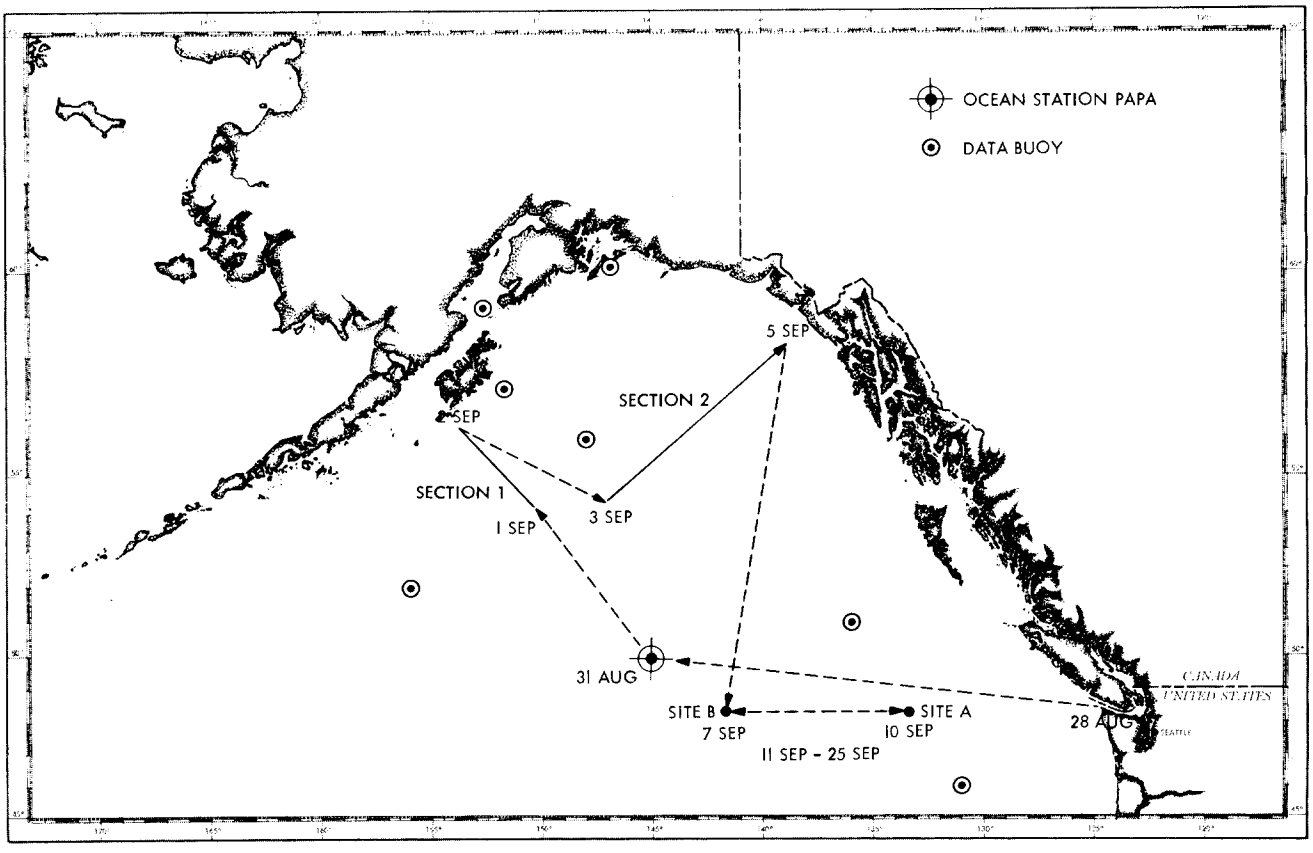

Figure 1. Operating Area of the Gulf of Alaska Experiment.

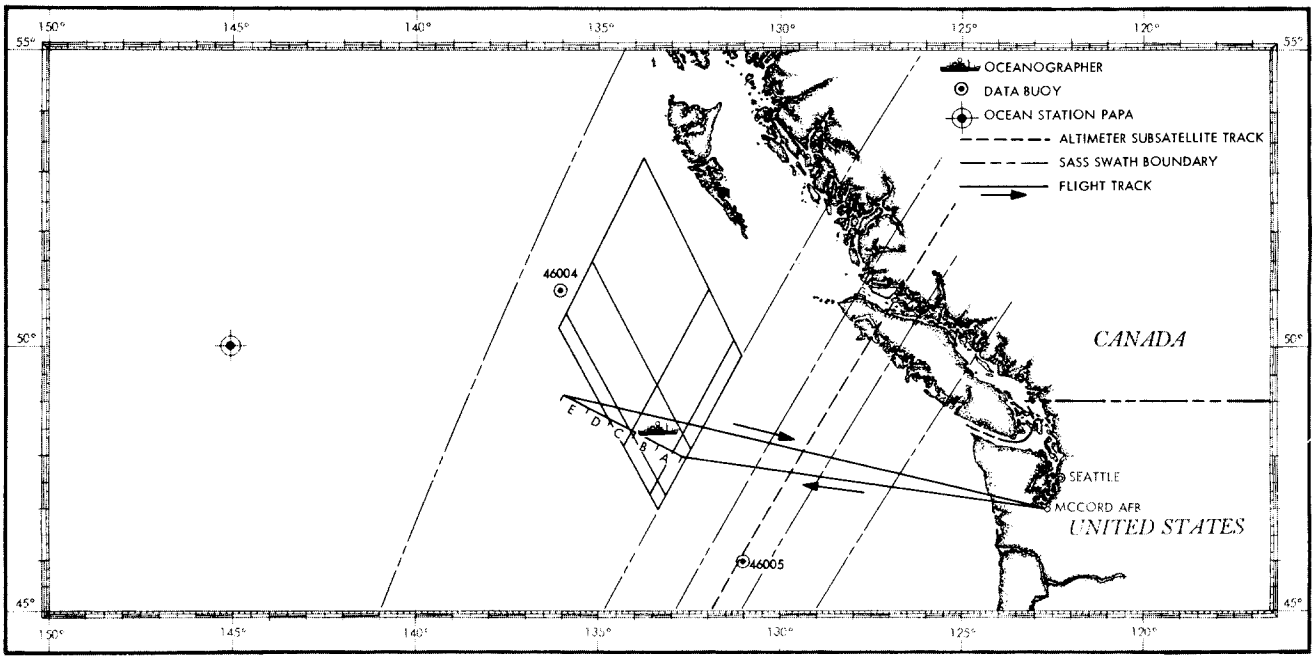

Figure 2. Typical Flight Plan for GOASEX.

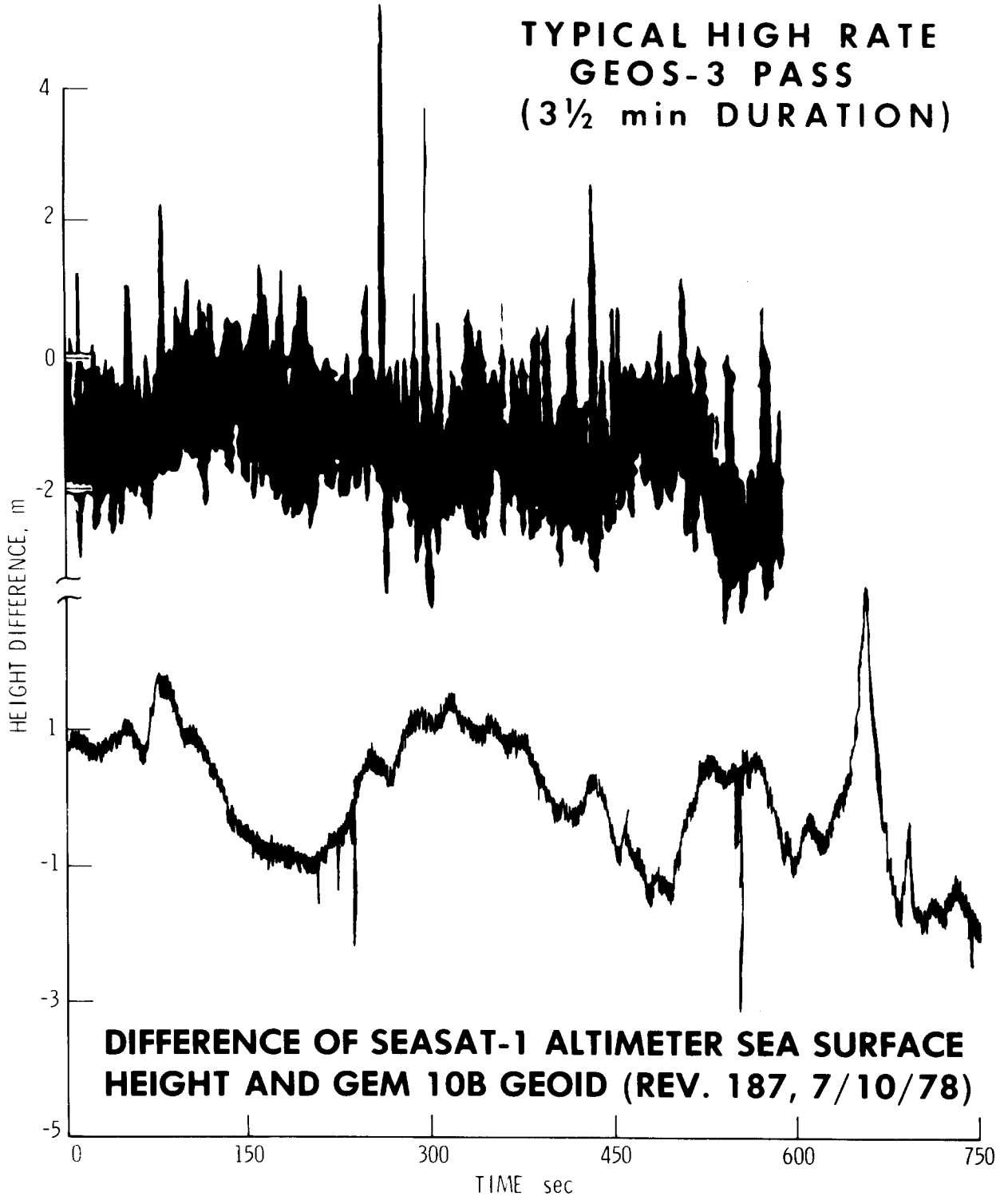

Figure 3. Comparison of GEOS-3 and Seasat Altimeter System Noise (Note Difference in the Abscissa Scale).

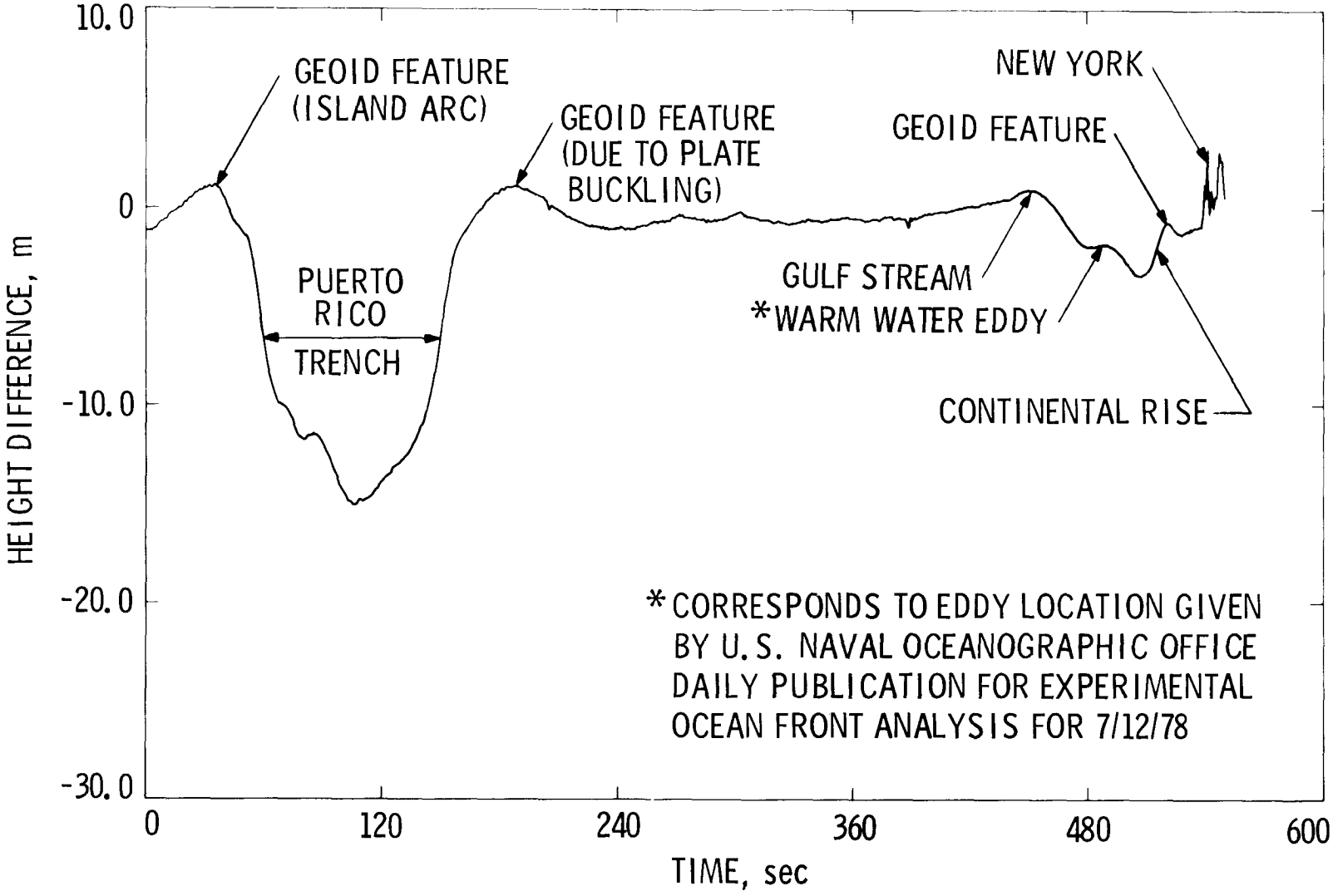

Figure 4. Difference of Seasat Altimeter Sea Surface Height and GEM 10B Geoid for North Atlantic Pass (7/10/78, Rev 191)

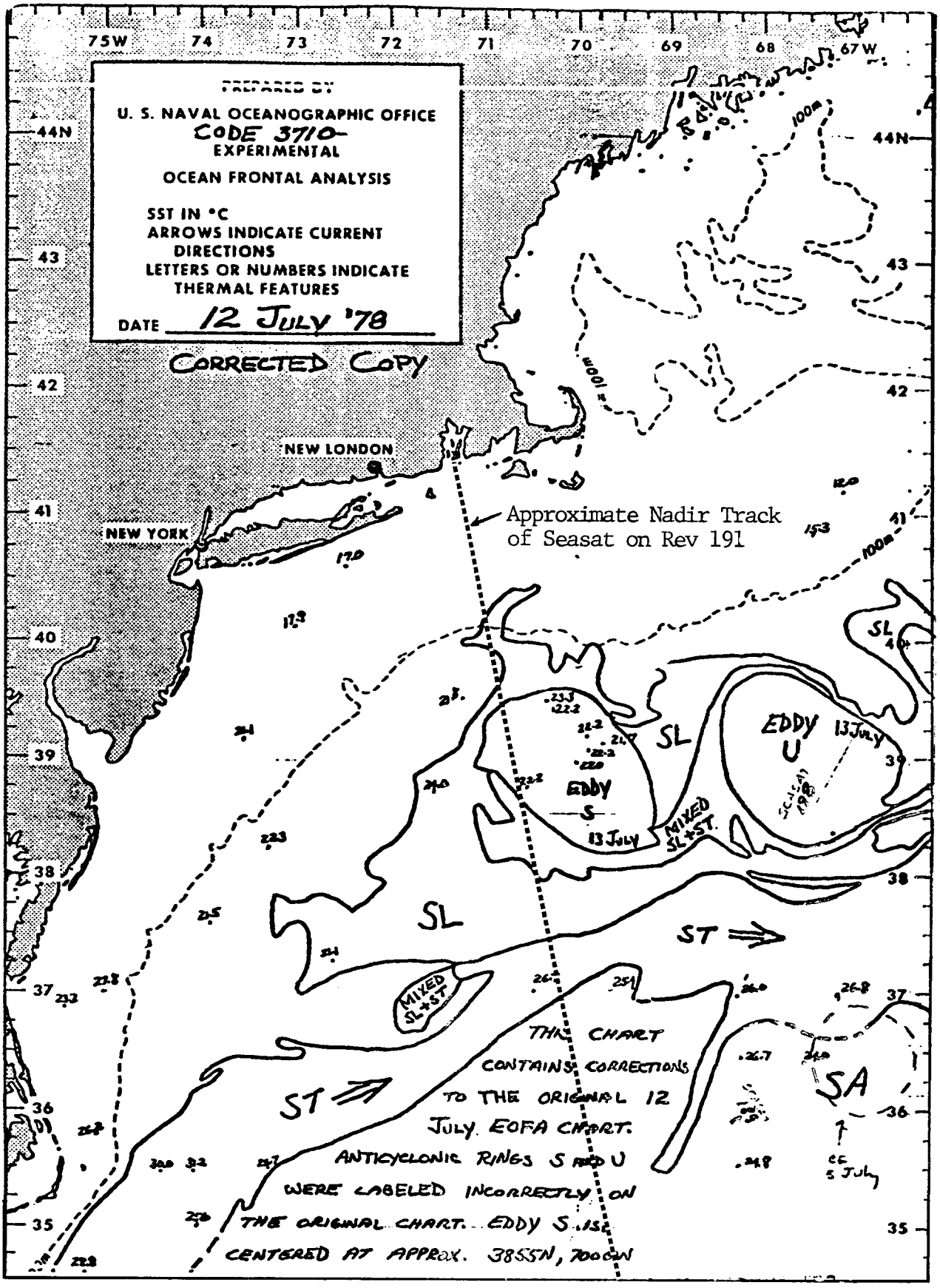

Figure 5. Ocean Frontal Analysis For July 12, 1978, with Approximate Location of Seasat Rev 191 on July 10, 1978.

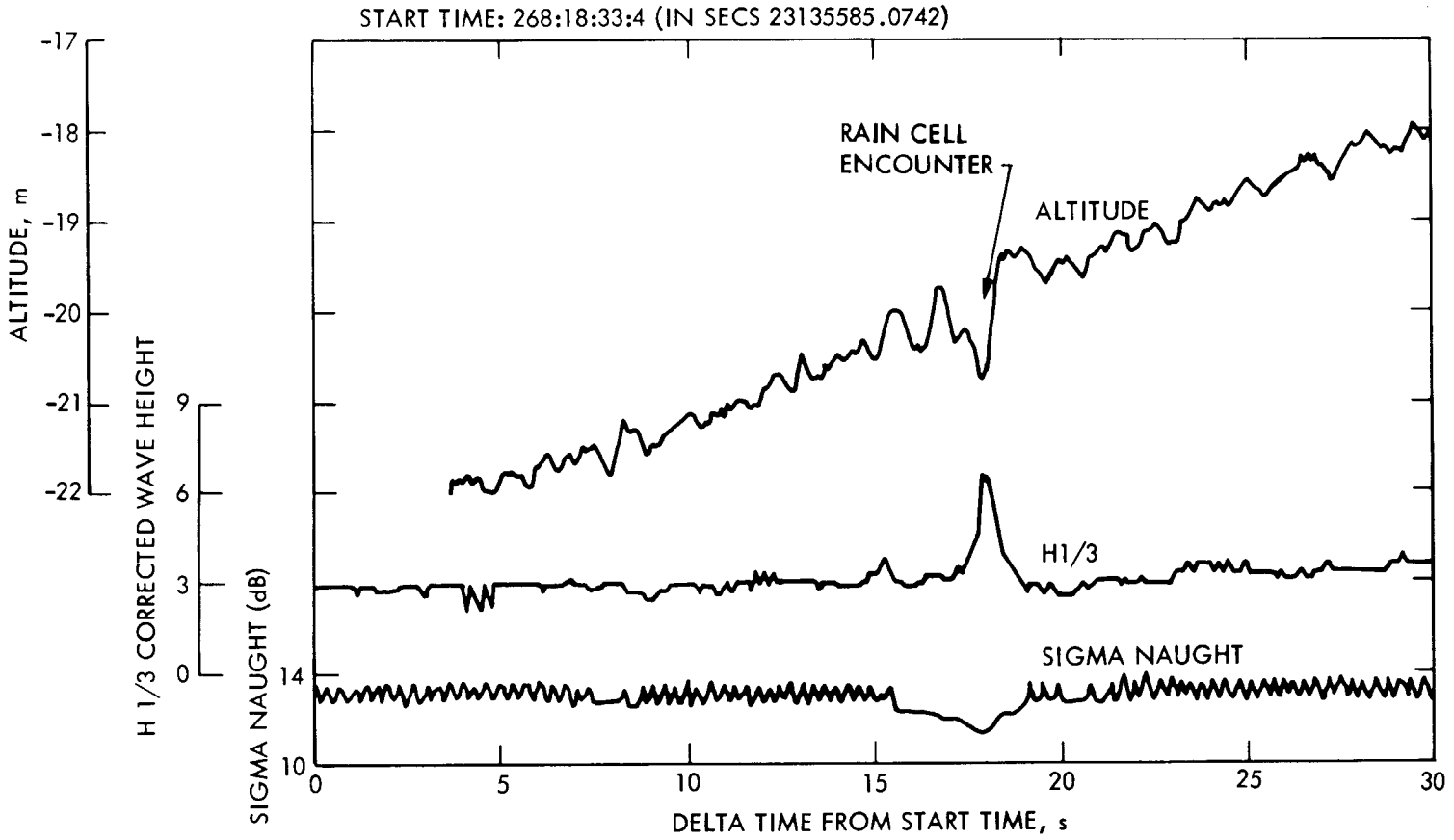

Figure 6. Response of Altimeter h, $H_{1/3}$, and σ_o to Rain Cell on Rev 1298.

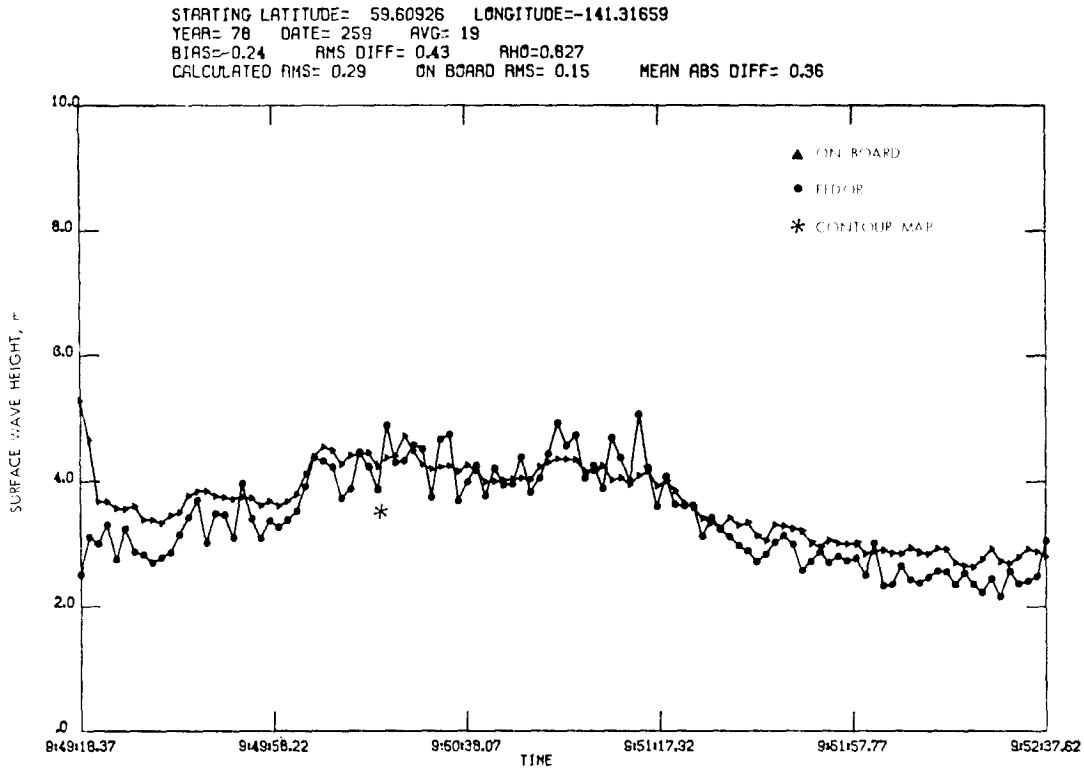

SWH - Onboard Processor and Fedor's Method, Rev 1164, Starting Latitude 59.6N

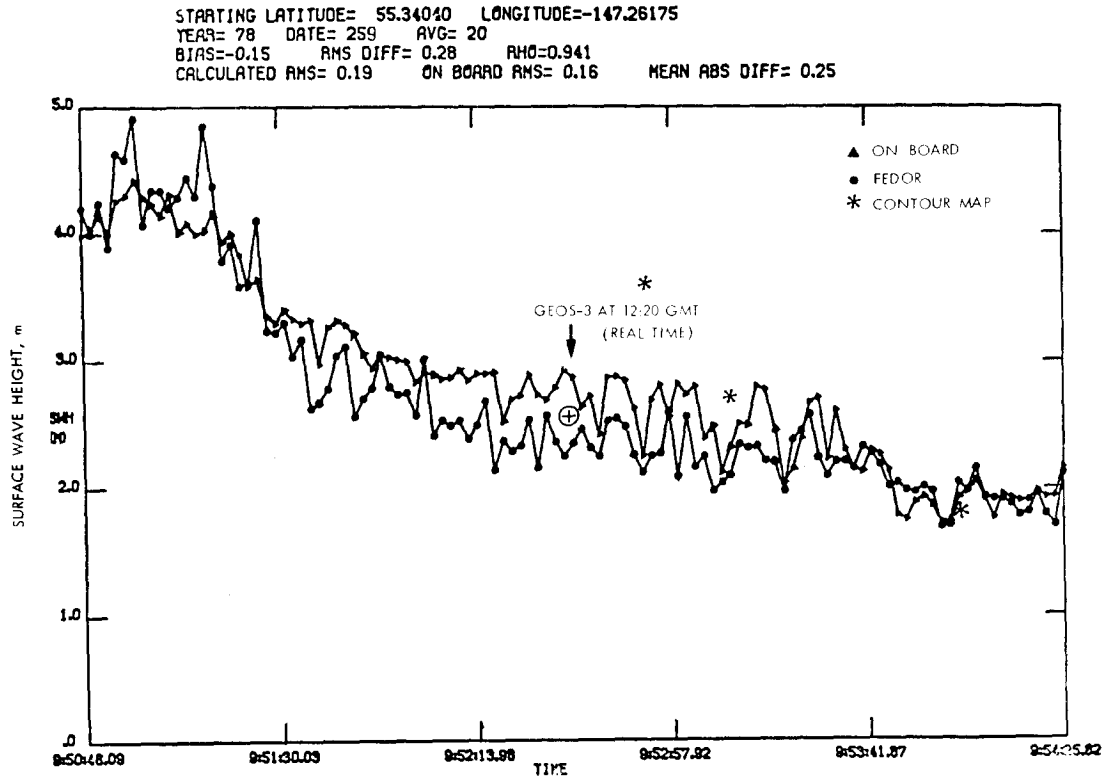

SWH - Onboard Processor and Fedor's Method, Rev 1164, Starting Latitude 55.3N

Figure 7. Two Examples of Significant Wave Height Measurement

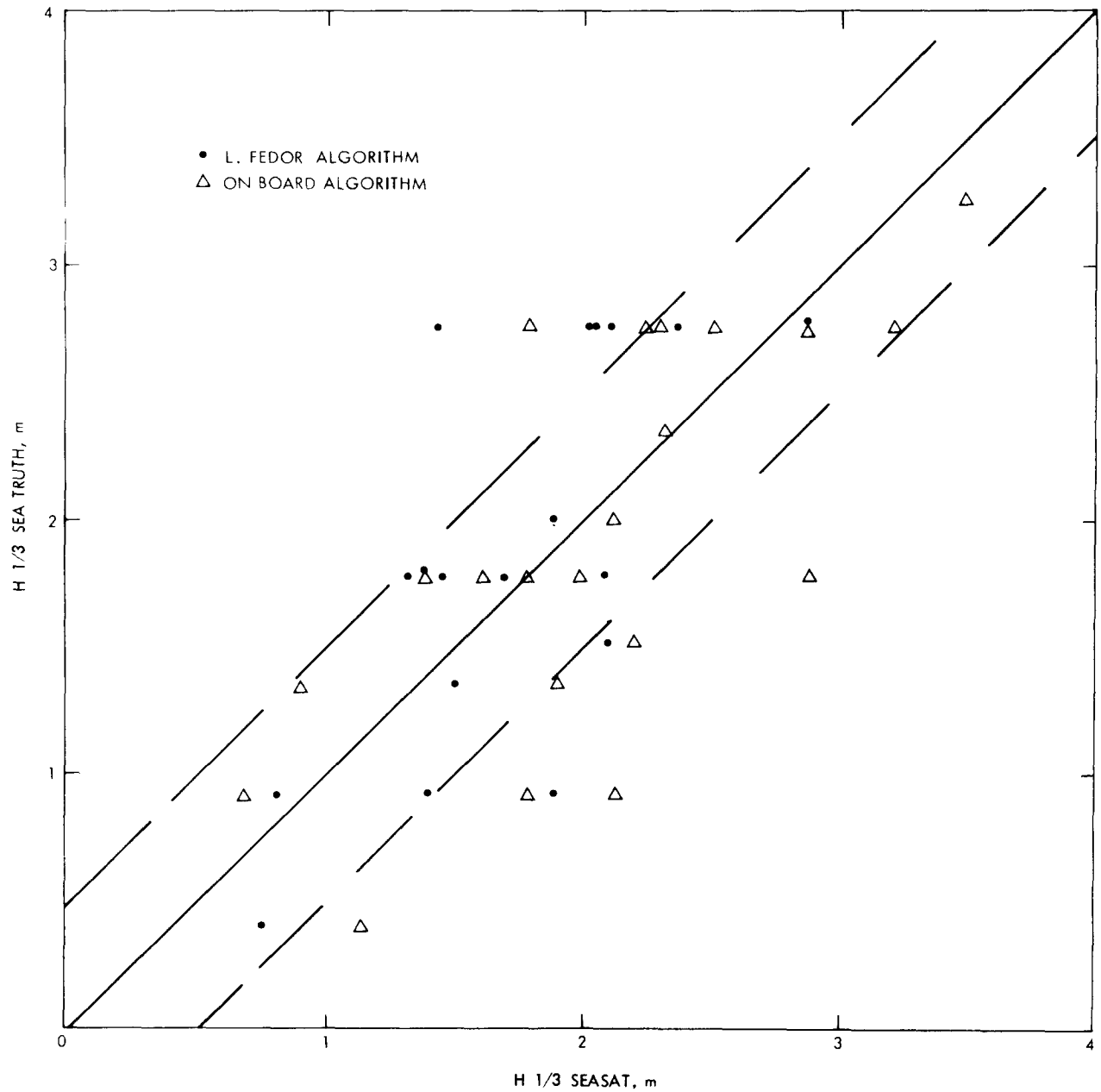

Figure 8. Scatter Diagram of Significant Wave Height Data

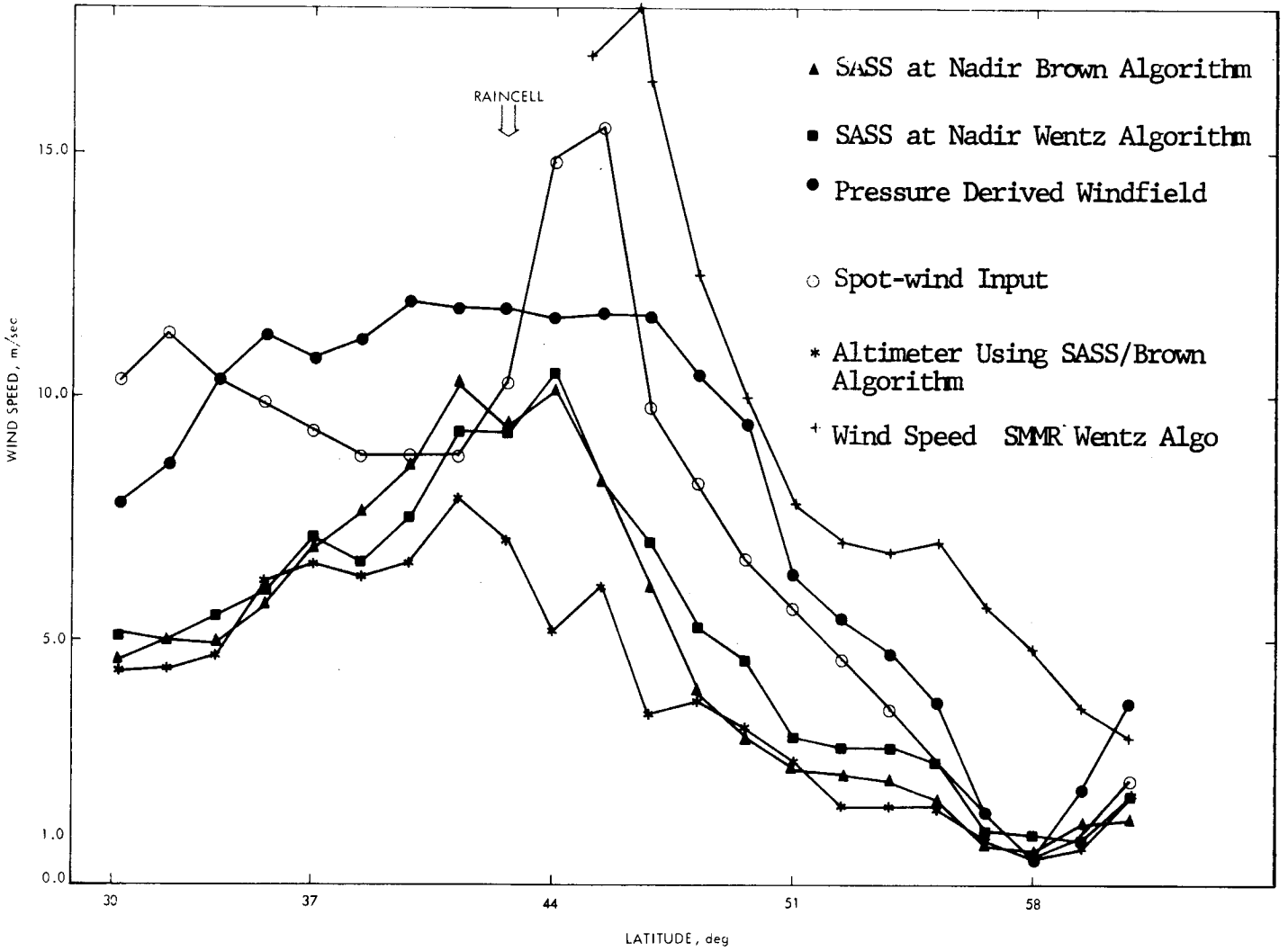

Figure 9. Wind Speed Comparisons (Rev 1298): SASS at Nadir Using Brown Algorithm; SASS at Nadir Using Wentz Algorithm; Pressure Derived Windfield; Spot-wind Input; Altimeter Using SASS (Brown) Algorithm; and SMMR Ground-track Wind Speed Using Wentz Algorithm.

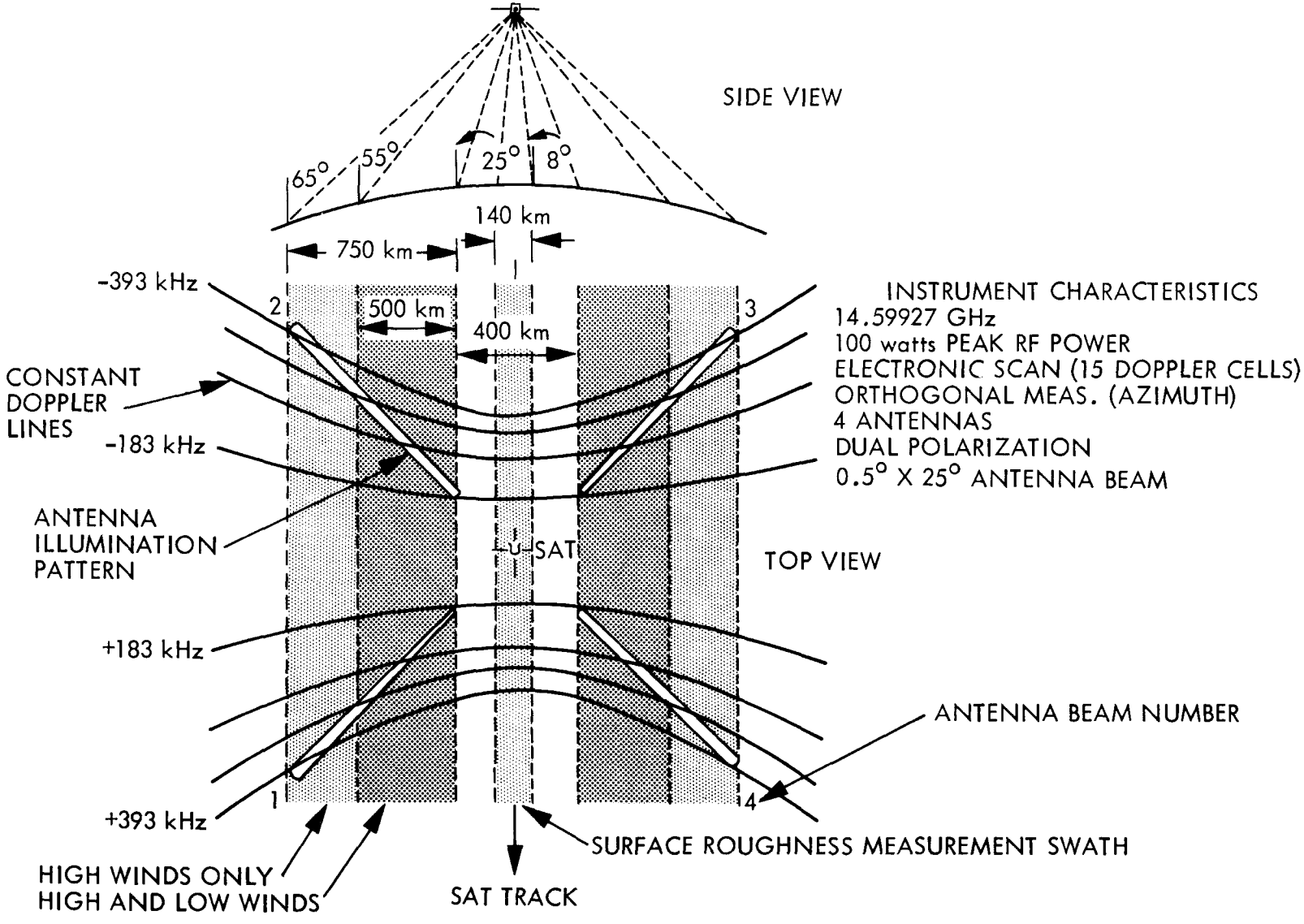

Figure 10. Geometry and Characteristics of SASS

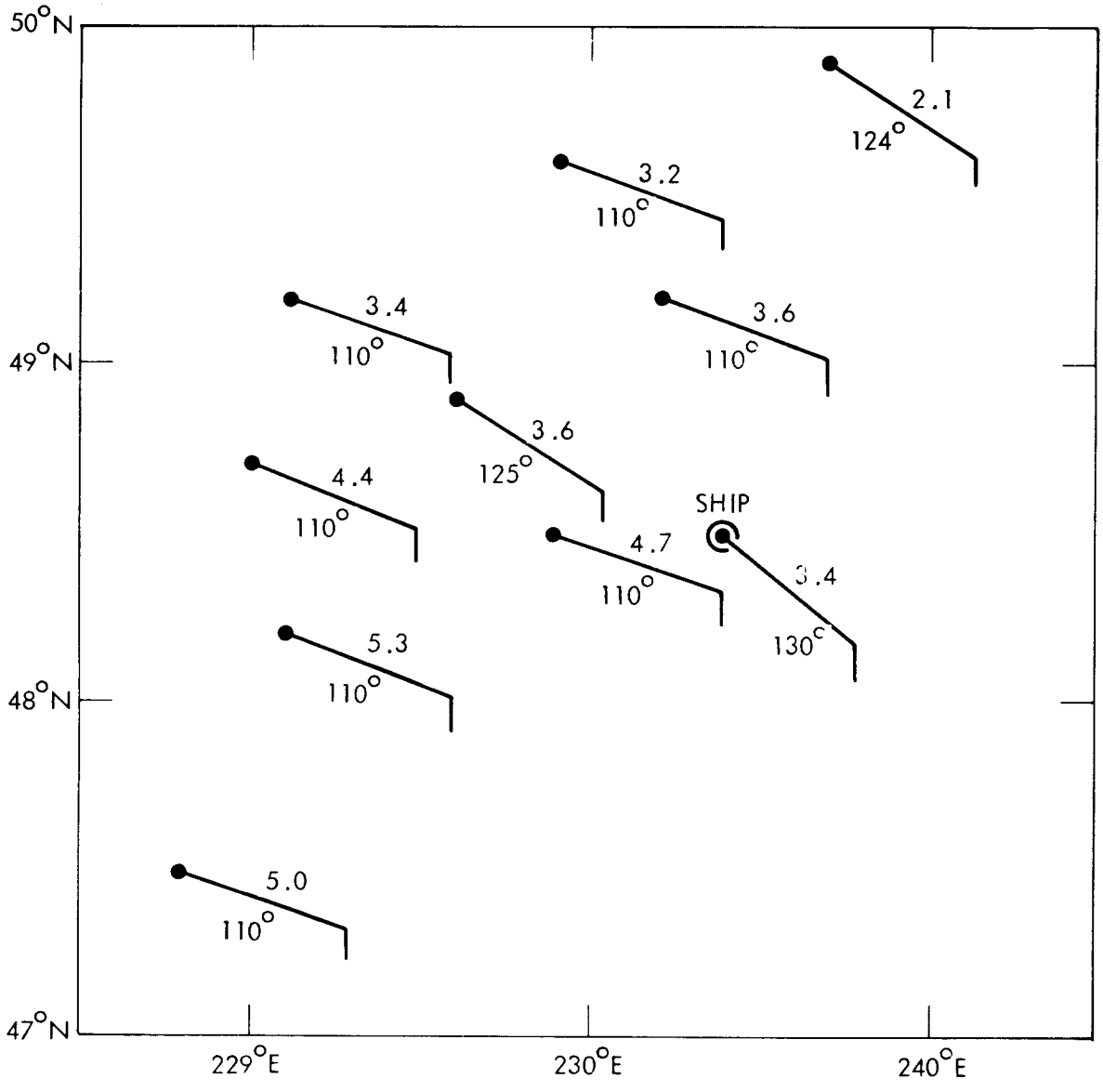

Figure 11. SASS Wind Field in the Vicinity of a Ship (Rev 1298)

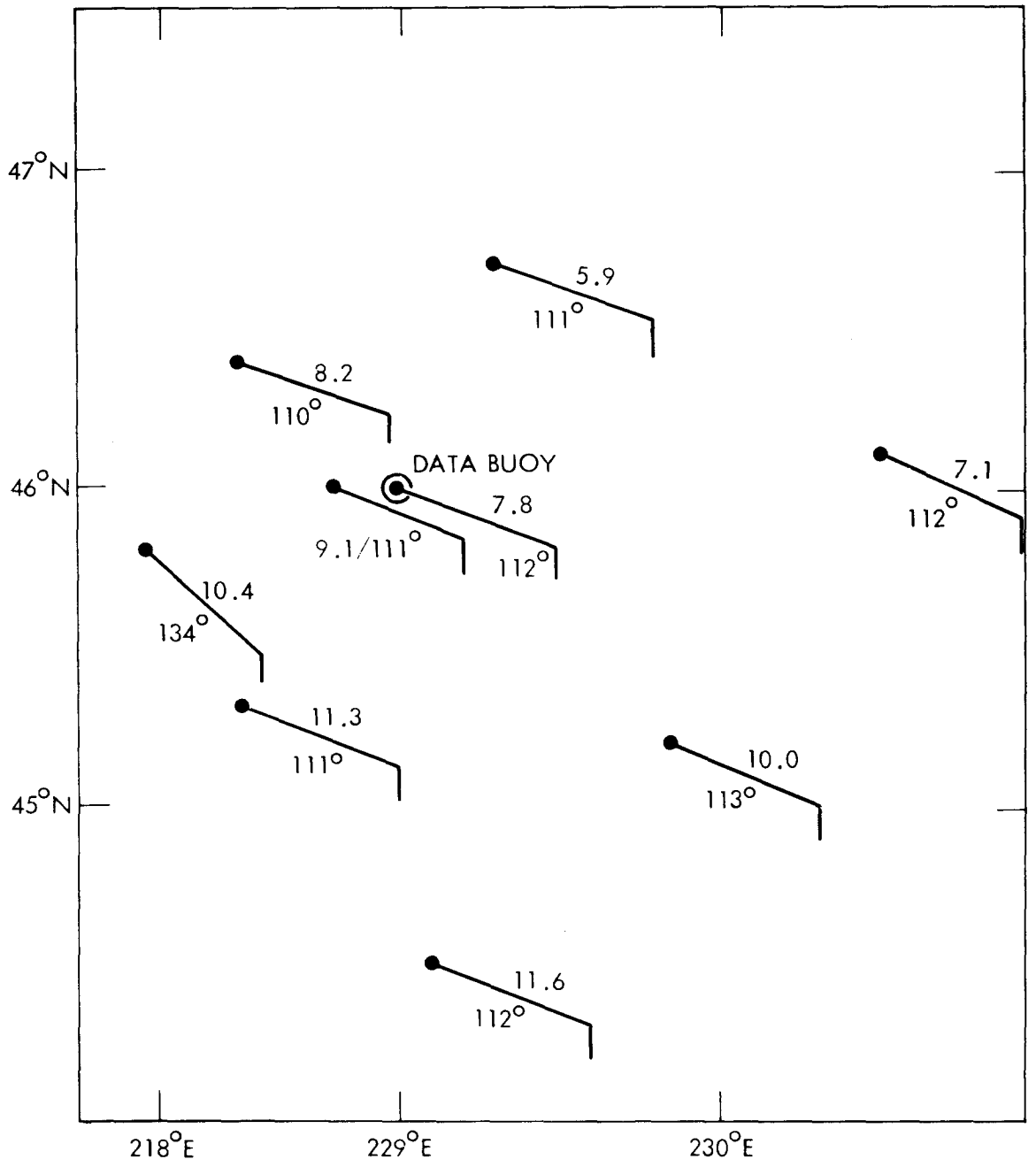

Figure 12. SASS Wind Field in the Vicinity of a Data Buoy (Rev 2198)

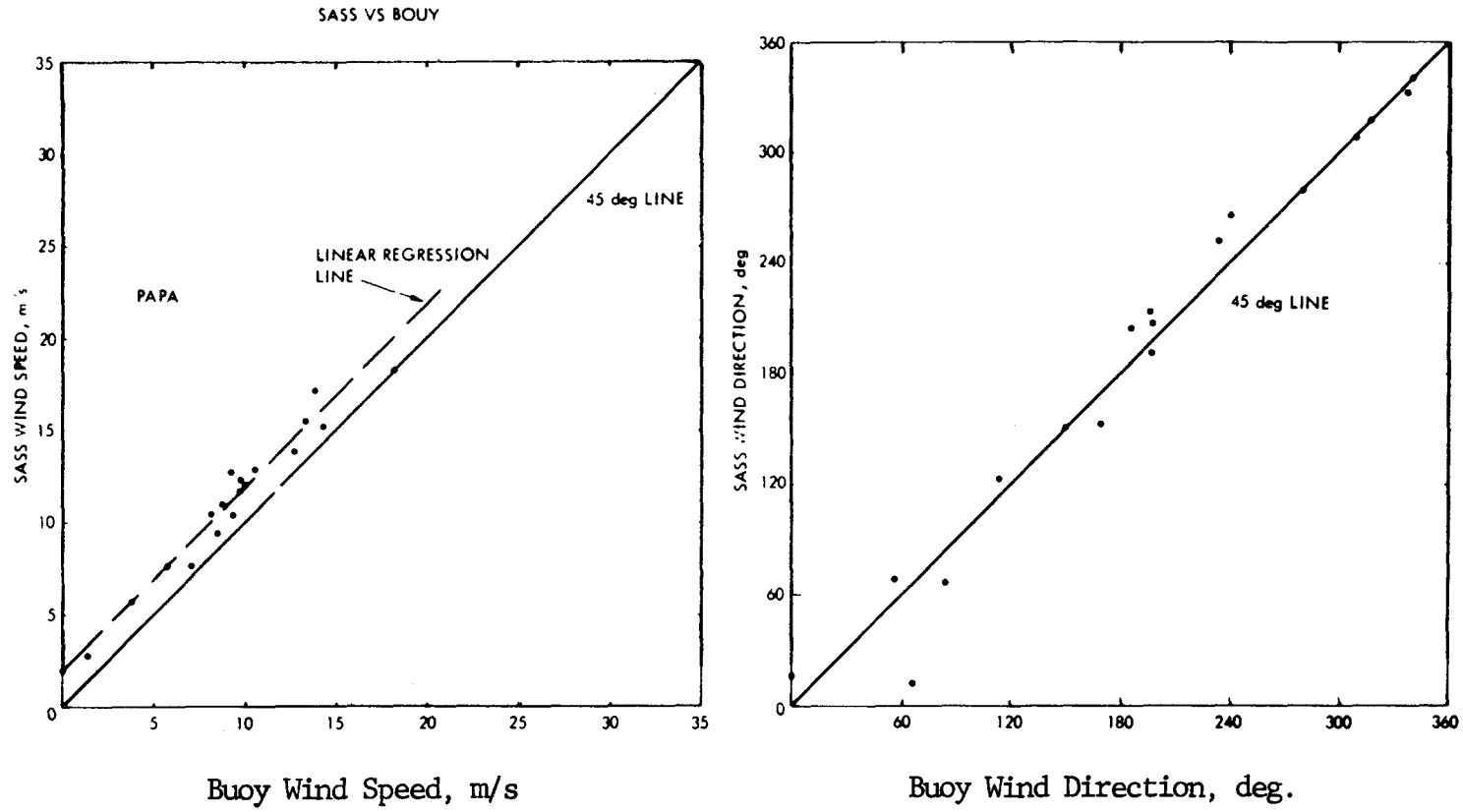

Figure 13. Comparison of SASS Derived Winds to Buoy Winds.

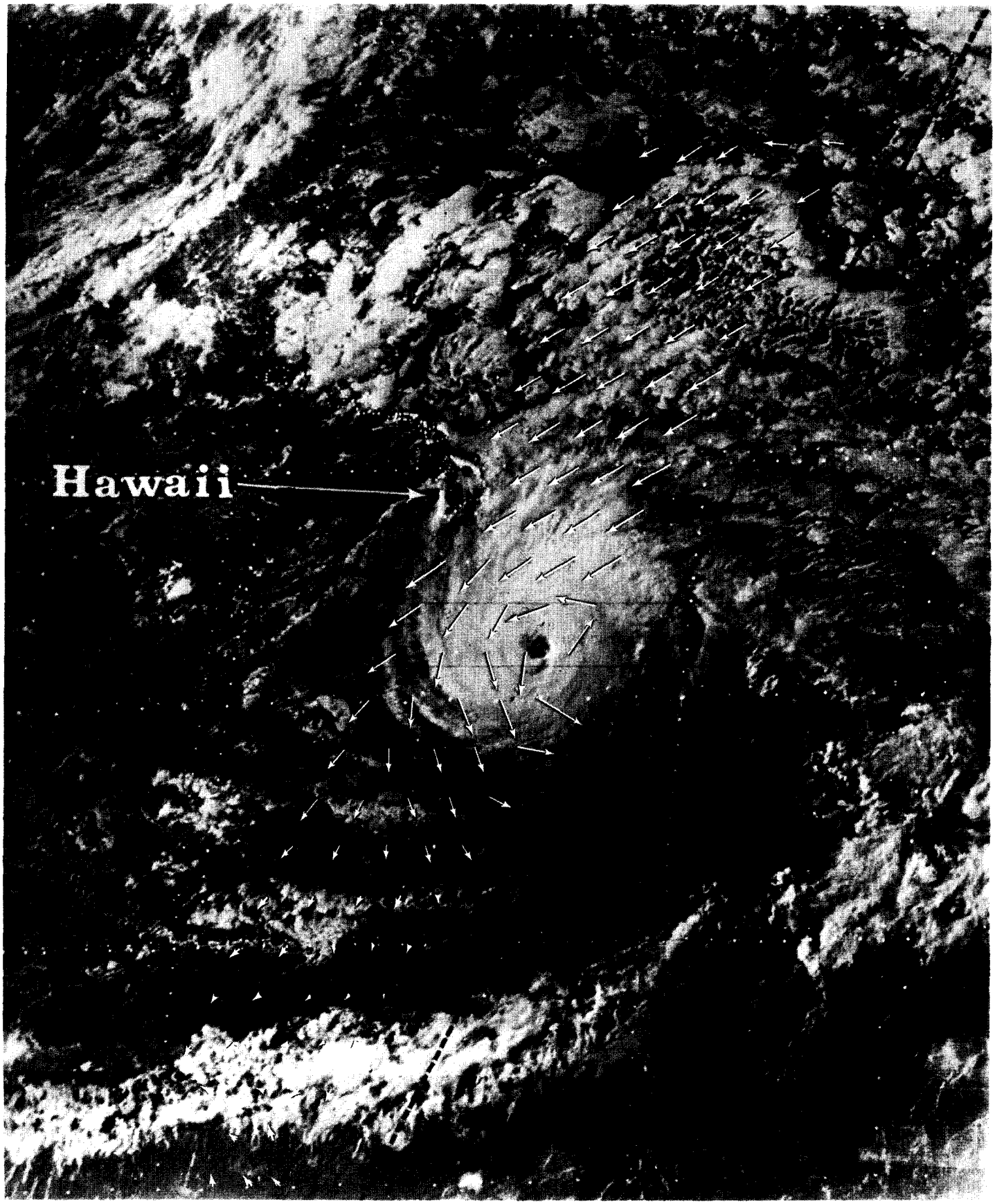

Figure 14. NOAA GOES Image of Hurricane Fico With SASS Derived Winds Superimposed On July 20, 1978.

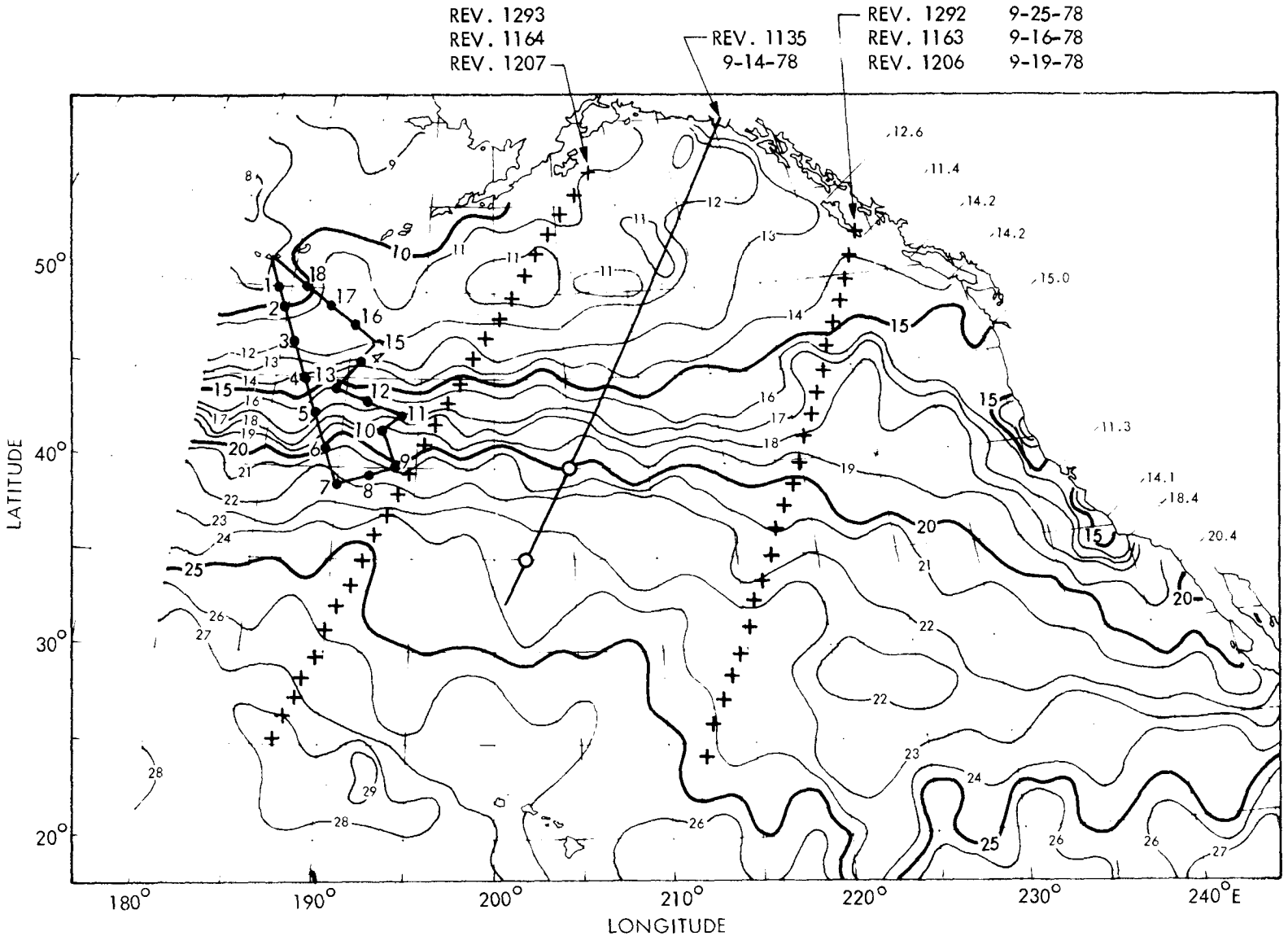

Figure 15. National Marine Fisheries Service (NMFS) analysis of sea surface temperature for September 1978. SMMR swath center tracks are superimposed for data used in this intercomparison report. In upper left is aircraft track and station numbers of higher quality air expendable bathy thermograph data used to verify NMFS analysis.

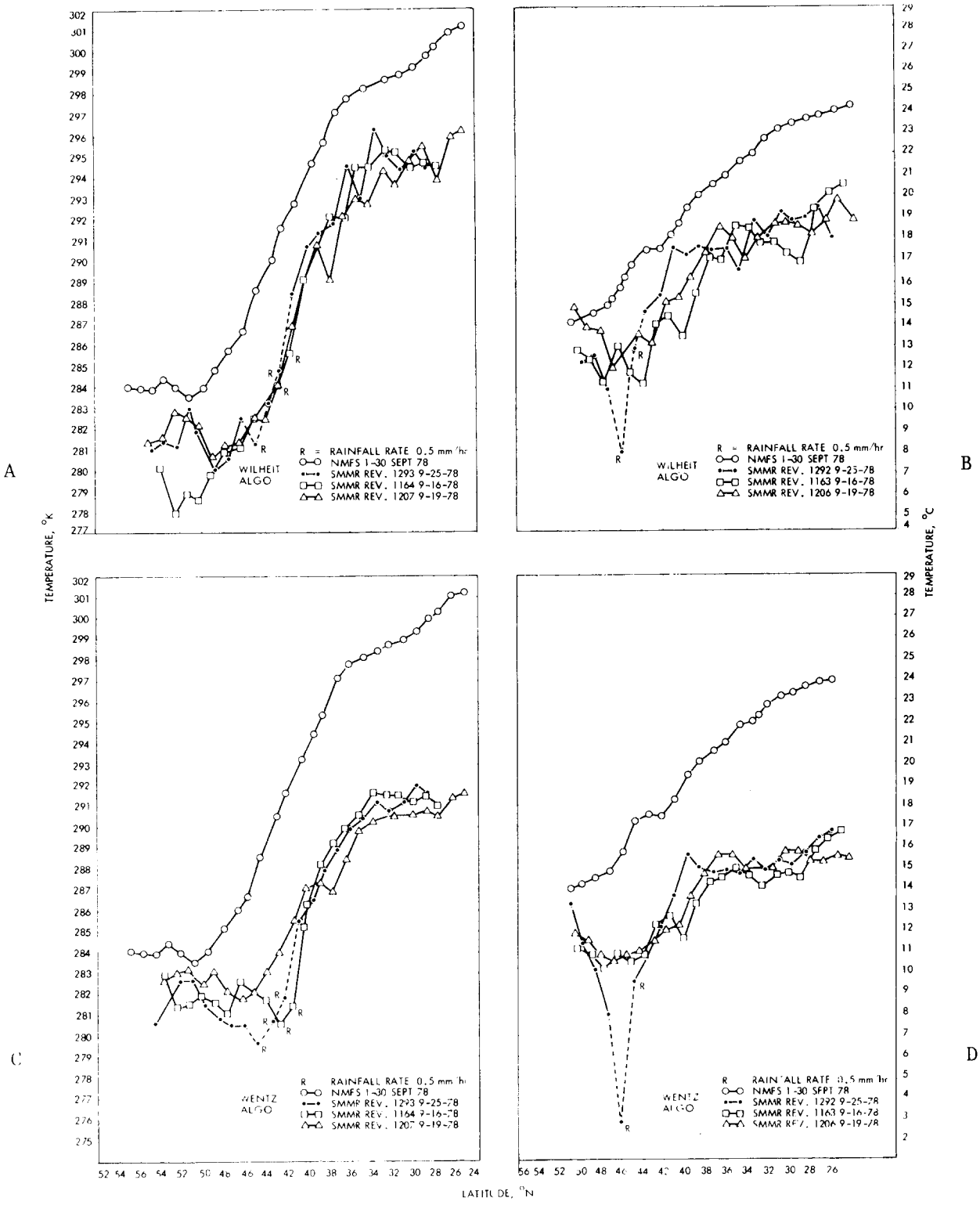

Figure **16.** Comparison of NMFS sea temperature analysis with SMMR data along west (a, c) and east (b, d) tracks of figure 8-6. Both Wilheit (a, b) and Wentz (c, d) algorithm results are displayed.

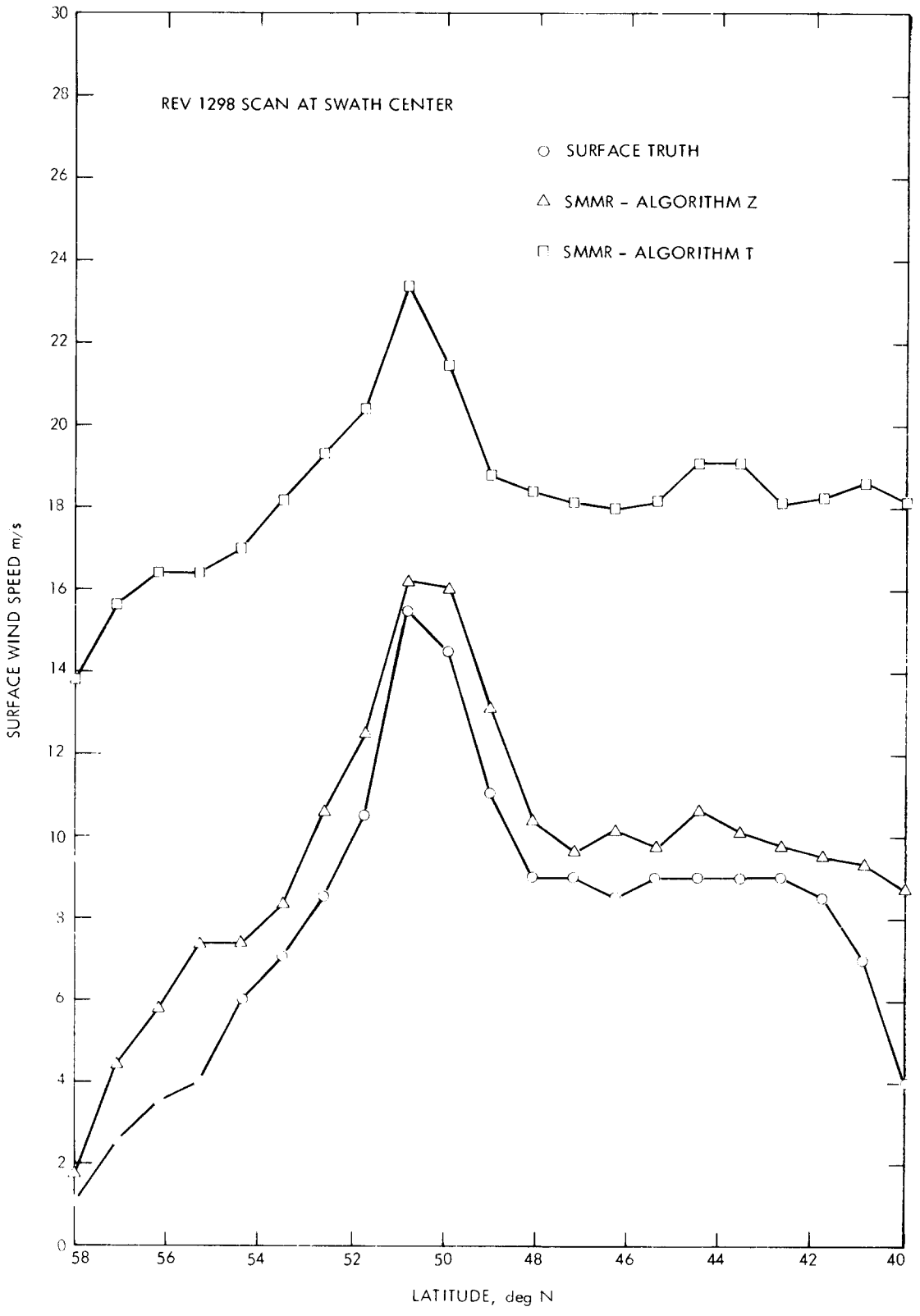

Figure 17. Seasat SMMR Wind Comparison (Rev 1298).

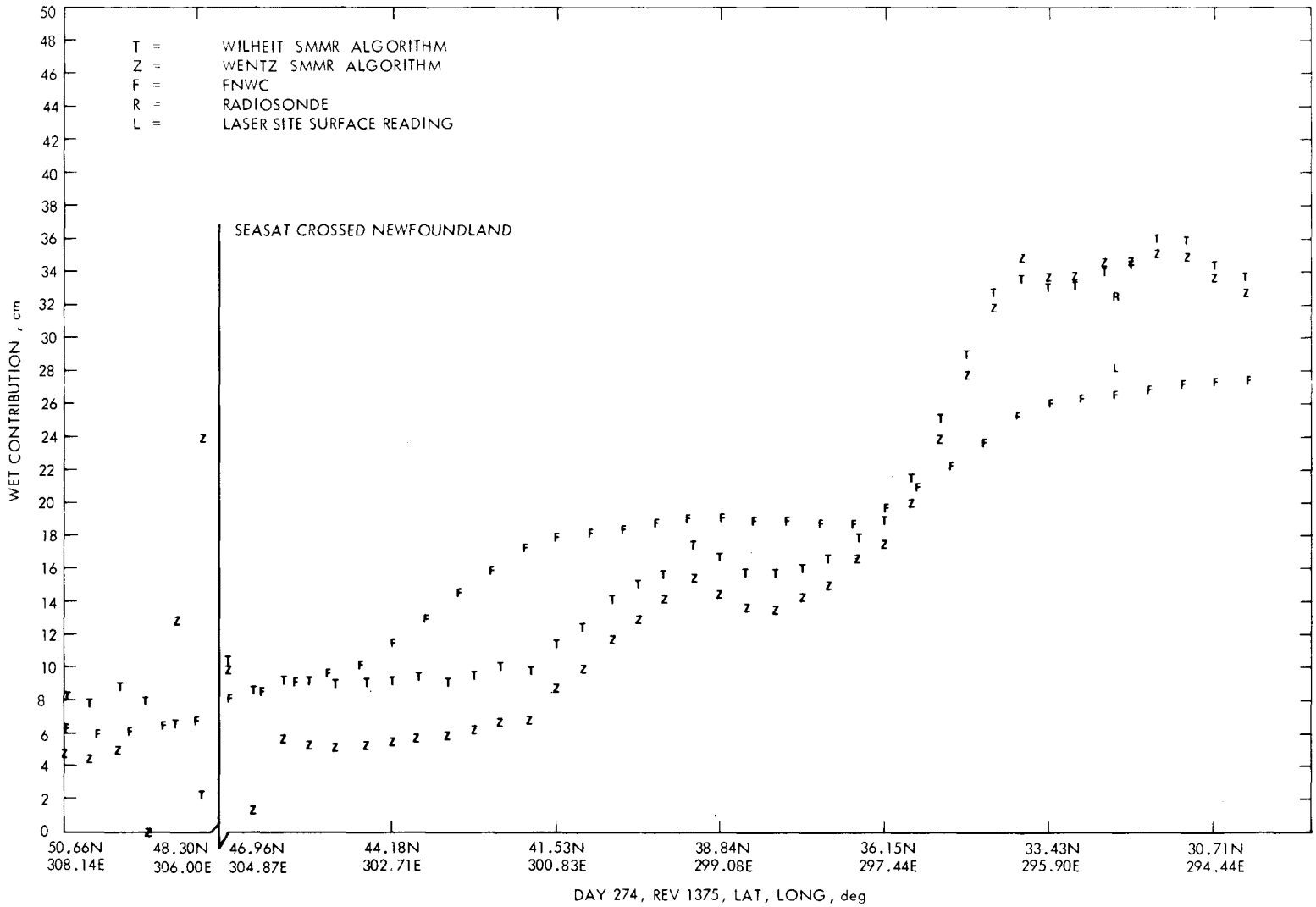

Figure 18. Comparison of altimeter path length correction determined from SMMR data by T and W algorithms with FNWC estimates.

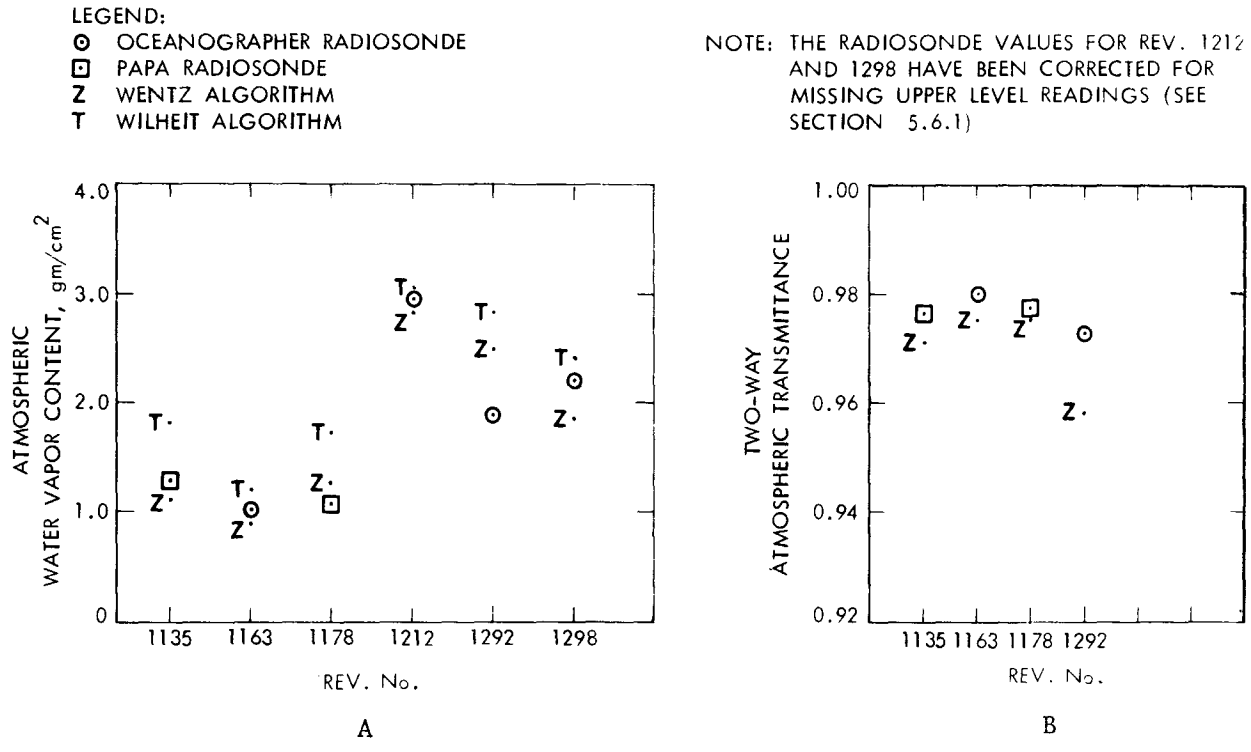

Figure 19. Comparison of integrated atmospheric water vapor obtained from radiosonde ascents (see text) with the SMMR/CV values obtained by Wilheit and Wentz's algorithms. Note: The radiosonde values for Revs 1212 and 1298 have been corrected for missing upper level readings.

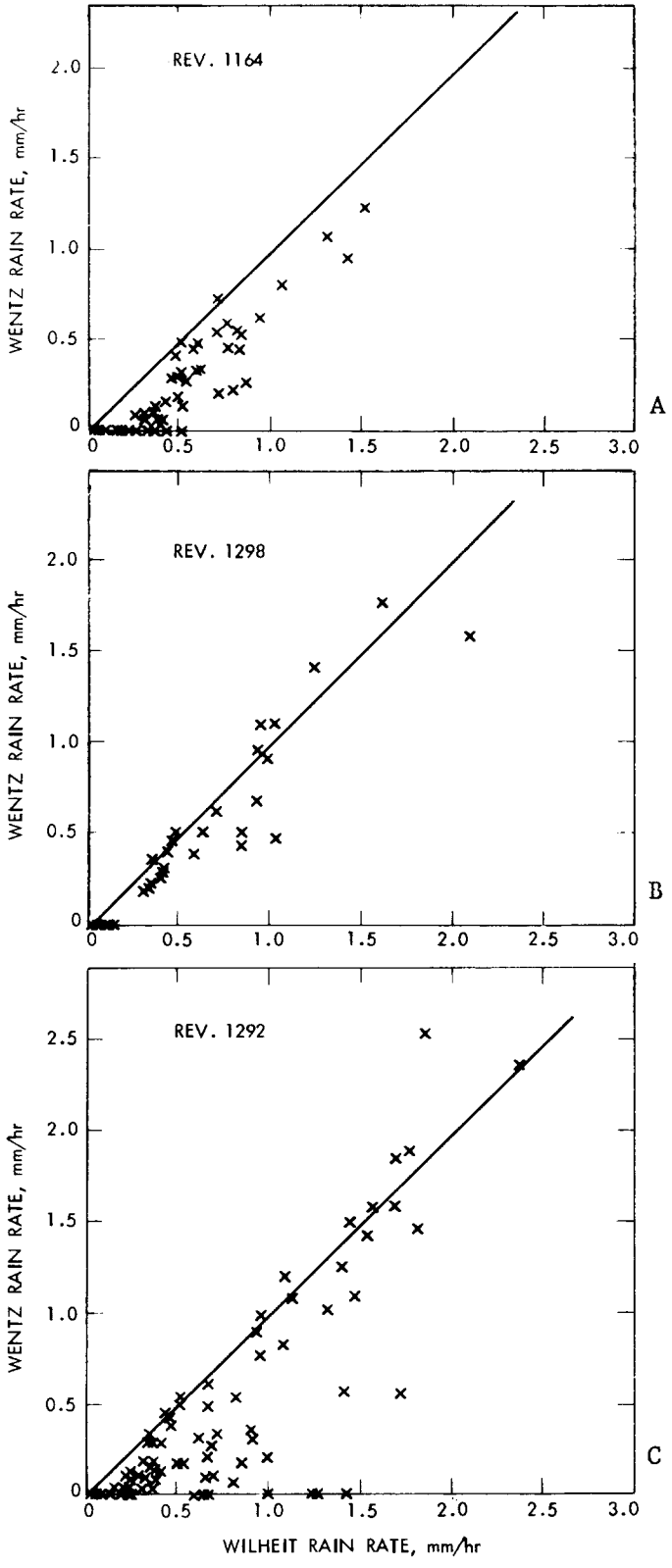

Figure 20. Comparison of the rain rate calculated with the Wentz and Wilheit algorithms

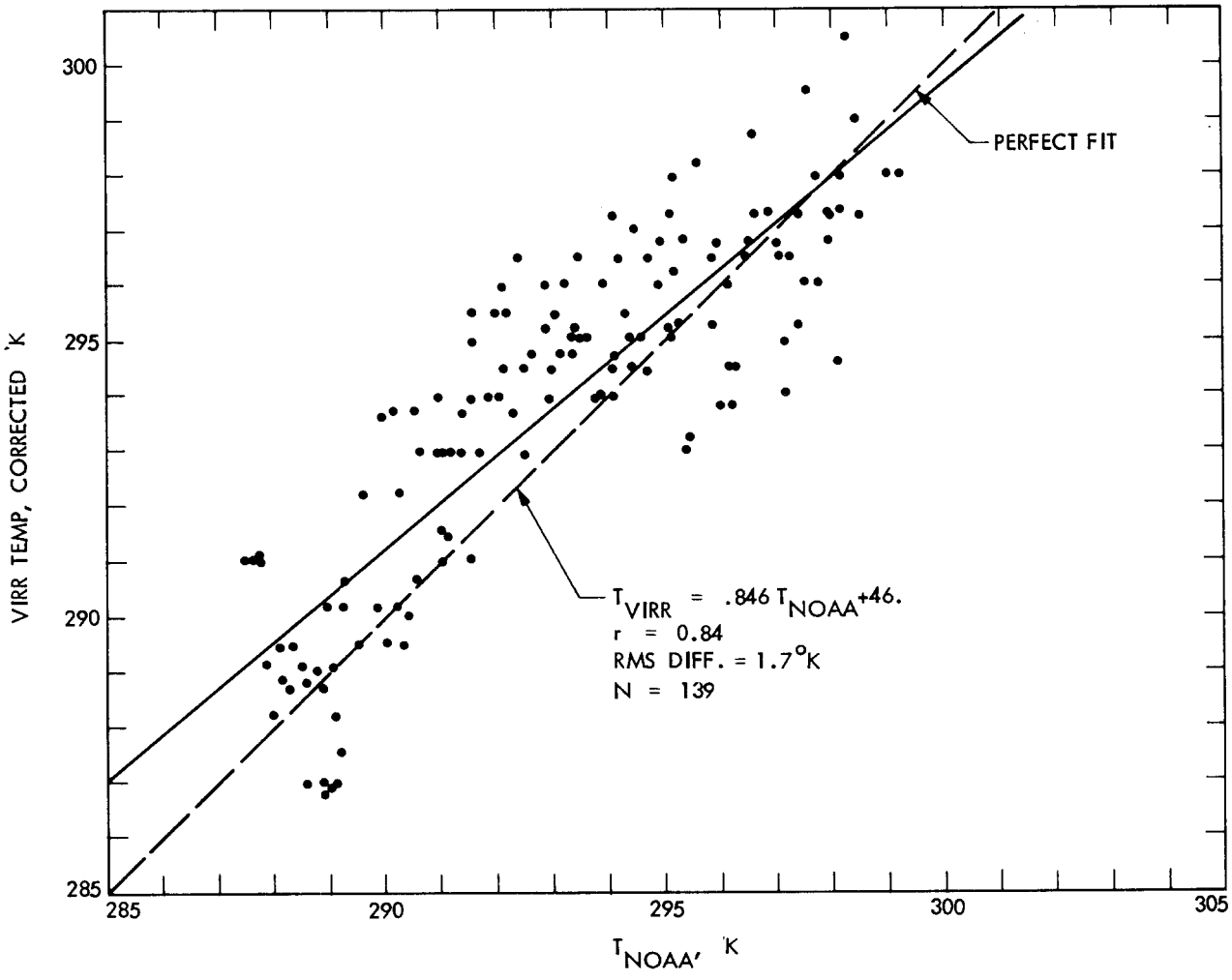

Figure 21. NOAA Temperature Field Estimates* Vs. Seasat-A VIRR Temperatures∓

*For Time Period July 5, 1978 - July 10, 1978

∓VIRR Day 188 (July 7, 1978) 22:49:45-22:51:55 GT

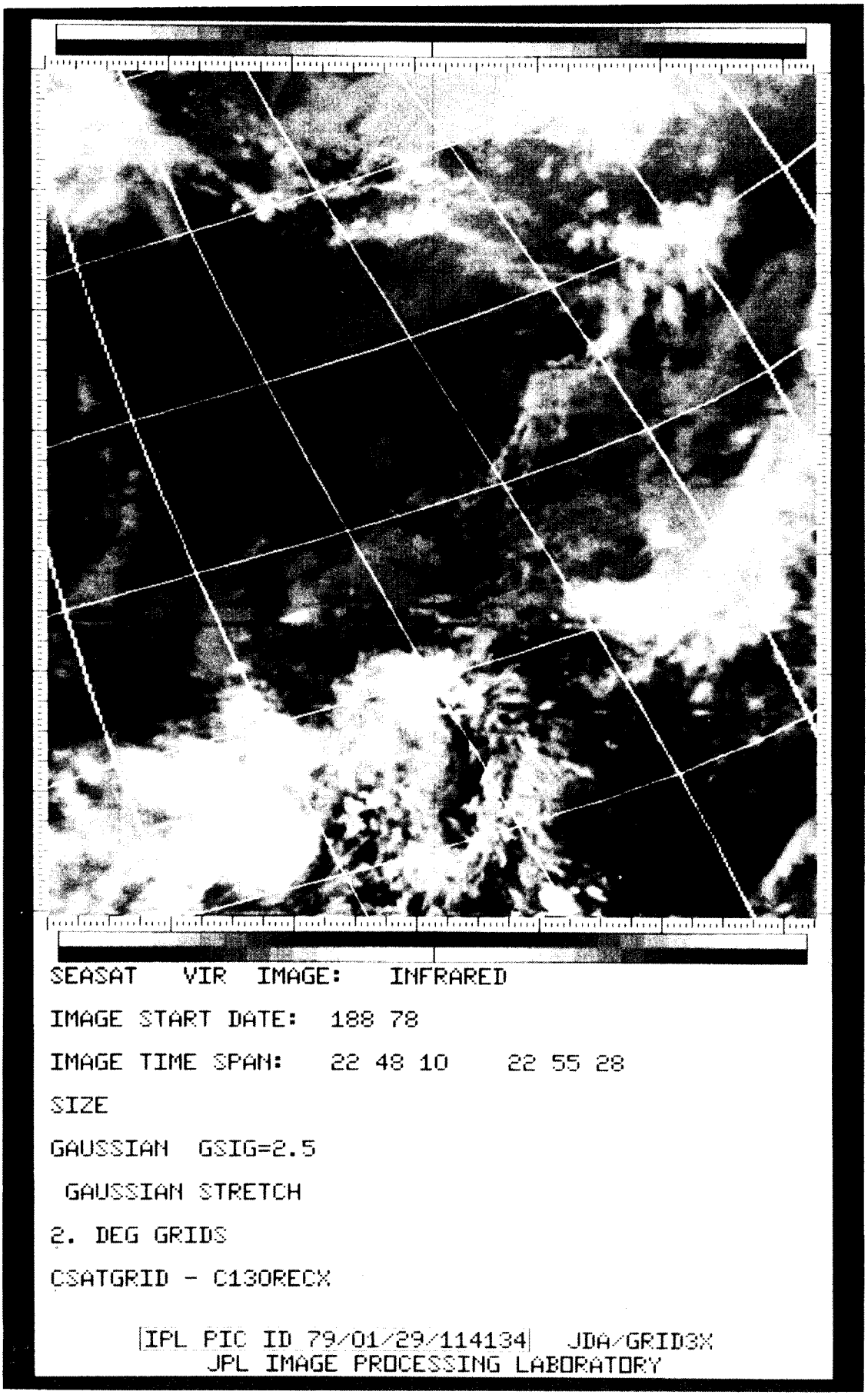

Figure 22. VIR Infrared Image of the Western North Atlantic. (Rev 156; July 7, 1978)

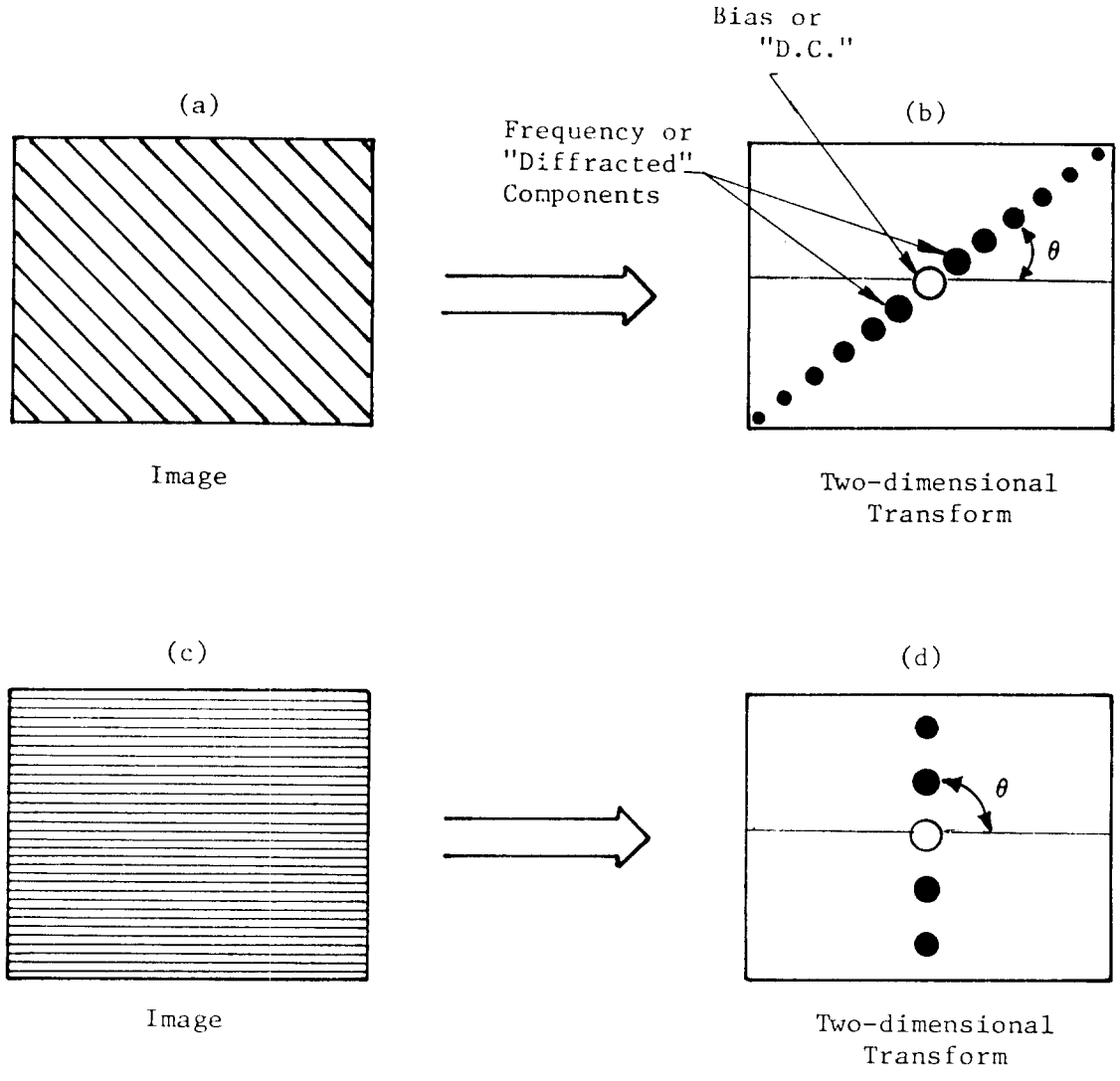

FIGURE 23. Diagrams of Linear Images and Corresponding Two-Dimensional Fourier Transforms. Note that the distribution in the two-dimensional Fourier transform is governed by the frequency and orientation of the spatial distribution of the images. Spacings of components in (b) and (d) are inversely proportional to spacings of lines in the images (a) and (c). The sizes of the dots indicate the amount of energy in the diffracted orders--smaller dots, smaller amount of energy.

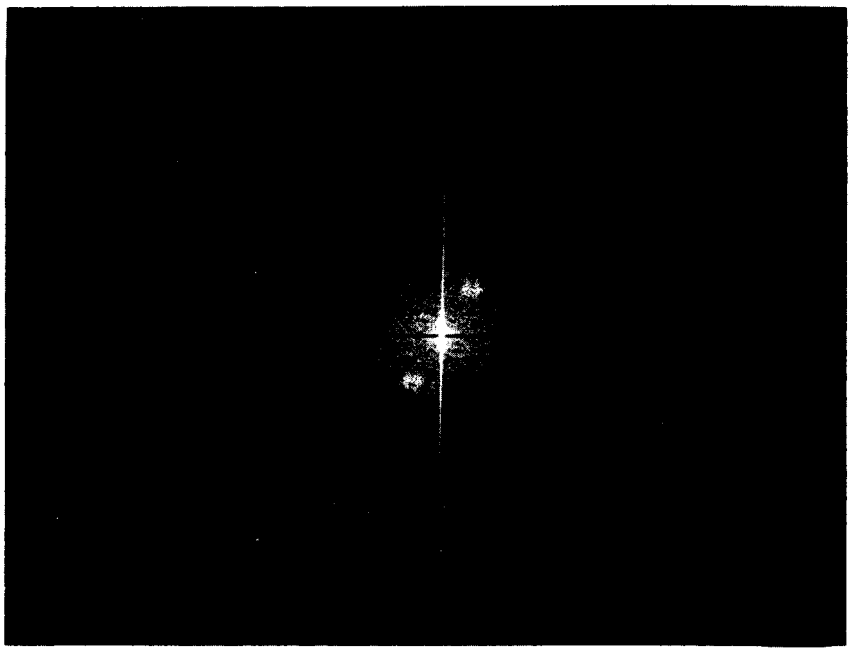

FIGURE 24. Optical Fourier Transform (OFT) of Subswath 4, Rev 1126, Approximate 94.5 cm from Start of Pass.

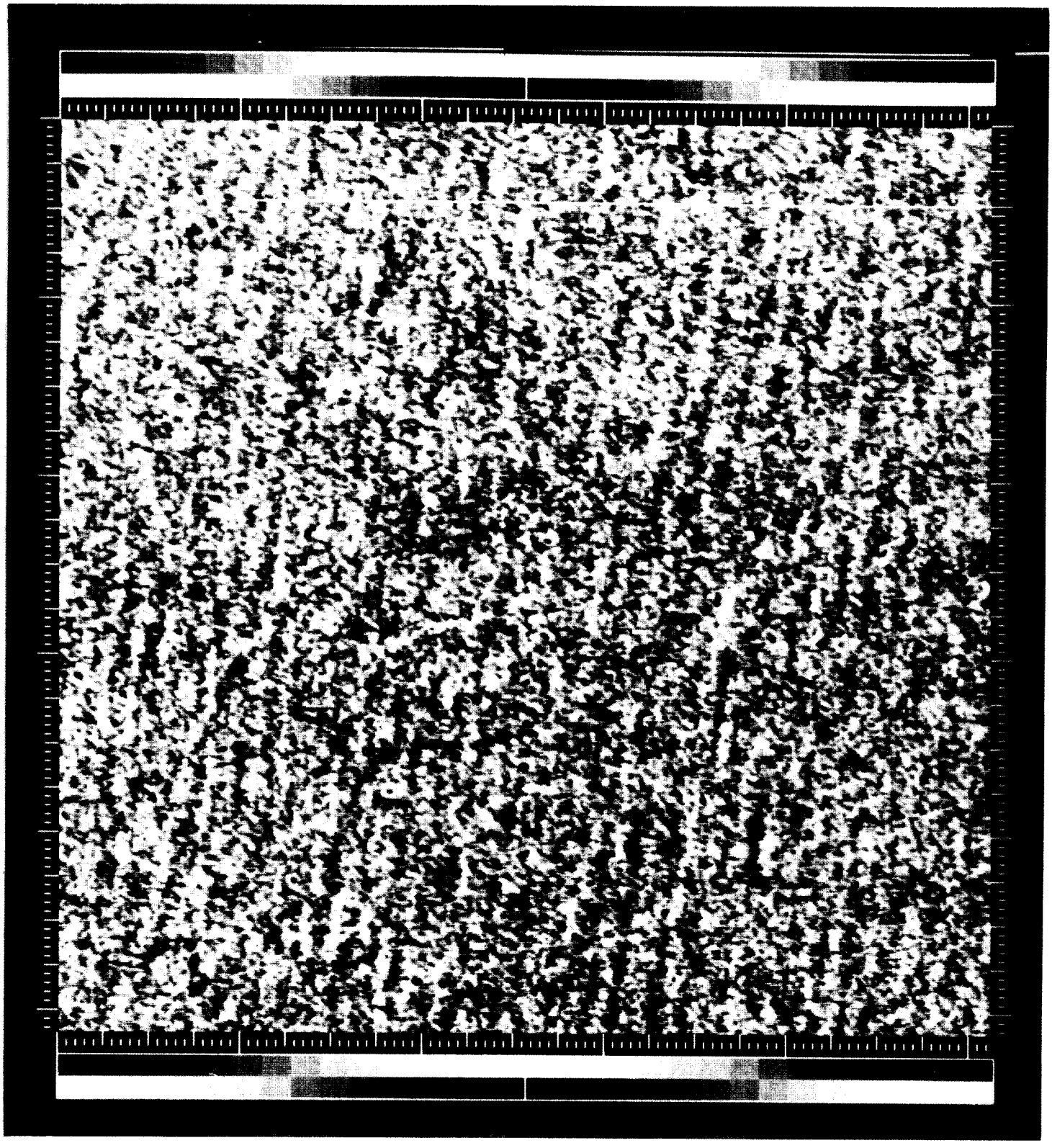

Figure 25. SAR Image of Waves From Hurricane Fico (Rev 251; July 14, 1978). Image is 5 x 5 km with Principle Waves of 160-m Wavelength.

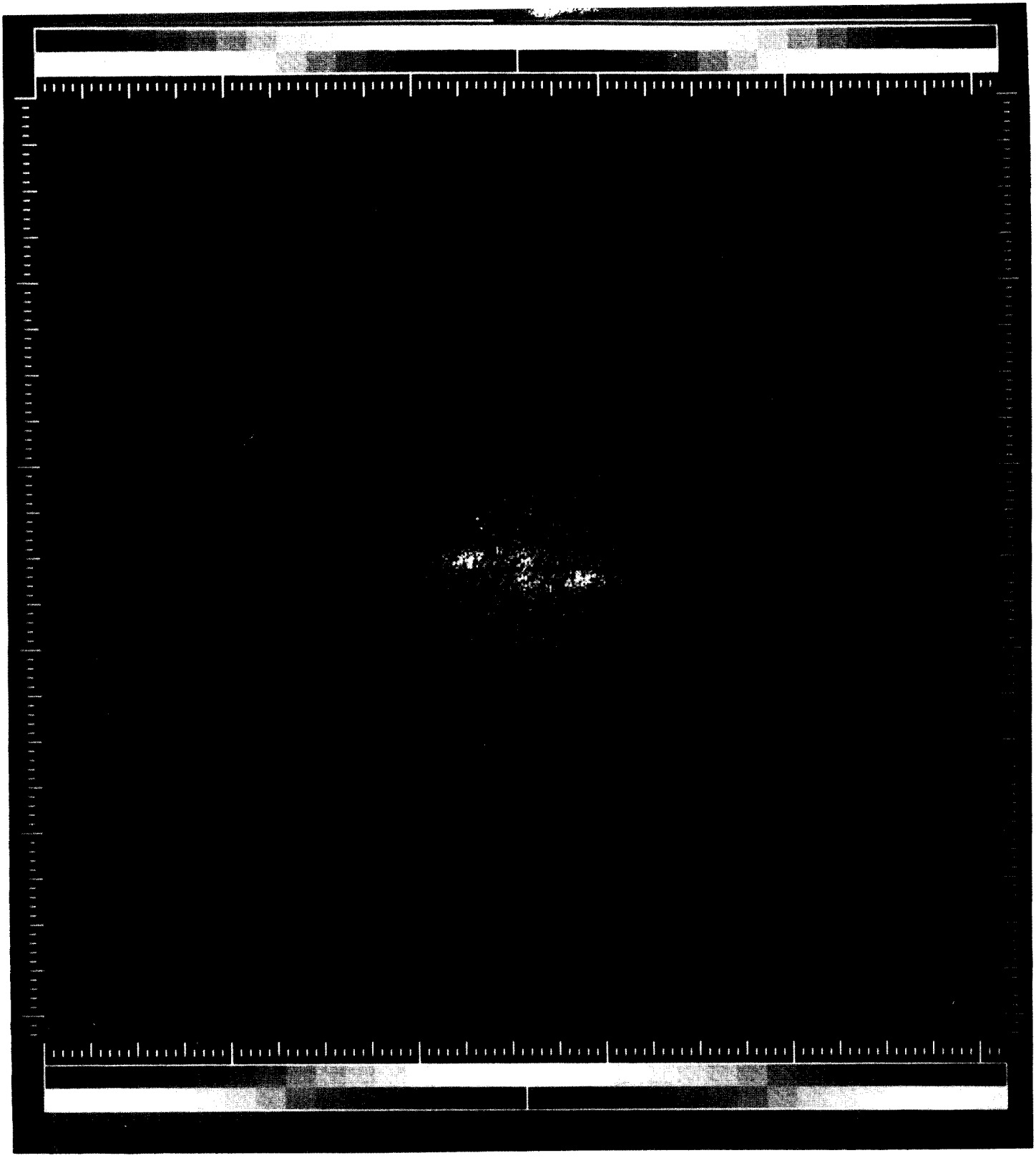

Figure 26. Optical Fourier Transform of the SAR Image in Figure 25.

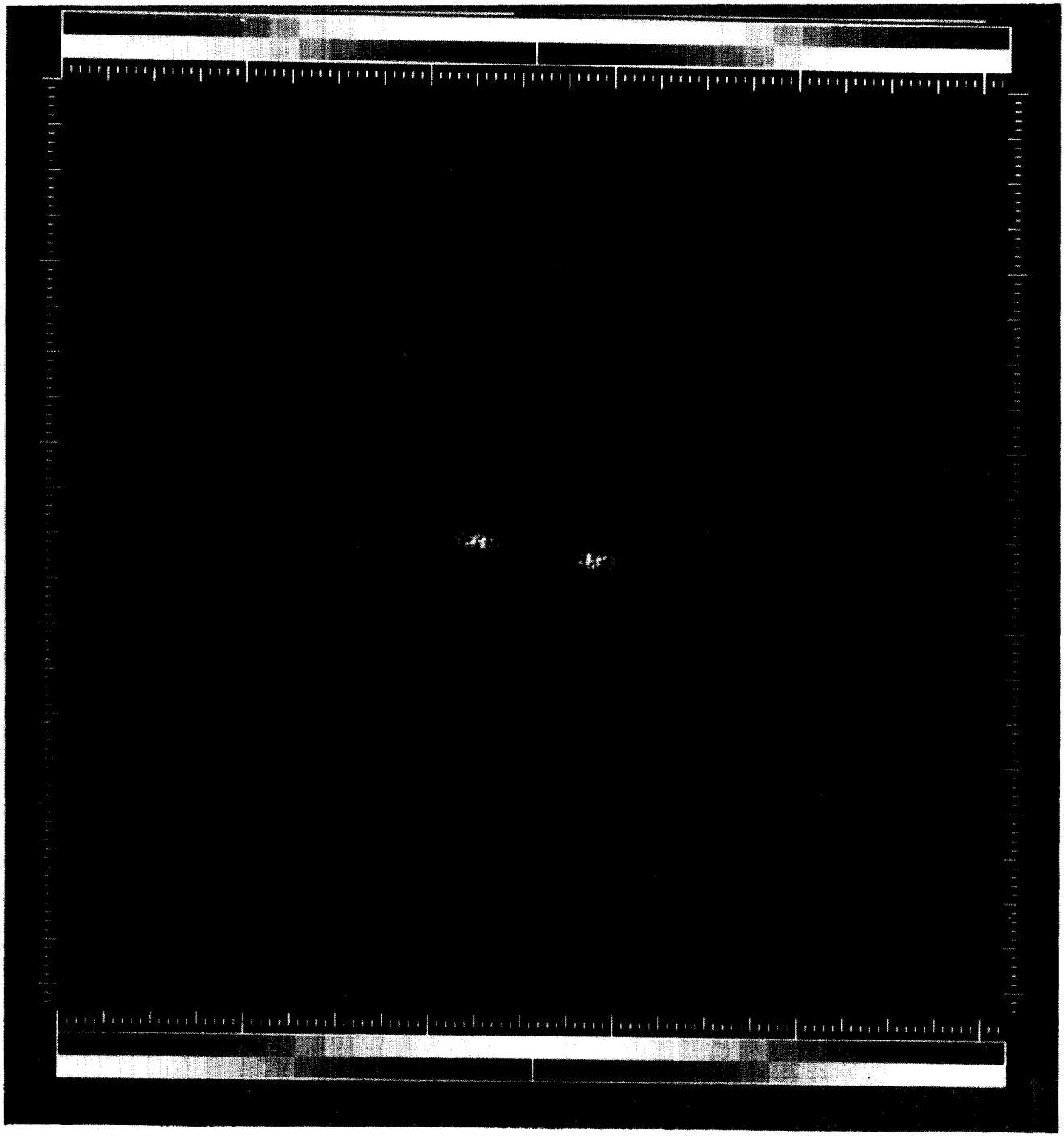

Figure 27. Optical Fourier Transform shown in Figure 26, but Filtered to the Principal Angular Component of Waves.

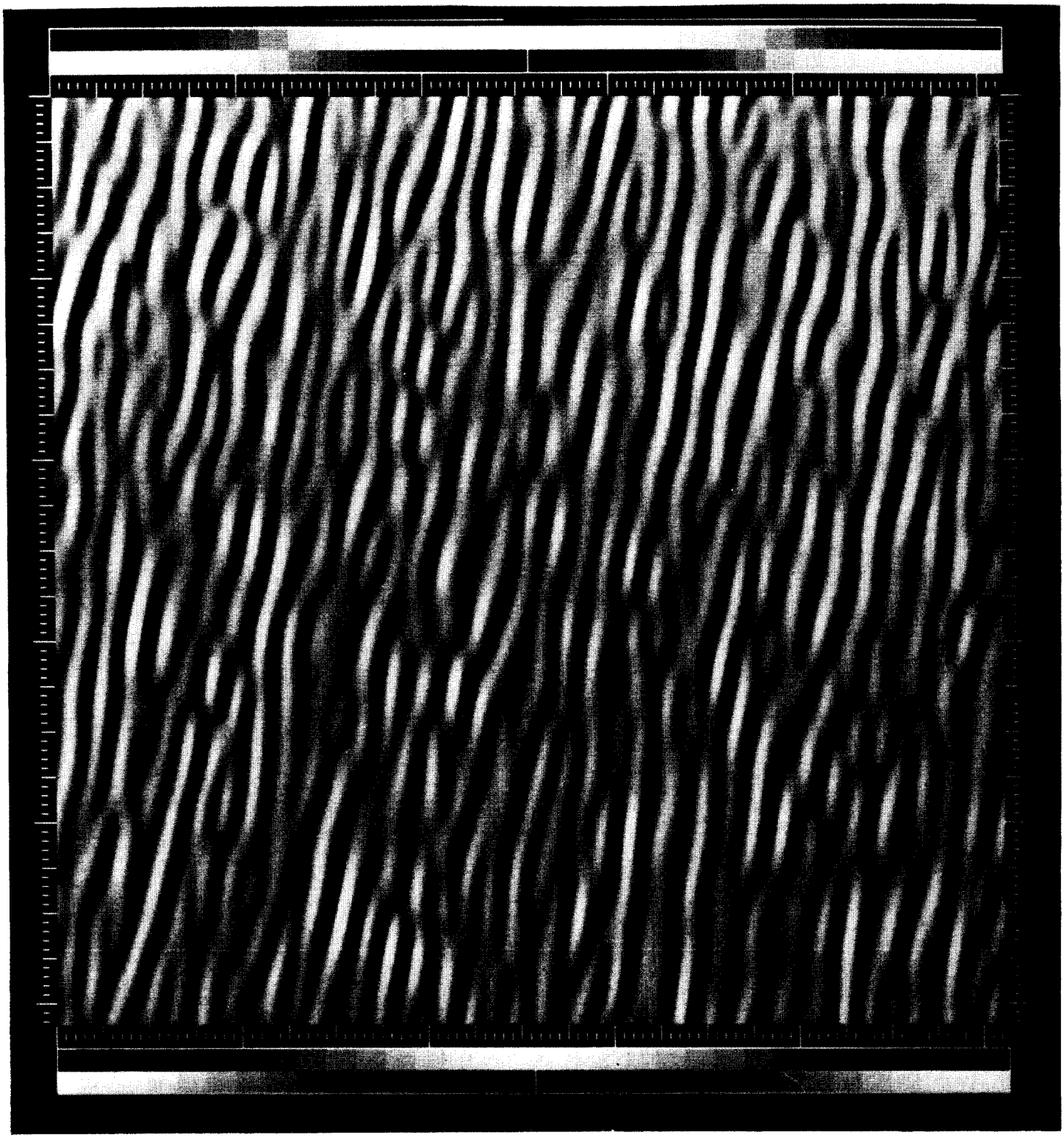

Figure 28. Enhanced Hurricane Fico Wave Image Using the Filtered Optical Fourier Transform of Figure 27.

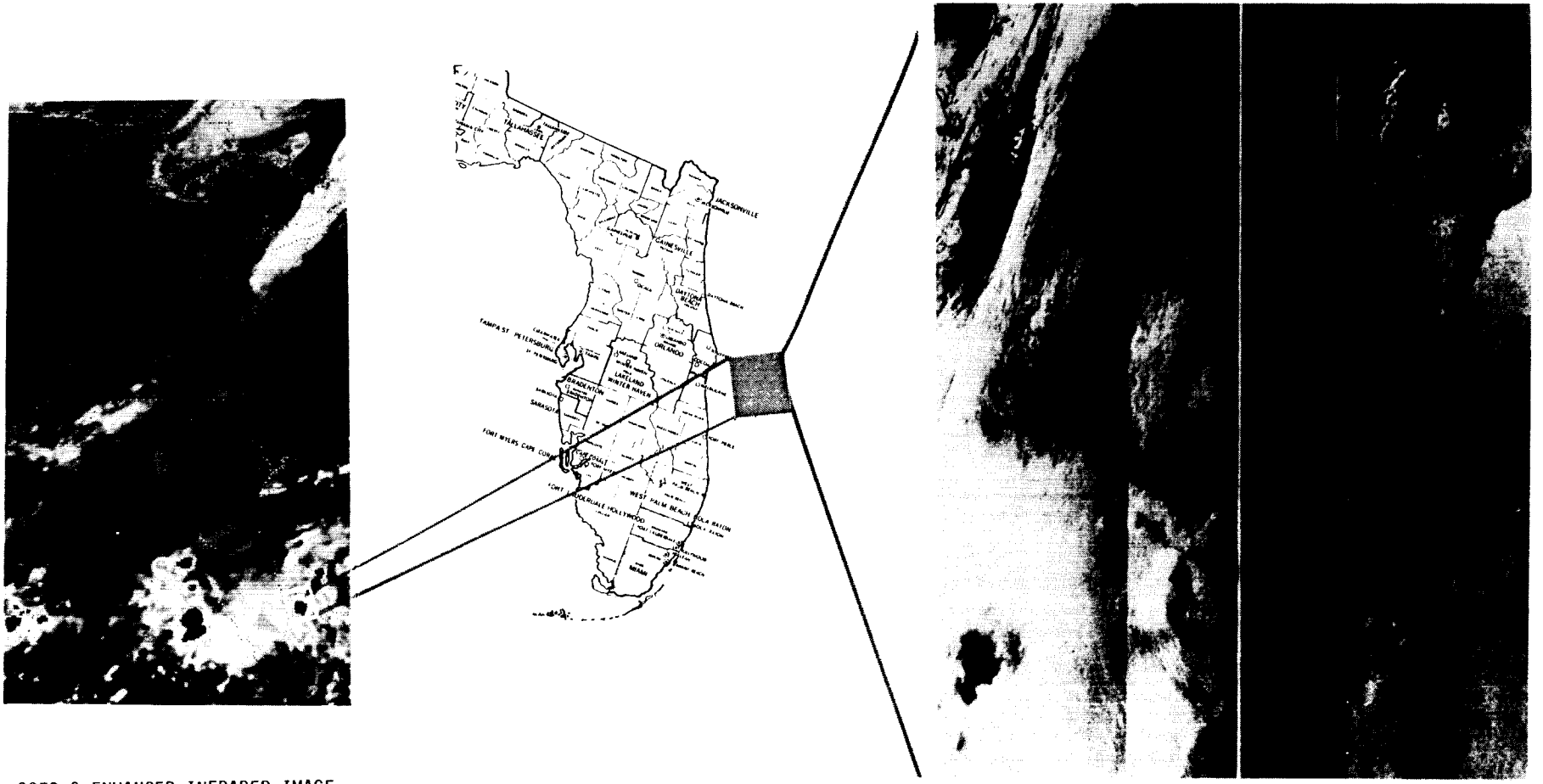

GOES 2 ENHANCED INFRARED IMAGE
0600 EDT-JULY 8, 1978

SEASAT SYNTHETIC APERTURE RADAR IMAGE
0604 EDT-July 8, 1978

Figure 29a. COMPARISON OF GOES 2 IMAGE WITH THE SEASAT IMAGE SHOWING THE ABILITY OF THE SEASAT MICROWAVE INSTRUMENT TO PENETRATE CLOUD COVER. THE GOES 2 IMAGE SHOWS THE DESIGNATED AREA COVERED BY CLOUDS. SEASAT SHOWS OCEAN SURFACE FEATURES SUCH AS GULF STREAM MOTION (UPPER LEFT) AND SURFACE ROUGHNESS (LOWER LEFT) DUE TO RAIN SHOWERS. THE BLACK AREAS WITHIN WHITE AREAS ARE RAIN SQUALLS.

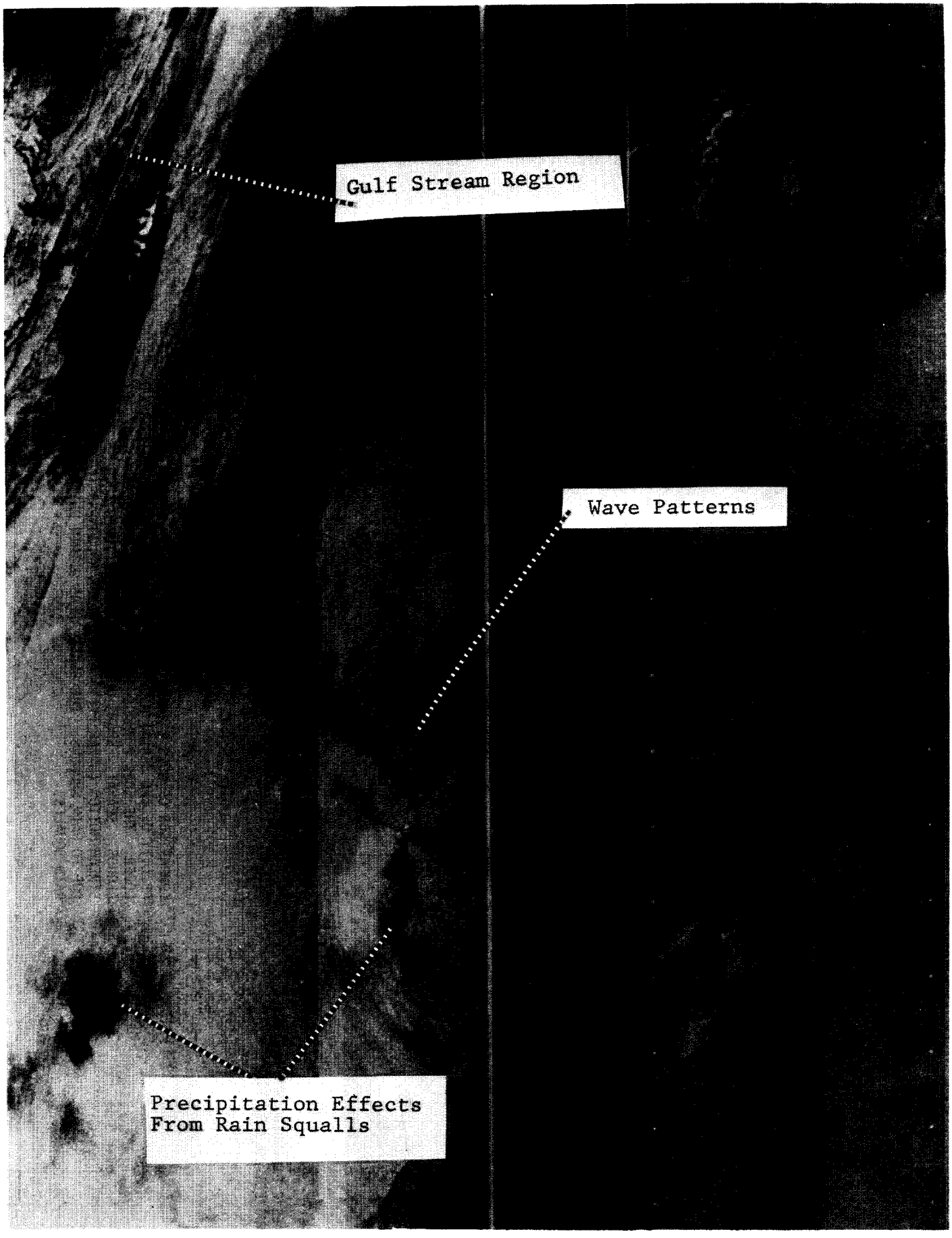

Figure 29b. Enlargement of SAR Image From Figure 29a.

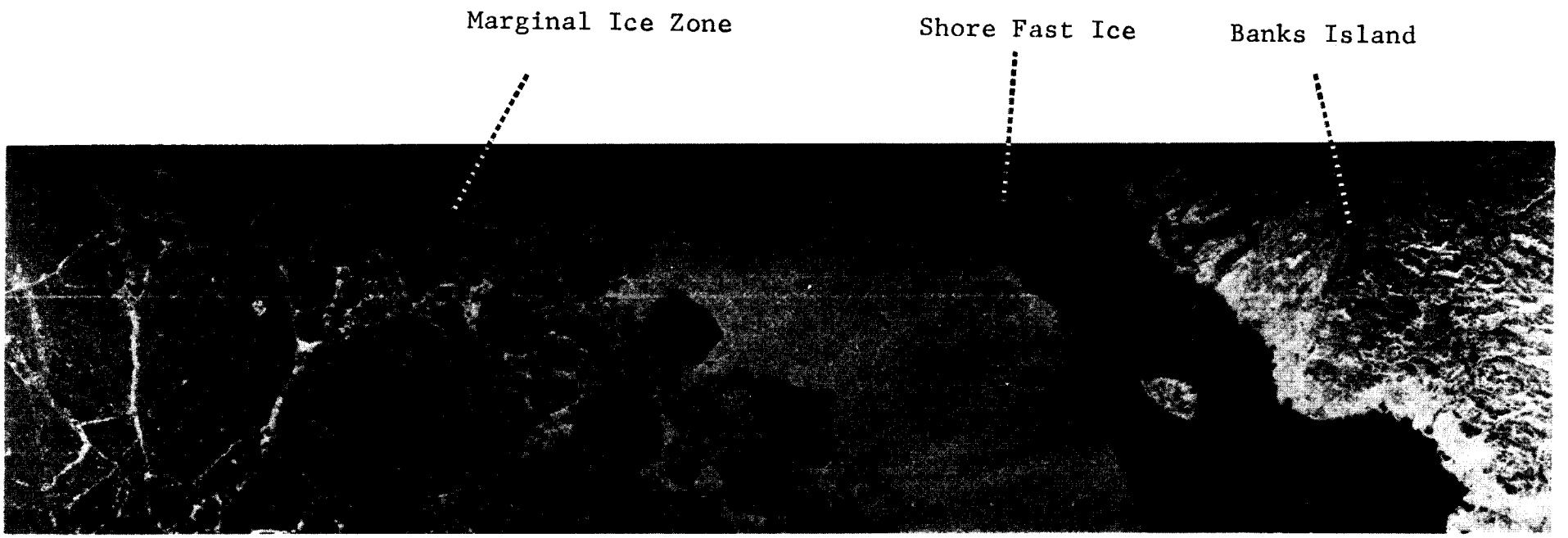

Figure 30. The Synthetic Aperture Radar (SAR) Image of Banks Island, Canada, And Various Types of Sea Ice on July 11, 1978.

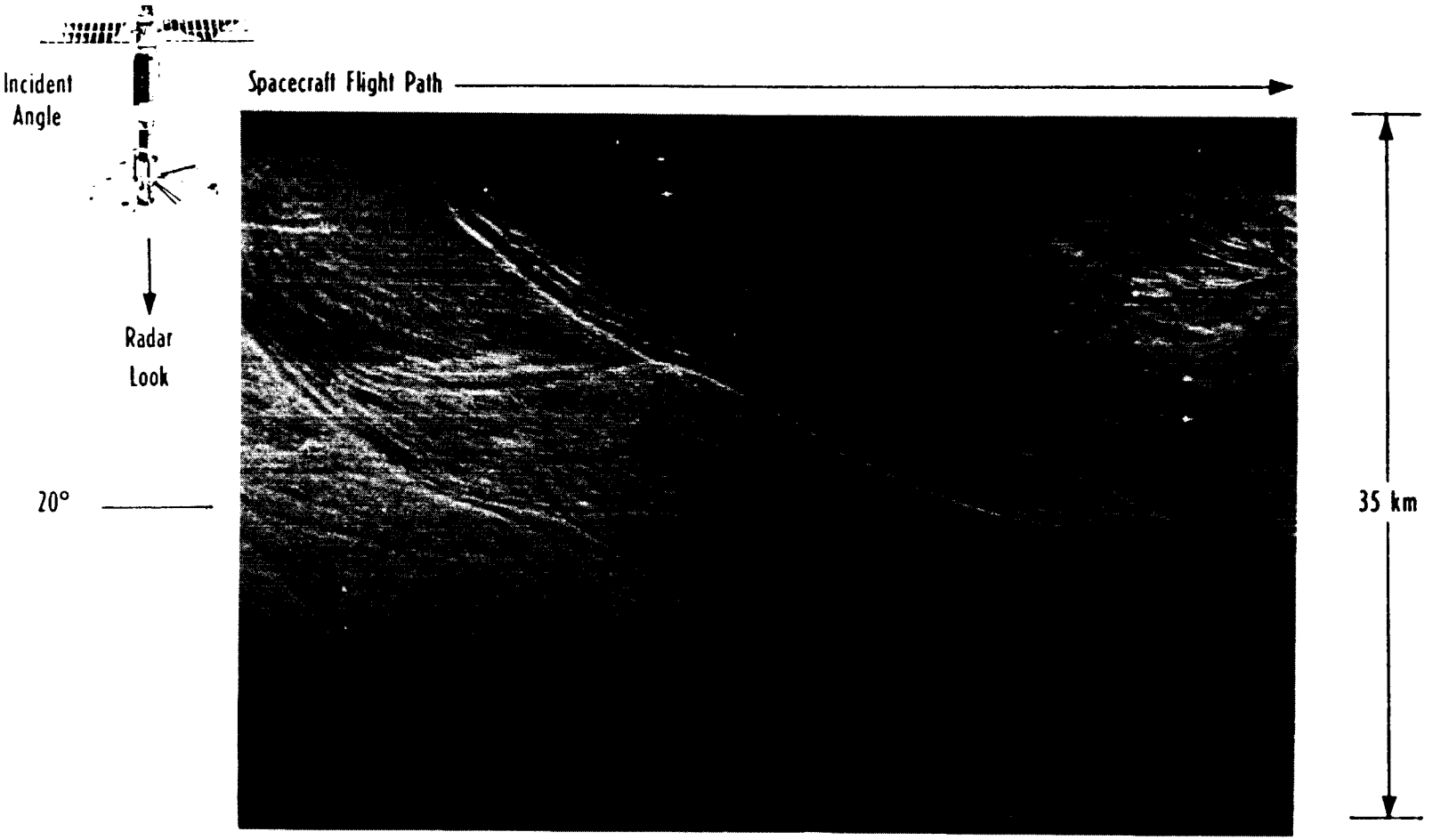

Figure 31. SAR Images of Hudson Canyon Area off the U.S. East Coast (Rev 1232; September 21, 1978).

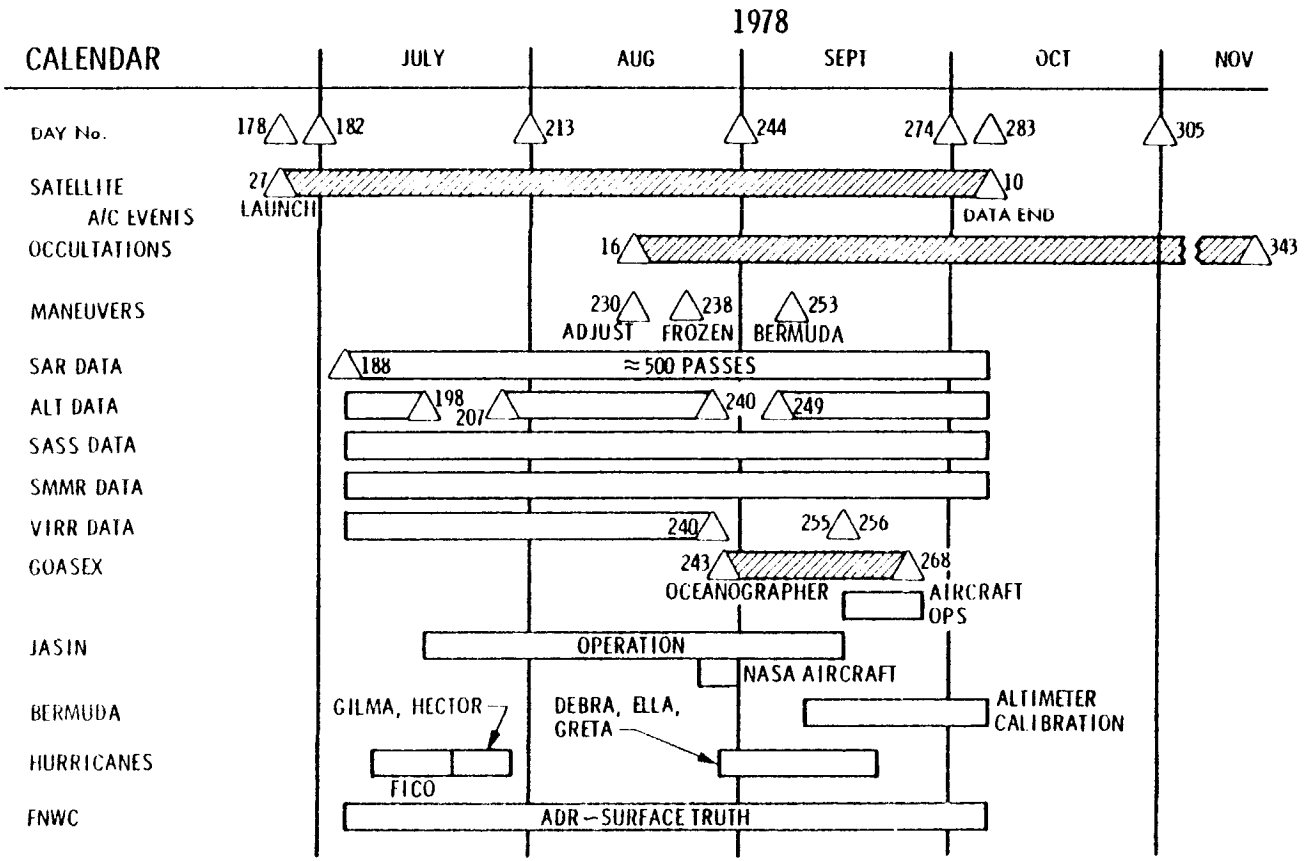

Figure 32. Seasat Mission Profile Showing Days of Data Collection.

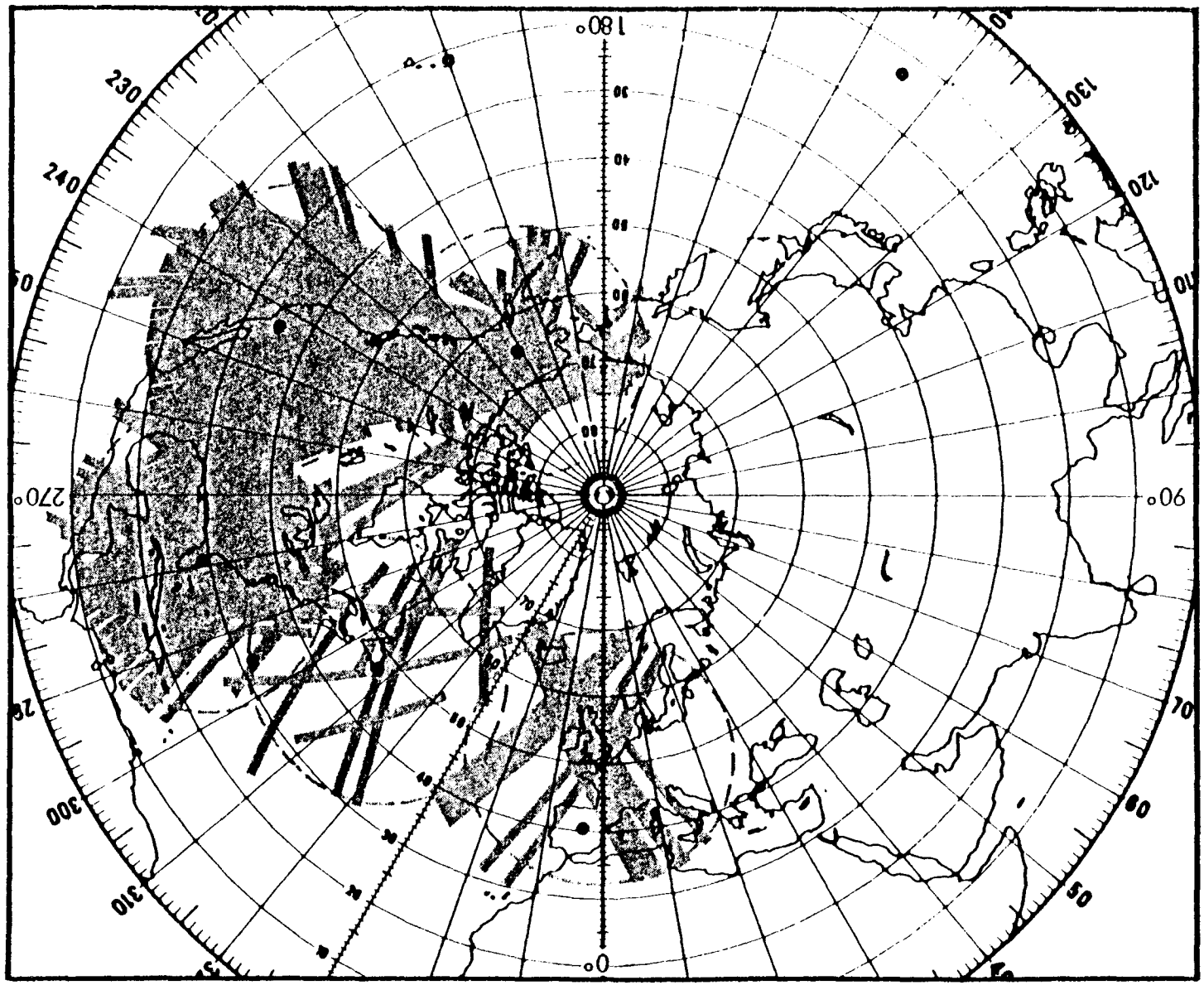

Figure 33. Seasat SAR Data 33 Collection Coverage from July 3rd to October 10th, 1978 (Revs 107-1502).

SURFACE TEMPERATURE DATA AND THEIR UTILIZATION IN SURFACE TUNNY FISHING IN THE TROPICAL EAST ATLANTIC

Jean-Michel STRETTA
Oceanographer, ORSTOM
Oceanographic Research Centre
BPV 18, Abidjan
Ivory Coast

1. INTRODUCTION

Concentrations of tunny are influenced by the temperature of the water and the food available (plankton, micronekton, sardines ...). For this reason the yellowfin tuna (Thunnus albacares) is usually found in waters with a surface temperature ranging between 23° and 29° C., whereas the listao (Katsuwonus pelamis) can move in much cooler waters (even 18°C.).

The problem of locating tunny food is difficult to solve by means of a direct approach; a theoretical approach is possible if we use our knowledge of surface temperature and sub-surface temperature structures such as the depth of the thermocline. This knowledge of the environment in time and space is at present available through the analysis of historical data and the use of satellites and aeroplanes equipped with infra-red radiometers which give synoptic repeated views of surface temperature conditions, the subjacent conditions being deducible with the help of hydrological models available for each region.

On the basis of a certain knowledge of the environment it is possible to demarcate the zones rich in phytoplankton and zooplankton where potential tunny food will abound. For instance, in certain parts of the Gulf of Guinea there may be oceanic upwellings causing a cooling of surface water. If these upwellings, which are usually rich, come into contact with warm water, a front appears (the front between the island of Sao-Tomé and Cape Lopez, Gabon, in June and July is an example). This front will be favourable to the development of plankton, which will serve as food for the small pelagic organisms and micronekton which will be the staple food of the Thunnidae (DUFOUR and STRETTA, 1973). The tunny will then be concentrated on the edge of the front, on the warm water side, for it will find there favourable temperature and feeding conditions (STRETTA et al., 1975, STRETTA, 1977).

2. ANALYSIS OF SURFACE TEMPERATURE DATA

The findings of oceanographic cruises to study the ecology of tunny and the findings of cruises undertaken jointly with aerial radiometry operations have given us a knowledge of the surface and sub-surface hydrological structures, which enables us to identify situations favourable to the formation of concentrations of tunny. Analysis of these situations placed in a forecasting model now enables us to seek new zones with a high fishing potential in the tropical Atlantic. This analysis is based on: historical temperature data, the temperature data of satellites and the data yielded by aerial radiometry.

2.1 Analysis of historical temperature data

In order to have a general idea of surface temperature trends in the tropical Atlantic we first use the various oceanographic atlases: MAZEIKA, 1968; HASTENRATH and LAMB, 1977; MERLE, 1978. However, the most suitable work for our type of study is that of MERLE, 1977. This author's block diagrams, based on the NANSEN data collected by the NODC, have the advantage of bringing out the monthly temperature trends from 5 to 200 m. per surface unit of 5° Longitude and 2° Latitude. With these data it is easy to identify the zones with considerable surface cooling and/or considerable upwellings of the thermocline in which the surface layers will be enriched.

As we know by means of the usual oceanographic data, the period of time which elapses between the appearance of surface cooling and the presence of potential tunny food (a period which varies according to the zone concerned), we can then draw up theoretical maps of month-by-month fishing probabilities for the whole of the tropical Atlantic.

2.2 Analysis of temperature data from satellites

On the basis of these theoretical findings, the data obtained by satellite enable us to identify any shift in space and in time of these potential fishing zones.

For this second analysis we use satellite data from three sources:

- weekly temperature maps supplied by the NOAA with the GOSSTCOMP system,
- weekly temperature maps from the satellite "METEOSAT" processed with software designed by ORSTOM,
- daily temperature maps from "METEOSAT" processed with software designed by the CNES (Centre National d'Etudes Spatiales), Toulouse, France.

Data from the first two sources arrive in Abidjan by mail, but data from the third are sent by telex a few hours after the information is picked up by the Centre de Météorologie Spatiale at Lannion, France.

A prerequisite of effective follow-up and forecasting of potential fishing sectors is regular receipt of reliable temperature maps. The presence of considerable cloud cover over the Gulf of Guinea often means large blank zones on the "METEOSAT" temperature maps or data corrupted by isolated cloud systems.

2.3 Analysis of temperature data obtained by means of aerial tele-detection

Zones recognized as favourable to concentrations of tunny are going to be analysed in more detail by an aeroplane with a long range belonging to the tunny fishing flotilla of France and the Ivory Coast as a whole and equipped with an infra-red radiometer.

These flights, at an altitude of 150 metres, make it possible to prospect the shoals of tunny at sight and draw up surface temperature maps accurate to within 0.2°C. These maps are then analysed and fitted into the general scheme of temperature trends of the sector concerned. In this way trends are revealed and certain strong points in the scheme which will be the zones favourable to concentrations of tunny will be made evident. The combined findings and forecasts then allow of drawing up flight schedules for the next few days, which have to be used most advantageously, having regard to the general temperature situation and the dispersal of the flotilla, and of readjusting the satellite data.

3. CURRENT DEVELOPMENT AND PROSPECTS

The work described above has been proceeding in an operational way for a year now and a Fishing Aid Office (Bureau d'Aide à la Pêche) has been established at the fishing port of Abidjan for this purpose. All the temperature and meteorological data centralized and analysed in this Office are made available to the tunny fishermen in the form of maps, when they are on land, or in the form of a forecasting bulletin broadcast to the flotilla as a whole on fishing potentials, as well as a general analysis of the situation on the fishing grounds.

BIBLIOGRAPHY

DUFOUR P. et STRETTA J. M., 1973. Fronts thermiques et thermohalins dans la région du cap Lopez (golfe de Guinée), juin-juillet 1972: phytoplancton, zooplancton, micronecton et pêche thonière. Doc. Scient. Centre Rech. Océanogr. Abidjan, vol IV n°3 : 99-142

HASTENRATH S. and LAMB P. J., 1977. Climatic Atlas of the tropical Atlantic and eastern Pacific Oceans. The University of Wisconsin Press.

MAZEIKA P. A., 1968. Serial Atlas of Marine Environment. Mean Monthly Sea Surface Temperature and Zonal Anomalies of the Tropical Atlantic. Folio 16, American Geographic Society.

MERLE J., 1977. Seasonal variations of temperature and circulation in the upper layers of equatorial Atlantic area (GATE Area). GATE Workshop Miami 28 Feb-10 Mar. 1977.

MERLE J., 1978. Atlas hydrologique saisonnier de l'océan Atlantique inter-tropical. Travaux et Documents de l'ORSTOM, n° 82, 184 p.

STRETTA J. M., NOEL J. et VERCESI L., 1975. Caractérisation des situations hydro-biologiques et potentialités de pêche thonière au cap Lopez en juin et juillet 1972 et 1974. Doc. Scient. Centre Rech. Océanogr. Abidjan, vol VI n°2 : 59-74

STRETTA J. M., 1977 : Température de surface et pêche thonière dans la zone frontale du cap Lopez (Atlantique tropical oriental) en juin et juillet 1972, 1974 et 1975. Cah. ORSTOM, série Océanogr. vol XV n°2 : 163-180.

A Need for Improved Quality of Sea-Surface Temperature Data from the World Oceans

S. Tabata
Institute of Ocean Sciences
Sidney, B.C., Canada

1. Introduction

In the past, sea-surface temperatures based upon merchant and naval ship observations have generally been used for the preparation of ocean climatology atlases (e.g. Laviolette and Seim, 1969), for correlating with fish abundances and catches (e.g. Owen, 1968; U.S. Nat. Mar. Fish. Service, 1977) and to explain climatic anomalies (e.g. Namias, 1963). Further, they are used daily in synoptic weather forecasting. In more recent years, they have been utilized a great deal as ground truth for satellite observations (Brown, 1975) and as one of the source data in global, numerical atmospheric circulation models (Rowntree, 1972; 1976). These last two applications in particular demand temperatures that should be more reliable and accurate than we have been accustomed to in the past. Yet, even today the quality of the ship-reported temperatures has not improved significantly over the past half century.

The present report comprises a summary of the results of a series of studies conducted on the quality of sea-surface temperatures based on data observed in the northeast Pacific Ocean from a number of platforms -- weatherships, research ships, anchored U.S. environmental buoys (NOAA buoys) and merchant-naval ships and employing a variety of instruments -- ordinary bucket thermometers, specially-designed bucket thermometers, reversing thermometers, engine-intake thermometers, expendable bathythermographs (XBT), salinity temperature depth recorder (STD) and thermosalinographs.

2. Variability of Temperatures in the Surface Mixed Layer

Bathythermograph (BT) data have always shown that the surface mixed layer of the ocean is generally isothermal to within ±0.1°C (e.g. Tabata and Giovando, 1963). However, until recently it was unknown to what greater degree, if any, the layer was isothermal.

In order to demonstrate to what degree the mixed layer was uniform and/or variable in temperature, oceanographic data obtained at Ocean Station P (50°N, 145°W) in the northeast Pacific Ocean during the 20 years (1956-1976) were examined. On the basis of data from 778 hydrographic stations (3265 observations) the temperature within the surface mixed layer was within ±0.02°C during the cooling season (October through March) and within ±0.03°C during the heating season (April through September) (Tabata, 1978e). The larger variability for the heating season was significantly greater (at the 95% confidence level) than for the cooling season. This was probably due to the greater radiational heating effects, by solar radiation, on the submerged thermometers used rather than to the actual greater variability during the heating season. The magnitude of variability in the mixed layer was numerically equalled to the accuracy of the thermometers employed; consequently, the water in the mixed layer at any time is isothermal and commensurate with the accuracy of the temperature measurements, provided that the radiational effects of thermometer mentioned above for the heating season actually account for the difference in the variability.

3. Sea-Surface Temperatures Observed with Bucket Thermometers

An analysis of sea-surface temperatures observed at Station P indicated that, even when temperature measurements were made by trained observers with an ordinary bucket thermometer, they contained relatively large errors (Tabata, 1978d). This can be construed from a comparison of surface temperatures measured with a bucket thermometer and the 10-m temperatures determined with reversing thermometers. From Section 2 the surface and the 10-m temperatures should be of the same magnitude except when observations are made during calm or light wind conditions. Yet, the observed difference between the surface and 10-m temperatures was relatively large when the surface observations were made with a bucket thermometer. This is shown in Fig. 1.

The main feature of the results shown in this figure is that while the mean differences and the associated standard deviations for the earlier period (1956 through mid-1969) were both relatively large, +0.12 and ±0.34°C, respectively, those of the subsequent period were only about one-third and one-fourth as large, +0.04°C and ±0.09°C, respectively. The remarkable convergence of the surface and 10-m temperatures for the later period indicated the vast improvement in the quality of surface temperatures taken after 1969 and demonstrates the effectiveness of observational techniques and the instruments employed in the later period.

It would appear initially that the main source of error in the determination of surface temperature was attributable to the use of an ordinary bucket thermometer. While this may be so to a certain extent, it is by no means the only one. It is probable that the other source of error lies in the use of improper procedures. In a recent cruise (August-September 1975) surface temperatures measured with an ordinary bucket thermometer were compared with those obtained with a calibrated salinity-temperature-depth recorder (STD). The results indicated that the bucket temperatures were, on the average, only 0.04°C higher than the STD observed temperatures, with a standard deviation of ±0.15°C. (Tabata, 1978a, 1978c). The results obtained during this cruise also indicated that there was a noticeable difference in the quality of surface observations with individuals (Tabata, *ibid*).

At Station P sea-surface temperature measurements were made regularly by the meteorological observers using specially-designed bucket thermometers. Their observations indicated that the surface temperatures were, on the average, 0.04°C higher than those measured with reversing thermometers, with a standard deviation of ±0.13°C (Tabata, 1978d). Considering that the bucket thermometers were read to only 0.1°C, their surface temperatures are as good as can be expected. The fact that surface temperatures observed with an ordinary bucket thermometer can yield results with the same accuracy indicates that, when measurements are made with care, the same degree of accuracy can be obtained by the use of ordinary bucket thermometers that are considered "crude" by some.

4. Comparison of Bucket and Engine-Intake Temperatures

Because of the high reliability of the bucket temperatures observed by the meteorological observers, they were utilized to compare with the corresponding engine-intake temperatures. In Table 1 is shown the summary of the results of this comparison. It is evident from the table that of the engine-intake temperatures from the four weatherships, the two former ships, C.C.G.S. *St. Catharines* and *Stonetown* and the two new ships, C.G.G.S. *Quadra* and *Vancouver*, those from one of the former ships (*St. Catharines*) and from one of the new ships (*Quadra*) were, on the average, equivalent to the corresponding bucket temperatures. The associated standard deviation from one of the former ships (*Stonetown*) was somewhat higher (±0.20°C) than those for the other ships (±0.12 - ±0.15°C). It is to be noted that the former ships were fitted with engine-intake thermographs whose costs were only a fraction of those of the new ships. Evidently the lower-cost thermographs appeared to be as good as the more expensive ones. As is evident from Table 1, even the temperatures measured with the relatively expensive thermosalinographs are not much better than those obtained with the less expensive thermographs.

5. Engine-Intake Sea Surface Temperatures Recorded by the Ship's Crew

In Fig.2 is shown the frequency distribution of the differences between the bucket and STD temperatures and between engine-intake and STD temperatures. The engine-intake temperatures were those obtained by the engine-room crew; the STD temperatures are considered to represent true values. Not only were the engine-intake temperatures, on the average overestimated (±0.30°C) but were also characterized with large variability (standard deviation = ±1.16°C), approximately an order of magnitude greater than those for the bucket data (±0.19°C). Such a high level of "noise" appears to be common in merchant-naval ship observations everywhere. For example, a comparison of the sea surface temperatures observed by merchant naval ships in the northeast Pacific Ocean were on the average, 0.2°C ±1.5°C larger than at the time series stations (Station P and 8 NOAA buoy stations) (Tabata, 1978b).

6. Sea Surface Temperatures Based on Expendable Bathythermographs (XBT)

According to a comparison of sea surface temperatures obtained by a limited number of XBT's (64) with the corresponding STD temperatures, it was noted that the former possessed a positive bias of 0.27°C with a standard deviation of ±0.14°C (Tabata, 1978a). They are, therefore, capable of measuring sea-surface temperatures to the same accuracy as the bucket thermometers, if this effect can be removed. Under operational conditions at sea, it is difficult to know whether such an effect is present in every XBT unless each XBT is tested before being used.

7. Recent Attempts to Measure Reliable Sea-Surface Temperatures Using the Engine-Intake Method

In view of the difference between the bucket and engine-intake temperatures noted in past observations from the weatherships (see Section 4), attempts were made to determine if the reliability of the intake temperatures could be improved. The resistance-type engine-intake temperature-measuring systems fitted to the two weatherships, *Quadra* and *Vancouver* were calibrated internally using known resistance values. The engine-intake temperatures subsequently observed were compared with reliable, corresponding bucket temperatures that were accurate to ±0.1°C. The results of this comparison is shown in Table 2. It is evident from this table that the mean difference between the bucket and engine-intake temperatures and the associated standard deviations for *Quadra* were both relatively small and consistent during the first 4 cruises over the 10 month period. The occurrence of the near-constant difference (0.08°C) during the first 10 months suggests that although the calibration held for 10 months the calibration itself was not performed as well as it could have been. The mean differences and the associated standard deviations for the *Vancouver*, on the other hand, both fluctuated appreciably from one cruise to another. This is attributed to the measuring system aboard this ship which has been known to have problems (Tabata, 1978d).

Considering that each weathership makes engine-intake temperature measurements using a pair of sensors alternately (starboard and port intakes) and considering that both the bucket and engine-intake temperatures are read to 0.1°C only, the difference and standard deviation indicated in the earlier cruises of *Quadra* are indeed very small. With the application of proper calibration the difference probably could have been eliminated.

8. Conclusions

Sea-surface temperatures measured routinely with specially-designed bucket thermometers are correct to within ±0.1°C. Those observed with an ordinary bucket thermometer are capable of attaining an accuracy of ±0.1°C only if observations are made with extreme care. The quality of engine-intake temperatures recorded by the ship's crew is not satisfactory. Such data are the mainstay of present day merchant-naval ship sea-surface temperature reports that find their way into the daily weather reports and eventually into the climatological archives. Yet, such data appear to be characterized by lack of precision everywhere. A recent test conducted on the engine-intake temperatures observed from the weatherships suggests that they can indeed provide data that are as accurate as those obtained from specially-designed bucket thermometers.

A knowledge of reliable sea-surface temperatures is becoming increasingly important to the study of the influence of ocean temperatures upon weather and climatic patterns where a difference of even a few degrees in climatic temperature anomaly can affect these patterns (Bjerknes, 1966; Namias, 1969; Rowntree, 1972; 1976). Further, the ships' data currently employed as ground truth for satellite observations are far too coarse (±2.0°C). They are also not sufficiently reliable for use in interpreting bathythermograph subsurface temperatures.

Although the conclusions drawn from our studies are based on data taken in northeast Pacific Ocean, the principal conclusions should be valid to data from other oceans as the data from this area are in no way unique from the standpoint of data quality to those elsewhere. There is no reason why the ships' sea-surface temperatures observed routinely cannot be improved. Methods are available to make reliable observations; all that is needed is a concerted effort amongst our part directed to obtaining such data.

Some suggestions for the improved technique and instrumentation for routine measurements of reliable sea-surface temperatures are:

1) As the size of ships increases it will become increasingly difficult to make reliable sea-surface temperatures employing ordinary bucket thermometers. For this reason it would be advisable to discontinue the use of the bucket method. If this is to be used, a well-insulated, specially-designed bucket thermometer should be used.

2) At wind speeds greater than 6 m/s, a surface mixed layer is usually thicker than 10m. Intake temperatures if observed at a depth of 10 m from the waterline should be identical to sea-surface temperatures. Because of the ease in making intake measurements its adoption for routine use is advisable.

3) However under calm or light wind conditions there should be a temperature gradient present in the upper several metres of the sea surface, especially during the warm summer months. In such cases, both the engine-intake and bucket temperatures should be taken.

4) There appears to be some reading errors associated with intake temperature observations by the ship's crew. A digital readout should be provided to reduce reading errors.

5) Although reliable, well-made platinum-resistance thermometers are available, their inherent low resistance makes them sensitive to small changes in the measuring system. A good quality thermistor having higher resistance is to be preferred.

6) Temperature sensors should not be fitted to the intake system where air pockets can occur. There is some suspicion that the air pockets can influence the measurements of temperature appreciably.

7) Frequent calibration (about twice per year) should be made to the intake temperature system.

8) Calibration of resistance-type engine-intake thermometers should be made using accurate thermometers rather than with known resistance values.

   Such calibration can be made by relating the engine-intake readings to the accurate bucket measurements. This is to be done when the surface mixed layer depth exceeds the intake depth.

9) Low-cost micro-computers (≈$600) are now commercially available. They can be incorporated into the temperature-measuring system so that the analogue data can be readily digitized and put on magnetic tape. Developments in the application of these computers should be monitored and their use for routine observations of sea-surface temperatures considered.

REFERENCES

Bjerknes, J., 1966. A possible response of the atmospheric Hadley circulation to equatorial anomalies of ocean temperature. *Tellus* , 18, 820-828

Brown, S.R., 1975. SST quarterly report, April-June 1975. Unpub. U.S. Dept. of Commerce, NOSS, NESS, Washington, D.C. 2 pp.

Laviolette, P.E. and S.E. Seim, 1969. Monthly charts of mean, minimum and maximum sea surface temperature of the North Pacific Ocean. Special Publ. SP-123, U.S. Naval Oceanogr. Office, Wash, D.C., 57 pp.

Namias, J., 1963. Large-scale air-sea interactions over the North Pacific from summer 1962 through the subsequent winter. *J. Geophy. Res.*, 68, 6171-6186.

1969. Seasonal interactions between the North Pacific Ocean and the atmosphere during the 1960's. *Mon . Wea. Rev.*, 97, 173-192.

Owens, R.W. Jr., 1968. Oceanographic conditions in the northeast Pacific and their relations to the albacore fishery. U.S. Fish. and Wildlife Service, *Fish. Bull.* 66, 503-526.

Rowntree, P.R. 1972. The influence of tropical east Pacific Ocean on the atmosphere. *Quart. J. Roy Meteorol.Soc.*, 98:290-321.

1976. Response of the atmosphere to a tropical Atlantic ocean temperature anomaly. *Quart. J. Roy Meteorol. Soc.* 102:607-625.

Tabata, S. and L.F. Giovando, 1963. The seasonal thermocline at Ocean Weather Station "P" during 1956 through 1959. Fish. Res. Bd. Can. Ms. Rep. Ser. Oceanogr. Limnol. 157, 27 pp.

Tabata, S., 1978a. An examination of the quality of sea-surface temperatures and salinities observed in the northeast Pacific Ocean. Pa. Mar. Sciences Report 78-3, Institute of Ocean Sciences, Patricia Bay, Sidney, B.C. 33 pp.

1978b. Comparison of observations of sea-surface temperatures at Ocean Station "P" and NOAA buoy stations and those made by merchant ships travelling in their vicinities, in the northeast Pacific Ocean. *J. Appl. Meteorol.* 17: 374-385.

1978c. On the accuracy of sea-surface temperatures and salinities observed in the northeast Pacific Ocean. *Atmosphere-Ocean* 16, 237-247.

1978d. An evaluation of the quality of sea surface temperatures and salinities measured at Station "P" and Line P in the northeast Pacific Ocean. *J. Phys. Oceanogr.* 8, 970-986.

1978e. On the variability of water properties in the surface wind layer at Station "P". *Limnol. Oceanogr.* 24, (in press)

U.S. National Marine Fisheries Service, 1977: *Fishing Information* , July 1977, No. 7, U.S. Dept. Commerce, NOSS Nat. Mar. Fish. Serv. Southwest Fish. Center, La Jolla, Calif., 13 pp.

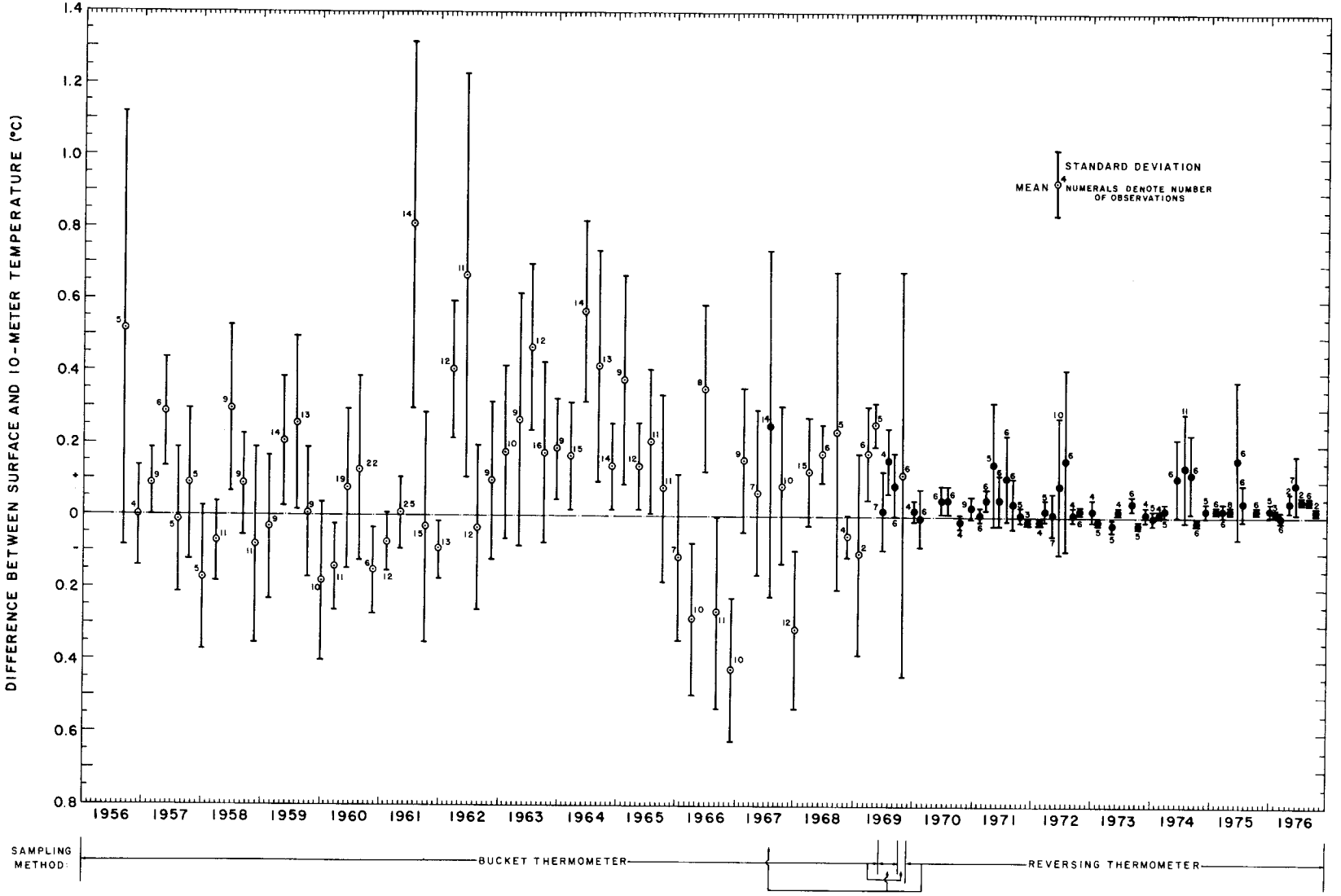

Fig. 1 Cruise mean differences between surface and 10-m temperatures (°C), and the associated standard deviations, for each cruise at Station"P" during the period 1956-1976. The methods used to determine the surface temperatures are also indicated. The closed circles represent surface temperatures measured with reversing thermometers. The 10-m temperatures were measured with one or two reversing thermometers. Two thermometers were utilized after mid-May 1969.

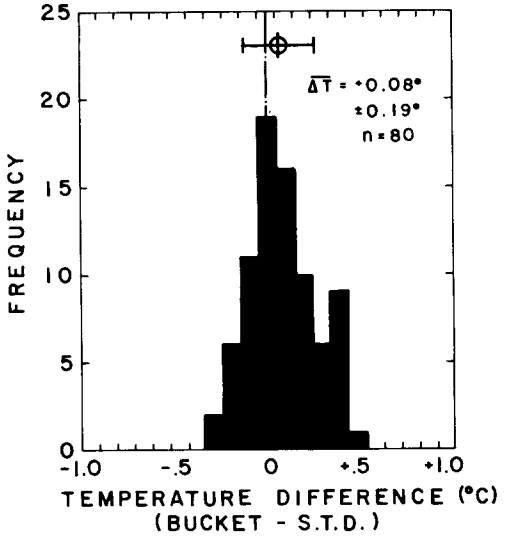

A

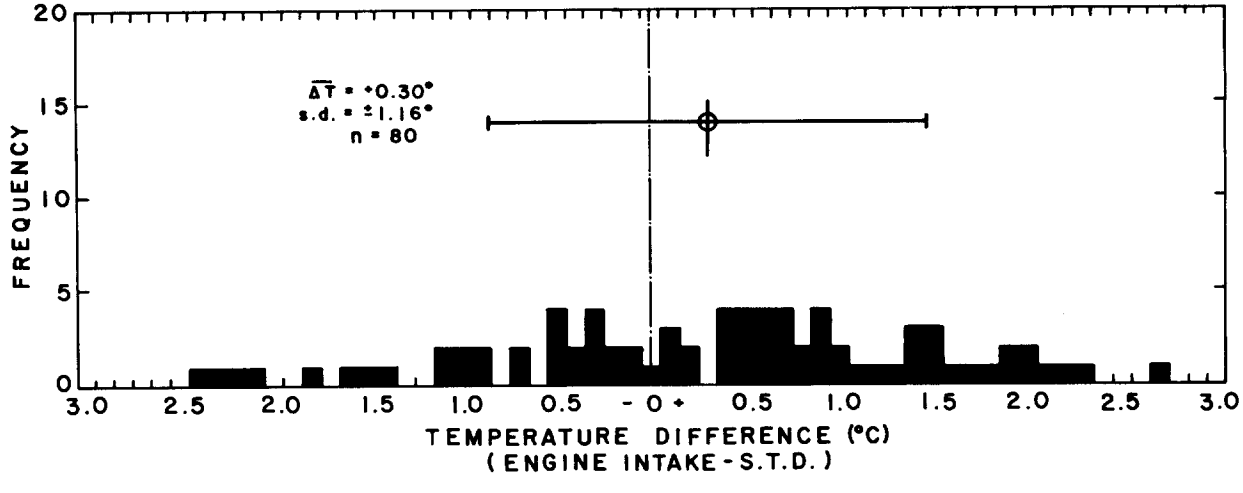

B

Fig. 2. Frequency distribution of differences between
A. bucket and STD temperatures (°C)
B. engine-intake and STD temperatures (°C)
Data obtained from C.F.A.V. *Endeavour* cruise of 19 August - 10 September, 1975.

Table 1. Mean cruise temperature difference (engine intake, thermosalinograph (seawater loop) minus bucket (°C) and the associated standard deviations (±°C) - from various ships.

Name of Ship	Temperature Difference (°C) (Engine Intake - bucket)	Standard Deviations (±°C)	Number of Observations
St. Catharines	-0.02	0.12	575
Stonetown	+0.18	0.20	1098
Vancouver	-0.02	0.15	1102
Quadra	-0.02	0.15	836

Name of Ship	Temperature Difference (°C) (Thermosalinograph - bucket)	Standard Deviations (±°C)	Number of Observations
Vancouver	-0.22	0.12	183
Quadra	+0.06	0.14	272
Parizeau	+0.08	0.13	91

Table 2. Mean cruise temperature difference (engine-intake minus bucket temperatures)(°C) and the associated standard deviations (±°C); data collected during February 1977 through October 1978 by the weatherships C.C.G.S. *Quadra* and *Vancouver*.

A. Observations by *Quadra*

Period of Observations	Temperature Difference (°C)	Standard Deviation (±°C)	Number of Observations
16 Feb.-30 Mar./77	0.07	0.08	311
6 May-23 June/77	0.07	0.09	379
30 July-14 Sept./77	0.09	0.07	370
22 Oct.-4 Dec./77	0.08	0.09	296
11 Jan.-13 Feb./78*	0.04	0.07	256
29 Mar.-7 May/78*	-0.08	0.11	312
20 June-30 July/78*	0.58	0.17	313
12 Sept.-22 Oct./78*	0.26	0.15	290

B. Observations by *Vancouver*

Period of Observations	Temperature Difference (°C)	Standard Deviation (±°C)	Number of Observations
26 Mar.-11 May/77	0.18	0.23	355
18 June-2 Aug/77	0.01	0.13	368
10 Sept.-26 Oct./77	0.09	0.09	358
3 Dec./77-10 Jan./78	0.10	0.16	309
6 May-21 June/78	-0.23	0.09	368
29 July-13 Sept./78	0.13	0.11	359

* No observations made enroute to and from Station P.

Observations and studies of the cyclogenesis in the Ligurian Sea.

Project of participation of the Belgian Station S.T.A.R.E.S.O.
(Station de recherches sous-marines et océanographiques de l'Université de Liège)

by Jean-Louis VAN HAMME,Dr.Sc.
Institut Royal Météorologique
3,Avenue Circulaire
1180 Bruxelles
Belgique

Cyclogenesis in the Ligurian Sea in Winter is a classic phenomenon (cf. for example: Sverre Petterssen-Weather analysis and forecasting, vol.1, fig.13.6.1 and 13.6.2) but the scales of the cyclones may be very different; in the following examples,we shall consider mainly the synoptic scale and the mesoscale (or an overlapping of this scales) but there are also many microscale aspects.
The influence on the weather of the european regions may also be very different because the cyclogenesis is generally coupled with different anticyclones.
If we want to simplify,we may consider two extreme examples:

1° an anticyclogenesis over Scandinavia and/or U.S.S.R. followed by the development of a large scale "blocking" situation; for example, at the end of november 1978 and the beginning of december (see weather map of 1/12/78) there was a "cold wave" on West-Europe as a result of a cyclogenesis above the western Mediterranean Sea coupled with an anticyclogenesis over Scandinavia.Such a "weather pattern" may sometimes maintain a "cold wave" during many weeks and even during many months (cf. winter period 1962-1963); moreover,such a "cold wave" appears often suddenly. Snow will appear or disappear in Western-Europe as a function of the position of the cyclone ("low pressure" or "depression"). This example confirms the importance of the study of cyclogenesis over the Mediterranean Sea for short-range,medium-and long-range weather forecasting.

2° a weakening of the " maritime " anticyclone of the Azores(with a ridge of high pressure until the Alps) appears very often when a cold front is undulating (while crossing the Alps) on the eastern side of the anticyclone.The anticyclone is then generally coupled with a " low pressure system " situated nearby Russia and polar air is streaming from the North Sea to the Mediterranean Sea (which is still rather warm in winter: watertemperature generally fluctuating between 10 and 15 degrees round about New-Year's Day). A "wave" on the cold front and a "secondary low" are then developing and a deep depression appears on the weather maps ; sometimes it is really a "cyclone" because the windspeed increases very rapidly and there is a storm of 10,11 and sometimes 12 Beaufort locally and a stormy sea.The path of such a depression is very often " from the Ligurian Sea to Turkey " (where it disappears by filling up) and the duration of the complete evolution is rather short (fluctuating between three days and a week).This stormy sea is very dangerous for the harbours and the coastal towns, for example for Venice when the center of the cyclone is situated on southern Italy and when so the south-easterly wind is blowing over the Adriatic Sea (cf.papers from Prof. Frasetto about this very important subject). If we consider the upper-air situation, for example at the 500 mb level,during this typical cyclogenesis, we observe the substitution of a well-marked ridge by an important trough and simultaneously a very cold air advection until North-Africa.
The figures of schematic "ground charts" and "upper-air charts at 500 mb" permit an easy analyse of the cyclogenesis in the Ligurian Sea during the period 29/12/74 to 2/1/75;in 24 hours (from 30/12 to 31/12/74) there was a pressure fall of 25 mb and a temperature fall of about 5 degrees (or more).The windspeed increased from 5 $msec^{-1}$ to 50 $msec^{-1}$ (two hours later) and the stormy sea damaged the belgian station situated at the "Pointe de la Revelatta" nearby Calvi in Corsica.The anemogram of the Cap Cavallo station permits to analyse the suddenly increase of windspeed. We must underline that the windspeed of 50 $msec^{-1}$ (and some observations of 12 Beaufort

given by voluntary ships) is probably a mesoscale or a microscale effect because at the "Calvi-Sainte Catherine Airport" (between the hills and the mountains, at a distance of nearly 10 km from our station) the maximum windspeed was about 29 $msec^{-1}$.

With the intention of a study of this cyclogenesis, an automatic "air-sea" buoy was anchored at a few miles from the coast (in the Mezzo Golfo) and an "air-sea" mesoscale observing station (with an anemometer) was implemented at the top of the Revelatta (190 meter) with the object of comparison with the Cap Cavallo anemometer (altitude: 300 meter) and with the Sint-Catharina Airport (58 meter) and also for measurements of the vertical component of the wind (Gill anemometer).

In the framework of the "COST 43-Mediterranean Sea-Group", a complete set of observations from the automatic buoy was sent to the "Service Météorologique Métropolitain" in Paris each day from 1 to 14/8/78 via Calvi-Airport meteo station at 9 a.m.(Greenwich Time) in code form.These observations plotted graphically and associated to STD (salinity-temperature-depth) measurements(Bisset-Berman) are very interesting for the interpretation of the passage of thundery troughs in summer (cf. 7 and 8/8/78) and the influence of "air-sea" interactions on the thermocline.The S.T.D.data were obtained on board of the oceanographic ship "Recteur Dubuisson" (CMM selected ship,with continuous meteorological records).
During the ALPEX subprogram of GARP,a sounding balloon will give continuous records of the boundary layer (1.000 meter) over the Mezzo Golfo .

Acknowledgments:
The author thanks warmly Prof.A.DISTECHE,Director of S.T.A.R.E.S.O. and his assistants for the S.T.D. measurements;he thanks also all the members of the "Air-Sea Interactions" working group for their participation in this project.

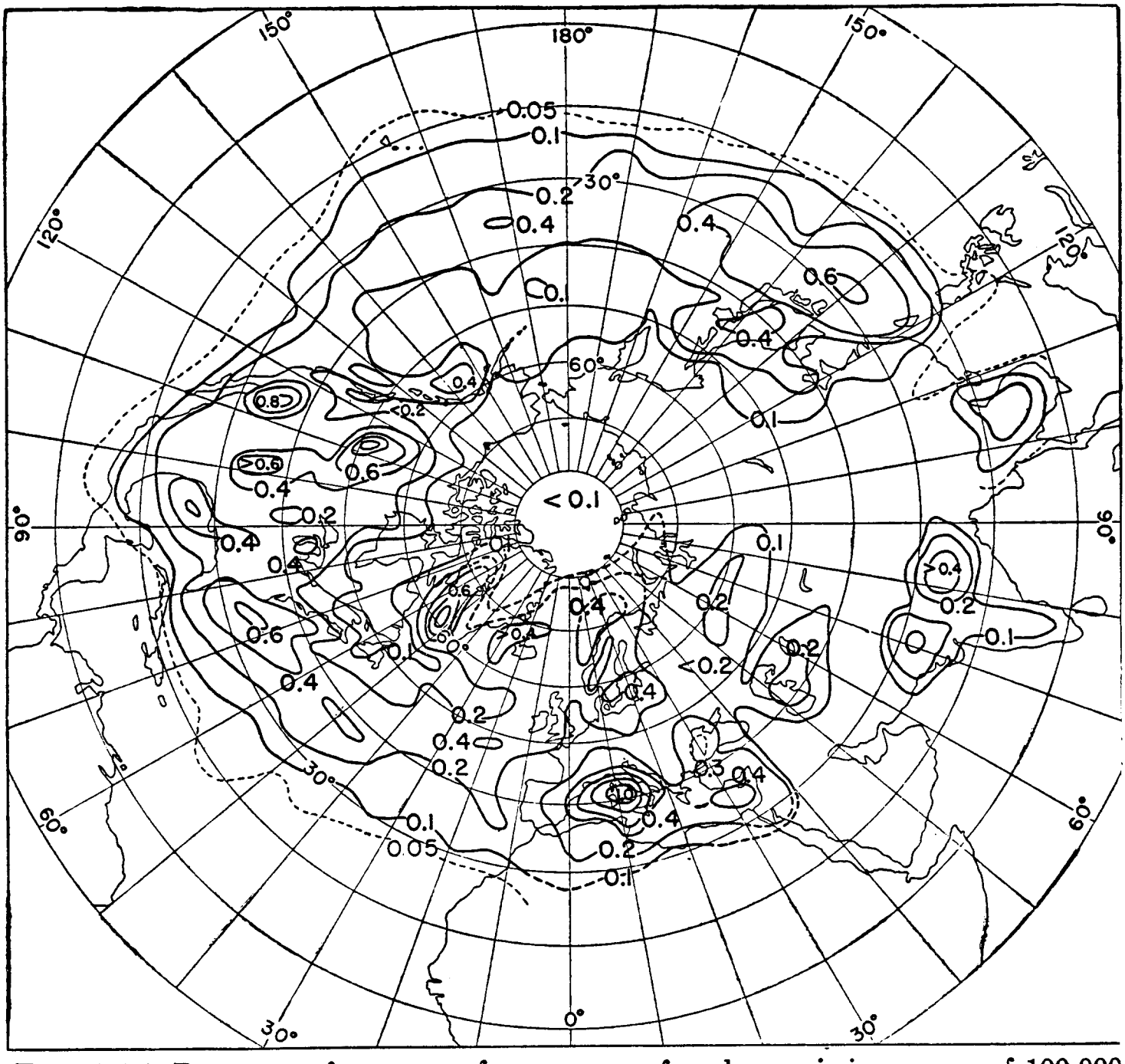

FIG. 13.6.1. Percentage frequency of occurrence of cyclogenesis in squares of 100,000 km² in winter (1899 to 1939).

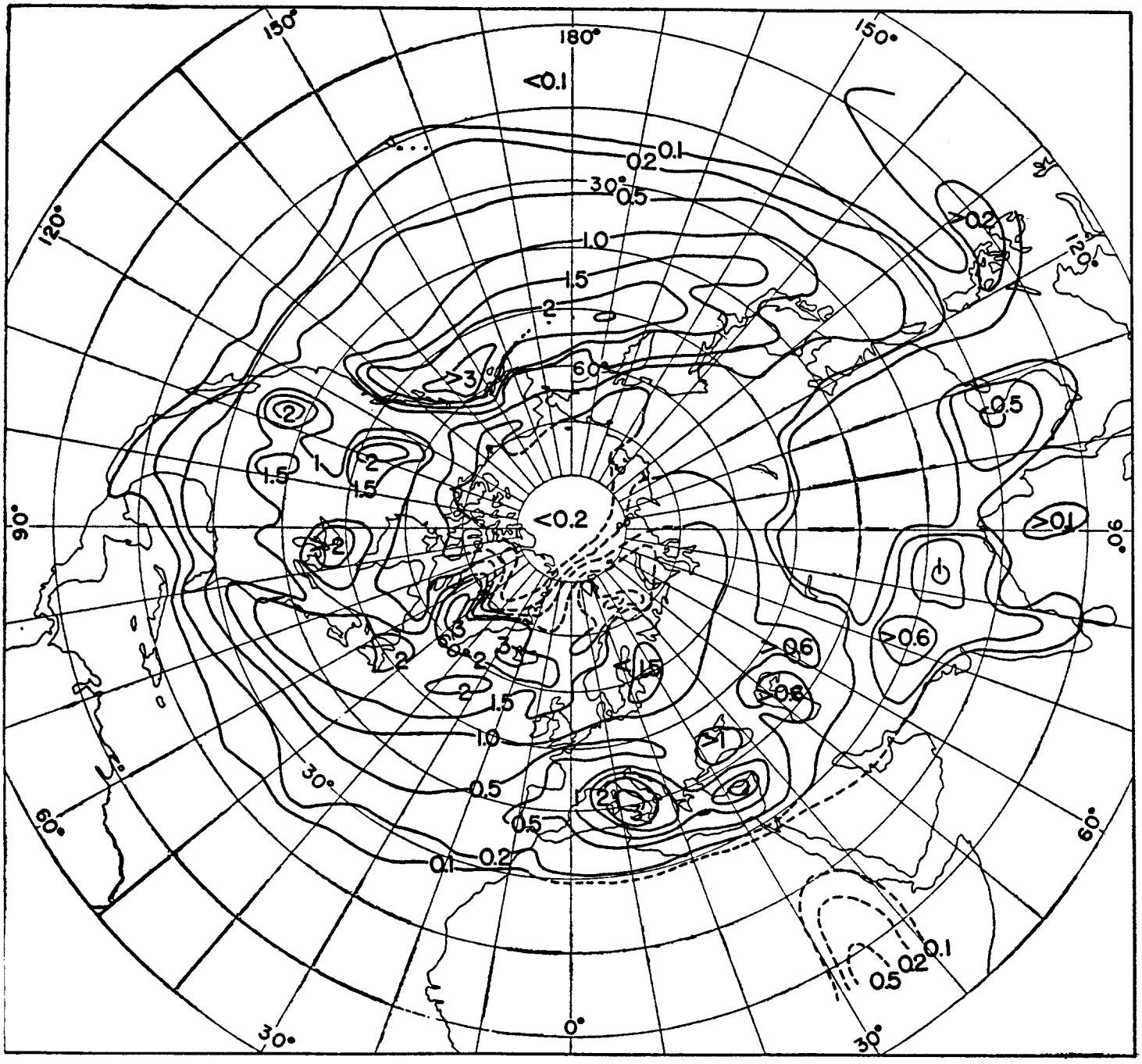

FIG. 13.6.2. Percentage frequency of cyclone centers in squares 100,000 km² in winter (1899 to 1939).

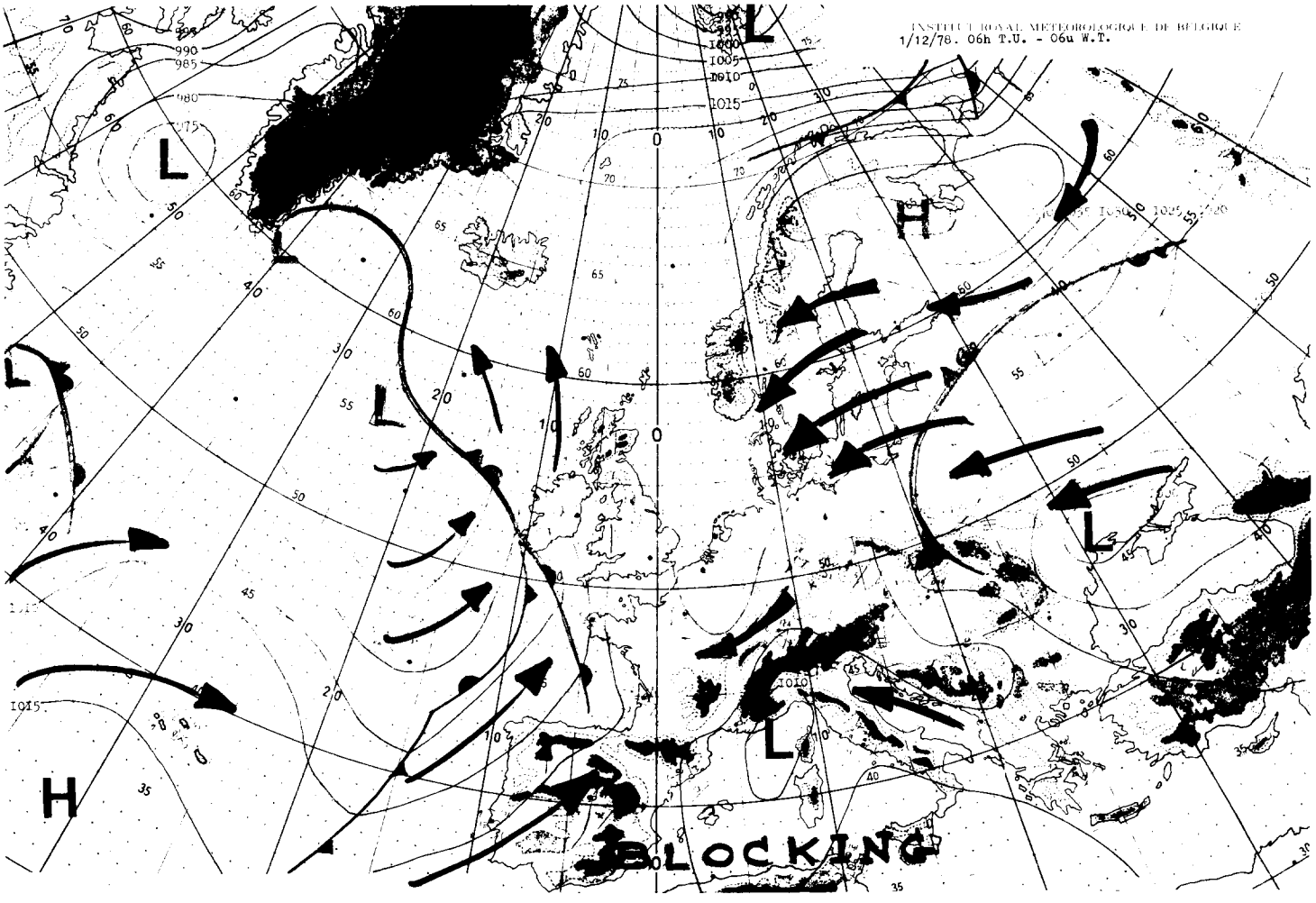
INSTITUT ROYAL METEOROLOGIQUE DE BELGIQUE
1/12/78. 06h T.U. - 06u W.T.
L
H
BLOCKING

Carte de surface 29/12/74

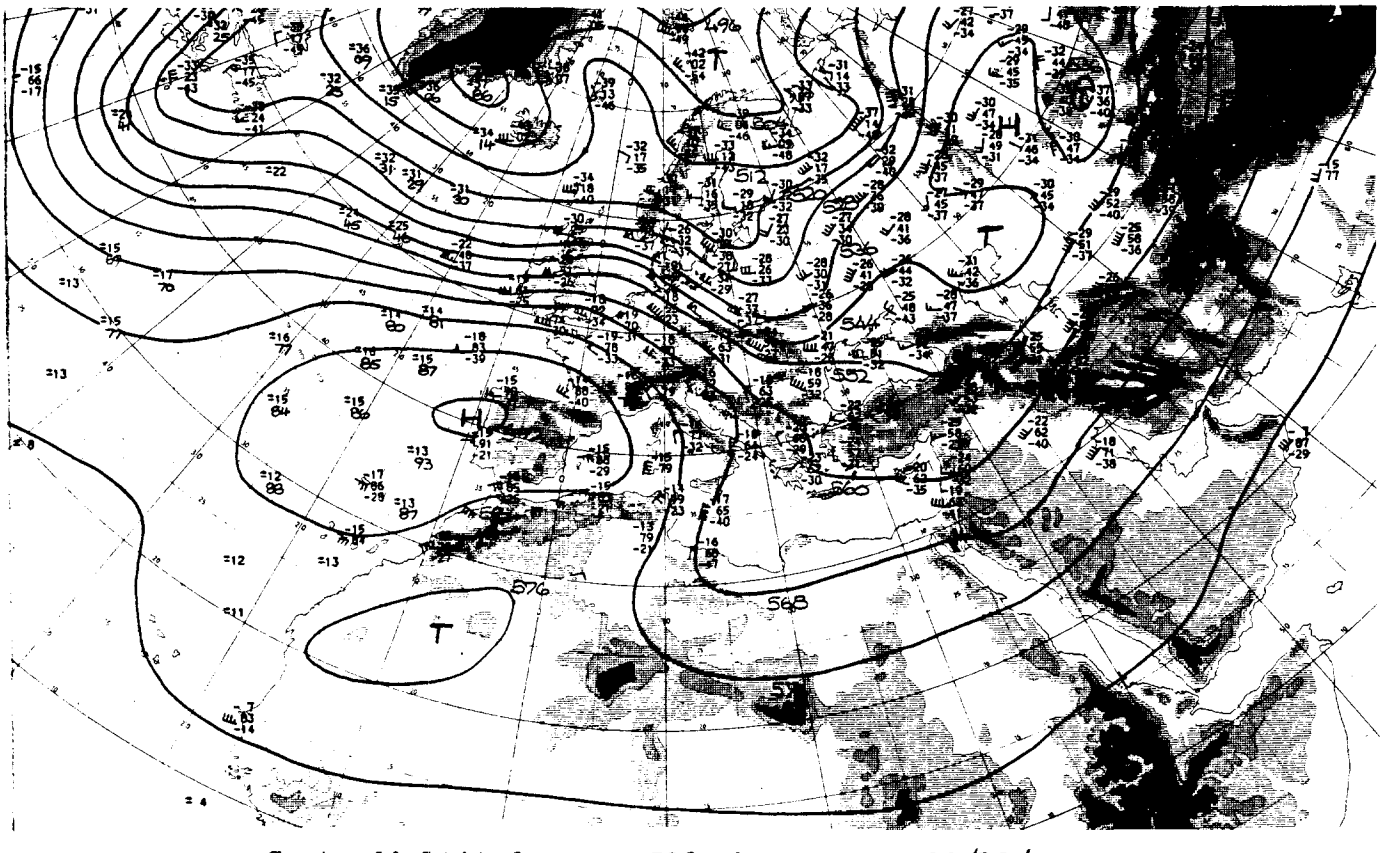

Carte d'altitude - 500 mb - 29/12/74

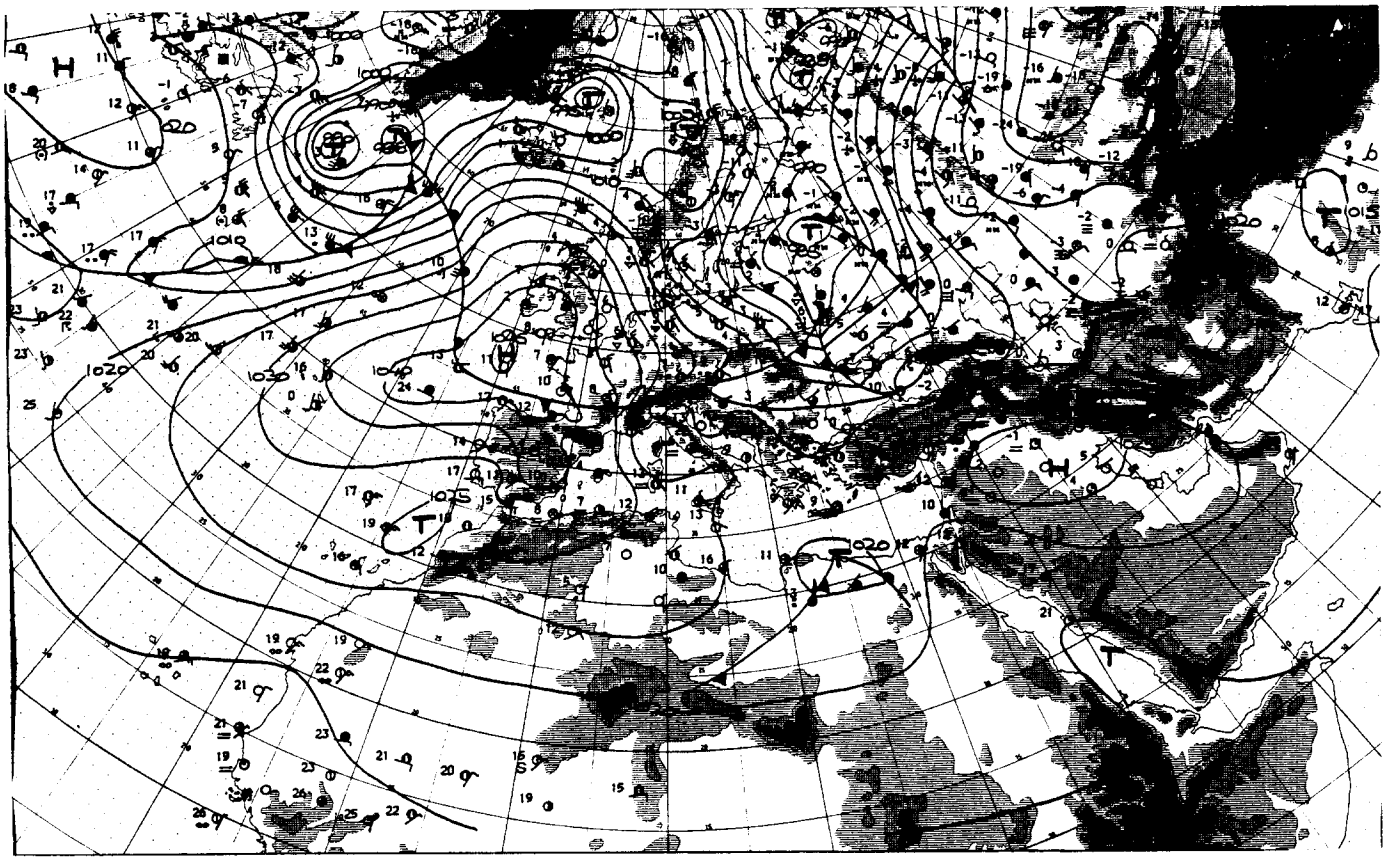

Carte de surface 30/12/74

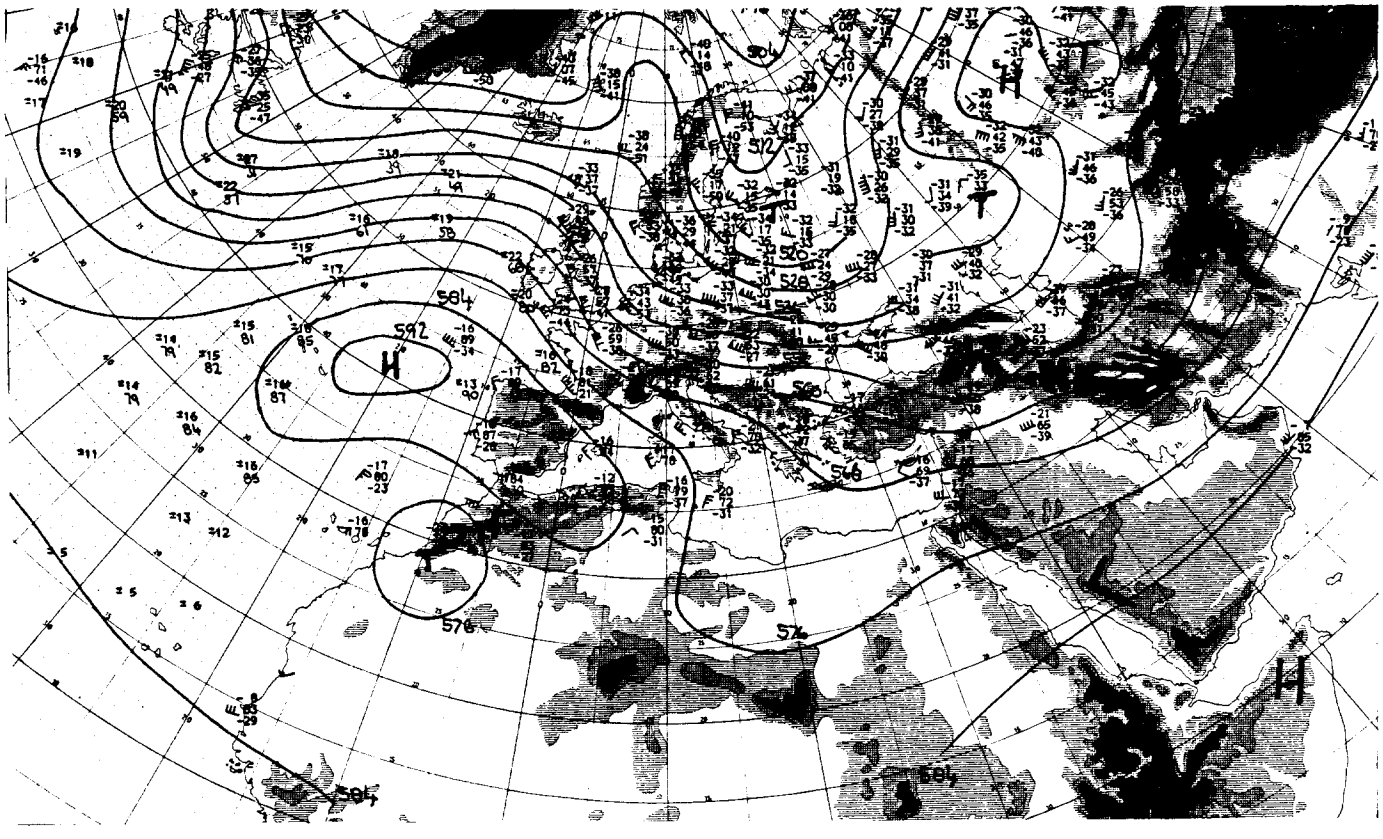

Carte d'altitude - 500 mb - 30/12/74

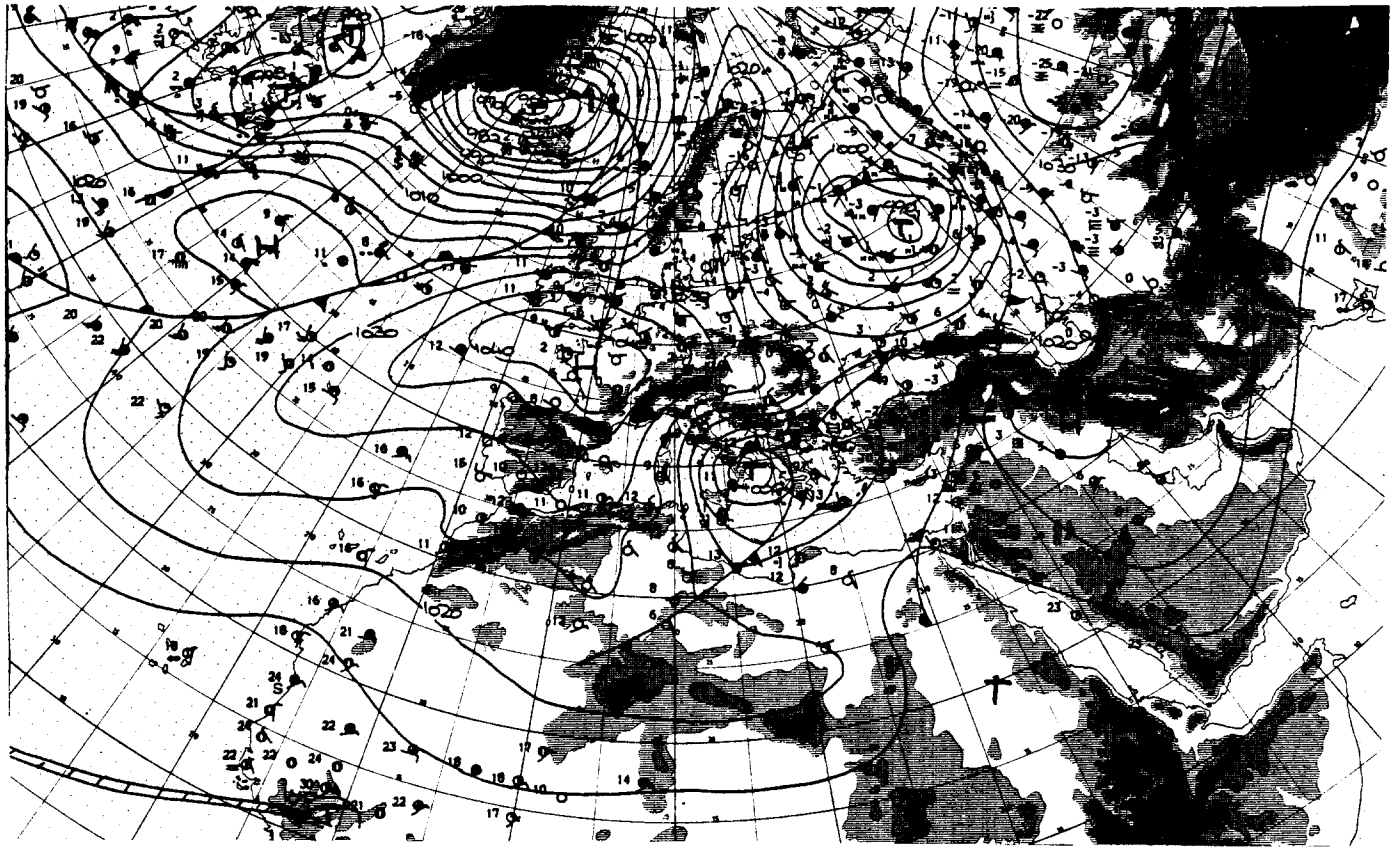

Carte de surface 31/12/74

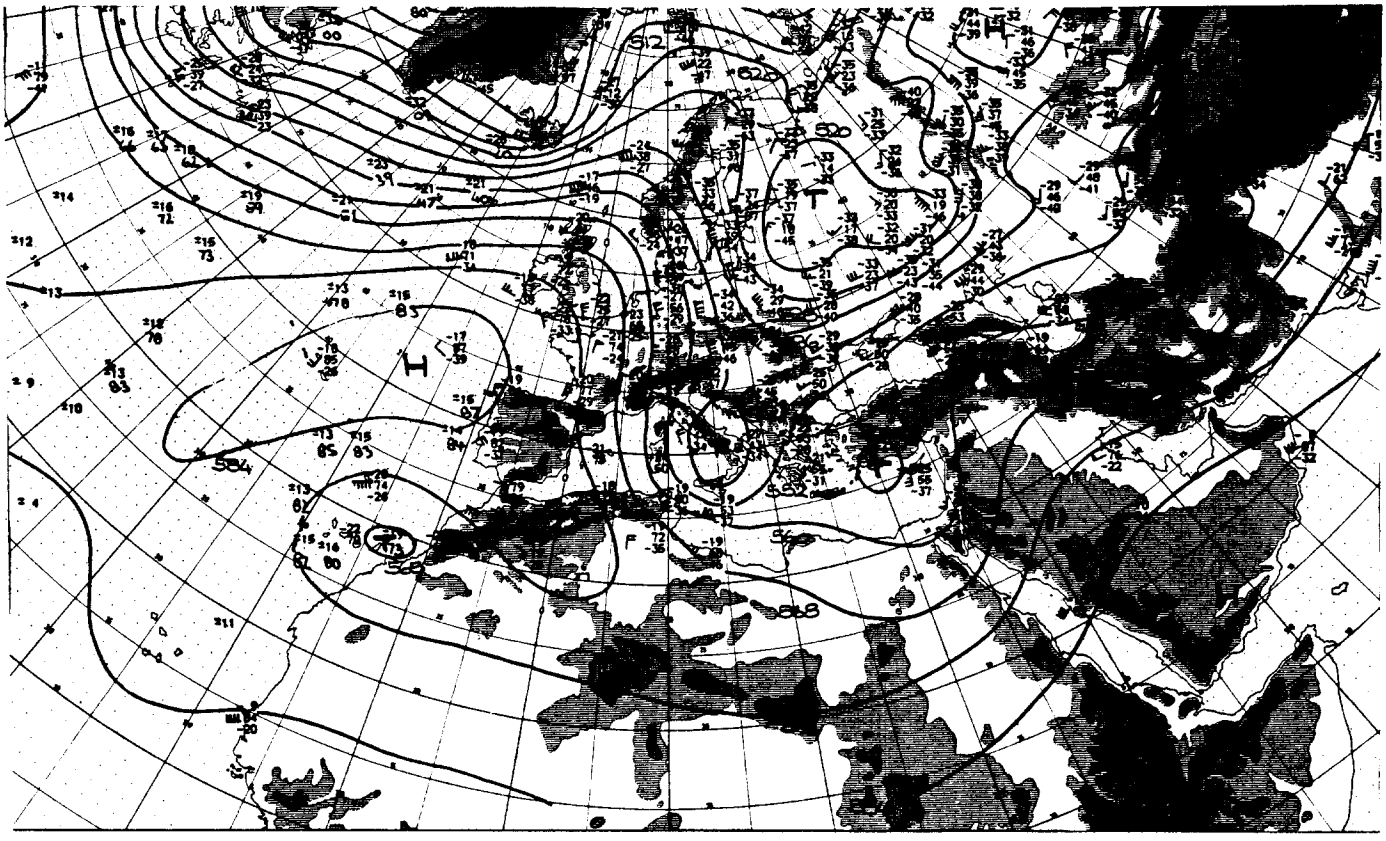

Carte d'altitude - 500 mb - 31/12/74

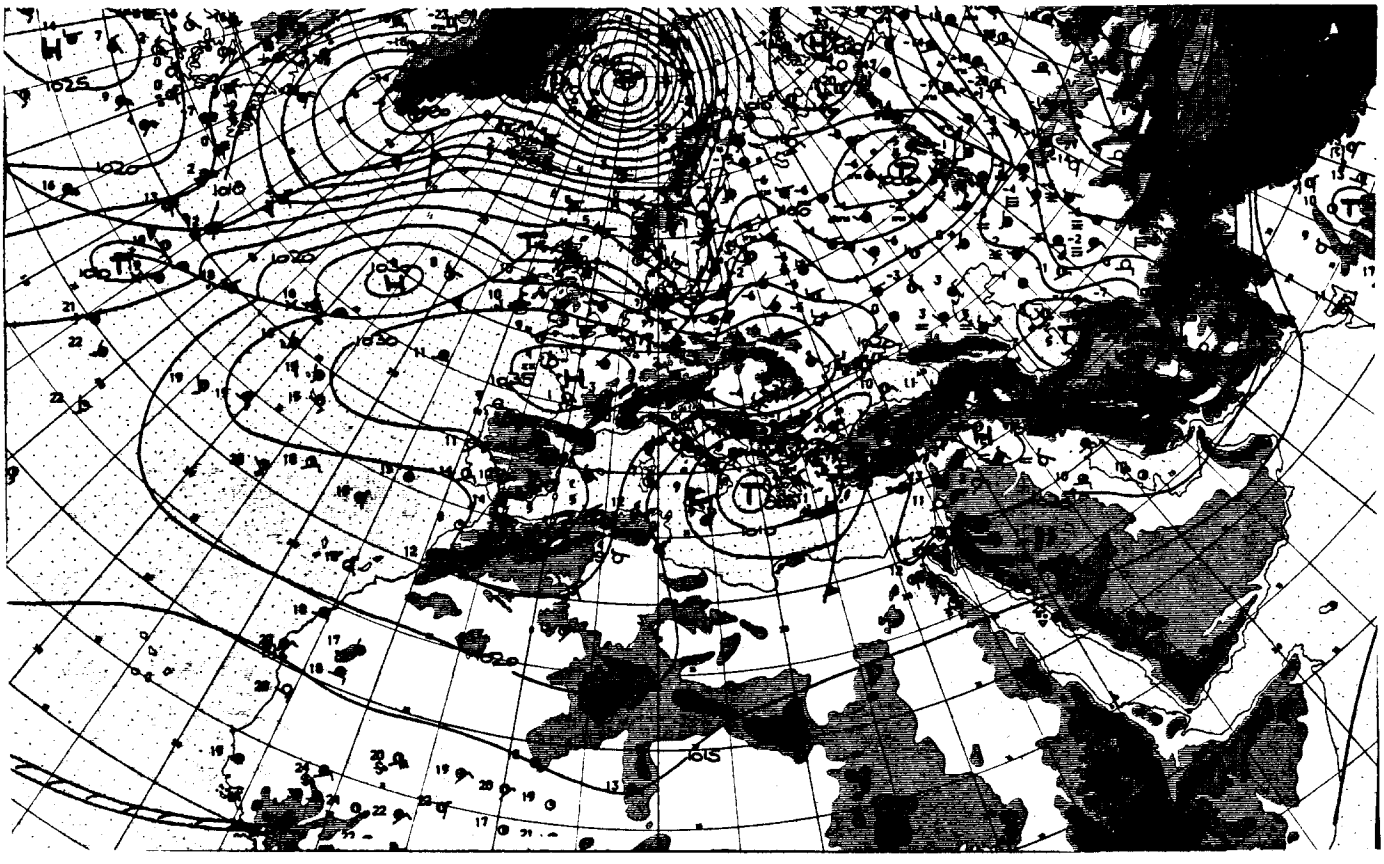

Carte de surface 1/1/75

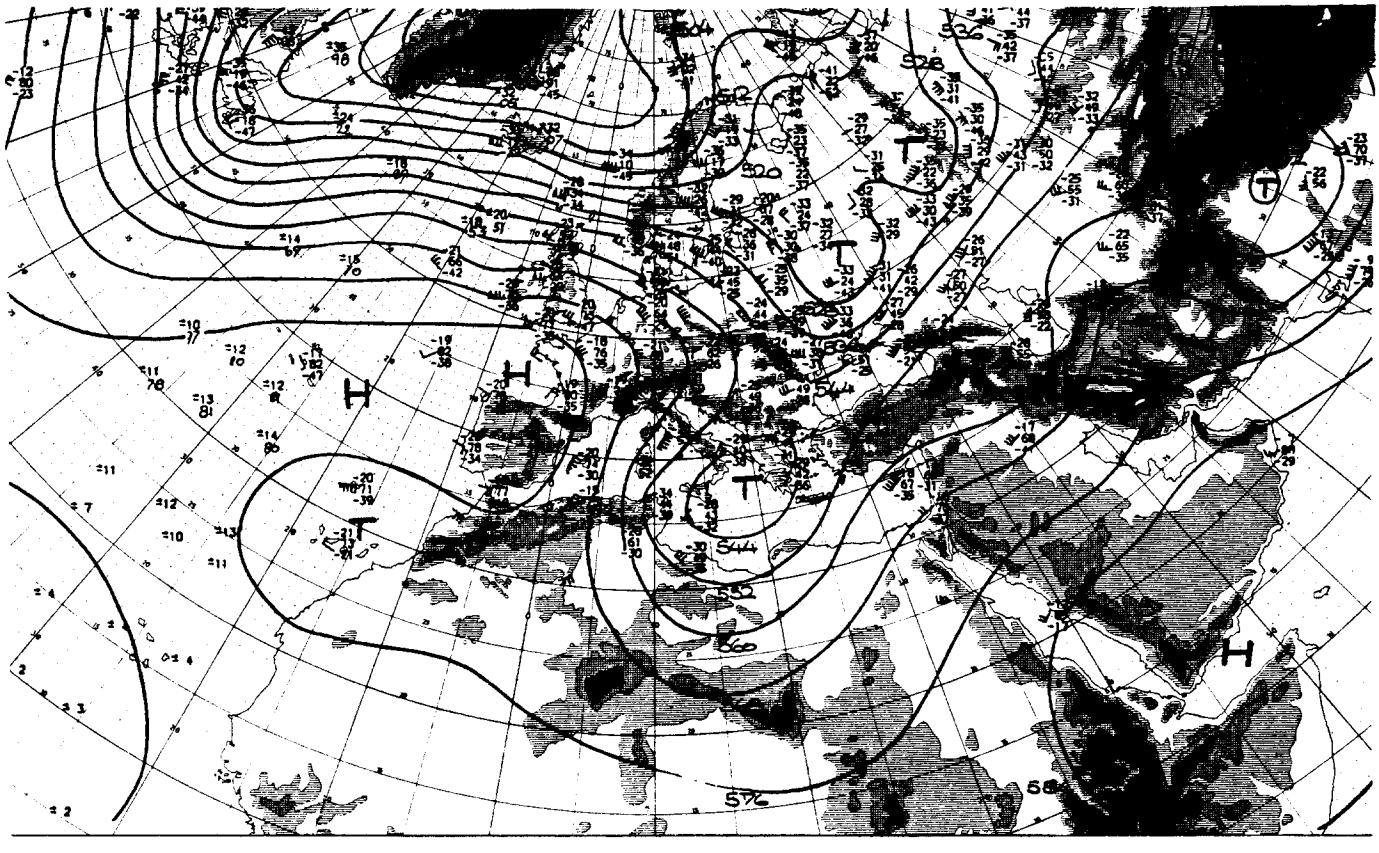

Carte d'altitude - 500 mb - 1/1/75

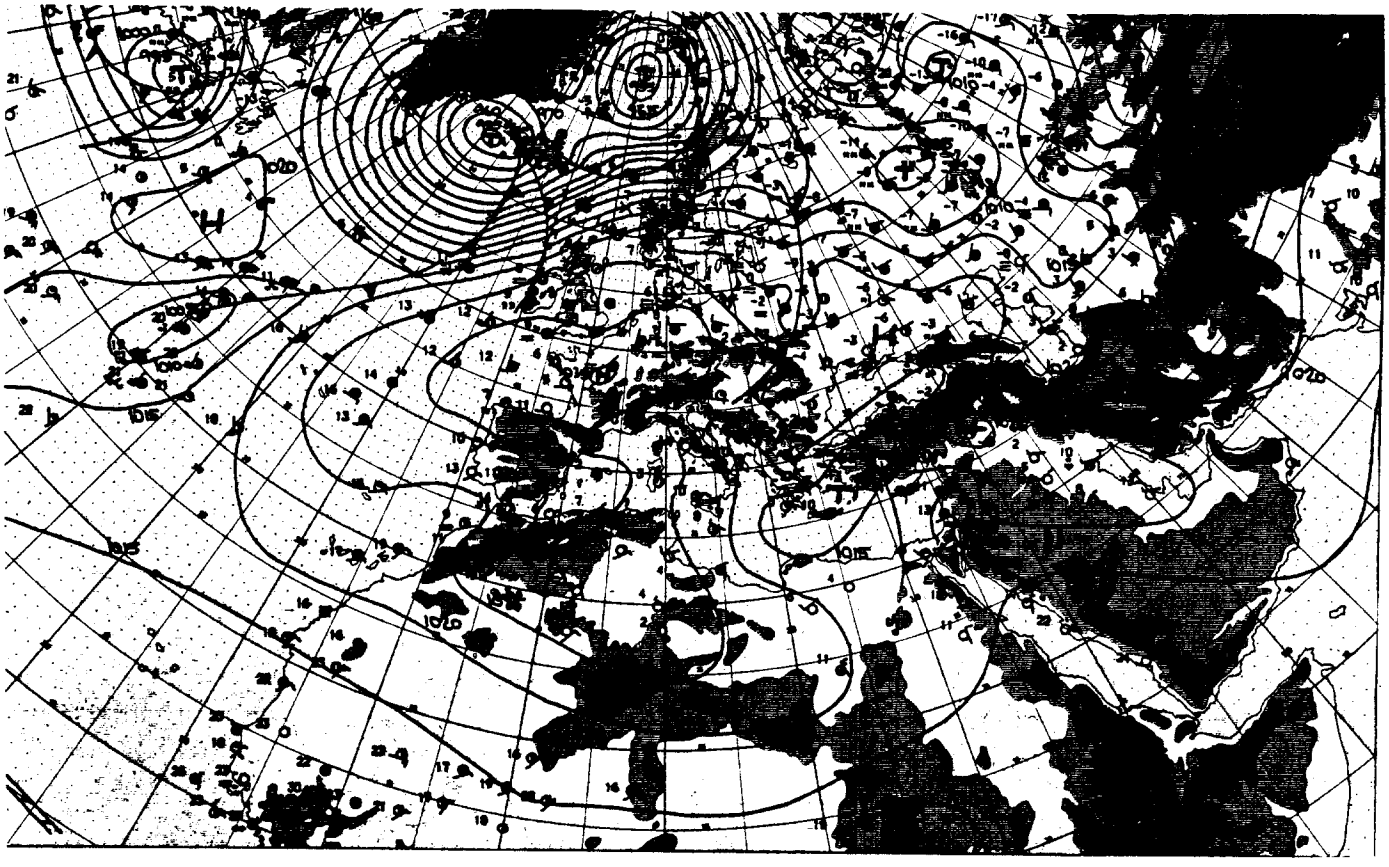

Carte de surface 2/1/75

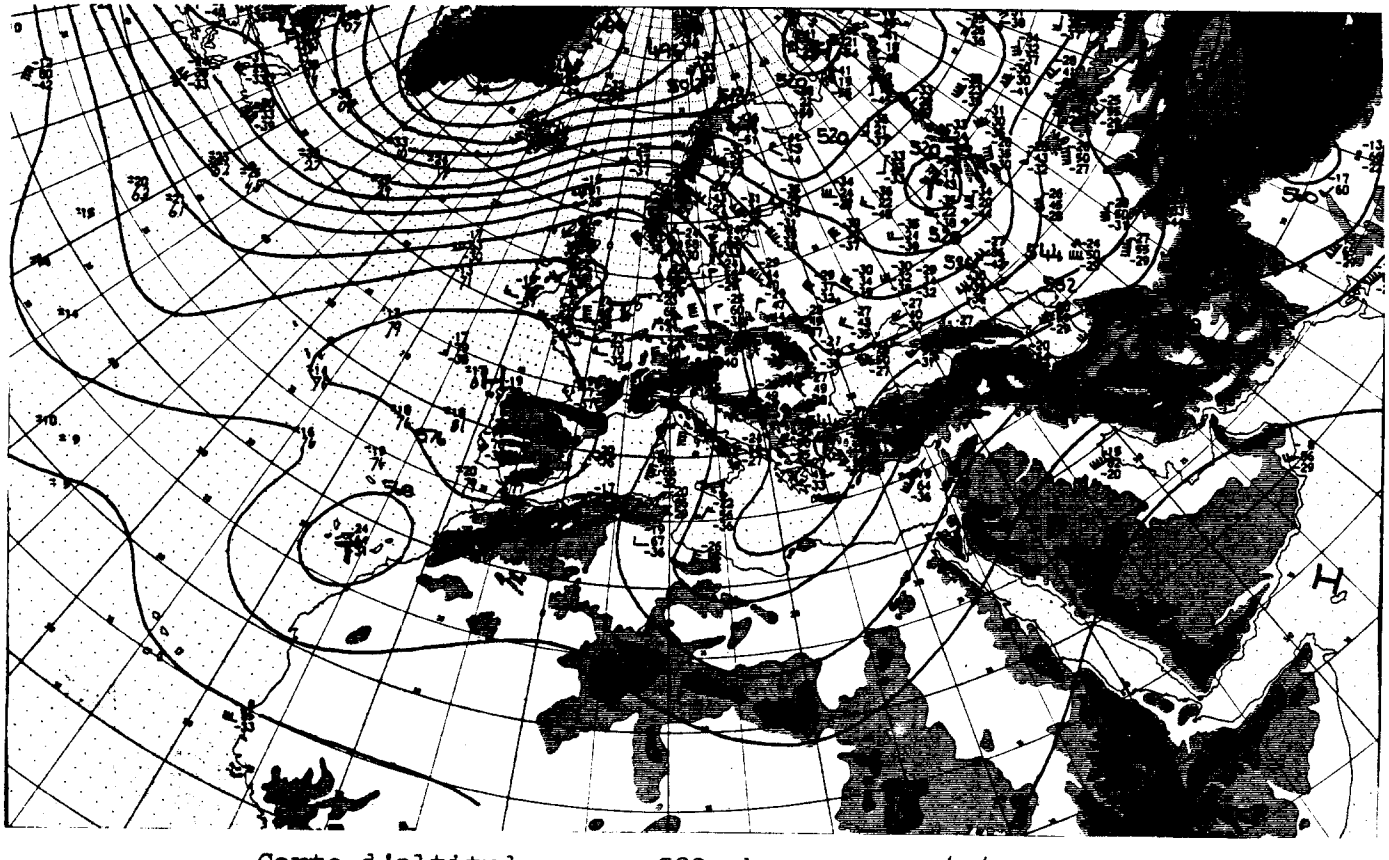

Carte d'altitude - 500 mb - 2/1/75

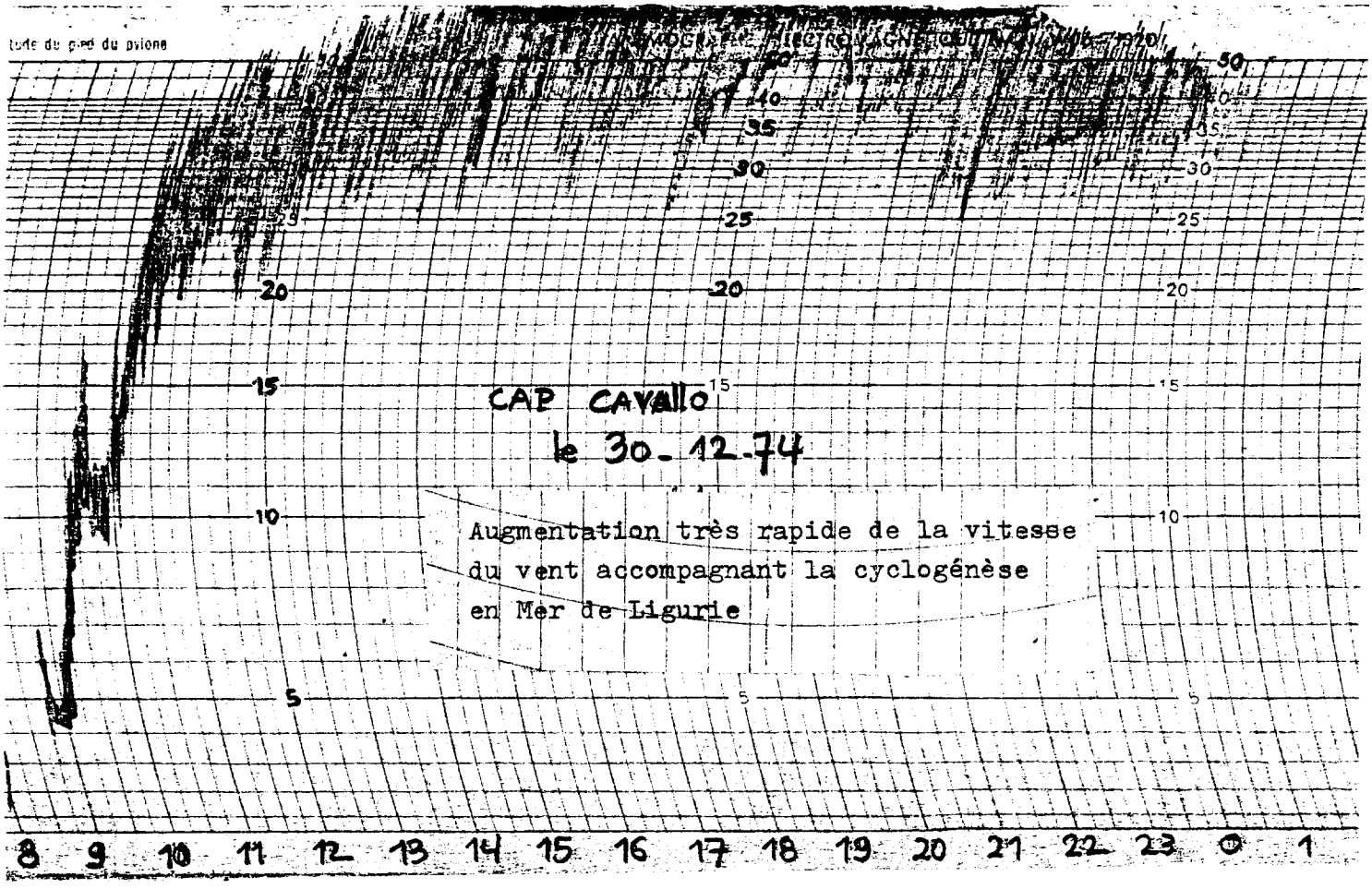
CAP CAVALLO
le 30-12-74
Augmentation très rapide de la vitesse
du vent accompagnant la cyclogénèse
en Mer de Ligurie

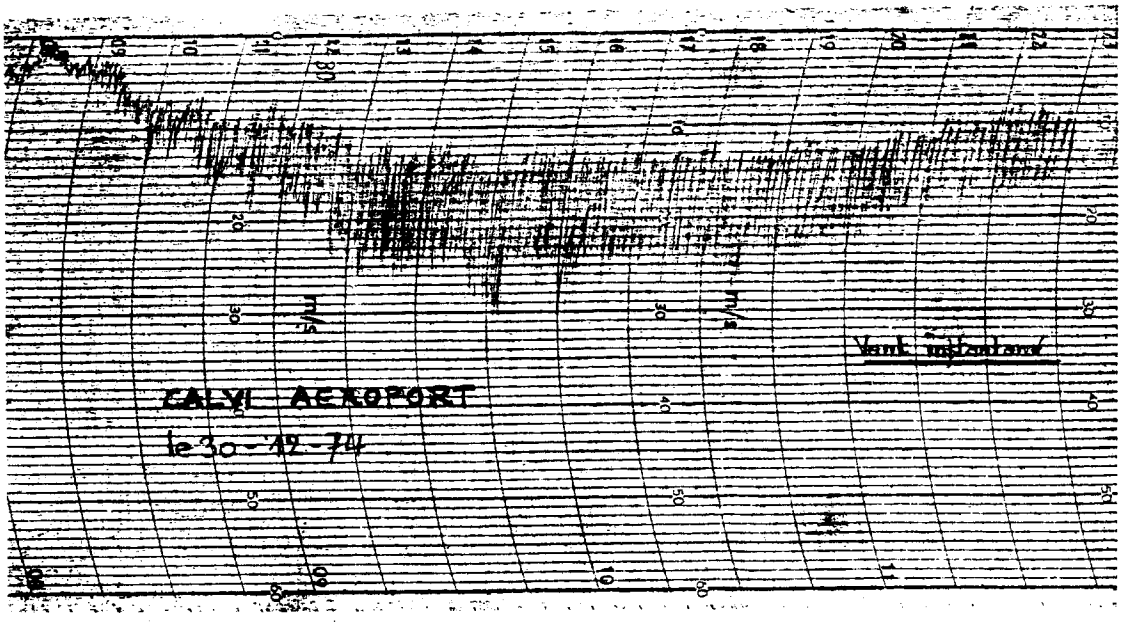
CALVI AEROPORT
le 30-12-74
Vent méridional

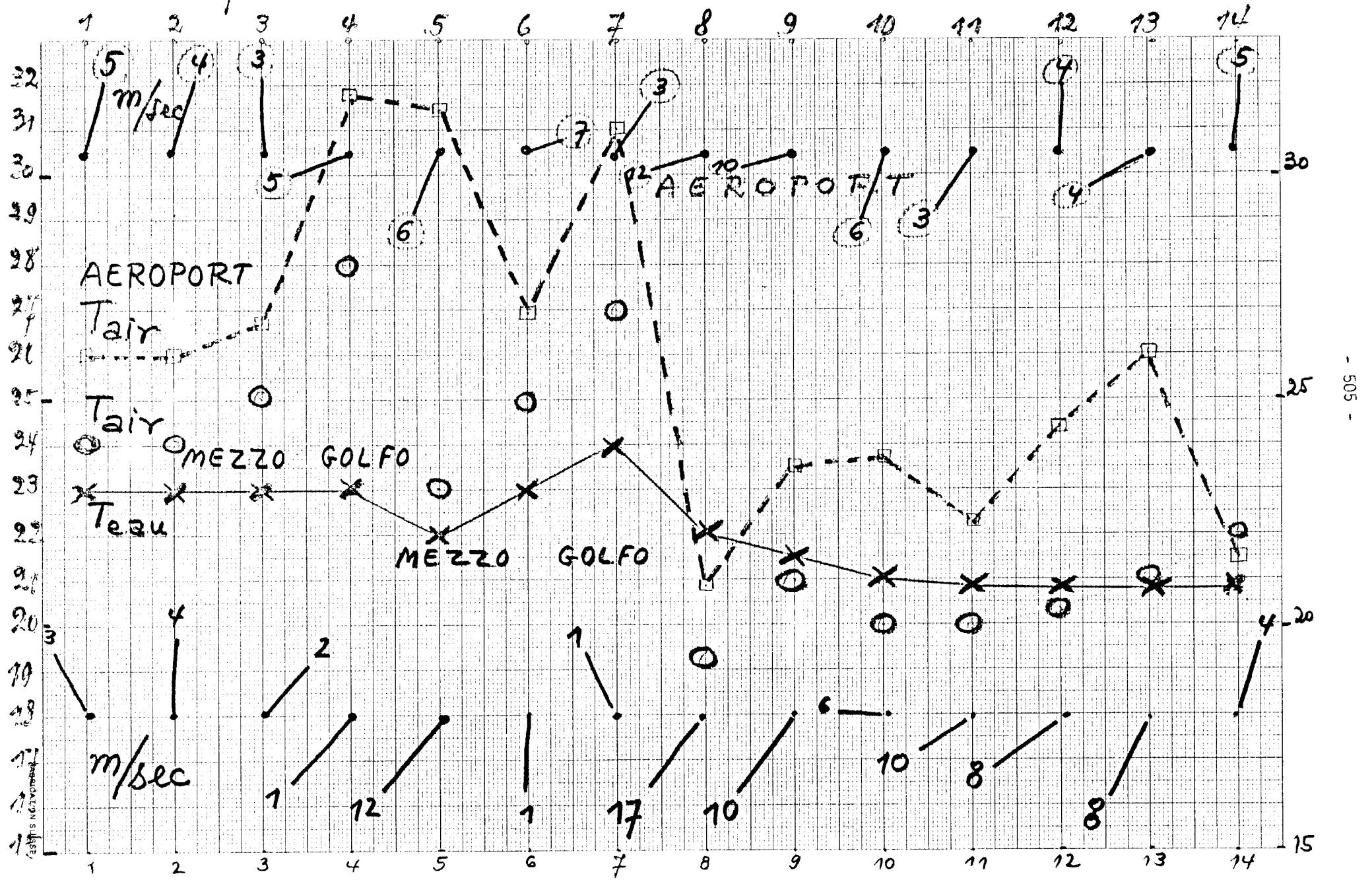
AOUT 1978
CALVI - CORSE
m/sec
AEROPORT
Tair
Tair
MEZZO
GOLFO
Teau
MEZZO
GOLFO
AEROPORT
m/sec

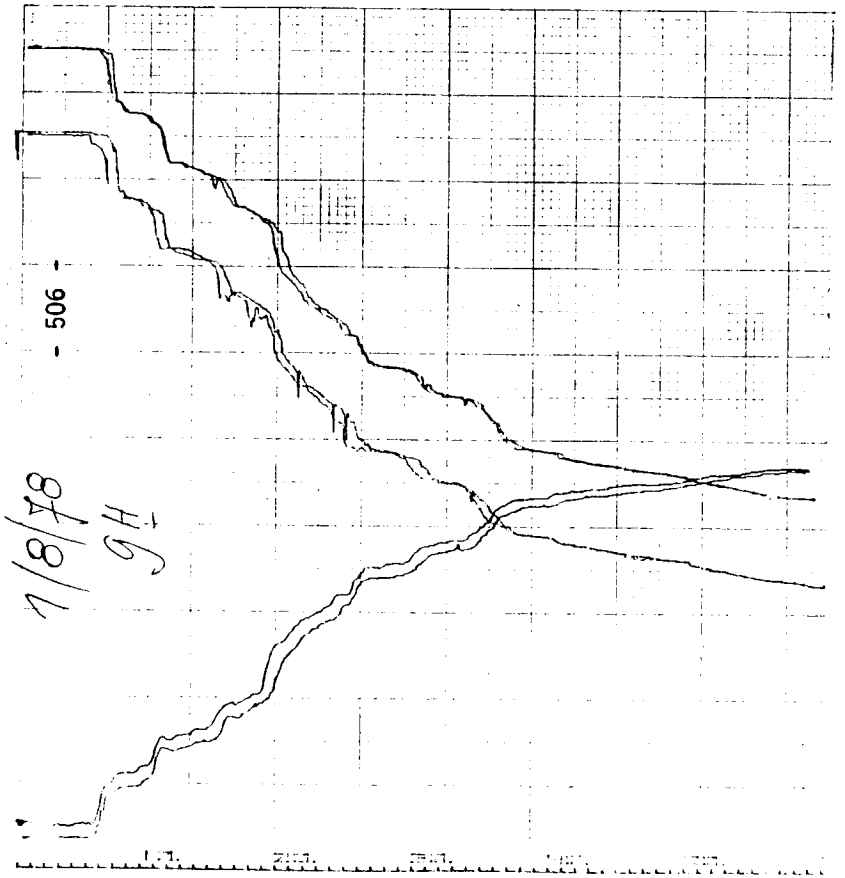
- 506 -
1/8/78
9H

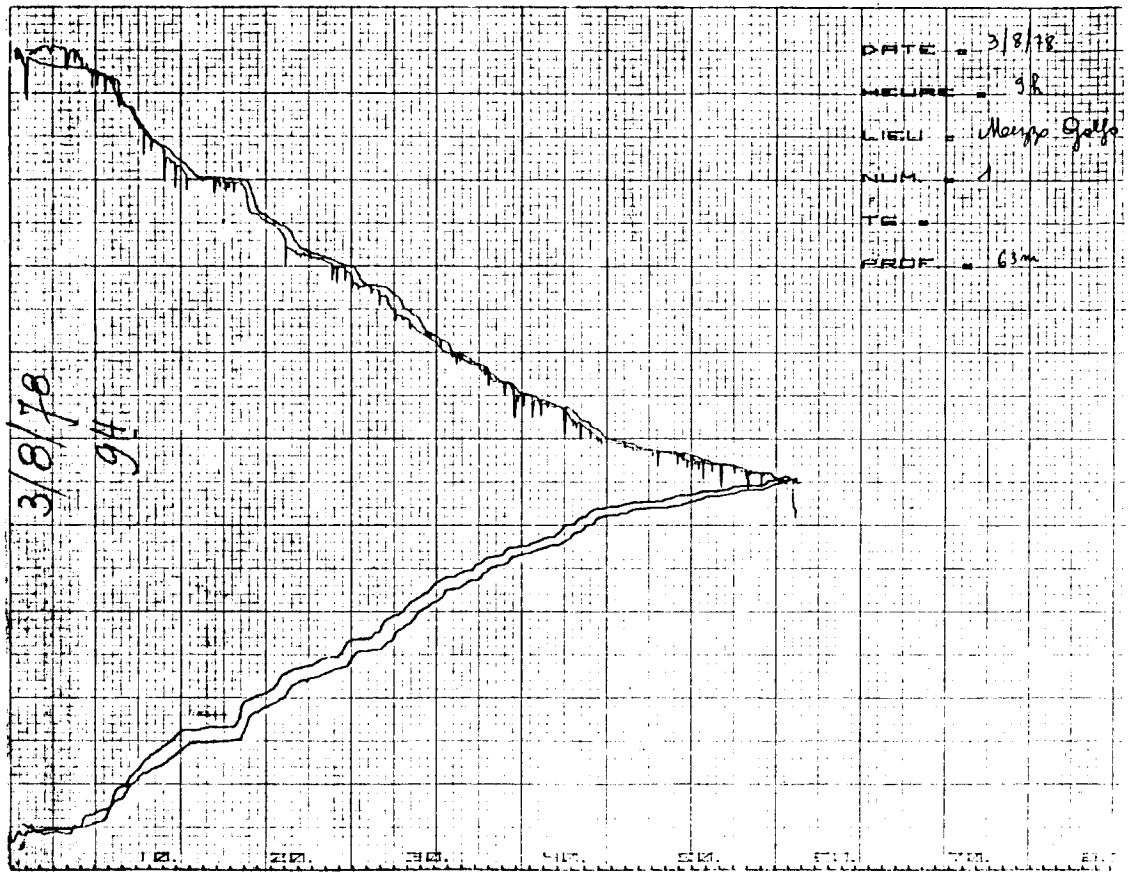
DATE - 3/8/78
HEURE - 9h
LIEU - Marina Golfe
NUM. - 1
TS -
PROF. - 63m
3/8/78
9H

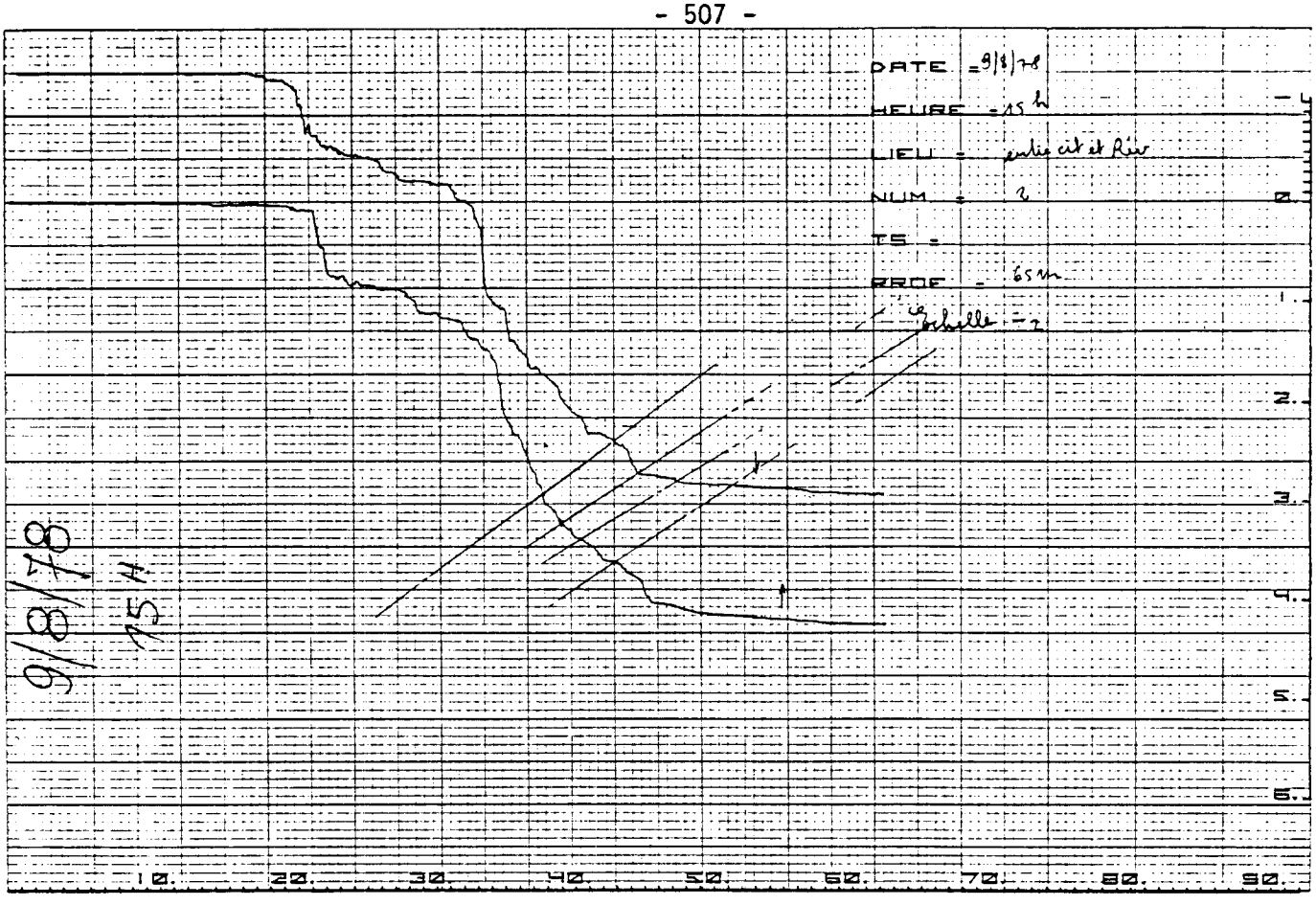
DATE = 9/8/78
HEURE = 15 h
LIEU = entre cit et Rive
NUM = 2
TS =
PROF = 65 m
échelle = 2
9/8/78 15 h
10. 20. 30. 40. 50. 60. 70. 80. 90.

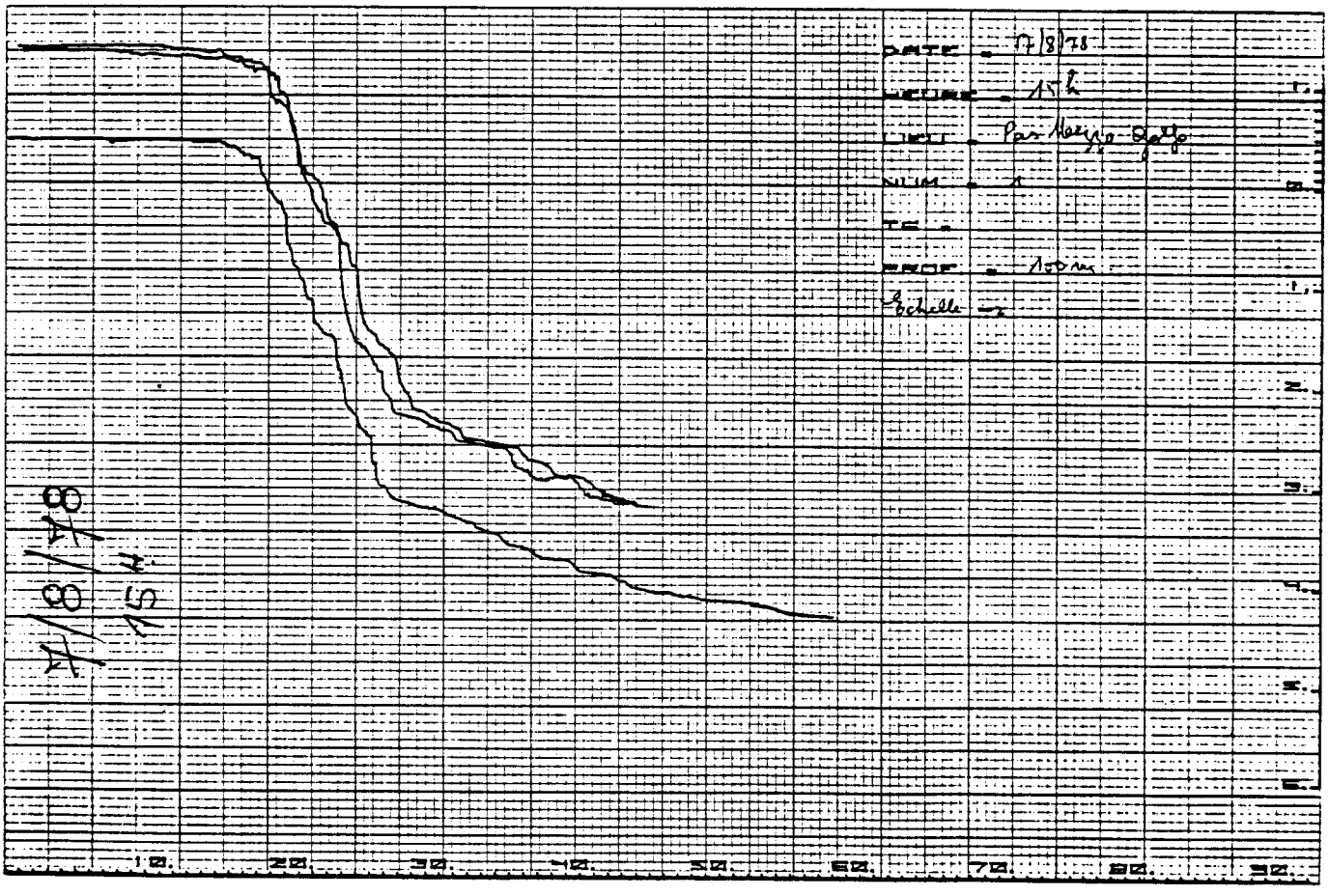
DATE = 7/8/78
HEURE = 15 h
LIEU = Par Verger Delta
NUM = 1
TS =
PROF = 120 m
échelle = 2
7/8/78 15 h
10. 20. 30. 40. 50. 60. 70. 80. 90.

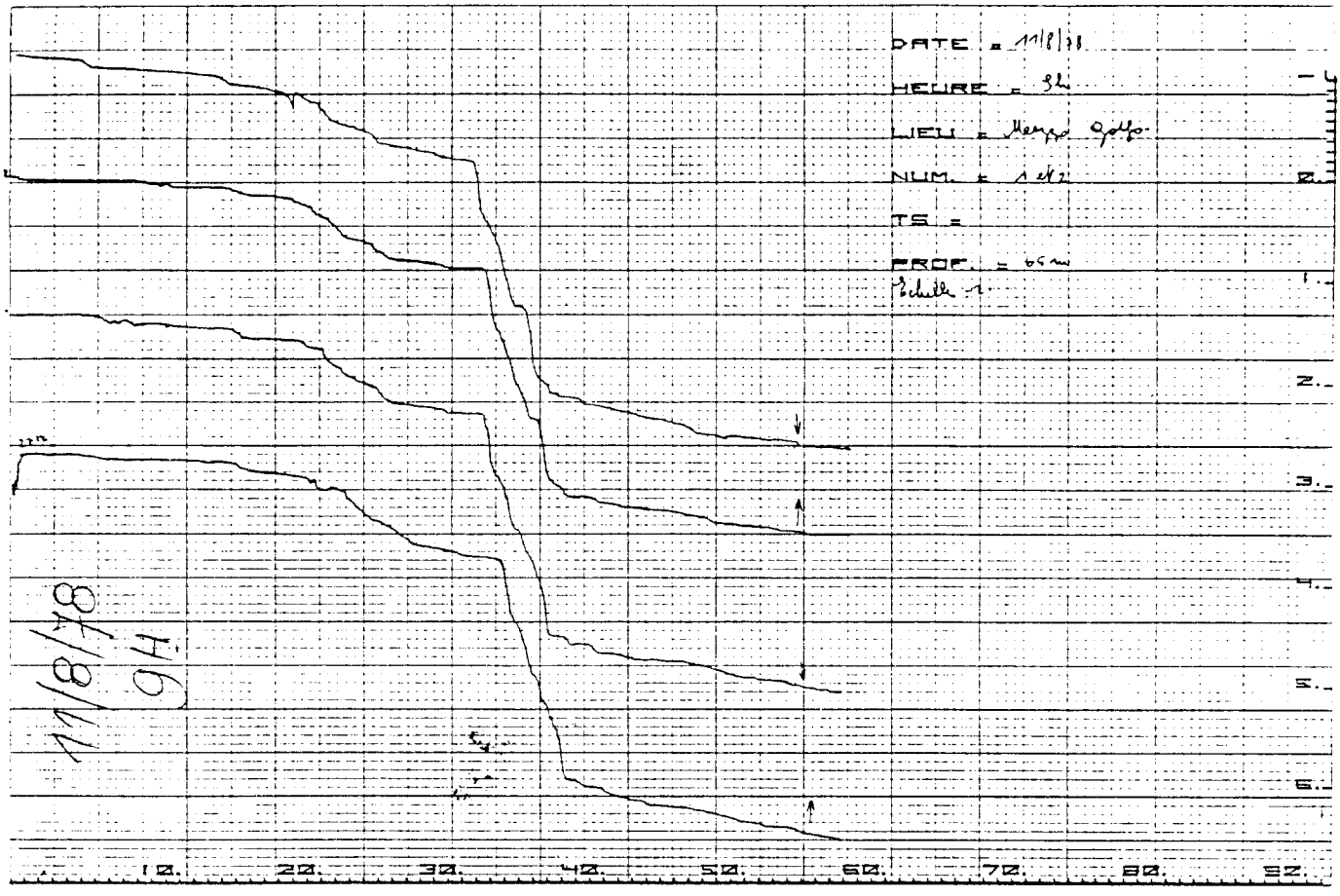
DATE = 11/8/78
HEURE = 9h
LIEU = Mergo golfo
NUM. = 1 et 2
TS =
PROF. = 65 m
Echelle 1:
11/8/78
9H
10.
20.
30.
40.
50.
60.
70.
80.
90.


DATE = 10/8/78
HEURE = 11h
LIEU = Mergo golfo
NUM. = 1 et 4
TS =
PROF. =
Echelle 1:
10/8/78
11H
10.
20.
30.
40.
50.
60.
70.
80.
90.

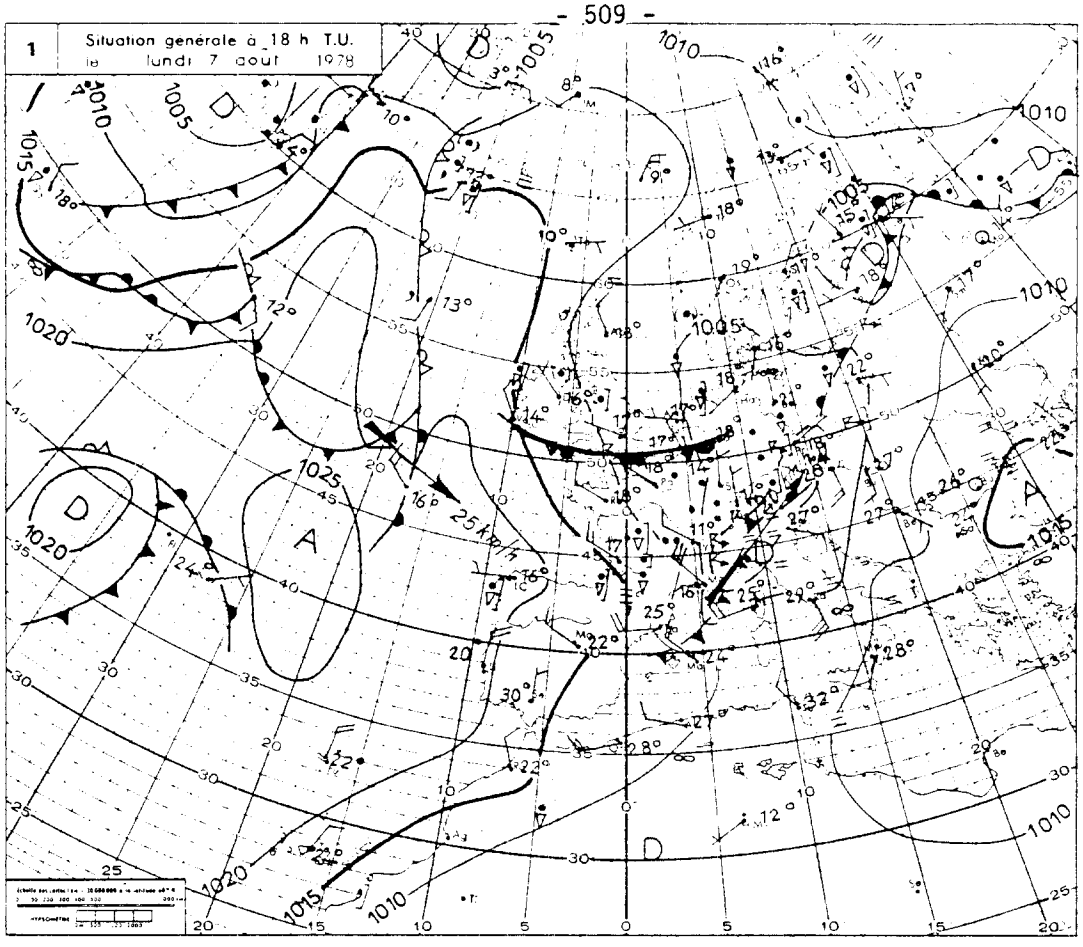
1
Situation générale à 18 h T.U.
le lundi 7 août 1978

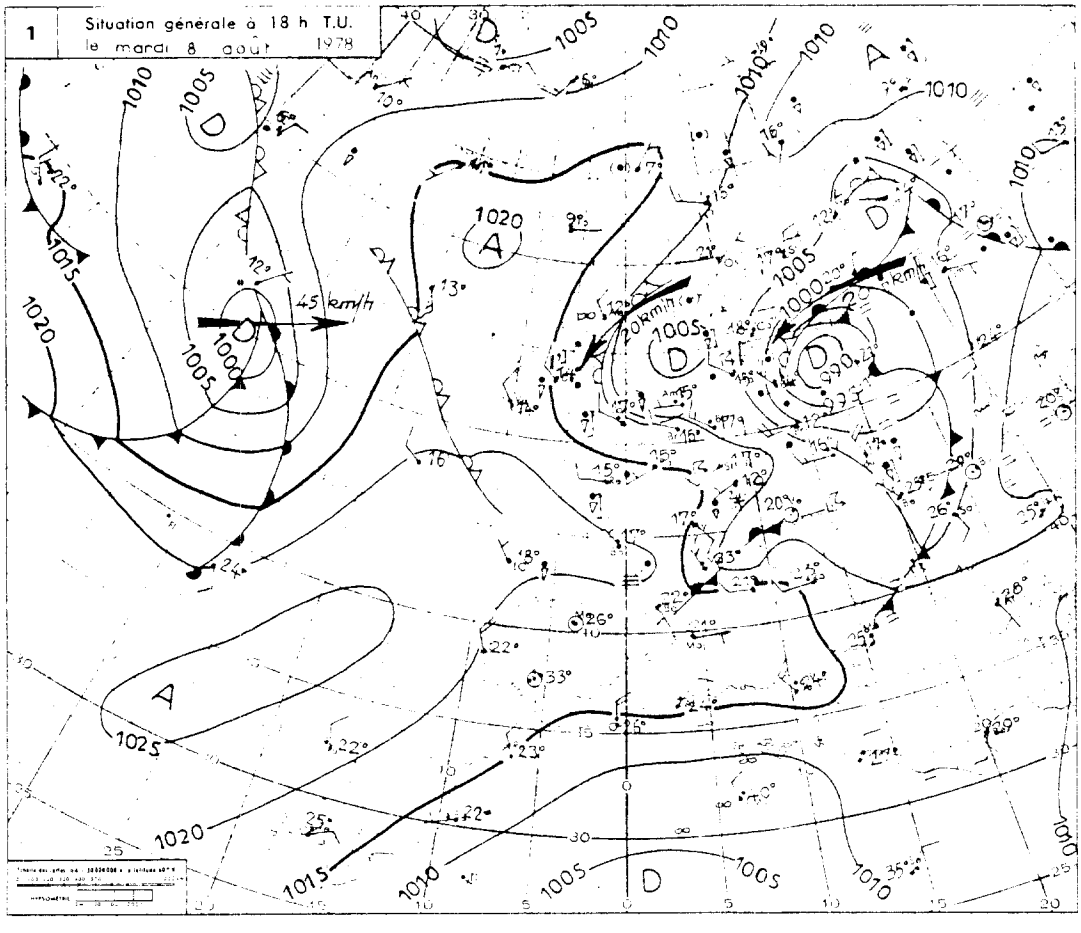
1
Situation générale à 18 h T.U.
le mardi 8 août 1978
45 km/h

REVIEW AND EVALUATION OF EXISTING OCEANOGRAPHIC PRODUCTS

by

K.P. Vasiliev

Chief, Department for Marine Forecasting
Hydrometeorological Centre of the USSR
(Moscow)

At the present time, oceanographic (hydrological) services to marine activities cover a wide scope of problems which characterize dynamical and thermal oceanic processes. These processes have an essen tial and sometimes a decisive impact on works at sea. Therefore the majority of marine Member-States issue oceanographic analyses and prognoses aimed at meeting the requirements of marine activities and rising their safety and economic effectiveness.

Services to various fields of marine activities with oceanographic products are being performed taking into account the specific character of the works. For this aim meteorological services of Member-States issue analyses and prognoses of:

- sea water temperature (in the surface and subsurface layers of the sea);
- sea conditions;
- sea ice conditions (formation and destruction of ice cover, ice thickness, position of ice edge and boundaries, ice navigability);
- sea level oscillations (periodical - tides, storm surges);
- currents;
- salinity.

Apart from these, a number of countries (Japan, USSR, USA, FRG) is performing services to fisheries and whaling at places of the catch. The USA, USSR, Netherlands and other countries have organized weather routeing of ships. At recent time, specialized services to works on reconnaissance and extraction of mineral raw materials at the shelf are rapidly developing.

The coverage of World Ocean areas by oceanographic products issued by Member-States is given below briefly.

At present, not all World Ocean areas are equally covered by oceanographic product broadcasts in pictorial, digital and textual forms. Oceanographic analyses (prognoses) for the Northern Hemisphere are being transmitted for the whole water area and many regions are overlapped by broadcasts of several countries, while for the Southern Hemisphere products are issued for limited areas adjacent to coasts of Africa, South America, Australia and New Zealand. It must be kept in mind that lack of meteorological and oceanographic observational data at oceanic areas of the Southern Hemisphere affects the quality of compiled analyses and prognoses.

For illustration of the above a chart is presented of coverage of the World Ocean by facsimile charts of analysis/forecasting of oceanographic parameters (see Fig.1).

To make a brief critical review of oceanographic products issued by meteorological centres of the world is a wide and difficult problem and under modern conditions, with ever growing marine activities both national and international, this problem has become especially complex.

Oceanographic products currently issued are based mainly on obser vational data and depend upon the method of making these observations with time and space. Today, sources of oceanographic information are observations of voluntary observing ships, research vessels, weather ships, stationary and drifting buoys, platforms and spacecraft (aircraft, satellites). However, in spite of abundance of sources, adequate information for preparation of qualitative analyses and prognoses is rarely available. It should be noted, that recently an essential progress is made due to information on sea ice, sea-surface temperature and state of sea (sea conditions) available from satellites. As regards salinity and surface current data there is an extremely inadequacy of these data and much has to be done to meet the requirements of users. The above results in the oceanographic products being limited, as a rule, to the following three oceanographic parameters: sea ice, sea conditions and sea water temperature (the latter mainly concerns sea surface temperature).

Let us consider in some detail the oceanographic products issued on a real-time basis.

ANALYSES

a) Sea-surface temperature. At present, only charts of sea-surface temperature distribution are operationally prepared at meteorological centres (because of the lack of adequate deep-sea observations, charts of sea water temperature distribution at various sea levels are not prepared operationally).

Techniques of compiling analysis charts are based on the synoptic method using climatic manuals for check and retrieval of deficient data (at individual squares). Apart from the above, the numerical analysis method is used in operational practices. It comprises the computerized primary processing of initial observational data (identification, interpretation and quality control) with further data averaging with respect to squares and extrapolation at grid points, drawing of the temperature field and introducing of this field, as an initial one, into the numerical prognostic model.

The main shortcoming of the existing methods for analysis of the sea-surface temperature field is their subjectiveness as well as lack of density of observations, and the latter does not permit to compile analyses for the standard time of observations. Therefore analyses are compiled from data averaged for 5 and more days, while for separate local regions for one day. Such a situation does not fully meet the requirements of users, especially fisheries.

Recently global charts of sea-surface temperature distribution for the World Ocean from satellite data have been compiled on the experimental basis. These charts are of great interest both for practical and especially for scientific aims. However, the accuracy of data derived is not yet sufficient ($\pm$ 2°C) and the correctness of data compatibility from different satellite paths is not clear. But one can suppose that satellite information is very perspective.

b) Sea conditions. The field of sea conditions is analysed for one time of observation (00 GMT), more rarely for two times of obser-

vation (00, 12 GMT), and only in the USSR analyses of the sea condition field are issued for 4 standard times of observation. Techniques of their compiling are based on synoptic or calculation methods. At squares where observational data are unavailable they are retrieved by calculation of wave heights from the surface pressure field.

Methods of objective analysis of sea condition field are not used in operational practices.

c) Sea ice. Analysis of sea ice conditions on freezing seas and oceanic areas is performed from aircraft reconnaissance data and/or TV satellite information. Usually, the ice edge (of drifting and fast ice) and boundaries of various concentration sea ice are drawn at ice charts. Apart from it, sea ice thickness, hummocking of ice, compacting, diverging, location of icebergs, deformation of ice, polynyas, leads and fractures may be plotted on ice charts. Unfortunately, up to now there are no common international ice symbols and the latter results in difficulties of utilizing sea ice charts by marine users.

d) Surface currents. Unavailability of surface current observational data does not permit to issue surface current analysis charts. The Japan Meteorological Agency issues episodically charts of factual measured surface currents at different points of the north-west Pacific Ocean.

e) Salinity. Charts of factual salinity distribution at present are not being compiled because of the absence of observational data.

FORECASTING

At present time, the development of methods for oceanographic forecasting is mainly directed to construction of simplified hydrodynamic models, far away from real conditions, or to finding statistical insufficiently founded relationships. Such a situation can, in the first place, be explained by unavailability and/or lack of observational data. The latter causes simplifications of our ideas on the dynamical and thermal processes of the ocean and their interrelationship with atmospheric processes. Therefore one is introducing simpli-

fications and idealizations into natural conditions in solving the set of classical hydrothermodynamic equations and revealing statistical relationships. These result in obtaining prognostic relationships which do not permit the calculation of oceanographic parameters with an accuracy which satisfies users.

a) Sea-surface temperature. The existing methods of short-range sea-surface temperature forecasting are based on calculations of heat balance components of the surface. In further investigations the role of different factors (advection, stratification) was revealed. However, the application of results from such advanced studies is practically difficult due to the absence of necessary observational data. A similar situation exists in methods of forecasting the vertical temperature profile which are based on initial data (sea-surface temperature distribution in the vertical), heat inflow through a surface and the atmospheric pressure field over sea.

Long-range forecasting of sea-surface temperature is based, as a rule, on empirical relationships of sea-surface temperature with air temperature and atmospheric circulation; during the cold season convective mixing is taken into account.

It should be noted that lack of initial data is handicapping the introduction of advanced numerical models of forecasting/calculating the oceanic thermal structure into operational practices.

b) Sea conditions. Prognoses of sea condition field are being compiled both by the synoptic-statistical method (calculating the surface pressure from prognostic charts) and on the basis of the spectral theory of waves. The skill score of issued forecasts is highly dependent on the forecast of the pressure field and ranges as follows: 84-92% for 24-hour forecasts and 76-84% for 48-hour forecasts. Taking into account the low quality of sea condition observations and the skill score of surface pressure field prognoses which do not exceed 85-90% for the first day, the results obtained may be assumed acceptable.

c) Sea ice. Present-day methods for sea ice forecasting are based on accounting heat losses by sea and the adequacy of heat supply i.e. on the balance method. This method yields good results in short-range forecasting (up to 5 days) the appearance of sea ice in coastal waters.

Long-range sea-ice forecasts are based on accounting the heat content of the active layer and on the rate of its cooling. Account of these components is performed either by calculation or using empirical relationships. The empirical methods take into account the heat content of sea by the sum of degree-days of heat, the rate of cooling - by the index of atmospheric circulation, or by the frequency of occurrences of wind and air temperature for the period preceding sea ice formation. Some other signs are used as well: sudden changes for autumn and for the pre-winter period, cold waves, years= analogues, course of air temperature, residual ice cover percentage.

Recently methods of sea-ice forecasting have been developed based on solution of hydrothermodynamic equations, but this methods still remain in the stage of research.

The main shortcoming of methods for long-range forecasting sea-ice conditions is their dependence on long-range weather forecasts (air temperature and wind) the verification score (skill score) of which remains low. Therefore various indices of hydrometeorological processes are being introduced into prognostic relationships which take into account indirectly expected synoptic processes (sequence of weather). Finally it should be noted that methods of long-range sea-ice forecasting used in operational practices do not fully meet the requirements of marine activities.

d) Surface currents. The first papers devoted to forecasting of surface currents demonstrated that in developing methods for surface current forecasting one encounters two serious difficulties:

- lack of knowledge of surface current regime and
- unavailability of surface current data.

Thus, the complexity and insufficient knowledge of surface currents demanded data obtained from theoretical investigations to be used in calculation and forecasting of surface current fields.

However for local regions, statistical relationships between surface currents with wind, pressure gradient and atmospheric pressu-

re field have been developed. Efforts in the theory of sea surface currents have been developed along three directions:

1) Ekman's theory and its generalizations;
2) Horizontal circulation theory;
3) Theory of the baroclinic ocean.

On the basis of Ekman's theory one can calculate the steady-state surface current, caused by a homogeneous wind field in a boundless sea of a constant depth. Results obtained make it possible to have a general idea on the character of drift, gradient and convective components of the complex picture of actual sea surface currents.

On the basis of the theory of the horizontal water circulation in the ocean a method has been developed for calculation of total fluxes of momentum which permits to calculate the horizontal circulation from the wind field.

The baroclinic ocean theory makes it possible to calculate the velocity field from the given wind and density fields.

e) Sea level. Methods of forecasting non-periodical sea-level oscillations being utilized in operational practices are based on the relationship of sea-level oscillations with meteorological factors. In this case, the sea is considered as a dynamical system, characteristics of the wind field - as a forcing random function, while sea-level oscillations - as the response of the system. Thus, giving the wind field as a function of time one can determine sea-level oscillations. In practice, relationships of sea level with local wind, pressure gradient and atmospheric pressure are being used.

Long-range forecasts (for 1-5 years) of sea-level changes are based on the water balance equation and on indices of atmospheric circulation.

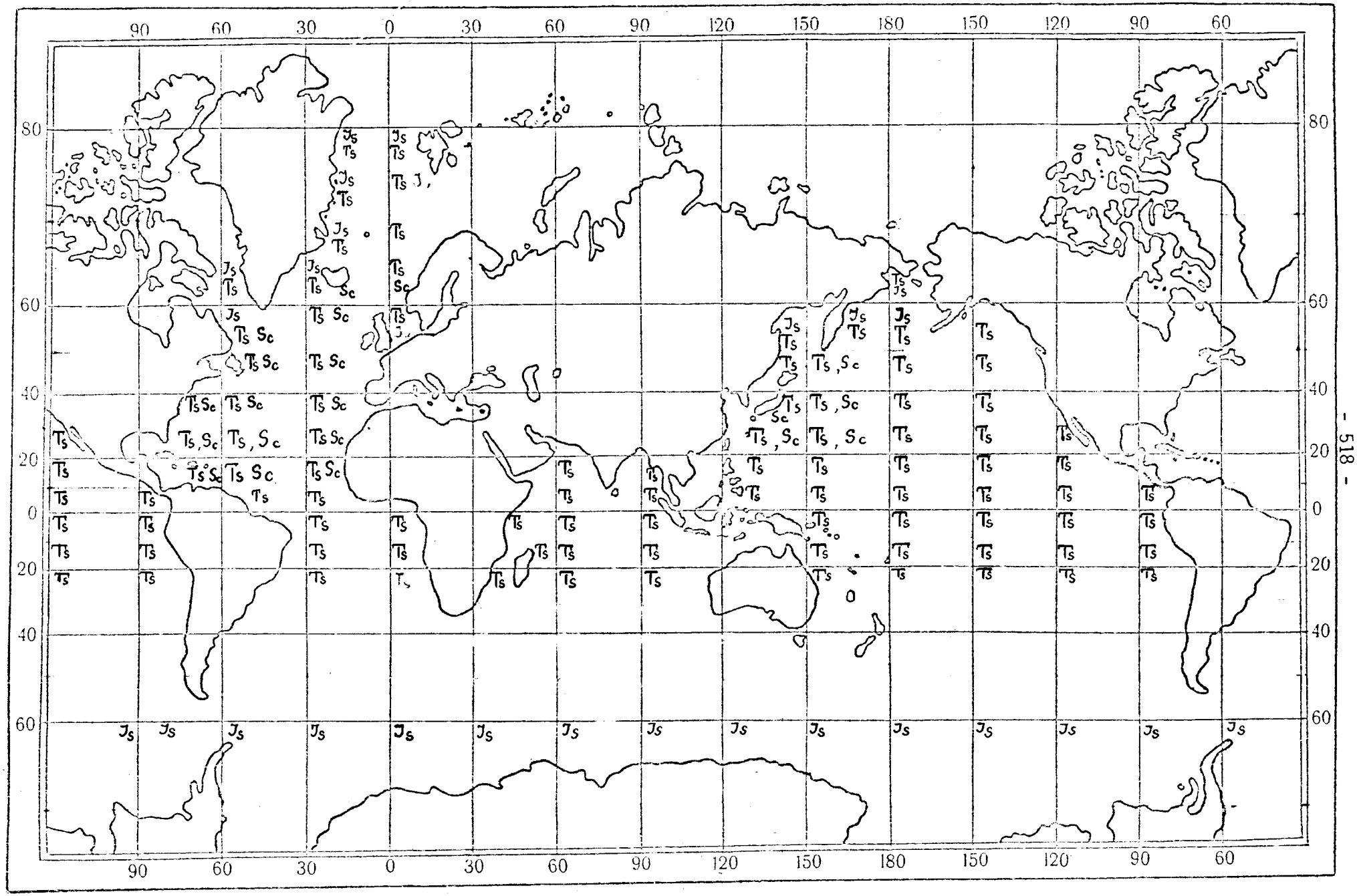

Figure 1 - (T_S - surface temperature; S_C - sea conditions; J_S - ice conditions)

The need of minimum data densities for the preparation of products and connected problems

By

Hans Walden

Summary

For most oceanographic products a certain minimum number of measurements is needed unless the observation of a whole ocean area (by satellite) is available or usable. This is also true of most products which are to serve operational purposes. Otherwise, the needed isolines could not be plotted which is mainly done by interpolation.- It is shown that the minimum data density depends on various factors: the required accuracy and the resolution of the product, by its purpose, by the length of the acceptable "synoptic interval" and by the representativity of a measurement which in turn is affected by the location with regard to boundaries of water masses; these factors can, moreover, vary for the different parameters. A survey of the necessary data densities in the various IGOSS branches is given. In discussing the question if minimum data densities can be defined examples of analyses and corresponding data densities are presented. The rôle of data with regard to numerical models and the influence of models on the need of data is shortly discussed.- The problem of the required data densities should be studied through a special scientific investigation.

The need of sufficient data for the preparation of analyses

On the basis of a very great number of single observations and single measurements which have been collected during a very long period of time we dispose of a survey on the average distribution of the most important oceanographic parameters in most sea areas of the earth at the time being. Their periodical fluctuations are also known to a great part, especially the seasonal cycles. Moreover, we know somewhat about the differences along rather small distances, for example those connected with micro-scale processes, but such knowledge is confined to certain selected sea areas. Furthermore, we know something about the effect of atmospherical phenomena and their flucatuations on the sea, and that not only at its surface, but also - to a certain degree - in deeper layers of the oceans.

However, for practical operational purposes whose characteristic feature it is to make a choice between two or frequently more operational possibilities and where it is desirable to determine the most favourable conditions for this decision, e.g. for ship routeing, pollutant transport, location of fish species to be harvested etc., one needs a good knowledge of the medium- and small-scale variability of oceanic processes and parameters; not enough with that: In order to be able to select and utilize the optimum conditions one needs - on a regular basis, their spatial distribution in the very presence and, much better, in the future.

For several operational purposes the presentation of the parameter pattern within an area at the surface will do; in other cases of application the third dimension, depth, will be needed. Climatic, i.e. average data, have a much confined value for present-time operational actions at sea. An example: A ship wishes to utilize a river-like current in the ocean, such as parts of the Gulf Stream, in an optimal way. As the current is meandering and, moreover, changes its course and as the positions of the meanders change as well, the ship's navigator wants the actual location of the current's core.

For perceiving these actual deviations from the average state of the ocean one single oceanographic measurement is of little help, because the representativity of such a single datum is restricted to a certain circuit, the size of which differs for the different oceanographic parameters.

In order to provide the needed distributions, i.e. products in the form of charts, cross sections and similar analyses, more than one single measurement is required. It is the decisive advantage of the availability of some various or a great number of single data that, between them, interpolation might be possible. Whether this is allowed or not depends on the distance of the observations. It is a difficult problem how far from each other those data can be located, so that interpolation yields realistic results. With a negative undertone one could also ask how uncertain inter- and extrapolated sections in such analyses are.

The influence of models on interpolation procedures will shortly be dealt with in a later section.

In this context another aspect is important: It is the question what accuracy the user requires for the information about the state of the interesting part of the ocean. For instance, for one purpose water temperature may be needed as precise as $\frac{1}{100}$ degree, but for other practical goals a 0.5 degree accuracy will certainly be sufficient. On principle similar examples could be given with respect to currents, ocean waves, water density etc. Accuracy is strongly related to the resolution of an analysis. Thus, the necessary minimum spatial distance of isolated data or - in other words - the minimum density of measurements is a function not only of the representativity but also of the resolution and of the accuracy demanded.

Next, there is also the problem of the simultaneousness (one could perhaps initiate the word "synopticity") of data. Many oceanographic processes take place slowly so that the tendency of conservation is rather great - with exception of all phenomena connected with tides. Therefore, the demands for simultaneousness of

data are not so severe as in synoptic meteorology, and the time interval within which data are considered "synoptic" should be permitted to be comparatively long. For example, the weekly SST charts of the Deutsches Hydrographisches Institut for the North Sea apply to data which originate from all seven days of the week (however weighted of course). Without the amplification of the "synoptic interval" the temperature data would, at least partly, not be located densely enough for the elaboration of the analysis.

It may be mentioned here that, on the open oceans, the representativity of the meteorological parameter being important for synoptical work is higher than that of the oceanographic ones. Thus, in many cases, weather maps can be prepared without a high spatial density of observations.

The spatial data density in the various IGOSS branches

What rôle does the areal or spatial density of data play in IGOSS ? IGOSS encompasses some various components or branches for which the situation regarding the data basis is quite different. Let us differentiate as follows:

1."Near-real-time" branch of IGOSS

1.1. One component consists of operational IGOSS projects within the scope of large scientific multi-ship cruises. IGOSS products can influence the research work. Frequently the measuring stations (ships, buoys, moorings etc.) may be located so close to each other that synoptic products can be afforded.

1.2. As another component the operational IGOSS can be considered, with emphasis on oceanographic sub-surface products and services which is thought to yield benefit to users in the fields of fishing, shipping, pollution monitoring etc. Generally, a benefit will be attainable only if the distribution(pattern) of the parameters of interest can be made available. This means that a certain minimum data density is indispensable for the preparation of useful products. This is not the case in most sea areas up to now. Special measures must be taken to improve the density; one of them is the concentration of measurements to selected sea areas.

1.3. Operational IGOSS for surface parameters can yield benefit for a variety of users. The data situation is rather favourable, because this IGOSS component can operate on the basis of the observational system of the WMO. In future, moreover, satellites will provide additional measurements which will embrace parameter patterns over large areas by means of one "image" or in a very short time.

2."Non-real-time" branch of IGOSS

2.1. In some marine research activities such as the FGGE (First GARP Global Experiment) oceanographic data are needed as a necessary auxiliary means when deriving scientific results. Here, the IGOSS data will mainly not be used before the end of the field experiment. The benefit of these ad hoc measurements is ensured. As many ships, buoys etc. participate, the data density can be influenced and correspondingly made sufficient.

2.2. In any case, IGOSS activities lead to "climatological" results so far as the data are collected during a very long time. The data density will increase rather steadily and will, after many years, be sufficiently high to render improved "hydroclimatic" products.

2.3. Another component of IGOSS serves medium and long-range weather forecasting. It consists of activities through which the large-scale distribution of near-surface parameters can be controlled and special extended anomalies be discovered. Although this component has an operational background, a real-time transmission or immediate collection of the relevant data is not considered necessary at present. A certain density of measurements is indispensable but even a few rather scattered data may be useful for numerical models and the subsequent forecasting.

Summarizing the statements about the data bases of the different IGOSS components one can say:

In 1.1 and 2.1, the data density can be managed,

in 1.3, the situation is favourable,

in 2.2, time leads to the necessary data density,

in 2.3, the data density is mainly orientated along meteorological aspects,

but in 1.2, the density is insufficient.

With a view to this latter statement, let us cast a glance at the BATHY-TESAC programme of IGOSS: On the whole, considerable numbers of BATHY-data have been available for some time. These data, however, are scattered nearly arbitrarily over some parts of the world ocean. Although there is some self-evident concentration of data along shipping lines, the data are so scattered that - with a few exceptions - it is not possible to prepare useful products.

Figure 1 is taken from the Joint IOC/WMO Circular Letter No. 78-49 of 18 October 1978 and shows the number of BATHYs per 10 degree areas, as they were received by the Deutsches Hydrographisches Institut, Hamburg during the first half-year 1978.

With the exception of four "squares" (two in the Gulf of Alaska, the other two in the northwestern Atlantic) the half-year totals lie below 500. 520 BATHYs, however, correspond to 20 BATHYs per week, on an average, and that in an area of 10° x 10°. Would these 20 BATHYs be distributed equally (regularly) there would be one single BATHY per 5 one-degree areas, or, in mid-latitudes, in a field of ca. 100 to 120 naut. miles. However, a total of 104 BATHYs, as e.g. approximately in the 10-degree area west of Gibraltar, yield only 4 BATHYs per week in this "square" or, correspondingly, one in a field of ca. 250 to 300 naut. miles. This is not sufficient to perceive the smaller, but frequent, spatial differences.
The lack of a sufficient number of data which can be referred to each other in a reasonable way, i.e. in a way which permits reliable interpolation is, in my opinion, the main reason for the lack of useful sub-surface products. In other words: The condition of minimum data density is not fulfilled.

Can a minimum data density be defined ?

It was explained before that, for operational applications of IGOSS products, "patterns" or "spatial distributions" of the oceanographic parameters are required. The means for presenting such distributions are usually isolines, in the three-dimensional space isoplanes. They are, of course, based on data and are drawn by interpolation.

It has been stated further that reliable interpolation requires a sufficient number of data which can be brought into a mutual reference. As this condition depends, inter alia, on the distance from each other, the minimum data density already repeatedly mentioned is necessary.

The question comes up: How can this minimum data density be defined ? To give a valid answer is very difficult due to the fact that the resolution of the analysis and the needed accuracy of the product affect such a density. The treatment of this combined problem would go far beyond the scope of this contribution and requires a special scientific investigation. Thus, I shall confine myself to considering the relation between minimum data density, mutual distances of measurements or data and, correspondingly, spatial (or area-related) differences of the parameters.
The latter ones are related to the parameter gradients.

These gradients are very different in the marine environment. For most parameters they are small within one and the same "water mass" and become extremely high in the neighbourhood of discontinuities or fronts in the ocean.

Far away from areas with strong gradients the representativity of one datum can be so great that the measuring stations can be located far from each other. In many (aero-)climate zones important

changes with time will also take place in a rather uniform way.

IGOSS has well taken into account the uniformity and small variability within distinct water masses when the positions of the IBON network were established.

On the other hand, in the vicinity of fronts, strong currents, eddies or whirls and where these phenomena use to change rapidly and frequently their location, a high density of data is indispensable.

This is a very simple and general statement, but it shows that the localization of measuring stations should not, if possible, be left to chance or planned along a schematic grid with uniform distances.

Looking into the FAO publication of "Environmental Analyses in Marine Fisheries Research", edited 1977 by Dr. G.H. Tomczak, one realizes that a great deal of analyses of various oceanographic parameters are already regularly prepared and disseminated. Most of those reprinted there contain isolines or fronts. Therefore, a considerable experience will exist on the representativity of isolated data for the various parameters.

A view onto some of the analyses represented in the FAO document may give a first idea of minimum data distances. Fig. 2 shows the surface isotherms (^{o}C) east of Australia in October 1973. Note the strong temperature differences along the 33th parallel of latitude, east of Newcastle, and compare with the SST distribution in September 1974 (Fig. 3). For perceiving such changes and differences below the sea surface, measurements at distances of less than 25 naut. miles are necessary.- Fig. 4 gives the distribution of SST in June 1974 east of Japan, elaborated by the Japanese Fisheries Information Service. If the resolution is considered sufficient, data distances of approximately 30 naut. miles are required.- Next figure (Fig. 5), also taken from the FAO publication mentioned and originating from OSTROM, contains SSTs in the Gulf of Guinea in July 1975. In order to perceive the different gradients one needs data distances between 10 and 20 naut. miles.- The cross section Honolulu - San Francisco (Fig. 6), ca. 1800 m long, observed in May 1976 by a US ship, is based on 29 XBT measurements whose distances to each other are in the vicinity of 60 naut. miles. Resolution and accuracy have apparently been considered sufficient.- Fig. 7 shows the copy of an SST chart for the North Sea, prepared by the Deutsches Hydrographisches Institut. The observations with whose help the isolines were drawn are included so that the observer can get an impression of the relation between the data distances and isotherms.- Fig. 8, also prepared by the Deutsches Hydrographisches Institut, presents anomalies of actual SSTs from a long-term average in the North Sea. The differences of $2^{o}K$ in the centre of

the North Sea indicates that data distances (or densities) of ca. 30 naut. miles are highly desirable.- Near the coast, especially where strong tidal currents use to run, and in upwellig areas strong hydrographic gradients and patchiness are to be expected so that a high data density must be demanded.

Other parameters than temperature may have quite deviating representativities. In Fig. 9 a mixed layer depth analysis of the US National Marine Fisheries Service for the eastern tropical Pacific is shown. It is an example of small resolution.-

Currents are frequently closely related to water masses; however, their distribution may largely differ from that of temperatures.- Ocean waves and the water level hardly depend on water mass properties so that the necessary data densities are ruled by factors which vary from those for the temperature. Fig. 10, a French product, also copied in the FAO document, is a sea state chart for the North Atlantic. Finer details are not discernible. However, one must be aware of the fact that near coasts, islands, shoals etc. the ocean waves can locally be extremely different; their representativity there is very small.

Data situation in the case of models

Mainly considering water levels and their prediction, W. Hansen defined "Wirkungspunkte" or (translated) "sites of effect". A "disturbance" occurring at the location of the "Wirkungspunkt" also appears, somewhat altered, in other areas of the ocean after some time. For predicting water levels at the German North Sea coasts by means of his hydrodynamic-numerical (HN-) models, Hansen needs, in order to take into account the long so-called external waves which enter from the Atlantic into the North Sea, only water level readings from one distinct location east of Scotland and, moreover, wind data from certain portions of the North Sea, but not from the whole North Sea. However, this "remote effect" is, as I see it, applicable only with water waves of a certain minimum length.

For several years, however, well experienced and fairly approved models serve as a tool to facilitate and improve the interpolation procedure of some oceanographic parameters so far as sufficient meteorological data are available. Hereby, the higher representativity and better interpolation suitability of some meteorological parameters are utilized. Basing on the usual peculiarities of the current pattern, current models can render information on how many measurements are at least necessary and at which geographical locations. For example, such a model for the German Bight (southeastern North Sea) needs current profile data from 3 locations which are situated ca. 40 naut. miles from each other and 30 to 40 naut. miles apart from the coasts. (Of course, it is the final goal of these

models to compute and predict the current pattern without any oceanographic measurements, merely using meteorological data.

However, such successfully approved models are not available in most parts of the ocean and not at all for all oceanographic parameters.

Final remarks

Thus, the problem of the data density as a basis of products for operational purposes has to be solved. As the necessary minimum density depends on several factors, it is a very complex problem. We remember from the statements made before, that the optimal or minimum data density is influenced by the required accuracy and the resolution of the product, by its purpose, by the length of the allowed "synoptic interval" and by the representativity of a measurement which in turn is affected by the location with regard to boundaries of water masses, and that it can vary for the different parameters. This great number of effects necessitates a special scientific investigation on the determination of the minimum data density. It is suggested that the meeting recommend to the Joint IGOSS Working Committee to ask IOC and WMO to take steps for the performance of such an extensive study.

Literature

W. Hansen, Über den Entwurf ozeanographischer Stationssysteme. Mitt.Inst.f.Meeresk. Univ.Hamburg, Hamburg 1970.

List of Figures

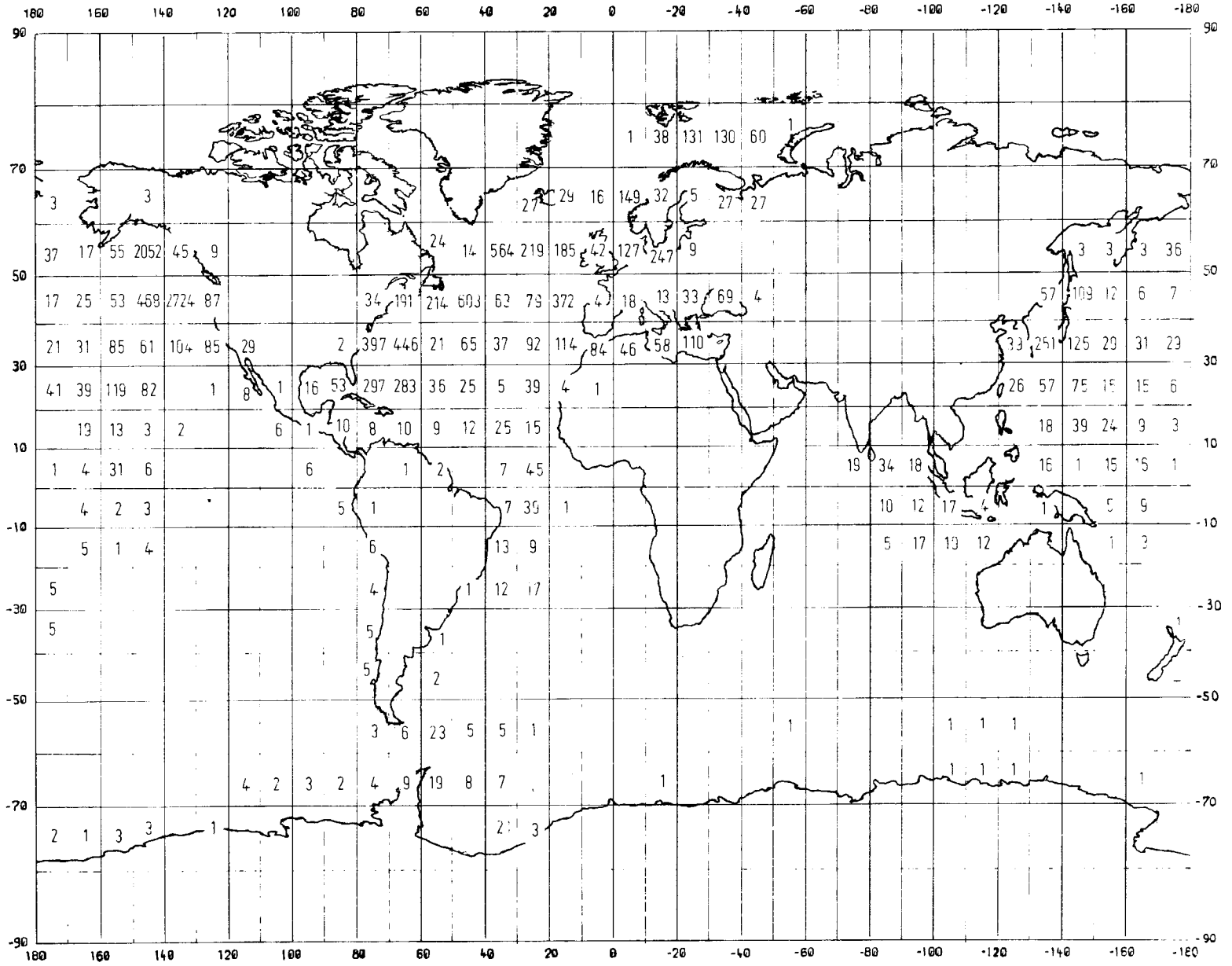

Geographical distribution of BATHY/TESAC reports received at the Deutsches Hydrographisches Institut from January to June 1978

Fig.1

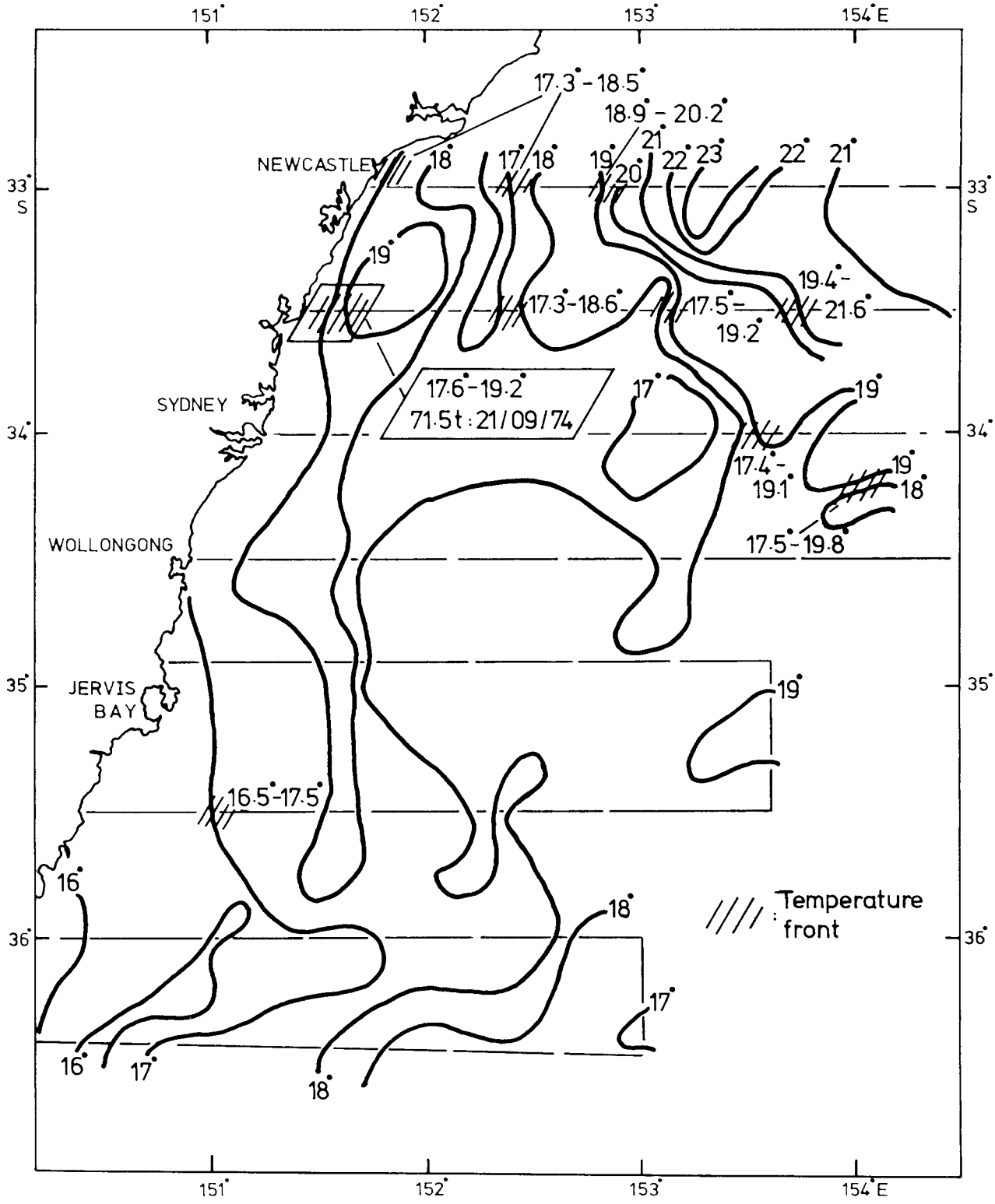

12. Aircraft flight paths and surface isotherms (°C), with tonnages and dates of Bluefin Tuna catches. 18-19/09/74

Fig.2

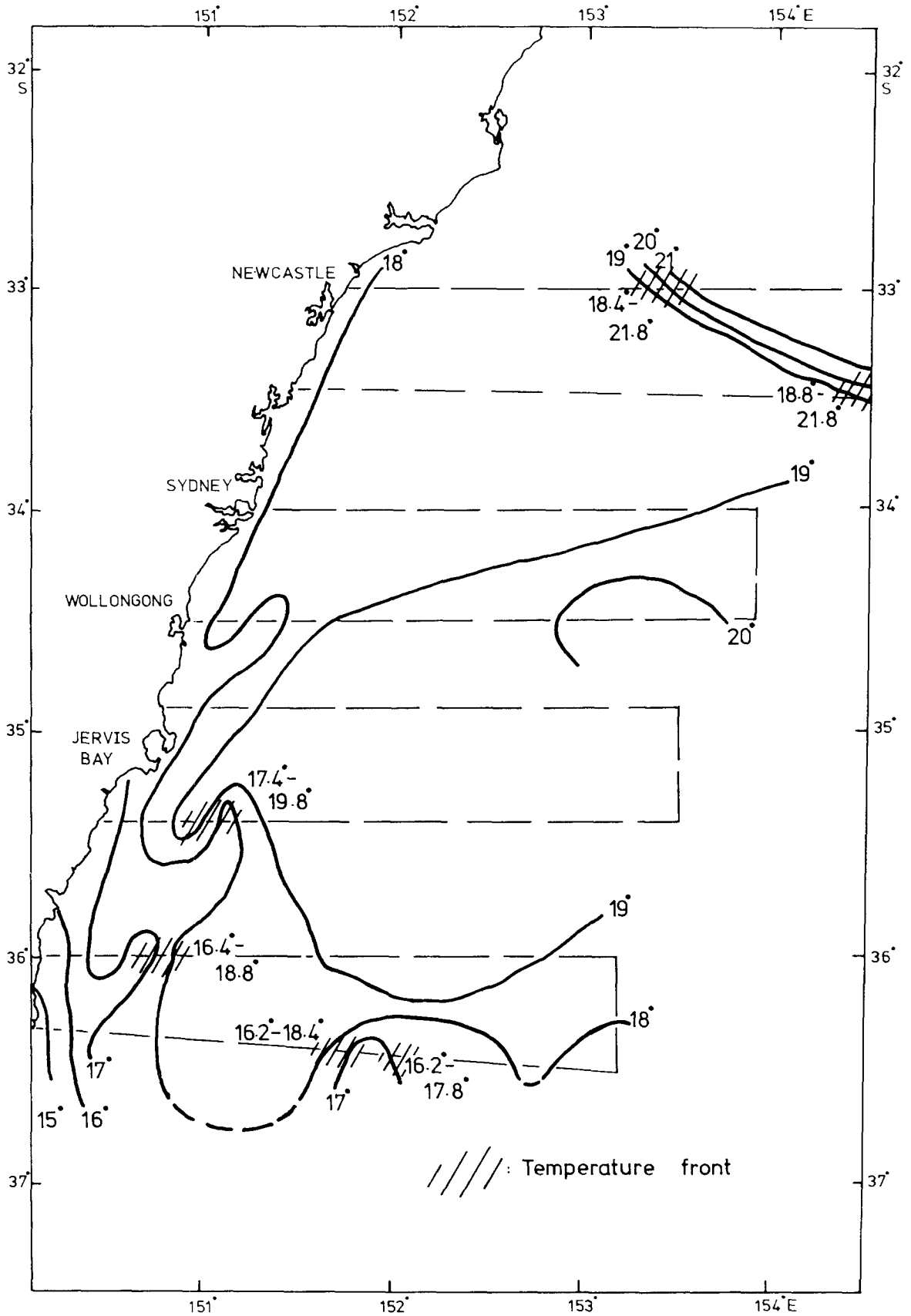

6. Aircraft flight path and surface isotherms (°C) 2-5/10/73

Fig.3

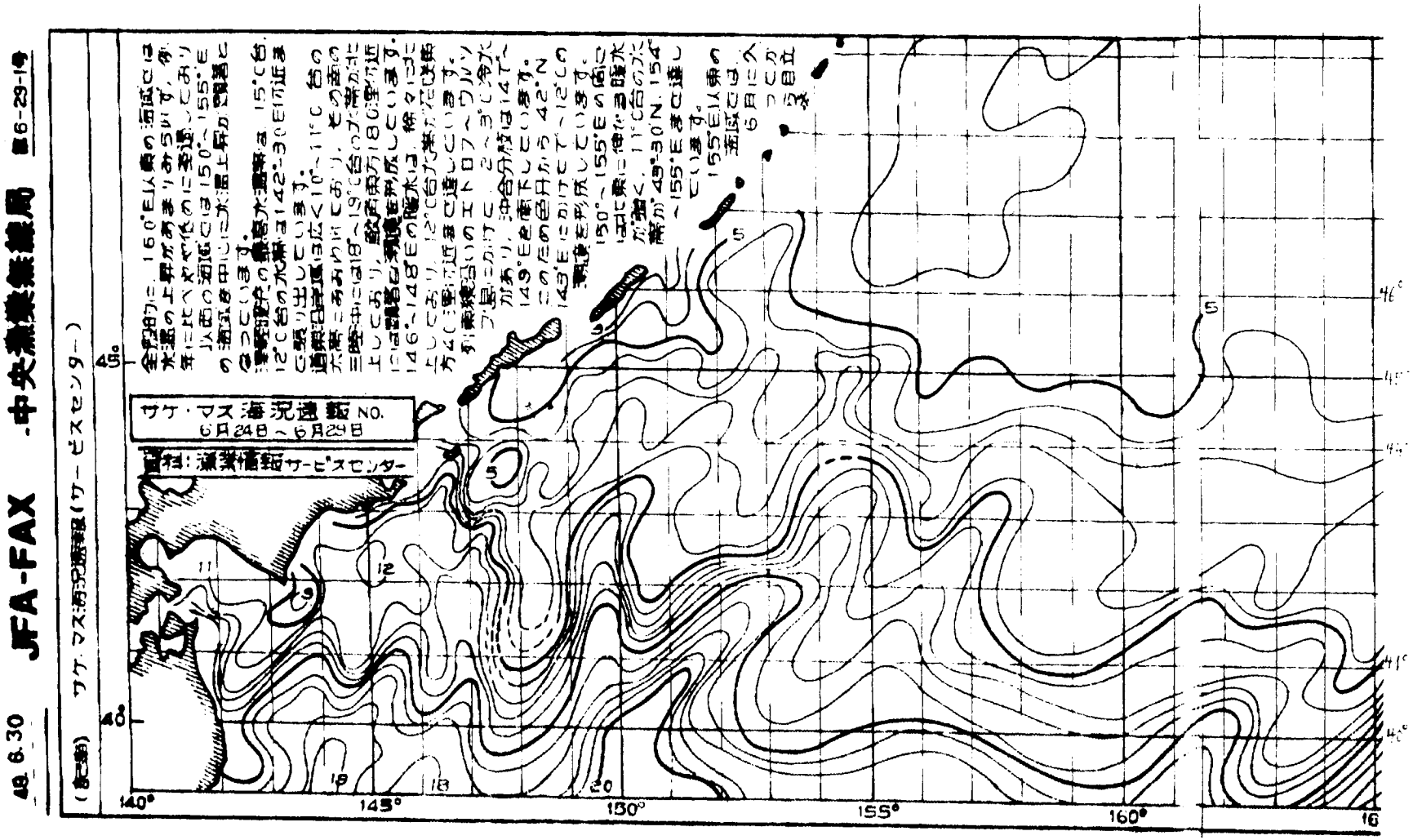

Figure 4: MAP C, Western North Pacific Ocean (Excerpt only: the original map covers the area from 140° to 180°E; for translation of Japanese text see Annex I)

Fig.4

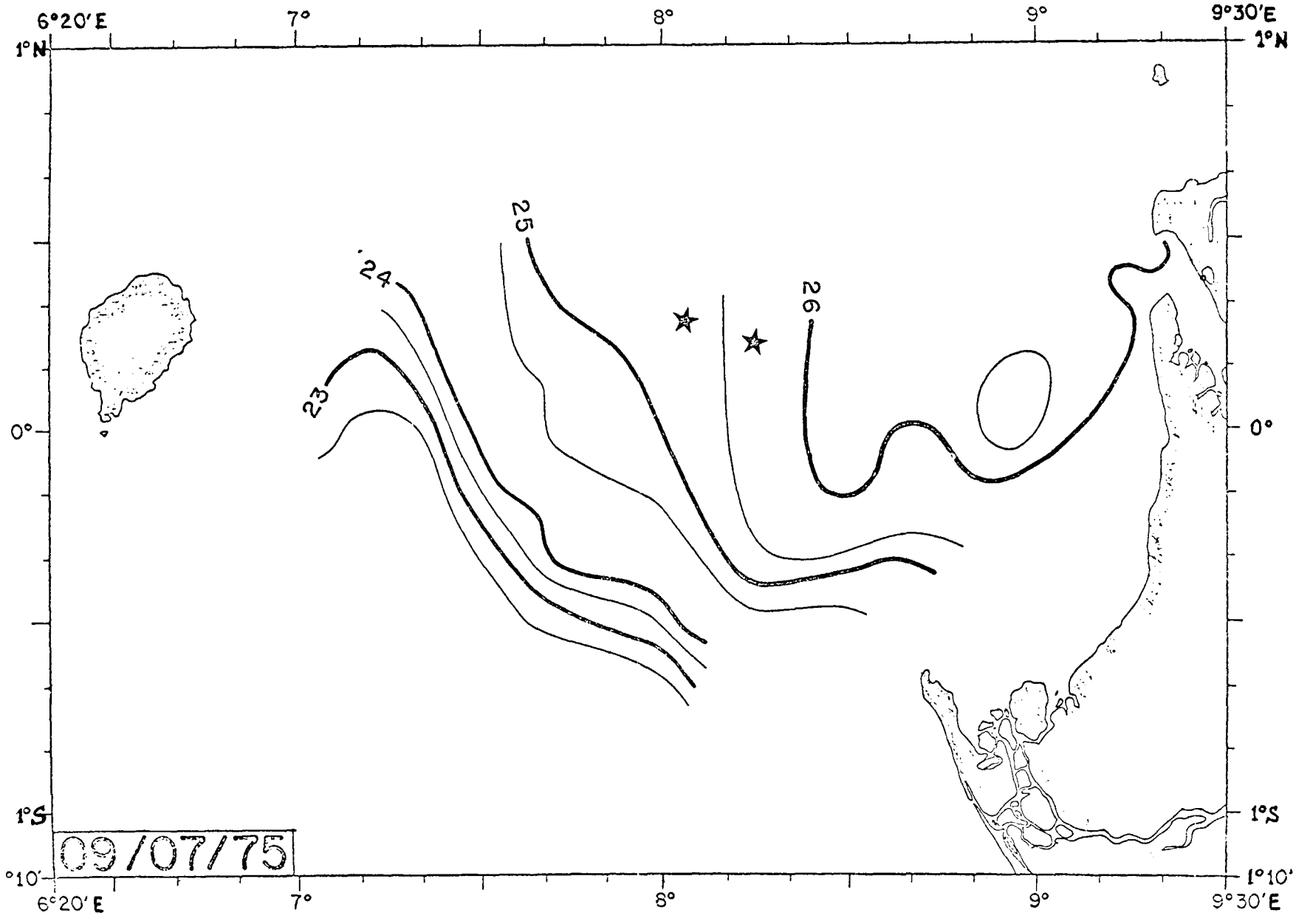

Figure 1: Sea surface temperature map for the Gulf of Guinea, 9 July 1975
(* = location of tuna fleet)

Fig.5

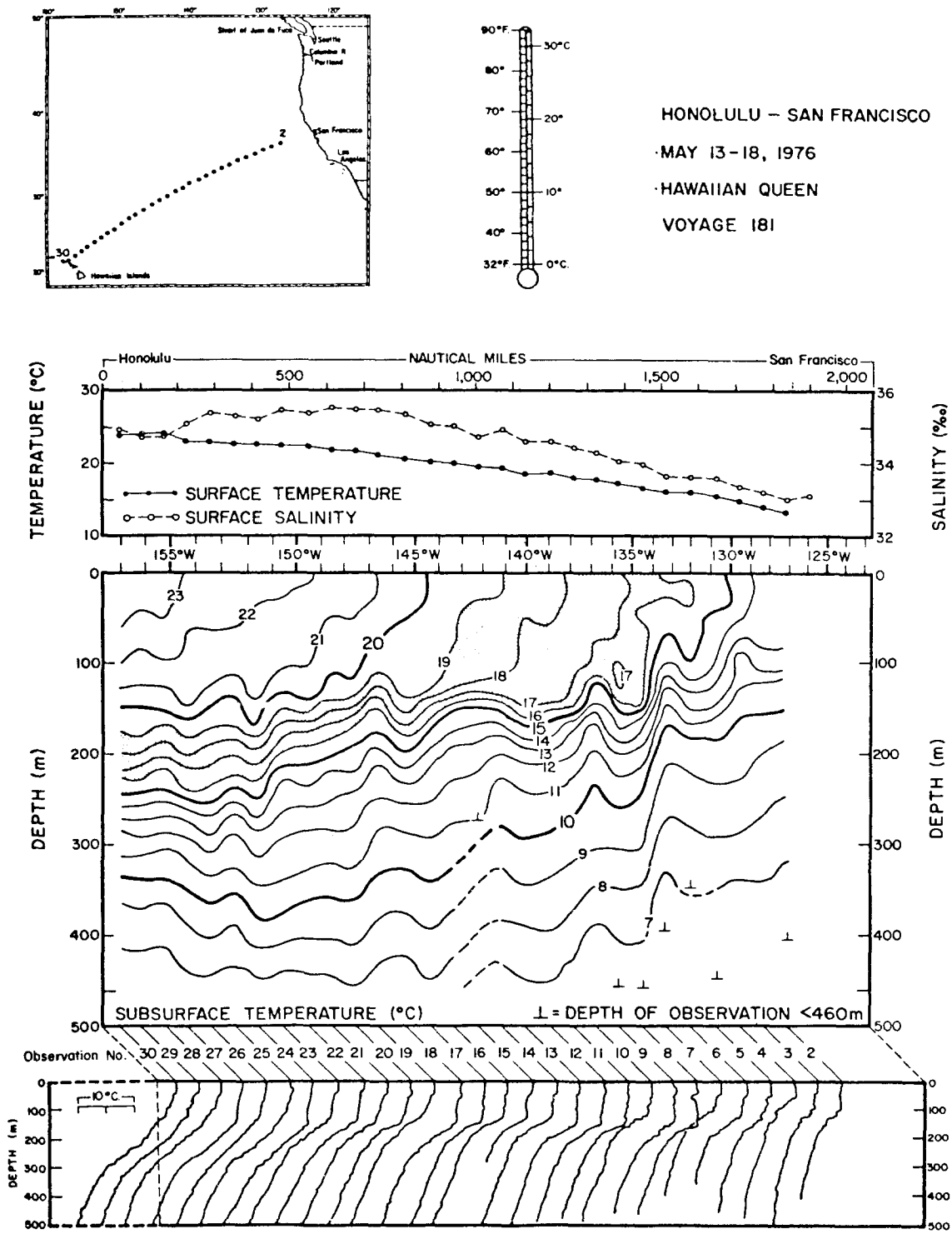

Figure 2b. Surface temperature and salinity and subsurface temperature structure from expendable bathythermograph observations between San Francisco and Hawaii.

Fig.6

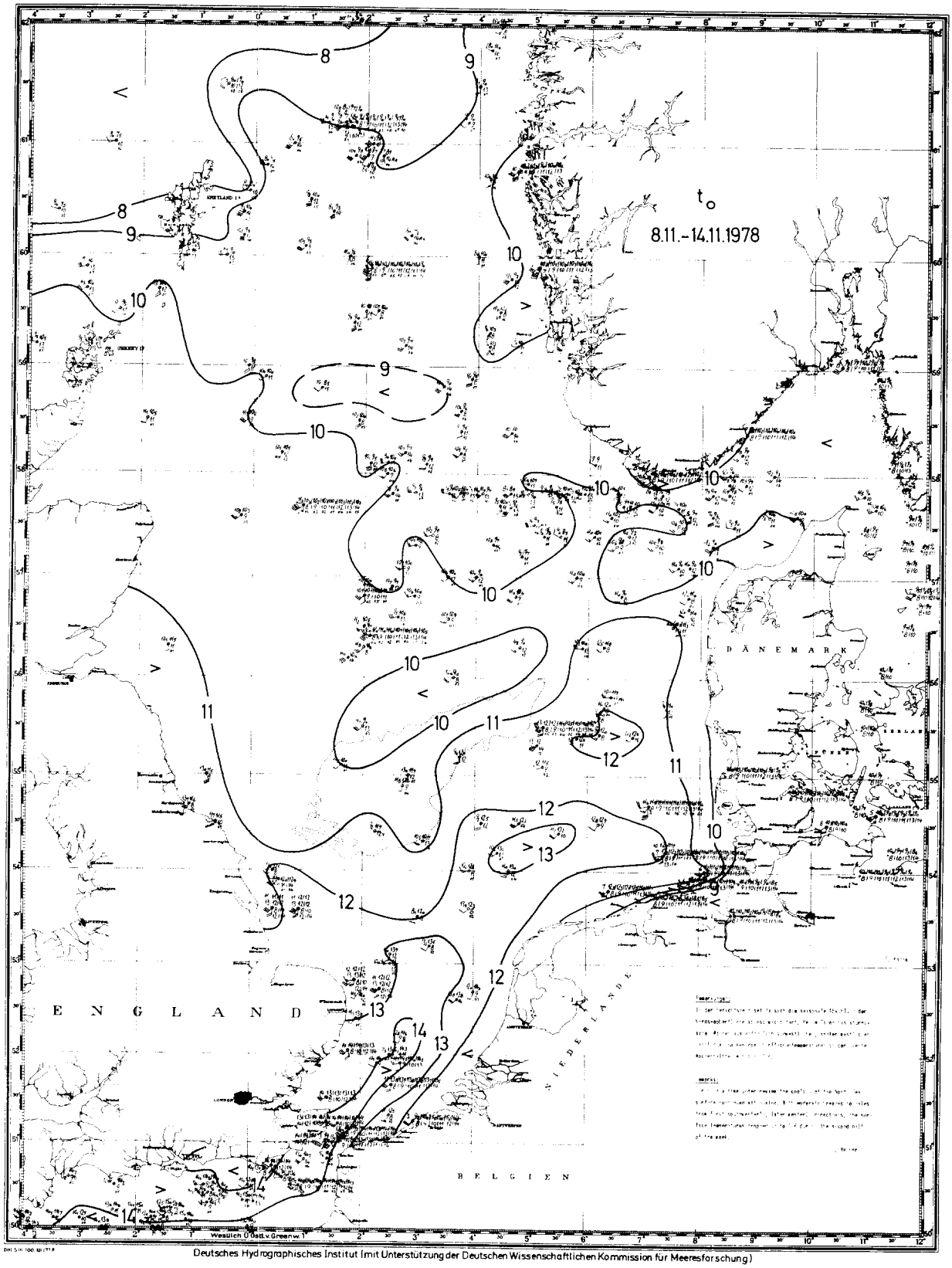

Deutsches Hydrographisches Institut (mit Unterstützung der Deutschen Wissenschaftlichen Kommission für Meeresforschung)

Fig.7 SST Chart North Sea (data reports entered)

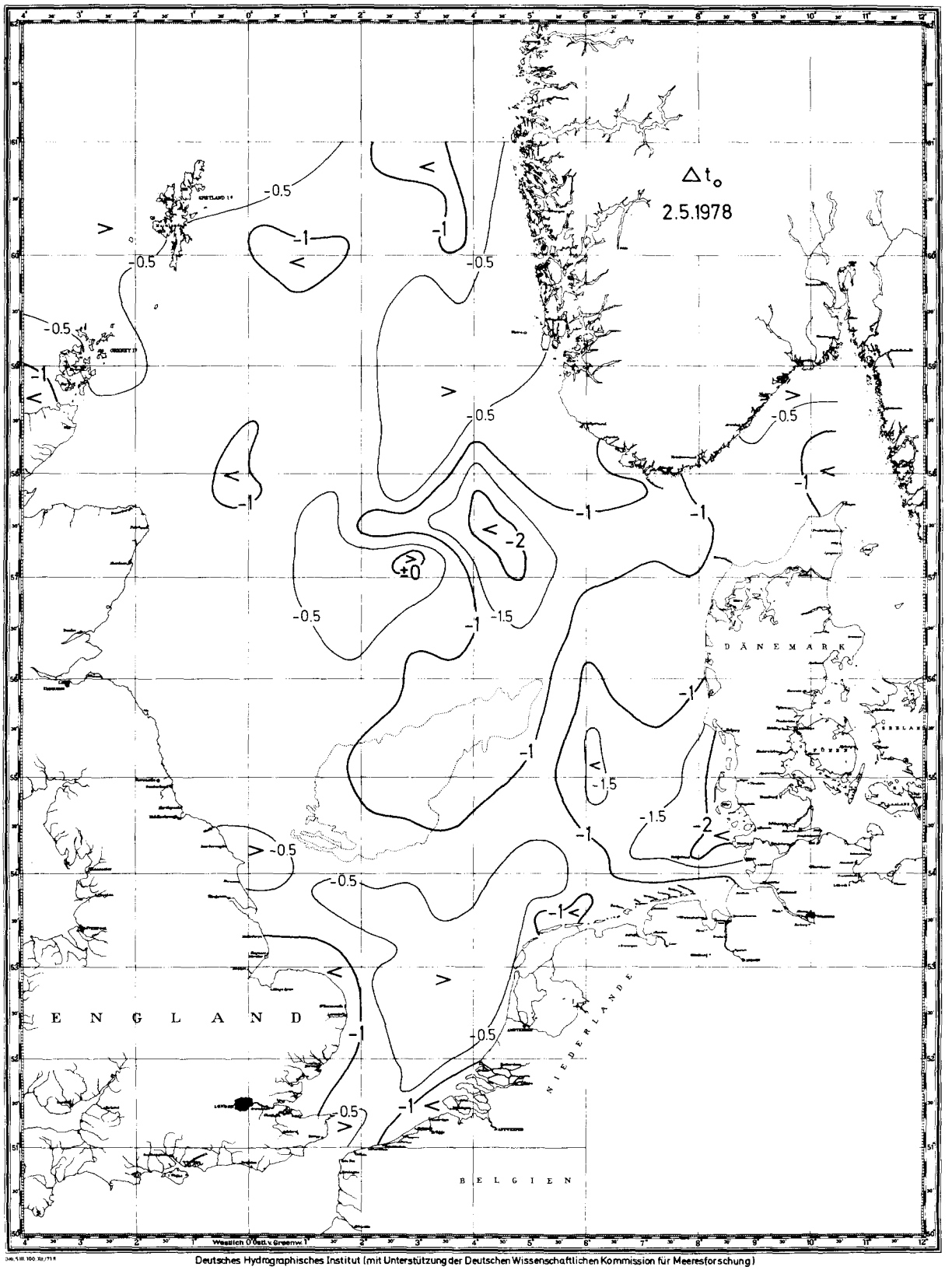

Fig.8 SST Anomalies North Sea

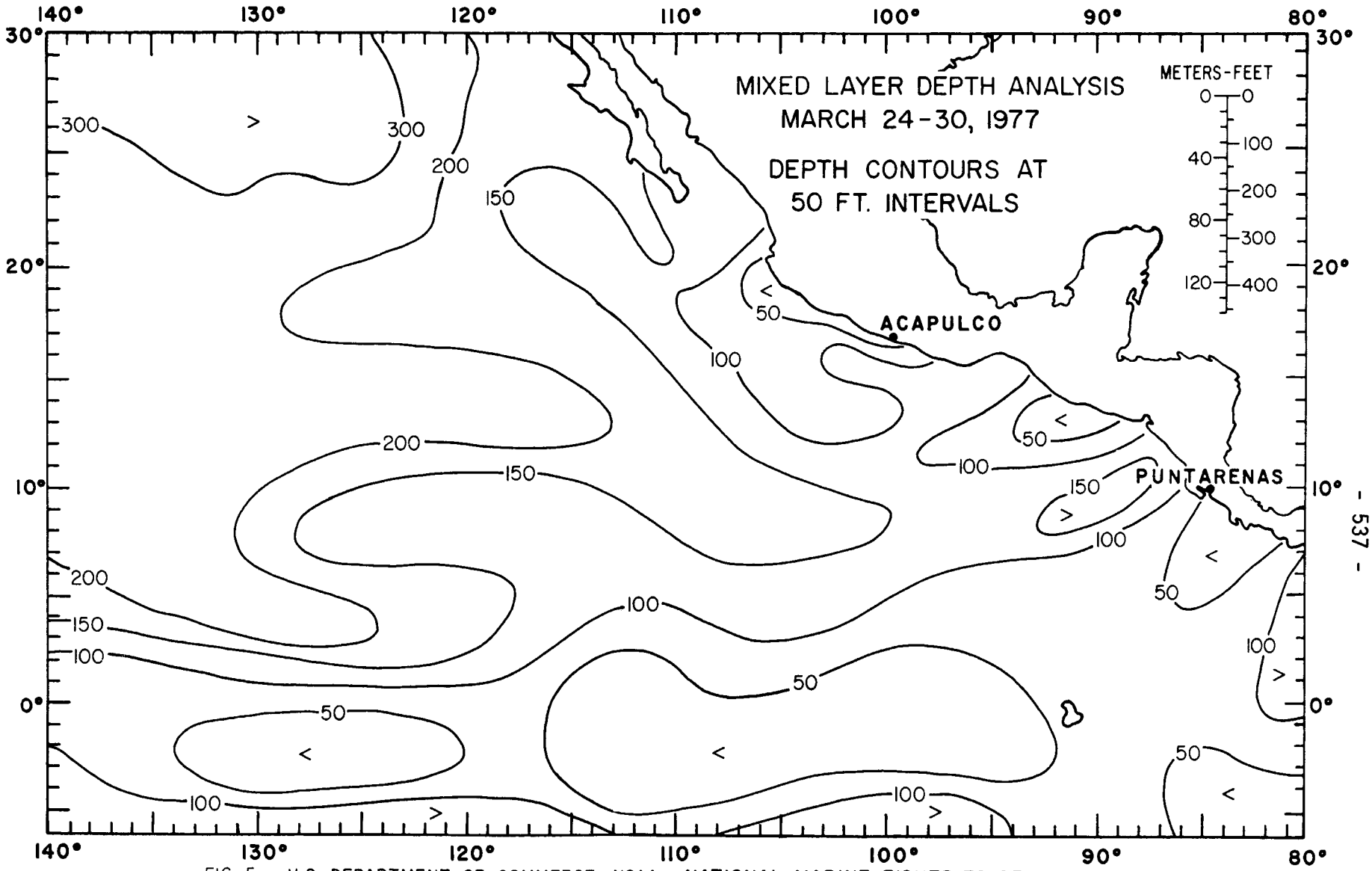

FIG. 5 : U.S. DEPARTMENT OF COMMERCE, NOAA NATIONAL MARINE FISHERIES SERVICE, FOC La Jolla, Calif.

Fig.9

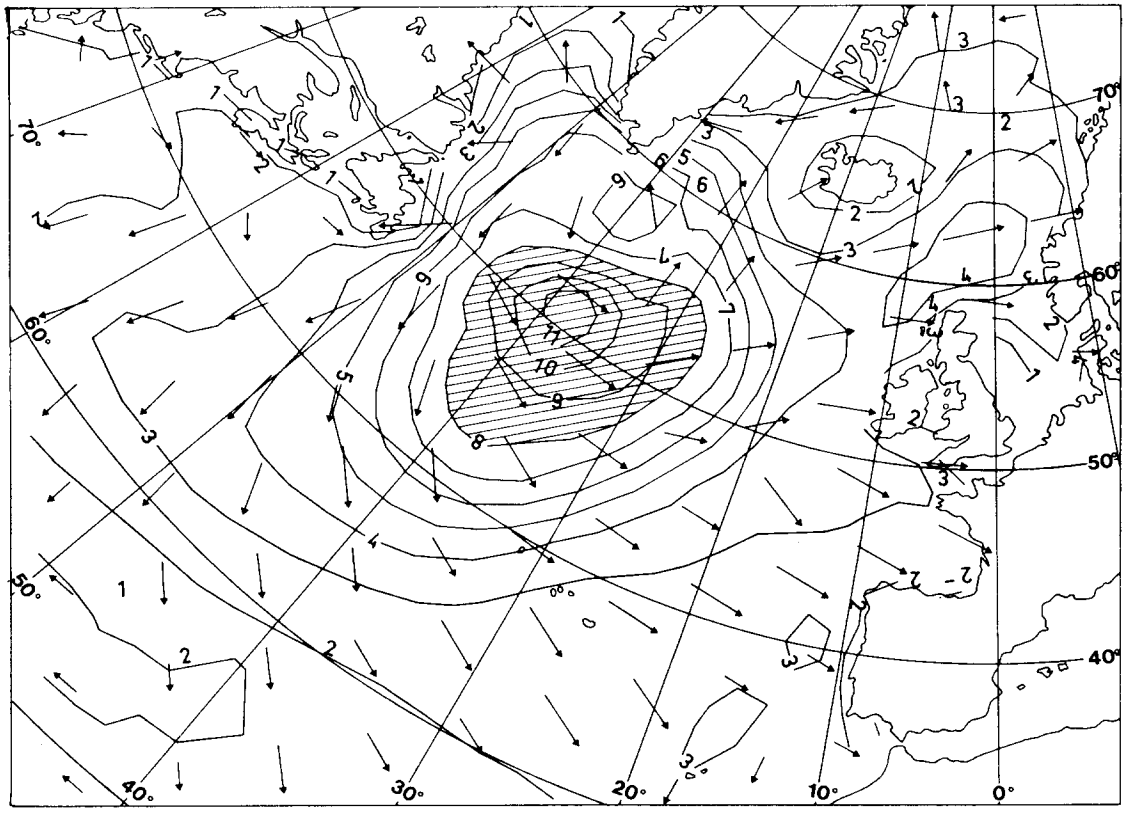

Figure 4: Chart showing the sea state in the North Atlantic Ocean on 15 June 1976 prepared by the French Meteorological Service for the facsimile distribution (Figures = wave height in metres; arrows indicating wave direction and, by the length of arrows, wave period). (Document Météorologie française)

Fig.10

TESTING ASSUMPTIONS OF THE WIND-DRIVEN GENERAL CIRCULATION IN THE INTERIOR OCEAN

by

Warren B. White

and

Stephen E. Pazan

Scripps Institution of Oceanography
La Jolla, California 92093
(714) 452-4826

and

Robert Haney

Naval Postgraduate School
Monterey, California
(408) 646-2308

1. It has been about one hundred years since the Challenger undertook "to investigate the physical conditions of the deep sea...in regard to...temperature, (and) circulation..." (Ritchie, G. S., 1957). Since so little was known about the ocean at that time the procedures used by the Challenger were exploratory in nature. This methodology has persisted pretty much intact to the present day. As enough data began to accumulate, the mean picture of the large scale temperature and circulation fields began to emerge, thereby allowing them to be modeled. Sverdrup, 30 years ago, showed that the circulation in the equatorial ocean are related to the rotational component of the wind. A few years later Munk showed that the Sverdrup theory could reproduce the qualitative features of the circulation over the entire North Pacific. This was later expanded to include most of the circulation features of the world's oceans.

Studies undertaken in the NORPAX program over the last 10 years have determined that large-scale year-to-year changes in the temperature and circulation fields of the ocean exist, have large amplitudes and are related to fluctuations in atmospheric climate. However, for the investigation of the transient ocean, it is no longer adequate to rely on the exploratory procedures developed during the Challenger era. It calls for a new approach for investigating the world ocean, involving new procedures and new tools. Procedurally, theoreticians and experimentalists must be influenced to work together in designing large-scale ocean experiments which test specific hypotheses. The results of experiments would be compared with theoretical models and then new hypotheses and new experiments would be formulated. Instrumentally, monitoring tools, such as satellite imagery, moored and drifting buoys and ship-of-opportunity expendable probes need to be developed and deployed in optimum fashion.

This utilization of monitoring tools in a process-oriented experiment is being conducted by the Anomaly Dynamics Study (ADS) in the mid-latitude North Pacific. ADS is a multi-university cooperative program within NORPAX, extending for 5 years from 1975-1980, containing both experimental and modelling components studying the transient behavior of the North Pacific Current. The ADS field experiment is investigating how the surface circulation and the structure of the main thermocline of the North Pacific Current respond to the very severe autumn/winter storm forcing by the Westerly Wind System. This is then compared to model results that depict how the North Pacific Current is supposed to respond. In this way the following hypotheses vital to the classical theory of the wind-driven general circulations are being tested:

(1) wind-driven transport moves 90° to the right of the wind, as theorized by Ekman in 1905;

(2) the thermocline is vertically displaced by the divergent action of the wind-driven surface currents, as theorized by Veronis and Stommel in 1956.

The validity of these hypotheses is not only fundamental to understanding how the atmosphere and ocean flow regimes interact on a year-to-year basis, but also to comprehending how the mean state of the general circulation is maintained. The accepted ideas that presently form the basis of ocean circulation theory state that mixing dictates the thermal structure in the surface layer (upper 100 meters) while convection does the same in the deep waters (greater than 1,000 meters). The main thermocline in between then is altered by the divergent action of the wind-driven surface currents. This latter action derives from sea-level pressure systems, whose associated winds (parallel to the isobars) push the surface waters to the right (at the surface) and thereby create regions of open-ocean upwelling or downwelling that discplaces the thermocline structure. This dynamic process is being tested.

The experimental program constitutes taking measurements for a period of five years of the surface wind-driven flow, the thermal structure in the upper 500 meters, and the surface wind and heating parameters needed to calculate the ocean/atmosphere exchange of heat, moisture, and momentum. The program also includes experiments with ocean circulation models that show how the upper ocean is supposed to respond to atmospheric forcing inputs. With the observed data, the models can be tested, hopefully confirming or disproving the hypotheses posed above.

2. The first year of the experimental program--1975--was dedicated to the design of a measurement program that would optimize the sampling rates and establish the reliability of the tools chosen for the experiment. This was essential, since an entirely new set of measurement tools was needed. Previously, following the Challenger's lead, field surveys usually utilized one or more research vessels that took a variety of oceanographic measurements in a local region for about a month at a time. This methodology is woefully inadequate for our purposes; rather, a measurement program was needed over the entire mid-latitude North Pacific, not unlike meteorological networks already in existence over land.

A new tool for measuring wind-driven surface currents was developed. It is a satellite-tracked, free-drifting buoy, containing a battery-powered transmitter whose position is monitored twice daily by the NIMBUS VI satellite for a period of up to a year-and-a-half. A new program for measuring the thermal structure of the ocean involved 25 commercial ships-of-opportunity (between North America and Japan) and Navy P-3 aircraft, each having an expendable bathythermograph (XBT) system that drops a temperature-measuring probe into the ocean while the ships and aircraft are underway. The probe relays temperature depth information back to the craft. In this way, 500 XBT probes

are deployed in the mid-latitude North Pacific each month. Another device utilized was the General Dynamics Monster buoy that measures the surface wind and surface heating parameters.

Oceanic measurements are worthless in this endeavor without reliable meteorological forcing estimates. Therefore, wind stress forcing over the North Pacific was obtained from synoptic geostrophic wind analyses made by the U.S. Fleet Numerical Weather Central. The FNWC surface wind analysis has been compared with independent, highly accurate measurements of winds from the General Dynamics Monster buoy located at 35°N, 155°W during October and November 1975. Friehe and Pazan found good agreement (±10%) with the six hourly synoptic FNWC winds, although larger errors in the FNWC analysis were found in extreme low pressure systems which apparently are routinely avoided by commercial shipping.

3. Preliminary studies in 1975 showed that the Anomaly Dynamics Study program was capable of making both the oceanic and atmospheric measurements needed to confirm or disprove our hypotheses. The effort began in earnest in June 1976 and during the subsequent autumn/winter period provided the first complete measurement of a significant ocean/atmosphere disturbance. During the autumn and winter of 1976-77, the storm forcing and the sea-surface temperature (SST) were often two to three standard deviations from normal in the North Pacific. In both seasons, between 30 to 50°N in the central portion of the ocean, sea-surface temperature was 2 degrees Celsius colder than normal, associated in some as yet unknown way with an atmospheric storm frequency that had four to six more storms per season than usual. What is perhaps most remarkable about this year is the persistence of the altered climatic conditions throughout the entire autumn/winter season. Namias has reported that this strength and persistence had been only seen rarely in the last 30 years.

The wind-driven surface currents during this time were measured by 32 satellite-tracked buoys put out by McNally and Kirwan, drogued both at the sea surface and at 30 meters depth. The trajectories of these buoys, along with surface currents, were remarkably laminar in nature, indicating the relative absence of horizontal turbulent processes that would have tended to separate adjacent buoys. During the winter, the buoys were found to move nearly in the direction of the wind (along the isobars) at 1-2% of the wind speed. This is different from that expected from Ekman. A distinct relationship between the surface wind and surface currents was found by comparing the monthly mean, vector-averaged, surface currents, as detected by the drifting buoys, with the average surface wind vector for that month. The resulting comparison finds the wind-driven currents directed 20-30 degrees to the right of the surface wind on average.

The thermal variability associated with this severe atmospheric disturbance was established by using data from the XBT temperature field measurement programs. White and Bernstein found that patterns of temperature disturbances (compared to the long-term monthly-mean norm) at the sea surface, 60, 120, 200, 300, and 400 meters, show a strong response to the autumn/winter sea level pressure disturbances (compared to the same norm as temperature). During this period, the oceanic layers above 120 meters became very much colder than normal, while the deeper layers (in the thermocline) became warmer than usual. This is an important result--the opposite of what would be expected from the divergent action of the surface wind-driven currents that accompanied the low pressure disturbances. A time sequence study of temperature profiles showed that the cooling at the surface and warming at depth (250 to 500 meters) occurred in association with a reduction in the vertical stratification, indicating that mixing processes existed within the main thermocline. Although the analysis of this autumn/winter disturbance is not yet complete, the foregoing results represent a significant departure from what was expected.

4. A numerical simulation of the 1976-77 autumn/winter disturbance was conducted by Haney and others in 1978, using a 10-level ocean model (based on the conservation of heat and momentum) in a closed rectangular basin the size of the North Paicfic. The model is driven by observed atmospheric wind forcing obtained from sea-level pressure maps. Observed ocean temperature disturbances in the upper 500 meters are introduced into the model in the beginning; thereafter, the model attempts to simulate their observed evolution. In modeling the 1976-77 event, the numerical simulation started from the observed September temperature disturbance pattern and utilized the observed wind forcing from the monthly mean sea-level pressure pattern. The resulting simulation develops a a widespread cold disturbance in the surface layers which resembles that observed. An examination of the model dynamics shows that the cold, sea-surface temperature disturbance in the model was generated by the displacement of cold water by anomalous southward-directed wind-driven surface currents. However, the model did not adequately simulate the deep, warm disturbance that occurred in the main thermocline. This had been tentatively attributed to the omission of vertical mixing processes in the model.

5. At this point, we are half-way through a five-year process-oriented experimental program designed to test some of the mechanisms that are thought to be important for ocean/atmosphere climate dynamics on a year-to-year basis. Relative to the initial hypotheses of this experiment, the results of the case study of the 1976/77 autumn/winter disturbance tentatively indicate the following:

1. The wind-driven flow in the upper 30 m moved 20 to 30 degrees to the right of the surface wind, less than that expected from Ekman in 1905.

2. Little evidence has been found that the thermocline structure was displaced vertically by the divergent action of the wind-driven surface currents in the manner predicted by Veronis and Stommel in 1956.

These results indicate that the classical theoretical concepts do not explain this particular autumn/winter climatic disturbance in the ocean thermal structure. The signature of the thermal response suggests that vertical mixing was important in altering the thermal structure. This is presently being investigated with a view toward incorporating these processes into new ocean climate models.

REFERENCES

Ritchie, G. S. 1957. Challenger, Clewes & Son, Ltd., 249 pp.

DATA REQUIREMENTS FOR ANALYSIS AND PREDICTION OF OCEAN CONDITIONS ON A WORLD-WIDE BASIS

P.M. WOLFF (USA)

February 1979
Monterey, California

I. INTRODUCTION

In 1975 Vasiliev and Wolff identified the coverage of underwater soundings needed on a routine synoptic basis in order to analyze ocean temperature structure. This chart is shown in Figure 1. Since that time the number of soundings available has decreased steadily while there has been an increase in the amount of data available on sea surface temperature. Table 1 shows typical counts of number of soundings available. Maximum numbers of observations were obtained in the early 70's with decreasing observations since that time. Meanwhile the uses of upper ocean temperature structure have become economically more important.

If analyses are to be prepared, new methods will be required which infer temperature structure from surface observations. An analysis aid is described here which can be used in such an indirect method. The method combines specially processed historical temperature structure with rules for its local use depending on the particular oceanographic factors which operate to change the temperature structure in a region. Limited applications of the technique for both engineering and climate modeling have been useful. Most of these tests have involved limited areas or less than full year data.

With the availability of soundings of ocean temperature as shown in Table 1 and Figure 2, it can be instructive to imitate the actions of meteorologists when their knowledge of the atmosphere was just beginning to increase due to the early upper air soundings. Much effort was directed in the late 1930's and 1940's to the construction of definitive charts showing normal conditions monthly for the atmosphere.

What is proposed here is the construction of a most probable monthly ocean temperature data base for many uses in oceanography and ocean engineering.

II. DATA BASE DESCRIPTION

The data base consists of tables of the most probable temperature at selected depths for each 1° Lat. Long. in the ocean. Certain additional information is attached to each record identifying areas with the following physical characteristics:

1. Areas containing edge of continental shelf.
2. Areas sometimes occupied by major current boundary.
3. Areas sometimes containing significant upwelling.
4. Areas where temperature distributions are not normal.
5. Areas with unusual air-sea interaction phenomena.

For each area the highest and lowest observed temperature at each depth is included along with a description of the type of distribution of the data at that level during each month. Additionally, a table of MLD records is attached for each area such as Table 3.

The most probable temperature tables are prepared using statistical techniques. In an area where the distribution of soundings is similar to that in Figure (3), there is no complex oceanographic analyses needed. The distributions are Gaussian at all depths and the seasonal progression is regular in the upper few hundreds of meters and absent at greater depths. There is no record of the large variations at a fixed depth which would accompany water mass or current boundaries or the existence of significant eddies.

In areas of more complex processes observed distributions of temperature are often not normal. Figure (4) shows the envelope of soundings for such an area. The warmer water on the right represents typical Caribbean soundings and shows little variability. The colder soundings are from the left side of the current and is more representative of Gulf of the Mexico water mass. Standard statistics are not very useful in such an area. In extreme cases the distribution of temperature observations may be bi-modal.

III. HOW THE DATA BASE IS USED

Some of the uses of the data base are described here. Some are tested and others should be regarded as speculative.

1. For quality control of newly received observations comparison with the data base information will identify data which exceed previous limits.

2. For climate models a realistic initial temperature structure can be provided on a 60 mile grid for each month of the year.

3. For climate models a comparison of predicted ocean temperature structure with the values from the standard ocean temperature data base has multiple diagnostic uses.

4. For oceanographic expeditions expected temperature structures along a track can be extracted readily such as the section in Figure (2).

5. For ocean temperature analysis models changes in the surface temperature can be related to the most probable structure with depth in order to produce analyses which have realistic vertical and horizontal temperature gradients.

IV. CHARACTERISTICS OF GOOD TEMPERATURE ANALYSIS PROCESS

In the construction of analyses of ocean temperature at any level certain properties are necessary. These are:

1. represent all valid data
2. use standard ocean data base for data checking and reject
3. show features down to limits of grid spacing
4. preserve horizontal gradient of standard ocean in uniform regions
5. provide realistic structures in regions with:
   a. current boundaries
   b. eddies
   c. shelf phenomena
   d. upwelling
6. preserve second derivative of temperature in the vertical from the standard ocean temperature climatology.
7. work out from valid observations
8. pass consistency and stability checks

Use of the Standard Ocean Temperature Climatology enables the construction of analyses having these essential properties.

V. EXAMPLES

This technique of using historical data has been applied in several engineering problems. One of these has been the Ocean Thermal Energy Project of the Department of Energy. Figures 6 and 7 show these charts for OTEC potential at 1000 meters and 500 meters. Additionally, the method has

has been used to prepare monthly climatology for each of the areas shown in Figure 8. Sufficient data was available in each area.

Another application is fisheries. The tuna have a strong temperature dependence shown in Figure 9. When this variable is combined with MLD optimum areas can be established. Figure 10 illustrates such an analyses.

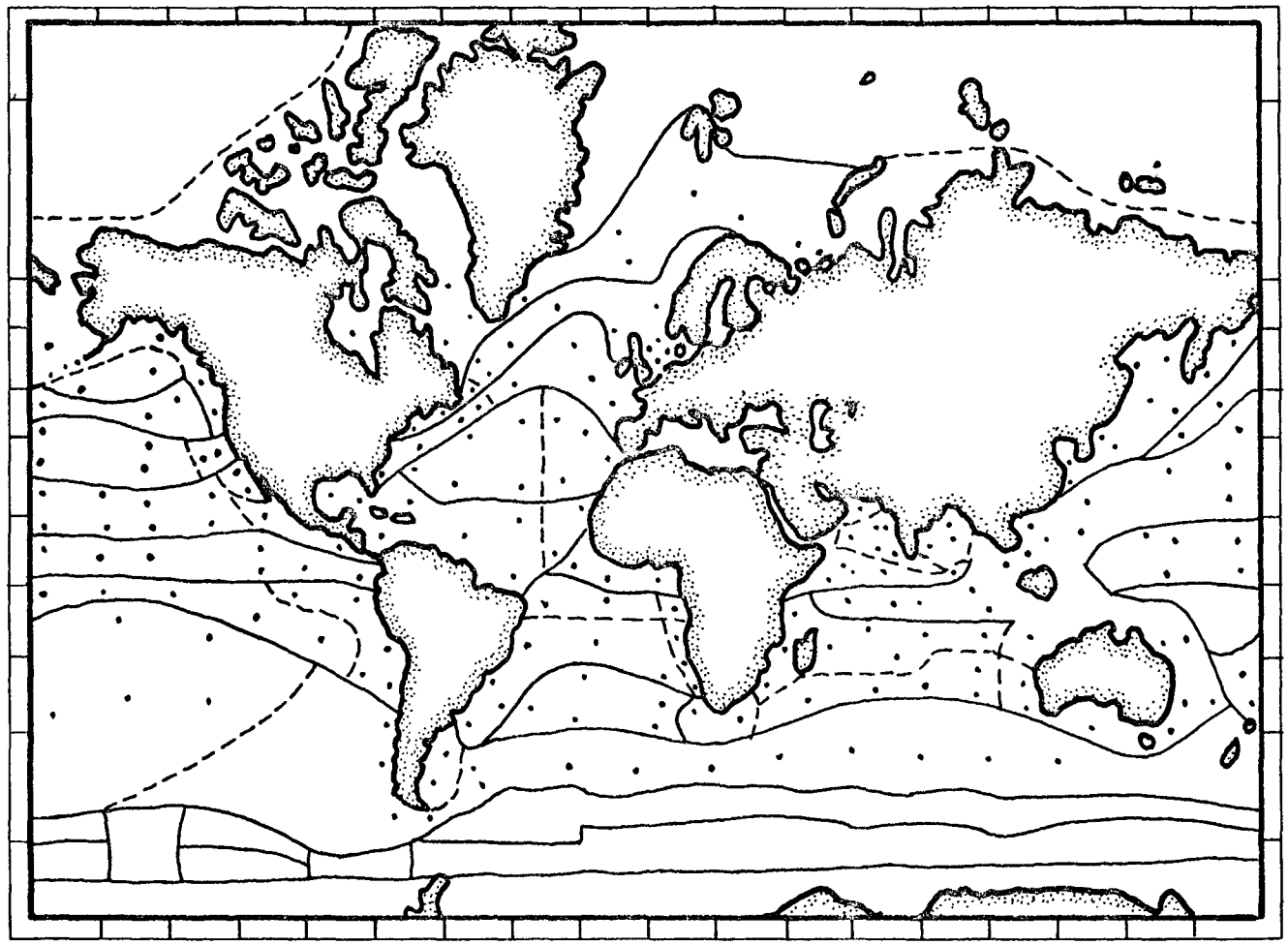

FIGURE 1: CHART SHOWING MAJOR WATER MASS AREAS WITH PROPOSED MINIMUM OBSERVATIONAL NETWORK FOR SUBSURFACE ANALYSIS. (Vasiliev and Wolff, 1975)

YEAR	XBT	NANSEN + STD	MBT
48	.	.	14.
49	.	10.	.
50	.	2.	32.
51	.	23.	.
52	.	11.	59.
53	.	26.	16.
54	.	1.	7.
55	.	.	18.
56	.	10.	31.
57	.	2.	202.
58	.	.	256.
59	.	1.	58.
60	.	.	56.
61	.	3.	199.
62	.	1.	195.
63	.	.	274.
64	.	14.	344.
65	.	85.	339.
66	3.	63.	461.
67	46.	46.	201.
68	49.	.	126.
69	86.	.	41.
70	244.	.	12.
71	182.	8.	1.
72	103.	.	15.
73	61.	1.	.
74	71.	.	.
75	37.	.	.
76	22.	.	.
77	.	.	.
	904.	307.	2857.

TABLE 1: DATA BASE OBSERVATIONS FOR 1° LATITUDE LONGITUDE AREA NEAR HAWAII

MONTH	1	2	3	4	5	6	7	8	9	10	11	12
0	24.2	23.6	23.5	23.8	24.1	24.9	25.3	26.3	26.0	25.7	25.4	24.2
10	24.2	23.6	23.5	23.8	24.1	24.9	25.3	26.3	26.0	25.7	25.4	24.2
20	24.2	23.6	23.5	23.8	24.1	24.9	25.3	26.3	26.0	25.7	25.4	24.2
30	24.2	23.5	23.5	23.8	24.1	24.5	25.3	26.3	26.0	25.7	25.4	24.2
40	24.2	23.5	23.5	23.4	23.9	23.9	25.2	26.3	26.0	25.7	25.4	24.2
50	24.0	23.5	23.1	23.1	23.6	23.5	25.0	26.3	25.0	25.7	25.4	24.2
60	23.9	23.4	22.8	22.9	23.4	23.0	24.5	25.3	24.5	25.7	25.4	24.2
70	23.7	23.4	22.6	22.8	23.1	22.4	24.0	24.8	24.0	25.2	25.4	23.2
80	23.6	23.4	22.3	22.6	22.9	22.2	23.6	23.6	23.6	24.7	24.5	22.7
90	23.2	23.3	22.1	22.5	22.5	22.0	23.3	23.0	23.2	24.2	23.0	22.2
100	22.8	23.1	21.9	22.3	22.2	21.8	23.1	22.7	22.8	23.6	22.5	21.8
150	20.2	19.5	20.5	21.6	20.2	20.1	21.0	21.0	19.8	21.3	19.8	19.4
200	17.0	17.1	18.2	20.6	17.4	18.0	19.0	19.2	16.8	19.3	16.8	16.7
250	14.2	13.3	15.8	17.0	13.5	14.6	15.4	16.0	14.2	16.8	14.3	13.7
300	11.4	11.2a	13.9	13.5	11.3	11.8	12.2	13.2a	11.8	14.0	12.0	11.6
350	9.6	9.7a	11.0	11.8	9.7	9.7	10.4	10.5a	9.8	10.6	10.5	9.7
400	8.7	8.6a	9.6	10.0	8.7	8.6	8.8	8.9a	8.5	9.5	9.0	8.5
450	7.4	7.6a	8.5	9.0	7.4	7.4	7.7	7.3a	7.2	8.0	8.0	7.4
500	6.6	6.3a	7.7	7.9	6.9a	6.7a	7.0	6.7c	6.4a	7.3a	7.1a	6.7a
600	5.5a	5.4a	6.0a	6.2a	5.8a	6.1a	5.6	5.6c	5.4a	6.0a	6.5a	5.6a
700	5.2a	5.2c	5.2a	5.6a	5.5a	5.2a	5.0a	5.0c	4.8a	5.2a	5.8a	5.0a
800	4.8c	4.7c	4.7a	5.0a	4.9c	4.7c	4.6a	4.6c	4.5a	4.4c	5.4c	4.6c
900	4.4c	4.5c	4.2a	4.5a	4.4c	4.3c	4.2a	4.2c	4.2a	4.6c	4.9c	4.2c
1000	4.0c	4.0c	4.0c	4.0a	3.9c	3.9c	3.9a	3.9c	4.0a	4.3c	4.7c	3.9c
1100	3.8c	3.8c	3.8c	3.8b	3.7c	3.6c	3.6b	3.7c	3.7b	4.1c	4.3c	3.7c
1200	3.5c	3.5c	3.5c	3.5b	3.5c	3.5c	3.4b	3.5c	3.5b	3.7c	4.0c	3.5c
1300	3.3c	3.3c	3.3c	3.3b	3.3c	3.3c	3.2c	3.3c	3.2c	3.4c	3.7c	3.3c
1400	3.1c	3.1c	3.1c	3.1b	3.1c	3.1c	3.1c	3.1c	3.1c	3.1c	3.3c	3.1c
1500	2.9c	2.9c	2.9c	2.9b	2.9c	2.9c	2.9c	2.9c	2.9c	2.9c	3.0c	2.9c

a EQUAL TO OR LESS THAN 1000M AND LESS THAN SEVEN REPORTS
b GREATER THAN 1000M AND LESS THAN FOUR REPORTS
c NO REPORTS AT THIS LEVEL (INTERPOLATED)

TABLE 2: EXAMPLE OF MOST PROBABLE MONTHLY TEMPERATURE DISTRIBUTION FOR A 1° SQUARE

SQ NO.		JAN	FEB	MAR	APR	MAY	JUN	JUL	AUG	SEP	OCT	NOV	DEC
14G	MOST PROB	90	110	110	30	30	20	20	20	40	50	70	80
	MIN	50	60	60	10	10	10	10	10	20	40	50	50
	MAX	200	140	150	70	60	40	40	30	70	60	100	120
					(Minimum depth in area=1310m; maximum depth=2660m)								
SQ NO.													
19G	MOST PROB	80	60	70	20	20	30	20	30	40	50	60	70
	MIN	30	40	50	10	20	30	20	10	20	30	30	40
	MAX	110	100	130	40	20	30	30	40	50	80	90	110
					(Minimum depth in area=1350m; maximum depth=3460m)								
SQ NO.													
20G	MOST PROB	90	80	90	40	40	40	30	40	40	50	60	70
	MIN	60	30	20	10	10	10	20	20	10	20	50	60
	MAX	110	150	190	90	70	60	50	50	40	70	70	70
					(Minimum depth in area=2950m; maximum depth=3500m)								
SQ NO.													
21G	MOST PROB	90	90	100	60	40	40	30	30	40	50	60	80
	MIN	40	40	30	20	20	20	20	10	20	20	20	30
	MAX	110	140	130	90	60	60	30	50	60	60	100	110
					(Minimum depth in area=2340m; maximum depth=3600m)								
SQ NO.													
22G	MOST PROB	70	115	90	30	20	20	20	30	40	40	60	60
	MIN	30	50	50	20	10	10	10	10	10	20	30	30
	MAX	100	120	110	60	60	50	40	60	60	60	80	100
					(Minimum depth in area=2490m; maximum depth=3460m)								

TABLE 3: EXAMPLE OF MIXED LAYER DEPTH (MLD) IN METERS, TABULATED FOR AREAS IN THE WESTERN GULF OF MEXICO.

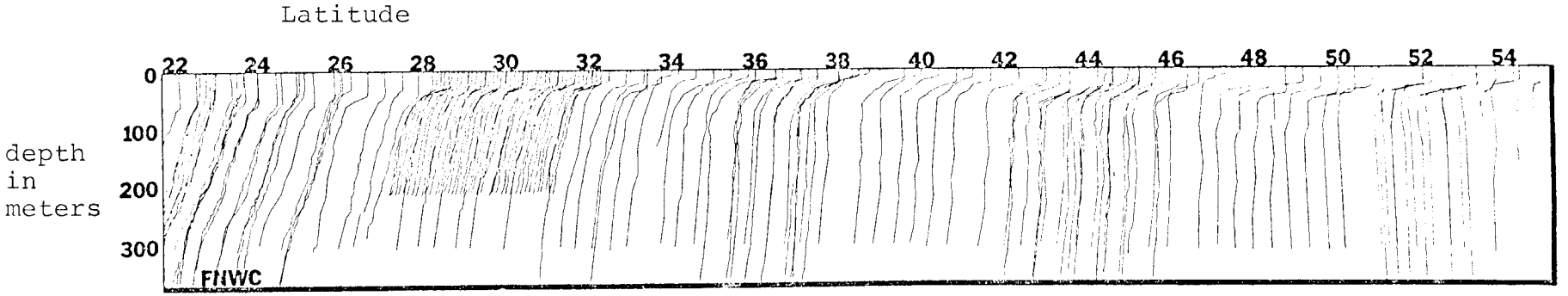

FIGURE 2: SECTION OF STD, XBT AND AXBT OBSERVATIONS
September 2, 1968

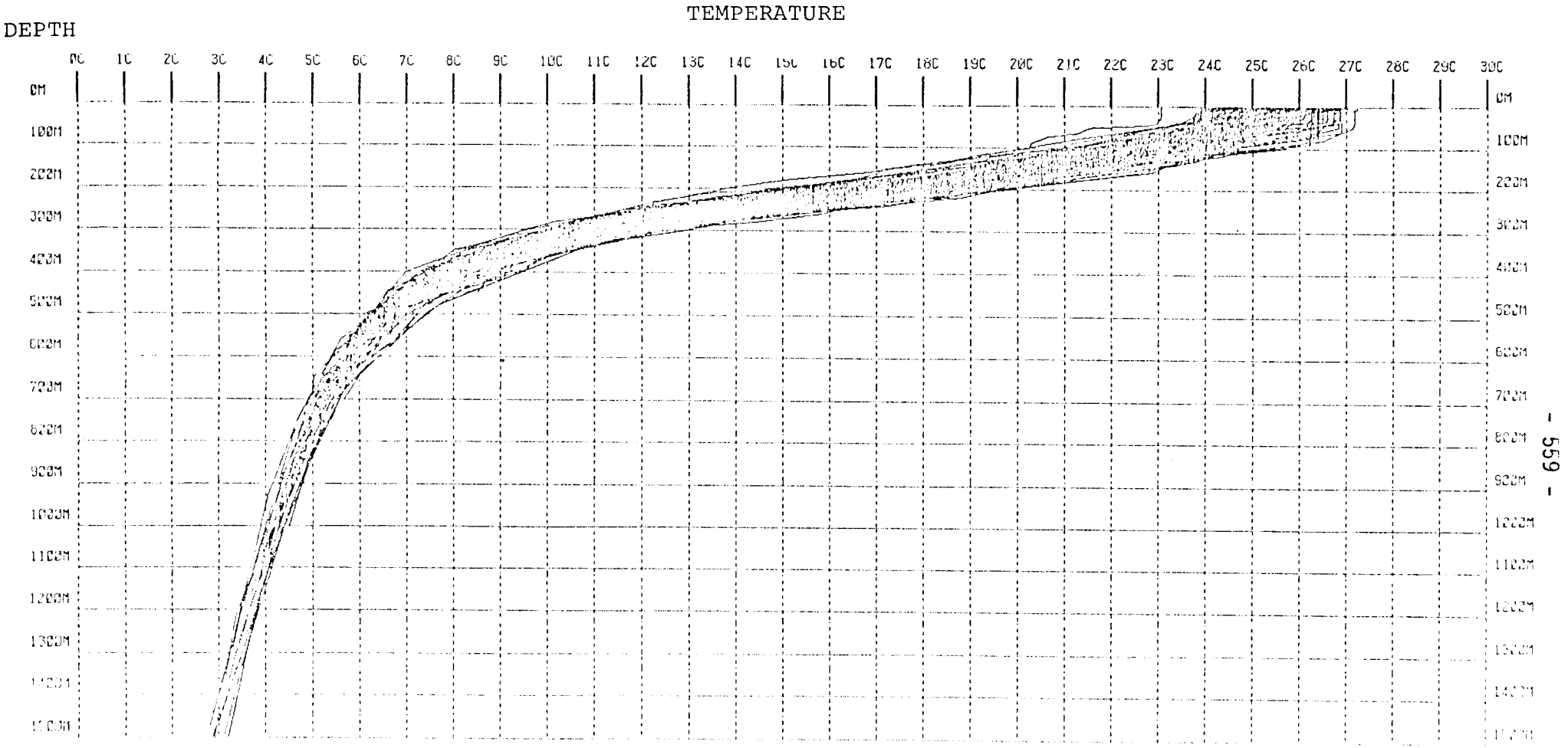

FIGURE 3: OVERPLOT FOR 1° AREA NEAR HAWAII

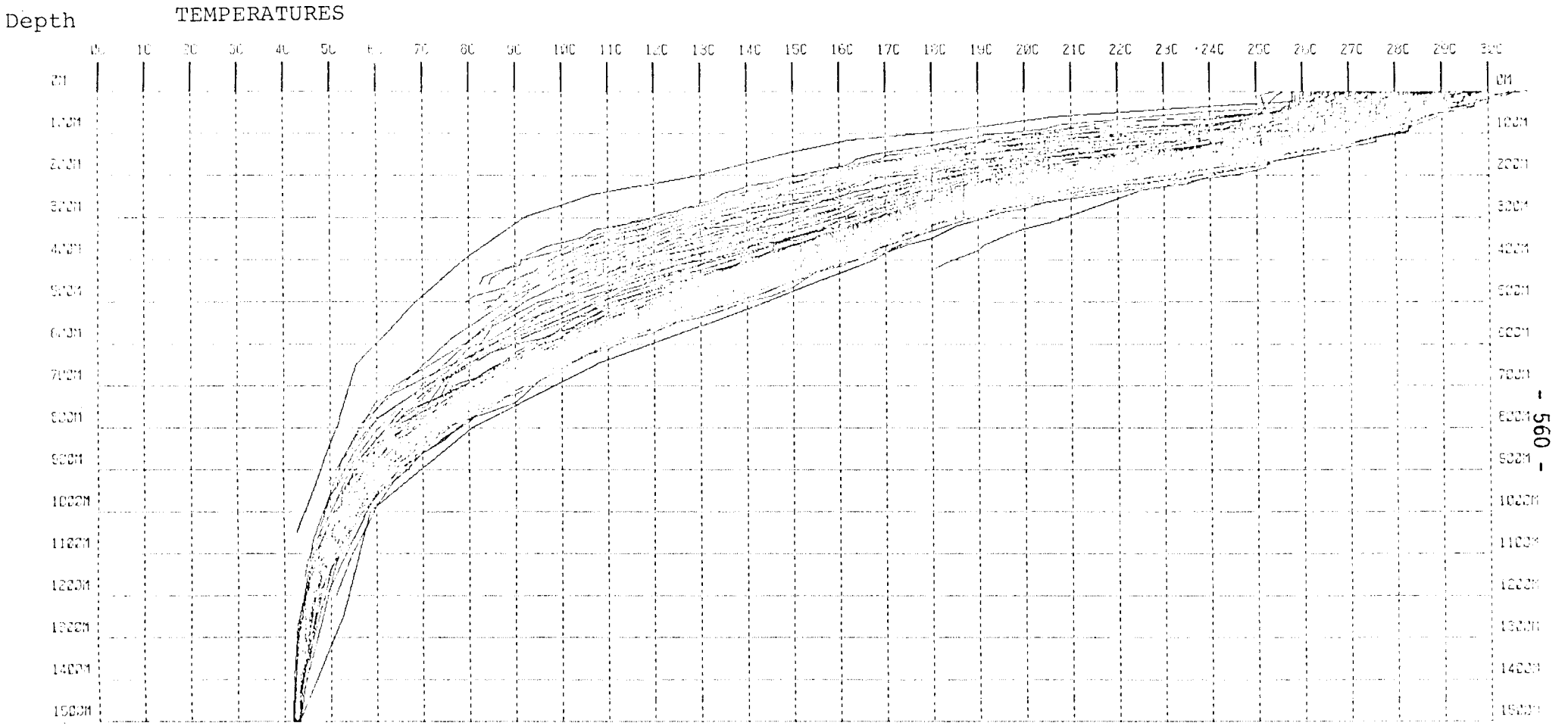

FIGURE 4: ANNUAL OVERPLOT FOR 1° AREA GULF OF MEXICO

CROSS-SECTION THROUGH GULF STREAM

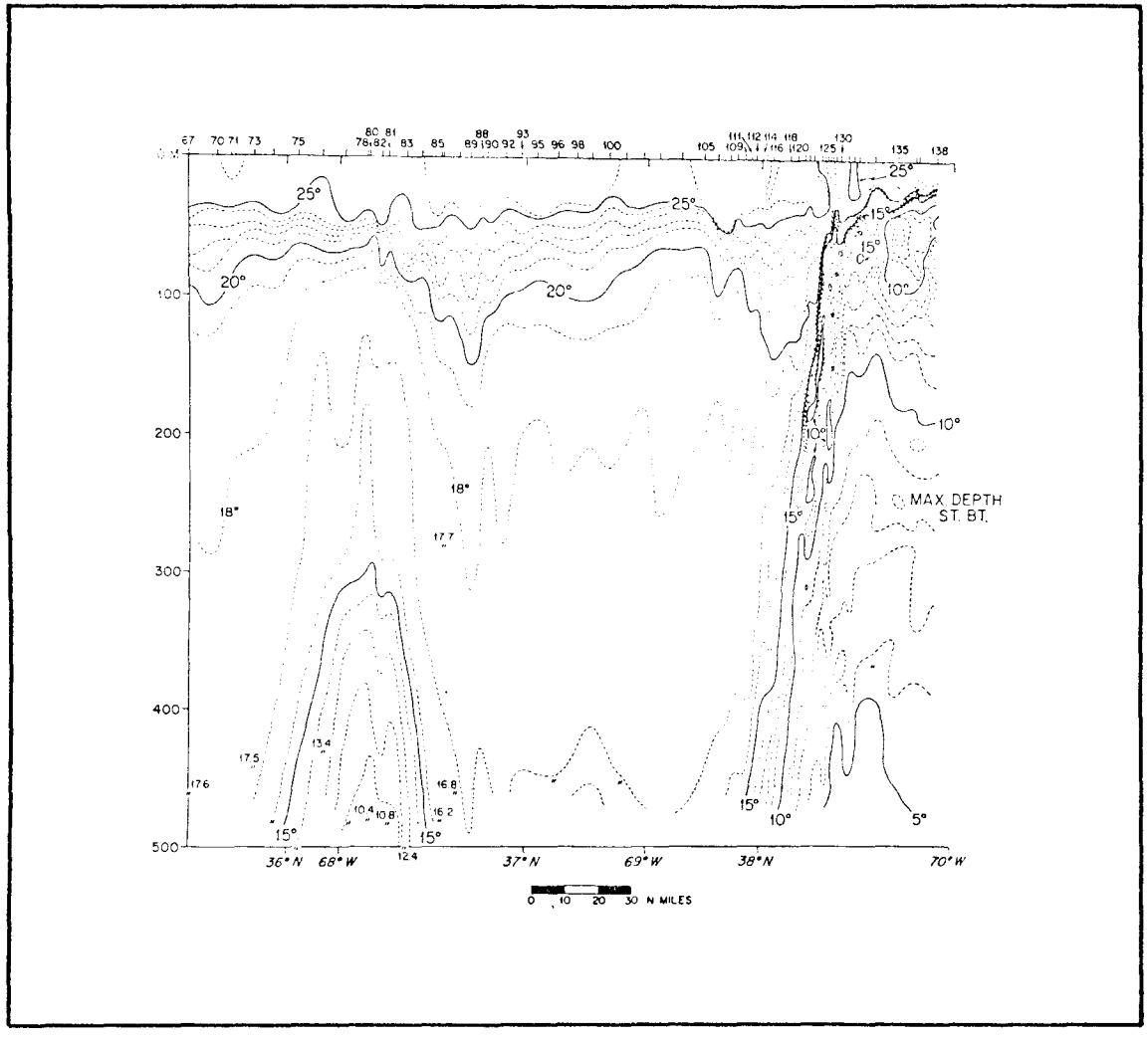

Numbers at top indicate the number and position of each expendable bathythermograph sounding. Vertical scale in meters; temperatures in degrees Celsius. (After Sippican and Wodds Hale Oceanographic Institute)

FIGURE 5: CROSS-SECTION THROUGH GULF STREAM

LARGE SCALE DISTRIBUTION OF

OTEC THERMAL RESOURCE

ΔT(°C) BETWEEN SURFACE AND 500 METER DEPTH

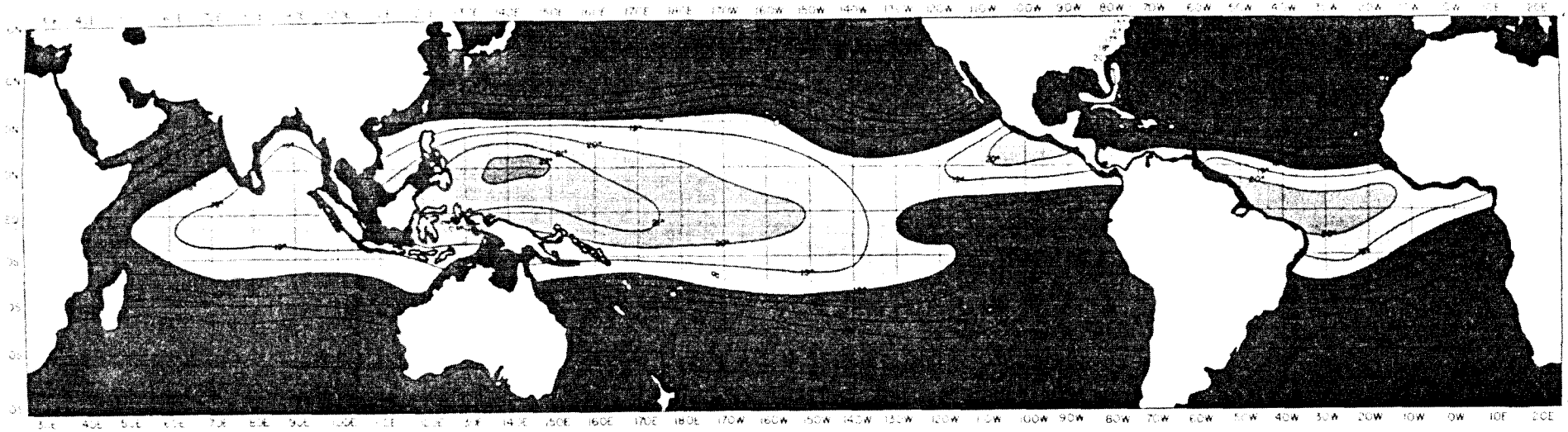

METHOD

SEA SURFACE TEMPERATURES WERE ANALYZED MONTHLY ON SPACE SCALES CONSISTENT WITH DATA AVAILABILITY. MEAN TEMPERATURES AT 500 METERS WERE ANALYZED ON SCALES OF 2½° LAT BY 2½° LONG IN AREAS WITH MORE DATA AND ON 5° LAT SCALES IN AREAS WITH FEWER OBSERVATIONS. MONTHLY AVERAGE ΔT VALUES WERE DETERMINED AND AVERAGED FOR 12 MONTHS. SEPARATE VALUES WERE DETERMINED FOR A 1° LAT RESOLUTION IN THE HAWAII, GULF OF MEXICO, FLORIDA AND PUERTO RICO AREAS.

SCALE AND ACCURACY

THIS GLOBAL SCALE CHART SHOWS THE GROSS RESOURCE AVAILABILITY AND DOES NOT ADEQUATELY PORTRAY FEATURES WHOSE SIZE IS LESS THAN 200 MILES. LOCAL VALUES ARE CONSIDERED ACCURATE TO LESS THAN 1°C IN DENSE DATA AREAS. BUT MAY BE LESS PRECISE IN REGIONS OF LARGE HORIZONTAL GRADIENTS.

WHEREVER THE ORANGE AREAS (ΔT > 20°C) INTERSECT THE GREEN AREAS (WATER DEPTH < 500 METERS), THERE WILL BE SOME PORTION OF THE GREEN AREA IN WHICH A ΔT OF 20°C EXISTS AT DEPTHS SHALLOWER THAN 500 METERS.

REFERENCES

FLEET NUMERICAL WEATHER CENTRAL (FNWC), MONTEREY, CALIFORNIA. FNWC and NATIONAL OCEANOGRAPHIC DATA CENTER DIGITIZED REPORTS (SOURCE FOR XBT DATA).

NATIONAL OCEANOGRAPHIC DATA CENTER DATA FILE BTG75A (SOURCE FOR MECHANICAL BATHYTHERMOGRAPH [MBT] DATA).

NATIONAL OCEANOGRAPHIC DATA CENTER DATA FILES SD40A5/0A6 FROM SD76A (9/30/76) - 3509 STA (SOURCE FOR NANSEN CASTS AND STD DATA).

ATWOOD, D.K. et al, 1976; OCEAN THERMAL ENERGY CONVERSION; RESOURCE ASSESSMENT AND ENVIRONMENTAL IMPACT FOR PROPOSED PUERTO RICO SITE, NSF GRANT NO. AER 75-00145

BATHEN, K., 1975; OCEANOGRAPHIC AND SOCIO-ECONOMIC ASPECTS OF AN OCEAN THERMAL ENERGY CONVERSION PILOT PLANT IN SUBTROPICAL HAWAIIAN WATERS.

COLBORN, J.G., 1974; THE THERMAL STRUCTURE OF THE INDIAN OCEAN.

LEIPPER, D.L., 1968; "HYDROGRAPHIC STATION DATA, FEBRUARY-MARCH NANSEN CASTS, 1965-1968"; "GULF OF MEXICO NANSEN CASTS AND STD, AUGUST-SEPTEMBER 1968", TEXAS A&M UNIVERSITY, REFERENCES 68-15T and 68-17T.

MOLINARI, R.L., 1977; "SYNOPTIC AND MEAN MONTHLY 20°C TOPOGRAPHIES IN THE EASTERN GULF OF MEXICO", NOAA ATLANTIC OCEANOGRAPHIC AND METEOROLOGICAL LABORATORIES.

ROBINSON, M., 1976; ATLAS OF NORTH PACIFIC OCEAN MONTHLY MEAN TEMPERATURES AND MEAN SALINITIES OF THE SURFACE LAYER, NAVAL OCEANOGRAPHIC OFFICE REFERENCE PUBLICATION 2, DEPARTMENT OF THE NAVY.

LEGEND

BLUE - AVERAGE OF MONTHLY ΔT's LESS THAN 18°C

YELLOW - AVERAGE OF MONTHLY ΔT's MORE THAN 18°C, LESS THAN 20°C

ORANGE - AVERAGE OF MONTHLY ΔT's MORE THAN 20°C, LESS THAN 22°C

LT RED - AVERAGE OF MONTHLY ΔT's MORE THAN 22°C, LESS THAN 24°C

DEEP RED - AVERAGE OF MONTHLY ΔT's GREATER THAN 24°C

GREEN - WATER DEPTH LESS THAN 1000 METERS

PREPARED BY
OCEAN DATA SYSTEMS, INC.
P.M. WOLFF, W.A. WOLFF, N.HANSON.

FIGURE: 6

LARGE SCALE DISTRIBUTION OF

OTEC THERMAL RESOURCE

ΔT(°C) BETWEEN SURFACE AND 1000 METER DEPTH

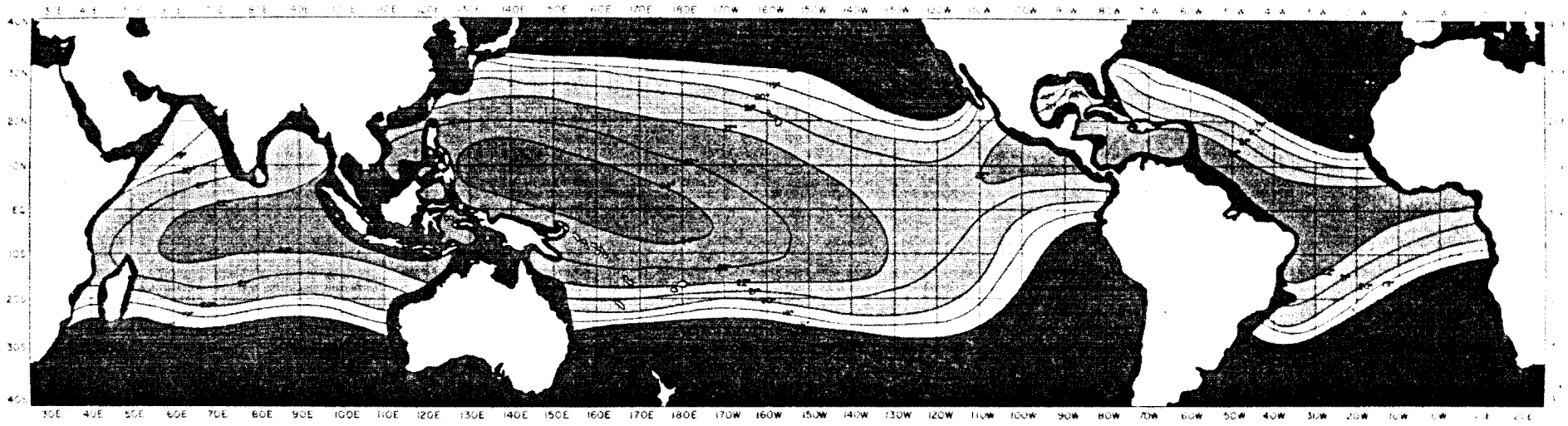

METHOD

SEA SURFACE TEMPERATURES WERE ANALYZED MONTHLY ON SPACE SCALES CONSISTENT WITH DATA AVAILABILITY. MEAN TEMPERATURES AT 1000 METERS WERE ANALYZED ON SCALES OF 2½° LAT BY 2½° LONG IN AREAS WITH MORE DATA AND ON 5° LAT SCALES IN AREAS WITH FEWER OBSERVATIONS. MONTHLY AVERAGE ΔT VALUES WERE DETERMINED AND AVERAGED FOR 12 MONTHS. SEPARATE VALUES WERE DETERMINED FOR A 1° LAT RESOLUTION IN THE HAWAII, GULF OF MEXICO, FLORIDA AND PUERTO RICO AREAS.

SCALE AND ACCURACY

THIS GLOBAL SCALE CHART SHOWS THE GROSS RESOURCE AVAILABILITY AND DOES NOT ADEQUATELY PORTRAY FEATURES WHOSE SIZE IS LESS THAN 200 MILES. LOCAL VALUES ARE CONSIDERED ACCURATE TO LESS THAN 1°C IN DENSE DATA AREAS, BUT MAY BE LESS PRECISE IN REGIONS OF LARGE HORIZONTAL GRADIENTS.

WHEREVER THE ORANGE AND RED AREAS (ΔT > 20°C) INTERSECT THE GREEN AREA (WATER DEPTH < 1000 METERS), THERE WILL BE SOME PORTION OF THE GREEN AREA IN WHICH A ΔT OF 20°C EXISTS AT DEPTHS SHALLOWER THAN 1000 METERS.

REFERENCES

FLEET NUMERICAL WEATHER CENTRAL (FNWC), MONTEREY, CALIFORNIA. FNWC and NATIONAL OCEANOGRAPHIC DATA CENTER DIGITIZED REPORTS (SOURCE FOR XBT DATA).

NATIONAL OCEANOGRAPHIC DATA CENTER DATA FILE BTG75A (SOURCE FOR MECHANICAL BATHYTHERMOGRAPH [MBT] DATA).

NATIONAL OCEANOGRAPHIC DATA CENTER DATA FILES SD40A5/0A6 FROM SD76A (9/30/76) - 3509 STA (SOURCE FOR NANSEN CASTS AND STD DATA).

ATWOOD, D.K. et al, 1976; OCEAN THERMAL ENERGY CONVERSION: RESOURCE ASSESSMENT AND ENVIRONMENTAL IMPACT FOR PROPOSED PUERTO RICO SITE, NSF GRANT NO. AER 75-00145

BATHEN, K., 1975; OCEANOGRAPHIC AND SOCIO-ECONOMIC ASPECTS OF AN OCEAN THERMAL ENERGY CONVERSION PILOT PLANT IN SUBTROPICAL HAWAIIAN WATERS.

COLBORN, J.G., 1974; THE THERMAL STRUCTURE OF THE INDIAN OCEAN.

LEIPPER, D.L., 1968; "HYDROGRAPHIC STATION DATA, FEBRUARY-MARCH NANSEN CASTS, 1965-1968"; "GULF OF MEXICO NANSEN CASTS AND STD, AUGUST-SEPTEMBER 1968", TEXAS A&M UNIVERSITY, REFERENCES 68-15T and 68-17T.

MOLINARI, R.L., 1977; "SYNOPTIC AND MEAN MONTHLY 20°C TOPOGRAPHIES IN THE EASTERN GULF OF MEXICO", NOAA ATLANTIC OCEANOGRAPHIC AND METEOROLOGICAL LABORATORIES.

ROBINSON, M., 1976; ATLAS OF NORTH PACIFIC OCEAN MONTHLY MEAN TEMPERATURES AND MEAN SALINITIES OF THE SURFACE LAYER, NAVAL OCEANOGRAPHIC OFFICE REFERENCE PUBLICATION 2, DEPARTMENT OF THE NAVY.

LEGEND

BLUE - AVERAGE OF MONTHLY ΔT's LESS THAN 19°C

YELLOW - AVERAGE OF MONTHLY ΔT's MORE THAN 18°C, LESS THAN 20°C

ORANGE - AVERAGE OF MONTHLY ΔT's MORE THAN 20°C, LESS THAN 22°C

LT RED - AVERAGE OF MONTHLY ΔT's MORE THAN 22°C, LESS THAN 24°C

DEEP RED - AVERAGE OF MONTHLY ΔT's GREATER THAN 24°C

GREEN - WATER DEPTH LESS THAN 1000 METERS

PREPARED BY
OCEAN DATA SYSTEMS, INC.
P.M. WOLFF, W.A. WOLFF, N.HANSON

FIGURE: 7

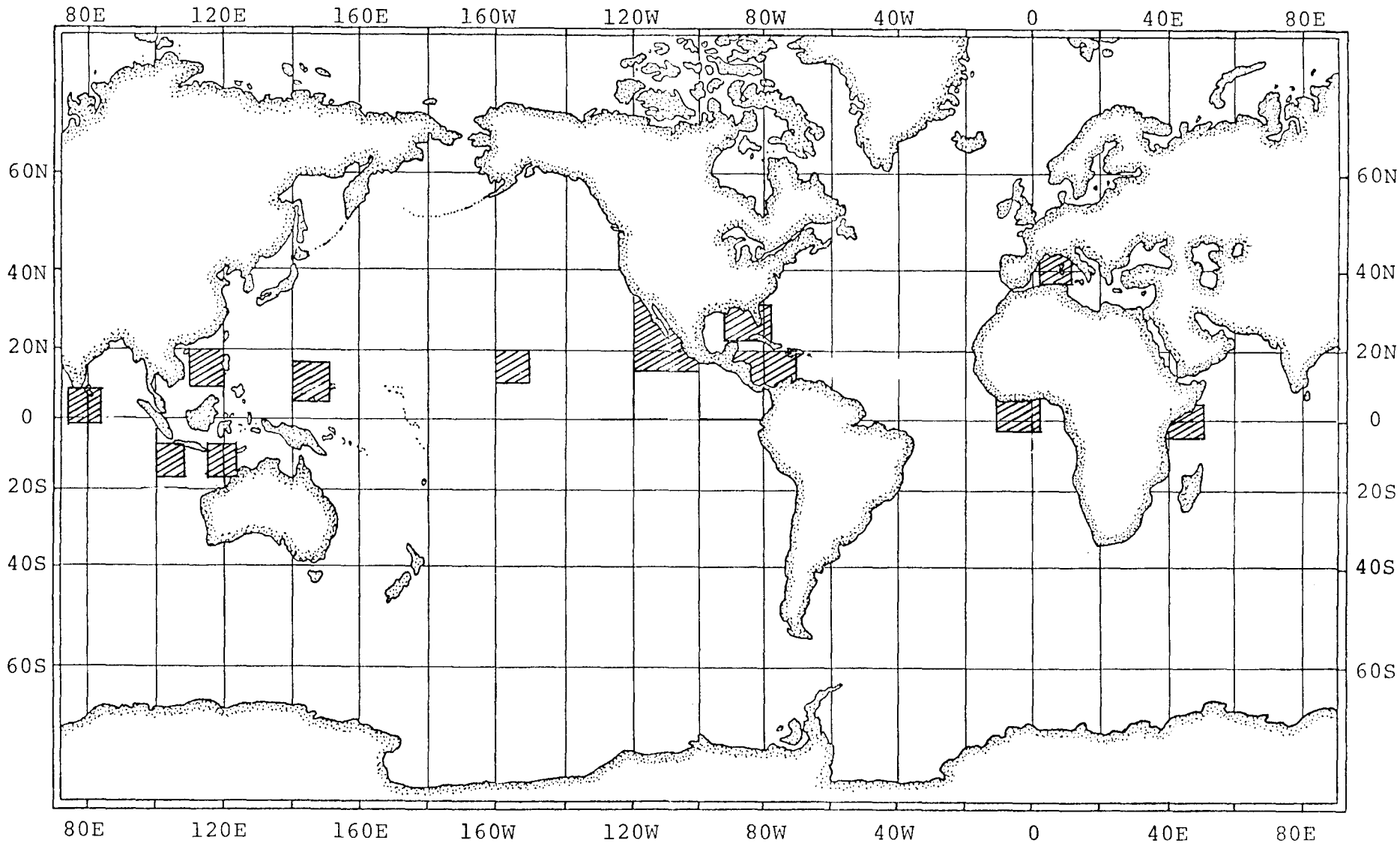

FIGURE 8: AREAS FOR WHICH STANDARD MONTHLY DATA BASE EXISTS

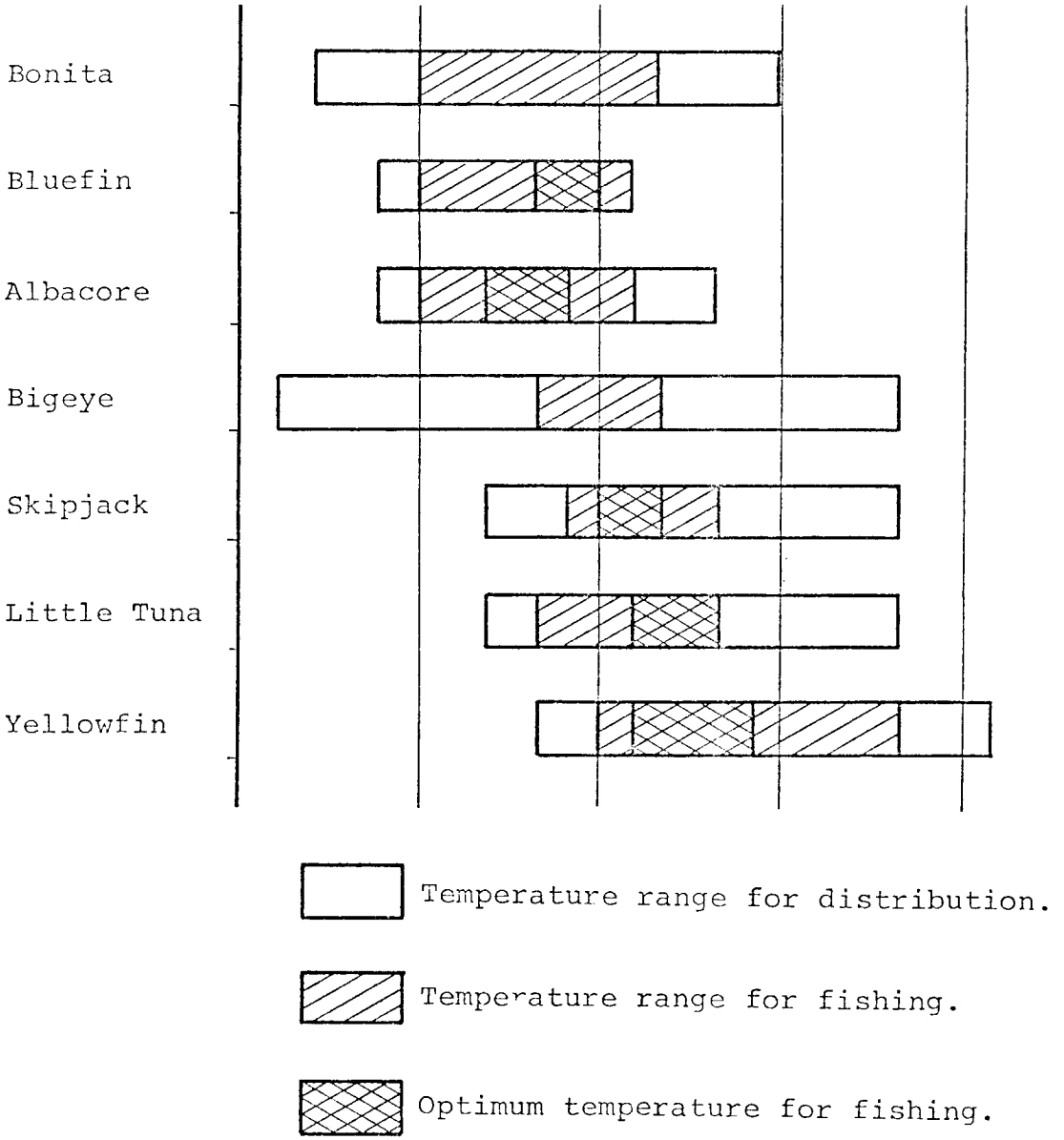

FIGURE 9: TEMPERATURE RANGE FOR DISTRIBUTION AND FISHING OF TUNA SPECIES (AFTER UDA).

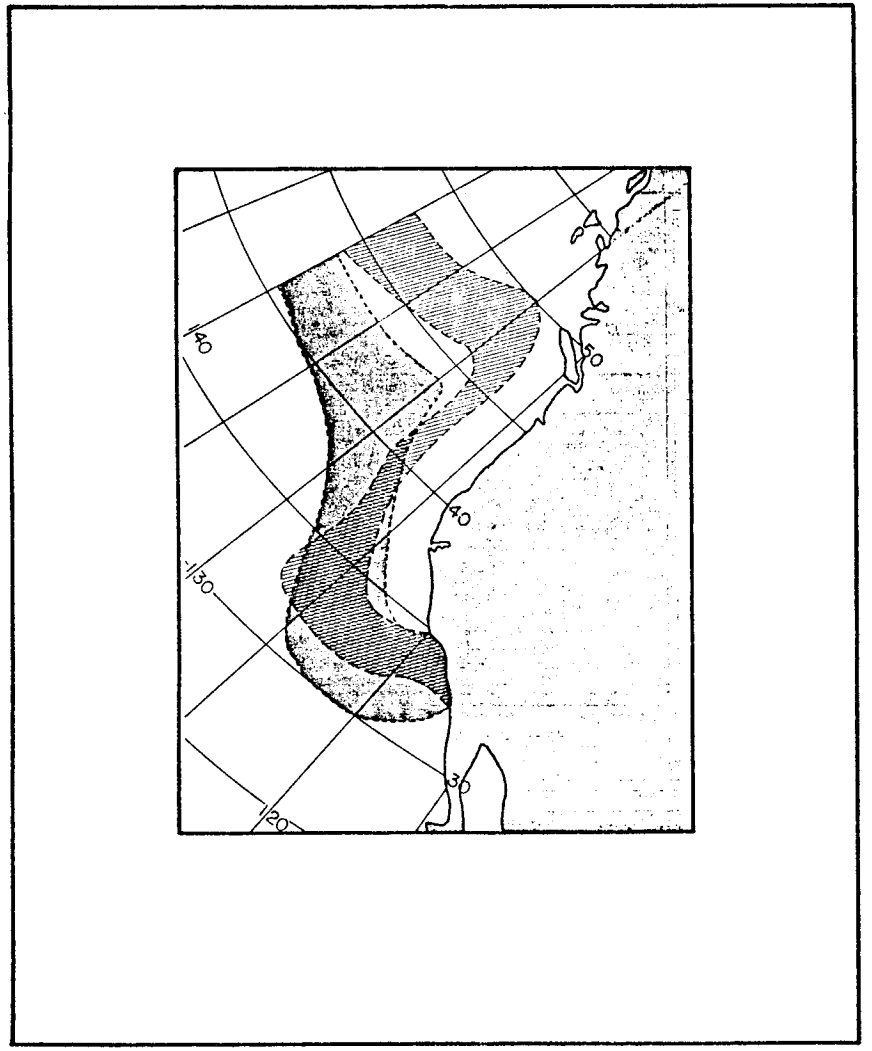

FIGURE 10: OPTIMUM FISHING AREAS FOR ALBACORE (CROSS HATCHED) FOR 20 TO 25 AUGUST 1967 AND FOR AN AVERAGE AUGUST

LIST OF PARTICIPANTS

ARGENTINA

R. NAWRATIL
Armada Argentina Servicio de Hidrografia Naval,
Avenida Montes de Oca 2124,
Buenos Aires

BELGIUM

J.-L. VAN HAMME
Chef de travaux, Département de météorologie appliquée,
Institut Royal Météorologique,
3, Avenue Circulaire,
1180 Bruxelles

BULGARIA

G.T. MANGOV
Institute for Hydrology and Meteorology,
66, Blvd. Lenin,
Sofia - 1113

CANADA

N.E.J. BOSTON
Suite 602, 1550 Alberni Street,
Beak Consultants Ltd.,
Vancouver, B.C. V6G 1A5

W.W. DENNER
Department of Physics,
Memorial University,
St. Johns, Newfoundland

J.A. HELBIG
Suite 602, 1550 Alberni Street,
Beak Consultants Ltd.,
Vancouver, B.C. V6G 1A5

E.J. SANDEMAN
Fisheries and Oceans Canada Research and Resource Services
P.O. Box 5667,
St. Johns, Newfoundland

S. TABATA
Institute of Ocean Sciences,
P.O. Box 6000, 9860 W. Saanich Rd.,
Sidney, B.C. V8L 482

DEMOCRATIC PEOPLE'S REPUBLIC OF KOREA	BANG JONG SAM Meteorological Organization DPRK, Pyong Yang
	KIM BEN CHEL Meteorological Organization DPRK, Pyong Yang
	KIM KI HWAN Meteorological Organization DPRK, Pyong Yang
	LI ZU HO Meteorological Organization DPRK, Pyong Yang
GERMAN DEMOCRATIC REPUBLIC	E. FRANCKE Institute of Marine Research of the Academy of Sciences of the GDR, DDR 2530 Rostock-Warnemünde
	J.-O. HOLZ Meteorological Service of the GDR, Marine Weather Office, 15 a, Seestrasse, DDR-253 Warnemünde
	H. VEIT Meteorological Service of the GDR, Albert-Einstein Strasse 42-44-46, DDR-15 Potsdam
FEDERAL REPUBLIC OF GERMANY	K. HUBER Deutsches Hydrographisches Institut, Bernhard Nochtstrasse 78, 2000 Hamburg
	H. WALDEN Tinsdaler Kirchenweg 233 a, D-2000 Hamburg 56
FRANCE	C. FONS Direction Météorologie Nationale, Service météorologique métropolitain, 2, Av. Rapp, 75007 Paris
	J.A.H. NOEL ORSTOM, 24, rue Bayard, Paris 8ème
	Y. TREGLOS Centre national pour l'exploitation des océans (CNEXO) 66, Av. d'Iéna, Boîte postale 107.16, 75763 Paris CEDEX 16

IRELAND	P. LYNCH National Board for Science and Technology, Shelbourne House, Shelbourne Road, Ballsbridge, Dublin 4
	O. SWEENEY National Board for Science and Technology, Shelbourne House, Shelbourne Road, Ballsbridge, Dublin 4
JAPAN	K. NAGASAKA Japan Meteorological Agency, Marine Department, 1-3-4, Otemachi, Chiyoda-ku, Tokyo 100
PAKISTAN	M.K. KHATTAK Embassy of Pakistan, Moscow
POLAND	B. WIŚNIEWSKI Marine Akademi, 70-500 Szczeciiz, Waty Chvobrego 1
THAILAND	M. HUNGSPREUGS Department of Marine Science, Chulalongkorn University, Bangkok 5
UNION OF SOVIET SOCIALIST REPUBLICS	P.D. AGAFONOV Oceanographic Committee of the Soviet Union, 11, Gorky Street, 103009 Moscow
	V.V. CHUDOV Ministry for Fisheries, 12, Rozhdestvensky Blvd., 103045 Moscow
	Yu.G. IONOV Head Office of Navigation and Oceanography of the U.S.S.R., 11 Linia, Vasilevsky Ostrov, Leningrad
	A.D. KHARLASHIN Hydrometeorological Centre of the U.S.S.R., 9-13 Bolshevistskaya Street, 123376 Moscow
	V.I. KLIMOK Computational Centre, Siberian Branch, Academy of Sciences of the U.S.S.R., 6 Prospect Nauki, 630090 Novosibirsk

UNION OF SOVIET SOCIALIST REPUBLICS (contd.)

V.S. KRASYUK
Hydrometeorological Centre of the U.S.S.R.,
9-13 Bolshevistskaya Street,
123376 Moscow

V.I. LAMANOV
World Data Centre,
6 Korolev Street,
249020 Obninsk, Kaluga District

Sh.A. MUSAELYAN
Hydrometeorological Centre of the U.S.S.R.,
9-13 Bolshevistskaya Street,
123376 Moscow

M.A. PETROSYANTS
Hydrometeorological Centre of the U.S.S.R.,
9-13 Bolshevistskaya Street,
123376 Moscow

V.M. POPOV
U.S.S.R. State Committee for Hydrometeorology and Control of the Natural Environment,
12 Pavlik Morozov Street,
123376 Moscow

K.P. RYZHKOV
U.S.S.R. State Committee for Hydrometeorology and Control of the Natural Environment,
12 Pavlik Morozov Street,
123376 Moscow

V.P. SADOKOV
Hydrometeorological Centre of the U.S.S.R.,
9-13 Bolshevistskaya Street,
123376 Moscow

K.P. VASILIEV
Hydrometeorological Centre of the U.S.S.R.,
9-13 Bolshevistskaya Street,
123376 Moscow

V.B. ZALESNY
Computational Centre, Siberian Branch,
Academy of Sciences of the U.S.S.R.,
6 Prospect Nauki,
630090 Novosibirsk

UNITED STATES OF AMERICA

A. BAKUN
Pacific Environmental Group, Southwest Fisheries Center
National Marine Fisheries Service, NOAA,
c/o F.N.W.C.,
Monterey, California 93940

W.J. EMERY
Department of Oceanography,
University of British Columbia,
Vancouver, B.C. V6T 1W5 (Canada)

UNITED STATES OF AMERICA

W.H. GEMMILL
National Meteorological Center,
National Weather Service, NOAA,
Washington D.C. 20233

E. HASHIMOTO
Office of Naval Research,
Naval Ocean Research Development Activity,
Bldg. 1100, Rm-115,
NSTL Station, MS 39529

R.E. HUNT Jr.
Pacific Marine Environmental Laboratory,
3711 15th Ave. NE,
Seattle, Washington 98105

R.C. JUNGHANS
NOAA, Office of Research and Development (RD1),
6010 Executive Blvd.,
Rockville, Maryland 20852

E. KHEDOURI
U.S. Naval Oceanographic Office,
NSTL Station,
Bay St. Louis, MS 39522

D.G. MOUNTAIN
U.S. Coast Guard Ocean Unit,
Bldg. 159 E, Navy Yard Annex,
Washington, D.C. 20590

J.E. OVERLAND
Pacific Marine Environmental Laboratory,
NOAA, 3711 15th NE,
Seattle, Washington 98105

S.E. PAZAN
Scripps Institute of Oceanography, A-030,
La Jolla, California 92093

S.A. PIACSEK
NORDA, Code 322,
NSTL Station,
Bay St. Louis, Mississippi 39529

W.G. PICHEL
NOAA/NESS, FOB No. 4 S123,
Suitland, Maryland 20233

D. ROSS
NOAA, Environmental Research Laboratories,
Atlantic Oceanographic and Meteorological Laboratories,
Richenbacker Causeway,
Miami, Florida

J.W. SHERMAN
NOAA, World Weather Building Rm 810,
Camp Springs, Maryland 20031

UNITED STATES OF AMERICA (contd.)	B.J. THOMPSON Oceanographic Services Branch, National Weather Service, Silver Spring, Md. 20910
	P.M. WOLFF Ocean Data Systems, 2400 Garden Road, Monterey, California 93940
INTERNATIONAL ORGANIZATIONS	
ICES	J. SMED International Council for the Exploration of the Sea, Charlottenlund Castle, 2920 Charlottenlund, Denmark
SECRETARIATS	
INTERGOVERNMENTAL OCEANOGRAPHIC COMMISSION	A. TOLKACHEV Assistant-Secretary, IOC, UNESCO, place de Fontenoy 75700 Paris, France
	G.W. WITHEE Assistant-Secretary, IOC, UNESCO, place de Fontenoy 75700 Paris, France
WORLD METEOROLOGICAL ORGANIZATION	S. MIZUNO Chief, Ocean Affairs Division World Weather Watch Department Case postale No. 5, Geneva 20, Switzerland